Molecular characterisation of eIF4A paralogues

Adrianna Dabrowska (BSc, MSc)

Thesis submitted in fulfilment of the requirements for the Degree of Doctor of Philosophy at the University of Glasgow

CRUK Beatson Institute

Institute of Cancer Sciences

School of Life Sciences

College of Medical, Veterinary and Life Sciences

University of Glasgow

September 2021

Abstract

Translation dysregulation is a common occurrence in the tumour environment. In cancer cells, numerous regulatory features are perturbed to increase protein output and thus enhance cellular growth. This can be achieved either through overexpression of certain translational factors or dampening translation repression. Importantly, translation initiation is the crucial step at which most regulatory elements converge. Moreover, highly structured 5'UTRs of oncogenic mRNAs often require helicase activity in order to be translated. Interestingly, humans have two highly identical helicases, eIF4A1 and eIF4A2, which have been shown to not only promote different outcomes for cancer patients but also to have divergent translational roles. eIF4A1 is the canonical factor associated with eukaryotic translation initiation complex eIF4F, whereas eIF4A2 has been shown to interact with CCR4-NOT complex, and thus has been implicated in miRNA-mediated translational repression.

The aim of this thesis was to understand what drives the distinct activities of the highly identical paralogues on a molecular level, and what influence the different interaction partners confer on the two helicases.

Using biochemical and structural approaches as well as cell imaging methods, the previously unexplored mechanisms that govern eIF4A2 and the distinct activities between the two paralogues were investigated.

The work presented in this thesis led to description and in-depth investigation of the novel RNA-dependent oligomeric formation of both paralogues. Most importantly, it was demonstrated that the potential to oligomerise dictates the catalytic properties of the paralogues, and that it is the RNA sequence and not the affinity that determines the extent of oligomerisation. Moreover, both helicases have different propensity to form oligomeric complexes. Additionally, regions responsible for divergent functions of eIF4A1 and eIF4A2 were identified. And the different functions imparted by their interaction partners were determined.

This study provides new understanding of the functions of eIF4A1 and eIF4A2 in the translational control and how functionally distinct oligomeric assemblies of the two paralogues can re-sculpture RNA landscapes.

Table of Contents

List of Tables

List of Figures

List of Equations

Acknowledgements

First of all, I would like to express my deepest appreciation for my supervisor Prof. Martin Bushell for investing in me as a scientist and his excellent mentorship along the way.

Next, my sincere gratitude goes to Dr Tobias Schmidt from whom I have learnt so much and who has always pushed me to better myself. Without a doubt, all past and present members of the Bushell lab have made my experience as a PhD student worthwhile and contributed to me becoming the scientist I am today. In particular, I would like to thank Dr Ania Wilczynska for being my good friend and often my voice of reason.

I would also like to thank the members of the Danny Huang lab, for providing great advice and support. My special thanks go to Dr Lori Buetow for battling the CNOT1 protein with me, and Dr Mads Gabrielsen for his humour and for introducing me to the world of SAXS.

I would like to express my gratitude and appreciation to my secondary supervisor Prof. Jim Norman and my panel advisors Prof. Daniel Murphy and Dr Justin Bower. Moreover, my thanks go to the members of the Beatson Institute Molecular Technology Services, Central Services, and the Beatson Advanced Imaging Resource as well as others who have helped me along the way, and the ones who have become my friends. It truly has been a wonderful experience to be a part of the Beatson Institute.

Many thanks go to the people outside of the Beatson Institute, my friends, and my family, who have checked up on me from afar, especially in the final stages of my PhD. Their support means a lot to me.

Last but not least, I owe my deepest thanks to my partner, Dr Ben Hawley, for our late-night scientific talks, for being there when I needed him, and so much more that I cannot express with words, but most importantly for believing in me.

Author's declaration

I hereby declare that the contents of this thesis are my own work unless specifically stated otherwise. This thesis has been submitted for the sole consideration of University of Glasgow.

Abbreviations

4E-BP	eIF4E-binding protein
Å	Ångström
aa	amino acid
aSEC	analytical gel filtration
ATP	adenosine-5'-triphosphate
bp / BP	base-pair
BSA	bovine serum albumin
CBC	cap binding complex
CCR4-NOT	Carbon Catabolite Repression—Negative On TATA-less
CDS	coding sequence
Da	Dalton
DDX	DEAD-box protein
DXH	DEAH-box protein
Dmax	maximum dimension
DMEM	Dulbecco's Modified Eagle Medium
DMSO	dimethyl sulfoxide
DTT	dithiothreitol
DUF	domain of unknown function
E. coli	*Escherichia coli*
EDTA	ethylenediaminetetraacetic acid
EGTA	ethylene glycol-bis(ß-aminoethyl ether)-N,N,N′,N′- -tetraacetic acid

eIF	eukaryotic translation initiation factor
eEF	eukaryotic translation elongation factor
EJC	exon junction complex
em	emission
EMSA	electrophoretic mobility shift assay
eRF	eukaryotic translation termination factor
ex	excitation
FBS	foetal bovine serum
FLIM	fluorescence lifetime imaging microscopy
FRET	fluorescence resonance energy transfer
FP	fluorescence polarisation
FT	flow through
GTP	guanosine-5'-triphosphate
HEPES	4-(2-hydroxyethyl)-1-piperazineethanesulfonic acid
hipp	hippuristanol
His	6x histidine tag
HPLC	high pressure liquid chromatography
I	scattering intensity
IgG	immunoglobulin G
IP	immunoprecipitation
IPTG	isopropyl ß-D-1-thiogalactopyranoside
IRES	internal ribosome entry site
K_D	dissociation constant
kDa	kilodaltons

L	litre
LB	lysogeny broth – bacterial medium
LDH	lactate dehydrogenase
M	molar concentration
m^6A	N6-methyladenosine
m^7G	7-Methylguanosine
mAU	mili absorbance units
mg/mL	milligram per millilitre
MIF4G / MIF	middle domain of eIF4G
MiliQ H_2O	ultra-pure water
min	minute
miRNA	microRNA
mL	mililitre
mM	milimolar concentration
mRNA	messenger RNA
mTOR	mammalian target of rapamycin
NADH	ß-Nicotinamide adenine dinucleotide, reduced
nm	nanometre
nt	nucleotide
OD_{600}	optical density at 600 nm
ORF	open reading frame
P(r)	pair-distance distribution function
PABP	polyA binding protein
PAGE	polyacrylamide gel electrophoresis
PBS	phosphate buffered saline

PCR	polymerase chain reaction
PDB	protein databank
PDCD4	programmed cell death protein 4
pI	isoelectric point
PIC	preinitiation complex
PK	pyruvate kinase
PMSF	phenylmethylsulfonyl fluoride
q	scattering vector
R_g	radius of gyration
RISC	RNA-induced silencing complex
RRM	RNA recognition motif
rRNA	ribosomal RNA
RT	room temperature
s	second
S6K	ribosomal protein S6 kinase beta-1
Sc	*Saccharomyces cerevisiae*
SAXS	small-angle X-ray scattering
SDS	Sodium dodecyl sulphate
SDS-PAGE	sodium dodecyl sulphate–polyacrylamide gel electrophoresis
SEC	size exclusion chromatography
silv	silvestrol
SUMO	small ubiquitin-like modifier
TCEP	Tris(2-carboxyethyl)phosphine
TEV	Tobacco Etch Virus protease

TOP	terminal oligopyrimidine
Tris	Tris(hydroxymethyl)aminomethane
tRNA	transport RNA
ULP1	ubiquitin-like-specific protease 1
UTR	untranslated region
µg/mL	microgram per millilitre
µL	microliter
µM	micromolar
WT	wild type

1. Introduction

1.1. Prelude

A major goal in biomedical science is to understand the biological mechanisms that lead to human disease. Protein synthesis is a cornerstone of biological processes and is discussed in **Chapter 1.3**. It is a tightly regulated mechanism that plays a crucial role in cell growth, proliferation, and differentiation. However, it is just one essential component of the gene expression pathway, and many upstream cellular gene expression decisions affect the translational response. Thus, in **Chapter 1.2**, the entirety of gene expression is briefly discussed, with focus on those steps that affect the translation pathway.

Aberrant protein synthesis is one of the many features of cancer, a disease that stems from within the organism, in which normal cells are transformed into cancer cells. In order to stop tumorigenesis, understanding how cancer exploits protein translation is indispensable (**Chapter 1.4**). As many cancer associated mRNAs contain features that require the activity of helicases, understanding how helicases function is crucial (**Chapter 1.5**). Helicases such as the eIF4A family, which have been shown to play opposite roles in cancer setting, are an attractive target for chemotherapeutic intervention. However, to better develop these drugs, we need to understand how these helicases work and how to target the appropriate one. Finally, in **Chapter 1.6**, the overarching aims of this thesis work are presented.

1.2. Gene expression

The processes within the cell that sustain and allow life are inherently chemical, catalysed by the activity of proteins within numerous and vast networks. The levels of each protein within these networks need to be carefully maintained for cellular homeostasis or modulated to adapt to changes in the environment. Thus, central to all cellular processes is the constant generation of new proteins. This involves the translation of the sequence within an mRNA that was in turn transcribed from a gene within the genomic DNA (**Figure 1.2-1**). This sequential flow of information from DNA to RNA to protein is true for all life and forms the central dogma of molecular biology (Crick, 1970).

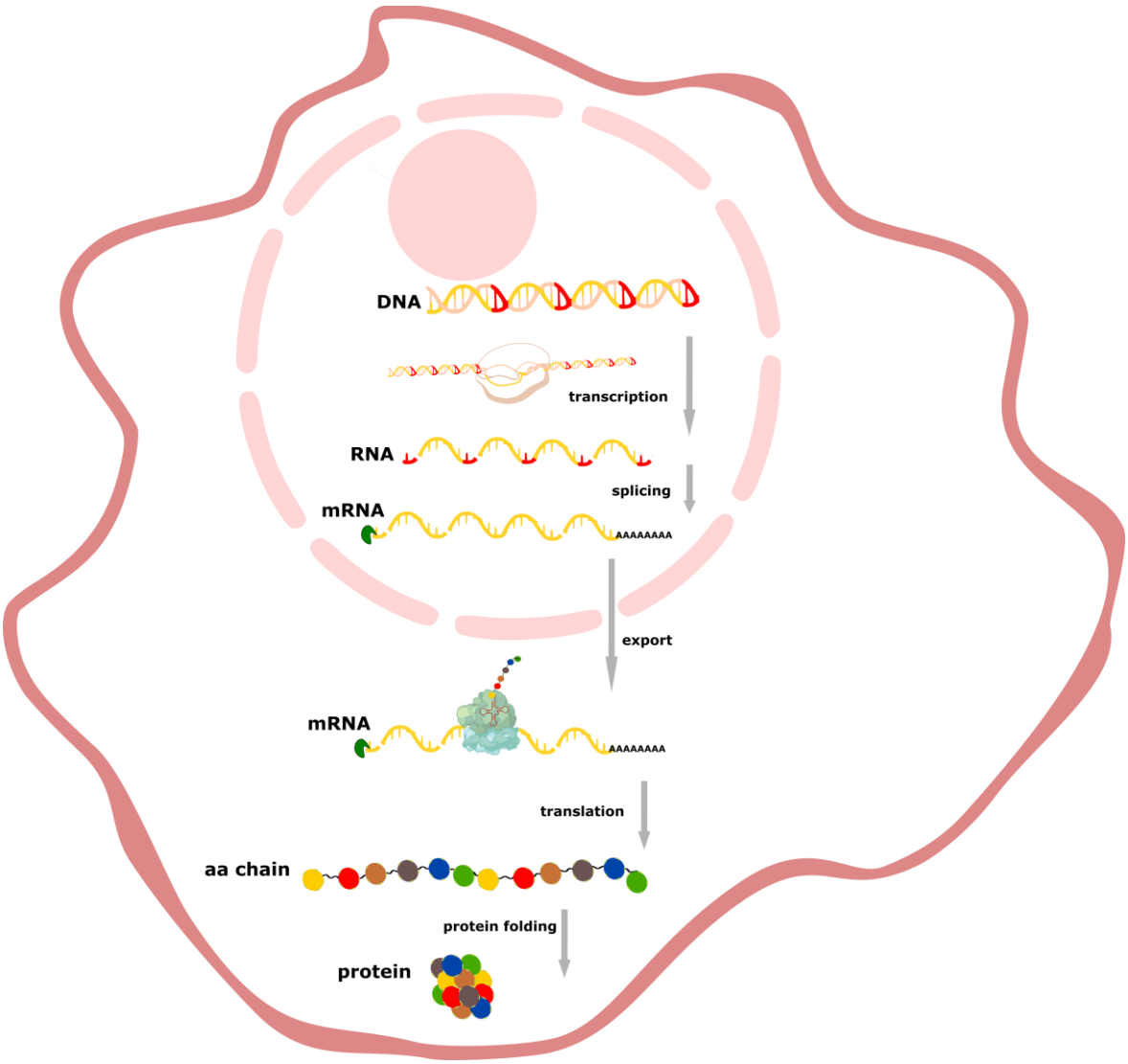

Figure 1.2-1 Central dogma of molecular biology

Central dogma of molecular biology is based on the unilateral flow of information. First, DNA is transcribed into RNA, containing both introns and exons. The splicing machinery removes introns, and mRNA is matured by adding the mRNA cap and polyA tail. The processed mRNA is subsequently exported from the nucleus into the cytoplasm where the mRNA translation into the polypeptide chain can begin. Finally, the amino acid (aa) chain can be folded into a functional protein. Figure drawn using Inkscape 1.1, ribosome outline exported from BioRender.

1.2.1. The human genome

The human genome consists of 22 pairs of autosomal chromosomes, the 23rd pair of sex chromosomes, and the mitochondrial DNA, totalling 3 billion base pairs of DNA sequence (Lander *et al.*, 2001; International Human Genome Sequencing Consortium, 2004; Miga *et al.*, 2020). The human genome comprises both protein-coding and non-coding DNA in the form of genes. As an oversimplified definition, genes are the units of information within the genome. While there are around 20,000 protein coding genes, this in fact only represents a small portion of the human genome (Ezkurdia *et al.*, 2014; Salzberg, 2018). The non-coding portion of the genome represents DNA that will never become a protein. Among the most prominent examples of non-coding DNA are genes transcribed into non-coding RNA like the portion of the genome encoding **1)** transfer RNA (tRNA), **2)** ribosomal RNA (rRNA), **3**) about 2300 human mature miRNAs (Alles *et al.*, 2019), and **4)** other regulatory RNAs (Li and Liu, 2019). Coding DNA is transcribed into mRNA and translated into proteins, whereas non-coding DNA is thought to take part in the regulation of gene expression.

Even though the majority of the genome does not encode a protein, the vast non-coding portion of the genome can affect protein translation; therefore, the small variations between the genomes of individual humans (Abecasis *et al.*, 2012; The 1000 Genomes Project Consortium, 2015) can affect their translational output.

The first step of gene expression involves the generation of numerous copies of a gene in the form of RNA. This process is known as transcription (**Chapter 1.2.2**).

1.2.2. Transcription and mRNA maturation

As this thesis pertains to regulation of protein translation, this transcription subchapter will introduce principles that lead to creation of a mature messenger RNA (mRNA), that in turn can be translated into a protein.

The transcription of a gene to form a mature mRNA is a complex, multi-step process that is subjected to regulation at every stage.

Generally, the genomic DNA can be found wrapped tightly around histones forming a structure referred to as chromatin. The purpose of chromatin is to condense and protect the genome, but also serves as the first regulatory hurdle that a gene must overcome to be expressed. When chromatin is in a highly condensed state the DNA itself is inaccessible and incapable of being transcribed. Thus, the first step of transcription is the unwinding of chromatin (Saha, Wittmeyer and Cairns, 2006; Wang, Allis and Ping, 2007; Phillips and Shaw, 2008). Chromatin remodelling factors modify the "tails" of histones with the addition or subtraction of several chemical modifications. Histone modifications are binding sites for further modifying factors that reinforce a histone "code" that dictates whether a particular genomic region is open and accessible (euchromatin), or condensed and inaccessible (heterochromatin) (Strahl and Allis, 2000; Jenuwein and Allis, 2001; Saha, Wittmeyer and Cairns, 2006; Tropberger and Schneider, 2013). Actively transcribing genes are thus found in euchromatin, while inactive genes are found in heterochromatin. This process is one of the major regulatory control points in the cell, acting through both histone and DNA modifications.

Once the DNA is found in a form of 'active' euchromatin it can be bound by RNA polymerase II (Pol II) and other transcription factors at the DNA promoter site (Travers, 1974; Kornberg, 1999; Sims, Mandal and Reinberg, 2004). Pol II, which is a multiprotein complex, proceeds to separate two strands of DNA by breaking the hydrogen bonds between the DNA base pairs. Subsequently, Pol II adds RNA nucleotides at the transcription start site, proximal to the DNA promoter (transcription initiation) and further translocates the DNA while transcribing its sequence into RNA (transcription elongation). The formed RNA strand is 5' to 3' and complementary bound to 3' to 5' DNA template strand. Subsequently the hydrogen bonds between the newly created RNA and DNA template strand are broken, and the newly synthetised RNA is released (transcription termination). Transcription termination by Pol II can occur in two different stages: **1)** recognition of the polyadenylation signal and joining of the cleavage and polyadenylation factor (CPF) and the cleavage factors IA, IB, **2)** 'torpedo' model, where Pol II is removed from the template by collision with other termination factors (Lykke-Andersen and Jensen, 2007).

It should be noted that, while the steps of transcription are often conceptualised as a linear progression of events, many steps occur concurrently. One of the examples of simultaneous processes are the so-called post-transcriptional modifications of the newly synthetised RNA.

The first of these is the important step of the addition of the cap structure. The cap is present on all mature human mRNAs (apart from mitochondrial mRNAs (Temperley *et al.*, 2010)) and is added by the capping enzyme complex (CEC) associated with Pol II. The CEC adds a non-templated guanosine to the 5'-most nucleotide and methylates this at the N7 position soon after the first few nucleotides are transcribed (Cho *et al.*, 1997). As will be described later (**Section 1.3.2**), the resulting mRNA m^7G cap is the docking point for the factors involved in translation initiation. Furthermore, it protects the mRNA from 5'-3' nucleolytic degradation in both the nucleus and the cytoplasm (Filipowicz *et al.*, 1976; Shatkin, 1976).

Additional modifications that are added co-transcriptionally and influence the translation of that mRNA are additional nucleotide methylations. One of the most common methylations is found on the N6 position of adenosine (m^6A), which is deposited by METLL3/METLL14 on around 25 % of all mRNAs (Dominissini *et al.*, 2012; Meyer *et al.*, 2012). This modification has been shown to have a strong role in destabilisation of the mRNA (Zaccara and Jaffrey, 2020).

A key stage of mature mRNA production is the splicing of the precursor mRNA (Berget, Moore and Sharp, 1977). The process of splicing involves the removal of introns (DNA segments located between two exons) by the spliceosome (Will and Luhrmann, 2011; Herzel *et al.*, 2017). Due to existence of the process called alternative splicing, a single precursor mRNA can become a range of mature mRNAs, which in turn could be translated into different proteins (Pan *et al.*, 2008). After the mRNA is spliced, a protein complex called exon junction complex (EJC) binds around the junction of the two exons (after intron excision), which can affect the translational output of the given mRNA (Nott, Le Hir and Moore, 2004; Tange, Nott and Moore, 2004).

Another important step is addition of the polyadenylate (polyA) tail to the 3' end of the newly synthetised mRNA (precursor mRNA) after its release by the above-mentioned cleavage and polyadenylation factors. As will be discussed later, the

polyA tail is a crucial *cis*-regulatory component of the mature mRNA (**Chapter 1.2.4**, **1.3.6**). The addition of polyA is performed by polyadenylate polymerase, which adds adenosine monophosphates to the RNA (Bienroth, Keller and Wahle, 1993; Balbo and Bohm, 2007). It is worth noting that, until recently, polyA tail was considered to be entirely homogenous; however, a recent publication (Lim *et al.*, 2018) demonstrated that the polyA can in fact be heterogenous.

1.2.3. Protein synthesis

Following transcription, the newly synthetised mRNA is subjected to one of the two fates: **1)** binding by a number of factors and nuclear export, **2)** degradation by the nuclear exosome in case of improper mRNA processing (Bousquet-Antonelli, Presutti and Tollervey, 2000; Liu, Luo and Wen, 2014). In the first instance, the newly synthesised cap of the mature mRNA is bound in the nucleus by the cap-binding complex (CBC), which is a heterodimer consisting of CBP20 and CBP80 (Izaurralde *et al.*, 1995). Similarly, the 3'end of the newly synthetised mRNA is bound by a nuclear polyA-binding protein, PABP2 (Dreyfuss, Kim and Kataoka, 2002). The mature RNA, ready for export, remains bound by the above-mentioned exon junction complex (**Chapter 1.2.2**). The nuclear export of mRNA is atypical and differs from the export of proteins, tRNA and miRNA and is mediated through the membrane associated protein TAP (Herold *et al.*, 2000). The presence of the CBC has also been implicated in the mediation of nuclear export (Izaurralde *et al.*, 1992). After the export from the nucleus through the nuclear pore complex, the mRNA can be translated by the ribosome to generate a protein.

All protein synthesis across all of life is catalysed by the ribosome. While there are differences between prokaryotes, archaea, and eukaryotes, the ribosome is broadly the same machine consisting of two subunits, each of which is made of ribosomal RNA (rRNA) and numerous proteins. The ribosome utilises transfer RNA (tRNA) to decode an mRNA and assemble the polypeptide chain that ultimately folds into a mature protein.

The pioneer round of translation (**Figure 1.2.3-1**), in contrast to the steady-state rounds of translation which generate the bulk of cellular proteins, offers a quality control of gene expression (Isken and Maquat, 2008). It is employed by the cell to detect splicing errors that resulted in the introduction of premature translation stop sequences (codons; see **Chapters 1.3.1**, **1.3.4**). The consequence of unchecked premature stop codons is that a nonsense protein could be made that may be detrimental to the cell. When the pioneering ribosome encounters this premature stop codon which is usually located at more than 50 nucleotides upstream of the EJC on that mRNA, a nonsense-mediated decay process is triggered (Maquat, Tarn and Isken, 2010). The CBC itself has been shown to play a role in nonsense-mediated decay of mRNA due to direct interaction between CBP80 and up-frameshift 1 (UPF1) nonsense-mediated decay factor, which is a part of SURF complex involved in recognition of premature stop codons (Lykke-andersen, Shu and Steitz, 2000; Hosoda *et al.*, 2005; Kashima *et al.*, 2006; Isken and Maquat, 2008).

If the pioneering ribosome completes translation of protein from a given mRNA without encountering premature stop codons, the canonical steady-state translation can begin. In that case the nuclear proteins are exchanged for cytoplasmic factors: **1)** CBC is replaced by eIF4E, **2)** nuclear PABP2 is exchanged for cytoplasmic PABP1, and **3)** EJC is displaced by the translating ribosome (Maquat, Tarn and Isken, 2010). Steady-state translation consists of 3 steps: initiation, elongation and termination and leads to production of polypeptide chain that can subsequently be folded into a mature protein. For the detailed description of steady-state cytoplasmic translation please refer to **Chapter 1.3**.

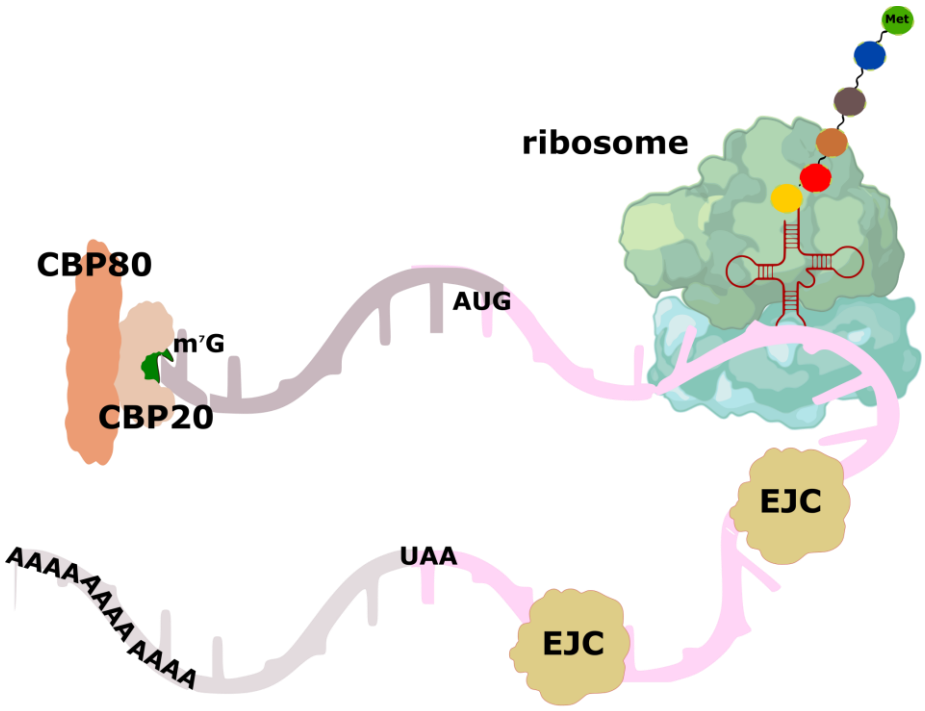

Figure 1.2.3-1 Pioneer round of protein translation

In the pioneer round of protein translation, the mature mRNA cap is bound by the CBC complex consisting of CBP20 and CBP80. The first round of translation consists of the same 3 steps as steady-state translation: initiation, elongation, and termination. During the pioneer round the ribosome encounters exon junction complexes (EJC) bound to the mRNA at the exon-exon junctions created after mRNA splicing. Ribosome dislocates EJC while it translocates the mRNA and produces first amino acid chain. Pioneer round of translation is used by the cell as a quality control measure to detect mRNAs with premature translation stop codons. Figure drawn using Inkscape 1.1; ribosome outline exported from BioRender.

1.2.4. mRNA turnover

Translation of a given mRNA into a protein is only one of its possible fates. To account for rapidly changing needs of the cell, mRNA can also be stored or degraded. In fact, the average mRNA half-life is around 4 hours (Herzog *et al.*, 2017), however this can vary from few minutes to days (Aviv *et al.*, 1976; Ross and Sullivan, 1985; Wisdom and Lee, 1991).

Actively translated mRNAs are bound by ribosomes and other translation factors, including **1)** the cap binding protein, which prevents mRNA decapping by the decapping enzymes DCP1/DCP2, and **2)** the polyA binding protein, which

prevents deadenylation (i.e., removal of 3' adenosines) (Parker and Song, 2004) (**Figure 1.2.4-1**). When the mRNA is 'unprotected' and deadenylation and decapping occur, the mRNA can be degraded either in a **1)** 3'-to-5' direction by the cytoplasmic exosome (Schmidt *et al.*, 2016; Zinder and Lima, 2017), or in **2)** 5'-to-3' direction by XRN1 exonuclease (Parker and Song, 2004; Mugridge, Coller and Gross, 2018). It is worth noting that recent reports suggest that mRNA degradation can happen co-translationally, meaning the ribosomes can still be detected on an mRNA that is degraded from 5'-to-3' direction (Hu *et al.*, 2009; Pelechano *et al.*, 2015; Tat *et al.*, 2016).

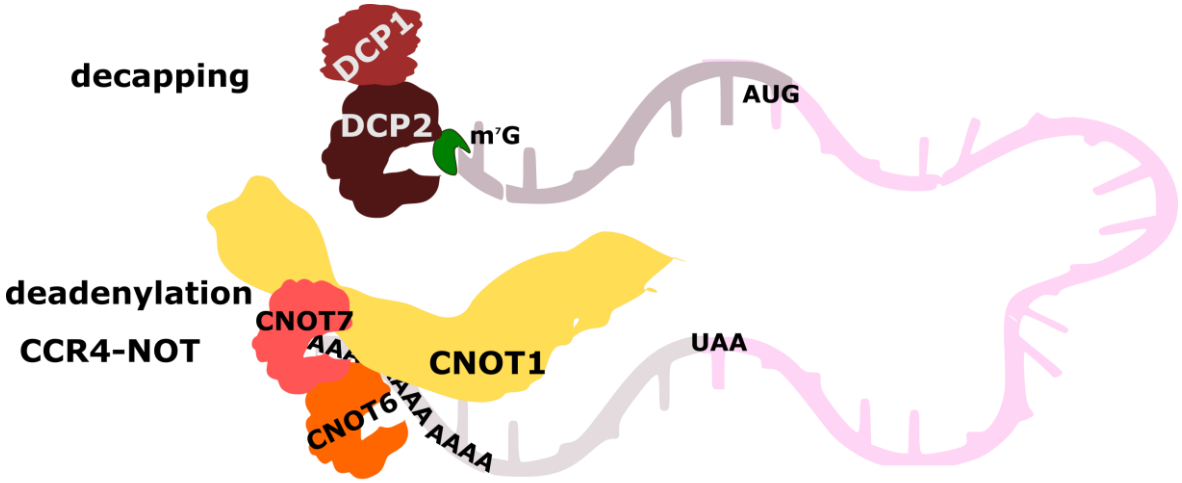

Figure 1.2.4-1 mRNA turnover

Simplified schematic of first steps of mRNA degradation. CCR4-NOT complex, presented here as CNOT1 scaffold protein with two deadenylases CNOT6 and CNOT7, and the decapping complex shown as DCP1/DCP2. Figure drawn in Inkscape 1.1.

Generally, in humans, deadenylation can be mediated by various enzymes such as the CCR4-NOT complex, polyA-specific ribonuclease (PARN), PAN2-PAN3 complex, Nocturin, or Angel (Godwin *et al.*, 2013; Shirai *et al.*, 2014). The bulk of deadenylation in mammalian cells is thought to be performed by PAN2-PAN3 and the CCR4-NOT complex. Previous reports suggested that PAN2-PAN3 primes the polyA tail for subsequent deadenylation by CCR4-NOT (Yamashita *et al.*, 2005; Bartlam and Yamamoto, 2010), however a more recent report proposed

deadenylation of different subsets of mRNAs by the two complexes (Yi *et al.*, 2018). Moreover, contrary to previous reports (Parker and Song, 2004), the polyA-binding protein has been show to promote deadenylation by inhibiting premature decay (Yi *et al.*, 2018). However, deadenylation is far from a simple process, where the recently described heterogeneity of polyA tail can impede removal or shortening of polyA tail (Lim *et al.*, 2018). Additionally, the length of polyA tail itself can play a role in mRNA stability, with both too-short and too-long polyA tails prompting mRNA degradation (Jalkanen, Coleman and Wilusz, 2014). This evidence further rationalises that the mRNA life is regulated not only in *trans*, i.e., through factors outside of the mRNA, such as RNA-binding proteins, but also in *cis* through the mRNA features themselves.

Depending on the type of degradation, deadenylation of an mRNA can trigger mRNA decapping. As written above, mRNA can be degraded in the 5'-to-3' direction following deprotection of the 5' end by removal of the m^7G cap. 5'-to-3' mRNA decay occurs during the above-mentioned nonsense-mediated mRNA decay (**Chapter 1.2.3**) that usually arises during the pioneer round of translation upon detection of premature RNA stop codons upstream of EJC (Karousis and Mühlemann, 2016). However, there have been reports in the literature about EJC-independent nonsense-mediated mRNA decay (Zhang *et al.*, 1998; Matsuda *et al.*, 2007; Karousis and Mühlemann, 2016).

Moreover, additional features of mRNA can promote or restrict degradation, i.e.,**1)** the described above m^6A found mostly in the 3'UTR of 25 % of all mRNAs (Zaccara and Jaffrey, 2020), **2)** the cap proximal modifications, as m^6Am, which enhances resistance to DCP2 decapping enzyme (Mauer *et al.*, 2017), **3)** AU-rich elements (AREs), which can be bound by RNA binding proteins like tristetraprolin (TTP), which in turn interacts with CNOT1, part of the CCR4-NOT complex (Fabian *et al.*, 2013), **4)** miRNA binding sites, which recruits miRNA-RISC complex, which in turn can recruit other complexes, like CCR4-NOT and prompt mRNA turnover (Wilczynska and Bushell, 2015). As miRNA can also mediate mRNA repression and not simply degradation, this concept is further explored in **Chapter 1.3.6**.

Moreover, mRNA can be damaged, e.g., through oxidation, or it can be simply degraded by endonucleases.

Finally, mRNA can also be stored in highly conserved cytoplasmic structures called P-bodies. Recent studies have implicated P-bodies as a storage location for mRNAs on which translation can be re-initiated (Brengues, Teixeira and Parker, 2005; Bhattacharyya *et al.*, 2006; Mozziconacci *et al.*, 2017). However, the precise role of P-bodies is still debated. Many mRNA decay factors such as the CCR4-NOT complex, DCP1/DCP2 decapping complex, and 5'-to-3' exonuclease XRN1 are found in P-bodies, which would suggest that mRNA can be degraded inside P-bodies (Morales, Kwon and Hecht, 1991; Ingelfinger *et al.*, 2002; Sheth and Parker, 2003; Cougot, Babajko and Séraphin, 2004; Andrei *et al.*, 2005). Therefore, more research is required to understand the precise function of P-bodies.

Moreover, upon cellular stress mRNAs can enter different cytoplasmic formations, called stress granules (SG). As with P-bodies, the exact function of mRNAs in SGs is widely debated, with some reports suggesting that SGs are a location of mRNA storage (Mollet *et al.*, 2008; Khong *et al.*, 2017; Lee and Seydoux, 2019) and others indicating that mRNA can actually be actively translated inside the SG (Mateju *et al.*, 2020).

In all, life of an mRNA is far from simple, with many regulatory elements dictating its fate, which in turn affects its final output – protein.

1.2.5. Protein turnover

The last component of gene expression is the degradation of a protein. Steady-state levels of a protein are a function of its synthesis rate and the degradation rate. The synthesis rate itself is determined by the rates of transcription, mRNA processing, and translation. While the modulation of translation rate determines a greater proportion of overall protein levels (Schwanhüusser *et al.*, 2011), degradation rate can be the major regulation step for subsets of proteins in particular conditions (Jovanovic *et al.*, 2015). For example, mitophagy during infection (Jovanovic *et al.*, 2015) or autophagy during starvation (Wang *et al.*, 2015; Kocaturk and Gozuacik, 2018; Chen, Chen and Huang, 2019).

Protein degradation is an active and predominantly controlled process, meaning there are cellular pathways to specifically deplete proteins in a regulated manner. This can be done to allow protein levels to be changed rapidly in response to stimuli. There are two major protein degradation pathways: **1)** the ubiquitin-proteasome pathway (UPP), and **2)** lysosomal proteolysis. The first UPP, is perhaps the most well understood, and starts with post-translational modification, called ubiquitination. Ubiquitin is a small, 8.6 kDa protein, that is covalently attached to the target protein's lysine residues by ubiquitin ligases (Goldstein *et al.*, 1975; Ciechanover *et al.*, 1980; Hershko *et al.*, 1980). This is a marker for degradation, however degradation-independent functions of ubiquitinylated proteins have been described, such as altered cellular localisation or inhibition of protein-protein interactions (Schnell and Hicke, 2003; Debdyuti and Howard, 2007). The protein marked for degradation is subsequently translocated to the proteasome, a large tube-like multimeric protein complex, and degraded through proteolysis (Glickman and Ciechanover, 2002). Unlike UPP, the second pathway, lysosomal proteolysis, is not selective in normal conditions, meaning that the protein does not need to bear a marker for degradation. Inside the lysosome, which is an organelle that contains a range of acidic proteases, proteins are entirely digested.

Interestingly, histones, which as described above (**Chapter 1.2.2**) modulate the structure of chromatin, can be ubiquitinated. This ubiquitination therefore alters the structure of chromatin and changes the transcription of genes (Hammond-Martel, Yu and Affar, 2012). This is an example how the end point of the gene expression pathway can affect the very start.

All proteins in the cell have a specific half-life, which can vary between individual proteins, and can be based on their intracellular location or function. The average range is between 4 and 14 hours, and the median at 8.7 hours (Chen, Smeekens and Wu, 2016). The notion that each protein has its half-life, affects also the proteins involved in protein translation. In fact, the median half-life of eukaryotic translation initiation factors is 7.1 hours (Chen, Smeekens and Wu, 2016), suggesting that a faster turnover of initiation factors might be another regulatory element of translation control.

1.3. Mechanisms in translation

Protein synthesis is a multistep process that involves the decoding of mRNA to generate the proteins that can carry out the majority of cellular processes. Practically every step of protein synthesis can be exploited in disease (**Chapter 1.4**). This chapter discusses how these mechanisms act in concert to produce the final protein.

The first step of translation is initiation, which is the process of ribosome loading onto the mRNA (**Chapter 1.3.2**). This is the rate-limiting step of translation and has the biggest impact on overall translation rates. Next, the assembled ribosome enters the elongation phase, and the polypeptide chain is formed (**Chapter 1.3.3**). Eventually, the ribosome terminates and can begin the cycle all over again (**Chapters 1.3.4** and **1.3.5**). Before these steps are discussed, the features of the mature mRNA that are relevant to translation are introduced (**Chapter 1.3.1**). Finally, an overview of mechanisms that repress translation to regulate synthesis rates is given (**Chapter 1.3.6**).

1.3.1. mRNA features

To understand protein translation, one must recognise and appreciate the features of mRNA and its regulatory elements that together with translation factors can dictate the protein output from a given mRNA.

Each mature mRNA consists of three regions: a 5' untranslated region (5'UTR), a coding sequence (CDS), and a 3' untranslated region (3'UTR) (**Figure 1.3.1-1**).

The 5'UTR starts with the m^7G cap, directly upstream of the first transcribed nucleotide. The length of the 5'UTR can vary between different mRNAs from a few nucleotides to hundreds of nucleotides, with the average human 5'UTR length of around 200 nt (Pesole *et al.*, 2001; Leppek, Das and Barna, 2018). Very short 5'UTRs can possess a "translation initiator of short 5'UTR" (TISU) element, found in around 4% of human genes (Elfakess and Dikstein, 2008; Elfakess *et al.*, 2011). The start of translation from TISU is independent of other 5'UTR features

and does not require some of the translation factors that are indispensable for translation from longer 5'UTRs (Elfakess *et al.*, 2011).

In contrast, the more numerous longer 5'UTRs can contain more regulatory elements. Apart from the cap and cap proximal modifications that act as translation regulators (**Chapter 1.2.2**), different RNA sequence motifs can be found in the 5'UTR. One of the most widely studied motifs, found immediately adjacent to the cap, is the TOP (terminal oligopyrimidine) motif. This group of mRNAs start with a cytosine followed by 4 to 14 uninterrupted pyrimidines (Levy *et al.*, 1991; Avni, Biberman and Meyuhas, 1997; Biberman and Meyuhas, 1999). The TOP motif is found on mRNAs encoding ribosomal proteins and translation factors, and is thought to be regulated by nutrient availability (Iadevaia *et al.*, 2008; Hsieh *et al.*, 2012; Thoreen *et al.*, 2012; Meyuhas and Kahan, 2015). Other examples of 5'UTR motifs occur further downstream of the mRNA cap, such as the pyrimidine-rich translational element (PRTE) (Hsieh *et al.*, 2012; Thoreen *et al.*, 2012), and the cytosine-enriched regulator of translation (CERT) motif (Truitt *et al.*, 2015). PRTE, as in the case of TOP motifs, confers regulation in *cis* depending on nutrient availability (Hsieh *et al.*, 2012; Thoreen *et al.*, 2012); in contrast the exact regulatory function of the CERT motif is unknown (Truitt *et al.*, 2015; Calviello *et al.*, 2021).

Longer 5'UTRs can also contain structured regions, such as stem loops, or G-quadruplexes (Wolfe *et al.*, 2014; Hinnebusch, Ivanov and Sonenberg, 2016; Leppek, Das and Barna, 2018; Waldron *et al.*, 2019). Structural elements are generally thought to be repressive elements that require activity of proteins to resolve the secondary structures (see **Chapter 1.5**). However, some mRNA structures are reported to act as an internal ribosome entry site (IRES), which allow for start of translation without the recruitment of the cap binding proteins. IRESs, which were first identified in viral genomes (Pelletier and Sonenberg, 1988), allow viruses to hijack human translation initiation factors to promote translation of viral RNA (Bushell and Sarnow, 2002; Kieft, 2008). However, later IRES structures have also been shown to exist in a subset of human mRNAs (Johannes and Sarnow, 1998; Jackson, 2013; Weingarten-Gabbay *et al.*, 2016). Additionally, a preference for IRES-mediated translation start has been observed after cell stress (Spriggs *et al.*, 2008).

Moreover, long 5'UTRs can contain upstream open reading frames (uORFs), which are coding sequences upstream of the main CDS. uORFs have been shown to be present in nearly 50% of human mRNAs (Iacono, Mignone and Pesole, 2005; Matsui *et al.*, 2007; Calvo, Pagliarini and Mootha, 2009). While uORFs could encode small peptides that may have a function, these peptides are not thought to be the primary role of uORFs. Instead, the process of translation of a uORF itself is inhibitory to translation from the main ORF (CDS) (see also **Chapter 1.3.5**); however, this is not always the case (Hinnebusch, Ivanov and Sonenberg, 2016).

The CDS encodes the part of mRNA that will be translated into protein. Three-nucleotide sequences (codons) encode different amino acids throughout the CDS. The CDS starts with a translation start site, for which the most common is an AUG (adenine, uracil, guanine) codon, that is read by the translation machinery as a methionine. Moreover, the AUG start codon in many mRNAs is flanked by a favourable sequence named Kozak consensus, i.e., GCC(A/G)CC**AUG**G (Kozak, 1986, 1989). The AUG start codons without the Kozak consensus are thought to be in 'poor context' and translation from those codons is not as efficient (Kozak, 2002). It should be noted that, translation can also start from a non-cognate (non-AUG) start codon, such as CUG, GUG, UUG, ACG, AUA, and AUU (Gerashchenko, Su and Gladyshev, 2010; Lobanov *et al.*, 2010; Ivanov *et al.*, 2011). Translation from non-cognate start codons has been thought to be very unfavourable, however a more recent study suggested that translation from non-cognate codons is more prevalent than originally thought (Kearse and Wilusz, 2017).

The 3'UTR region of mRNA starts right after the translation termination codon. There are three translation stop codons in humans, UAA, UAG, UGA, with the exception of the two mitochondrial codons: AGA, AGG (Barrell, Bankier and Drouin, 1979). Unlike other codons, the stop codons, do not correspond to any amino acids, with the exception of UGA, which can be read as selenocysteine (Zinoni *et al.*, 1986; Copeland, 2003). However, in humans there are only 25 identified selenoproteins (Kryukov *et al.*, 2003), and the incorporation of selenocysteine requires specific structural motif (selenocysteine insertion sequence - SECIS) in mRNA in the proximity of the UGA stop codon (Mix, Lobanov and Gladyshev, 2007). The presence of selenoproteins adds to growing evidence

that not only coding sequence matters when it comes to protein translation but also the structural and sequence elements of the mRNA.

Similarly, as with the 5'UTR, the length of 3'UTR can vary between different mRNAs. On average the 3'UTR is longer at around 800 nucleotides in humans (Mignone and Pesole, 2018), spanning between 60 and 4000 nucleotides between different mRNAs (Hesketh, 2005). As 3'UTRs are long, they can contain many regulatory elements, like the above-mentioned (**Chapter 1.2.4**) destabilising AREs or miRNA binding sites. Binding of miRNAs to the 3'UTR can lead to translation repression, which is described further in **Chapter 1.3.6**. Alike the 5'UTR, the 3'UTR can contain ORFs (downstream ORF – dORF) (Bazzini *et al.*, 2014; Mackowiak *et al.*, 2015; Chen *et al.*, 2020). Unlike uORFs, dORFs are proposed to enhance the protein translation from the main ORF (Wu *et al.*, 2020). Albeit the identification of dORFs and their functions is a new and rapidly growing field, therefore full influence of their presence on mRNA stability and translation cannot be assessed.

Finally, the most well-known 3'UTR feature is the polyA tail, which acts as a stabiliser of mRNA and provides a binding location for other regulatory proteins.

Apart from the described features of specific regions of mRNA, *cis* and *trans* regulatory elements can act in concert to provide a link between 5'- and 3'UTR. This link, known as mRNA circularisation (Wells *et al.*, 1998; Tomek and Wollenhaupt, 2012; Alekhina *et al.*, 2020) happens through interactions of proteins bound to the 5'UTR with the proteins bound to the 3'UTR of a given mRNA (see **Chapter 1.3.2**), which bring the two ends of mRNA closer together.

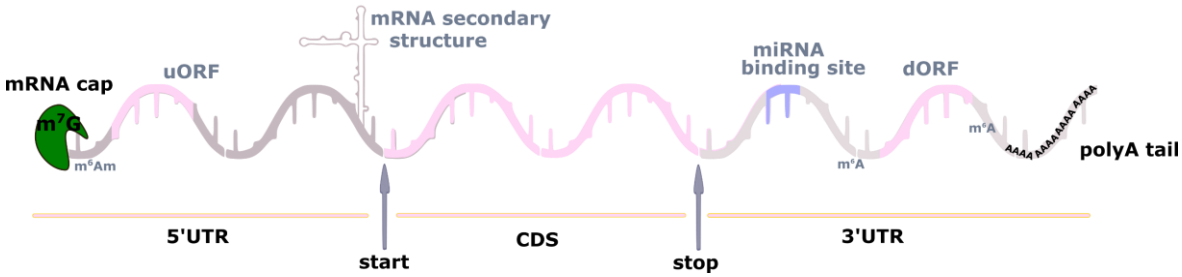

Figure 1.3.1-1 mRNA features
Mature mRNA consists of **1)** 5'untranslated region (5'UTR), also known in the literature as mRNA leader, **2)** coding sequence (CDS), that encodes the genetic information of a protein, and **3)** 3'untranslated region (3'UTR). Each mRNA has m^7G cap (with exception of mitochondrial mRNAs) and a polyA tail, length, and homogeneity of which can vary. Additionally, mRNAs can have upstream or downstream open reading frames (uORF, dORF), which are a coding sequence outside of the main CDS and can lead to creation of different isoforms of the same protein, inhibition of translation from the main ORF, or to translation of small peptides. Moreover, mRNAs can have secondary structures, usually found in the 5'UTR, miRNA binding sites (typically found in the 3'UTR), and post-transcriptional modification, as commonly found in 3'UTR m^6A or, modifications close to the mRNA cap. Features of all mRNAs labelled in black, features not present in all mRNAs labelled in grey. Figure drawn in Inkscape 1.1.

1.3.2. Translation initiation

Translation initiation is considered to be the most complex phase of protein translation, as it requires a large number of protein factors and is highly controlled (Sonenberg and Hinnebusch, 2009; Jackson, Hellen and Pestova, 2010). Being the most controlled stage of translation, initiation is also considered to be rate-limiting. The rates of initiations can vary depending on presence of regulatory elements in the 5'UTR (as described in **Chapter 1.3.1**) as well as on availability and activity of translation initiation factors. Translation initiation is a consecutive process, where each stage has to precede the next. Translation initiation on the majority of mRNAs can be divided in a few basic steps: **1)** mRNA binding by the cap binding complex – eIF4F, **2)** formation of 43S preinitiation complex (43S PIC) consisting of 40S ribosomal subunit, cofactors and methionine-bearing tRNA, **3)** recruitment of the 43S PIC to the mRNA, **4)** ribosome scanning through the 5'UTR in order to localise the initiation codon, and **5)** joining of the 60S ribosomal subunit to form the fully mature 80S ribosome to enable elongation (**Figure 1.3.2-1**) (Jackson, Hellen and Pestova, 2010; Dever and Green, 2012; Hinnebusch and Lorsch, 2012; Zhang *et al.*, 2019).

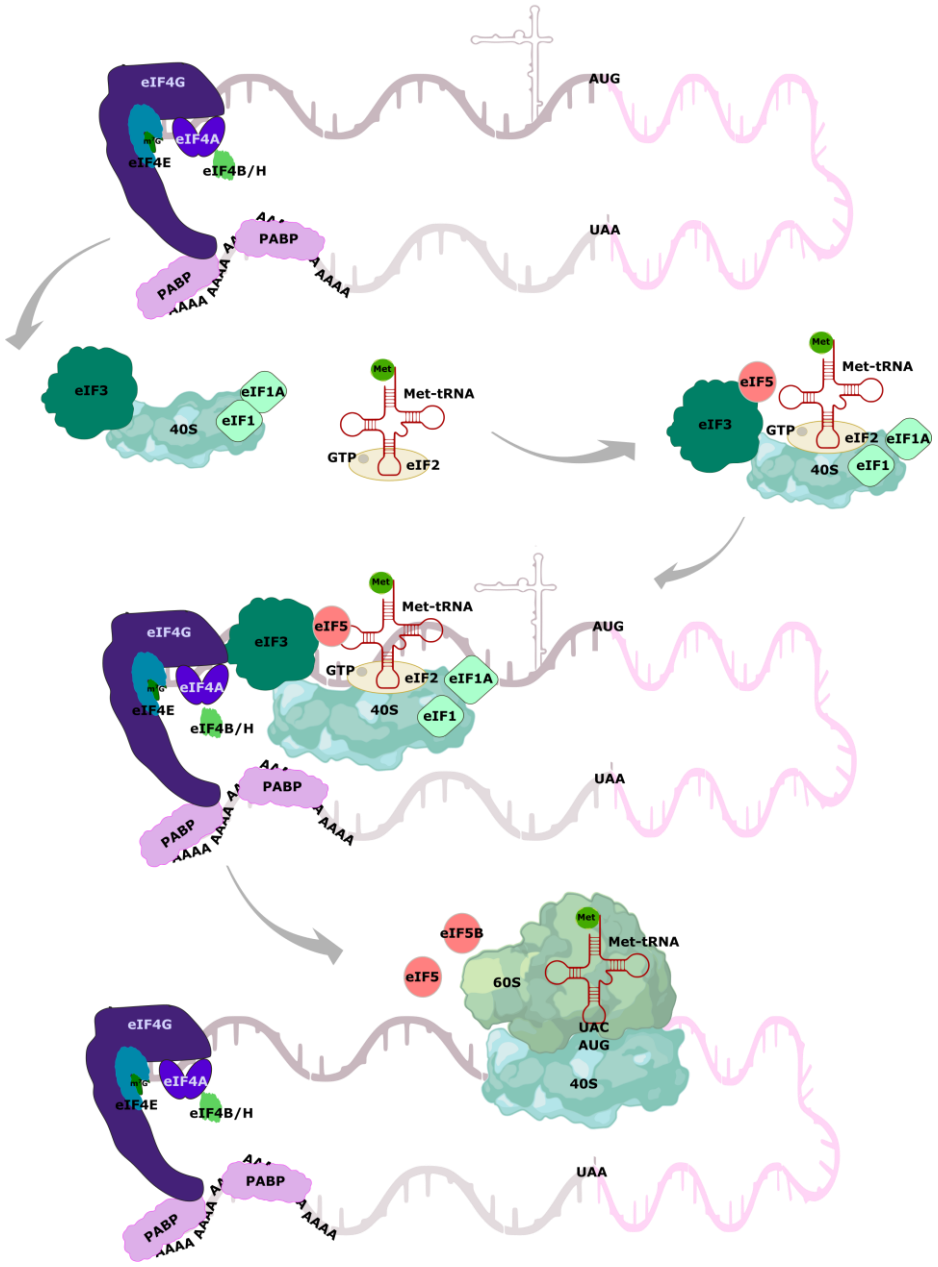

Figure 1.3.2-1 Stages of translation initiation

Translation initiation is the most rate-limiting step of protein synthesis and requires the largest amount of highly specialised translation factors. Cap-dependent translation starts by eIF4E cap-binding protein binding m^7G, which is joined by eIF4G and eIF4A, forming together eIF4F complex. On the other end of mRNA, PABP protein binds the polyA sequence and due to interaction between eIF4G and PABP, mRNA can be circularised. Separately, 43S PIC is assembled from 40S ribosomal subunit, and translation initiation factors eIF1, eIF1A, eIF3, eIF5, joined by the ternary complex (eIF2-GTP Met-tRNA). Assembled 43S PIC is subsequently recruited to the mRNA due to interaction between eIF4G and eIF3, as well as the help of eIF4A. Next, secondary structures within the 5'UTR are unwound by the helicases involved in translation, like eIF4A or DHX29 (not shown). Unwinding of the structures allows for translocation of 43S PIC along the 5'UTR to find translation start codon (marked as AUG). Upon binding of the AUG, 60S ribosomal subunit is recruited to the 40S with help of eIF5B, and due to activation of eIF2 by eIF5. Assembled 40S and 60S form 80S translation competent ribosome. Figure drawn in Inkscape 1.1; ribosome outline exported from BioRender.

In the first step the 25 kDa cap binding protein eIF4E recognises and binds the m^7G cap on the 5' end of the mRNA. Interestingly, eIF4E is the least abundant initiation factor and has been thought to be the limiting factor for mRNA translation (Duncan, Milburn and Hershey, 1987). However, this observation has been challenged. It has been reported that only about a quarter of total eIF4E in rabbit reticulocyte lysate associates with ribosomes, and eIF4E depletion has only a moderate effect on protein translation (Rau *et al.*, 1996). Similarly, a more recent study (Truitt *et al.*, 2015), showed that 50 % of the normal level of eIF4E is not detrimental to the global protein synthesis or normal development.

eIF4E is joined by another subunit of the eIF4F complex, eIF4G. However, it is not clear whether the cap binding is necessary for eIF4G recruitment, or whether the complex binds to the cap together. eIF4G, at 220 kDa, is the largest component of the heterotrimeric eIF4F and joins eIF4E opposite to the eIF4E's cap binding pocket (Marcotrigiano *et al.*, 1999). eIF4G is considered to be a scaffold protein, as it provides binding sites for other proteins involved in translation (Gingras, Raught and Sonenberg, 1999), such as **1)** eIF4A, another component of the eIF4F complex, **2)** the polyA binding protein PABP, which interaction, as mentioned above (**Chapter 1.3.1**), allows for mRNA circularisation, **3)** eIF3, a thirteen subunit multi protein complex, and **4**) mitogen activated protein kinase interacting kinase 1 – Mnk1 (**Figure 1.3.2-2**) (Lamphear *et al.*, 1995; Imataka, Olsen and Sonenberg, 1997; Imataka, Gradi and Sonenberg, 1998; Pyronnet *et al.*, 1999; Korneeva *et al.*, 2001).

The only factor known to have a catalytic activity in the eIF4F complex is the 46 kDa DEAD-box RNA helicase eIF4A (Rogers, Richter and Merrick, 1999; Rogers *et al.*, 2001). Its canonical role, which is often aided by auxiliary factors eIF4H, eIF4B, and the other components of eIF4F (Korneeva *et al.*, 2005; Nielsen *et al.*, 2011; Özeş *et al.*, 2011; Feoktistova *et al.*, 2013), is to unwind secondary structures within the mRNA to offset their repressive influence on protein translation. However, a recent report suggested an additional RNA unwinding-independent role of eIF4A helicase in mRNA recruitment to the ribosome (Sokabe and Fraser, 2017).

To add to the complexity of translation initiation and different functions performed by the proteins in the eIF4F complex, each of the components of eIF4F has their own paralogues. The differences can be minor, such as the ones between eIF4G1 and eIF4G3, or larger, with the paralogue missing multiple binding sites for interaction partners, as is the case with eIF4G2 (**Figure 1.3.2-2**). This could lead to formation of multiple different, specialised eIF4F complexes (Robert *et al.*, 2020), with different paralogues, performing diverse functions (Imataka, Olsen and Sonenberg, 1997; Osborne *et al.*, 2013; Liberman *et al.*, 2015; Alard *et al.*, 2019). However, as this thesis pertains to investigation of eIF4A, the following text is focused solely on differentiation between the three eIF4A paralogues, i.e., eIF4A1, eIF4A2, and eIF4A3. eIF4A1 is the more abundant paralogue (Nielsen and Trachsel, 1988; Galicia-Vazquez *et al.*, 2012), thought to be the dominant one in the eIF4F complex, while the 90% identical eIF4A2 has a recently identified role in translational repression (Meijer *et al.*, 2013, 2019; Wilczynska *et al.*, 2019), and the 60% identical eIF4A3, forms a part of the exon junction complex (Holzmann *et al.*, 2000; Chan *et al.*, 2004). The eIF4A helicases are discussed in detail in **Chapter 1.5.2**.

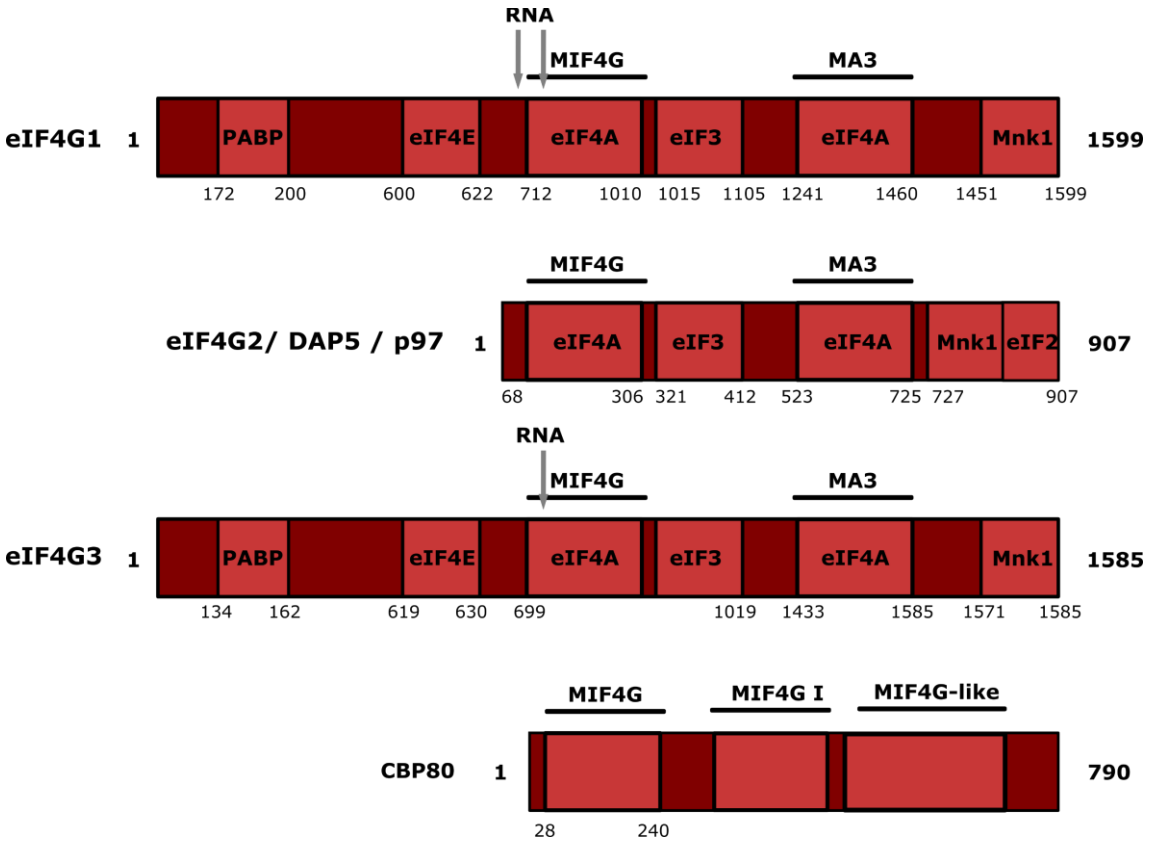

Figure 1.3.2-2 eIF4G paralogues

Schematic of human eIF4G paralogues, i.e., eIF4G1, DAP5, eIF4G3; and CBP80, a protein involved in the pioneer round of translation. Regions responsible for recruitment of eIF4G interaction partners marked in light red boxes, with amino acid boundaries underneath. Conserved domains marked above, with RNA binding regions pointed with an arrow. Regions responsible for interactions taken from Nielsen *et al.*, 2011; Shatsky *et al.*, 2014; and UniProt database: The UniProt Consortium, 2021. As an important aside, it should be noted that there is a discrepancy in the scientific literature, with some publications referring to eIF4G3 as eIF4G2.

The primed mRNA, loaded with the eIF4F complex, is ready for joining by the 43S PIC. However, first the 43S PIC has to be assembled. To appreciate how the different initiation factors influence the ribosomal subunit and together form the 43S PIC, understanding how the ribosomal subunit can interact with RNA is indispensable. The mRNA binding and decoding site is located across the 40S ribosomal subunit (Fraser *et al.*, 2007; Lorsch and Dever, 2010). The ribosome has three sites, identified as the transfer RNA (tRNA) binding sites i.e., tRNA exit site – E, peptidyl-tRNA site – P, aminoacyl-tRNA site – A; each occupied by adjacent codons (three bases) within the mRNA coding sequence (**Figure 1.3.2-3**).

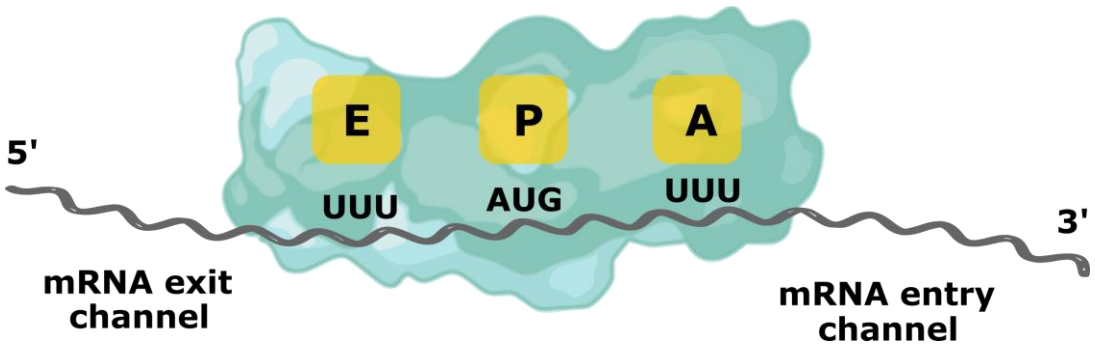

Figure 1.3.2-3 tRNA binding sites on a ribosome

Each ribosome has 3 tRNA binding sites **1)** tRNA exit site E, **2)** peptidyl-tRNA site P, **3)** aminoacyl-tRNA site A. Figure drawn in Inkscape 1.1, 40S ribosomal subunit outline exported from BioRender.

The ternary complex (eIF2-TC), formed with **1)** initiator tRNA charged with methionine and bearing anticodon for the start codon AUG, **2)** eIF2, and **3)** GTP binds the 40S ribosomal subunit independently or as a part of a larger complex with eIF1, eIF3 and eIF5 (Asano *et al.*, 2000; Sokabe, Fraser and Hershey, 2012). The initiator tRNA binds in the P site of the 40S, and the eIF2, which itself has 3 subunits (α, β, γ), interacts with GTP, tRNA, and the 40S (Kapp and Lorsch, 2004). eIF1 and eIF1A aid the interaction between eIF2-TC and 40S, as well as alter the mRNA decoding site by opening the mRNA entry channel, which in turn facilitates the mRNA to enter the ribosomal subunit (Pestova, Borukhov and Hellen, 1998; Passmore *et al.*, 2007). eIF3, consisting of 13 individual subunits (eIF3a to eIF3m), is involved in almost all of the steps of translation. eIF3 stabilises interaction between eIF2-TC and 40S, binds both eIF1 and eIF1A, as well as prevents premature 80S ribosome formation together with eIF1 and eIF2 (Benne and Hershey, 1978; Valasek *et al.*, 2004; Kolupaeva *et al.*, 2005). From the site of 60S ribosomal subunit, eIF6, bound to the 60S, inhibits premature ribosome formation (Miluzio *et al.*, 2009; Gartmann *et al.*, 2010).

The recruitment of the 43S PIC to the primed mRNA happens through the interaction between eIF4G and eIF3 (see **Figure 1.3.2-3**). However, additional interactions can be bridged through eIF4B, i.e., a stimulating cofactor of eIF4A helicase (Rogers *et al.*, 2001; Nielsen *et al.*, 2011), and eIF3, 40S and PABP (Methot, Song and Sonenberg, 1996; Le *et al.*, 1997; Bushell *et al.*, 2001), bringing all the complexes together. Moreover, the interaction between 40S and

mRNA is suggested to be additionally mediated through eIF4A (Sokabe and Fraser, 2017).

At this stage mRNA is stably bound to the decoding region of the 40S ribosomal subunit, containing the initiator tRNA. From there, the 40S ribosomal subunit translocates the mRNA in the 5'-to-3' direction in order to locate the translation start codon. The generally accepted mechanism of start codon recognition indicates that the initiator tRNA sample base-pairs the mRNA until it finds perfect complementarity to AUG codon (Mark, Lan and F., 1988). As only single-stranded mRNA can be bound to the ribosomal decoding site, any secondary structure present on that mRNA needs to be unwound before it enters the ribosome entry site. In the literature (Marintchev *et al.*, 2009; Jackson, Hellen and Pestova, 2010; Aitken and Lorsch, 2012; Marintchev, 2013), there are two models of how the mRNA can be de-structured in order to enter the ribosome: **1)** the 'ratchet' model in which initiation factors are bound to the mRNA upstream of the ribosome, preventing backwards motion, and 'pulling' the mRNA through the ribosome, **2)** RNA helicases dependent model in which helicases such as eIF4A, or DHX29 (Pisareva *et al.*, 2008; Parsyan *et al.*, 2009) unwind mRNA secondary structure. The recent CryoEM structure (Querido *et al.*, 2020) supports the 'ratchet' model, where the eIF4F complex is found behind the 40S ribosomal subunit. However, the importance of RNA helicases in translation of the mRNAs with highly structured 5'UTRs suggests that the second model is preferred. Thus, none of the current data can exclude the possibility of the two models coexisting. In fact, the authors of the CryoEM structure of 48S PIC (43S with eIF4F complex) (Querido *et al.*, 2020) did not exclude a possibility of additional eIF4A molecules, which exist in high excess in cells at 3 eIF4A per ribosome (Roger Duncan and Hershey, 1983), carrying out functions ahead of the ribosome (**Figure 1.3.2-4**).

Another major question that has for long perplexed many scientists, was recently solved. Until recently, the literature could not agree what happens with the eIF4F-eIF3 complex once the 40S ribosome is loaded onto mRNA and scans for the start codon. Recent translation complex profile sequencing studies (Bohlen *et al.*, 2020; Wagner *et al.*, 2020), proposed a revised model in which the eIF4F-eIF3 complex remains bound to the 43S PIC, and subsequently 80S until it has translocated approximately 12 amino acids, at which point these factors

are released (**Figure 1.3.2-4**). The implication of this is that only one initiation event can occur at a time, i.e., that initiation rates alone dictate the majority of overall translation rates. As an interesting aside, these studies also explain the long-standing mystery about how translation of the main ORF could be reinitiated after uORF translation (**Chapter 1.3.5**).

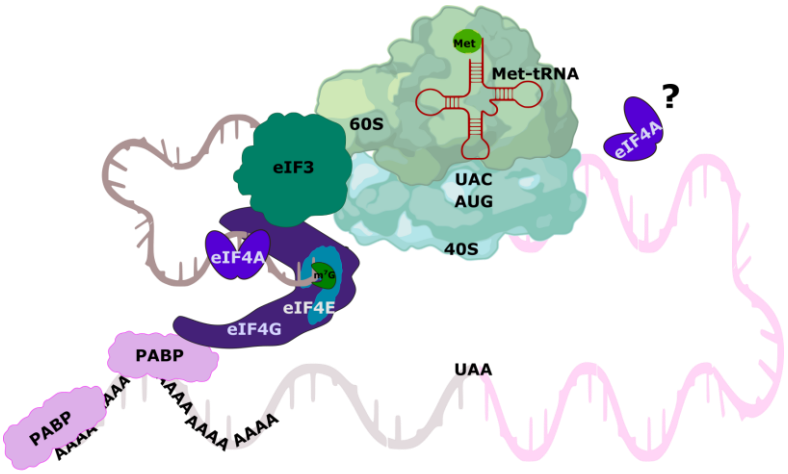

Figure 1.3.2-4 Alternative model of translation initiation – 5' end-tethered

Schematic of an alternative model of translation initiation. eIF4F complex remains bound to both the mRNA cap and eIF3, linking the eIF4F with the scanning ribosome. In this model the mRNA is looped around. Possibility of additional eIF4A next to the mRNA entry channel of the ribosome cannot be excluded, here presented with a question mark. Figure drawn in Inkscape 1.1; ribosome outline exported from BioRender.

As the ribosome scans for the codon, regulatory elements in both the *cis* and *trans* are important in the codon selection. As previously mentioned (**Chapter 1.3.1**), the sequence context of the start codon plays a role in translation start from that codon. Additionally, eIF1 prevents translation start from non-cognate codons, and AUG codons in poor context (Pestova, Borukhov and Hellen, 1998). Upon base-pairing between the initiator tRNA and the start codon of the mRNA, eIF1, which was bound closely to P-site, is displaced, causing conformational change in the 40S (Passmore *et al.*, 2007). This affects the position of eIF1A and eIF5, as well as activation of eIF2 GTPase. The release of the phosphate from GTP triggers dissociation of eIF1, and subsequent dissociation of eIF2-GDP (Algire, Maag and Lorsch, 2005). The released eIF2-GDP can be regenerated by eIF2B to be available for new rounds of translation initiation (Proud, 2005).

After recognition of the translation start codon and dissociation of the above-mentioned cofactors, the 60S ribosomal subunit can finally join the 40S ribosomal subunit to form the mature translation-competent 80S ribosome. The joining of the subunits is mediated by eIF5B-GTP, which binds between the two subunits, and upon GTP hydrolysis leaves the fully assembled 80S ribosome (Pestova *et al.*, 2000). Finally, eIF1A dissociates (Acker *et al.*, 2009), leaving behind the 80S ribosome, which in the revised model might be bound by eIF3 and eIF4F (see **Figure 1.3.2-1**).

1.3.3. Translation elongation

After the assembly of the 80S ribosome with the initiator tRNA positioned in the ribosome P-site and paired with the start codon, the next paired aminoacyl-tRNA (charged tRNA) can join the vacated ribosome A-site. Elongation has been shown to be overall a consistent and invariant process, with each round of elongation consisting of: **1)** delivery of a charged tRNA by GTP-bound eEF1A to a complimentary codon on an mRNA in the ribosomal A-site, **2)** GTP hydrolysis upon codon-anticodon recognition mediated by eEF1A and 60S ribosomal subunit, leading to eEF1A/GDP release, **3)** formation of a peptide bond by peptidyl transferase centre in 60S ribosomal subunit, **4)** ribosome translocation by one codon induced by peptide bond formation and mediated by GTP-bound eEF2, **5)** GTP hydrolysis and eEF2 release, **6)** change in tRNA position in the ribosomal E, P, A sites, following the translocation, with site E occupied by uncharged tRNA, ready to be released, P site occupied by peptidyl tRNA, and A site empty for new round of elongation (Zhang, Dunkle and Cate, 2009; Voorhees *et al.*, 2010; Chen *et al.*, 2012; Dever and Green, 2012; Voorhees and Ramakrishnan, 2013) (**Figure 1.3.3-1**).

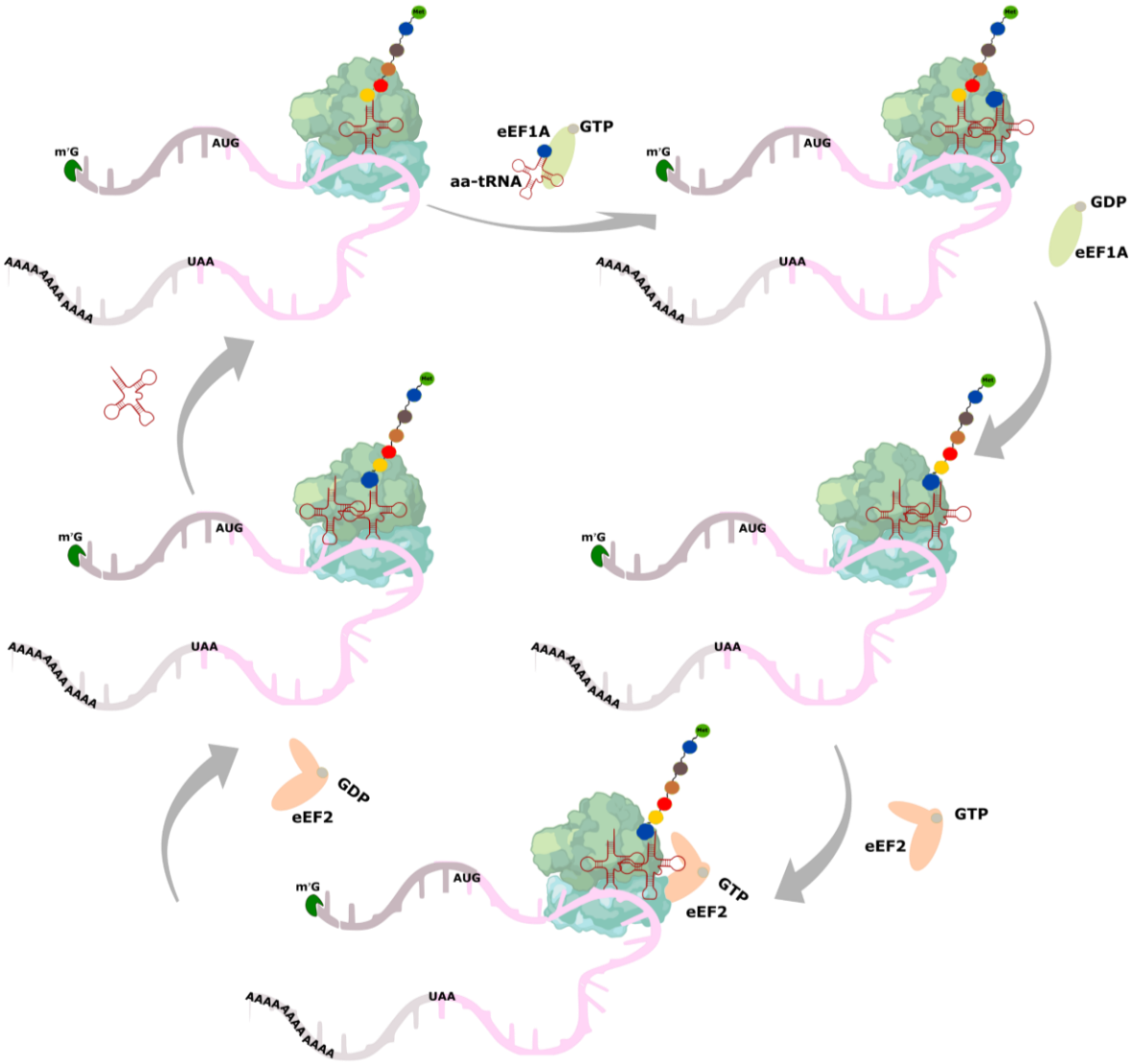

Figure 1.3.3-1 Translation elongation cycle

Elongation starts after assembly of the 80S ribosome and continues as a cycle until the translation stop codon is encountered by the ribosome. Each elongation cycle consists of (starting from the top left): **1)** charged tRNA (aa-tRNA) being brought to the ribosomal A site by eEF1A-GTP, **2)** positioning of the aa-tRNA in the A site, through the hydrolysis of GTP and release of eEF1A-GDP, **3)** formation of the peptidyl bond between the newly deposited aa and the polypeptide chain, **4)** GTP-eEF2 mediated ribosome translocation and eEF2-GDP release, **5)** change in the position of tRNAs on the ribosomal tRNA binding sites, with emptying of the A channel, and release of deacylated tRNA from the E channel. Figure drawn in Inkscape 1.1; ribosome outline exported from BioRender.

The ribosome decodes the coding sequence by interpreting every three bases (codons) as one of the 21 amino acids (including the rare selenocysteine (Copeland, 2003; Longtin, 2004)). As there are 64 possible codons and only 21 amino acids, there is inherent redundancy in the codon code.

The elongating ribosome proceeds through the coding sequence with an average incorporation rate of six amino acids per second (Bostrom *et al.*, 1986; Ingolia, Lareau and Weissman, 2011). However, there are some notable exceptions to this rule: **1)** ribosomes can pause for several seconds, allowing for binding of co-translational chaperones (Ingolia, Lareau and Weissman, 2011), **2)** incorporation of certain amino acids can cause elongation pausing, i.e., proline has been shown to have a slow incorporation rate and peptide bond formation (Pavlov *et al.*, 2009) which causes the ribosome to stall (Artieri and Fraser, 2014), and **3)** the abundance of particular charged tRNAs may be lower than the mRNA codon requirements (Torrent *et al.*, 2018; Torres *et al.*, 2019; Behrens, Rodschinka and Nedialkova, 2021). This last concept is related to a phenomenon where some mRNAs are enriched in certain codons and thus require more of a particular tRNA than there is available in the charged tRNA pool for a given cell type. When the ribosome encounters these codons, it will stall as the A site will remain empty for longer (Koutmou, Radhakrishnan and Green, 2015; Yu *et al.*, 2015). The tRNA abundance and existence of rare tRNAs is related to codon optimality, a concept in which more optimal codons are correlated with more efficient translation efficiency (Gingold *et al.*, 2014; Saikia *et al.*, 2016; Hanson and Coller, 2018; Medina-Muñoz *et al.*, 2021).

The elongation process continues until the A site of the ribosome is occupied by a stop codon and termination begins.

1.3.4. Translation termination

When the A site of the ribosome encounters one of the three stop codons, i.e., UAA, UAG, UGA, it is joined by eukaryotic release factors eRF1 and eRF3-GTP (Frolova *et al.*, 1996; Alkalaeva *et al.*, 2006; Mitkevich *et al.*, 2006; Pisareva *et al.*, 2006; Jackson, Hellen and Pestova, 2012) (**Figure 1.3.4-1**). eRF1 mimics tRNA and positions in the ribosomal A site which induces GTP hydrolysis by eRF3 (Frolova *et al.*, 1996; Song *et al.*, 2000). Next, eRF3 is released from the complex, which triggers full accommodation of eRF1, which promotes peptide hydrolysis and release (Song *et al.*, 2000). Generally, stop codon recognition is

highly efficient and there is little to no evidence for stop codon read-through in human cells.

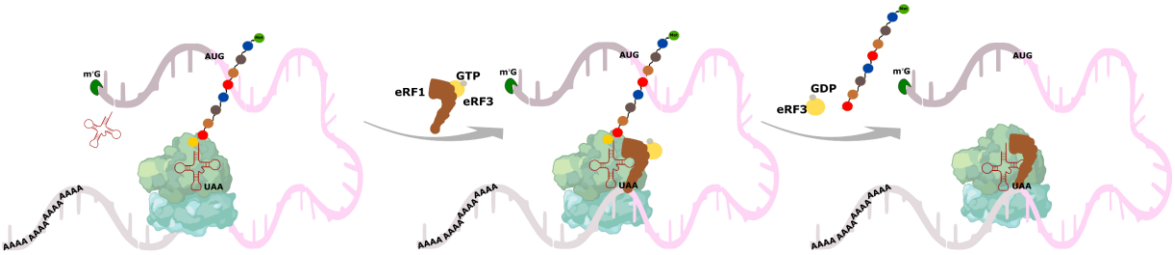

Figure 1.3.4-1 Translation termination

Translation termination begins with encountering of one of the translation stop codons UAA, UAG, UGA in the ribosome A site. As there are no tRNAs recognising the stop codons (apart from rare selenocysteine, see **Chapter 1.3.1**), the ribosome is joined by eRF1 resembling tRNA, and eRF3-GTP. After GTP hydrolysis and eRF3-GDP release, full accommodation of eRF1 triggers polypeptide chain release. Figure drawn in Inkscape 1.1; ribosome outline exported from BioRender.

1.3.5. Ribosome recycling and reinitiation

After peptide release both eRF1 and uncharged tRNA remain bound to the 80S ribosome in its A and P sites, respectively. This prompts joining of the ATP-binding cassette subfamily E member 1 (ABCE1), which acts as a ribosome recycling factor, by separating the 40S and 60S ribosomal subunits in an ATP-dependent manner (Pisarev *et al.*, 2010) (**Figure 1.3.5-1**). Additional eukaryotic translation factors have been implicated in having a role in full ribosomal subunits disintegration. eIF1 is thought to release the tRNA from the 40S ribosomal subunit, eIF1A is supposed to help with dissociation of eRF1 (Jackson, Hellen and Pestova, 2012), and eIF3j has been shown to aide with mRNA release from the 40S ribosomal subunit (Fraser *et al.*, 2007).

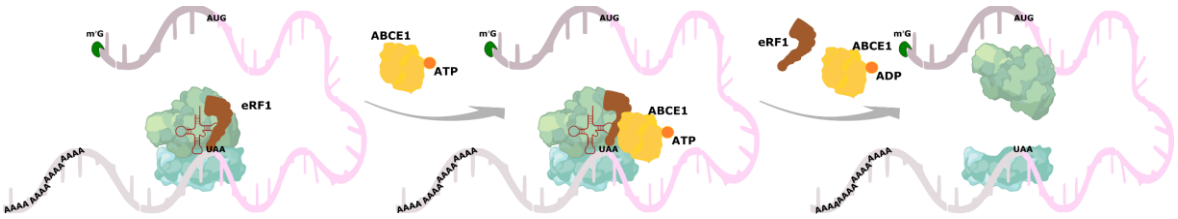

Figure 1.3.5-1 Ribosome recycling

After polypeptide chain release ribosome with deacylated tRNA and eRF1 remains bound to the mRNA, this prompts joining of ABCE1 complex which upon ATP hydrolysis separates 40 and 60S ribosomal subunits, which can be reused in new rounds of translation. Figure drawn in Inkscape 1.1; ribosome outline exported from BioRender.

As described in **Chapter 1.3.1** many mRNAs contain additional ORFs (uORF and dORFs). The newly described model in which eIF4F and eIF3 remain bound to the ribosome (see **Chapter 1.3.2** and **Figure 1.3.2-4**), provide a model for how multiple ORFs can be translated. Albeit due to presence of the initiation factors directly downstream of the 40S, the translation from a new ORF could happen only in the 5'-to-3', prohibiting start from a start codon directly upstream of stop codon. Indeed, whether translation can be reinitiated at the next available ORF depends on a few factors, such as the distance between the ORFs, presence of secondary structures, and length of the ORF itself (Kozak, 2001).

A famous example of uORF control of translation, requiring reinitiation is translation of a transcription factor ATF4 (Vattem and Wek, 2004). Human ATF4 contains two uORFs upstream of the main ORF. Therefore, the translation of the second uORF would only happen if the ribosome can be reassembled and there is abundance of the eIF2-TC. However, translation of the second uORF causes lack of translation from the main ORF, as the AUG start codon of the main ORF is located within the coding sequence of the second uORF. This causes repression of the main ORF, that is dependent on reinitiation. In a situation of cellular stress, with low eIF2-TC, the second uORF is not translated, and ATF4 is translated instead.

This control of transcription factor by translation of uORFs and ribosome reassembly is a perfect example of how the intricate cellular processes are interconnected.

1.3.6. Translational repression

One mechanism to ensure the correct translation rate is the repression of translation. Many pathways of translational repression exist in cells, however in this chapter, main focus is emphasised on the repression of translation involving the eIF4A paralogues.

This regulation can occur at several stages, typically at the level of initiation. The most well-known control is exerted through nutrient availability, i.e., if nutrients are high, translation is unrestricted, however when nutrients are deprived, translation is significantly hindered to conserve energy. The major sensor of nutrient availability is the mTOR (mammalian Target Of Rapamycin) pathway (Sabatini *et al.*, 1994). The mTOR complexes (mTORC1 and mTORC2) can sense amino acid levels, and signals related to levels of glucose and ATP. mTOR itself is a kinase that is active during times of nutrient availability. Among the many mTOR substrates are proteins directly associated with translational repression (**Figure 1.3.6-1**). These are the eIF4E binding proteins (4EBP1-3), and LARP1 (Hara *et al.*, 1998; Fonseca *et al.*, 2015). When the 4EBPs and LARP1 are phosphorylated, they are inactive and eIF4E-dependent translation proceeds as normal (Pause *et al.*, 1994; Gingras *et al.*, 1999; Hong *et al.*, 2017). When mTOR is inactivated due to starvation, these mTOR targets are unphosphorylated and are now able to repress translation. In this case, 4EBP1-3 can bind eIF4E by displacing eIF4G, thus repressing downstream initiation (Mader *et al.*, 1995). More recently, LARP1 has been shown to specifically repress the translation of TOP mRNAs, which themselves are present on mRNAs encoding proteins involved in translation, by displacing eIF4E from the cap of these transcripts (Lahr *et al.*, 2015, 2017; Smith *et al.*, 2021). Additional indirect control of translation through mTOR pathway is the influence exerted on eIF4A helicase. In the case of active mTOR, S6K (ribosomal protein S6 kinase beta-1) is phosphorylated (Hara *et al.*, 1998), which subsequently phosphorylates PDCD4, rendering it inactive (Hannan *et al.*, 2003; Dorrello *et al.*, 2006). PDCD4 in its active form has been shown to inhibit eIF4A (Yang *et al.*, 2002; LaRonde-LeBlanc *et al.*, 2006; Suzuki *et al.*, 2008; Fay *et al.*, 2014). An additional modulation of eIF4A function through mTOR is the activation of eIF4B by S6K (Shahbazian *et al.*, 2006).

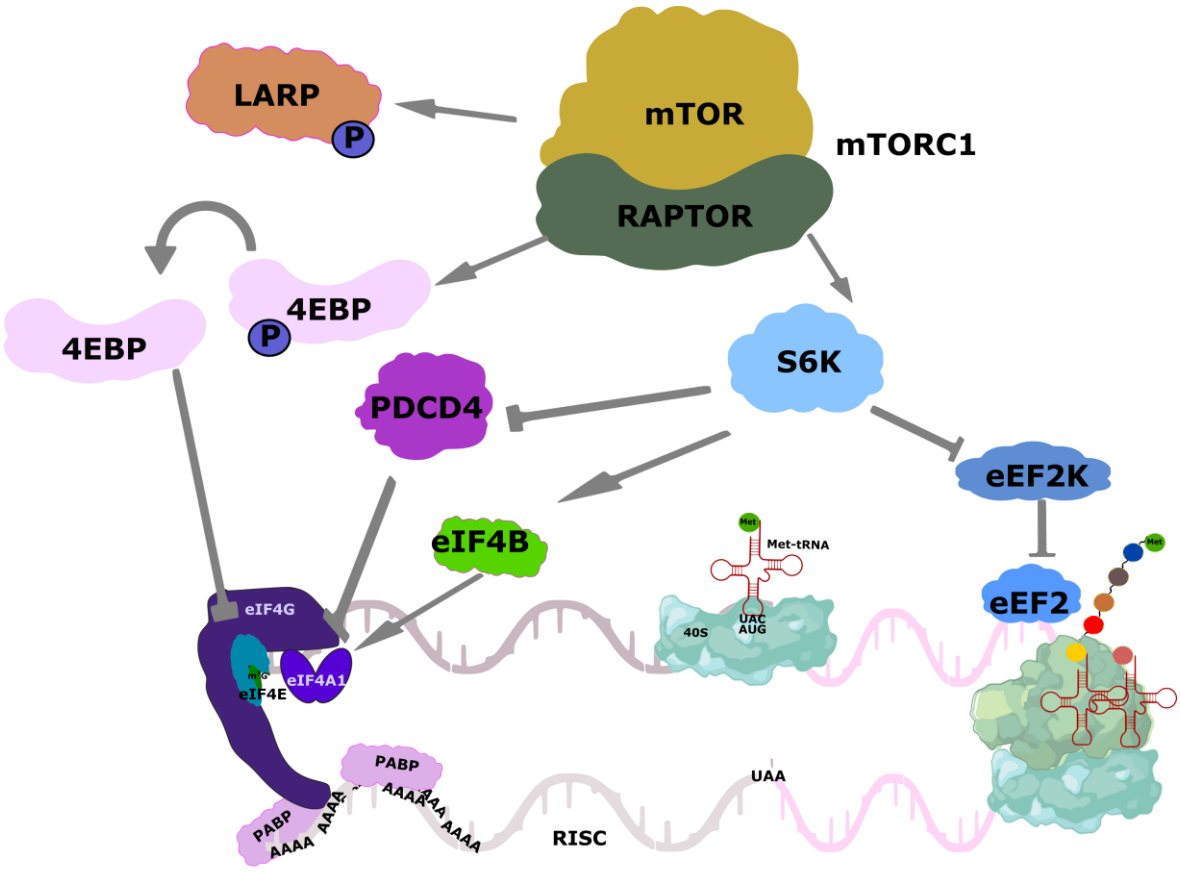

Figure 1.3.6-1 mTOR mediated regulation of protein synthesis

Schematic of translation regulation through mTOR. Active mTOR can phosphorylate proteins directly involved in repression of translation, such as 4EBP, which in its phosphorylated state does not inhibit eIF4E activity, or LARP which in its phosphorylated state does not repress TOP-motif mRNAs. mTOR imparts also indirect activity through phosphorylation of S6K kinase which itself phosphorylates **1)** PDCD4, rendering it incapable of eIF4A repression, **2)** eIF4B, in order to activate it, **3)** eEF2K, which is then prohibited from inhibiting elongation factor eEF2. Upstream signalling pathways not shown. Figure drawn in Inkscape 1.1; ribosome outlines exported from BioRender.

Another major pathway is the microRNA (miRNA) mediated translational repression (**Figure 1.3.6-2**). miRNA are small (around 22 nt) single-stranded, non-coding RNAs (Lagos-Quintana *et al.*, 2001), that are processed from longer double-stranded regions by the Drosha and Dicer endonucleases (Rana, 2007; Park *et al.*, 2011; Kwon *et al.*, 2016). Following processing by Dicer, a single strand of the miRNA duplex is loaded into one of the four main miRNA effector proteins known as Argonaute (Ago1-4). The miRNA-Ago complex is known as the RNA-induced silencing complex (RISC) (Pratt and MacRae, 2009). The loading of a

single strand of the miRNA duplex is reported to involve additional factors such as helicases, as was reported for the DEAH-box helicase DHX9 (Fu and Yuan, 2013). After assembly of the complex, RISC scans cytoplasmic mRNA until a target is located. This process involves base-pair recognition between the target mRNA and the approximately 5-8 nt region of the miRNA known as the seed sequence (Lewis, Burge and Bartel, 2005; Didiano and Hobert, 2006). The consequence of such a short seed sequence means that at least around 30% of human protein coding genes can be miRNA targets (Lewis, Burge and Bartel, 2005). When a stable RISC-mRNA interaction is made, translational repression can occur. This relies on the further recruitment of factors such as TRNC6A-C, which additionally interacts with PABP and CCR4-NOT complex (Braun *et al.*, 2011; Chekulaeva *et al.*, 2011; Fabian *et al.*, 2011). The translational repression may require the activity of other auxiliary factors, which interact with CCR4-NOT, including helicases such as DDX6 or eIF4A2 (Meijer *et al.*, 2013; Chen *et al.*, 2014; Rouya *et al.*, 2014; Kuzuoğlu-Öztürk *et al.*, 2016; Wilczynska *et al.*, 2019). The precise downstream mechanisms of miRNA-mediated repression are still debated. However, it has been shown that translational repression associated with eIF4A2 happens at translation initiation (Meijer *et al.*, 2013; Wilczynska *et al.*, 2019). Albeit no evidence so far excluded the possibility of repression mediated through other auxiliary factors existing at different stages of translation. Moreover, the translational repression has been shown as a primary event, which can lead either to storage of repressed mRNAs or to their degradation (Mathonnet *et al.*, 2007; Selbach *et al.*, 2008; Djuranovic, Nahvi and Green, 2012; Larsson and Nadon, 2013; Meijer *et al.*, 2013).

Curiously, miRNA have been shown to promote dissociation of both eIF4A1 and eIF4A2 from their target mRNAs (Fukao *et al.*, 2014), yet in the study from the Bushell lab (Wilczynska *et al.*, 2019) the messages bound by eIF4A2 where shown to be repressed. Moreover, eIF4G1 was implicated in facilitating miRNA mediated translational repression (Ryu *et al.*, 2013), however how this role is related to the function of eIF4A is unknown.

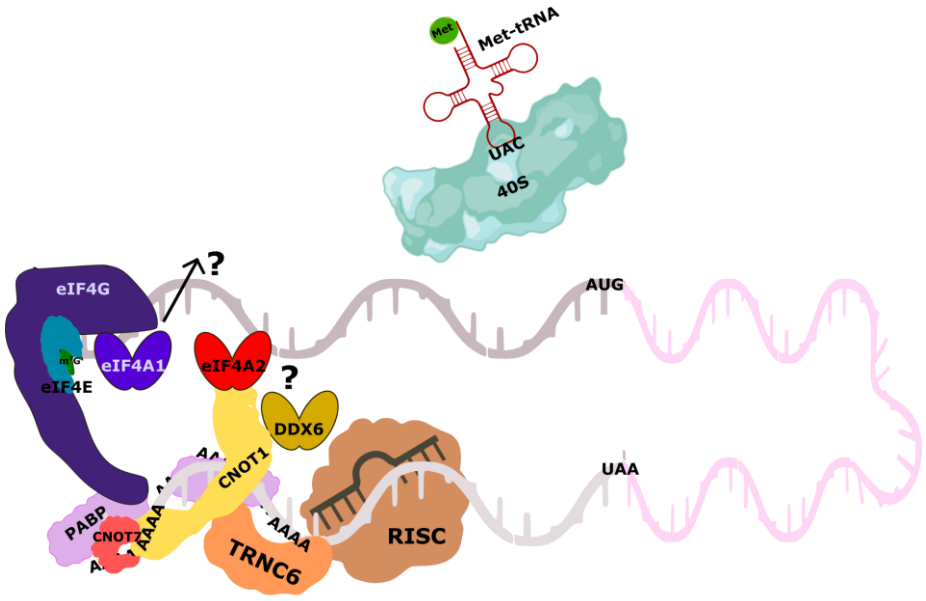

Figure 1.3.6-2 Translational repression via miRNA pathway

Schematic of translational repression via miRNA pathway. Upon recognition of miRNA binding site in the 3'UTR of an mRNA the RISC complex recruits TRNC6. That further recruits CCR4-NOT (presented here as CNOT1 and CNOT7), as well as associated helicases eIF4A2, or DDX6 (question mark indicates that it might depend on the type of repression which helicase is preferred by the complex). That can possibly promote dissociation of eIF4A1 from the translated message (possibility indicated with a question mark). The translational repression leads to dissociation of the 40S. Figure drawn in Inkscape 1.1; 40S ribosomal subunit outline exported from BioRender.

1.4. Dysregulation of translation in cancer

Translation, as described in **Chapter 1.3** is a highly controlled process, driven by *cis* regulatory elements, the ribosome, tRNA availability, translational factors, and their interaction partners. Any dysregulation of this intricate process can lead to production of aberrant proteins, or overexpression of proteins that can promote malignancy. In normal cells, translation initiation and repression act in concert to maintain homeostasis. As a major hallmark of cancer is proliferation (Hanahan and Weinberg, 2011), the protein output demand of the cancer cell is significantly higher than in a normal cell. Thus, to meet these demands, the delicate balance between initiation and repression is tipped in favour of unrestricted translation of favourable proteins.

Cancer exploits many pathways, however here the main focus will be on dysregulation of translation initiation, as both eIF4A1 and eIF4A2 are thought to exert their functions at translation initiation. As increased demand for protein synthesis requires more translation factors, many of the factors involved in the rate-limiting steps of initiation are oncogenes themselves. For example, even modest overexpression of eIF4E is transformative (Lazaris-Karatzas, Montine and Sonenberg, 1990; Ruggero *et al.*, 2004), and as shown in Truitt *et al.*, 2015, eIF4E haploinsufficient mice are protected from oncogenesis without a detrimental effect on their development. This indicates that interventions to reduce eIF4E levels would hinder cancer growth without causing distress to regular cells. Intriguingly, eIF4E is post-translationally modified by phosphorylation at serine 209 by the kinases MNK1/2. This phosphorylation has been shown to be critical for the oncogenic activity of eIF4E (Wendel *et al.*, 2007). For these reasons, perturbation of MNK1/2 has great promise as a cancer therapy (Ueda *et al.*, 2010; Knight *et al.*, 2021), and already a specific and potent MNK1/2 inhibitor has entered clinical trials (Reich *et al.*, 2018).

Another pathway that can modulate eIF4E activity is the described in **Chapter 1.3.6** mTOR pathway. Interestingly, there are two major signalling pathways, i.e., the PI3K-AKT and RAS-MAPK pathways, which converge on the TSC complex immediately upstream of the master nutrient sensor complex, mTORC1/2 (Inoki *et al.*, 2002; Ma *et al.*, 2005). Notably, the RAS-MAPK pathway is also directly

upstream of MNK1/2. Activation of PI3K-AKT and RAS-MAPK pathways lead to inhibition of TSC, which prevents it from deactivating mTORC1/2. While these signalling complexes are beyond the scope of this thesis, it should be noted that the PI3K-AKT and RAS-MAPK pathways are frequently mutated and constitutively active in cancers (Barault *et al.*, 2008; Yuan and Cantley, 2008; Prior, Lewis and Mattos, 2012). The result of this is a constitutive activation of mTORC1/2. This can lead to indirect inhibition of PDCD4 via the S6K intermediate, and activation of eIF4A through eIF4B. Hyperactive mTOR1/2 is thus a constitutively de-repressed translation initiation complex, leading to the high protein synthesis rates that a cancer cell demands. Many pro-oncogenes contain repressive mRNA features such as highly structured 5'UTRs. This the case for c-Myc the transcription factor (O'Leary *et al.*, 2019), translation of which is promoted in state of high eIF4A activation. This a beautiful example, of how cancer can harness translational control in order to amplify proteins involved in transcription, which themselves can control for production of more mRNAs, which encode proteins, that can aide cancer progression. Intriguingly, overexpression of eIF4A2, the eIF4A paralogue implicated in miRNA-mediated translational repression (**Chapter 1.3.6**) has been shown to also have negative influence on cancer progression (consult **Table 1.5.1-1**). Interestingly, eIF4A2 is not the only one of the many paralogues of translation initiation factors that has been shown to have cancer repressive role. Indeed, eIF4E3 has also been reported to have antitumorigenic properties (Osborne *et al.*, 2013). However other cofactors of eIF4A, involved in translation initiation, such as eIF4H, or eIF4G1 as well as many other factors, have also been shown to have pro-tumourigenic roles (Fukuchi-Shimogori *et al.*, 1997; Silvera *et al.*, 2009; Wu *et al.*, 2011; Gatza *et al.*, 2014; Sendoel *et al.*, 2017).

Amplification of initiation factors is only one of the mechanisms that lead to dysfunction of the protein synthesis pathway. Another broad mechanism that cancers exploit to enhance translation is perturbation of the RNAs themselves. For example, aberrant ribosomal RNA modifications, which are guided by other small RNAs, can also lead to cancer (McMahon *et al.*, 2019). Moreover, it has been observed in cancer cells that mRNAs encoding proteins beneficial for cancer undergo alternative polyadenylation, resulting in shortening of 3'UTRs, and a loss of miRNA binding sites, thus leading to upregulation of these

oncogenes (Mayr and Bartel, 2009; Lembo, Di Cunto and Provero, 2012). Interestingly, cancer cells can also exploit the miRNA pathway by expression of pseudogenes which titrate away the miRNA destined to repress an oncogene (Poliseno *et al.*, 2010).

1.5. RNA helicases

RNA helicases are one of the largest groups of enzymes that participate in mRNA metabolism (Tanner and Linder, 2001; Jankowsky, 2012; Bourgeois, Mortreux and Auboeuf, 2016) and exist in virtually all classes of organisms (Anantharaman, Koonin and Aravind, 2002). Contrary to their name, RNA helicases have been shown to not only unwind secondary structure within the mRNA but also to anneal, clamp, and remodel RNA as well as alter RNA-protein complexes (Jankowsky, 2012; Bourgeois, Mortreux and Auboeuf, 2016). Due to their impact both on the RNA as well as ribonucleoprotein complexes they serve as molecular switches, that can impact the entire gene expression pathway.

This thesis is focused primarily on the activity of two DEAD-box helicases, eIF4A1 and eIF4A2, which have been shown to play a crucial role in both translation initiation as well as repression (**Chapters 1.3.2**, **1.3.6**). To understand the experiments and rationales in this thesis, recognising the important characteristics of this group of enzymes (**Chapter 1.5.1**), as well as the already established differences between the paralogues (**Chapter 1.5.2**) is indispensable.

1.5.1. DEAD/H-box helicases

All helicases belong to six superfamilies, categorised by the differences in their structures and function (Corbalenya and Koonin, 2007; Singleton, Dillingham and Wigley, 2007). Out of those six, two are represented by RNA helicases, i.e., Superfamily 1, and Superfamily 2 (SF1, SF2). Eukaryotic RNA helicases belonging to SF1 and SF2 are non-ring forming, a structural characteristic associated mostly with eukaryotic DNA helicases (Corbalenya and Koonin, 2007; Jankowsky, 2012). One of the largest helicase families in humans belong to SF2; these are the DEAD-box and closely related DEAH-box (DHX) helicases (Fairman-Williams, Guenther and Jankowsky, 2011; Linder and Jankowsky, 2011; Jankowsky, 2012).

DEAD-box proteins are so named due to the presence of conserved DEAD (Asp-Glu-Ala-Asp) sequence motif. DEAD-box helicases have two similar RecA domains named after a particular fold of the recombination protein RecA (Singleton, Dillingham and Wigley, 2007). The two domains form the helicase core and are joined by a flexible linker, which allows the domains to modify their position to each other (Andreou and Klostermeier, 2012). The conserved helicase core has a total of nine amino acid sequence motifs (**Figure 1.5.1-1**, panel A) (Linder *et al.*, 1989; Tanner *et al.*, 2003). Motifs Ia, Ib, IV, V are responsible for RNA binding, with motif VI involved in both RNA binding and ATP binding and hydrolysis. Other motifs of dual function are motif II, involved in both ATP binding and hydrolysis, and Mg^{2+} coordination; and motif III, responsible for ATP-dependent RNA unwinding. The final two motifs, I, Q, are involved in ATP binding and hydrolysis. These conserved motifs structurally fall inside the helicase core, creating the ATP and RNA binding pocket (**Figure 1.5.1-1**, panel B) (Schütz *et al.*, 2010). The positioning of the pocket permits the DEAD-box helicases to shift though the conformational cycle through RNA binding and release, coupled with ATP hydrolysis (Theissen *et al.*, 2008; Hilbert, Karow and Klostermeier, 2009; Andreou and Klostermeier, 2012; Henn, Bradley and De La Cruz, 2012). However, the presence of interaction partners has also been demonstrated to shift DEAD-box proteins through their conformation (Rudolph and Klostermeier, 2015; Wurm, Glowacz and Sprangers, 2021).

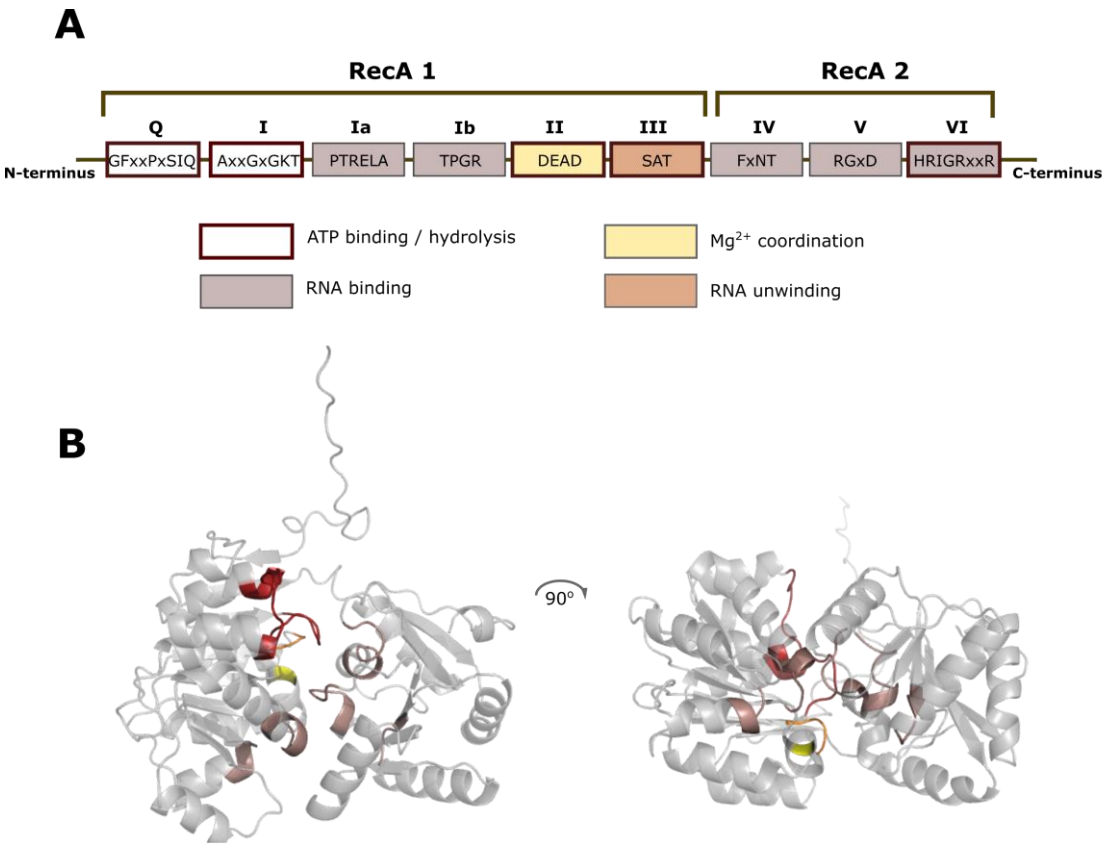

Figure 1.5.1-1 DEAD-box helicase motifs

A. Nine conserved motifs in DEAD-box RNA helicases. Each motif is represented by a box, with colour coded function represented in the scheme. Names of the motifs above each box and conserved amino acid sequence in one letter code presented inside the box, x – amino acid varying between different helicases.

B. AlphaFold 2.0 predicted structure of eIF4A2 (AF-Q14240-F1), with conserved motifs indicated in colour: motifs Q, I – *deep red*, Ia, Ib, IV, V, VI – *light brown*, II – *yellow*, III – *orange*. Structure presented with 90°C rotation.

Outside of the helicase core, i.e., the two RecA domains, the DEAD- (as well as DHX-) box proteins can have additional regions that modulate their functions. Examples of alternative functions regulated through extensions include **1)** DHX36 with an N-terminal extension that binds specific RNA structures, i.e., G-quadruplexes (Lattmann *et al.*, 2010), **2)** DDX21 with its additional GUCT domain, which despite similarities to RNA recognition motif (RRM) is not thought to interact with RNA but rather with other proteins (Ohnishi *et al.*, 2009), **3)** DDX5 and its P68HR domain responsible for interaction with m^6A writer METTL3 and nuclear localisation, and **4)** DDX3 and its autoinhibitory domain (Floor *et al.*, 2016) as well as its low complexity domain that is thought to have a function in phase-separation (Hondele *et al.*, 2019). On the other side of the spectrum is the eIF4A family which is considered to be a minimal helicase (Tanner and Linder, 2001) with only about 50 amino acids proceeding the Q motif and around 40 amino acids downstream of motif VI (**Figure 1.5.1-1**, panel A). The described minimal functional core of the DEAD-box helicases starts two amino acid upstream of a conserved phenylalanine of the Q motif and ends 35 amino acids beyond motif VI (Banroques *et al.*, 2011). Therefore, the N-terminal regions of the eIF4A paralogues should not be overlooked as possible regions promoting divergent functions.

Generally, DEAD-box helicases are thought to bind the substrate through an interaction with the nucleic acid phosphate backbone, therefore implicating a lack of sequence specificity (Peck and Herschlag, 1999; George W. Rogers, Lima and Merrick, 2001; Hilbert, Karow and Klostermeier, 2009). However, the direct contact with 2'OH group of the ribose allows for discrimination against DNA as a potential substrate (Peck and Herschlag, 1999; George W. Rogers, Lima and Merrick, 2001). In contrast to the above-mentioned lack of RNA sequence specificity, some of the DEAD/H-box helicases have been shown to preferentially bind specific RNA sequences. For example, the implicated in RISC assembly DHX9 (also known as RNA helicase A, or RHA) is thought to be RNA sequence specific in the conserved region of the DEAD- and DEAH- box proteins (Parsyan *et al.*, 2011). In contrast, other RNA-sequence specific DEAD/H-box helicases are thought to confer their substrate specificity through regions outside of the main helicase core, such as is the case with Vasa (*Drosophila melanogaster* orthologue of human DDX4) and its C-terminal region (Liu, Han and Lasko, 2009), or DDX43,

which KH domain facilitates substrate specificity (Yadav *et al.*, 2021). Interestingly, even the 'minimal' helicases eIF4A2 and eIF4A3, as is discussed in greater detail below (**Chapter 1.5.2**), has been shown to have a sequence preference (Saulière *et al.*, 2012; Wilczynska *et al.*, 2019).

As this conserved group of enzymes plays a role in practically all parts of mRNA metabolism, it is perhaps not surprising that aberrations of DEAD-box helicases have been shown to have a function in cancer (**Table 1.5.1-1**). Interestingly, some of the helicases can have positive influence on outcome for cancer patients. Crucially, specific helicases can have opposite effect depending on the type of cancer, suggesting that those enzymes can act as molecular 'double agents' which action is imparted upon them based on their environment or interaction partners. Most importantly, from the published data (**Table 1.5.1-1**), that seems to be the crucial difference between the paralogues eIF4A1 and eIF4A2, which are the subject of this thesis.

Table 1.5.1-1 Role of DEAD-box helicases in cancer

Helicase	Cancer	Study	Outcome
DDX1	breast	(Germain *et al.*, 2011)	relocalisation has negative impact
	testicular	(Tanaka *et al.*, 2009)	overexpression has negative impact
	ovarian	(Han *et al.*, 2014)	miRNA axis – positive impact on outcome
DDX2A / eIF4A1	breast	(Modelska *et al.*, 2015)	overexpression has negative impact
	cervical	(Liang *et al.*, 2014)	
	endometrial	(Lomnytska *et al.*, 2012)	
	gastric	(Gao *et al.*, 2020)	
	lung	(Ji *et al.*, 2003)	
DDX2B / eIF4A2	breast	(Yan *et al.*, 2011)	downregulation has negative impact
	lung	(Shaoyan *et al.*, 2013)	
	breast	(Liu *et al.*, 2019)	overexpression has negative impact
	colorectal	(Chen *et al.*, 2019)	
	oesophageal	(Lyu *et al.*, 2020)	
eIF4A3 / DDX48	bladder	(Kanellis *et al.*, 2021)	overexpression has negative impact
	brain		
	colon		
	breast	(Lin *et al.*, 2018; Ling *et al.*, 2020; Zhu, Ren and Yang, 2021)	
DDX3	breast	(Botlagunta *et al.*, 2008)	overexpression has negative impact
	colorectal	(Wu *et al.*, 2016)	
	liver	(Huang *et al.*, 2004)	
	lung	(Bol *et al.*, 2015)	
	liver	(C.-H. Chan *et al.*, 2019)	loss has negative impact
DDX5	colorectal	(Causevic *et al.*, 2001; Yang, Lin and Liu, 2005)	overexpression has negative impact
DDX6	colorectal	(Nakagawa *et al.*, 1999)	overexpression has negative impact
	gastric	(Tajirika *et al.*, 2018; Taniguchi *et al.*, 2018)	
	liver	(Miyaji *et al.*, 2003	
DDX9	lung	(Wei *et al.*, 2004)	overexpression has negative impact
DDX17	colon	(Shin *et al.*, 2007)	overexpression has negative impact
	breast	(Wortham *et al.*, 2009)	overexpression has positive impact
DDX20	breast	(Cai *et al.*, 2017)	loss has negative impact
	liver	(Takata *et al.*, 2012)	
DDX27	colorectal	(Tang *et al.*, 2018)	overexpression has negative impact
DDX32	leukaemia	(Abdelhaleem, 2002)	downregulation has negative impact
DDX43	bladder	(Martelange *et al.*, 2000)	overexpression has negative impact
	head and neck		
	lung		
	sarcoma		
DDX53	gastric	(Cho *et al.*, 2003)	demethylation and overexpression have negative impact
	liver		
DDX56	osteosarcoma	(Zhu *et al.*, 2020)	overexpression has negative impact

1.5.2. eIF4A

As described throughout this chapter there are three eIF4A paralogues in humans: eIF4A1 and eIF4A2, which share 90% amino acid sequence identity, and the less identical eIF4A3, with 60% amino acid sequence identity. eIF4A1 is the most abundant and well-recognised paralogue, the function of which is thought to be mainly within the eIF4F complex, reviewed in **Chapter 1.3.2**. In contrast, eIF4A2 has been shown to associate with CCR4-NOT complex and therefore take part in miRNA-mediated translational repression (**Chapter 1.3.6**). Despite, the differences in the preferable binding partners, both paralogues have been shown to associate with eIF4F (Yoder-Hill *et al.*, 1993; Wilczynska *et al.*, 2019; Robert *et al.*, 2020), possibly forming different complexes. Opposite to this, eIF4A3 role is mainly within the exon junction complex (Chan *et al.*, 2004).

Intriguingly, the overexpression of both eIF4A1 and eIF4A3 is associated with negative outcomes for cancer patients (see **Chapter 1.4** and **Table 1.5.1-1**). This is contrary to the few instances where eIF4A2 overexpression had a positive impact on the outcome for cancer patients (**Table 1.5.1-1**). Albeit as eIF4A2 overexpression has also been shown in other studies to instead have a negative impact, a possible double role of eIF4A2 cannot be disregarded.

As this thesis is focused mainly on discerning the molecular mechanisms that drive the distinct functions of eIF4A1 and eIF4A2, this chapter describes the known differences between those two paralogues. Moreover, as plethora of data in the protein translation field pertains to the yeast system, some important discoveries about the *Saccharomyces cerevisiae* eIF4A, named for the purpose of this thesis *Sc* eIF4A, are explored.

As has been described in the literature, eIF4A1 and not eIF4A2 is the dominant paralogue which associates with eIF4G (Galicia-Vazquez *et al.*, 2012). However, as has been observed (Galicia-Vazquez *et al.*, 2012) the two proteins are interconnected on a transcriptional level, where knockdown of eIF4A1 enhances both transcription and the protein levels of eIF4A2. However, this compensatory upregulation of eIF4A2 is not capable of rescuing the primary function of eIF4A1 in translation initiation (Galicia-Vazquez *et al.*, 2012). Moreover, it has been observed that complete loss of eIF4A1 is detrimental to cell growth, which has

not been observed for eIF4A2 (Galicia-Vazquez *et al.*, 2012). From the other side, depletion of eIF4A2 cannot be rescued by eIF4A1 for the activity of the miRNA-mediated translational repression pathway (Meijer *et al.*, 2013). eIF4A2 but not eIF4A1 has been implicated in uORF translation and the mRNAs bound by eIF4A2 are demonstrated to be both miRNA targets, and translationally repressed (Wilczynska *et al.*, 2019). Moreover, eIF4A2 has been shown to preferentially bind polypurine (AG) motifs and confer its repressive functions through those motifs (Wilczynska *et al.*, 2019). Interestingly, chemical inhibition of eIF4A1 renders it polypurine selective, reminiscent of the uninhibited eIF4A2 (Iwasaki, Floor and Ingolia, 2016; Wilczynska *et al.*, 2019). Although the exact mechanism of eIF4A2-mediated repression remains elusive, it has been demonstrated that eIF4A2 inhibits the deadenylase activity of CCR4-NOT complex (Meijer *et al.*, 2019). This suggests that the repressive activity of eIF4A2 leads to mRNA storage rather than mRNA degradation (**Chapter 1.3.6**).

The sequence specificity of eIF4A2 contrasts with what was described above for other DEAD-box helicases (**Chapter 1.5.1**), which are thought to be mostly sequence unspecific. However, it is worth noting that the third eIF4A paralogue, eIF4A3, has been shown to also preferentially bind polypurine motifs, as well as specifically clamp them (Saulière *et al.*, 2012). It is possible that conserved regions between eIF4A2 and eIF4A3 could be responsible for this sequence preference.

Interestingly, despite the high degree of identity between the eIF4A1 and eIF4A2 amino acid sequence, there are many differences between the two paralogues on the transcriptional level, perhaps those differences could explain how the two paralogues are transcriptionally linked. eIF4A2 is located on chromosome 3, whereas eIF4A1 transcript is on chromosome 17. Moreover, the two paralogues differ in the untranslated regions of their mRNAs. Curiously, both paralogues have short and unstructured 5'UTRs, with 5'UTR of eIF4A1 at only 17 nucleotides and 5'UTR of eIF4A2 at 34 nucleotides, suggesting that the translation of both is not dependent on helicase activity or even the scanning mechanism of 40S ribosomal subunit. However, eIF4A2 3'UTR, unlike eIF4A1, has a miRNA binding site (miR-21) (Cho, 2007; Yan *et al.*, 2011). Moreover, the 5'UTR of eIF4A2 has a TOP motif. Both the presence of miRNA binding site and the TOP motif in case of the eIF4A2, makes both of the paralogues subject to different forms of

translational control. Additionally, the coding sequence of the two mRNAs vary greatly due to the use of alternative codons (NCBI RefSeq). The implication of this is that the two paralogues require a different pool of charged tRNA. As discussed in **Chapter 1.3.3**, this mode of regulation is known as codon optimality. Those differences could perhaps explain the divergent expression of eIF4A1 in proliferative cells, and eIF4A2 in differentiated cells (Williams-Hill *et al.*, 1997).

In yeast, only a single eIF4A orthologue exist. *Sc* eIF4A has been shown to be a conserved ATP-dependent DEAD-box helicase. Its activity is also modulated by co-factors, which enhance its catalytic activity and alter its conformation (Schutz *et al.*, 2008; Andreou and Klostermeier, 2012, 2014; Harms *et al.*, 2014). In contrast to the human orthologues, no RNA sequence specificity has been observed for *Sc* eIF4A. However, the catalytic activities are thought to be modulated, similarly to the human eIF4As, through length of the single-stranded region as well as the stability of the RNA duplex (Andreou, Harms and Klostermeier, 2019). Additionally, apart from the considered canonical unwinding role of the helicase, both human and yeast eIF4A have been implicated in unwinding-independent loading of mRNAs onto the ribosome (Sokabe and Fraser, 2017; Yourik *et al.*, 2017). Perhaps, the most interesting difference between human and yeast proteins can stem from their interaction partners. Human eIF4G bears two eIF4A binding sites (**Figure 1.3.2-2**) whereas the yeast orthologue has only one eIF4A binding MIF4G domain (Schutz *et al.*, 2008; Shatsky *et al.*, 2014). Intriguingly, CNOT1, the scaffold protein of CCR4-NOT complex, shown to interact with eIF4A2 (Meijer *et al.*, 2019), has both MIF4G, and MA3 domain, however only MIF4G domain has been shown to interact with DDX6 helicase, and the role of MA3 domain in this context is unexplored (Mathys *et al.*, 2014).

Despite the known differences between the human paralogues, the mechanism of how they exert their specific functions remains unsolved. Furthermore, the question of whether it is the features of each eIF4A that drives the differences or whether it is imparted by the interaction partners remains open.

1.5.3. eIF4A inhibitors

Due to the overwhelming evidence implicating overexpression of eIF4A1 in promoting malignant growth, targeting eIF4A pharmacologically has been a major goal. Several natural compounds have been shown to inhibit eIF4A, and many synthetic analogues are currently under investigation.

Interestingly, despite inhibiting translation, many small molecule inhibitors exert completely different function on eIF4A. Some of the most well-known eIF4A inhibitors are hippuristanol, pateamine A and a large group of compounds known as rocaglamides.

Hippuristanol, isolated from the coral *Isis hippuris* (M. Bordeleau *et al.*, 2006) binds to the C-terminal domain of eIF4A and serves as an allosteric inhibitor by impeding ATP-binding (Lindqvist *et al.*, 2008). Lack of ATP binding impedes eIF4A RNA binding and unwinding. Moreover, hippuristanol has been shown to lock eIF4A in a closed conformation (Sun *et al.*, 2014).

Pateamine A (PatA), isolated from the sea sponge *Mycale hentscheli* has been shown to inhibit cap-dependent translation (Northcote, Blunt and Munro, 1991; Bordeleau *et al.*, 2005). PatA has been shown to increase the affinity of eIF4A for both ATP and RNA, and this strong association between eIF4A and RNA was demonstrated to sequester eIF4A from the eIF4F complex (M. E. Bordeleau *et al.*, 2006). Moreover, PatA has been shown to increase eIF4A helicase activity (Bordeleau *et al.*, 2005), implying that translational repression can be achieved through both inhibitors of gain and loss of function.

Rocaglamides belong to the class of flavaglines, isolated from *Agalia* genus of plants (Ebada *et al.*, 2011). Rocaglamide A (RocA) has been shown to interact with both eIF4A and RNA and bind in the molecular cavity of eIF4A (Iwasaki *et al.*, 2019), as well as induce RNA-sequence specific clamping of eIF4A (Iwasaki, Floor and Ingolia, 2016). Similar RNA-sequence specificity can be induced by silvestrol, another flavagline family member (Wilczynska *et al.*, 2019).

As eIF4A inhibition seems to be beneficial in reducing growth of cancer cell lines, there is a growing search for new inhibitors that are better suited for chemotherapeutic application. Some of these are of natural origin (Chu *et al.*,

2019) whereas others are synthetic derivatives (Zhang *et al.*, 2019; Müller *et al.*, 2020). Another synthetised eIF4A inhibitor, eFT226 (Zotatifin) (Ernst *et al.*, 2020) is currently undergoing clinical trials for COVID-19 (Effector Therapeutics NCT04632381).

Thus, eIF4A inhibitors show a promising avenue for repressing malignant growths. However, none of the available inhibitors seem to differentiate between the paralogues, as is the case of rocaglamides which target the conserved region. Due to the divergent roles of eIF4A1 and eIF4A2, as well as their differential effect on cancer there is a major need to understand how the inhibitors target each paralogue, and to preferentially find a paralogue-specific inhibitor. However, this need to differentiate between the paralogues and how they are targeted only recently became apparent in the scientific community (Cunningham, Chapman and Schatz, 2018).

1.6. Project aims

The overarching aim of this thesis is to understand the molecular processes that drive the different functions of the eIF4A paralogues. As eIF4A2 is underexplored in comparison to eIF4A1, the initial goal was to establish properties of eIF4A2 before moving on to comparisons between the two helicases.

Specific aims:

I. To determine the biochemical properties that drive the functions of the mostly unexplored eIF4A2.

II. To investigate how both the canonical eIF4A interaction partners, as well as the miRNA pathway related CNOT1 influence the activities of eIF4A2.

III. To compare the activities of eIF4A1 and eIF4A2 and further our understanding in their divergent functions by exploring their activities alone and in presence of interaction partners. As well as to investigate the specific regions of the helicases that could be responsible for the divergent functions *in vivo*. And finally, to examine whether the functions of human eIF4As could be conserved between the species.

2. Materials and Methods

2.1. Preparation of plasmid constructs

All primers used in this thesis were purchased from Sigma-Aldrich and contain appropriate restriction site with an overhang for digestion efficiency. Primers 10 to 16 were designed for the purpose of this thesis (**Table 2.1-1**).

Table 2.1-1 List of all the primers used in this thesis

No	Primer name	Sequence
1	eIF4A1_fw	TTGGTCTCATGGTTCTGCGAGCCAGGATTCC
2	eIF4A1_rv	AATAGCGGCCGCTCAGATGAGGTCAGCAACATTG
3	eIF4A2_fw	TTGGTCTCATGGTTCTGGTGGCTCCGCGGATTATAAC
4	eIF4A2_rv	AATAGCGGCCGCTTAAATAAGGTCAGCCACATTCATGG
5	eIF4A1_FLIM_fw	GTTGAAGCTTCATCTGCGAGCCAGGATTCC
6	eIF4A1_FLIM_rv	GAATAGGATCCTCAGATGAGGTCAGCAACATTG
7	eIF4A2_FLIM_fw	GTTGAAGCTTCATCTGGTGGCTCCGCGGATTATAAC
8	eIF4A2_FLIM_rv	GAATAGGATCCTTAAATAAGGTCAGCCACATTCATGG
9	Citr/turq_to_SUMO_fw	TTGGTCTCATGGTGTGAGCAAGGGCGAG
10	Sc_eIF4G_fw	TTGGTCTCATGGTCTTGTTCCAAGTGCTAATAGGTG
11	Sc_eIF4G-M_rv	AATAGCGGCCGCTTAGTTCCAGTTCTTGTCGT
12	Sc_eIF4G-MC_rv	AATAGCGGCCGCTTACTCTTCGTCATCACTTTCTCC
13	eIF4A1_D265R_E268K_fw	AGCTGGACACACTATGTCGCTTGTATAAAACCCTGACCATC
14	eIF4A1_D265R_E268K_rv	GACTGCCTGGGTGATGGTCAGGGTTTTATACAAGCGACATAGTGTG
15	eIF4A1_D296A _T298K_fw	CACCGAGAAGATGCATGCTCGAGCTTTCAAGGTATCCGCCATG
16	eIF4A1_D296A _T298K_rv	CATATCTCCATGCATGGCGGATACCTTGAAAGCTCGAGCATGCATC

To prepare constructs used in this thesis for cloning into expression vectors for either protein production or in cell work PCR reactions and site directed mutagenesis were performed (see **Tables 2.1-2**, **2.1-3**, **2.1-4**, **2.1-5**), using constructs presented below and primers (**Table 2.1-1**):

- previously cloned in the Bushell lab constructs of eIF4A1 1-18 A2 and eIF4A2 1-18 A1 were cloned into petSUMO expression plasmid using primers no 3 and 2 or 1 and 4, respectively,

- *Sc* eIF4G constructs were cloned from a vector purchased from Addgene (#37232) (Mitchell *et al.*, 2010) using primers no 10, 11 for shorter construct, and 10, 12 for longer construct into petSUMO vector,
- mCitrine and mTruquoise2 containing vectors were purchased from Addgene (#54587 and #54842) (Griesbeck *et al.*, 2001; Goedhart *et al.*, 2012) and used for cloning in eIF4A1 and eIF4A2, with primers no 5, 6 and 7, 8 correspondingly,
- mTurquoise2-eIF4A2 and mCitrine-eIF4A2 were also subcloned from the vector backbone into petSUMO plasmid for protein expression using primers no 9, 4,
- using primers, no 13, 14 and 15, 16 mutagenesis on petSUMO-eIF4A1 plasmids were performed to obtain eIF4A1 mutants deficient in eIF4G binding,
- eIF4G binding deficient mutants were also cloned into vectors containing mTurquoise2 and mCitrine using primers no 7, 8 (**Table 2.1-1**).

It should be noted that the vectors purchased from Addgene arrive as an agar stab culture and preparation of plasmid according to the manufacturer's guidelines is needed prior to any cloning.

Table 2.1-2 PCR reaction settings used for cloning of different constructs

Step	Temperature	Time	Cycles
Initial denaturation	98°C	1 min	1
Denaturation	98°C	30 s	30
Annealing	$T_a = T_m - 3°C$	30 s	
Polymerisation	72°C	30 s per 1 kb	
Elongation	70°C	5 min	1
Hold	10°C	∞	1

T_a – annealing temperature is based on calculated T_m (melting temperature) of primers, IDT OligoAnalyzer Tool was used for determination of T_m

Table 2.1-3 Example of site directed mutagenesis reaction mix

Component	Supplier & Cat. No.	Final amount
Phusion HF polymerase	NEB M0530	1 U (0.5 µL)
5 x Phusion HF or GC buffer	NEB B0518 or B0519	1 x
DNA template	-	~ 100 ng
dNTP (10 mM stock of each)	Thermo Scientific R0182	0.2 mM
Forward primer	Sigma-Aldrich	0.5 µM
Reverse primer	Sigma-Aldrich	0.5 µM
H_2O (nuclease-free)	Invitrogen AM9937	Up to 50 µL

Note that the polymerase should be added last

Table 2.1-4 Site directed mutagenesis settings

Step	Temperature	Time	Cycles
Initial denaturation	95°C	1 min	1
Denaturation	95°C	30 s	40
Annealing	66°C	30 s	
Polymerisation	68°C	7 min	
Elongation	72°C	15 min	1
Hold	10°C	∞	1

T_a – annealing temperature is based on calculated T_m (melting temperature) of primers, IDT OligoAnalyzer Tool was used for determination of T_m

Table 2.1-5 Example of PCR reaction mix

Component	Supplier & Cat. No.	Final amount
PfuTurbo	Agilent 600250	2.5 U (1 µL)
10 x PfuTurbo buffer	Agilent 600250	1 x
DMSO	NEB B0515	1.5 µL
DNA template	-	~ 10 ng
dNTP (10 mM stock of each)	Thermo Scientific R0182	0.2 mM
Forward primer	Sigma-Aldrich	0.3 µM
Reverse primer	Sigma-Aldrich	0.3 µM
H_2O (nuclease-free)	Invitrogen AM9937	Up to 50 µL

Note that the polymerase should be added last

After PCR and site directed mutagenesis 2 µL of DpnI (Agilent 500402) were added to the reaction mix, and the samples were incubated for 1 h at 37°C. DpnI recognises methylated DNA and therefore cleaves the DNA template leaving the PCR product intact. Subsequently the PCR reaction mix was purified either using QIAquick PCR Purification Kit (Qiagen 28104) or resolved on 1.2% w/v agarose (Melford 9012-36-6) gel with SYBR Safe DNA gel stain (Thermo Fisher Scientific

S33102) in TAE buffer (provided by Beatson Central Services). For identification of sizes of PCR products HyperLadder 1kb (Bioline BIO-33026) DNA marker was used. If agarose gel was resolved, PCR products were extracted from the gel using Zymoclean Gel DNA Recovery Kit (Zymo Research D4008) or QIAquick Gel Extraction Kit (Qiagen 28706). The concentration of purified PCR product was estimated by A260 nm measurements using Nanodrop (Thermo Scientific ND-ONE-W).

Next, double enzymatic digestions were performed:

- for cloning into petSUMO vector and the petSUMO vector itself with BsaI-HFv2 (NEB R3733) and NotI-HF (NEB R3189),
- for cloning into the mCitrine and mTurquoise2 plasmids and the vectors themselves with HindIII-HF (NEB R3104) and BamHI-HF (NEB R3136).

Enzymatic digestions were assembled in CutSmart buffer (NEB B6004) and performed at 37°C for at least 2 h. The amount of enzyme used was based on the quantity of PCR product and manufacturer's guidelines. After digestion, the enzymes were inactivated by heating up the samples to 80°C for 20 min. Next, the samples were purified using either QIAquick PCR Purification Kit or gel extraction method, as above. Vectors were purified using gel extraction method.

Next, ligation reactions were performed using 3 to 1 insert to vector ratio (see **Equation 2.1-1**). Ligations were performed using LigaFast Rapid DNA Ligation System (Promega M8221) at RT for 10 min and subsequently half of the mixture was used for bacterial transformations. Alternatively, T4 DNA Ligase (NEB M0202) was used at 16°C overnight, after which the samples were inactivated for 10 min at 65°C before transformation.

Equation 2.1-1 Determination of insert and vector amounts for ligation

$$\frac{ng\ of\ vector\ *\ \ kb\ insert}{kb\ vector} * \frac{1}{3} = ng\ of\ insert$$

Transformations into *E. coli* DH5α were performed using standard protocol, i.e., **1)** thawing of the bacteria on ice, **2)** adding of the ligation mix or plasmid to the bacteria, **3**) incubation on ice for 10 to 20 min, **4)** heat-shock for 45 s in 42°C, **5)**

outgrowth step in S.O.C medium (Invitrogen 15544034) at 37°C for 1 h with vigorous shaking, **6**) spreading bacteria on agar plates with appropriate antibiotics, **7)** overnight incubation at 37°C.

Next, 5 mL LB media with appropriate antibiotic in culture tubes (Falcon 352051) were inoculated with single colony each and grown overnight at 37°C with shaking. Subsequently, DNA was purified by the Beatson Institute Molecular Technology Services using Qiagen Universal Robot and sequenced on an Applied Biosystems 3130xl sequencer. When necessary, for cell work, plasmids were regrown at larger scale, purified by the Beatson Institute Molecular Technology Services using Invitrogen Purelink HiPure Plasmid Filter Purification Kits and sequenced again.

2.2. Protein expression and purification

The properties of all the protein constructs used in this thesis are presented in **Table 2.2-1**. Residues denote the amino acid limits of each construct. Mass in Da can be used for estimation of either elution profile on size exclusion chromatography or migration on SDS-PAGE. Extinction coefficient (ε) is needed for estimation of molar concentration using the Beer-Lambert equation (**Equation 2.2-1**). The isoelectric point (pI) allows for determination of electrical charge of the protein at a given pH, which is useful for determination which ion exchange resin should be used in a purification step. In pH higher than pI the protein should be negatively charged, in pH lower than pI positively charged and at pH equal to pI the protein should remain neutral. Mass, ε and pI presented here are calculated using ExPASy Server, ProtParam tool (Gasteiger *et al.*, 2005).

Equation 2.2-1 The Beer-Lambert law

$$A = \varepsilon\ (M^{-1}cm^{-1})\ \times l\ (cm)\ \times\ C\ (M)$$

Table 2.2-1 Properties of all the proteins used in this thesis

Construct	Residues	Mass (Da)	ε (M^{-1} cm^{-1})	pI
eIF4A1	1 - 406	46153	34630	5.32
eIF4A2	1 - 407	46402	40130	5.33
eIF4A1 Δ N-20	21 - 406	44005	34630	5.60
eIF4A2 Δ N-21	22 - 407	44241	38640	5.62
eIF4A1 1 – 18 A2	1 - 406	46065	36120	5.39
eIF4A2 1 – 18 A1	1 - 407	46490	38640	5.26
eIF4A2-7-mut	1 – 407	46308	40130	5.32
eIF4A1 4G-mut	1 – 406	46194	34630	5.75
eIF4A1 DQAD	1 – 406	46152	34630	5.40
mTurquoise2-eIF4A2	1 - 655	74181	66155	5.50
mCitrine-eIF4A2	1 - 655	74318	63635	5.60
Sc eIF4A	1 - 395	44697	18005	5.02
eIF4G-MC	674 - 1599	104179	74995	7.89
***Sc* eIF4G-MC**	572 – 952	43358	36690	6.03
***Sc* eIF4G-M**	572 – 853	32098	35200	5.48
eIF4H	1 – 248	27385	14440	6.66
PDCD4	1 - 469	51735	40255	5.07
CNOT1 MIF	1093 – 1317	26084	23950	6.62
CNOT1 MA3	800 - 999	23732	23505	7.88
CNOT1 MA3-MIF	800 – 1312	58793	47580	8.40
CNOT7	1 - 285	32745	39225	4.77
DDX6	1 - 483	54416	30745	8.85
CNOT1 ma3-mif_1	842 – 1317	54596	42080	7.32
CNOT1 ma3_1	800 – 1057	29520	23505	8.85
CNOT1 ma3_2	842 - 1092	28529	18005	7.87

Parameters calculated using Expasy ProtParam tool (Duvaud *et al.*, 2021)

2.2.1. Protein expression

Transformations of *E. coli* BL21 Codon Plus RP (strain containing more Met-tRNA and Arg-tRNA) with 10 ng of plasmids were performed as described above (**Chapter 2.1**). Constructs that were not tested previously, were subjected to test expressions: **1)** 5 mL bacterial cultures were grown overnight with antibiotics at 37°C, and subsequently **2)** used for inoculation of fresh antibiotic free 5 mL LB and grown at 37°C for 5 hours, **3)** the day culture was split into two samples with one induced with 1 mM IPTG (Indofine MB1008), **4)** cultures were grown for additional 2 hours. 50 µL samples were collected before induction and after 2 h expression. Collected samples were mixed in 4 to 1 ratio with SDS-

loading buffer (100 mM Tris pH 6.8, 40% w/v sucrose, 8 % SDS, 0.3% bromophenol blue, 2 mM EDTA, 20% ß-mercaptoethanol) and heated to 95°C for 5 min. Subsequently 20 µL of each sample was applied onto a gel and resolved using SDS-PAGE. The non-induced culture corresponding to the highest level of expression of the correct protein was used for preparation of a stock. In general, once transformed and tested, bacteria expressing the correct proteins were kept as a glycerol stock, i.e., 0.5 mL of bacterial sample collected in the growth phase mixed with 0.5 mL of 50% sterile glycerol, frozen in dry ice and stored at -80°C.

Biomass production for large scale protein purification was as follows: 200 - 500 mL LB containing 20 µg/mL kanamycin and 20 µg/mL chloramphenicol were inoculated from a glycerol stock and grown over night in 37°C, 5% CO_2, with shaking 225 rpm. In the morning cultures were poolled together and the optical density at 600 nm (OD600) was measured. Fresh LB media (3 – 12 L) was inoculated from the overnight culture to OD_{600} ~ 0.1 and grown without antibiotics in 37°C, 5% CO_2, with shaking 225 rpm, till either OD_{600} around 0.8, or OD_{600} around 0.4 if the cultures were to be cooled before the induction (refer to **Table 2.2.1-1** for details about individual proteins). Subsequently 1 mM final concentration of IPTG was added to the cultures and proteins were expressed at temperature and time as stated in **Table 2.2.1-1** in 5% CO_2, with 225 rpm shaking. After expression, bacteria were pelleted by centrifugation in 1 L tubes at 4°C, 15 minutes, 4000 rpm in J6-MI centrifuge (Beckman JS-4.2 swing bucket rotor). The process was repeated until the whole culture was spun down. Subsequently pellets were resuspended in ice cold PBS, transferred into 50 mL conical-bottom tubes and centrifugated again at the same settings. PBS was decanted, the tubes with pellets were placed in a tub with dry ice and ethanol mixture. Pellets were left for 10 minutes to freeze and subsequently stored at -80°C.

Table 2.2.1-1 Expression conditions and tags used for protein purification

Construct	Expression	Tags
eIF4A1	4 h, 37˚C	His-SUMO
eIF4A2	4 h, 37˚C	His-SUMO
eIF4A1 Δ N-20	4 h, 37˚C	His-SUMO
eIF4A1 1 – 18 A2	4 h, 37˚C	His-SUMO
eIF4A2 1 – 18 A1	4 h, 37˚C	His-SUMO
eIF4A2-7-mut	4 h, 37˚C	His-SUMO
eIF4A1 4G-mut	4 h, 37˚C	His-SUMO
mTurquoise2-eIF4A2	3 h, 37˚C	His-SUMO
mCitrine-eIF4A2	3 h, 37˚C	His-SUMO
eIF4G-MC	16 h, 18˚C	His-SUMO
***Sc* eIF4G-MC**	16 h, 18˚C	His-SUMO
***Sc* eIF4G-M**	16 h, 18˚C	His-SUMO
eIF4H	4 h, 37˚C	His-SUMO
PDCD4	4 h, 37˚C	His-SUMO
CNOT1 MIF	4 h, 37˚C	His-SUMO
CNOT1 MA3	4 h, 37˚C	His-SUMO
CNOT1 MA3-MIF	4 h, 37˚C; 4h, 30˚C; 16 h 18˚C	see figure legends
CNOT7	4 h, 37˚C	His (TEV cleavage)
DDX6	4 h, 37˚C	His-SUMO
CNOT1 ma3-mif_1	4 h, 37˚C; 4h, 30˚C; 16 h 18˚C	see figure legends
CNOT1 ma3_1	4 h, 37˚C	His-SUMO
CNOT1 ma3_2	16 h, 18˚C	His-SUMO

2.2.2. Protein purification

Proteins were purified in buffers as stated below prepared out of: Tris-HCl (prepared by Beatson Institute Central Services), HEPES (Sigma-Aldrich H4034), KCl (Sigma-Aldrich P9541), NaCl (Fisher Scientific 7647-14-5), imidazole (Sigma-Aldrich 1047161000), EDTA (prepared by Beatson Institute Central Services), glycerol (Fisher Scientific G/0600/17), DTT (Sigma-Aldrich D0632), TCEP (Melford T26500).

A. 20 mM Tris-HCl, pH 7.5, 1 M NaCl, 30 mM imidazole, 10 % w/v glycerol
B. 20 mM Tris-HCl, pH 7.5, 0.1 M NaCl, 500 mM imidazole, 10 % w/v glycerol
C. 20 mM Tris-HCl, pH 7.5, 10% w/v glycerol, 0.1 mM EDTA, 1 mM DTT

D. 20 mM Tris-HCl, pH 7.5, 0.1 mM KCl, 1% w/v glycerol, 0.1 mM EDTA, 1 mM DTT
E. 20 mM Tris-HCl, pH 7.5, 1 M KCl, 1% w/v glycerol, 0.1 mM EDTA, 1 mM DTT
F. 20 mM Tris-HCl, pH 7.5, 0.1 mM KCl, 1% w/v glycerol, 0.1 mM EDTA, 1 mM TCEP
G. 20 mM Tris-HCl, pH 7.5, 0.1 M KCl, 30 mM imidazole, 1 % w/v glycerol
H. 20 mM Tris-HCl, pH 7.5, 0.1 M NaCl, 30 mM imidazole, 1 % w/v glycerol
I. 20 mM Tris-HCl, pH 7.5, 0.25 mM KCl, 1% w/v glycerol, 0.1 mM EDTA, 1 mM TCEP

The frozen bacterial pellets were thawed on ice with addition of buffer A supplemented with 1 mM PMSF (Sigma-Aldrich 93482) and 1 tablet of Complete™ EDTA-free Protease Inhibitor Cocktail (Roche 5056489001) per 50 mL of buffer. After the pellets were dissolved final 1 mg/mL lysozyme (Sigma-Aldrich 62971) was added, the bacterial mixture was incubated for 30 min at RT, and subsequently for 30 min on ice. After the incubation time bacterial cells were lysed either **1)** using a microfluidizer (Microfluidics M-110P) set on 20000 psi, with each sample lysed twice, in the case of a large-scale, or **2)** in the case of a small-scale purification, using a sonicator (Sonics Vibra-cell VCX 130) set to 60 % amplitude with 10 pulses of 10 s on 10 s off, repeated 4 times, with sample cooling in between. Subsequently bacterial lysates were pre-cleared by centrifugation for 35 minutes at 4°C either at **1)** 19 000 rpm in a Beckman Avanti J-25 or J-25i Beckman centrifuges (rotor Beckman JA-25.5, fixed angle) or in Thermo Scientific SORVALL RC 6+ centrifuge (rotors Thermo Scientific F21-8x50y, SORVALL SS-34) in the case of large-scale purification, or **2)** at 13 300 rpm in Thermo Scientific Fresco 17 centrifuge (75003424 rotor) in the case of small scale. Supernatant from centrifugation was filtered through 0.45 µm pore filter.

- In the case of small-scale purification, the filtered lysate was applied to washed in buffer A Ni^{2+} resin (Ni-NTA Agarose Qiagen 30210), and incubated with rotation for 30 min at RT. Subsequently, the supernatant was collected, and 3 washes in buffer A were performed. Final wash was done in 200 µL of buffer H with 5 µL of 80 µM ULP1 protease and incubated for 1 h at room temperature with gentle rotation. Next,

supernatant was collected off the Ni^{2+} resin, and remaining fraction bound was eluted in buffer B.

- In the case of large-scale purification filtered lysate was applied on an equilibrated in buffer A HisTrap HP column (GE Healthcare / Cytiva 29-0510-21) using a peristaltic pump. All large-scale purifications (unless otherwise stated in the figure legend) were performed using either ÅKTA Explorer purification system (GE Healthcare) or NGC Chromatography System (Bio-Rad). Columns were washed in buffer A, and subsequently bound fractions were eluted in a linear gradient of buffer B. Pooled fractions containing protein of interest were diluted twice in buffer C and subjected to His-SUMO tag cleavage with ULP1 protease or His cleavage with TEV protease; for either 1 h at RT or 4°C overnight. Subsequently proteins were diluted again to a final dilution of 5 to 6 in buffer C. Next the diluted proteins were subjected either to reverse affinity chromatography using buffers G or ion exchange chromatography in buffer D, with a linear gradient elution using buffer E. Size exclusion chromatography was usually the final step of purification, performed in buffer F.

All columns were equilibrated before applying the samples: HisTrap HP either in buffer A, G or H, ion exchange columns (anion – RESOURCE Q; Cytvia 17117901; cation – HiTrap Heparin; Cytvia 17040701) in buffer D, and size exclusion column (Superdex S200 HiLoad 16/600; Cytvia 28989335) in buffer F. For information about purification of individual proteins consult **Table 2.2.2-1**. eIF4G-MC was eluted from SEC and stored in buffer I.

As a final step, all proteins were concentrated using either Vivaspin or Amicon Ultra centrifugal filters with an appropriate molecular weight cut off (MWCO). And concentrated proteins were aliquoted into 500 µL tubes (aliquot size between 10 and 200 µL), snap frozen in liquid nitrogen and stored at - 80°C.

Absorbance spectra (230 – 350 nm) of final products were measured and molar concentrations were calculated based on **Equation 2.2-1**. Moreover, nucleic acid contaminations were estimated using OD260 to OD280 ratio, and proteins used for further studies were deemed to not have contaminants.

Additionally, throughout the purification steps, SDS-PAGE was used to determine the purity and fractions containing the purified proteins. For this, gels were cast (see **Table 2.2.2-2**) and resolved in SDS-PAGE running buffer (25 mM Tris, pH 8.3, 0.192 M glycine, 0.1% SDS). Alternatively, pre-cast gels were used (NuPAGE 4 – 12 % Bis-Tris, Invitrogen NP0322BOX, NP0323BOX, NP0335BOX) and resolved in MOPS (Invitrogen NP0001) for larger proteins, or MES (Invitrogen, NP0002) for smaller proteins. Gels were either stained with Coomassie stain (5 volumes of methanol, 1 volume of acetic acid, 5 volumes of H_2O, and 1 g per 1L of stain Brilliant blue) and de-stained with de-staining buffer (3 volumes of methanol, 1 volume of acetic acid and 6 volumes of H_2O). Alternatively, gels were stained with InstantBlue (Abcam ab119211) and de-stained with H_2O. Precision Plus Protein Dual Color Standards (Bio-Rad 1610374) was used as marker.

Table 2.2.2-1 Purification steps of proteins used in this thesis

Construct	Affinity	Ion exchange	SEC	Additional
eIF4A1	Ni^{2+} column	Anion	+	-
eIF4A2	Ni^{2+} column	Anion	+	-
eIF4A1 Δ N-20	Ni^{2+} column	Anion	+	-
eIF4A1 1 – 18 A2	Ni^{2+} column	Anion	+	-
eIF4A2 1 – 18 A1	Ni^{2+} column	Anion	+	-
eIF4A2-7-mut	Ni^{2+} column	Anion	+	-
eIF4A1 4G-mut	Ni^{2+} column	Anion - FT	+	+
mTurquoise2-eIF4A2	Ni^{2+} agarose	-	-	-
mCitrine-eIF4A2	Ni^{2+} agarose	-	-	-
eIF4G-MC	Ni^{2+} column	Cation	+	-
***Sc* eIF4G-MC**	Ni^{2+} column	-	+	Reverse affinity
***Sc* eIF4G-M**	Ni^{2+} column	-	+	Reverse affinity
eIF4H	Ni^{2+} column	Cation	+	-
PDCD4	Ni^{2+} column	Anion	+	-
CNOT1 MIF	Ni^{2+} column	Anion - FT	+	Reverse affinity + SEC
CNOT1 MA3	Ni^{2+} column	Anion - FT	-	Reverse affinity
CNOT1 MA3-MIF	Ni^{2+} column	Anion - FT	+	-
CNOT7	Ni^{2+} column	Anion	+	-
DDX6	Ni^{2+} column	Cation	+	-
CNOT1 ma3-mif_1	Ni^{2+} column	Anion - FT	+	+/-
CNOT1 ma3_1	Ni^{2+} column	-	-	-
CNOT1 ma3_2	Ni^{2+} column	Anion - FT	+	-

FT means that the protein of interest was found in the flow through from that purification step

Table 2.2.2-2 SDS-PAGE gel casting protocol for 2 gels

Components	Supplier & Cat. No.	Resolving gel	Stacking gel
H_2O MiliQ	-	5 mL	1.5 mL
buffer *	-	5 mL	1.5 mL
30 % acrylamide	ProtoGel 37.5:1 National Diagnostics EC-980	10 mL	3 mL
10% w/v APS	Sigma-Aldrich A3678	200 µL	60 µL
TEMED	Sigma-Aldrich T22500	30 µL	10 µL

* 4 x resolving buffer (1.5 M Tris, pH 8.8, 1% SDS), 4 x stacking buffer (0.25 M Tris, pH 6.8, 1% SDS)

Resolving gel was cast first and after polymerisation stacking gel was cast on top (stacking gel was about 20% of the length of the whole gel).

2.3. *In vitro* methods

2.3.1. RNA binding assays

All RNA binding assays were performed in the binding buffer: 20 mM HEPES (Sigma-Aldrich H4034), 100 mM KCl (Sigma-Aldrich P9541), 1 mM $MgCl_2$ (Sigma-Aldrich M8266), 1 mM DTT (Sigma-Aldrich D0632), supplemented with 1 mM AMP-PNP (Sigma-Aldrich A2647), unless stated otherwise in the figure legends. For binding in presence of ATP 1 mM ATP (Sigma-Aldrich A2647) was used instead of 1 mM AMP-PNP. RNAs used in all RNA binding assays can be found in **Table 2.3.1-1**, and were purchased from Integrated DNA Technologies (IDT). All the reactions containing 0 µM protein had equivalent volume (to the volume of protein) of protein storage buffer (buffer F in **Chapter 2.2.2**) added.

Table 2.3.1-1 Single-stranded RNAs used in binding assays

RNA name	RNA sequence	Length (nt)	Label	Application
$(AG)_{10}$	AGAGAGAGAGAGAGAGAGAG	20	Dy780	EMSA
$(AG)_{10}$	AGAGAGAGAGAGAGAGAGAG	20	-	aSEC
$(AG)_{10}$	AGAGAGAGAGAGAGAGAGAG	20	FAM	FP, EMSA
$(CAA)_6CA$	CAACAACAACAACAACAACA	20	Dy680	EMSA
$(CAA)_6CA$	CAACAACAACAACAACAACA	20	-	aSEC
$(CAA)_6CA$	CAACAACAACAACAACAACA	20	FAM	FP, EMSA
$(AG)_5$ / 10 nt AG	AGAGAGAGAG	10	Dy780	EMSA
$(AG)_5$ / 10 nt AG	AGAGAGAGAG	10	-	aSEC
$(AG)_{7.5}$ / 15 nt AG	AGAGAGAGAGAGAGA	15	Dy780	EMSA
$(AG)_{7.5}$ / 15 nt AG	AGAGAGAGAGAGAGA	15	-	aSEC
$(AG)_{25}$ / 50 nt AG	AGAGAGAGAGAGAGAGAGAG AGAGAGAGAGAGAGAGAGAG AGAGAGAGAG	50	Dy780	EMSA
$(AG)_{25}$ / 50 nt AG	AGAGAGAGAGAGAGAGAGAG AGAGAGAGAGAGAGAGAGAG AGAGAGAGAG	50	-	aSEC
A_{20}	AAAAAAAAAAAAAAAAAAAA	20	-	aSEC
A_{20}	AAAAAAAAAAAAAAAAAAAA	20	FAM	EMSA
$(GAAG)_5$	GAAGGAAGGAAGGAAGGAAG	20	-	aSEC
$(GAAG)_5$	GAAGGAAGGAAGGAAGGAAG	20	FAM	EMSA
$(GUGCU)_4$	GUGCUGUGCUGUGCUGUGCU	20	-	aSEC
$(GUGCU)_4$	GUGCUGUGCUGUGCUGUGCU	20	FAM	EMSA
$(AGUG)_5$	AGUGAGUGAGUGAGUGAGUG	20	FAM	FP, EMSA
$(UCUC)_5$	UCUCUCUCUCUCUCUCUCUC	20	FAM	FP, EMSA
$(UGUU)_5$	UGUUUGUUUGUUUGUUUGUU	20	FAM	FP, EMSA
$(AG)_5U_{10}$	AGAGAGAGAGUUUUUUUUUU	20	FAM	EMSA
$U_5(AG)_5U_5$	UUUUUAGAGAGAGAGUUUUU	20	FAM	EMSA
$(AG)_2U_{12}(AG)_2$	AGAGUUUUUUUUUUUUAGAG	20	FAM	EMSA
$(AG)_2U_8(AG)_2U_4$	AGAGUUUUUUUUAGAGUUUU	20	FAM	EMSA
$(AG)_2U_4$	AGAGUUUUAGAGUUUUAGAG	20	FAM	EMSA
$(AG)_2U_2$	AGAGUUAGAGUUAGAGUUAG	20	FAM	EMSA
$(AGU)_6AG$	AGUAGUAGUAGUAGUAGUAG	20	FAM	EMSA

2.3.1.1. Electrophoretic mobility shift assay

Electrophoretic mobility shift assay (EMSA) is a technique that allows for visualisation of protein – nucleic acid complexes in their native state.

RNA protein complexes were assembled as presented in **Table 2.3.1.1-1** and preincubated for 1 hour at room temperature. After the preincubation 2.5 µL of 5% w/v Ficoll 400 (Sigma-Aldrich F2637) solution was added to the reaction. Prepared samples were loaded on a 7% acrylamide native gel (**Table 2.3.1.1-2**) and resolved for 45 minutes at 100 V. Separation of complexes on a native gel is based on both the mass of the complex and its charge. The resolved native gels were visualised using Li-COR Odyssey and respective channels (700 for Dy680, 800 for Dy780) or Typhoon FLA7000 imager (for FAM labelled RNAs). Band shifts can be observed on the gels corresponding to **1)** negatively charged nucleic acids that migrate to the bottom to the gel **2)** eIF4A-RNA complexes that stay in the upper part of the gel due to the positive charge of the proteins at pH 7.5.

Table 2.3.1.1-1 Example of assembly of RNA binding reaction for use in EMSA assay

Components	Volume (µL)
10 x binding buffer	1
10 mM AMP-PNP / ATP	1
DMSO / 10 mM silv	0.1
100 nM RNA (Dy680 or Dy780)	2.5
protein (10 x µM conc)	1
H_2O RNAse free	4.4

Reactions were often assembled as a master mix with omission of a varying component, which was pipetted separately to the tubes.

In the case of reactions with competition RNA 3.4 µL of H_2O was used, and 1 µL of competitor RNA was added after initial preincubation for 45 min and incubated for another 45 min before applying the sample to a gel.

Silvestrol (silv) purchased from Generon, DMSO (Sigma-Aldrich D2438).

Table 2.3.1.1-2 Native gel protocol for two 7% gels

Components	Supplier & Cat. No.	Volume (mL)
40% acrylamide	AccuGel 19:1 National Diagnostics EC-850	3.5
5x TB buffer	Supplied by CRUK BI central services	4
RNAse free H_2O	RNAse free MiliQ	12.28
10% w/v APS	Sigma-Aldrich A3678	0.2
TEMED	Sigma-Aldrich T22500	0.02

Additionally, the K_D of the protein for RNA was calculated from EMSAs where protein titration (0, 0.01, 0.02, 0.06, 0.2, 0.5, 1, 3, 5, 7 μM) was used. For this, fraction bound was assessed using analysis feature in Image Studio Lite Ver 5.2. Briefly, the signal of unbound (free RNA at the bottom of the gel) and the bound (complexes, top of the gel) was calculated. The obtained values were added, and fraction bound was calculated by dividing the signal of bound fraction by total. Subsequently fraction bound data were exported to GraphPad Prism (versions from 7 to 9.2) and K_D was calculated by applying Hill equation to the data (**Equation 2.3.1.1-1**).

Equation 2.3.1.1-1 Hill equation

$$Y = \frac{B_{max} \times X^h}{{K_D}^h + X^h} + offset$$

X – concentration of titrant
Y – specific binding
B_{max} – maximum binding
K_D – dissociation constant
h – hill coefficient

2.3.1.2. Analytical size exclusion chromatography

Analytical gel filtration chromatography (aSEC), alike EMSA allows for visualisation of native complexes. However, advantageously in aSEC RNA substrates do not need to be labelled and if a chromatography system (here, ÅKTA Explorer from GE Healthcare) with multiple wavelength detection is used both RNA (at 260 nm) and protein (at 280 nm or peptide bonds at 220 nm) can be observed in the sample. In a size exclusion chromatography larger molecules (complexes) elute faster, at a smaller retention volume, and smaller molecules

are trapped in the pores of the chromatography column resin and are eluted at higher retention volume.

Reactions were set up as presented in **Table 2.3.1.2-1** and incubated for 1 h at RT. Subsequently, complexes were loaded on a preequilibrated in the binding buffer 2.2 mL size exclusion column (Superdex™ 200 Increase 3.2/300 Cytvia 28990946). Samples were run at a maximum flow rate of 50 µL/min.

Table 2.3.1.2-1 Example of aSEC sample preparation

	Final concentration	
Components	**protein only**	**protein-RNA complexes**
binding buffer	1 x	
AMP-PNP	1 mM	
DMSO / 10 mM silv	100 µM (equal volume in case of DMSO)	
Unlabelled RNA	0 µM	4 µM
protein	16 µM	
H_2O RNAse free	to 70 µL	

Some of the obtained chromatograms were additionally analysed to estimate protein to RNA ratio as well as the proportion of different complexes in the sample. For this exported chromatograms data were analysed using the area under curve function in GraphPad Prism (versions from 7 to 9.2), with setting limits for analysis of individual peaks. For complexes ratio analysis data from A 260 nm was used. The contribution of each complex was calculated by dividing area under curve of individual peak by the combined areas of all peaks in the sample. To understand the protein to RNA ratio in each complex molar concentrations of proteins and RNA were calculated in each peak based on the total concentrations in the sample and the ratio of area under the curve of individual peaks (A 260 nm for RNA, and A 220 nm for protein).

2.3.1.3. Fluorescence Polarisation

Fluorescence polarisation (FP) is a method that allows for measuring of molecules binding in solution. However, in this method distinction between different complexes that can contribute to the observed binding cannot be

made. FP is based on the changes in polarisation upon molecules binding (in this case protein and RNA) due to the change in the rotation of the fluorophore and can be described by **Equation 2.3.1.3-1**. Briefly, upon excitation with polarised lights, small, unbound molecules (with fluorescent probes, in this case FAM), rotate rapidly in solution therefore the emitted light is depolarised resulting in low FP value. When the fluorescently labelled molecule (short RNA) is bound by a larger one (protein) the rotation is slower, leading to emission of polarised light and high FP signal.

Equation 2.3.1.3-1 Fluorescence polarisation

$$FP = \frac{(F_{\parallel} - F_{\perp})}{(F_{\parallel} + F_{\perp})}$$

$F_{\parallel}$ - fluorescence intensity parallel to the excitation plane
$F_{\perp}$ - fluorescence intensity perpendicular to the excitation plane
Often F is referred as I for intensity, however here F was used to not confuse with I – scattering intensity

Complexes for fluorescence polarisation assays were assembled in a similar manner as presented in **Table 2.3.1.1-1**, with the difference in total reaction volume (20 µL) and use of 50 nM final concentration of FAM RNA. Reactions here were also prepared as master-mixes excluding variable elements (such as proteins) which were mixed separately. For the competition experiments either 0, equimolar amount, 10-fold excess or 50-fold excess of competitor RNA was used. For the competition experiments master-mixes were prepared as follows: buffer, FAM-RNA, DMSO, AMP-PNP, and H_2O were mixed together, then separated into 4 tubes and appropriate amount of competitor RNA added. Subsequently mixture was added to the different concentrations of proteins (titration from 0 to 10 µM). In the case of eIF4As binding in presence of additional proteins (for example CNOT1 or eIF4G both human and yeast) the additional proteins were included in the master-mix and preincubated for 5 - 10 minutes before pipetting the master-mix to the appropriate concentrations of eIF4As.

For reactions with AMP-PNP measurements after 1 hour of incubation were used, for ATP measurements were performed within the first 5 – 10 minutes of reaction assembly. FP was measured on either PerkinElmer 2030 Explorer or

Tecan Spark, with excitation at 485 nm and emission at 535 nm. Reactions were measured in 384-well plates (black, round bottom, non-binding surface; Corning #4514), covered with transparent film to avoid evaporation (Optical Adhesive Covers, Applied biosystems 4360954), at 30°C. Obtained data was analysed in GraphPad Prism, and K_D values were calculated using Hill equation (**Equation 2.3.1.1-1**).

2.3.2. RNA release assay

RNA release experiments were performed employing FP method (**Chapter 2.3.1.3**). RNA release assays were measured using Tecan Spark, and 384-well plates (Corning #4514), covered with optical adhesive film.

In this case either free RNA or RNA with 5 μM of either eIF4A1 or eIF4A2 or their mutants were used. The reactions were assembled in the same manner as for the FP assays with the only difference in the reaction start. Reactions were started with addition of either 1 mM ATP or 1 mM AMP-PNP. Subsequently kinetic measurements were performed at 30°C with intervals between 2.5 to 10 min for 15 hours. Obtained data was fitted to the 'Dissociation – One phase exponential decay' model in GraphPad Prism 9.2 (**Equation 2.3.2-1**) and half-lives were calculated.

Equation 2.3.2-1 Dissociation – One phase exponential decay

$$Y = (Y_0 - NS) \times \exp(-K \times X) + NS$$

X – time
Y – binding
Y_0 – binding at time 0
NS – binding at a long time (plateau)
K – rate constant (decay constant)

2.3.3. Unwinding assays

Unwinding assays were performed using Tecan Spark and PerkinElmer 2030 Explorer. 384-well plates with transparent bottom (Corning CLS3544 and Thermo Scientific 242764), covered with optical adhesive film were used. It should be noted that use of different machines, plates or adhesive films can affect the result, therefore, to make obtained measurements comparable internal controls need to be present in each experiment, such as sample with free RNA, free buffer, and maximal fluorescence reference control. Unwinding reactions were assembled and preincubated for 30 – 60 min before the reaction start with Mg^{2+}/ATP. After kinetic cycles were measured with intervals between 45 – 120 s for at least 1 h, with excitation wavelength at 535 nm and emission at 595 nm.

2.3.3.1. RNA annealing

All RNAs used in the unwinding assays were purchased from IDT as single stranded RNAs which were either unlabelled or labelled with fluorophore (Cy3) or quencher (BHQ2) (**Table 2.3.3.1-1**).

To use the RNAs in unwinding reactions a double-stranded region is necessary. Therefore, the RNAs presented in **Table 2.3.3.1-1** were mixed in an annealing buffer (20 mM Tris acetate pH 7.5, 100 mM KCl, 2 mM DTT) with a 1.1 : 1 : 1 ratio of unlabelled overhang strand, reporter, and quencher respectively. For overhang RNA substrates labelled with 3'BHQ 1.1 to 1 of overhang to reporter ratio was used. For reference strands only overhang strand and reporter strand were mixed. That mixed RNAs with a final concentration of at least 500 nM each were heated to 85 – 90 °C in a water bath and cooled slowly to RT (at least for 5 h, often overnight). Annealed RNAs were stored either at -80°C or at -20°C if the substrates were used in the next couple of weeks.

Table 2.3.3.1-1 List of RNA oligos used in unwinding and ATPase assays

RNA name	RNA sequence	Label and position
5'$(AG)_{10}$ overhang	AGAGAGAGAGAGAGAGAGGAAAAAAUUAAAAAAUUAA AAAACUCGGAGGGGCCGGUGGGGCC	-
5'$(CAA)_6$CA overhang	CAACAACAACAACAACAGAAAAAAUUAAAAAAUUAAA AAACUCGGAGGGGCCGGUGGGGCC	-
5'$(AGUG)_5$ overhang	AGUGAGUGAGUGAGUGAGUGGAAAAAAUUAAAAAAUUAA AAAAC	3' BHQ2
5'$(UCUC)_5$ overhang	UCUCUCUCUCUCUCUCUCGAAAAAAUUAAAAAAUUAA AAAAC	3' BHQ2
5'$(UGUU)_5$ overhang	UGUUUGUUUGUUUGUUUGUUGAAAAAAUUAAAAAAUUA AAAAAC	3' BHQ2
3'$(AG)_{10}$ overhang	CCGGGGUGGCCGGGGAGGCUCAAAAAAUUAAAAAAUUAA AAAAGACAACAACAACAACAACAAC	-
3'$(CAA)_6$CA overhang	CCGGGGUGGCCGGGGAGGCUCAAAAAAUUAAAAAAUUAA AAAAGGAGAGAGAGAGAGAGAGAGA	-
3' reporter	CUUUUUUAAUUUUUUAAUUUUUUG	5' Cy3
3' quencher	AGCCUCCCCGGCCACCCCGG	3' BHQ2
5' reporter	GUUUUUUAAUUUUUUAAUUUUUUC	5' Cy3
5' quencher	GGCCCCACCGGCCCCUCCGA	3' BHQ2

2.3.3.2. Unwinding reaction and analysis

Unwinding reactions were assembled in 20 µL reactions as presented in (**Table 2.3.3.2-1**). Reactions were started with adding Mg^{2+}/ATP as the binding buffer for unwinding reactions was depleted of $MgCl_2$. As mostly protein titrations (from 0 to 15 µM) were performed, master-mixes of reactions presented in in (**Table 2.3.3.2-1**) were made. As ATPase reactions were performed in conjunction to unwinding reactions, ATPase mix (as described in **Chapter 2.3.4**) was added straight to the wells designated for ATPase measurements before addition of other components of reaction. Wells without ATPase mix had 1 x binding buffer instead.

Unwinding reactions with competitor RNAs were assembled in a way where eIF4A was preincubated for 45 min with the RNA substrate and other components of the reaction (excluding Mg^{2+}/ATP) and then for another 45 min with competitor RNA. In reactions with interaction partners the proteins were preincubated together for 15 - 30 min before preincubation for 1 h with other components.

Wells in which no proteins were added (RNA only control) had an equivalent volume of protein storage buffer added instead of proteins (see buffer F **Chapter 2.2.2**).

Table 2.3.3.2-1 Example of unwinding reaction assembly

	Volume per single well (µL)		
Components	normal	With competitor	With interaction partners
4 x binding buffer	5	5	5
DMSO / 10 mM silv	0.2	0.2	0.2
500 nM annealed RNA	2	2	2
H_2O RNAse free	up to 20 µL total		
protein (10 x µM conc)	2	2	2
10 mM ATP	2	2	2
Competitor RNA (10 x µM conc)	0	2	0
interaction partner 1 (10 x µM conc)	0	0	2
interaction partner 2 (10 x µM conc)	0	0	0/2
ATPase mix	0/2	0/2	0/2

Obtained data were analysed using GraphPad Prism (versions 7 to 9.2). First, a baseline (value measured before the start of the reaction multiplied by 0.9 to account for dilution) was removed from each sample. Next, values were normalised to references. Reference value (total signal change) was calculated by subtracting the average of final reaction points for RNA only conditions (0 µM protein; the lowest fluorescence signal obtained for RNA) from the average of final points in the reaction of highest protein concentration with RNA substrate that did not contain quencher strand (the highest signal obtained for that RNA). The obtained reference value was used to normalise the unwinding results and allowed for comparison of fraction unwound. Next, first 200 s of reactions were fitted using linear model (**Equation** 2.3.3.2-1), where $Y_{intercept}$ was set to 0. Obtained slope value from straight line fitting corresponded to fraction unwound per s (initial velocity of unwinding reaction).

Equation 2.3.3.2-1 Straight line fitting

$$Y = Y_{intercept} + X \times slope$$

Y – value on Y axis
$I_{ntercept}$ – value at which Y axis is crossed
X – value on X axis
Slope = $(Y_{max} - Y_{min})/(X_{max} - X_{min})$

Initial velocity plotted against titrant protein concentration was further analysed with Hill equation (**Equation 2.3.1.1-1**), which resulted in obtaining a Hill coefficient (h, measurement of cooperativity), and an apparent K_D for the unwinding substrate in the unwinding reaction.

2.3.4. ATPase assays

ATPase reactions were performed in conjunction with unwinding reactions (**Chapter 2.3.3**) from the same master-mix (**Table 2.3.3.2-1**) in separate wells on a 384-well plate supplemented with ATPase mix. Here, dependency of NADH conversion and ATP conversion was employed (**Figure 2.3.4-1**). ATPase mix contains final concentrations of 1 mM NADH (Sigma-Aldrich 43420), 1 mM PEP (Alfa Aesar B20358) and 1/250 v/v enzyme mix PK/LDH (pyruvate kinase and lactic dehydrogenase) (Sigma-Aldrich P0294). Reactions were started in the same manner and at the same time as the unwinding reactions. Each reaction containing ATPase mix had its separate control without Mg^{2+}/ATP. The turnover of NADH was monitored by measuring absorbance at 340 nm during the same kinetic cycles as unwinding.

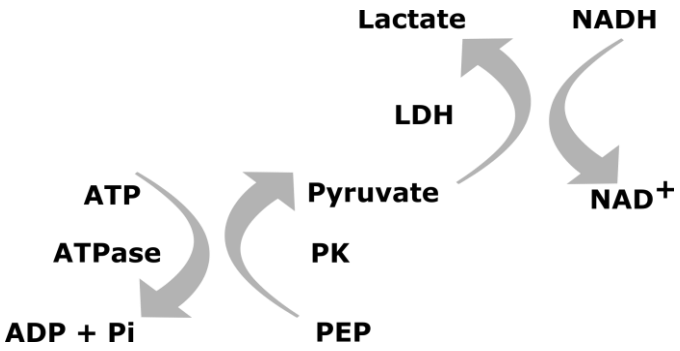

Figure 2.3.4-1 Dependence of ATP conversion and NADH conversion

NADH has absorbance at 340 nm, which decreases with NADH conversion. In the ATPase NADH coupled assay ATP hydrolysis is coupled with oxidation of NADH, therefore decrease in absorbance at 340 nm can be used for ATPase measurements.

Obtained data were analysed in GraphPad Prism (versions 7.0 – 9.2). The raw absorbance data (see example **Figure 2.3.4-2**) were converted to the concentration of NADH using machine and plate specific ε of 0.62 mM for Thermo Scientific plates and 1.22 mM for Corning plates. Next, the slope in the linear region between 1000 and 3600 s was measured (**Equation 2.3.3.2-1**). The ATPase was calculated using **Equation 2.3.4-1** for each individual condition.

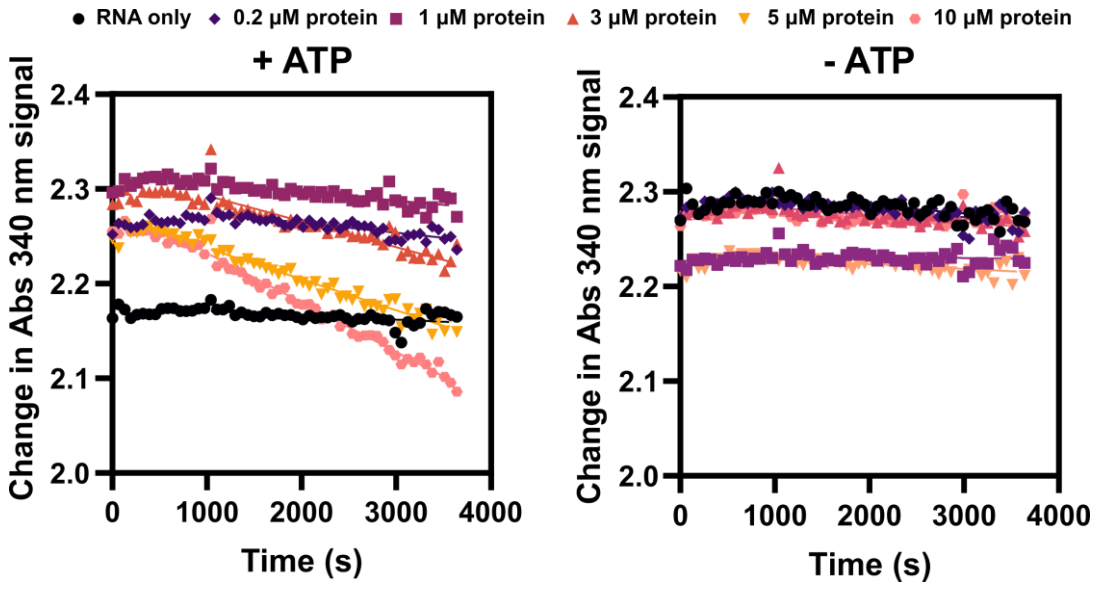

Figure 2.3.4-2 Example of raw ATPase data

Change in Abs at 340 nm for selected protein concentrations, with ATP (*left*) and without ATP (*right*).

Equation 2.3.4-1 Calculation used for determination of ATPase activity

$$ATPase = -(slope_{+ATP} - slope_{-ATP})$$

Slope calculated from line fitting

2.3.5. Small-angle X-ray scattering

Small-angle X-ray scattering (SAXS) experiments were performed to obtain structural information about protein-RNA complexes in solution. From a SAXS experiment information about size, shape, flexibility, and aggregation of the complex can be obtained.

All samples were prepared in the binding buffer (20 mM HEPES pH 7.5, 100 mM KCl, 2 mM $MgCl_2$, 1 mM DTT) and preincubated for an hour, to allow for complexes formation. Sample containing free protein was diluted to final concentration of 100 µM eIF4A2 in 100 µL of binding buffer. Sample containing ATP-bound state was prepared in the manner as the free protein supplemented with 1 mM AMPPNP (non-hydrolysable ATP analogue). Samples containing RNA, were also prepared in the binding buffer, containing 1 mM AMP-PNP, with final ratio of RNA to protein of 1:1 and 1:3 for monomeric, and oligomeric conditions, respectively. The concentration of RNA varied, while the concentration of protein was kept at ~ 100 µM. RNAs used in SAXS experiments are presented in **Table 2.3.5-1**. Subsequently the samples were snap frozen in liquid nitrogen and shipped on dry ice together with 50 mL of 10 x concentrated binding buffer to Diamond Light Source (DLS) in Oxford, UK. At DLS samples were run on size exclusion column Superdex 200 increase 3.2 coupled with X-ray radiation (SEC-SAXS) on B21 beamline. 620 frames were collected for each sample. The collected data were analysed with the use of Scatter IV and ATSAS 3.0.3 package deposited at EMBL (Manalastas-Cantos *et al.*, 2021).

Table 2.3.5-1 Unlabelled RNA oligos used in SAXS studies

RNA name	RNA sequence
$(AG)_{10}$	AGAGAGAGAGAGAGAGAGAG
$(CAA)_6CA$	CAACAACAACAACAACAACA
$(AG)_{10}$24BP	AGAGAGAGAGAGAGAGAGAG**GUUUUUUAAUUUUUUAAUUUUUUC CUUUUUUAAUUUUUUAAUUUUUUG**
$(AG)_5$24BP	AGAGAGAGAG**GAAAAAAUUAAAAAAUUAAAAAAC CUUUUUUAAUUUUUUAAUUUUUUG**
$(CAA)_6CA$24BP	CAACAACAACAACAACAACA**GAAAAAAUUAAAAAAUUAAAAAAC CUUUUUUAAUUUUUUAAUUUUUUG**

Unlabelled RNAs ordered from IDT. RNAs were ordered either as single-stranded or as double-stranded. The double stranded regions are indicated in bold.

The obtained data represent the intensities of the scattered X-rays after the beam hits the sample. Scattering Intensity (I) was collected for both the complexes and the buffer. First, scattering intensity of the buffer was subtracted from the protein scattering intensity. Scattering intensity, I, is represented as a function with scattering vector q. Next, frames corresponding to the peak with eluted protein and most constant radius of gyration (R_g) were selected. R_g represents the distance from the centre of gravity of the molecule, in this case protein or protein complex. Radius of gyration changes upon protein folding, conformational change, or formation of a complex. Generally, 10 % difference in radius of gyration for small proteins (~50 kDa) is considered a significant change. Next, the Guinier region (region at low q values, close to 0 scattering angle) was analysed (Guinier, Fournet and Yudowitch, 1955; Putnam *et al.*, 2007; Behrens *et al.*, 2012; Kachala, M., Valentini, E. and Svergun, 2015; Kikhney and Svergun, 2015). In the Guinier region a linear region was determined at the $q*R_g$ limit of 1.3. For this only the very first few points at the starting q^2 value were removed (Kachala, M., Valentini, E. and Svergun, 2015). The fit in the Guinier region provides information about sample aggregation (**Figure 2.3.5-1**, panel A), in this case no aggregation in the collected samples was observed. From this analysis information about both the R_g as well as I(0), intensity at 0 scattering angle can be extracted. After determination of R_g different samples were compared in the dimensionless Kratky plot. Here, based on the shape of the curve and changes between the samples information about the proteins folded state, globularity or existence of multiple domains was derived (**Figure 2.3.5-1**, panel B). Next, flexibility analysis was performed in by searching for plateau in one of the three plots: Porod-Debye, Kratky-Debye, or

SIBYLS plot. Here, the flexibility of the protein is determined based on the plot in which plateau was reached first (Rambo and Tainer, 2011; Brosey and Tainer, 2019). Proteins which reach plateau first in the Porod-Debye plot are considered to be rigid, proteins with plateau in Kratky-Debye are disordered, and the ones with plateau in SIBYLS plot are characterised as being flexible and often multidomain. After flexibility analysis pair distance distribution P(r) was analysed, which provides information about the real dimension, (maximum distance, d_{max}) of the sample (**Figure 2.3.5-1**, panel C).

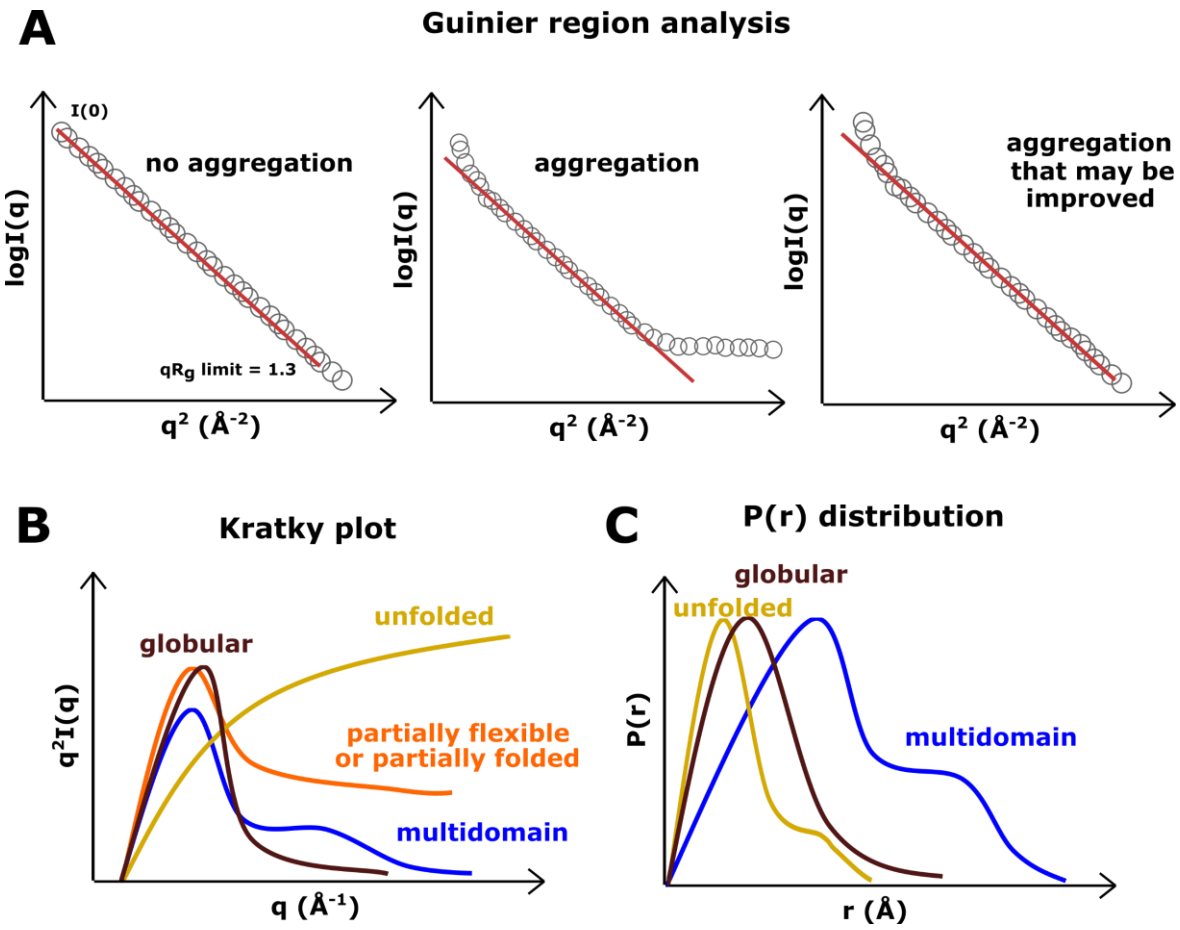

Figure 2.3.5-1 Example of SAXS data evaluation

Representative examples of protein behaviour in SAXS experiment and the interpretation of data. Figures created in Inkscape 1.1 and based on Putnam *et al.*, 2007. I – intensity, q – scattering vector, r – radius, P(r) – pair distance distribution.

A. Interpretation of $\log_{10}$ intensity plots in the low q region (Guinier region). Sample that follows a linear trend is not aggregated (*left*), sample that skews out of the linear region is aggregated (*middle*), sample that skews from the linear fit at the lowest q value (*right*) might be ameliorated by changing the conditions (for example protein concentration or buffer). In case on the *right* if aggregation is very small, sometimes data can be clipped and processed further (Putnam *et al.*, 2007).

B. Example of a Kratky plot for proteins that are globular (*burgundy*), multidomain (*blue*), partially folded or partially flexible (*orange*), or unfolded (*yellow*).

C. Example of pair distance distribution function (P(r)) for proteins that are globular (*burgundy*), multidomain (*blue*) or unfolded (*yellow*). The P(r) provides information about protein's d_{max} (maximum distance). Here, in the Scatter IV d_{max} was determined by analysis of the curve, and the Chi-square score for the possible d_{max} calculated, the lower the score, the better d_{nax} value fits the data. Notice the smooth end of the globular and multidomain proteins versus the sharp edging of the unfolded protein.

After these analyses dummy atom envelope models were calculated that corresponded to the shape and size of molecules. Briefly, the data from previous analyses are read by the DAMMIF package from ATSAS 3.0.3 (Franke and Svergun, 2009; Manalastas-Cantos *et al.*, 2021). The DAMMIF program was set to run 17 possible iterations of data interpretation, which resulted in creation of 17 .pdb files. Then programs from DAMAVER (Volkov and Svergun, 2003) package were executed. DAMSEL was used to compare all 17 models and determine the most probable model and find the outliers. DAMSEL also provides information about resolution (Tuukkanen, Kleywegt and Svergun, 2016), all resolved envelopes had a resolution around 40 Å. Next, DAMSUP was used to align the models with the most probable one. Then, DAMAVER averaged the aligned models and provided information about probability of fit. DAMFILT filtered the average model and generated the most representative envelope. This processes can be repeated for refinement. Additionally, obtained envelopes were superposed using SUBCOMB package from ATSAS 3.0.3.

2.3.6. Deadenylation assay

Deadenylation assay is an assay that allows for visualisation of deadenylation activity of proteins by using labelled RNA substrates (**Table 2.3.6-1**), which can be visualised on a gel. Removal of the polyA tail can be seen as a migration of the RNA substrate on a gel similar to the migration of the deadenylated marker.

Table 2.3.6-1 RNAs used for deadenylation assay

RNA name	RNA sequence
Dy780-(CAA)6CA-C20-A20	CAACAACAACAACAACAACACCCCCCCCCCCCCCCCCCCCAAAAAAAAAAAAAAAAAAAA
Dy680-(CAA)6CA-C20	CAACAACAACAACAACAACACCCCCCCCCCCCCCCCCCC

RNAs ordered from IBA life science.

Here, the helicases and CNOT1 constructs were mixed at 3 µM each, with 1 µM deadenylation RNA substrate and 1 mM AMP-PNP in the binding buffer (20 mM HEPES pH 7.5, 100 mM KCl, 1 mM $MgCl_2$, 1 mM DTT) and pre-incubated for 1 h at RT. In case of reaction without a helicase (or both helicase and CNOT1 construct) an amount of protein storage buffer (buffer F, see purification **Chapter 2.2.2**) corresponding to the volume of a protein was added. After 1 h pre-incubation an aliquot (5 µL) of the reaction mix was taken and mixed in 1 to 1 ratio with stop solution (0.5 x TBE, 10 mM EDTA, 0.2 % w/v SDS, 85 % v/v formamide) – timepoint 0 min. After taking an aliquot, 0.5 µM CNOT7 deadenylase was added to reaction and 5 µL aliquots were taken at time points 20 min, 40 min and 60 min and mixed immediately with 5 µL stop solution. Samples were then heated at 95°C for 2 min and loaded on an acrylamide-8M-urea TBE gels (see below for gel details). After electrophoresis gels were scanned immediately using Licor Odyssey (channel 700 for deadenylation marker and channel 800 for deadenylation substrate).

The 20% gels were assembled from SequaGel UreaGel Sequencing System (Scientific laboratory supplies NAT1138) by mixing 4 volumes of Concentrate with 0.5 volume of Diluent and 0.5 volume of Buffer. After polymerisation gels were pre-warmed by running in 0.5 x TBE at 400 V (~40 W) for at least 1 h. Temperature of the gel was assessed by reading from a temperature indicating strip (Bio-Rad) attached to the glass plate of a gel above the buffer line in the electrophoresis tank. After loading the samples gels were run at 400 V for 45 min.

2.3.7. Recombinant protein immunoprecipitation

Recombinant protein immunoprecipitations (IP) were used to examine interactions between CNOT1 protein constructs and the helicases. In an IP a mounted antibody binds to the protein and any other proteins that interact with the protein of interest stay bound with it.

All IP and beads coating steps were done in Protein LoBind Tubes (Eppendorf 0030108116 and 0030108094). First, 50 µL of Dynabeads Protein G (Invitrogen 10004D) superparamagnetic beads per IP were washed three times in binding

buffer supplemented with 0.1% v/v IGEPAL CA-630 (Sigma-Aldrich I3021). IGEPAL CA-630 is a non-ionic and non-denaturating detergent, which here reduces nonspecific binding. Magnetic rack was used to remove liquid without aspirating the magnetic beads. After the washes the beads were coated with anti-IgG (control), anti-eIF4A2, or anti-DDX6 antibodies (see **Table 2.4.6-1** for details about antibodies) by incubating the beads with antibodies in binding buffer with IGEPAL CA-630 for 10 min at RT with gentle rotation. After incubation, excess of unbound antibodies was washed off (three washes). Next, the protein reactions (**Table 2.3.7-1**) were added to the beads and incubated for 15 min at RT with gentle rotation. After incubation beads were washed four times with buffer with IGEPAL CA-630 to reduce unspecific binding of proteins. Next beads were mixed with 3 times diluted SDS loading buffer (see **Chapter 2.2.1** for loading buffer details). Next samples were heated to 95°C for 5 min and subjected to SDS-PAGE (pre-cast gels used: Invitrogen NuPAGE 4 – 12 % Bis-Tris); Precision Plus Protein Dual Color Standards (Bio-Rad 1610374) was used as a marker. Care was taken to not aspirate the beads and not load them on a gel. After electrophoresis gels were stained with InstantBlue Comassie (Abcam ab119211) and de-stained with H_2O. Bands were visualised using Licor Odyssey.

Table 2.3.7-1 Reaction assembly for recombinant proteins IP

Components	Final concentration	Volume (µL)
10 x binding buffer	1 x	22
$(AG)_{10}$ RNA (10 µM)	0 /1 µM	0 / 22
helicase (50 µM)	5 µM	22
H_2O RNAse free	up to 220 µL total reaction volume	
AMP-PNP / ADP + Pi / AMP (10 µM)	0 / 1 µM	0/ 22
interaction partner 1 (50 µM)	5 µM	22
interaction partner 2 (50 µM)	0 / 5 µM	0 / 22

Each reaction was prepared in 220 µL – 100 µL per IP and 10 µL for input lane (10 µL excess for pipetting errors). For components in each lane see figure legends. AMP-PNP (Sigma-Aldrich A2647), ADP + Pi (Sigma-Aldrich A2754), AMP (Sigma-Aldrich A1752).

2.4. Cell based methods

2.4.1. Cell culture

HeLa cells were purchased from ATCC and additionally authenticated by the Beatson Institute of Molecular Technology Service using Promega GenePrint 10. Additionally, cells were tested for mycoplasma on a regular basis. No mycoplasma contamination was detected.

HeLa cells were cultured in DMEM (Gibco, 21969035), supplemented with 10 % v/v FBS (Gibco 10270-106) and 2 mM final concentration of L-glutamine (Gibco 25030024), and passaged when cells reached around 90% confluency. For detaching the cells, for passaging and seeding, trypsin (Gibco 15090046) was used. Stock aliquots of early cell passages were frozen in 90% v/v FBS and 10% v/v DMEM and stored in liquid nitrogen. Cells were kept in tissue culture incubator with settings: 37°C, 5% CO_2. All reagents were warmed up to 37°C (or RT in case of transfection reagent) before applying to the cells.

2.4.2. Plasmid transfection

HeLa cells were transfected with:

- 1 µg of plasmid, or 1 µg of each plasmid in case of co-transfection for FLIM-FRET assays, and Wester Blots – per 35 mm dish,
- 6 µg of plasmid, or 6 µg of each plasmid in case of co-transfection for IPs – per 15 cm dish,

using GeneJammer (Agilent 204131) at a reagent (in µL) to plasmid (in µg) ratio of 3 to 1, according to the manufacturer's guidelines. Briefly, HeLa cells were seeded with cell density of ~120,000 cells per 35 mm sterile dish with glass bottom (MatTek P35G-1.5-20-C), or ~5 million cells per 15 cm sterile dish. After 24 h post seeding, the media were exchanged, and transfection protocol was followed. Pre-warmed reagents were mixed as follows for 35 mm dish (A) and 15 cm dish (B).

A. 3 µL of GeneJammer were mixed with 97 µL of DMEM (without FBS or L-glutamine) and incubated for 5 min at RT; subsequently the appropriate amount of plasmid diluted in 10 µL sterile H_2O was added.
B. 18 µL of GeneJammer were mixed with 582 µL of DMEM (without FBS or L-glutamine) and incubated for 5 min at RT; subsequently the appropriate amount of plasmid diluted in 60 µL sterile H_2O was added.

After 40 min incubation the transfection mixture was added dropwise onto the pre-plated cells. 48 h post transfection media were exchanged, and cells were used for further assays.

2.4.3. Protein extraction

Protein extraction differed depending on whether samples were subsequently used only for Western Blot (WB) analysis (A) or for immunoprecipitation followed with WB (B).

A. Transfected HeLa cells and untransfected controls were detached from the 35 mm dishes using trypsin and transferred to 1.5 mL tubes. Next the cells were washed twice in ice cold PBS with centrifugation steps (0.8 rpm for 5 min in Eppendorf MiniSpin plus) to remove PBS. Subsequently cell pellet was either frozen in dry ice / ethanol and stored at -80°C for further processing or immediately used. To lyse cells 100 µL RIPA buffer (50 mM Tris pH 7.5, 150 mM NaCl, 1% Triton X-100 (Sigma-Aldrich X100), 0.5 % sodium deoxycholate (Sigma-Aldrich, D6750), 0.1 % SDS), supplemented with 5 mM DTT, 0.5 mM PMSF, 5 mM NaF and Protease Inhibitor cocktail (Roche 11873580001, from a made stock to final concentration 1x) was used per sample. Cells were incubated on ice for 20 min and subsequently sonicated in an ultrasonic bath (Diagenode Bioruptor CD-200TM-EX) for 10 min at medium setting. Lysed cells were centrifugated at 13 300 rpm for 10 min at 4°C in an Thermo Scientific Fresco 17 centrifuge. Supernatant from centrifugation (containing soluble material, i.e., proteins) was used for subsequent analysis.

B. Transfected HeLa cells and untransfected controls were scraped from 15 cm dishes in total 12 mL ice-cold PBS using cell scrapers, transferred to 50

mL conical tubes and centrifugated for 5 min at 4°C at 1500 rpm in Eppendorf 5810R centrifuge (swing bucket rotor A-4-62). Pellet was resuspended in 1 mL of ice-cold PBS and transferred to 1.5 mL tubes and centrifugated at 2000 rpm for 5 min at 4°C in Thermo Scientific Fresco 17 centrifuge (75003424 rotor). Next each sample of cell pellet was resuspended in 1 mL of lysis buffer (20 mM Tris pH 7.5, 200 mM NaCl, 2.5 mM $MgCl_2$, 0.5 % Triton-X100) supplemented with 1 mM DTT, 5 mM NaF, 1 x Roche Inhibitor cocktail (from a stock). Each sample was then split into 2 tubes containing 0.5 mL lysis buffer/cell mixture and either 2 µL of RNAse inhibitor (RiboLock, 40 U/µL, Thermo Scientific EO0381) or 10 µL of RNAse 1 (100 U/µL, Invitrogen AM2295) was added to the samples. Samples treated with RiboLock were incubated on ice and samples treated with RNAse 1 were incubated at RT. Total incubation time for both was 20 min. At this point 50 µL from each sample was taken for RNA analysis (see **Chapter 2.4.4**). Next, the cell lysates were centrifugated for 15 min at 5000 rpm at 4°C in Thermo Scientific Fresco 17 centrifuge. Supernatant was used for subsequent analysis.

Protein concentrations were determined using Bio-Rad Protein Assay (#5000006), based on Bradford assay, and following manufacturer's guidelines. Briefly, 970 µL of the diluted reagent (5 x concentrated stock) was added to a 10 times diluted protein sample of total volume 30 µL in a cuvette. Equal volume of BSA with known concentrations (0, 20, 50, 70, 100, 300, 500, 700, 1000 µg/mL) was used to establish protein concentration in the samples. After 5 min incubation, absorbance of all the samples and controls was measured at 595 nm.

2.4.4. RNA integrity analysis

For the control of RNA stability and digestion in the IP samples 50 µL of each sample after RNAse / RNAse inhibitor treatment was subjected to RNA extraction using RNeasy Mini Kit (Qiagen 74104). The concentration of eluted RNA was measured using Nanodrop (Thermo Scientific ND-ONE-W). Subsequently 500 ng of RNA from each sample was resolved on 1.2% w/v agarose (Melford 9012-36-6) gel with SYBR Safe DNA gel stain (Thermo Fisher Scientific S33102) in TAE buffer for

35 min at 200 V. The RNA on the gels was exposed using ChemiDoc (Bio-Rad 1708370). Integrity of RNA was assessed based on visibility of 28 and 18S rRNA.

2.4.5. Immunoprecipitations

Similarly, as for recombinant proteins immunoprecipitations (**Chapter 2.3.7**) Dynabeads Protein G (Invitrogen 10004D) were washed three times (using magnetic rack to avoid bead aspiration) in IP lysis buffer (see **Chapter 2.4.3**) supplemented with 10 % w/v BSA. Again, all the steps were performed in LoBinding tubes and 18 µL of Dynabeads per IP was used. Next, 4 µg of appropriate antibody (**Table 2.4.6-1**) diluted in 200 µL of lysis buffer (containing BSA) was added to the Dynabeads and incubated for 1 to 2.5 h at 4°C with gentle rotation. After incubation time lapsed unbound antibodies were removed by washing the beads three times in lysis buffer (without BSA). Next, the equal protein concentration of each sample (in equal volume, samples of different concentrations were diluted in lysis buffer to match) was added to the beads and incubated for 30 min at 4°C with gentle rotation. Next, the supernatant containing unbound proteins was discarded and beads were washed three times in 600 µL per wash of lysis buffer. The final wash was removed and 50 µL of 3 times diluted SDS-PAGE loading buffer was added (see **Chapter 2.2.1** for components of loading buffer). Samples were heated to 95°C for 5 minutes and subjected to SDS-PAGE electrophoresis, again care was taken to avoid aspiration of the beads. Pre-cast gels were used, either NuPAGE 4 – 12 % Bis-Tris (Invitrogen) or Criterion 4-15 % (Bio-Rad #5671084), and Precision Plus Protein (Bio-Rad 1610374) was used as a marker.

2.4.6. Western blotting

Western blotting (WB) was performed to visualise results from immunoprecipitations as well as to test the transfection efficiency (HeLa cells treated with RIPA buffer).

First the SDS-PAGE was performed (as described for IP **Chapter 2.4.5**, similarly RIPA extracted lysates were run on NuPAGE gels). Next, a wet transfer from the gels onto 0.45 µm nitrocellulose membranes (Amersham Protran, Cytvia GE106 00002) was performed in a pre-chilled transfer buffer (50 mM Tris pH 8.3, 192 mM glycine, 20 % methanol, 1 % SDS) for 1 h 15 min with settings 100 V / 0.8 A. Transfer quality was checked by staining the membranes with Ponceau S solution (Sigma-Aldrich P7170) for 5 min after which the stain was washed off with H_2O. The membranes were blocked in 5 % w/v milk (Marvel) in TBST (supplied by the Beatson Institute Central Services) for 30 to 60 min at RT while gently nutating. Next, the blocking solution was decanted, and membranes were washed in TBST. Subsequently primary antibodies (directed against epitopes of proteins of interest; **Table 2.4.6-1**) were diluted in blocking solution and applied to membranes. Membranes were incubated with antibodies, while gently nutating, for 1 h at RT or 4°C (only anti-eIF4A1/2 and anti-GFP antibodies could be used for 1 h RT incubation). Next, the membranes were washed five times in TBST (2 quick rinses, and 3 longer ~10 min washes) and incubated with secondary antibody (directed against an epitope on primary antibody, secondary antibodies are directed against host species of primary antibody), while nutating. After incubation the membranes were washed again in TBST (5 washes as above), and the results were visualised using LI-COR Odyssey (with 700 and 800 channels).

Anti-GFP antibody was used for detection of mTurqoise2 and mCitrine due to large similarities of epitopes (in general, 227 out of 238 amino acids matched for mTurquoiseC2 and GFP and 230 out of 238 for mCitrineC1 and GFP).

Table 2.4.6-1 List of antibodies used in this thesis

Antibody	Supplier	Cat. No.	Host	Application	Dilution
eIF4A1	Abcam	ab31217	rabbit	WB	1:2000 WB
eIF4A1	Abcam	ab31217	rabbit	IP	4 µg per cell IP
eIF4A2	Abcam	ab31218	rabbit	IP	4 µg per cell IP
eIF4A2	Abcam	ab31218	rabbit	IP	5 µg per *in vitro* IP
eIF4A2	Santa Cruz	137148	mouse	WB	1:1000
GFP	Abcam	ab290	rabbit	IP	4 µg per cell IP
GFP	Abcam	ab6556	rabbit	IP	4 µg per cell IP
GFP	Abcam	ab6556	rabbit	WB	1:5000 WB
GFP	Abcam	ab13970	chicken	WB	1:5000
eIF4G1	CST	2498	rabbit	WB	1:1000
eIF4G2	CST	5169	rabbit	WB	1:1000
PDCD4	Abcam	ab51495	rabbit	WB	1:2000
DDX6	Abcam	ab70455	rabbit	IP	5 µg per in vitro IP
Vinculin	Abcam	ab12900	rabbit	WB	1:10000
IgG	CST	2729	rabbit	IP	4 µg per cell IP
IgG	CST	2729	rabbit	IP	5 µg per *in vitro* IP
IRDye800CW	LI-COR	926-32212	donkey anti-mouse	WB – secondary antibody	1:10000
IRDye800CW	LI-COR	926-32213	donkey anti-rabbit	WB – secondary antibody	1:10000
IRDye800CW	LI-COR	926-32218	donkey anti-chicken	WB – secondary antibody	1:10000
IRDye680RD	LI-COR	926-68070	goat anti-mouse	WB – secondary antibody	1:10000
IRDye680RD	LI-COR	926-68071	goat anti-rabbit	WB – secondary antibody	1:10000
IRDye680RD	LI-COR	926-68028	donkey anti-chicken	WB – secondary antibody	1:10000

2.4.7. FLIM-FRET

Fluorescence lifetime imaging microscopy – fluorescence (Förster) resonance energy transfer (FLIM-FRET) was used to assess protein-protein interactions in live cells.

Measurements were performed using Nikon TE2000 microscope (60 x magnification) with the Lambert Instruments Fluorescence Attachment system equipped for FLIM frequency domain method. Briefly, to use the frequency domain the system has to be equipped in a modulated light source and a modulated detector. Then the sample (and reference) can be excited with light that is modulated in intensity, which causes the fluorescence emission to be intensity-modulated. As the emission decays the emitted light displays a phase-shift (time delay) and a decrease in modulation-depth (in reference to excitation light). Both the phase shift and the decrease in modulation depth are directly contingent on the decay constants of the fluorophore (fluorescence lifetime) as well as on the modulation frequency. As those parameters depend also on the fluorophore decay constants with each measurement a reference of a known fluorescence lifetime needs to be used (**Figure 2.4.7-1**). For experiments contained in this thesis 10 μM fluorescein (in Tris, pH above 11) was used (provided by the Beatson Institute Advance Imaging Resource), with a known fluorescence lifetime τ of 4.0 ns.

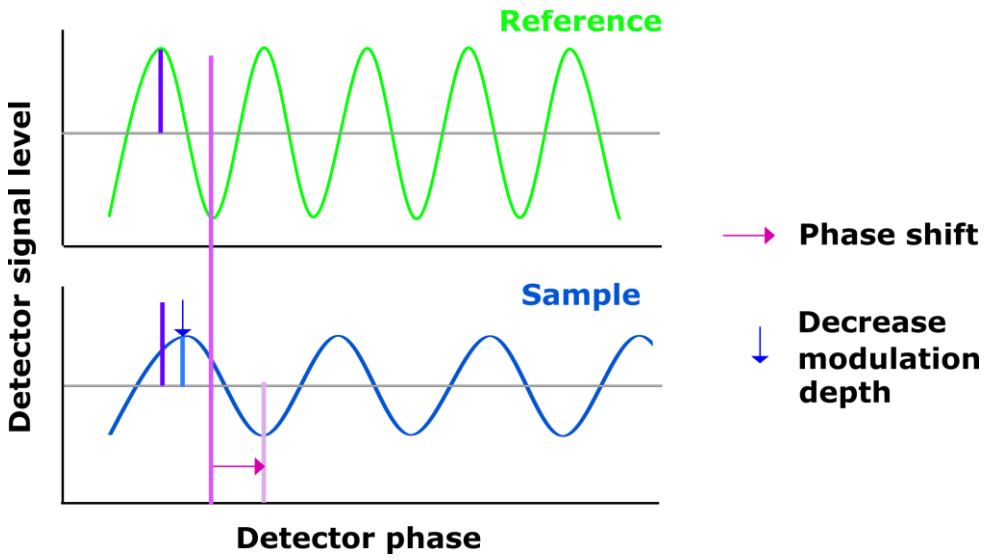

Figure 2.4.7-1 Frequency domain FLIM

A schematic of phase shift observed between a reference of a known fluorescence lifetime and the sample, as well as the observed decrease modulation depth. Schematic based on (Lambert Instruments).

To perform a FLIM-FRET experiment a good pair of spectrally overlapping fluorophores needs to be chosen. For experiments used in this thesis mTurquoise2 was chosen as a donor (ex 437, em 474) and mCitrine as an acceptor (ex 516, em 529) (**Figure 2.4.7-2**).

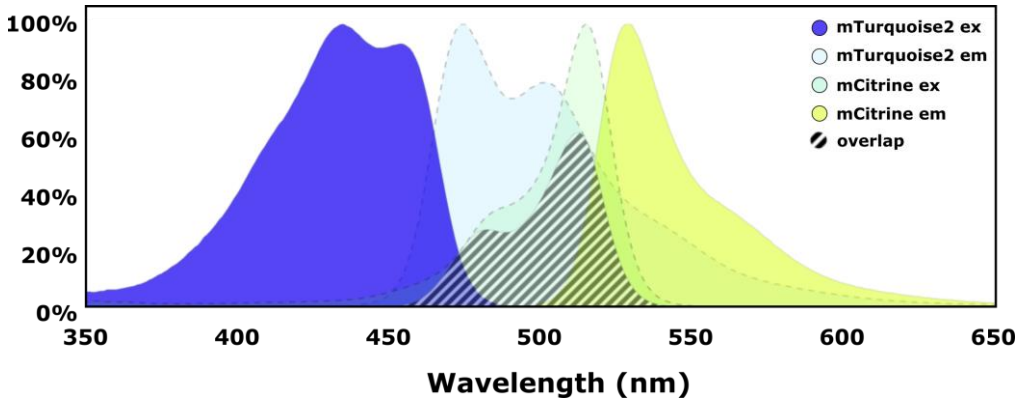

Figure 2.4.7-2 Overlapping spectra of mTurquoise2 and mCitrine

Excitation spectrum (ex) of mTurqoise2 show in blue, with emission (em) in light blue, ex of mCitrine show in light green, and its excitation in yellow. Overlap of mTurqoise2 emission and mCitrine excitation is show with stripe pattern. Figure created using FPbase FRET Calculator (FPbase).

48 h post-transfection (as described in **Chapter 2.4.2**) cells were subjected to FLIM-FRET experiment. Each sample (as well as the reference) were excited with LED light source at 445 nm (bandwidth 20 nm). Per each dish (dishes in technical duplicate) 3 to 4 regions were chosen and imaged. For total amount of cells measured for each experiment refer to figure legends. The information about the fluorescence lifetime of individual cells was extracted using LI-FLIM software (version 1.2.12.30; Lambert Instruments), which automatically calculated the phase shift and decrease in modulation depth of selected region and compared it to the reference. From each image, selected regions corresponded to different cells (one large region per cell). Next, images were exported in a cyan-magenta lifetime scale (setting the limits of fluorescence lifetime from 3.6 to 3.9 ns). The collected data from each individual image was exported as a .csv file. As that created a large (hundreds) number of files, lifetime values from individual experiments were combined in one .csv file and analysed using R. For statistical analysis two-tailed, unpaired t-test was used.

3. Characterisation of eIF4A2

3.1. Chapter introduction

Translation dysregulation is a common feature of tumourigenesis (Bhat *et al.*, 2015) with cancer cells adjusting to the cellular environment and enhancing their growth by increasing the production of pro-survival proteins (see also **Chapter 1.4**). Many mRNAs of pro-oncogenes are characterised by highly structured 5' untranslated regions (5'UTRs) (Wolfe *et al.*, 2014). As many mRNA structures in the 5'UTR are inhibitory to translation (Pelletier and Sonenberg, 1985; Taliaferro *et al.*, 2016; Leppek, Das and Barna, 2018), and the translation initiation is the most rate limiting step of protein synthesis (Shah *et al.*, 2013; Alekhina *et al.*, 2020), the expression of oncogenes is especially dependent on proteins which can resolve these structures, including helicases (**Chapter 1.5**).

One of the helicases that has been shown to play a role in cancer development and progression is eIF4A1 (Liang *et al.*, 2014; Modelska *et al.*, 2015; Gao *et al.*, 2020). eIF4A1 is a part of the heterotrimeric eukaryotic translation initiation complex 4F (eIF4F), responsible for cap-dependent translation initiation. eIF4F comprises the mRNA cap-binding protein eIF4E, the scaffold protein eIF4G and the DEAD-box helicase eIF4A1 (Grifo *et al.*, 1983). Recent studies have shown that eIF4A1 acts both as a helicase to unwind secondary structure within the 5'UTR of the mRNA and as an ATP-dependent protein that facilitates mRNA loading onto the ribosomes (Sokabe and Fraser, 2017; Yourik *et al.*, 2017). This dual role of the eIF4A1 and its involvement in tumourigenesis makes it an ideal target for anti-cancer therapies. Indeed, there is a growing search for eIF4A1 inhibitors. Currently, the available inhibitors are being tested *in vitro* and in pre-clinical studies, showing promising results (Jin *et al.*, 2013; Cunningham, Chapman and Schatz, 2018; Chu *et al.*, 2019; K. Chan *et al.*, 2019; Zhang *et al.*, 2019; Naineni *et al.*, 2020). However, the efficacy of eIF4A1 inhibition could be compromised by presence of highly similar eIF4A1 paralogue, eIF4A2. Intriguingly, the existing inhibitors lack specificity towards one paralogue. However this has been largely overlooked with only a few instances where the influence of the inhibitors on both paralogues was examined (Bordeleau *et al.*, 2005; Cunningham, Chapman and Schatz, 2018; Chu *et al.*, 2019).

The high similarity between the eIF4A paralogues (90 % of amino acid sequence identity) has led many researchers to believe that they are functionally redundant. Surprisingly, recent discoveries, demonstrated eIF4A2 to have an opposing translational function to eIF4A1 (Meijer *et al.*, 2013, 2019; Wilczynska *et al.*, 2019). eIF4A2 assembles with the Ccr4-Not complex and is involved in miRNA-mediated translational repression, executed at the stage of translational initiation (Meijer *et al.*, 2013). Moreover, the paralogues are associated with different states of the cell, i.e., eIF4A1 being associated with a proliferative state of the cell and eIF4A2 with a differentiated one (Galicia-Vazquez *et al.*, 2014). Additionally, high expression of eIF4A1 (Modelska *et al.*, 2015) and low expression of eIF4A2 (Shaoyan *et al.*, 2013) has been associated with poor cancer patient prognosis (see also **Table 1.5.1-1**), further emphasising the requirement to find inhibitors targeting one paralogue without affecting the other.

In contrast to the studies describing repressive function of eIF4A2, there have been a few recent reports linking eIF4A2 overexpression in colorectal and oesophageal cancers with poor cancer patients prognosis (Chen *et al.*, 2019; Liu *et al.*, 2019; Lyu *et al.*, 2020). This may suggest that eIF4A2 performs a dual role, depending on the type of cancer, or the complex it is in, as a suppressor of translation in some events and as a protein that promotes tumourigenesis, calling for further investigation of the two paralogues.

While structural information of eIF4A1 alone (Schütz *et al.*, 2010; Iwasaki *et al.*, 2019; Jiang *et al.*, 2019) and in complex with its interacting partners (LaRonde-LeBlanc *et al.*, 2006; Schutz *et al.*, 2008; Chang *et al.*, 2009) have been generated, only a single C-terminal domain of eIF4A2 has been resolved (Schütz *et al.*, 2010). Considering the ability of paralogues to interact with different co-factors in cells, understanding the structural differences may hold a key to distinguishing the paralogues and their behaviour, while providing an information necessary to design inhibitors targeting the right paralogue at the right time.

As eIF4A2 has for long been considered functionally redundant, and it is believed to have low expression in many cell types (Sudo, Takahashi and Nakamura, 1995) it has not been studied extensively in the past. The quest to distinguish the paralogues, understand their functions, mechanisms of action and target them in an appropriate manner where necessary, with reduction of pro-oncogenic

activities without inhibiting potential anti-oncogenic ones is still open. Therefore, the aims of this PhD project were to elucidate the mechanisms governing eIF4A2 to uncover the activities that distinguish it from eIF4A1.

As it has been shown previously (Wilczynska *et al.*, 2019), eIF4A2 has an inherent preference for binding polypurine RNAs. Therefore, pivotal to this project were biochemical approaches to uncover how eIF4A2 interacts with different RNA substrates, how it performs its helicase activity and what influences its ATPase activity.

The heterologously produced eIF4A2's binding capacity to different RNA sequences was examined, using biochemical and biophysical techniques such as electrophoretic mobility shift assay (EMSA) (Fried and Crothers, 1981; Garner and Revzin, 1981), analytical size exclusion chromatography (aSEC) (Lathe and Ruthven, 1955; Eisenstein, 2006), and fluorescence anisotropy (Albrecht, 1961; Lea and Simeonov, 2011). In an EMSA a fluorescently labelled RNA is used to form complexes with the protein of interest, and subsequently visualised on a native polyacrylamide gel (see also **Chapter 2.3.1.1**). The separation on a native gel is based on the electric charge of the molecules involved in the reaction, as well as their size and shape. A negatively charged free RNA will migrate to the bottom of the gel, whereas a protein bound one, due to the positive charge of the protein, will stay in an upper part of the gel. Alternatively, aSEC allows for separation of the molecules based on their size, disregarding the charge of the molecules (see also **Chapter 2.3.1.2**). Additionally, absorbance of the sample can be measured, to distinguish RNA and protein parts of the complex. Here, bigger molecules elute faster from the chromatography column resin, whereas smaller ones are trapped in the pores. The fluorescence anisotropy, or fluorescence polarisation, is a solution-based method, used to study molecular interactions. It relies on the change exerted on a labelled RNA molecule by binding of the protein, where the degree of polarisation of a fluorophore is inversely related to its molecular rotation. The molecule rotation is dependent on its size. Quantitatively, fluorescence polarisation is the difference in fluorescence intensity (emission light) parallel and perpendicular to the excitation light plane (see **Chapter 2.3.1.3**).

Pivotal to this chapter was structural characterisation by small-angle X-ray scattering (SAXS) of how eIF4A2-RNA complexes are assembled on various RNA substrates (see also **Chapter 2.3.5**). Here, the pre-equilibrated complexes were set up with a use of a non-hydrolysable ATP analogue, AMP-PNP, that allows for stable eIF4A2-RNA complex formation by inhibiting ATP hydrolysis thus prohibiting RNA release. Therefore, the complexes are trapped in an RNA-bound state. SAXS allows for measuring complexes in solution, which omits the crystal formation, a step necessary for crystallography methods. Additionally, as the measurements are done in solution instead of a solid crystal, the obtained structure models resemble a more natural, unpacked state. SAXS does not provide atomic resolution, however the easiness of sample preparation is a great benefit as it allows for rapid detection of various complexes. Moreover, the resolved SAXS structure models are of high enough resolution to distinguish conformational changes between differently formed complexes.

Furthermore, advanced imaging approaches were utilised to establish eIF4A2 behaviour in live cells. In fluorescence lifetime imaging microscopy – fluorescence resonance energy transfer (FLIM-FRET) (Bastiaens and Squire, 1999) live cells are transfected with two variants of a protein of interest, one tagged with a donor and the other one with the acceptor, that together form a FRET pair (see also **Chapter 2.4.7**). For this the excitation of an acceptor molecule has to overlap with the emission spectrum of the donor (Bajar *et al.*, 2016) (see also **Figure 2.4.7-2**). Additionally, it is important that the donor fluorophore chosen for FLIM-FRET has a high quantum yield (QY), defined as a ratio of the number of photons emitted to the ones absorbed (Lakowicz, 2006, p.10). In this project, mTurquoise2 with a QY = 0.93 (Bajar *et al.*, 2016) was used. Moreover, it is vital that the fluorophores exist in the monomeric state, as the oligomerisation of the fluorophores can mask real interactions happening in the cells.

Finally, unwinding and ATPase assays were performed *in vitro* to further understand the enzymatic activities of eIF4A2. For this various RNA substrates containing double-stranded region were used following established protocols (Özeş *et al.*, 2014). Briefly, RNA unwinding was measured by monitoring the change in fluorescence over time of the reaction, in which ongoing strand separation correlated with de-quenching of the substrate (see also **Chapter**

2.3.3). These measurements provide quantitative value of velocity of unwinding (fraction unwound per second), measured as the linear region in the first few timepoints (200 s) of a reaction, as well as fraction unwound (change between the starting and end value normalised to the reference) that can be compared for different RNA substrates. ATP-turnover (ATPase) was measured UV-spectroscopically by monitoring the ATP-dependent conversion of NADH to NAD^+ at 340 nm in an enzyme-coupled reaction. For this, unwinding reactions were supplemented with ATPase mix (see also **Chapter 2.3.4**).

In all, this chapter, provides an extensive characterisation of eIF4A2 DEAD-box helicase, providing important information about eIF4A2 molecular mechanisms.

3.2. eIF4A2 purification

As molecular activities of eIF4A2 have not previously been described in great detail, *in vitro* characterisation of its function was necessary. To study the enzymatic activity of eIF4A2, a previously cloned full length eIF4A2 construct (pET-SUMO-eIF4A2, performed by Dr Tobias Schmidt) containing a His-SUMO tag was expressed in *E. coli* strain BL21 DE3 RP codon+. The bacterial pellet after lysis, centrifugation and filtration of the supernatant (see **Chapter 2.2.2**) was subjected to the affinity chromatography, where the lysate was applied on a Ni^{2+} column and eluted in a linear imidazole gradient (**Figure 3.2-1**, panel A). Flow-through from the column and the wash contained unbound proteins. His-SUMO tagged eIF4A2 eluted from the column in a linear imidazole gradient and was subsequently treated with ULP1 (ubiquitin like protease 1) to cleave off the His-SUMO tag. After the cleavage eIF4A2 was subjected to ion exchange chromatography (**Figure 3.2-1**, panel B, *left*). As eIF4A2 (pI = 5.33) is negatively charged in pH = 7.5 it bound to anion exchange column (ResourceQ) and was eluted from the column in a linear gradient of increasing potassium chloride concentration. Fractions of interest were visualised using SDS-PAGE (**Figure 3.2-1**, panel B, *right*) and chosen for the next purification step. The final step comprised size exclusion chromatography (**Figure 3.2-1**, panel C) followed by protein concentration. The final product of purification was analysed by SDS-PAGE (**Figure 3.2-1**, panel D). Purity of the protein was determined, and no detectable protein contaminants were visible in the gel. Additionally, absorbance spectrum from 230 to 350 nm was measured (**Figure 3.2-1**, panel E). A clear peak at 280 nm and the 260/280 ratio of below 0.6 (0.55) indicated absence of nucleic acid contamination. Together, this indicates that the eIF4A2 protein is highly pure and suitable for biochemical studies.

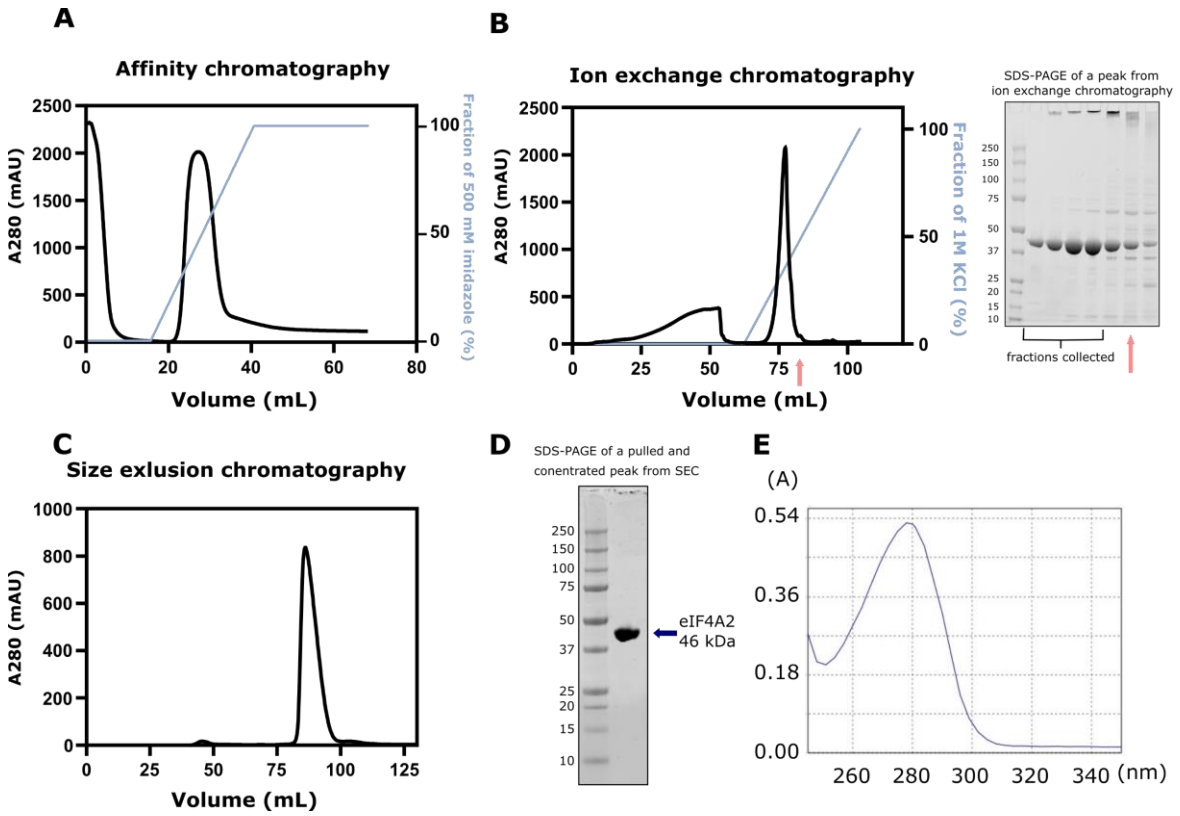

Figure 3.2-1 eIF4A2 3-step purification

A. Representative chromatogram of an elution profile of His-SUMO tagged eIF4A2 using a linear imidazole gradient on a 5 mL HisTrap HP column.

B. Peak fractions pooled from HisTrap HP shown in panel **A** were subjected to cleavage by ULP1 at room temperature for 1 hour and subsequently loaded on a 6 mL ResourceQ anion exchange column. The elution profile in presented chromatogram of eIF4A2 eluted in linear potassium chloride gradient shows signs of peak tailing (marked by a red arrow). Fractions were collected and subsequently run on SDS-PAGE (shown on the right). Pooled fractions (marked on the gel) were run on size exclusion chromatography column. Numbers on the left side of the gel represent the kDa sizes of the protein marker. The apparent aggregation in the wells is caused by high KCl concentration and disappeared after buffer change.

C. Representative size exclusion chromatography elution profile on Superdex S200 HiLoad 16/600 column. Purified eIF4A2 elutes around 85 mL.

D. Representative Coomassie stained SDS-PAGE gels of purified, full length, tag free, 46 kDa eIF4A2. Numbers on the left indicate sizes of the protein marker.

E. Representative absorbance spectrum (230 – 350 nm) of 12 times diluted eIF4A2 sample, with clearly visible peak at 280 nm indicating pure protein.

3.3. eIF4A2 unwinds secondary structure of RNA

Many previous reports have focused solely on the enzymatic activities of eIF4A1 and disregarded the highly identical paralogue eIF4A2 (Grifo *et al.*, 1984; Abramson *et al.*, 1987; Rogers, Richter and Merrick, 1999; G. W. Rogers, Lima and Merrick, 2001). First, to answer a question about the activity of purified eIF4A2, its unwinding activity was scrutinised. In a similar manner to published data about eIF4A1 (Rogers, Richter and Merrick, 1999; Özeş *et al.*, 2011) the unwinding activity was tested with the protein in excess over the RNA substrate. Previous studies revealed a preference of eIF4A to bind single-stranded RNA (Rogers, Richter and Merrick, 1999; Andreou, Harms and Klostermeier, 2019). Thus, the RNA substrate for the unwinding reaction was designed to contain a single-stranded overhang (**Figure 3.3-1**, panel A). Additionally, the substrate included a fluorophore labelled double-stranded region (Cy3-reporter) and guanidine-rich double-stranded region with a fluorophore quencher (BHQ-quencher). The choice of the single-stranded RNA sequence (overhang) was based on a study, in which the authors performed an RNA bind-n-seq experiment to determine eIF4A binding preferences (Iwasaki, Floor and Ingolia, 2016). The study suggested that polypurine-rich motifs are preferentially bound by the helicase. Therefore, the unwinding activity of eIF4A2 was tested on a double-stranded substrate containing a polypurine $(AG)_{10}$ single-stranded 5'overhang (**Figure 3.3-1**, panel B). As expected, an increase of the unwinding activity (measured as initial velocity) with increasing eIF4A2 concentration was observed. Notably, the obtained result resembled a sigmoidal shape, indicative of potential cooperativity. To test this, the Hill equation was fitted to the data. The derived Hill coefficient is a measurement of cooperativity in the reaction (Hill, 1913; Giraldo, 2008; Prinz, 2010). In a situation without cooperativity in the reaction the curve does not follow a sigmoidal trend and the Hill coefficient is less or equal to 1. Alternatively, a Hill coefficient above 1 for sigmoidal curves, suggests cooperativity in the reaction (**Figure 3.3-1**, panel C). Indeed, the calculated Hill coefficient (2.60 ± 0.31) for eIF4A2 unwinding reaction on the $(AG)_{10}$ 5'overhang substrate indicated cooperativity of the protein. As eIF4A2 has a single unwinding core (see also **Figure 1.5.1-1**), the co-operativity points to the possibility that more than one eIF4A2 molecule might be needed for unwinding the double-stranded RNA fragment.

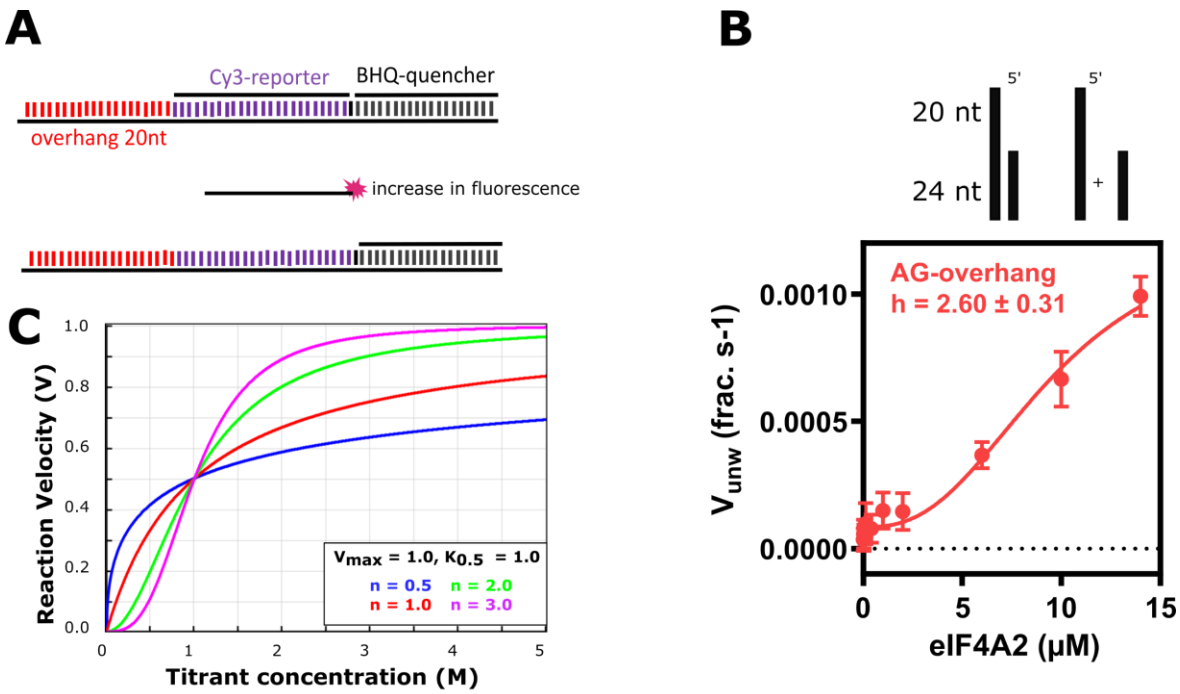

Figure 3.3-1 eIF4A2 can unwind RNA substrates in a cooperative manner

A. Schematic of the unwinding substrate consisting of a 20 nt single-stranded overhang (loading) RNA region, a double-stranded Cy3-labelled region, and double-stranded region labelled with Black Hole Quencher (BHQ).

B. Unwinding activity of eIF4A2 on an RNA substrate with $(AG)_{10}$ single-stranded region plotted as velocity of the unwinding versus the concentration of the helicase. The obtained Hill coefficient for the reaction marked as h, showed in the upper left corner, suggests co-operativity in the reaction. Each point n=3, with error bars as SEM, fit – Hill equation.

C. Schematic of plotted velocity of reaction versus titrant concentration. Graph shows the change in the shape of a reaction curve where V_{max} and $K_{0.5}$ is the same, but the Hill coefficient (labelled as n) varies. Graph created using an online calculator (PhysiologyWeb).

3.4. eIF4A2 can bind to RNA as a multimeric enzyme

The observed cooperativity in unwinding (**Chapter 3.3**), in a situation wherein the protein does not have multiple catalytic cores performing the same function, could be a sign of a possible co-operation between separate proteins. Such co-operation can potentially indicate protein multimerisation (Giraldo, 2008, 2013). To understand how the cooperativity is exerted and whether it is possible that multiple eIF4A2 act on one RNA, the binding of eIF4A2 to single-stranded RNA was tested. For this purpose, electrophoretic mobility shift assays (EMSA) were employed. This technique allows for a visualisation of pre-formed complexes in a native state in a polyacrylamide gel. Upon protein binding, a band shift of a labelled RNA is observed, with each subsequent protein molecule binding to the RNA seen as further shifts. A series of titrations of eIF4A2 on two different single-stranded RNA sequences (selection based on the bind-n-seq experiment from Iwasaki, Floor and Ingolia, 2016) $(AG)_{10}$ and $(CAA)_6CA$ labelled with Dy780 and Dy680 respectively was performed (**Figure 3.4-1**). With increasing eIF4A2 concentration multiple shifts were observed, suggesting binding of multiple eIF4A2 molecules to the single-stranded RNA and thus potential protein oligomerisation. Two sequences promoted oligomer formation to a different extent, with $(AG)_{10}$ being more stimulating.

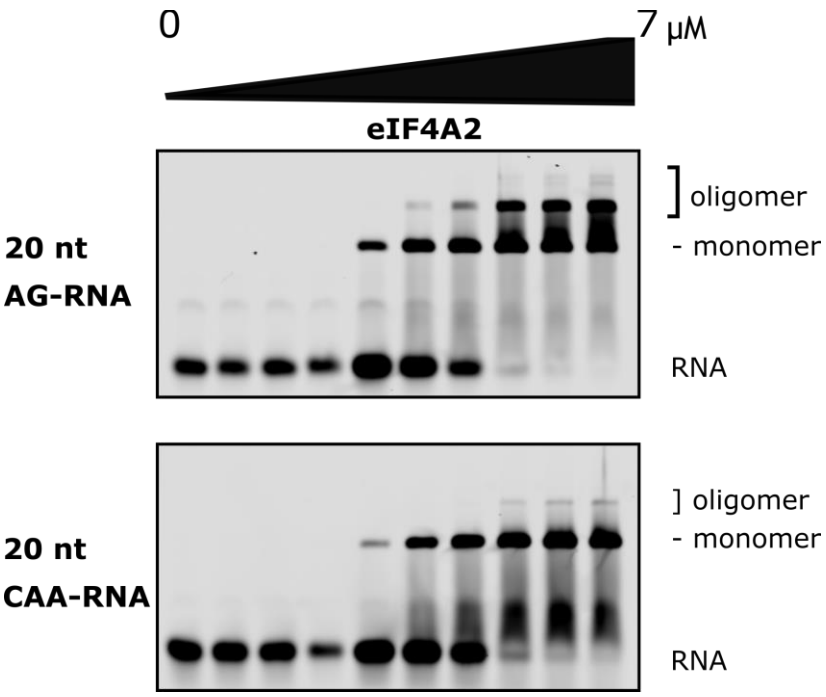

Figure 3.4-1 eIF4A2 has capacity to bind to a single-stranded RNA both as a monomer and oligomer

Electrophoretic mobility shift assay of increasing concentration of eIF4A2 bound to single-stranded RNA, $(AG)_{10}$ upper panel and $(CAA)_6CA$ lower panel. Each incremental band shift corresponds to higher-order complex formation. Complexes were pre-incubated for 1h at room temperature in presence of 1 mM AMP-PNP and subsequently run on 7% native polyacrylamide gels, for 50 minutes at 100 V, and visualised using Licor Odyssey. Representative gels, n = 3.

3.5. eIF4A2 multimerises in presence of RNA and it is dependent on its sequence and length

To further understand how eIF4A2 oligomers are formed, a series of analytical gel filtrations were performed. This technique allows for detection of the formed complexes and their separation by size. One of the advantages of analytical gel filtration over an EMSA is the possibility to detect unlabelled proteins and RNA by monitoring the UV-absorbance at 260 nm for RNA and at 280 nm for protein, as well as at 220 nm to observe peptide bonds. Bigger complexes elute faster, with smaller retention volume, whereas smaller molecules, for example monomers, are trapped in the resin pores and elute later, in a higher retention volume.

To answer whether eIF4A2 can form oligomers independently of RNA a sample containing 16 µM eIF4A2 in the binding buffer (see **Chapter 2.3.1**) was applied to a Superdex 200 increase 3.2/300 column resin. This resulted in a single peak eluted at 1.6 mL of retention volume (**Figure 3.5-1**, panel A, *brown A220, orange A260*). The previously run reference sample of Ovalbumin (45 kDa) similarly eluted at 1.6 mL, which suggested that the observed peak of eIF4A2 contains monomeric protein and that eIF4A2 does not form oligomers without presence of RNA. Given that the oligomers observed in the EMSAs (**Figure 3.4-1**) appeared with increasing concentration of eIF4A2, a mixture containing eIF4A2 (16 µM) in excess over RNA (4 µM) was applied to the resin. Intriguingly, this time multiple peaks were recorded on the chromatogram (**Figure 3.5-1**, panel A, *A220 red, A260 pink*). The previously run as a reference Conalbumin (76 kDa) eluted at 1.5 mL, and the free AG-RNA at 2.05 mL. This suggested that eIF4A2, based on the peaks' elution, is capable of forming at least detectable monomeric, dimeric, and trimeric complexes. To explore the stoichiometry of the formed complexes the molar ratio of protein and RNA in monomeric, dimeric, and trimeric peaks was calculated (**Figure 3.5-1**, panel B). As expected, in the monomeric peak there was an excess of protein over RNA, which could be explained by contribution of unbound fraction. As eIF4A2 did not form multimeric complexes without RNA, the assumption that all the RNA is bound in the dimeric and trimeric complexes can be made. As there is a 2.3 – 4-

fold excess of protein over RNA in those conditions, multiple proteins are involved in formation of oligomer on a single RNA.

In all, this implies that eIF4A2 oligomerisation is dependent on RNA being present, and when the helicase is in excess over RNA, which allows for multiple proteins oligomerising on a single RNA substrate.

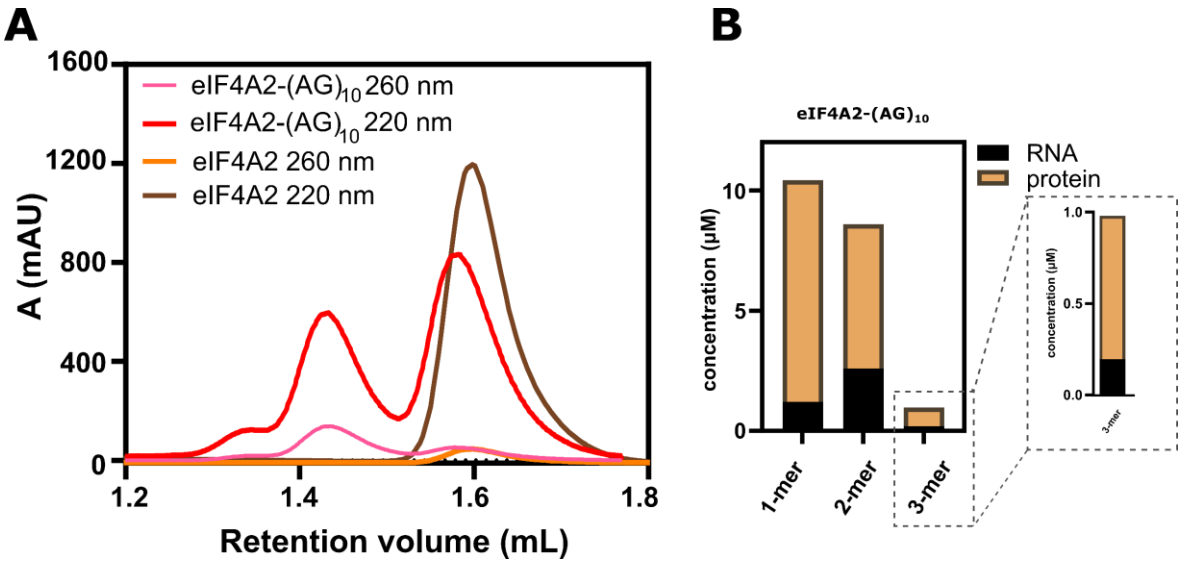

Figure 3.5-1 eIF4A2 forms oligomeric complexes only in the presence of RNA

A. 16 μM of free eIF4A2 (A_{220} *brown*, A_{260} *orange*) and 16 μM of eIF4A2 in presence of 4 μM $(AG)_{10}$ single-stranded AG-RNA (A_{220} *red*, A_{260} *pink*) run on a Superdex 200 increase 3.2/300 column. The free helicase eluted as a single – monomeric peak, whereas the RNA-bound eIF4A2, formed multiple complexes, corresponding to monomeric, dimeric, and trimeric eIF4A2. Note that the observed shift in retention volume between RNA free and RNA-containing eIF4A2 sample indicates presence of the RNA-bound state of monomeric eIF4A2 in the presence of RNA. Trace for eIF4A2-$(AG)_{10}$ recorded by Dr Tobias Schmidt.

B. eIF4A2 forms dimers and trimers in excess over RNA. Area under the curve for each individual peak (monomer, dimer, and trimer) for the eIF4A2-RNA sample from panel **A** was calculated, using GraphPad Prism. Molar concentrations of both protein and RNA in each peak were calculated based on the ratio of areas of each peak; with total of 16 μM protein and 4 μM RNA present in all three peaks. In the monomer there is a great excess of protein over RNA which suggests presence of the unbound fraction. In case of the dimer, there is twice as much protein in the sample than RNA, and in the case of trimer at least 3 proteins are formed on one RNA. The graph on the right is the zoomed in data representing trimer.

As eIF4A2 oligomerises only in presence of RNA (**Figure 3.5-1**) and the previously tested $(AG)_{10}$ and $(CAA)_6CA$ RNA (**Figure 3.4-1**) induced oligomerisation to a different extent, the propensity to multimerise in presence of different RNA sequences was investigated. This time, aSEC was performed on eIF4A2 complexes formed on adenosine only RNA – $(A)_{20}$, polypurine RNA containing more adenosine nucleotides than guanosine ones – $(GAAG)_5$, RNA without adenosines - $(GUGCU)_4$, as well as the previously tested $(AG)_{10}$ and $(CAA)_6CA$. The traces presented in **Figure 3.5-2**, panel A were recorded by Dr Tobias Schmidt. Here, similarly as in **Figure 3.5-1** distribution of RNA and protein differed (**Figure 3.5-2**, panel A, *A220 left, A260 right*). As the protein was in excess over RNA (16 µM and 4 µM respectively), the contribution of unbound protein in the monomeric fraction was to be expected. As previously, $(AG)_{10}$ RNA supported oligomerisation to the highest extent, with creation of trimeric complexes. Trimeric complexes were also detected in the samples with $(GAAG)_5$ and $(GUGCU)_4$ RNA.

Next, the contribution of the monomer (1-mer), dimer (2-mer), and trimer (3-mer) was quantified (**Figure 3.5-2**, panel B) based on the distribution of RNA to exclude the influence of unbound protein (**Figure 3.5-2**, panel A, right). Additionally, previously obtained in the Bushell lab dissociation constants (K_D) for RNAs used in **Figure 3.5-2**, panel A were compared to the formation of oligomers on tested sequences (**Figure 3.5-2**, panel B). Oligomerisation did not follow a trend, where the RNAs with higher K_D (lower affinity) would not form oligomers. As an example, trimers formed on $(GAAG)_5$ and $(GUGCU)_4$ but did not form on $(CAA)_6CA$ RNA, regardless of the lower K_D in the case of $(CAA)_6CA$.

As an additional way of visualisation of oligomer formation, eIF4A2-RNA ($(AG)_{10}$, $(CAA)_6CA$, $(GUGCU)_4$, $(A)_{20}$, $(GAAG)_5$) complexes were scrutinised by an EMSA (**Figure 3.5-2**, panel C). As in an EMSA the detection is dependent on the labelled RNA, the detection can depend on the label itself. Moreover, in this assay it is not clear how much of an unbound protein is in the sample. However, one undeniable advantage of an EMSA is that the samples can be prepared, incubated, and visualised at the same time on the same gel. It should be noted that the results from both experiments differed (i.e., not detectable dimer for $(CAA)_6CA$ RNA in these conditions), therefore a detailed validation of the

obtained results with use of variety of techniques was applied throughout this thesis. Here (**Figure 3.5-2**, panel C), again, all of the tested RNAs (apart from $(CAA)_6CA$) supported dimer formation, however the trimeric complexes were only detected on $(AG)_{10}$ RNA.

In all, sequence of the RNA is the main determinant of oligomer formation, and the collected data suggest that the oligomerisation is independent of affinity. Again, the $(AG)_{10}$ RNA supported oligomerisation to the greatest extent, however other sequences supported formation of at least a dimer. Furthermore, validation of the results, proved that different techniques have different sensitivity, and care should be taken while analysing obtained data.

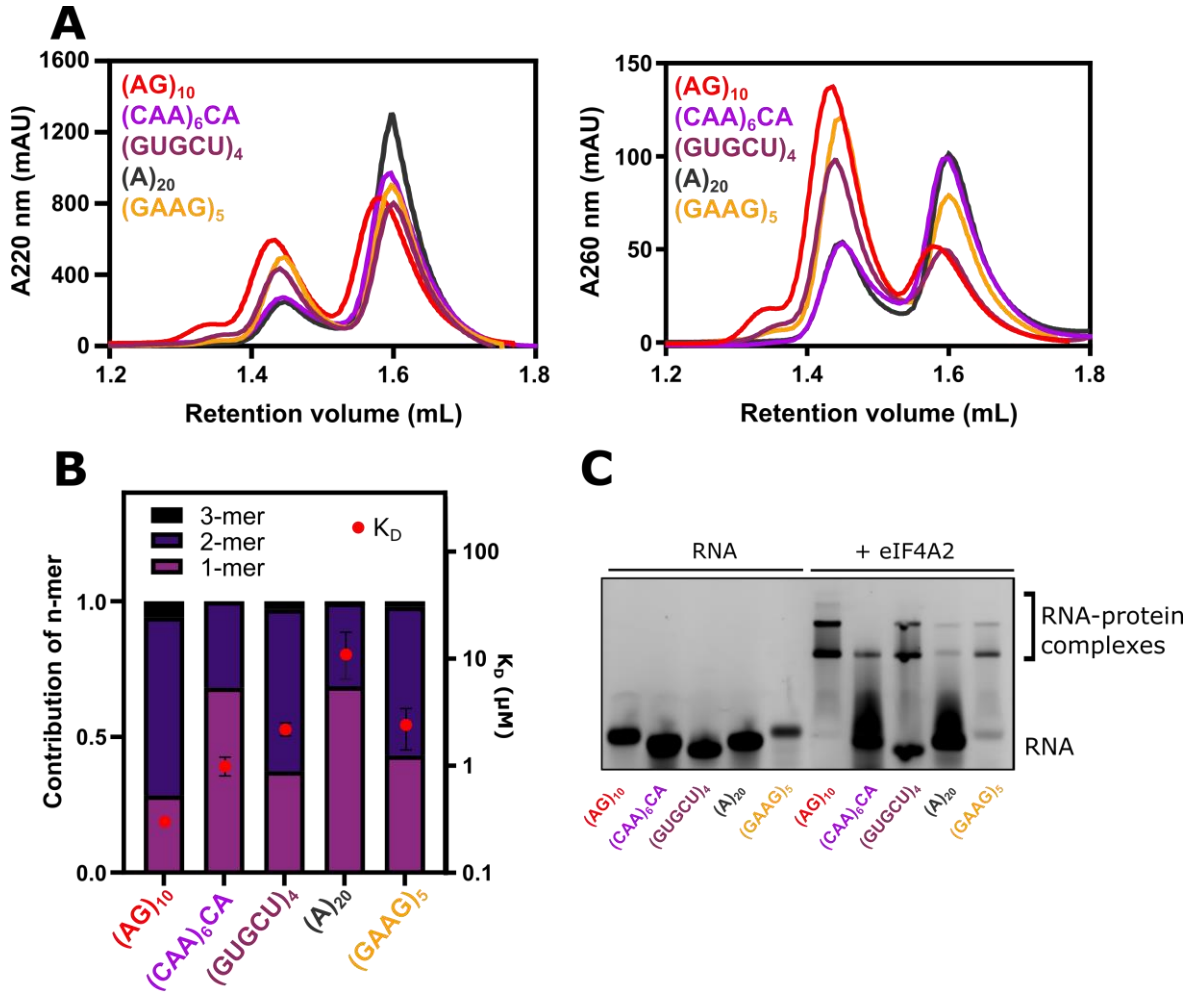

Figure 3.5-2 RNA sequence determines the extent of eIF4A2 oligomerisation

A. Representative aSEC run on a Superdex 200 increase 3.2/300 column of 16 μM eIF4A2 in complex with 4 μM 20 nucleotide single-stranded RNA of the following sequences: $(AG)_{10}$, $(CAA)_6CA$, $(GUGCU)_4$, A_{20}, $(GAAG)_5$. Panel on the left corresponds to A220 for protein detection (peptide bonds), panel on the right corresponds to A260 for RNA detection.
Note that the monomeric peak in the A220 is higher than the dimer due to contribution of unbound protein.
Various RNAs promote oligomerisation to a different extent, with $(AG)_{10}$ having the greatest propensity to induce trimer formation.

B. Quantification of contribution of monomer (1mer), dimer (2mer) and trimer (3mer) to the total of formed complexes for each RNA in aSEC experiment from A260 panel **A** (left axis) with dissociation constant (K_D) marked for each RNA as a red dot (right axis).

C. Representative EMSA for 1 μM free RNAs used in panel **A** and RNA-eIF4A2 complexes (with concentrations of 1 and 5 μM respectively). RNAs used were 5'FAM labelled, samples were prepared and run in the same manner as in the **Figure 3.4-1** and visualised using Typhoon FLA 7000, n = 2.

Next, to understand more about the binding interface of eIF4A2 and how the oligomers are formed, a series of EMSAs and analytical gel filtrations were performed (**Figures 3.4-1**, **3.5-3, 3.5-4, 3.5-5**). RNA substrates of different lengths were employed to identify whether the oligomerisation happens through multiple proteins binding to the same RNA next to each other or through protein-protein interactions. Here, in the case of eIF4A2 binding to the RNA substrate independently next to each other, the formation of multimeric complexes should only be observed on RNAs that provide multiple binding sites. Additionally, the K_D should remain constant if the full binding site is provided.

Increasing length of RNA was found to be necessary to support oligomerisation (**Figures 3.5-3**, **3.5-4**), with trimeric complexes of eIF4A2 forming only on the 20 nucleotide AG-RNA stretch (**Figure 3.5-4**, panel A). However, the measured binding affinities towards 10, 15, 20, and 50 nucleotide AG-RNA stretches showed an increase in the binding affinity of eIF4A2, i.e., a decrease in K_D, on AG-RNAs from 10 to 15 nucleotides (**Figure 3.5-4**, panels B, C). Additionally, as shown in one study (Iwasaki *et al.*, 2019) 6 and 8 nucleotide AG-RNA stretch did not support binding of eIF4A1, suggesting that increase of the RNA length from 10 to 15 nucleotide does not provide an additional independent binding site. The binding affinity remained the same from 20 to 50 nucleotides, however, the 50 nucleotide RNA stretch supported binding of up to 6 visible proteins (**Figure 3.5-5**, panel A), in turn suggesting possible formation of two trimers. This supports a model in which the RNA binding interface increases from 10 to 15 nucleotides (Abramson *et al.*, 1987; A. Z Andreou and Klostermeier, 2013), with the full binding site allowing for oligomer formation. As the 20 nucleotide AG-RNA stretch allows for trimer formation, in the case of multiple binding sites, in saturating conditions on different RNA sequences (as shown **Figure 3.5-2**) formation of trimers would be expected. However, the lack of trimeric complexes suggests that 20 nt RNA stretch is not long enough to accommodate multiple binding sites of eIF4A2 and hints at oligomers forming through protein-protein interaction. This leads to creation of a model in which at least one of the protomers in the oligomer needs to come into direct contact with RNA and allow for binding of other protomers (**Figure 3.5-5**, panel B). In case of RNA length permitting for two optimal binding sites formation of 2 oligomeric species

(6 proteins bound to RNA) is visible. This concept is further explored in section **3.9** (**Figure 3.9-2**).

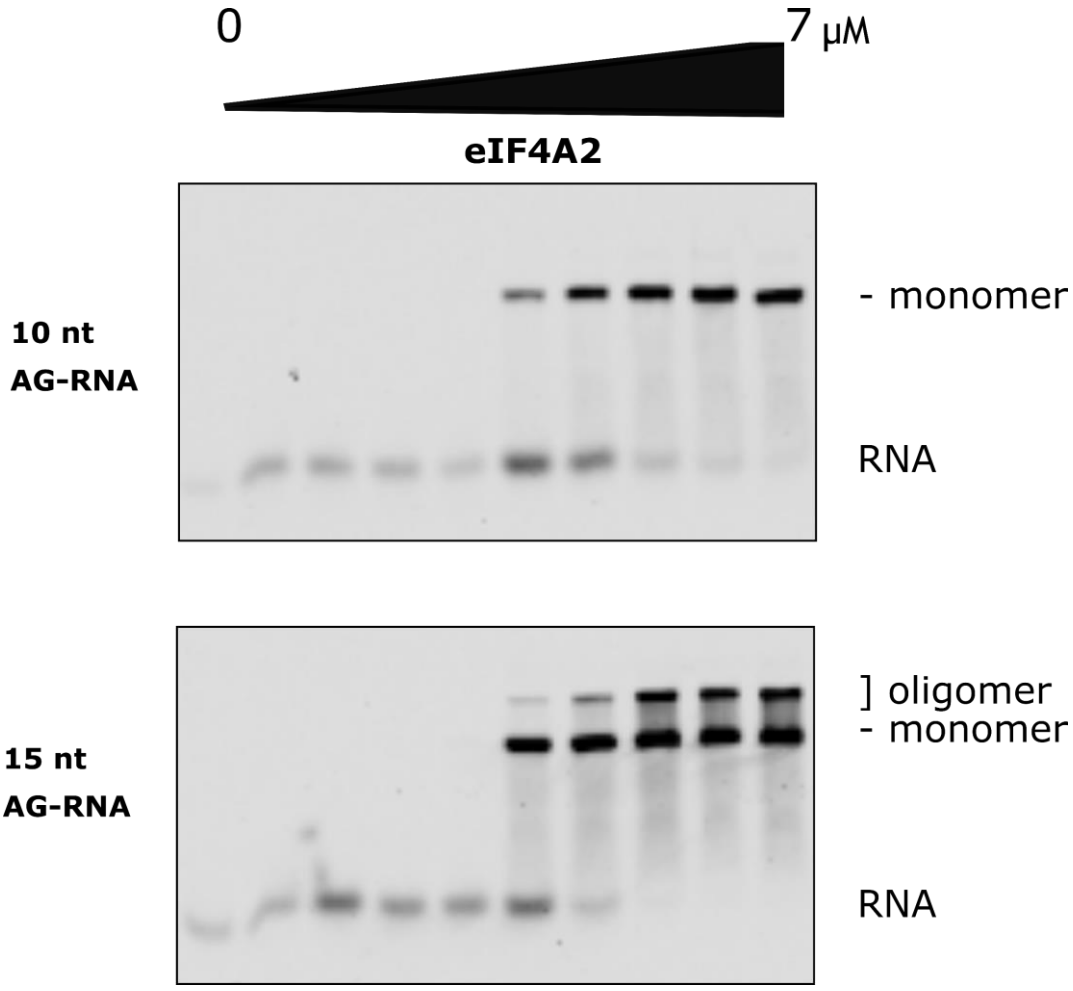

Figure 3.5-3 eIF4A2 requires optimal length of RNA to fit into the binding site to oligomerise

Representative EMSAs of eIF4A2 binding to polypurine (AG) RNA of 10 nt length (*top panel*) and 15 nt length (*bottom panel*), n = 3. Titration of eIF4A2 from 0 to 7 μM, constant concentration Dy780 labelled AG RNA (25 nM). Complexes were preincubated for 1h at room temperature in the binding buffer (20 mM HEPES, pH 7.5, 2 mM $MgCl_2$, 100 mM KCl, 1mM DTT), supplemented with 1 mM AMP-PNP. Complexes were resolved on 7% native EMSA for 50 minutes, at 100V. 10 nt RNA stretch does not provide optimal binding site to for higher order complexes.

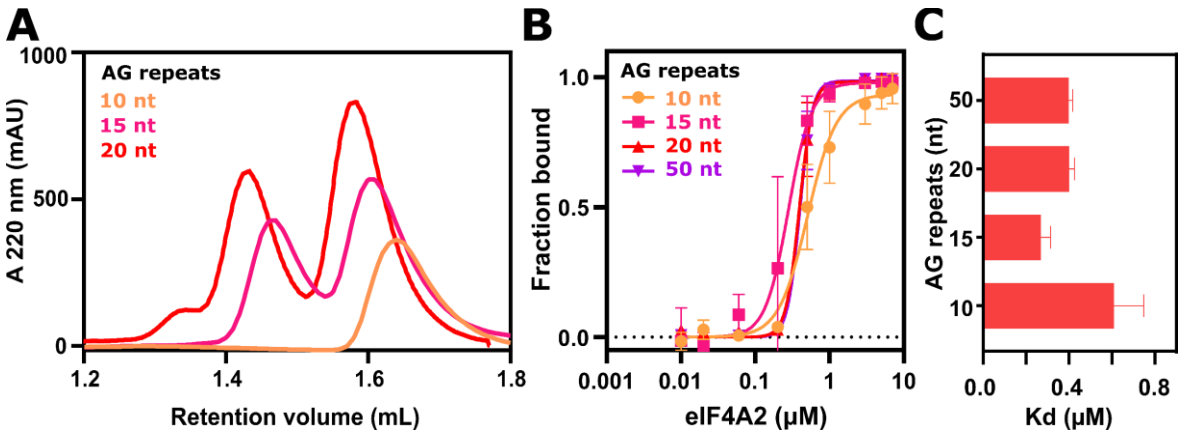

Figure 3.5-4 Optimal RNA length for the binding site correlates with oligomerisation

A. Representative (n = 3) elution profiles from aSEC on a Superdex 200 increase 3.2/300 column of 16 μM eIF4A2 in complex with 4 μM AG-repeat single-stranded RNA of varying length (10, 15, 20 nucleotides). Complexes were incubated for 1 hour at room temperature in presence of binding buffer (20 mM HEPES pH 7.5, 100 mM KCl, 2 mM $MgCl_2$, 1 mM DTT) and 1 mM AMP-PNP, and subsequently injected onto the column.

B. Representation of fraction bound based on the image analysis of EMSAs (n = 3 for each condition) of titration of eIF4A2 (0 to 7 μM) in presence of 10, 15, 20, 50 nucleotide AG-RNA (25 nM) as shown in **Figure 3.4-1**, **Figure 3.5-3**, **Figure 3.5-5**. Error bars – SEM, fit – Hill equation.

C. Dissociation constants obtained from image analysis of EMSAs as shown in the panel **B**, analysed using Hill equation in Graph Pad Prism. N = 3, error = SEM.

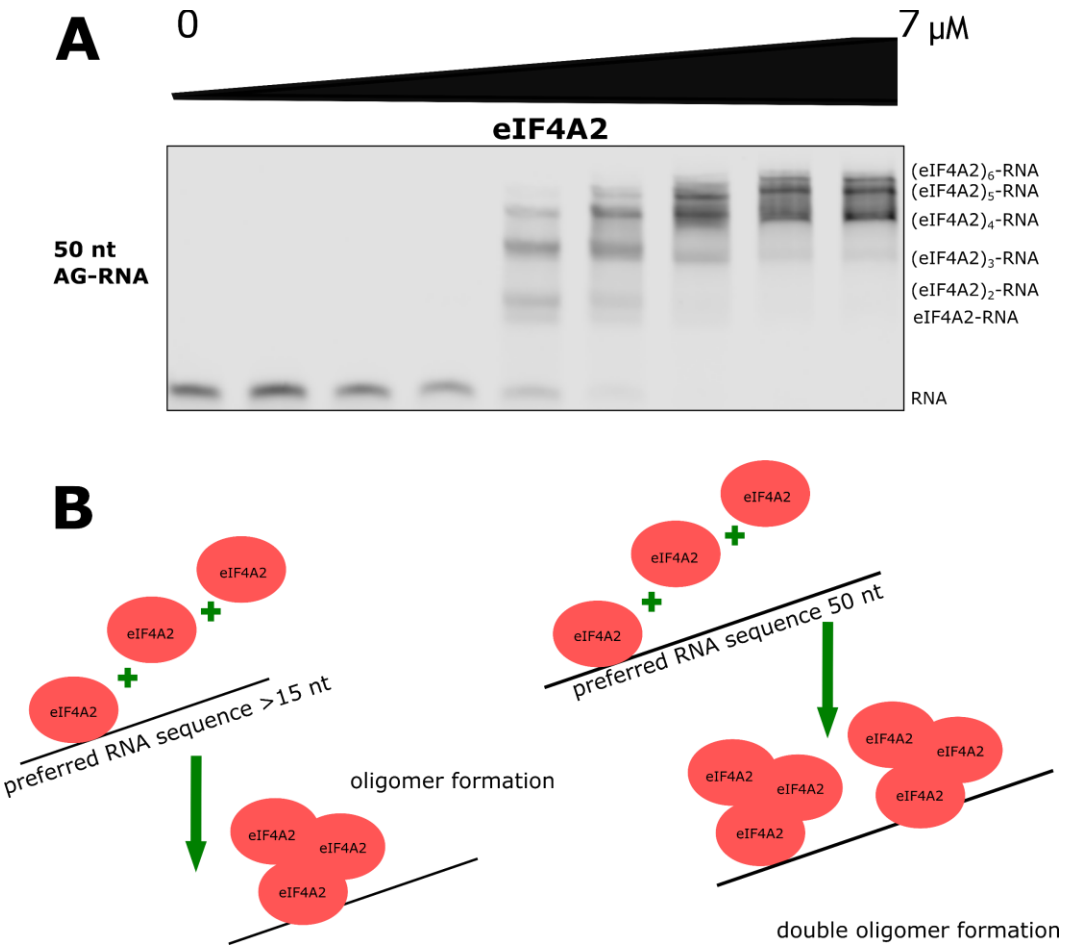

Figure 3.5-5 RNA containing double binding site for eIF4A2 promotes formation of multiple oligomers

A. Representative EMSA of eIF4A2 binding to 50 nucleotide AG RNA. Experiment performed as in the **Figure 3.5-3**. RNA that comprises multiple binding sites allows for formation of multiple oligomeric species next to each other, n = 3.

B. Model of eIF4A2 binding to RNA, where RNA needs to comprise optimal binding site, and have a preferred sequence. Upon RNA binding, subsequent eIF4A2 protomers can bind, forming an oligomer. Where the RNA length allows for multiple binding sites formation of more than one oligomer next to each other is possible.

Since **1)** the polypurine-rich AG-RNA promotes oligomerisation to the highest extent, **2)** a 10 nucleotide AG-RNA stretch allows for binding of one protein but does not support oligomerisation, **3)** and native mRNA substrates rarely have long stretches of uninterrupted polypurine motifs, it was essential to understand whether eIF4A2 tolerates different sequence arrangements to form oligomers. To achieve that, EMSAs on 20 nucleotide long RNAs with varying polypurine motifs were performed (**Figure 3.5-6**, panel A). This showed that eIF4A2 oligomerisation can be achieved on different sequences containing AG-stretches**.** However, differences in the extent of oligomerisation were observed. Sequences in wells 1, 3, and 6 promoted oligomerisation the most. A visible difference between sequences in wells 2 and 3 was observed. Both sequences contain the same number of uninterrupted purines, however only for sequence 3 trimeric complex and clearly defined dimer are visible. This difference could be explained by the location of polypurine motif within the RNA sequence. Given that eIF4A2 binds preferentially (with the highest affinity) to AG-repeats it is probable that in the case of sequence 2 eIF4A2 binds the RNA exactly at the external 10-nucleotide polypurine motif, and therefore does not have the full binding interface. The situation is different in the case of sequence 3, where the polypurine motif is internal and flanked by uracil. This could be further explained by very low oligomerisation on sequence 4, where the external purines flank a long stretch of uracil. Furthermore, sequences 5, 6, and 7 promote oligomerisation to a greater extent than sequence 8. Here, the dissimilarity stems from length of AG-stretches, where sequences 5-7 contain motifs of 4 purines, whereas sequence 8 has only 2 purines next to each other. Additionally, previously obtained in the Bushell lab by Dr Tobias Schmidt eIF4A2 affinities towards sequences 1-6 presented in **Figure 3.5-6**, panel B, further demonstrated that oligomerisation is independent of the K_D. Sequences 3 and 4 have similar affinities yet differ in propensity to promote oligomerisation. Similarly, sequences 5 and 6 have higher dissociation constant than sequence 4, which promotes mostly monomeric binding.

In all, eIF4A2 is capable of oligomerisation on interrupted polypurine motifs, however the presence of flanking regions, and the length of polypurine motifs themselves matter.

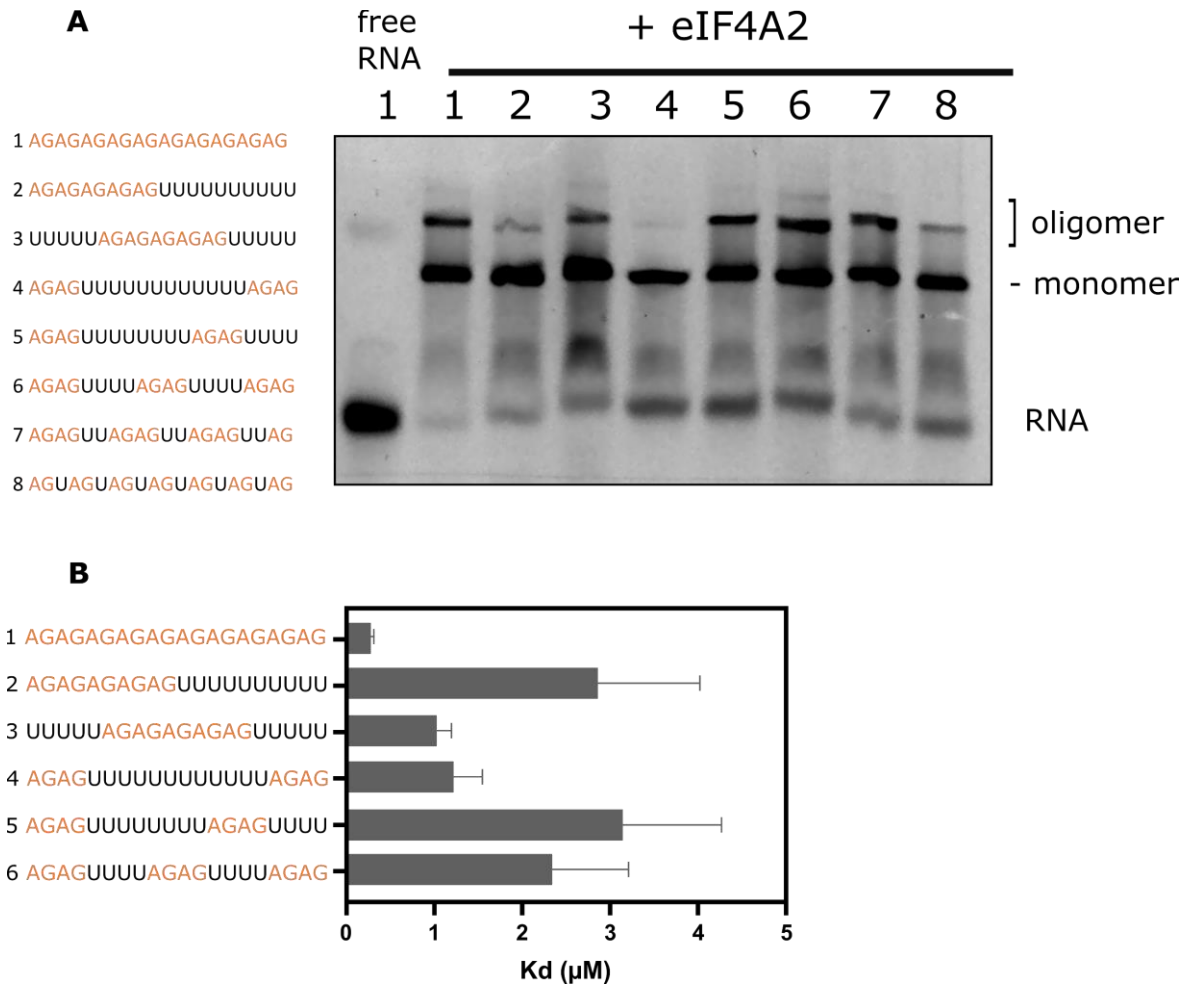

Figure 3.5-6 eIF4A2 oligomerises on RNAs containing different arrangements of AG-repeats

A. Representative (n = 2) EMSA of 5 μM eIF4A2 formed complexes with 1 μM 5'FAM labelled RNAs containing different arrangements of AG-motifs. The samples were prepared and visualised in the same manner as in **Figure 3.5-2**, panel C.

B. Dissociation constants (n = 3), obtained by Dr Tobias Schmidt through titrations of eIF4A2 to the same amount of 5'FAM labelled RNAs, measured by anisotropy change.

To sum up, eIF4A2 oligomerises only in presence of RNA, and when the protein is in excess over RNA allowing for formation of both the dimer and trimer in these conditions. It is still unclear what causes the disparities in oligomerisation on various RNA sequences. As the differences in K_D do not seem to correlate with the extent of oligomerisation, it appears that the RNA sequence itself plays a crucial role in stimulating the oligomerisation, with AG-RNA having the greatest propensity to induce trimeric complexes. Another good example is the $(A)_{20}$ RNA, that had the highest K_D amongst the tested RNAs and a large fraction of the RNA remained unbound, however it promoted dimer formation.

Moreover, an optimal length of the RNA is necessary to provide full binding interface to induce oligomerisation. Interestingly, as shorter RNA fragments (less than 8 nt) do not support binding, the formation of a dimer on RNA as short as 15 nt suggests that the oligomerisation happens through the protein-protein interactions. Expanding the length of RNA allows for formation of multiple oligomers, however the amount of bound eIF4A2 does not grow linearly, providing further evidence towards a model of protein-protein interaction induced oligomerisation.

Finally, the specific preferences of eIF4A2 to the particular arrangements of AG motifs, regardless of K_D, point again towards the RNA sequence being the largest determinant of the extent of oligomerisation.

3.6. Oligomers have different shape and conformation than monomers

The previous results described RNA dependent oligomerisation of eIF4A2 and pointed towards the RNA sequence being the main determinant of formation of oligomers. However, how the oligomers are formed and whether distinct RNA binding modes can be responsible for differences in oligomerisation still remained elusive. To explore the potential differences a structural approach was indispensable. Here, the changes in shape and size of eIF4A2 under free, AMP-PNP bound, monomeric, and oligomeric (bound to various RNAs) conditions were investigated using small-angle X-ray scattering (SAXS). This technique provides structural information in solution, without the need of crystal formation, making it advantageous in this aspect over crystallography. Additionally, the structures may resemble a more natural state without experiencing crystal packing widely observed in crystallography. The simplicity of sample preparation without the need to grow crystals allows for obtaining data for various conditions, i.e., different RNA substrates, in a shorter time. However, SAXS does not provide as high resolution as crystallography, rendering it not suitable for determination of atomic resolution. Overall, the sample preparation, the resolution high enough to observe conformational changes, and the possibility to couple the obtained information with the biochemical data, made it the preferred method to use in this project.

Here, preincubated complexes were snap frozen in liquid nitrogen, and shipped on dry ice to Diamond Light Source (DLS) in Oxford, UK. Collected data on DLS Beamline B21 were analysed with the use of Scatter IV and ATSAS 3.0.3 package deposited at EMBL (Bioisis: Tutorial, Manalastas-Cantos *et al.*, 2021). Samples containing apo-eIF4A2 (free protein), AMP-PNP-bound eIF4A2, monomeric eIF4A2 bound to $(AG)_{10}$ and $(CAA)_6CA$ as well as oligomeric eIF4A2 bound to $(AG)_{10}$ were reanalysed for the purpose of this thesis and consistency between the samples, based on a previous analysis by Dr Mads Gabrielsen using Scatter III. More details about the method, sample preparation and analysis can be found in the **Chapter 2.3.5**.

The SAXS experiments at the DSL are coupled with size exclusion chromatography (SEC-SAXS), which allows for separation and analysis of multiple

species in heterogenous sample. The eluted sample from the SEC column is subjected to X-ray radiation, which in turn results in SAXS data embedded within the SEC profiles of the samples.

First the elution profile of apo-eIF4A2 was examined (**Figure 3.6-1**, panel A). A main peak corresponding to the monomeric eIF4A2 was observed (at around 450 frames – frames correspond to the SAXS frames collected), additional, very minor peaks, i.e., small molecule contaminants were observed (around 550 frames). Next, a region of the peak (**Figure 3.6-1**, panel B, *pink selection*) was selected for further analysis. Selected region corresponded to the frames with most constant R_g (radius of gyration; distance from the centre of gravity of a molecule), assuring similarity between the analysed data (Bioisis: Tutorial). After the selection of the frames, the first step of analysis consisted of determining the Guinier region (**Figure 3.6-1**, panel C). This is the most important step that allows for scaling the data and further analysis. For the Guinier region analysis, the scattering data is analysed in the region where the scattering angle is close to zero (Guinier, Fournet and Yudowitch, 1955; Putnam *et al.*, 2007; Behrens *et al.*, 2012) (see also **Chapter 2.3.5**). This analysis provides information about both the R_g and intensity (I) at zero scattering angle (I(0)), as well as allows for detection of aggregation in the sample. Here, the R_g was determined, and no aggregation was observed. The same initial analysis was performed for AMP-PNP-eIF4A2, monomeric eIF4A2 bound to $(AG)_{10}$ and $(CAA)_6CA$ as well as oligomeric eIF4A2 bound to $(AG)_{10}$ (see **Appendix 1 Figures 1-1**, **1-2**, **1-3**, **1-4**).

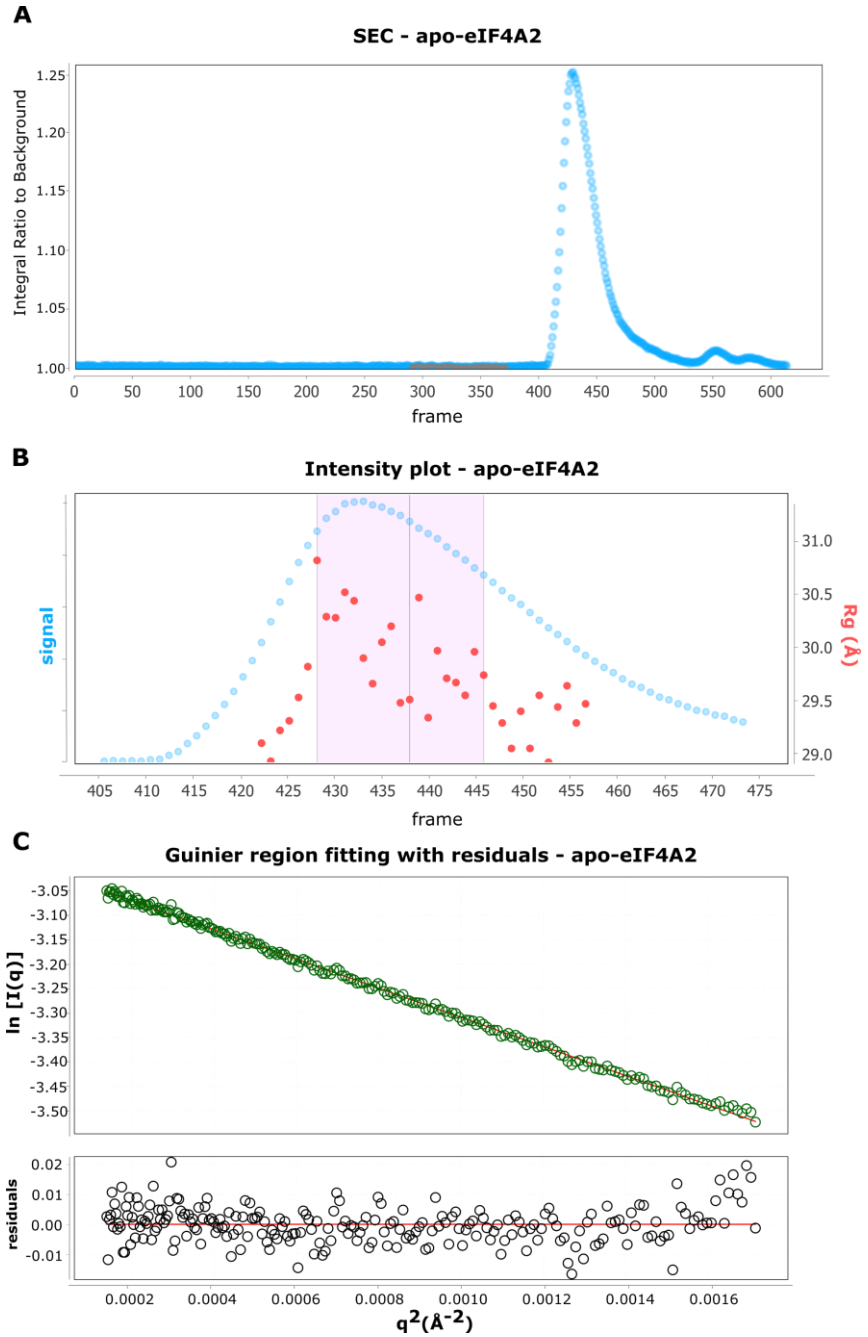

Figure 3.6-1 Apo-eIF4A2 forms a single monomeric species in solution

A. Size exclusion chromatography (Superdex 200 increase 3.2) of the sample containing 100 µM eIF4A2 in binding buffer (20 mM HEPES pH 7.5, 100 mM KCl, 2 mM $MgCl_2$, 1 mM DTT) run at the Diamond Light Source (Oxford, UK) before the sample was subjected to X-ray radiation, frame corresponds to fraction collected during SAXS. One main peak is visible, eluting around 450 frames, corresponding to monomeric eIF4A2. Grey region corresponds to buffer subtracted as background.

B. Intensity plot of the sample presented in panel **A**. Frames with most constant R_g (red dots) selected for further analysis (marked in light pink).

C. Guinier region fitting (*top*) with residuals of the linear fit (*bottom*) of the sample from panel **A**. It shows the linearisation of scattering data in the region close of scattering angle close to 0. Establishing the correct region is important for all further analysis and comparisons. I = Intensity, q = scattering vector.

As the initial analysis was performed, and the Guinier region was determined, the samples could be compared between each other. In **Figure 3.6-2**, panel A, Intensity plots were compared between apo-eIF4A2 (*dark green*) and AMP-PNP-bound state (*lime green; graph on the left*), free eIF4A2 and monomeric eIF4A2-$(AG)_{10}$ (*blue-violet; middle graph*) and monomeric and oligomeric (*purple*) eIF4A2-$(AG)_{10}$ (*graph on the right*). The log_{10} intensity plots provide the information about the shape of the proteins and possible aggregation. None of the samples had any aggregation. Signs of aggregation would be visible both in the intensity plot and Guinier analysis in the low q region as the absence of linear dependence of log(I(q)) versus q^2 (Putnam *et al.*, 2007; Grishaev, 2012). Additionally, the shape of the proteins could be determined from the log_{10} intensity plots (Volkov and Svergun, 2003; Putnam *et al.*, 2007; Kikhney and Svergun, 2015). Apo-eIF4A2, AMP-PNP-bound, and monomeric follow the same trend, however oligomeric $(AG)_{10}$-bound eIF4A2 seems to be the least globular (see the difference in graph on the right, **Figure 3.6-2**, panel A).

Next, the dimensionless Kratky plots (**Figure 3.6-2**, panel B) provide information about the folded state of the complexes (Volkov and Svergun, 2003; Putnam *et al.*, 2007; Kikhney and Svergun, 2015) (see **Figure 2.3.5-1**). Here, both the apo-eIF4A2 and AMP-PNP-bound eIF4A2 (*panel on the left*) seem to follow a partially unfolded trend (upward trend) in the Kratky plot, whereas $(AG)_{10}$-bound monomeric (*middle panel*) seems to follow a more folded trend. Finally, both the $(AG)_{10}$ formed monomer and oligomer follow a similar, folded trend (*graph on the right*). However, the oligomer could be potentially less folded (higher values for $q*R_g$ ~ 4). Additionally, both oligomer and monomer seem to be rigid, however, similarly as described in publication by Behrens *et al.*, 2012, there might be some degree of flexibility in the monomeric species due to slight upturn of the data in high $q*R_g$ (~7-8).

Finally, the P(r) distribution (pair distance distribution function) of each sample was assessed. This analysis allows for representation of real space and determination of the maximum distance in the analysed particle (d_{max}) (Kachala, M., Valentini, E. and Svergun, 2015). To discover the correct P(r) it is necessary to find the d_{max} value that provides a distribution above 0 and is smooth (no sharp changes in the curve) (Bioisis: Tutorial). To obtain the positive distribution, appropriate d_{max}, and minimise artefacts data at high q can be

trimmed (Bioisis: Tutorial). Using the programme Scatter IV, each fit is assigned a Chi-square score (the lower score the better). After finding the distribution that is positive and has low score, the value can be further refined. Here, in the **Figure 3.6-2**, panel C, P(r) shows that fits for all the samples are positive. Additionally, for apo-eIF4A2 and the AMP-PNP-bound state the P(r) plot suggests that the majority of the distances between the atoms of the sample are around 30 Å. However, the distribution also suggests that there are parts of the protein that extend over the 30 Å core (more for the apo-eIF4A2), with d_{max} reaching 104 Å and 99 Å, respectively. Monomeric eIF4A2 has a less pronounced peak at 30 Å, suggesting more even distribution of distances, with the d_{max} reaching 108 Å. Lastly, the distribution for oligomeric eIF4A2 shows that the peak is shifted to 40- 50 Å, the distribution is broader both suggesting that the particle is bigger than apo-eIF4A2, and additionally, the calculated d_{max} is the largest from the measured samples, reaching 131 Å.

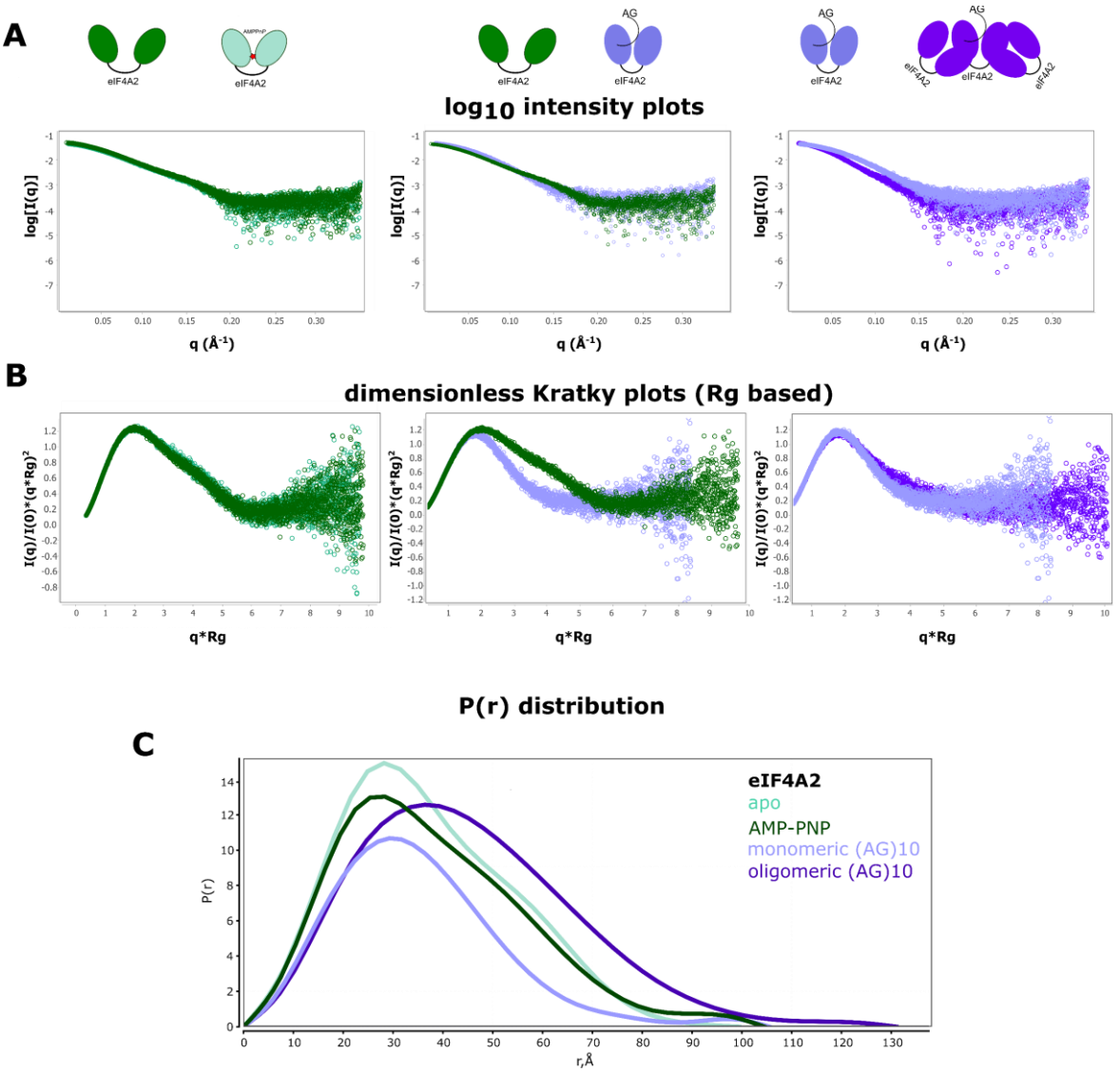

Figure 3.6-2 Monomeric RNA bound eIF4A2 differs from the free species and the oligomer

- **A.** Comparison of scattering curves (log_{10} intensity plots) of (from left to right) 1) apo-eIF4A2 and AMP-PNP bound eIF4A2, 2) apo-eIF4A2 and monomeric $(AG)_{10}$ bound eIF4A2, 3) monomeric and oligomeric eIF4A2 bound to $(AG)_{10}$. The biggest difference is visible between the monomeric and oligomeric eIF4A2. The curves suggest that there is no aggregation in the samples.
- **B.** Dimensionless Kratky plots based on the Guinier regions. Compared samples correspond to the same samples as in panel **A**. Monomer adopts more globular shape, whereas the free protein and AMP-PNP bound one follow partially unfolded trend in the dimensionless Kratky plot. There is a difference visible in the compactness of monomer and oligomer.
- **C.** P(r) distribution, that allows for determination of d_{max} (maximum distance in the sample) for the samples analysed in panel **B** and **C**. Oligomer has the longest d_{max}.

Analysed SAXS data allows for modelling of dummy atom models (envelopes) that represent the shape of measured molecules at a low resolution (Svergun and Stuhrmann, 1991; Svergun, 1999). The calculated models represent a fit to the experimental curves analysed above. Here, the data was modelled first using the DAMMIF method (17 individual runs per sample), further refined by DAMAVER package to obtain the highest confidence in the models (Volkov and Svergun, 2003; Franke and Svergun, 2009). Obtained envelopes are presented in **Figure 3.6-3**. In panel A, apo-eIF4A2 can be seen with two visible RecA domains in an open conformation (see **Chapter 1.5.1**), with a region expanding out of the main core, further demonstrating the elongated nature as described by the P(r) (**Figure 3.6-2**, panel C). In panel B of **Figure 3.6-3** the AMP-PNP-bound state is presented. The change in conformation upon AMP-PNP binding is elucidated. In panel C, a more closely shaped and rigid monomeric eIF4A2 is visible. A clear change in conformation upon RNA binding is detected. And finally, in panel D, oligomeric $(AG)_{10}$ bound eIF4A2, proves that the shape, size and conformation of oligomeric species differs from the monomeric ones.

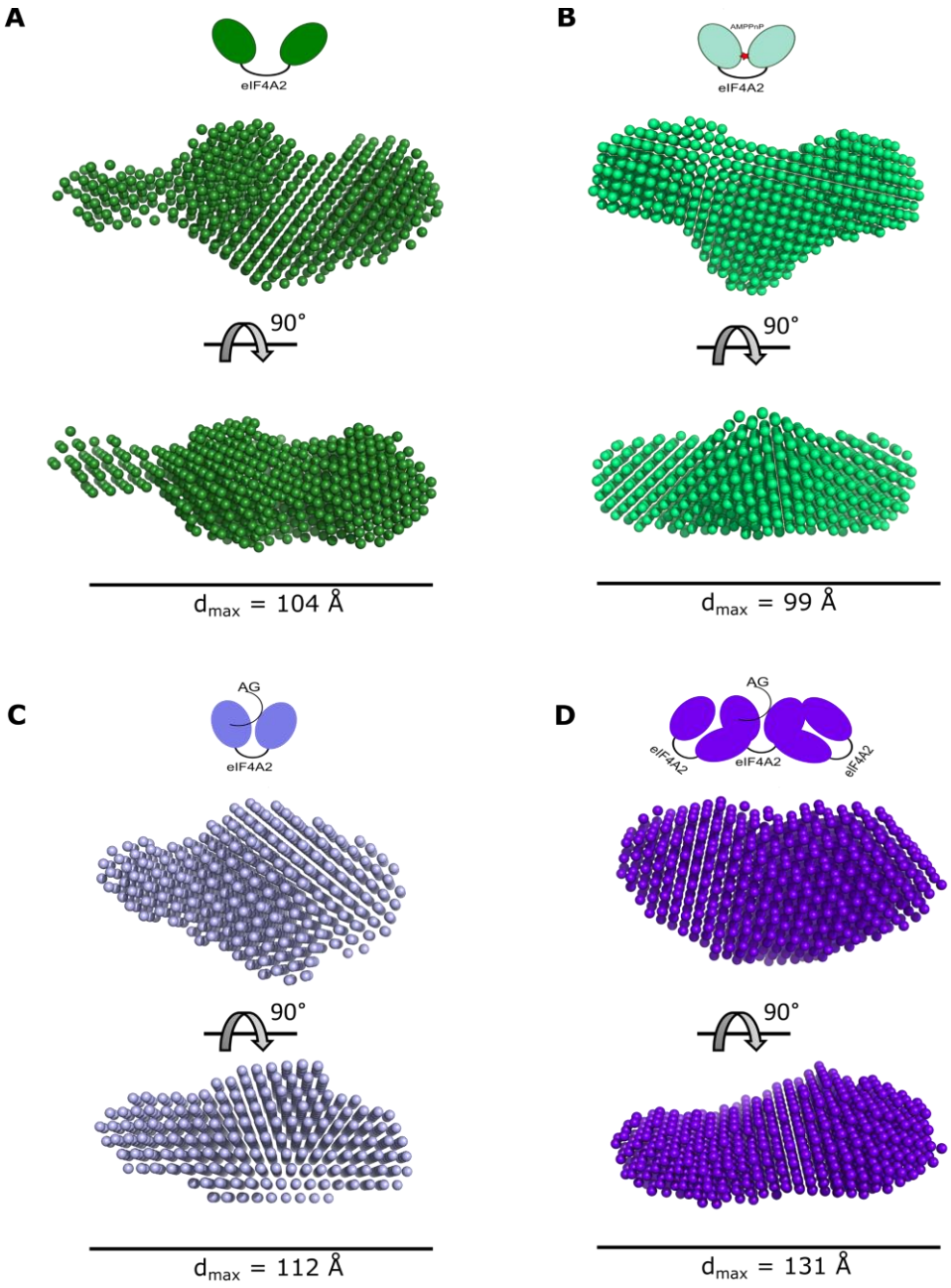

Figure 3.6-3 Envelope models of eIF4A2 support differences in shape, size, and conformation of eIF4A2 depending on the AMP-PNP, RNA binding and oligomerisation status

Envelope models (dummy atom model fitting using DAMMIF and DAMAVER packages from ATSAS 3.0.3) – for more information about analysis please refer to **Chapter 2.3.5**. Models created based on the Guinier region analysis and P(r) distribution.

- **A.** Apo-eIF4A2. Extended region is visible.
- **B.** AMP-PNP-bound eIF4A2.
- **C.** $(AG)_{10}$ monomeric eIF4A2. RNA bound state adopts more globular, closed shape.
- **D.** $(AG)_{10}$ bound oligomeric eIF4A2.

As previous studies have shown a preference of eIF4A2 to bind to polypurine motifs (Wilczynska *et al.*, 2019), the potential differences between the monomer bound to $(AG)_{10}$ and $(CAA)_6CA$ was examined. For this, a sample with equimolar concentration of eIF4A2 and $(CAA)_6CA$ was prepared in the same manner as the previous samples and analysed using SAXS. Again, the size exclusion profile was examined, and the Guinier region was established (see **Appendix 1 Figure 1-4**).

As before, the intensity and dimensionless Kratky plots of the two monomers were compared (**Figure 3.6-4**, panel A and B). The monomers followed the same trend in the intensity plot, suggesting that both tested conditions yield globular proteins without sings of aggregation. A slight difference was detected in the dimensionless Kratky plot, similar to the one between $(AG)_{10}$ formed monomer and oligomer, indicating that the $(CAA)_6CA$ monomer could potentially be less compact than the one on $(AG)_{10}$ RNA. In addition, a flexibility comparison was performed for those two conditions (**Figure 3.6-4**, panel C). For this analysis, using Scatter IV, it is assessed in which of the following three correlation plots (see below) the data reach a plateau: Porod-Debye, Kratky-Debye, SIBYLS plots. Depending on which of the graphs produces a plateau, the flexibility of the sample can be determined: Porod-Debye - rigid, globular, Kratky-Debye - disordered formation, SIBYLS - ordered and disordered elements (Rambo and Tainer, 2011; Brosey and Tainer, 2019). Here, in the **Figure 3.6-4**, panel C, both of the monomers reach the plateau in the Porod-Debye plot, suggesting that both monomers are rigid and well-defined.

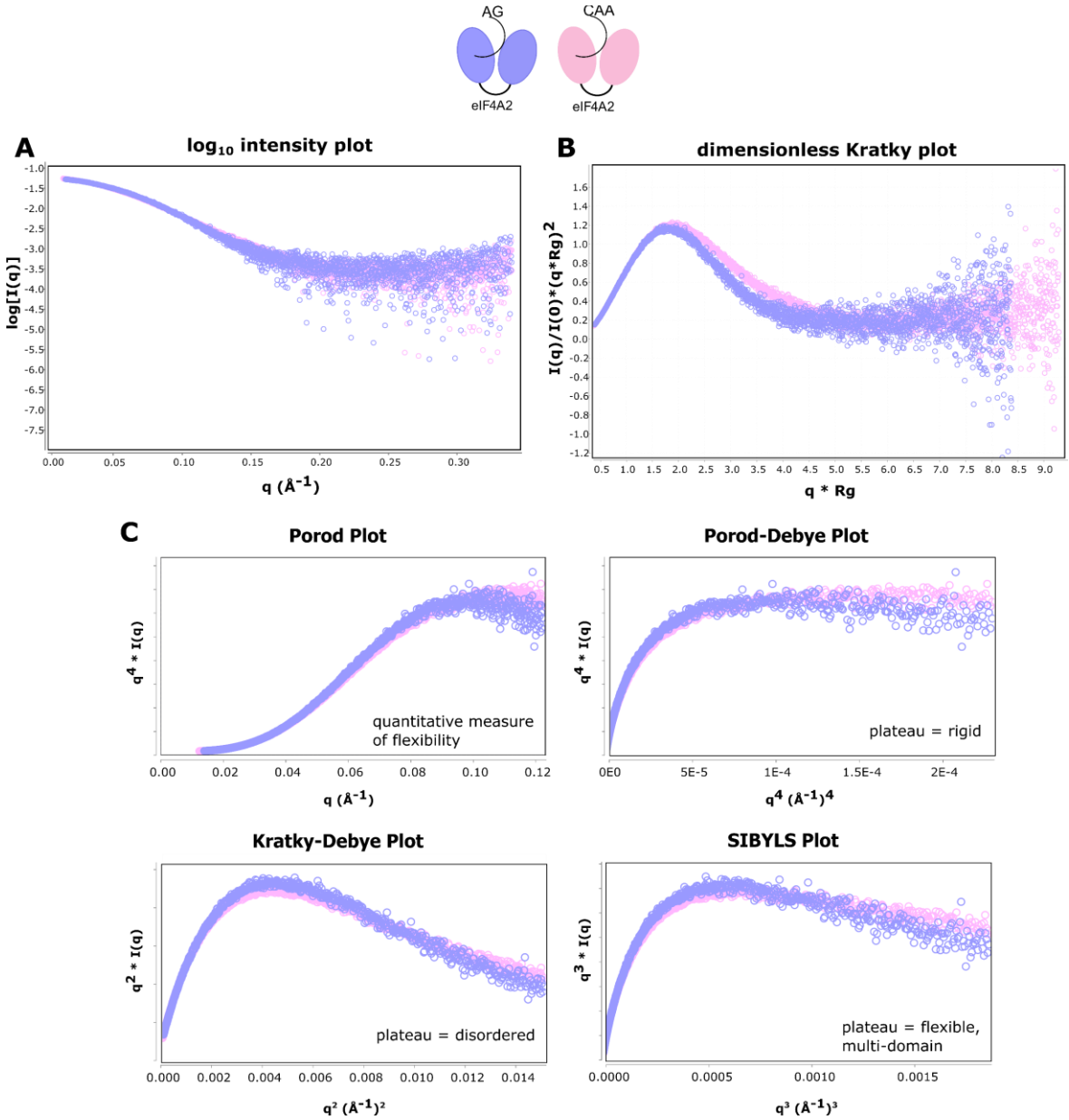

Figure 3.6-4 Monomers of eIF4A2 formed on $(AG)_{10}$ and $(CAA)_6CA$ RNA follow similar pattern.

- **A.** Comparison of scattering curves (log_{10} intensity plots) of monomeric $(AG)_{10}$ bound eIF4A2 and monomeric $(CAA)_6CA$ eIF4A2. Scattering plots follow identical trend. No aggregation in the samples is visible.
- **B.** Dimensionless Kratky plots based on previous analysis of the Guinier regions.
- **C.** Flexibility analysis based on Porod, Porod-Debye, Kratky-Debye, SIBYLS plots. Plateau of both samples in the Porod-Debye plot suggests that the monomers are rigid and well-defined, mostly globular complexes.

Lastly, the envelope model of $(CAA)_6CA$ monomer was created in the same way as previous samples (**Figure 3.6-3**). In the **Figure 3.6-5**, panel A, globular shape is observed, with a small extension. Subsequently, monomers formed on $(AG)_{10}$ and $(CAA)_6CA$ RNA were superimposed onto each other using SUPCOMB package (Kozin and Svergun, 2001). Both monomers seem to adopt a very similar shape and conformation regardless of the sequence of bound RNA (**Figure 3.6-5**, panel B).

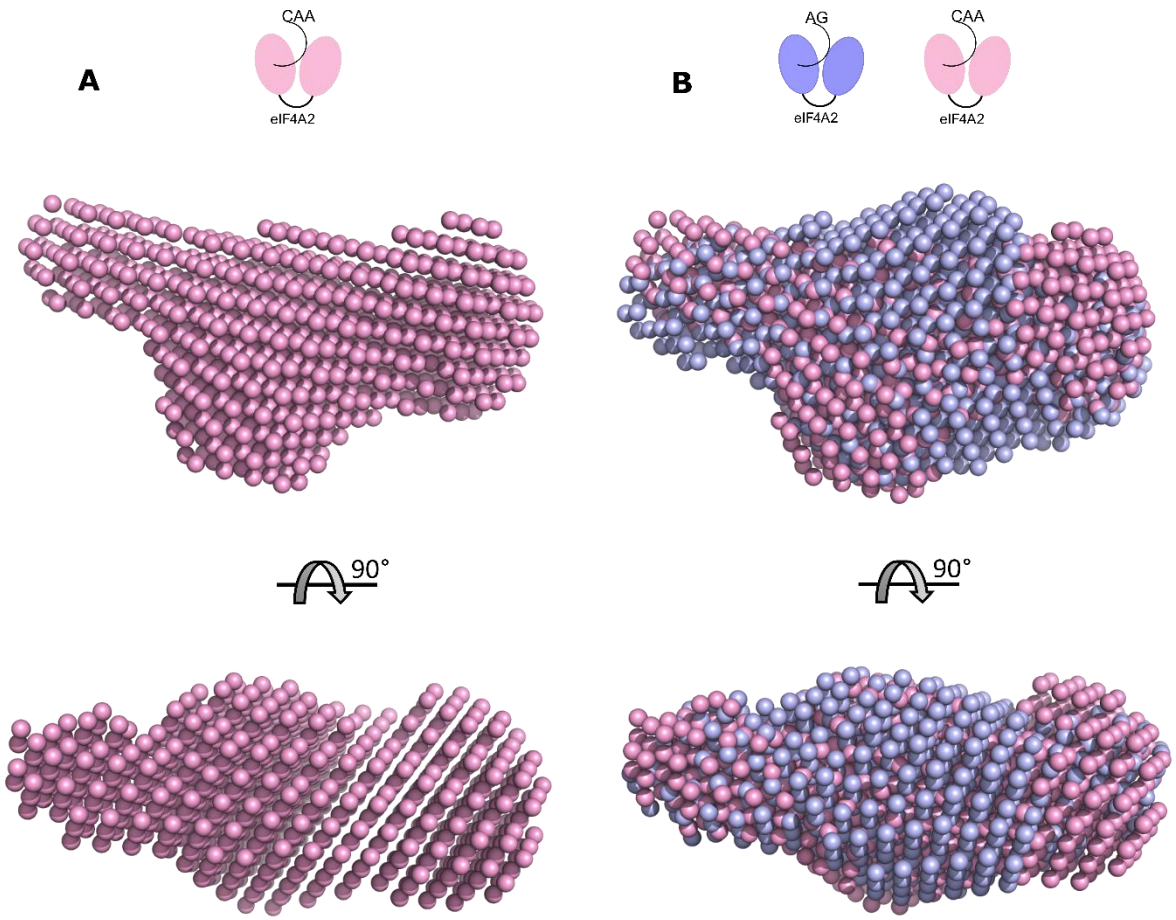

Figure 3.6-5 Envelope models of $(AG)_{10}$ and $(CAA)_6CA$ eIF4A2 monomers show high similarities

Envelope models (dummy atom model fitting using DAMMIF and DAMAVER packages from ATSAS 3.0.3) – for more information about analysis please refer **Chapter 2.3.5**.

- **A.** Envelope model of $(CAA)_6CA$ bound monomer.
- **B.** Superposition of envelope models of the eIF4A2 monomers bound to $(AG)_{10}$ (blue) and $(CAA)_6CA$ (pink). Superposition created using SUPCOMB package from ATSAS 3.0.3.

As eIF4A2 is a helicase that is believed to unwind double-stranded regions within mRNAs it was important to test whether a longer RNA substrate containing a double-stranded region influences the conformation and the variety of protein species formed. First, eIF4A2 complexes were formed on an RNA substrate containing 24 bp double-stranded region with a 5'$(AG)_{10}$ single-stranded overhang (RNA sequence as previously used in **Figure 3.3-1**) in a protein to RNA ratio supporting oligomer formation. As shown in **Figure 3.6-6**, panel A, two distinct peaks were observed, spanning between 350-470 frames. As only two peaks were detected, covering the same region in which the sample of oligomeric eIF4A2-AG_{10} RNA revealed three peaks, it was not possible to determine whether the sample consisted of monomers and dimers, or trimers or mixtures of few species. For the next analysis, the two regions were selected and analysed separately as oligomer and monomer (**Figure 3.6-6**, panel B), and Guinier analysis was performed (**Figure 3.6-6**, panel C). Larger biomolecules are characterised by linear region at lower q^2 (Putnam *et al.*, 2007). Here, the linear region of the oligomer is achieved at q^2 0.0010 versus 0.0016 for the monomeric species. The same analysis was performed for complexes formed on $(CAA)_6CA$ 24BP (RNA sequence as previously used in **Figure 3.3-1**), and a substrate with shorter single-stranded overhang $(AG)_5$ 24BP (see **Appendix 1 Figures 1-5**, **1-6**). As seen in the size exclusion profiles of complexes formed on both $(CAA)_6CA$ 24BP and $(AG)_5$ 24BP, oligomeric complexes were formed less readily than on the $(AG)_{10}$ 24BP RNA.

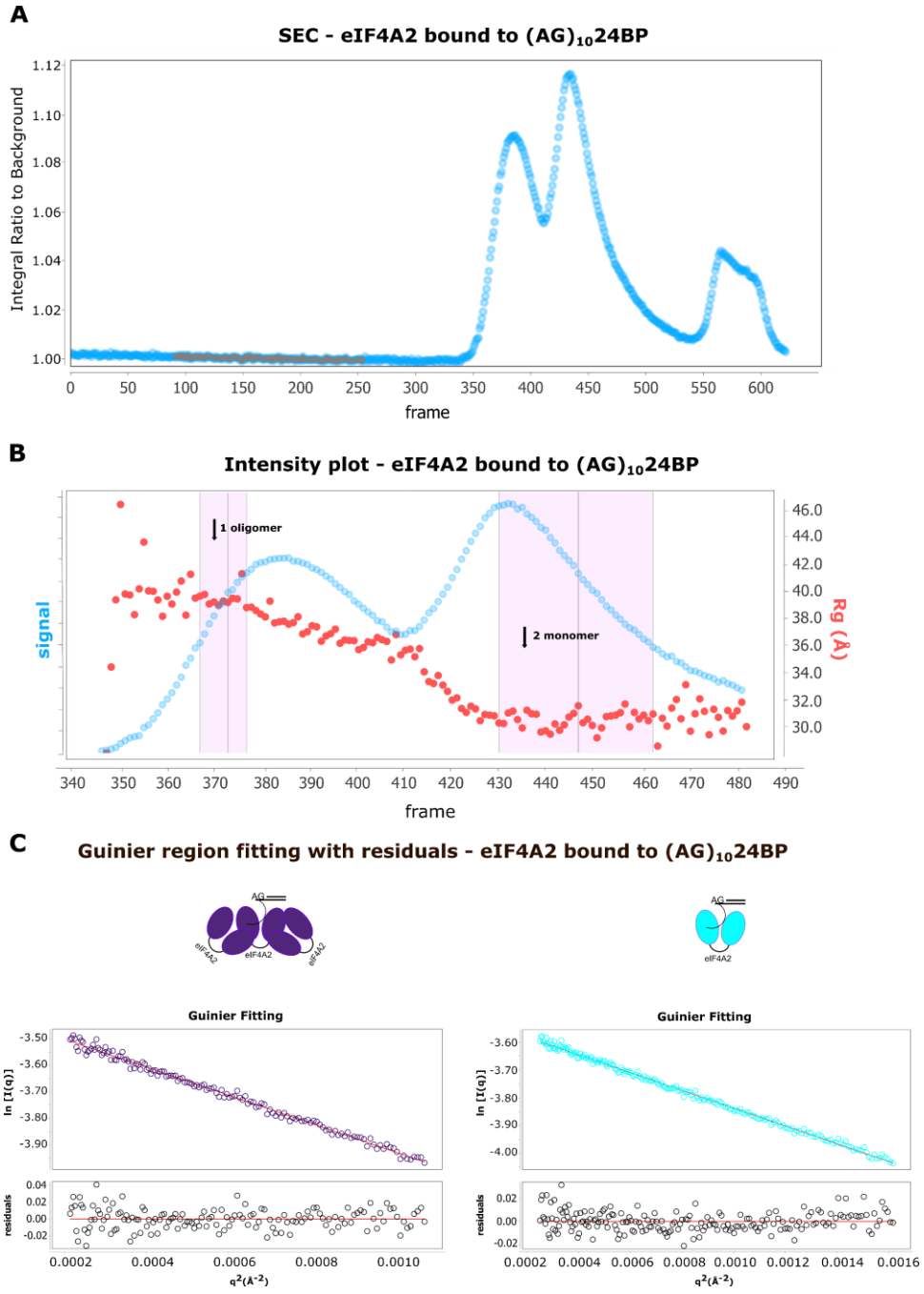

Figure 3.6-6 eIF4A2 forms oligomers more readily on a substrate with double-stranded region

A. Size exclusion chromatography (Superdex 200 increase 3.2) of the sample containing 90 μM eIF4A2, 30 μM $(AG)_{10}$ 24BP RNA, and 1 mM AMP-PNP run at the DLS before the sample was subjected to X-ray radiation, frame corresponds to frames collected during SAXS. Two peaks are visible, spanning from 350 to 450 frames. Grey region corresponds to buffer subtracted as background.

B. Intensity plot of the sample presented in panel **A**. Frames with most constant R_g (red dots), corresponding to the monomer, and oligomer, selected for further analysis (marked in light pink).

C. Guinier region fitting (*top*) with residuals in linear region (*bottom*) of the samples from panel **A**, oligomer on the left (*deep purple*) and monomer on the right (*cyan*).

Next, the log_{10} intensity and normalised Kratky plots were compared between the obtained oligomers and monomers for each RNA respectively (**Figure 3.6-7**, panel A for log_{10} intensity plots and panel B for dimensionless Kratky plots). The obtained data for the complexes formed on $(AG)_{10}$ 24BP (panel A and B*, graphs on the left*), suggest that the monomer was both less globular and less folded than the oligomer. In the case of eIF4A2 complexes formed on $(CAA)_6CA$ 24BP RNA (panel A and B*, graphs in the middle*) the monomer is less globular but more folded than the oligomer. Finally, for complexes formed on $(AG)_5$ 24BP the monomer was less globular, however both the monomer and oligomer had the same folded state (panel A and B*, graphs on the right*). However, as the distinction between the peaks for complexes formed on $(CAA)_6CA$ 24BP and $(AG)_5$ 24BP was less pronounced than for the ones formed on $(AG)_{10}$ 24BP (**Appendix 1 Figures 1-5**, **1-6** and **Figure 3.6-6**, panel A), caution has to be taken with interpretation of this data. Nonetheless, the obtained complexes, provide further evidence that both the RNA sequence as well as length of the single-stranded region play a role in enhancing oligomerisation.

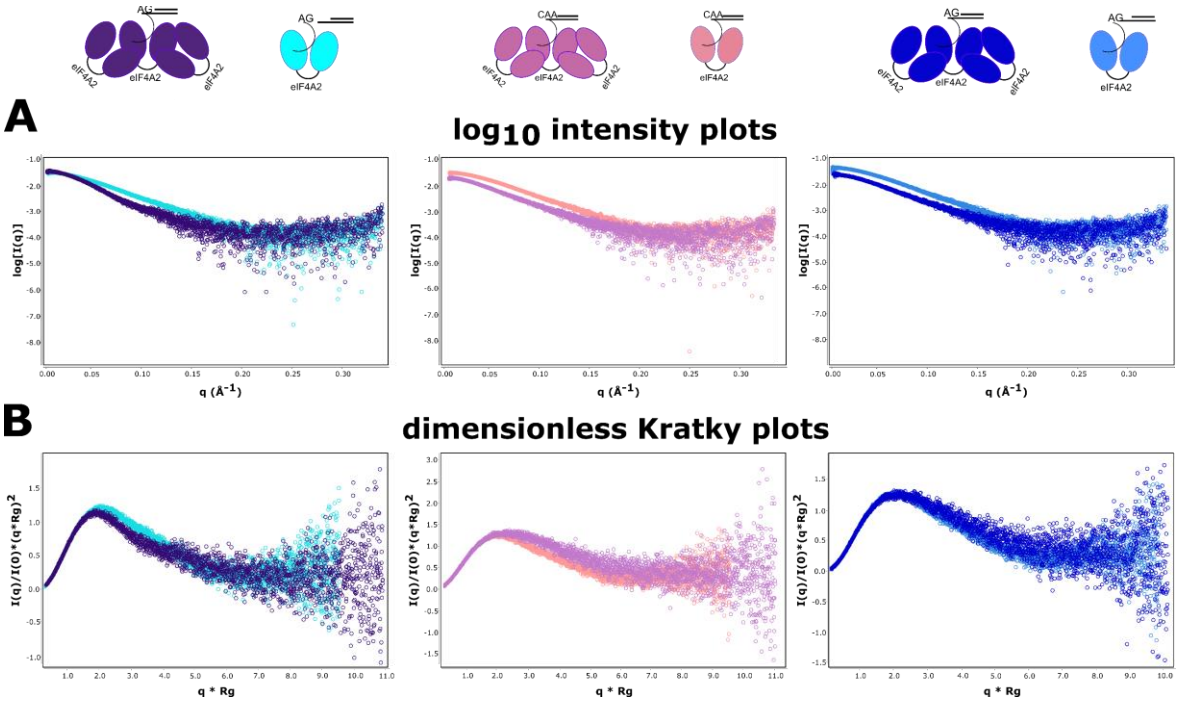

Figure 3.6-7 Monomers and oligomers formed on substrates with double-stranded region differ

A. Comparison of scattering curves (log_{10} intensity plots) of monomers and oligomers of eIF4A2 formed on $(AG)_{10}$ 24BP (left, *monomer - cyan, oligomer - deep purple*), $(CAA)_6CA$ 24BP (middle, *monomer - salmon, oligomer – deep pink*), and $(AG)_5$ 24BP (right, *monomer - blue, oligomer – navy blue*).

B. Dimensionless Kratky plots based on the Guinier region analysis (see **Appendix 1 Figure 1-5**, **1-6**). Each graph corresponds to the same samples from panel A.

Next, comparisons between all of the monomers and oligomers formed on the substrates with double-stranded region were produced (**Figure 3.6-8**). Based on the analysis and data gathered in the log_{10} intensity and dimensionless Kratky plots (panel **A** and **B** respectively), all of the monomers (*graphs on the left*) behaved in exactly the same manner and had the same characteristics when it comes to the shape and folded state. However, there were visible differences between the formed oligomers (*graphs on the right*), suggesting distinct shape. The oligomer formed on the substrate containing $(AG)_{10}$ single-stranded region was the most distinct, being the most globular and the most folded. However, caution has to be taken with interpretation of this data, as there is a possibility that the oligomers formed on $(AG)_{10}$ 24BP and $(AG)_5$ 24 BP as well as $(CAA)_6CA$ 24BP can be of different species – trimer versus dimer (see **Figure 3.6-6** and **Appendix 1 Figure 1-5**, **1-6**).

Additional flexibility analysis was performed, similarly as in the **Figure 3.6-4**, panel C between the eIF4A2 oligomers formed on $(AG)_{10}$ 24BP and $(CAA)_6CA$ 24BP. Here (**Figure 3.6-8**, panel C) the $(AG)_{10}$ 24BP oligomer (*purple*) reached plateau in the Porod-Debye plot, suggesting a rigid and well-defined structure, however the $(CAA)_6CA$ 24BP oligomer (*dark pink*) achieved plateau first in the SIBYLS plot suggesting both flexible and inflexible regions (Rambo and Tainer, 2011; Brosey and Tainer, 2019). This indicated that the oligomers created on $(AG)_{10}$ 24BP RNA not only form more readily but additionally are more rigid, suggesting greater stability of the formed complexes on this RNA.

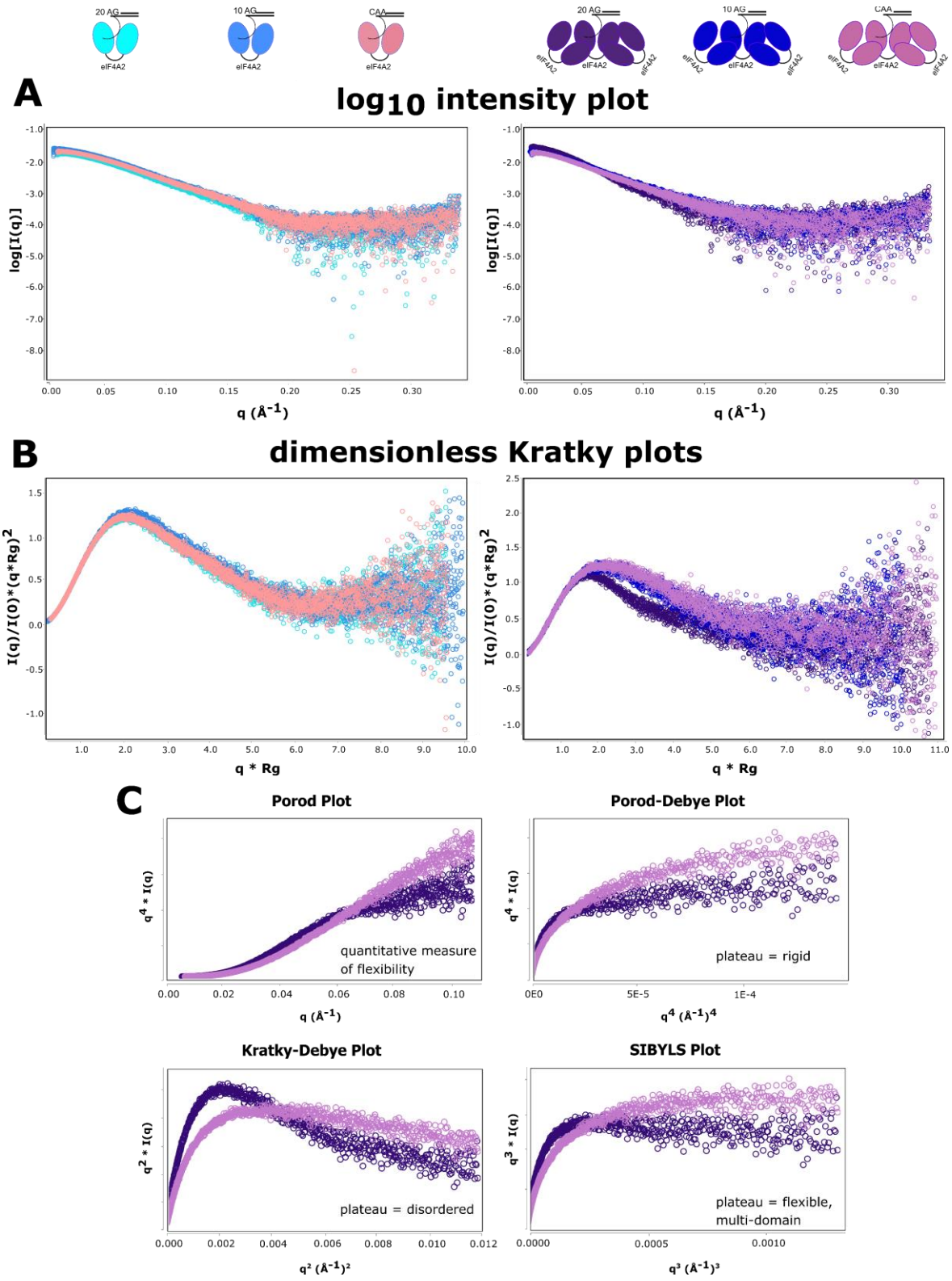

Figure 3.6-8 Comparison of scattering data for eIF4A2 monomers and oligomers formed on substrates with 24 BP double-stranded region

A. Comparison of scattering curves (log_{10} intensity plots) of eIF4A2 monomers (graph on the left) formed on $(AG)_{10}$ 24BP (*cyan*), $(CAA)_6CA$ 24BP (*pink-salmon*), and $(AG)_5$ 24BP (*blue*), and oligomers (graph on the right) formed on $(AG)_{10}$ 24BP (*deep purple*), $(CAA)_6CA$ 24BP (*deep pink*), and $(AG)_5$ 24BP (navy *blue*). No aggregation in the samples is visible, all the monomers followed the same trend, slight differences are visible in the oligomer samples.

(figure legend continues on the next page)

B. Dimensionless Kratky plots based on the Guinier regions analysis, graph on the left presenting monomers, and graph on the right portraying oligomers. Colour scheme the same as in panel **A**. All monomeric samples follow the same trend, associated with globular proteins. Oligomer formed on $(AG)_{10}$ 24 BP substrate again shows a distinct trend to the other oligomers.

C. Flexibility analysis eIF4A2 oligomer formed on $(AG)_{10}$ 24BP (*deep purple*), and $(CAA)_6CA$ 24BP (*dark pink*). The analysis shows plateau in SIBYLS plot for $(CAA)_6CA$ 24BP suggesting mixture of flexible and inflexible domains, whereas plateau in the Porod-Debye plot for the $(AG)_{10}$ 24 BP oligomer suggests that this oligomer is more rigid.

Finally, envelope models were created, as described above (**Figure 3.6-3**). For envelope models of each individual complex please refer to **Appendix 1 Figure 1-7**. Superimposed monomeric eIF4A2 complexes formed on RNAs with double-stranded region adopt similar conformation, however the $(AG)_{10}$ 24 BP substrate formed one is the largest of the three (**Figure 3.6-9**, panel A). As **1)** the complexes were formed with the use of AMP-PNP, i.e., non-hydrolysable ATP analogue, permitting RNA binding, but hindering RNA release, **2)** the d_{max} of the tested monomers is larger than the one of free protein (see **Table 3.6-1**), and **3)** eIF4A does not bind directly to the double-stranded RNA (Lorsch and Herschlag, 1998a), it is possible that the extended region corresponds to the double-stranded region of the RNA. Next, the $(AG)_{10}$ 24BP oligomer was compared to the oligomer formed on $(CAA)_6CA$ 24 BP (**Figure 3.6-9**, panel B, *left*) and to the oligomer formed on $(AG)_5$ 24BP (*right*). Clear distinction in size and shape was observed in both instances. The lesser distinction of the size exclusion chromatography peaks (see **Appendix 1 Figure 1-5**, **1-6**) of the complexes formed on $(CAA)_6CA$ 24 BP and $(AG)_5$ 24BP RNA, the clear smaller size based on the created envelope models (**Figure 3.6-9**, panel B), and the differences in the R_g and d_{max} (**Table 3.6-1**) suggest that the oligomeric complexes possibly represent different species. As the collected d_{max} values (**Table 3.6-1**) were larger than the ones of the monomeric species, the oligomer in this case could represent a dimer.

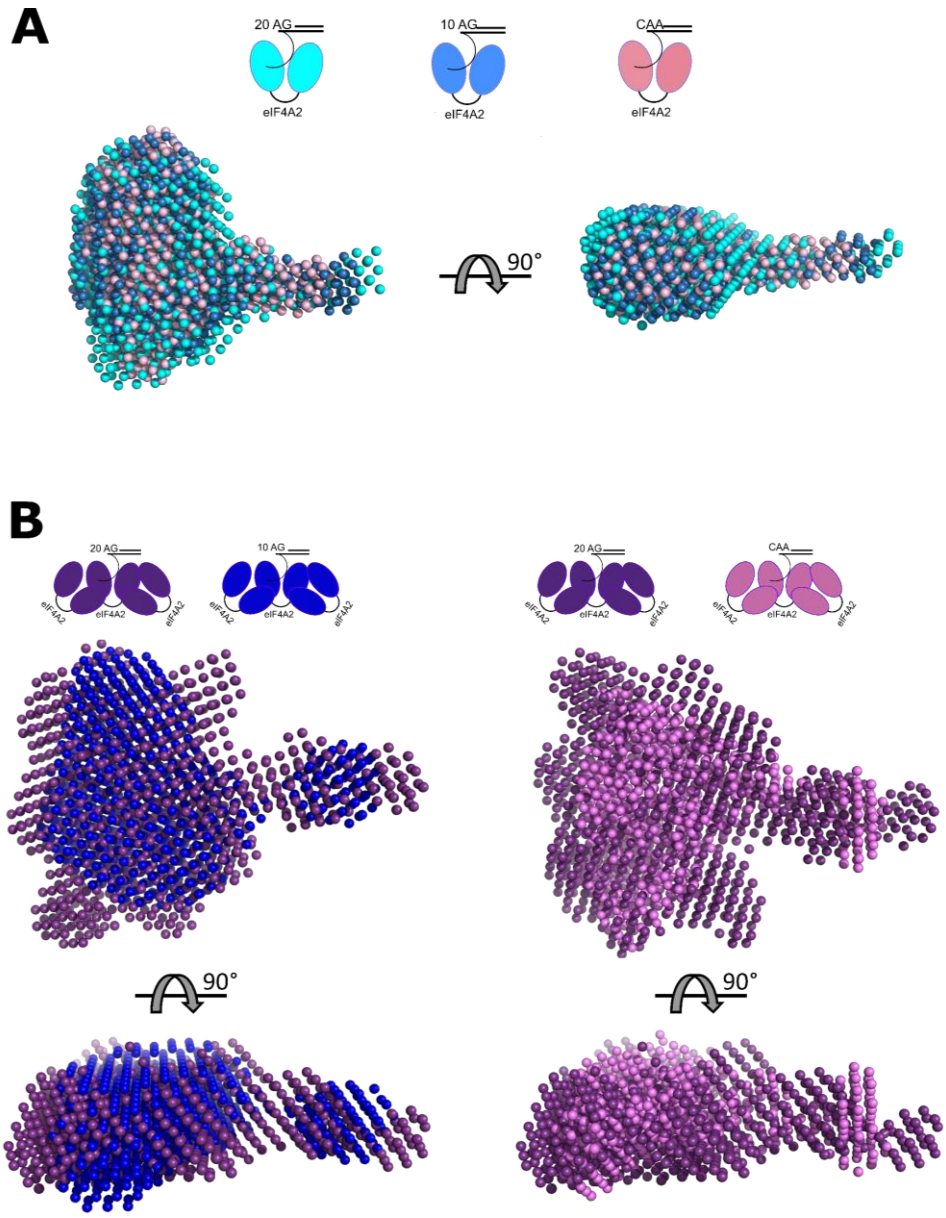

Figure 3.6-9 eIF4A2 adopts different conformation based on RNA substrate and oligomerisation status

Envelope models (dummy atom model fitting using DAMMIF and DAMAVER packages from ATSAS 3.0.3) – for more information about analysis please refer to **Chapter 2.3.5**. Superposition created using SUPCOMB package from ATSAS 3.0.3.

- **A.** Superposition of monomers formed on $(AG)_{10}$ 24BP (cyan), $(AG)_5$ 24BP (blue) and $(CAA)_6CA$ 24BP (pink). Monomers adopt similar conformation, however the monomer created on $(AG)_{10}$ 24BP seems to be the largest.
- **B.** Superposition of oligomers formed on $(AG)_{10}$ 24BP (deep purple), $(CAA)_6CA$ 24BP (dark purple – left, and oligomers formed on $(AG)_{10}$ 24BP (deep purple), $(AG)_5$ 24BP (navy blue) – right. Oligomer formed on $(AG)_{10}$ 24BP appears to be the largest, possibly due to different state of oligomerisation (trimer versus dimer).

Table 3.6-1 R_g and D_{max} values obtained from SAXS analysis of eIF4A2 complexes

Sample	R_g (Å)	d_{max} (Å)
apo-eIF4A2	30.1	104
AMP-PNP bound eIF4A2	30	99
$(AG)_{10}$ monomeric eIF4A2	27	112
$(AG)_{10}$ oligomeric eIF4A2	34.2	131
$(CAA)_6CA$ monomeric eIF4A2	27.5	97
$(AG)_{10}$ 24BP monomeric eIF4A2	29.6	114
$(AG)_{10}$ 24BP oligomeric eIF4A2	39.1	139
$(CAA)_6CA$ 24BP monomeric eIF4A2	29.1	117
$(CAA)_6CA$ 24BP oligomeric eIF4A2	35	134
$(AG)_5$ 24BP monomeric eIF4A2	30.5	109
$(AG)_5$ 24BP oligomeric eIF4A2	30.2	132

In conclusion, SAXS was proven to be a method with sufficient resolution to distinguish different dimensions (**Table 3.6-1**) of the investigated samples. Additionally, distinct shapes and conformations were detected between apo-eIF4A2 and AMP-PNP bound state suggesting that this method has satisfactory sensitivity to detect small changes upon binding of different RNAs. The extended arm of apo-eIF4A2 disappeared upon AMP-PNP binding, and the monomeric RNA bound samples are more globular than the RNA unbound state. The analysis of monomeric species formed on single-stranded $(AG)_{10}$ and $(CAA)_6CA$ RNA however did not show large differences between the formed complexes. The flexibility analysis suggested that both investigated monomers are rigid and globular. The monomers also have similar R_g, indicating similar mass distribution around the centre of gravity of both monomers, suggesting that the conformation adopted on distinct RNAs as a monomer might not influence oligomerisation potential (see different oligomerisation propensity **Figures 3.4-1**, **3.5-2**). However, the maximum dimension and slight difference in the dimensionless Kratky plot (**Table 3.6-1**, **Figure 3.6-4**, panel B), could potentially indicate that those small variances can indeed play a role in oligomerisation. Additionally, the oligomeric $(AG)_{10}$ bound eIF4A2 was more rigid, folded, and most importantly larger than the monomeric species.

Finally, as a cooperativity was observed in an unwinding reaction (**Figure 3.3-1**), the propensity of eIF4A2 to form oligomeric complexes on RNA substrates with double-stranded region was investigated. The double-stranded substrate

containing $(AG)_{10}$ single-stranded region (sequence and length that promoted oligomerisation to the highest extent, **Figures 3.5-2**, **3.5-4**) did not promote formation of additional species not seen on single-stranded RNA (compare **Appendix 1 Figure 1-3** and **Figure 3.6-6**). Further suggesting that eIF4A2 interacts mostly with the single-stranded region, and this interaction promotes oligomerisation. Additionally, double-stranded RNA substrate with $(AG)_5$ single-stranded overhang did not produce oligomers as readily as $(AG)_{10}$ single-stranded region (compare **Appendix 1 Figure 1-5** and **Figure 3.6-6**), further emphasising the importance of single-stranded RNA in oligomerisation. However, as the d_{max} - (**Table 3.6-1**) between monomeric and oligomeric (possibly dimeric) $(AG)_5$ 24BP sample differed and no oligomers were detected on single-stranded 10 nt AG-RNA (**Figures 3.5-3**, **3.5-4**) at least partial influence of the double-stranded region cannot be excluded. Intriguingly, regardless of the similarities between monomers formed on RNAs with double-stranded regions, oligomers formed on substrates with $(AG)_{10}$ and $(CAA)_6CA$ single-stranded overhangs differed significantly, with oligomers forming on $(CAA)_6CA$-containing RNA less readily (**Appendix 1 Figure 1-6**). Finally, the extended region in all of the complexes formed on RNA with double-stranded region, as previously described, is possibly the double-stranded RNA itself. As there is only one extension visible both per monomeric and oligomeric complex, this suggests again (see **Figure 3.5-1**) that the oligomers are formed through protein-protein interaction on single RNA.

In all, information gathered through SAXS experiments provided another level of assurance that eIF4A2 can form oligomeric complexes, and that their existence is dependent on the sequence and length of a single-stranded region of RNA. Moreover, the different capacities to form oligomeric species in presence of double-stranded region indicate the need to explore the influence of presence of oligomeric species on helicase activities of eIF4A2.

3.7. eIF4A2 interacts in live cells supporting oligomerisation model

As phenomena observed *in vitro* do not always turn out to be true in cells, and the *in vitro* research serves as a tool to discover how things might work *in vivo*, it was important to determine whether eIF4A2 can oligomerise in live cells. For this a FLIM-FRET (fluorescence lifetime imaging microscopy – fluorescence resonance energy transfer) method was used. It is a technique that allows to study molecular interactions between two fluorescently tagged proteins of interest in live cells. In this method it is the fluorescence lifetime of a donor molecule that is measured. The principles of this method are shown in the **Figure 3.7-1** (see also **Chapter 2.4.7**). For the purpose of this thesis the method is explained with the use of eIF4A2 as the protein of interest. As shown in **Figure 3.7-1**, panel A (*left*), in which cells transfected with donor-eIF4A2 only, the donor molecule transitions from the ground state (S_0) to the excited state (S_2) through the absorption of energy in the form of light. Subsequently the donor molecule undergoes internal conversion (change from S_2 to S_1) and emits a photon (S_1 to S_0). The time the donor molecule remains in the excited state before emitting a photon is called fluorescence lifetime, τ. Conversely, when **1)** a suitable pair of donor and acceptor molecules are present in the same cell, i.e. the donor has a high quantum yield and its emission spectrum overlaps with the acceptor excitation spectrum, and **2)** they are in a close proximity (less than 10 nm) (Förster, 1948; Spiegel *et al.*, 2016), the donor molecule can relax from the excited state by non-radioactive transfer of energy to the acceptor (FRET). As the process of energy transfer to the acceptor is faster than the emission of a photon (as in the case of no FRET), the donor molecule returns to S_0 in shorter time, in turn decreasing the fluorescence lifetime (**Figure 3.7-1**, panel A, *right*). In **Figure 3.7-1**, panel B a situation is described in which the two fluorophores do not come into direct contact with each other. It is important to choose fluorophores which do not dimerise on their own. In this case, due to absence of interaction, a change between the fluorescence lifetime in cells transfected with the donor molecule alone and the ones transfected with both donor and acceptor is not likely.

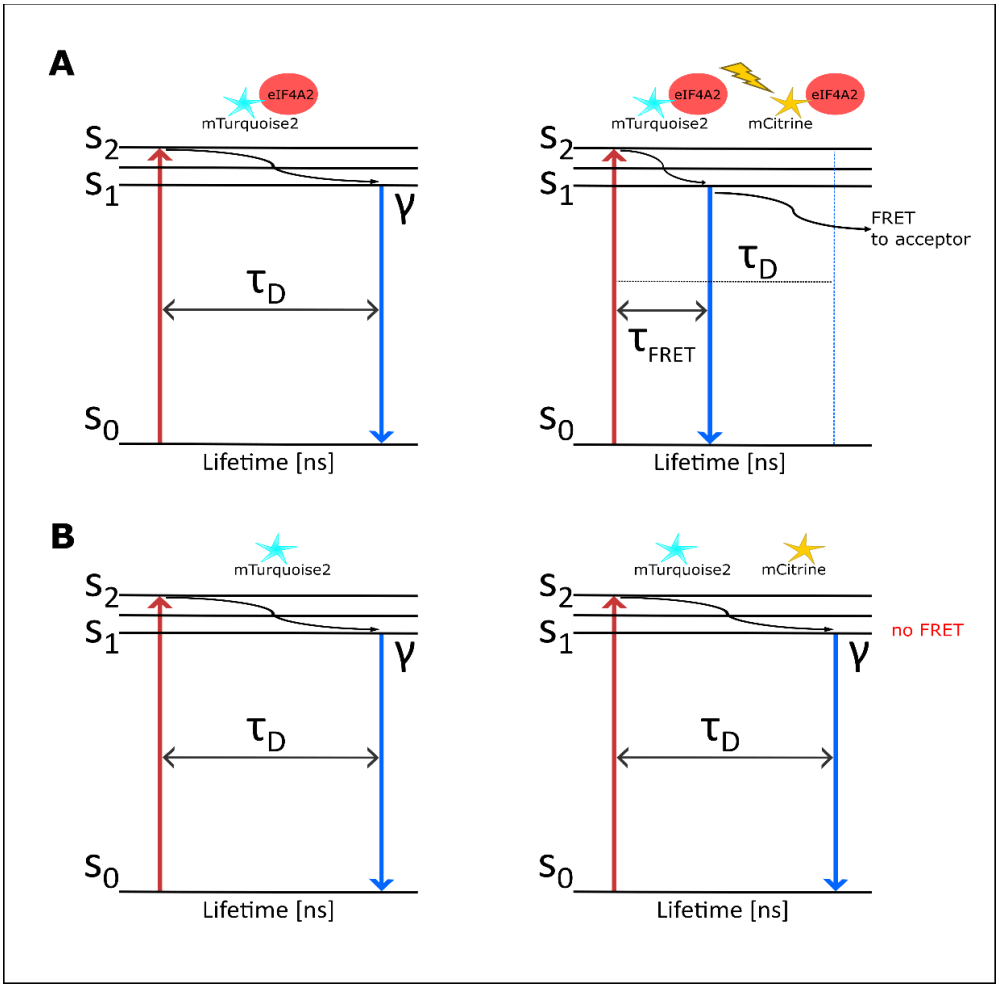

Figure 3.7-1 Diagram of mechanism behind FLIM-FRET method

A. The diagram on the left presents a situation in which eIF4A2 is N-terminally tagged with a donor molecule (mTurquoise2). When the cells are excited with light at 436 nm (20 nm bandwidth), the donor molecule absorbs a photon and changes its electronic state from ground (S_0) to the excited one (S_2). Then the molecule transfers through the internal conversion (change from S_2 to S_1) and emits a photon (S_1 to S_0). The period of existence in the excited state is called fluorescence lifetime of a donor, τ_D.
The diagram on the right portrays the situation in which cells were transfected with mTurquoise2-eIF4A2 (donor) and mCitrine-eIF4A2 (acceptor). Here, due to expected interaction of two eIF4A2 proteins, and the mTurquoise2 and mCitrine being a suitable FRET pair, the donor returns to the ground state not through emission of a photon but to transfer of energy to the acceptor molecule. This, in turn, results in shortened fluorescence lifetime.

B. The two diagrams represent cells transfected with either mTurquoise2 or both mTruquoise2 and mCitrine. Here, due to lack of interaction between the donor and acceptor molecules, the decrease of fluorescence lifetime is not to be expected. The donor in both cases (left for donor alone, and right for both donor and acceptor) needs to emit a photon to return to the ground state.

First, a suitable pair of fluorophores was chosen, mTurquoise2 was selected as a donor (Goedhart *et al.*, 2012), and mCitrine as an acceptor (Hoffmann, Chen and Campbell, 2018). The monomeric features of both fluorophores make them ideal candidates for determining oligomerisation of eIF4A2. Additionally, the high quantum yield, i.e., the ratio of photons absorbed to the ones emitted, of mTurquoise2 means that the fluorophore is brighter and has a strong signal. Another advantage of mTurquoise2 is its sufficiently long fluorescence lifetime (4 ns).

Next, the possibility of a tag interfering with eIF4A2 oligomerisation had to be excluded. Since **1)** the recombinant eIF4A2 was N-terminally tagged (His-SUMO) through the first step of purification and this did not interfere with obtaining active protein and **2)** many published reports (Li, Belsham and Proud, 2001; Oberer, Marintchev and Wagner, 2005; Hosmillo *et al.*, 2016) used N-terminally tagged eIF4A, it was decided to place the fluorophore on the N-terminus. Therefore, to test the oligomerisation, mTurquoise2-eIF4A2 and mCitrine-eIF4A2 were cloned and then purified using agarose resin (see **Chapter 2.2**, **Figure 3.7-2**, panels A, B). The proteins were cleaved of the resin and assessed to be of sufficient purity to use in this test.

Next, unlabelled eIF4A2 (WT), mTurquoise2-eIF4A2, mCitrine-eIF4A2, or an equimolar mixture of both mTurquoise2-eIF4A2 and mCitrine-eIF4A2 were incubated with Dy780 labelled $(AG)_{10}$ RNA for 1 hour in binding buffer (20 mM HEPES pH 7.5, 100 mM KCl, 2 mM $MgCl_2$, 1 mM DTT) supplemented with 1 mM AMP-PNP. Subsequently, the prepared samples were visualised using EMSA (**Figure 3.7-2**, panel C). For the WT eIF4A2 three bands were observed, suggesting formation of monomer, dimer, and trimer. For the fluorophore-tagged eIF4A2 two bands of different size were visible. The change in size in comparison to WT could be explained due to the larger size of the fluorophore-tagged eIF4A2 (46 kDa for WT and 73 kDa for the tagged one). Additionally, the lack of the third band could potentially stem from **1)** the inability of eIF4A2 to form trimers when tagged, **2)** formation of only two species, i.e., either monomer and dimer or monomer and trimer, **3)** apparent lower concentration of tagged eIF4A2, or **4)** size of the protein being too large to resolve fully on 7% acrylamide gel.

In the first, and second case, if the tagged eIF4A2 could form any of the multimeric species, the fluorophore tagged eIF4A2 was still a good candidate for FLIM-FRET studies. As the detection of interaction can only be seen between two tagged proteins, any of the permutations of an interaction would be sufficient to detect a change in fluorescence lifetime as long as the complex consists of at least one donor and one acceptor.

In the third case, as the concentration was determined UV-spectroscopically using protein specific extinction coefficients calculated with Expasy PotParam (Duvaud *et al.*, 2021), the active concentration could be masked by contaminants from purification. One way to avoid this situation would be to purify the proteins through the regular multi-step purification used for other proteins in this thesis. Alternatively, **1)** a ratio of the protein of interest to the contaminants could be calculated from the Coomassie stained gel, **2)** protein concentration could be then established with a Bradford method, **3)** the obtained mg/mL concentration of tagged-eIF4A2 could be calculated using the established ratio, **4)** it could be converted to molar concentration using the provided above extinction coefficients. Trying to establish concentration without including contaminants simply from absorption at 280 is not recommended as extinction coefficients and the amount of aromatic amino acids of contaminants are not known.

The fourth, and probably the easiest explanation of lack of clearly visible three bands could be resolved by choosing a different type of native gel: either of lower percentage of acrylamide or gradient percentage.

In all, the clearly visible multimeric complexes, proved the N-terminally tagged eIF4A2 to be a good candidate to test whether eIF4A2 oligomerises in cells using FLIM-FRET.

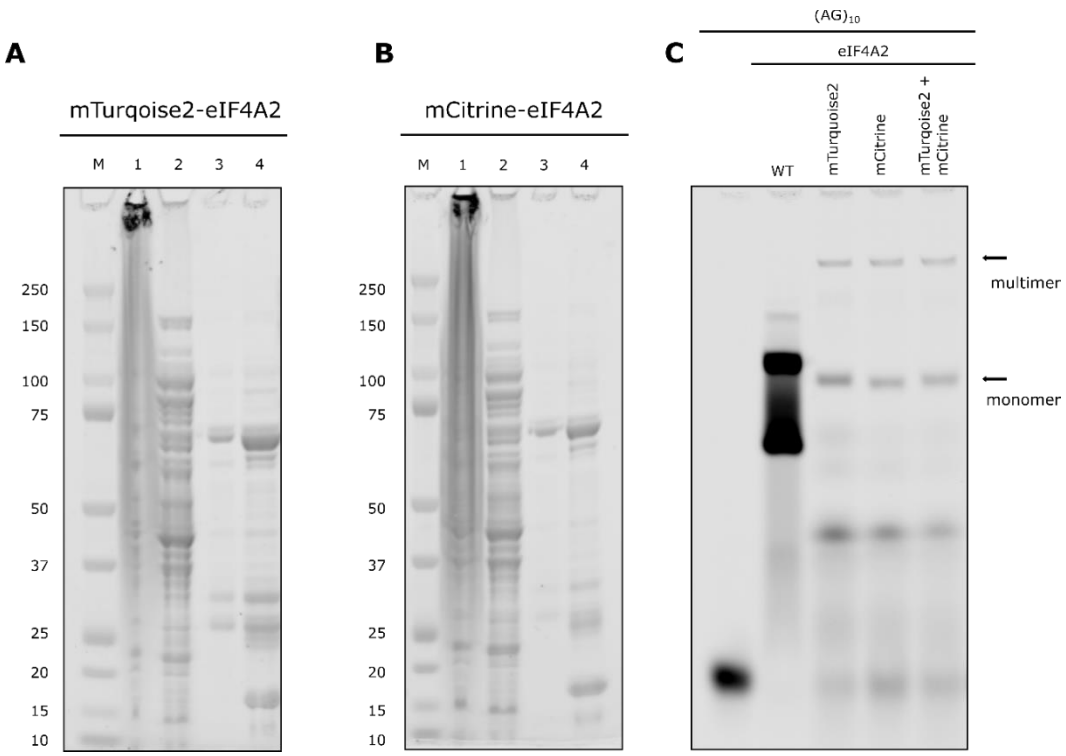

Figure 3.7-2 N-terminally tagged eIF4A2 is capable of oligomerisation

A. Purification of mTurquoise2-eIF4A2, using agarose resin. Lane 1 shows the flow through collected from resin. Lane 2 indicates the wash 1 from the resin. After 2 washes subsequent washes, ULP1 protease was added to the resin in the buffer containing reduced salt concentration. Lane 3 represents the supernatant containing cleaved mTurquoise2-eIF4A2. Additionally, lane 4 corresponds to elution from the resin. Protein visible in lane 3 was used for subsequent tests.

B. Purification of mCitrine-eIF4A2. All the steps were done in the same manner as in the panel **A**. The lanes 1, 2, 3, and 4 correspond to the same steps as in the mTurquoise2-eIF4A2 purification.

C. Test EMSA showing RNA binding of eIF4A2 (WT and fluorophore-tagged) to Dy780 labelled $(AG)_{10}$ RNA. Proteins (5 µM total per lane) were preincubated with the RNA (25 nM) for 1 h at room temperature in the binding buffer with 1 mM AMP-PNP. The shift corresponding to the protein-RNA binding is visible in all the lanes in comparison to the RNA only one. Two arrows indicate monomer and multimer in the tagged-eIF4A2 lanes. Note the visible change between the WT monomer and the fluorophore-eIF4A2 is due to the larger size of the tagged eIF4A2.

To address the question of whether eIF4A2 can oligomerise in cells, FLIM-FRET was performed. Briefly, HeLa cells were transfected with either a plasmid containing mTurquoise2-eIF4A2 or both the mTurquoise2-eIF4A2 and the mCitrine-eIF4A2 plasmids for 48 hours (see **Chapter 2.4.2**). Next, fluorescence lifetime of the donor was measured using a FLIM Lambert system. Here, the mTurquoise2 donor was excited with LED emitting at 445 nm. Together with each experiment, a reference fluorophore with known fluorescence lifetime was measured to calibrate the instrument. Representative images from 3 different experiments (4 experiments in total) are presented in **Figure 3.7-3**, panel A, left, each donor-eIF4A2 (*top*) is paired with donor-eIF4A2 and acceptor-eIF4A2 (*bottom*) measured on the same day. As expected, eIF4A2 fluorescence was restricted to the cytoplasm, indicating these constructs follow the proteins endogenous localisation. Quantification of FLIM-FRET showed that the donor-eIF4A2 alone had the expected average fluorescence lifetime of around 3.9 ns. However, in cells co-transfected with both donor and acceptor tagged eIF4A2 a statistically significant decrease of fluorescence lifetime to around 3.7 ns was observed (**Figure 3.7-3**, panel A, *right*). As FRET can only occur between fluorophores in close proximity, this decrease in fluorescence lifetime suggests that eIF4A2 may indeed multimerise in cells. Moreover, the observed change was similar to what has been communicated for other interactions using mTurquoise2 as a donor (Bertolin *et al.*, 2019). As described in the study Bertolin *et al.*, 2019, mTurquoise2 coupled in a tandem construct with superYFP (a fluorophore that as mCitrine belongs to the YFP family) reached the change of fluorescence lifetime of 0.6 ns. In the case of in cell interaction, the change was only around 0.2 ns.

As a control, HeLa cells were transfected with a free donor (mTurquoise2) or co-transfected with free donor (mTurquoise2) and free acceptor (mCitrine). Unlike tagged-eIF4A2, free fluorophores were dispersed throughout the cell (**Figure 3.7-3**, panel B, *left*, each donor (*top*) is paired with corresponding donor and acceptor (*bottom*)). Furthermore, co-expression of the free fluorophores did not result in a significant change of fluorescence lifetime. This indicates that FLIM-FRET is not driven by chance. Together, these findings support that the decrease observed for the samples with fluorophore-eIF4A2 stems from the interaction between the two eIF4A2.

Additionally, transfection efficiency for both the tagged-eIF4A2 as well as free fluorophores was tested through **Figure 3.7-3**, panel C. Briefly, HeLa cells were treated in the same way as the ones used for FLIM-FRET, samples were collected, and Western Blot was performed using a standard protocol (see **Chapters 2.4.3**, **2.4.6**). Anti-vinculin antibody was used to determine the loading control. Anti-eIF4A2 antibody detected 2 bands. Bands visible in all the lanes just below 50 kDa marker corresponded to WT eIF4A2. Additional bands around the marker size 75 kDa in wells containing cells with eIF4A2 transfections matched the tagged-eIF4A2 with the calculated size of 73 kDa. Since the anti-GFP antibody can effectively detect GFP derivatives like m-Turquoise2 and m-Citrine due to high similarity between them anti-GFP antibody was used. It detected bands between 25 and 37 kDa marker size in lanes with fluorophores transfections, as well as the tagged-eIF4A2 in lanes with eIF4A2 transfections. Less eIF4A2 was observed in lanes with free fluorophores transfection, however the amount of loading control (vinculin) seems to be lower in those lanes as well. In all, eIF4A2 with both tagged fluorophores, as well as both of the free fluorophores seem to have similar transfection efficiency.

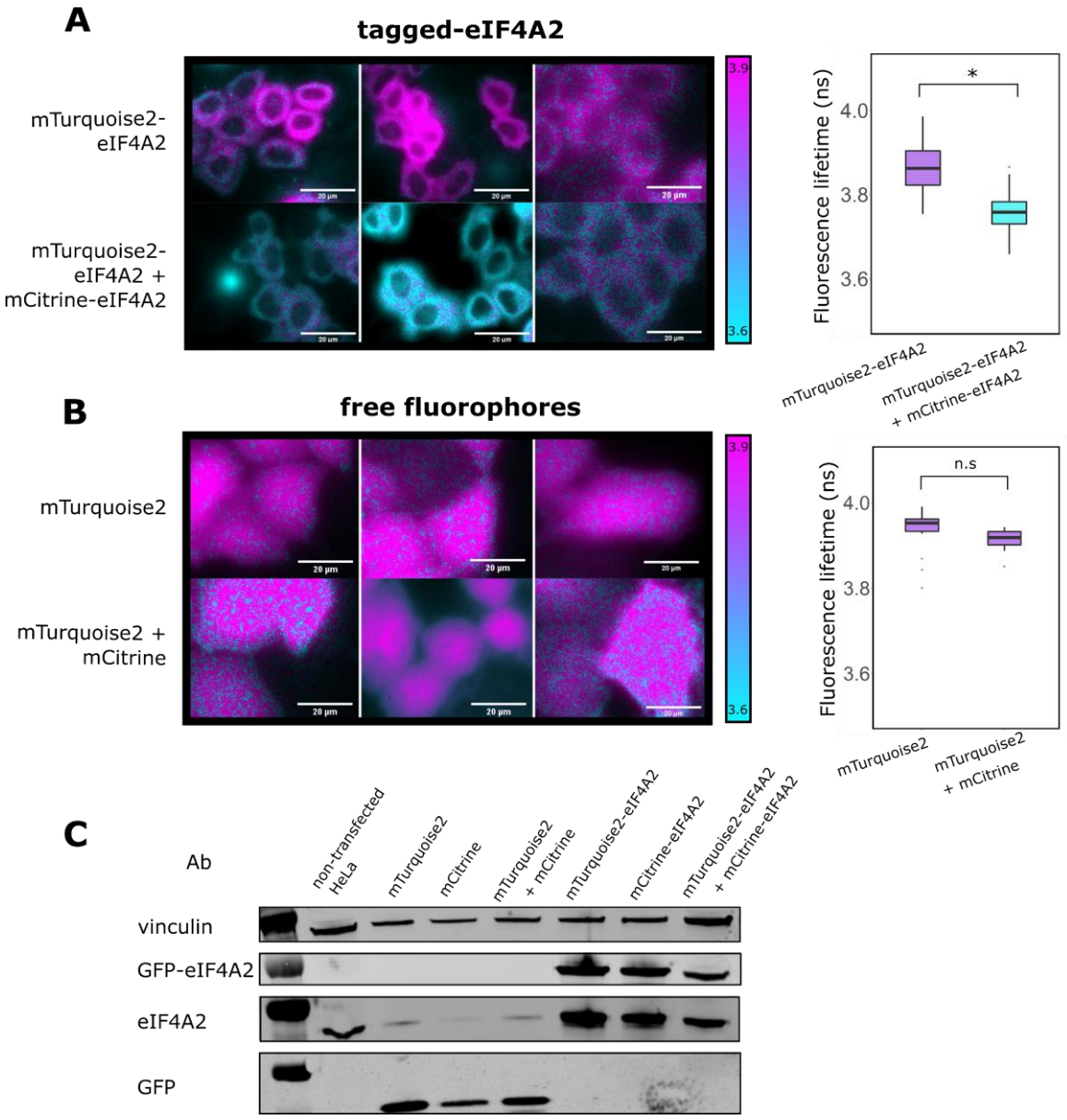

Figure 3.7-3 eIF4A2 oligomerises in live cells

A. Fluorophore tagged eIF4A2 oligomerises in live cells. Left side of the panel contains representative images of transfected HeLa cells expressing either mTurquoise2-eIF4A2 (*top*) or both mTurquoise2-eIF4A2 and mCitrine-eIF4A2 (*bottom*). The images are presented from three separate experiments, each top panel with a corresponding bottom panel from the same experiment. Images have a scale bar of 20 μm and are colour coded with a magenta fluorescence lifetime scale from 3.9 to 3.6 ns. Right side of the panel shows box plot with median as a black bar for each condition. Each box contains all the measured fluorescence lifetimes, collected from 4 different experiments, with the total of 131 cells measured for the mTurquoise2-eIF4A2 and 146 cells for the co-transfection. The p-value = 0.029 was calculated using T-test (two-tailed distribution, two-sample equal variance).

(figure legend continues on the next page)

B. Free mTurqoise2 and mCitrine do not oligomerise. This panel is presented in the same way as the panel A. The p-value = 0.1, calculated in the same manner proved the change in fluorescence lifetime for free fluorophores as not significant. Data presented in the box plot was collected from 5 separate experiments, with the average of 2 to 3 regions per 35 mm dish (samples in technical duplicates) per experiment. The total cells measured for the mTurquoise2 was 95, and 87 for both fluorophores.

C. Western blot representation of transfection efficiency. Anti-vinculin antibody was used as a loading control. Anti eIF4A2 antibody detected WT band in all the samples. Bands for the fluorophore-tagged eIF4A2 were detected with both anti-GFP and anti-eIF4A2 antibody below the marker size of 75 kDa. Anti-GFP antibody detected bands corresponding to the free fluorophores. In the non-transfected HeLa cells only the bands corresponding to vinculin and WT eIF4A2 were observed.

As **1)** the detected change in fluorescence lifetime for tagged-eIF4A2 was significant and not detected for free fluorophores, **2)** the extent of the change was similar to what was reported in the literature for in cell interaction (Bertolin *et al.*, 2019), and **3)** the overexpression of both tagged-eIF4A2 was on a similar level, all the gathered data so far were indicative of eIF4A2-eIF4A2 interaction in cell. However, a question remained why the change in fluorescence lifetime in cell was not as large as the one reported for the tandem construct (Bertolin *et al.*, 2019). One of the reasons could be the fact that for the full change the donor has to interact specifically with the acceptor. In a situation where two donors (or two acceptors, or a donor and a WT) interact with each other the change of fluorescence lifetime would not be visible.

To understand the possible interactions a series of immunoprecipitations (IPs) were performed. Briefly, HeLa cells were treated in a similar manner as for the FLIM-FRET experiment and IPs were carried out as described in **Chapters 2.4.5**, **2.4.6**, with use of **1)** anti-IgG, **2)** anti-eIF4A1, **3)** anti-eIF4A2 4) anti-GFP antibodies (**Figure 3.7-4**, panel A, *left*). Here, the input lanes for non-transfected HeLa cells only detected WT eIF4A2, whereas the input lanes for all the other conditions contained both WT eIF4A2 and fluorophore-eIF4A2. As expected, only the WT eIF4A2 was detected in eIF4A2 IP lane for non-transfected condition. The eIF4A2 IP lanes in all of the transfected conditions detected both WT and fluorophore tagged eIF4A2. In the GFP IP lanes in the transfected conditions not only the fluorophore tagged eIF4A2 but also the WT were detected. This suggested that the tagged eIF4A2 can interact with the WT.

Thus, giving a potential explanation why the observed reduction in fluorescence lifetime was smaller than the one theoretically expected. Additionally, eIF4A1 IP lanes detected only WT eIF4A1, further suggesting, that the interaction is specific.

As the RNA in the tested conditions was intact (**Figure 3.7-4**, panel A, *right*), another reason for the interaction in cell had to be considered, i.e., the observed interaction could stem from binding to the same long mRNA. This time, the cells were lysed in presence of RNase 1 to degrade the RNA and treated in the same way as described above. Interestingly, the same result was observed in the RNase 1 samples (**Figure 3.7-4**, panel B, *left*), which suggests that the interaction is not only due to the two proteins being bound to the same RNA at the same time but through actual protein-protein interaction. Understandably, RNase 1 should not digest the RNA completely, which should still permit for the RNA fragments that were occupied by the protein, and necessary for the oligomerisation to remain untouched. To verify this result, RNA integrity test was performed, and clear degradation was observed (**Figure 3.7-4**, panel B, *right*).

In all, eIF4A2 is capable of interaction in live cells, the N-terminal tag does not inhibit the interaction between the tagged proteins, as well as between the tagged protein and WT. Additionally the true extent of oligomerisation, might be greater, and it is not mediated by the proteins being bound to the same RNA next to each other. The gathered data provide a basis for further investigation of oligomeric eIF4A2 and its activities.

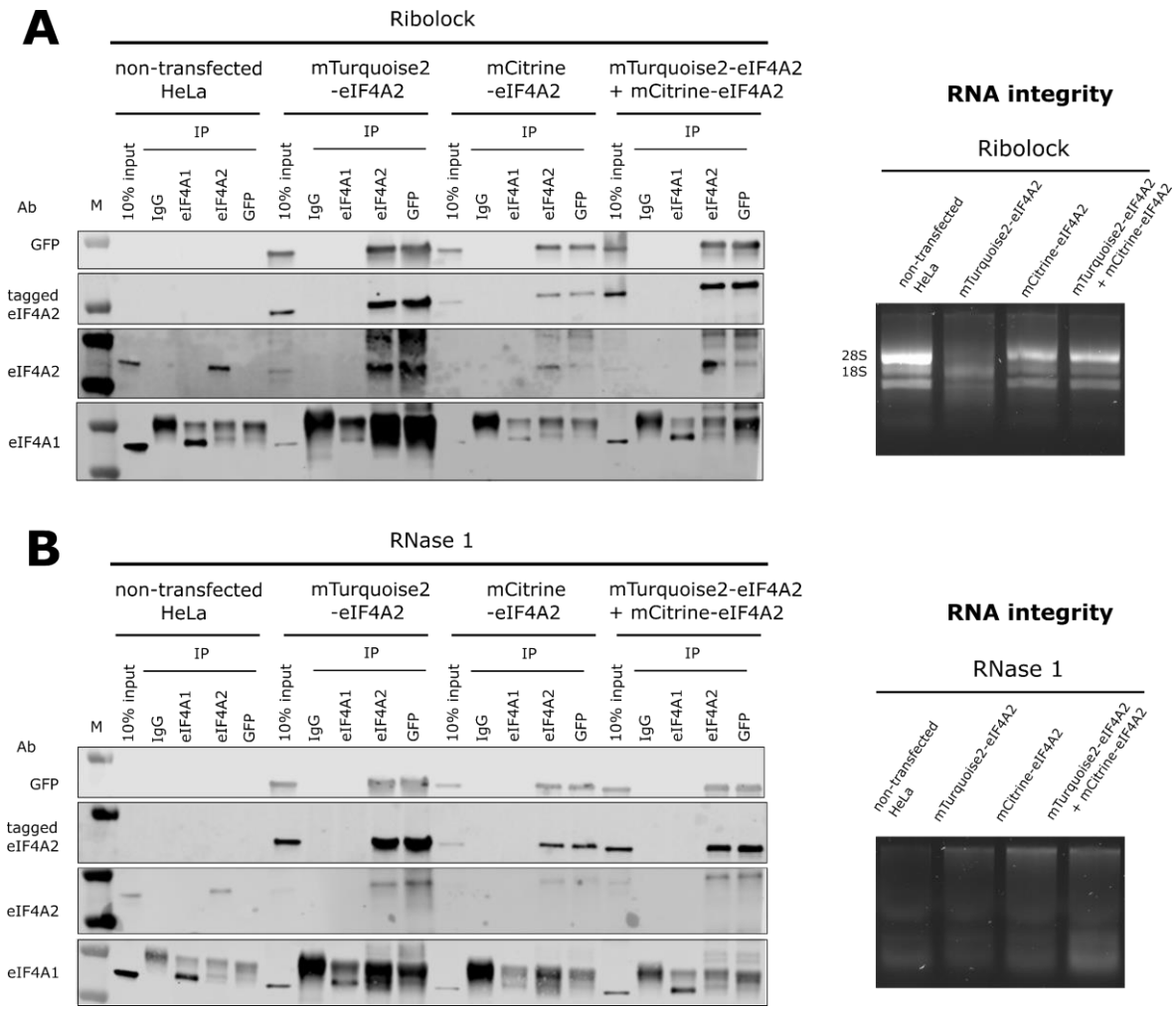

Figure 3.7-4 Fluorophore tagged eIF4A2 interacts with WT in cells

HeLa cells were either non-transfected or transfected with indicated fluorophore-eIF4A2 and treated in the same manner as for the FLIM-FRET experiments. Single 15 cm^2 dish was used for each condition. After cells collection, each dish was divided in half and lysed in presence of either 80 U Ribolock (to block activity of RNases and inhibit RNA degradation) or 1000 U RNase 1. After the lysis, protein concentration in each sample was measured with the Bradford method. Subsequently, the same amount of protein from each sample was used for IPs. RNA samples were collected for each condition.

A. The Western Blot (*left*) represents samples treated with Ribolock. In the input and IP lanes for non-transfected HeLa cells, only the WT eIF4A2 was detected. In all other samples the input contained both WT eIF4A2 and tagged-eIF4A2 (tagged-eIF4A2 can be detected with both anti-eIF4A2 and anti-GFP antibodies). IgG lanes in all the tested conditions did not show unspecific immunoprecipitation of proteins. In all the tested conditions in the GFP IP a co-pull down of WT eIF4A2 was observed. In the eIF4A1 IP both the WT and the tagged-eIF4A2 was not detected. The RNA remained intact (*right*).

B. The Western Blot (*left*) represents samples treated with RNase 1. The obtained IP result is the same as in panel A. Degradation of the RNA (lack of distinguishable 28S and 18S bands) is clearly visible (*right*).

3.8. Catalytic activities of oligomeric eIF4A2

In the previous subchapter, interaction of eIF4A2 was demonstrated to exist in cells, suggesting that there may be a potential function associated with those complexes (**Chapter 3.7**). Additionally, eIF4A2 was shown to form oligomeric complexes on the RNA substrates with double-stranded regions, indicating that those complexes can form on single-stranded RNA adjacent to the double-stranded one (**Chapter 3.6**). Moreover, different RNA sequences were shown to induce oligomerisation to a different extent (**Chapters 3.5**, **3.6**). Finally, as observed in the **Chapter 3.3** the unwinding activity of eIF4A2 is performed in a co-operative manner. Taken together, these data provide the evidence needed for further exploration of the activities of the oligomeric eIF4A2.

To understand how the oligomerised species of eIF4A2 behaves enzymatically, and whether the extent of oligomerisation matters in the catalytic capacities of eIF4A2, its unwinding and ATPase activities were tested. To achieve the oligomerised state, eIF4A2 concentration was kept above the concentration of the RNA substrate (see **Figure 3.5-1**).

As shown in the **Chapters 3.4** and **3.5** (**Figures 3.4-1, 3.5-2**), the AG-RNA induced oligomerisation to the highest extent, and the oligomers did not form as readily on the $(CAA)_6CA$ RNA. Therefore, the differences in unwinding and ATPase on double-stranded substrates, with $(AG)_{10}$ and $(CAA)_6CA$ single-stranded regions were investigated (RNA substrates as shown in **Figure 3.3-1**, panel A). The used substrates differed only in the sequence of the single-stranded region.

Unwinding and ATPase reactions were performed by a titration of eIF4A2 on $(AG)_{10}$ overhang substrate (**Figure 3.8-1**, panel A and B, respectively) and on a $(CAA)_6CA$ overhang substrate (**Figure 3.8-1**, panel C and D, respectively). eIF4A2 exhibited higher unwinding activity on the RNA substrate containing AG single-stranded region compared to $(CAA)_6CA$ one (**Figure 3.8-2**, panel A). Additionally, the obtained Hill coefficient for $(CAA)_6CA$-containing RNA was smaller than for $(AG)_{10}$ in the unwinding reaction (h_{CAA} = 1.5 ± 0.3 in comparison to h_{AG} = 2.6 ± 0.3). A similar pattern was observed for eIF4A2 ATPase activity (**Figure 3.8-2**, panel B). Additionally, the ATPase activity on the substrate with AG overhang followed a sigmoidal shape with Hill coefficient h_{AG} = 2.5 ± 0.47, whereas this

pattern was not observed for the $(CAA)_6CA$ RNA where the Hill coefficient was found to be only 0.5 ± 0.24. This in turn suggested that the cooperativity in the ATPase activity is dependent on the RNA substrate, as no indication of cooperativity was observed on the substrate with $(CAA)_6CA$ overhang.

In general, the Hill coefficients for both the ATPase and unwinding activity were higher for $(AG)_{10}$ overhang substrate, which correlated with the higher extent of oligomerisation on single-stranded AG-RNA (**Figure 3.4-1**), as well as on $(AG)_{10}$ 24BP RNA (**Figures 3.6-6**, **3.6-9**, and **Appendix 1 Figure 1-3**). This in turn, suggested that more readily formed oligomers correlated with greater outcome of both the unwinding and the ATPase. However, the dissociation constant for both overhangs differed (as presented earlier in Wilczynska *et al.*, 2019), with higher affinity towards $(AG)_{10}$ containing substrate ($(AG)_{10}$ K_D = 0.27 ± 0.03 and $(CAA)_6CA$ K_D = 1.04 ± 0.21). As previously shown, the oligomerisation of eIF4A2 was not dependent on affinity towards the RNA substrate but on its sequence (**Figure 3.5-2**). However, in this case, the possibility that the activities are simply dependent on the affinity towards the RNA could not be excluded.

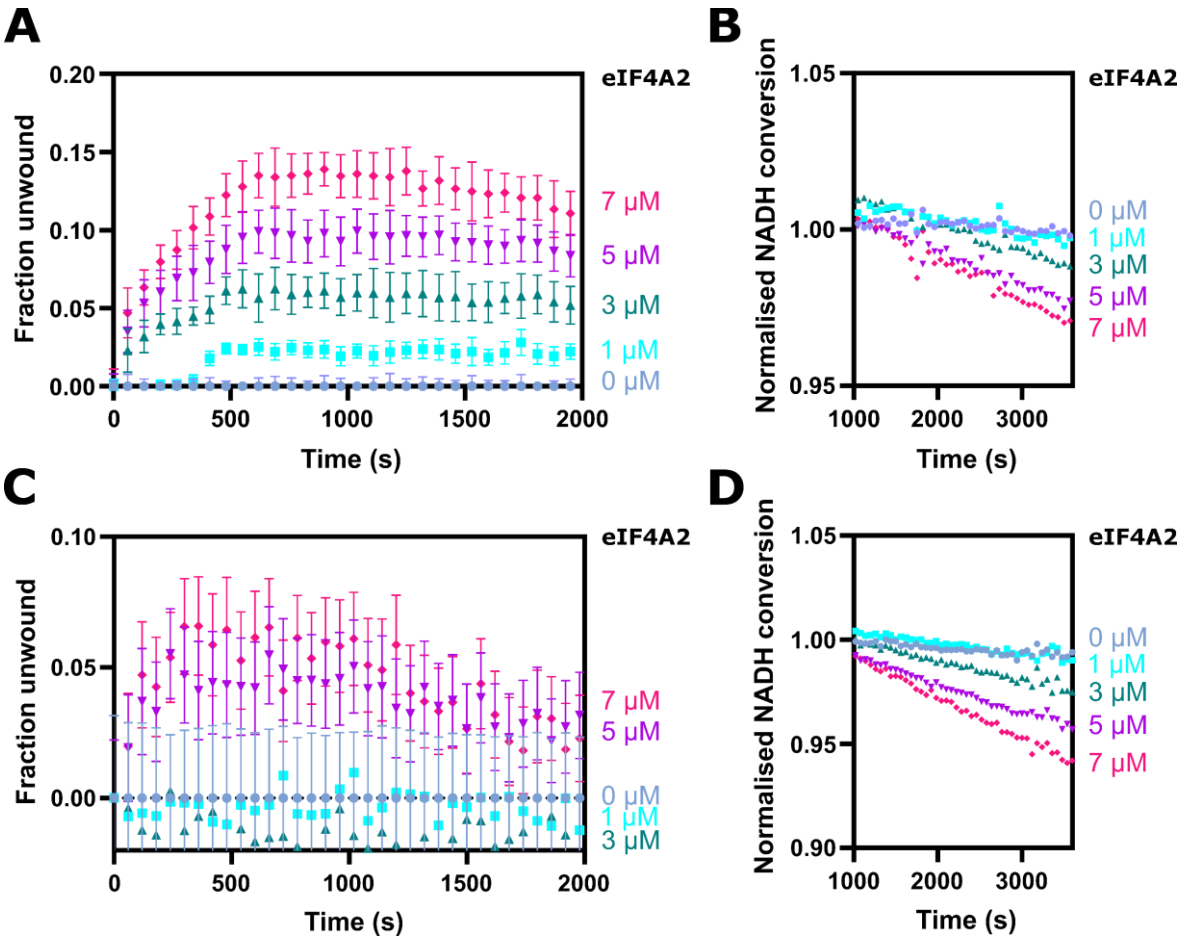

Figure 3.8-1 Unwinding and ATPase activity of eIF4A2 increases with protein concentration

A. Unwinding activity of eIF4A2 on $(AG)_{10}$ 24BP RNA substrate presented as fraction unwound over time with indicated concentrations of eIF4A2. Representative graph, n = 4, error bar – SEM from technical duplicate. For more details how the reactions were performed please refer to **Chapter 2.3.3**).

B. Representation of ATPase activity of indicated concentrations of eIF4A2 on a $(AG)_{10}$ 24BP RNA substrate. The raw data were normalised to the respective starting value of each dataset. Trend with no error bars is shown. The raw data were used for further analysis in this chapter to obtain nM of ATP used per second. For more details about the analysis and an example of raw ATPase activity data please refer to the **Chapter 2.3.4**. Representative graph, n = 3.

C. Unwinding activity of eIF4A2 on $(CAA)_6CA$ 24 BP RNA substrate presented as fraction unwound over time with indicated concentrations of eIF4A2. Very limited unwinding activity was detected for 1 and 3 μM eIF4A2 (error bars for those two concentrations removed for clarity of presentation). Representative graph, n = 3, error bar – SEM from technical duplicate.

D. Representation of ATPase activity of indicated concentrations of eIF4A2) on a $(CAA)_6CA$ 24BP RNA substrate, presented as in the panel **B**. Representative graph, n = 3.

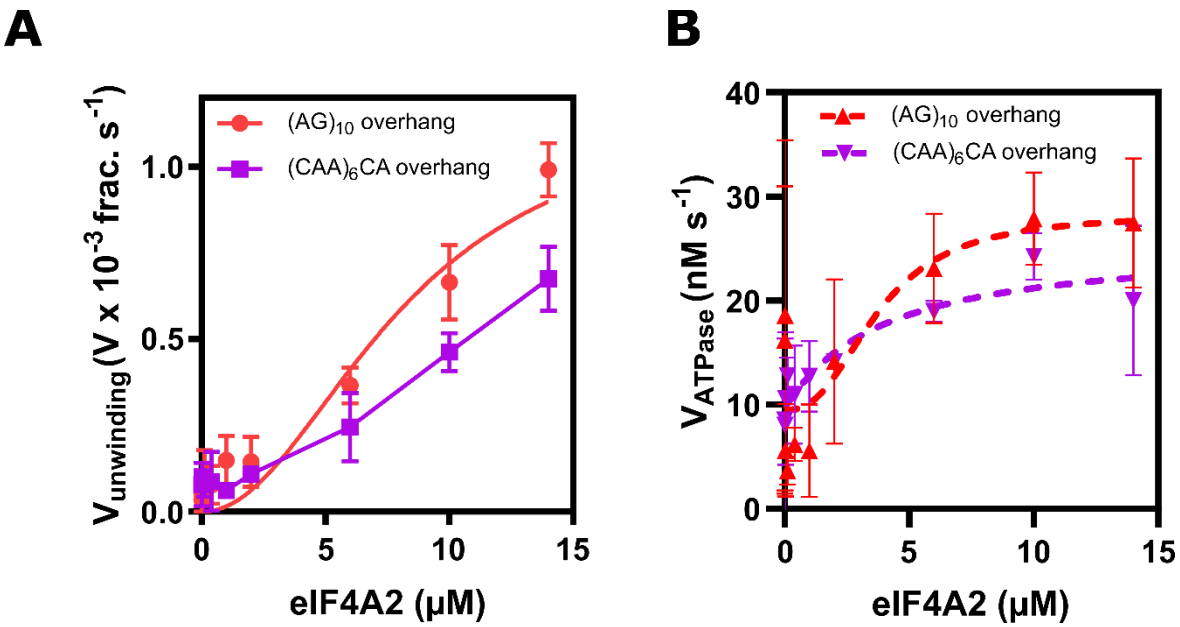

Figure 3.8-2 Unwinding and ATPase activity of eIF4A2 is greater on $(AG)_{10}$ overhang substrate than on the $(CAA)_6CA$ one

A. Unwinding activity presented as velocity of unwinding (fraction unwound per second) versus eIF4A2 concentration on $(AG)_{10}$ and $(CAA)_6CA$ overhang containing RNA substrate. Reactions were started with 1 mM ATP, eIF4A2 was in excess over RNA substrate (50 nM). Data collected from 3 individual replicates for $(CAA)_6CA$ 24BP and 4 replicates for $(AG)_{10}$ 24BP, error bar – SEM, fit – Hill equation.

B. ATPase activity on the same RNA substrates as in the panel **A**. Reactions were performed at the same time as unwinding reactions, in wells supplemented with ATPase mix (please see **Chapter 2.3.4** for more details). Activity presented as velocity of ATPase (nM of ATP used per second) versus eIF4A2 concentration, n = 3, error bar – SEM, fit – Hill equation.

As both the extent of oligomerisation and the different K_D for the two tested RNA substrates could not be excluded as the main determinant of differences in their catalytic activities, further RNA substrates were employed. This time, the velocity of unwinding and K_D was compared for substrates with 20 nt $(AGUG)_5$, $(UCUC)_5$, or $(UGUU)_5$ single-stranded overhangs (**Figure 3.8-3**, panel A). As before, the double-stranded component of the RNA substrate was the same for all permutations. The RNA substrate with the greatest sequence similarity to the AG-RNA, $(AGUG)_5$, was found to have the lowest measured K_D, and the highest measured velocity. This further suggests there is a correlation between unwinding activity and K_D. However, for the other two tested substrates an inverse correlation was observed. The unwinding activity on $(UGUU)_5$-containing RNA substrate was lower than the one observed on $(UCUC)_5$-containing one. However, the measured K_D was lower (higher affinity) on $(UGUU)_5$. This result suggests the unwinding activity does not correlate with eIF4A2 affinity towards the RNA substrate. It should be noted that the differences in the measurements of K_D were greater than those for the unwinding reaction.

The next question was whether oligomerisation could instead drive the extent of RNA unwinding. For this, pre-formed eIF4A2-RNA complexes were resolved using EMSA (**Figure 3.8-3**, panel B). As expected, oligomeric complexes were formed most readily on the similar $(AG)_{10}$ and $(AGUG)_5$ RNAs (see **Figure 3.5-6**). All three complexes (monomer, dimer, and trimer) were detected on $(UGUU)_5$ RNA, and no RNA binding was observed on $(UCUC)_5$. Therefore, the gathered data suggests that neither the measured K_D, nor the extent of oligomerisation correlated with the unwinding activity.

As the question of what drives the unwinding reaction remains open, there are certain possibilities worth considering. Perhaps the differences observed in the dimensionless Kratky plot, or the different dimensions of the obtained complexes could play a role (**Figure 3.6-4**, **Table 3.6-1**). Additionally, as RNA unwinding is a dynamic process performed by eIF4A2 only in the presence of ATP, a question was posed whether the AMP-PNP RNA bound state could reflect what complexes actually take part in the reaction. As shown in **Figure 3.8-3**, panel C, complexes formed in presence of AMP-PNP are more stable than those formed in presence of ATP. Moreover, complexes resolved using EMSA are pre-incubated for an hour before visualisation, whereas the change in fluorescence

as measured in the unwinding assays can be observed in the first minutes of the reaction (see **Figure 3.8-1**, panel A and C). The measured AMP-PNP bound state allows for measurements of K_D excluding the influence of ATPase activity and the RNA binding dynamics. However, this could potentially mean that the measured AMP-PNP bound state does not reflect possible different k_{on} and k_{off} rates of eIF4A2 binding to RNA substrates. Thus, the RNA binding capacity and the K_D in presence of hydrolysable ATP could be different. To test this, eIF4A2 RNA binding was measured in presence of either ATP or AMP-PNP (data presented in **Table 3.8-1**). The K_D in presence of ATP for $(AG)_{10,}$ $(CAA)_6CA$, and $(AGUG)_5$ was found to be greater than the one measured in presence of AMP-PNP. The trend of affinity for different RNA substrates remained the same. Surprisingly, the K_D for $(UCUC)_5$ and $(UGUU)_5$ was smaller in presence of ATP compared to of AMP-PNP, further suggesting that different RNA sequences can employ different binding dynamics.

In all, eIF4A2 unwinding velocity differs depending on the sequence of the single-stranded region proceeding the double-stranded RNA. The unwinding activity was greater on substrates containing AG motifs. Similarly, the ATPase activity was higher for $(AG)_{10}$ than for the $(CAA)_6CA$ containing RNA. Additionally, for RNAs with single-stranded $(AG)_{10}$, $(AGUG)_5$ as well $(CAA)_6CA$ regions the unwinding activity correlated with both oligomerisation propensity as well as K_D. However, for other RNA substrates, i.e., $(UCUC)_5$, $(UGUU)_5$, the unwinding activity did not correlate with the oligomerisation nor the K_D, suggesting that further exploration of the dynamic eIF4A2-RNA complexes is necessary.

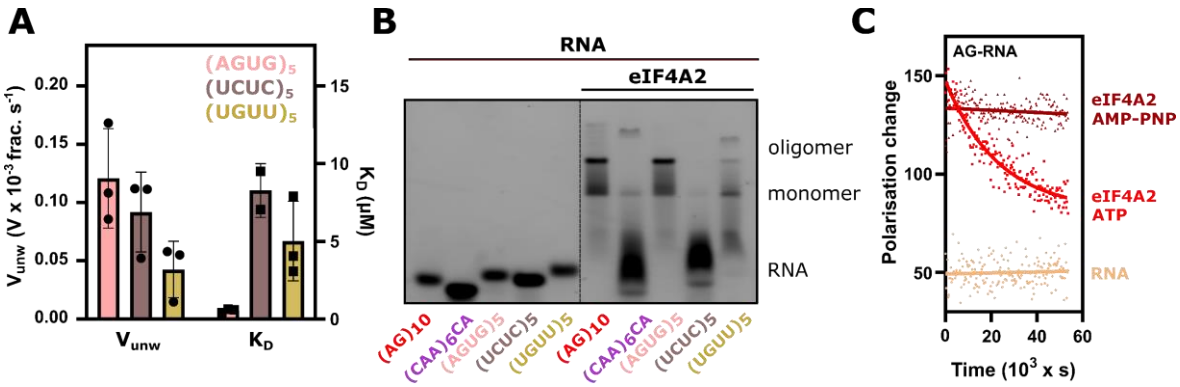

Figure 3.8-3 Unwinding activity does not follow K_D nor oligomerisation extent

A. Unwinding activity does not follow K_D. Unwinding activity (velocity) presented on left axis, and K_D (right axis) of eIF4A2. Unwinding activity was measured for a single concentration of eIF4A2 (5 μM) on 50 nM double-stranded RNA substrate, differing in the sequence of the single-stranded region: $(AGUG)_5$, $(UCUC)_5$, $(UGUU)_5$. K_D was measured by titrating eIF4A2 on the single-stranded RNAs, i.e., $(AGUG)_5$, $(UCUC)_5$, $(UGUU)_5$, in the presence of AMP-PNP. K_D was derived from Hill equation. N = 3.

B. Oligomerisation is dependent on RNA sequence. EMSA representing eIF4A2 (5 μM) formed complexes on 1 μM 20 nt single-stranded RNAs, i.e. $(AG)_{10}$, $(CAA)_6CA$, $(AGUG)_5$, $(UCUC)_5$, $(UGUU)_5$ in presence of AMP-PNP. Free RNAs on the left side of the gel. N = 2. Unrelated lanes removed for clarity. Note the surprising formation of a monomer and trimer on $(CAA)_6CA$ RNA in this experiment.

C. AMP-PNP formed complexes are more stable than ATP formed one. Representative (n = 3) RNA binding over a span of 60000 s. Free FAM-labelled RNA has polarisation around 50 and does not change over time (*yellow*). eIF4A2 (5 μM) bound to AG-RNA (50 nM) in presence of AMP-PNP is shown in *burgundy*, and in presence of ATP in *red*.

Table 3.8-1 Dissociation constant (K_D) of eIF4A2 to various RNA substrates

RNA	K_D (μM) AMP-PNP	K_D (μM) ATP
$(AG)_{10}$	0.75 ± 0.05	3.82 ± 0.42
$(CAA)_6CA$	3.24 ± 0.32	6.11 ± 0.61
$(AGUG)_5$	0.53 ± 0.12	2.59 ± 0.31
$(UCUC)_5$	8.27 ± 1.22	4.43 ± 0.47
$(UGUU)_5$	5.02 ±1.47	3.10 ± 0.36

K_D from polarisation experiments of eIF4A2 binding to $(AG)_{10}$, $(CAA)_6CA$, $(AGUG)_5$, $(UCUC)_5$, $(UGUU)_5$ in presence of AMP-PNP, measured after 1 hour of pre-incubation, n = 3, and immediately after assembling complexes in presence of ATP, n = 1. K_D obtained from Hill equation fitted to the data. Error = SEM from 3 individual replicates for AMP-PNP, and from technical duplicate for ATP. Note that the K_D for $(AG)_{10}$ differs from the one obtained previously using a different method (see Figure 3.5-4, panel C). Due to slight differences in the reaction conditions (see **Chapters 2.3.1.1**, **2.3.1.3**) the K_D for both $(AG)_{10}$ and $(CAA)_6CA$ is different to the one reported in Wilczynska *et al.*, 2019. The trend of K_D for $(CAA)_6CA$ RNA being much higher than for $(AG)_{10}$ one is consisted with what was observed previously for eIF4A1 in Iwasaki, Floor and Ingolia, 2016.

The sequence of the single-stranded overhang on a double-stranded RNA substrate drove the outcomes of unwinding reactions. This led to a question of whether the RNA sequence was the main determinant of the outcome. As previously reported (Rozen *et al.*, 1990; Rogers, Lima and Merrick, 2001) eIF4A is a bi-directional helicase. However, the concept of bi-directionality has not been explored for eIF4A2, and the influence of the single-stranded region's sequence on unwinding of substrates from 3' to 5' direction is currently not known. Additionally, employing RNA substrates that differ only through the positioning of the single-stranded region form the substrates used in **Figure 3.8-1** and **Figure 3.8-2** could potentially help to understand the importance of the sequence of single-stranded region in the unwinding and ATPase activities.

As a first step to addressing this, the activity of eIF4A2 on double-stranded RNA substrates, differing in the location of the single-stranded overhang was assessed. As **1)** the outcome of unwinding and ATPase activity, **2)** the propensity to oligomerise, and **3)** the K_D differed between substrates with $(AG)_{10}$ and $(CAA)_6CA$ 5'-overhangs differed, these single-stranded sequences were explored. Thus, unwinding and ATPase assays were performed for 3'$(AG)_{10}$ or 3'$(CAA)_6CA$ overhangs RNA substrates (**Figure 3.8-4**).

These experiments revealed that eIF4A2 exhibits 3'-to-5' helicase activity. Furthermore, a preference for the 3'overhang sequence was observed, with the initial velocity being the largest for 3'$(AG)_{10}$ RNA (**Figure 3.8-5** and **Table 3.8-2**). Moreover, the collected data suggests that eIF4A2 prefers 3' overhang substrate over the RNA sequence. However, when comparing only 5' overhangs or only 3' overhangs to each other, in both cases, $(AG)_{10}$ sequence was preferred by the helicase. As the affinities for the overhangs should remain the same (see **Table 3.8-1**) regardless of the direction, the obtained results unexpectedly point to a preference for unwinding in 3'-to-5' direction.

Next, the ATPase activity between tested RNA substrates was compared. Since, greater unwinding activity on the 5'$(AG)_{10}$ overhang substrate was associated with slightly higher ATPase activity (**Figure 3.8-2**), a similar outcome was expected for substrates with 3' single-stranded overhang. Surprisingly, the ATPase activity of both substrates with 3' overhang followed very closely the same trend (**Figure 3.8-5**, panel B). In general, despite the observed differences

in unwinding activity between RNA substrates with 5' and 3' overhangs, the ATPase activity was similar (**Table 3.8-2**, **Figure 3.8-5**, panel B).

In sum, the sequence of the single-stranded region on a double-stranded RNA substrate seems to be the main determinant of the outcome of the unwinding reaction. RNAs containing AG-motifs, i.e., $(AG)_{10}$ or $(AGUG)_5$ promote unwinding to the highest extent. Similarly, for the tested AG-RNAs both eIF4A2 affinity and the extent of eIF4A2 oligomerisation was greater than for the other tested RNAs. Moreover, this preference towards $(AG)_{10}$ containing RNA was also visible in the RNA substrates with 3' overhangs. Unexpectedly, the unwinding activity for both the $(AG)_{10}$ and $(CAA)_6CA$ 3'overhangs substrates was greater than the ones with 5'overhangs, suggesting that the unwinding activity can be modulated by the positioning of the single-stranded overhang. More broadly, this implicates eIF4A2 as a predominantly 3'-to-5' helicase. Finally, despite the clear differences in unwinding activity of eIF4A2 on the tested RNA substrates the variation in ATPase activity was lower. This suggested that the ATPase activity is less dependent on the outcomes of unwinding reaction as well as on the sequence of single-stranded overhang.

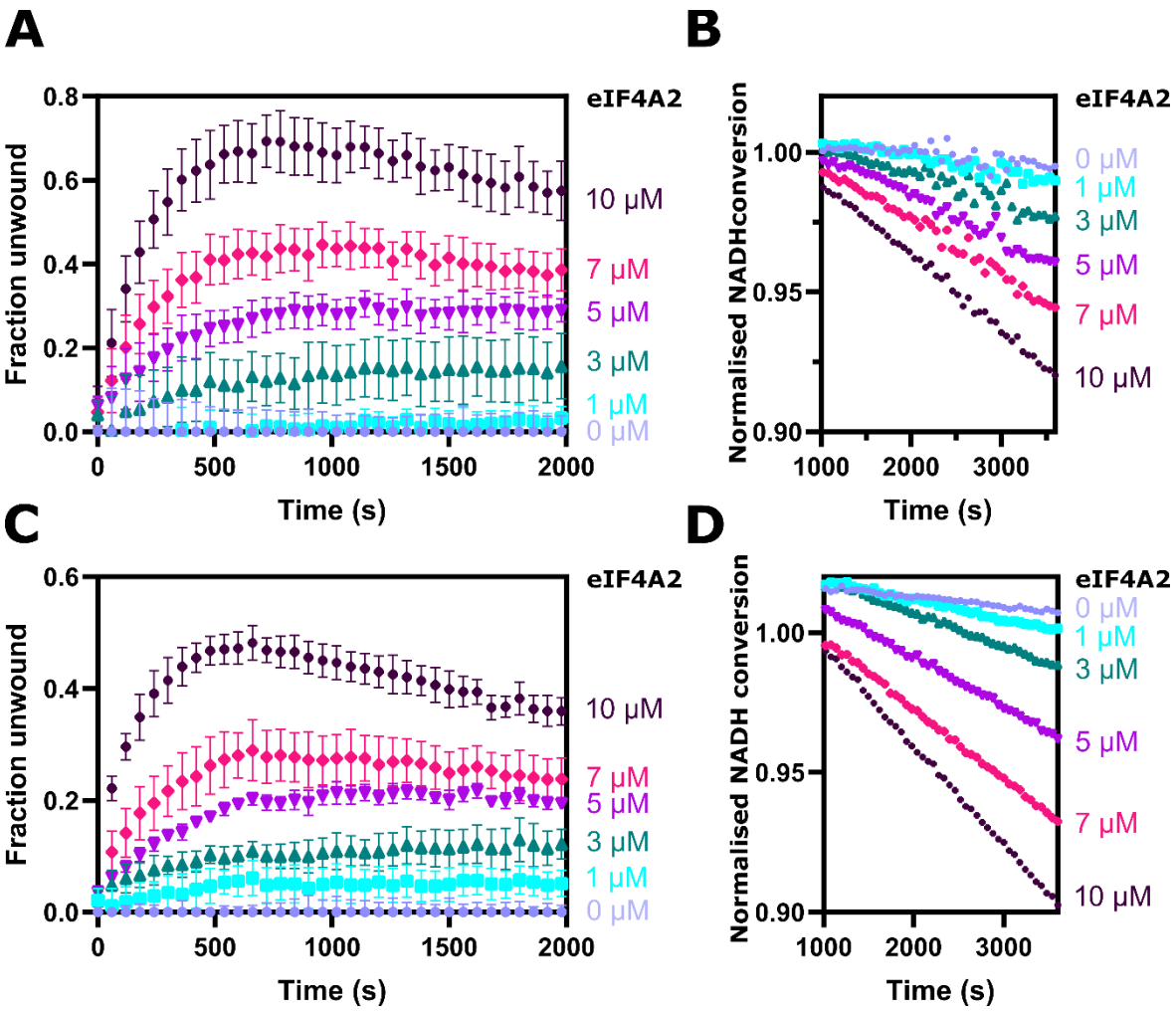

Figure 3.8-4 Oligomerised eIF4A2 performs unwinding and ATPase activities on RNA substrates with 3' single-stranded overhangs

- **A.** Unwinding activity of eIF4A2 on 3'$(AG)_{10}$ 24 BP RNA substrate presented as fraction unwound over time with indicated concentrations of eIF4A2. Data points are the mean and error of a technical duplicate. Representative graph, n = 3.
- **B.** Representation of ATPase activity of selected concentrations of eIF4A2 (0, 1, 3, 5, 7, 10 μM) on a 3'$(AG)_{10}$ 24 BP RNA substrate, presented in the same way as in **Figure 3.8-1**. Representative graph, n = 3.
- **C.** Unwinding activity of eIF4A2 on 3' $(CAA)_6CA$ 24 BP RNA substrate presented as fraction unwound over time with indicated concentrations of eIF4A2. Representative graph, n = 3, error bar – SEM from a technical duplicate.
- **D.** Representation of ATPase activity of selected concentrations of eIF4A2 (0, 1, 3, 5, 7, 10 μM) on 3' $(CAA)_6CA$ 24 BP RNA substrate, presented in the same way as in **Figure 3.8-1**. Representative graph, n = 3.

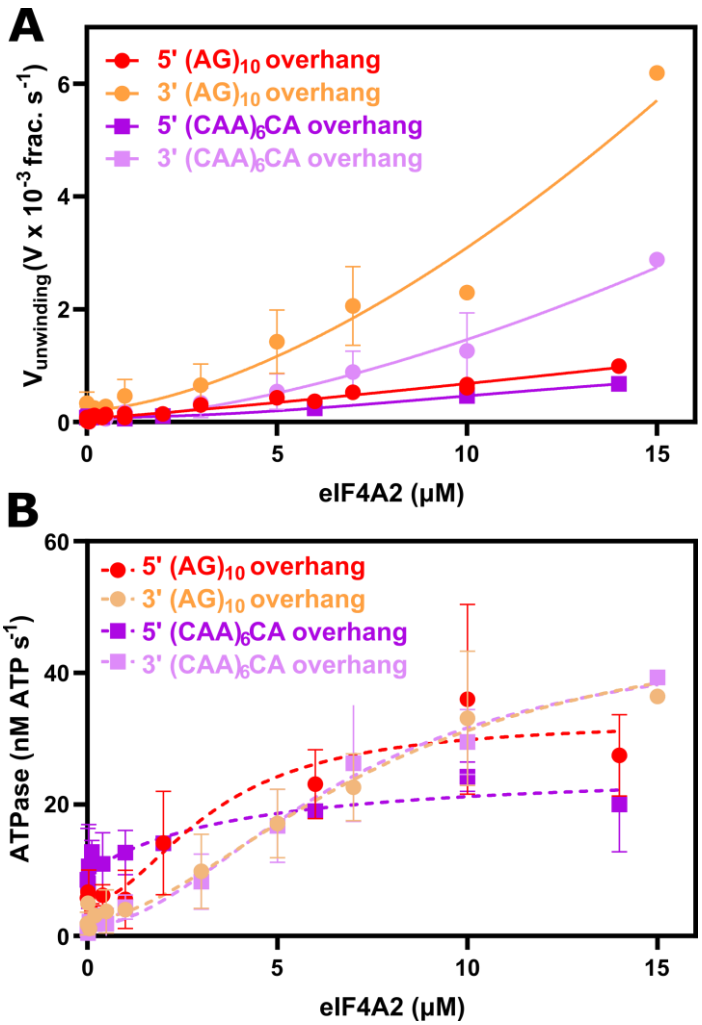

Figure 3.8-5 Unwinding activity but not ATPase of eIF4A2 is greater on a substrate with 3' overhang single-stranded region.

A. eIF4A2 unwinding activity presented as velocity of unwinding versus eIF4A2 concentration on RNA substrates with 5' and 3' single-stranded overhang. Hill equation was fitted to visualise the trend. N = 3, error = SEM.

B. ATPase activity performed simultaneously in separate wells on the same RNA substrates as in panel A, presented as nM ATP consumed per second versus eIF4A2 concentration, fit - Hill equation, n = 3, error = SEM.

Table 3.8-2 Velocity of unwinding and ATPase of 10 μM eIF4A2 on RNA substrates with 5' and 3' single-stranded overhangs

24BP RNA substrate overhang	V x 10^{-3} frac. s^{-1}	nM ATP s^{-1}
5'$(AG)_{10}$	0.651 ± 0.046	25.570 ± 5.055
5'$(CAA)_6CA$	0.463 ± 0.039	24.225 ± 2.227
3'$(AG)_{10}$	2.295 ± 0.084	33.100 ± 10.227
3'$(CAA)_6CA$	1.259 ± 0.678	29.500 ± 4.950

3.9. eIF4A2 activity is modulated by natural family of eIF4A inhibitors

High overexpression of eIF4A1 in many types of cancer is driving a growing interest in eIF4A inhibitors (Liang *et al.*, 2014; Modelska *et al.*, 2015; Cunningham, Chapman and Schatz, 2018; Gao *et al.*, 2020). As eIF4A2 has 90% of amino acid sequence identity with eIF4A1, the effect of the inhibitors on eIF4A2 was further explored. As the data presented so far probed the new and unexpected ability of eIF4A2 to oligomerise a major question was to examine the effect of inhibitors in the context of oligomerisation.

Two of the known eIF4A inhibitors have opposite mechanisms of action (see **Chapter 1.5.3**). Silvestrol, a rocaglate derivative, is known to induce tighter RNA binding (clamping) with longer half-life of eIF4A on RNA (Iwasaki, Floor and Ingolia, 2016; Wilczynska *et al.*, 2019) and hippuristanol, has been shown to inhibit the eIF4A RNA binding activity altogether (Cencica and Pelletier, 2016). Therefore, the effect of the two inhibitors on eIF4A2 RNA binding activity in oligomerised conditions was tested.

As shown in the **Figure 3.9-1** silvestrol stimulated formation of eIF4A2 oligomers on both $(AG)_{10}$ and CAA RNA. In turn, hippuristanol almost completely abolished RNA binding of eIF4A2 with most of the substrate remaining unbound and no oligomeric complexes detected. Since silvestrol had a direct influence on the oligomerisation potential of eIF4A2 its effect was explored further.

As silvestrol induced formation of trimeric complexes on AG-RNA as well as on the less preferred $(CAA)_6CA$ one, the question was posed whether it can stimulate oligomer formation on less-than-optimal binding interfaces. As previously (**Chapter 3.5**) eIF4A2 was incubated with RNAs of varying length of AG repeats and the obtained complexes were resolved using EMSA (**Figure 3.9-2**, panel A). In the presence of silvestrol, a dimer band was detected on the gel with the shorter 10 nt long RNA substrate. As 10 nt long RNA comprises single binding site for eIF4A, formation of oligomeric complexes on this RNA further supports protein-protein interaction mediated oligomerisation. As an additional control analytical gel filtration of eIF4A2 complexes formed on 10, 15, 20 nt long AG-RNA in presence of silvestrol was performed (**Figure 3.9-2**, panel B, see also

Figure 3.5-4). This technique supported that silvestrol enhances the oligomerisation potential of eIF4A2.

Subsequently, the K_D on RNA substrates in presence of silvestrol were quantified and compared to the conditions without the inhibitor (**Figure 3.9-2**, panel C, D see also **Figure 3.5-4**, panel C). Silvestrol improved the binding affinity (reduced dissociation constant) of eIF4A2 to each of the tested RNA substrates, however the largest reduction in K_D was observed for the shortest of the tested substrates.

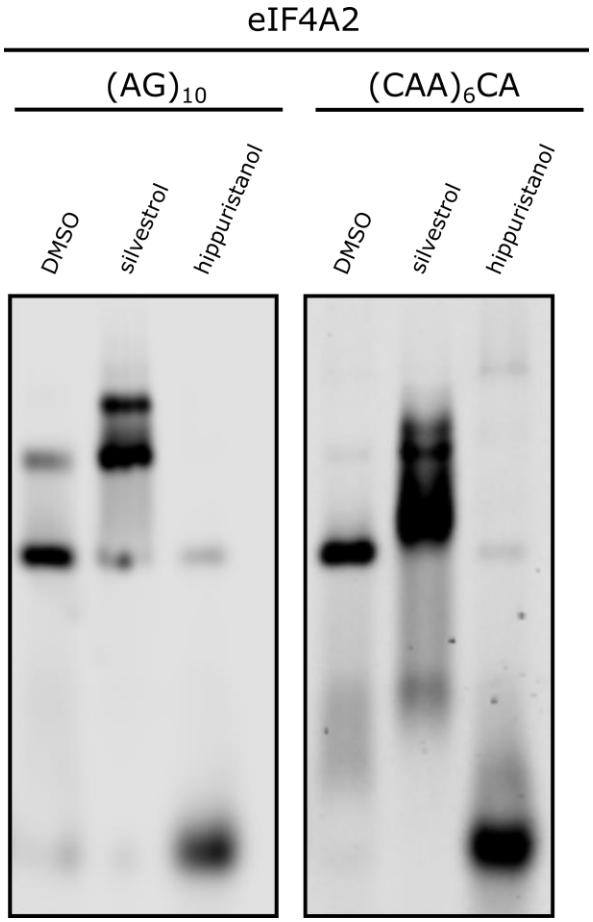

Figure 3.9-1 Silvestrol improves RNA binding and oligomerisation status of eIF4A2

EMSAs of 5 µM eIF4A2 in presence of either Dy780 labelled $(AG)_{10}$ (*left panel*) or Dy680 labelled $(CAA)_6CA$ (*right panel*); eIF4A2-RNA in the absence of inhibitors (DMSO), or in the presence of silvestrol (100 µM) or hippuristanol (50 µM). The protein was simultaneously incubated with 25 nM RNA, binding buffer (100 mM KCl, 2 mM $MgCl_2$, 20 mM HEPES pH=7.5), 1 mM AMP-PNP and inhibitors for 1 h at room temperature and the obtained complexes were subsequently resolved on 7% native acrylamide gel (100 V, 45 minutes) and visualised using Licor Odyssey.

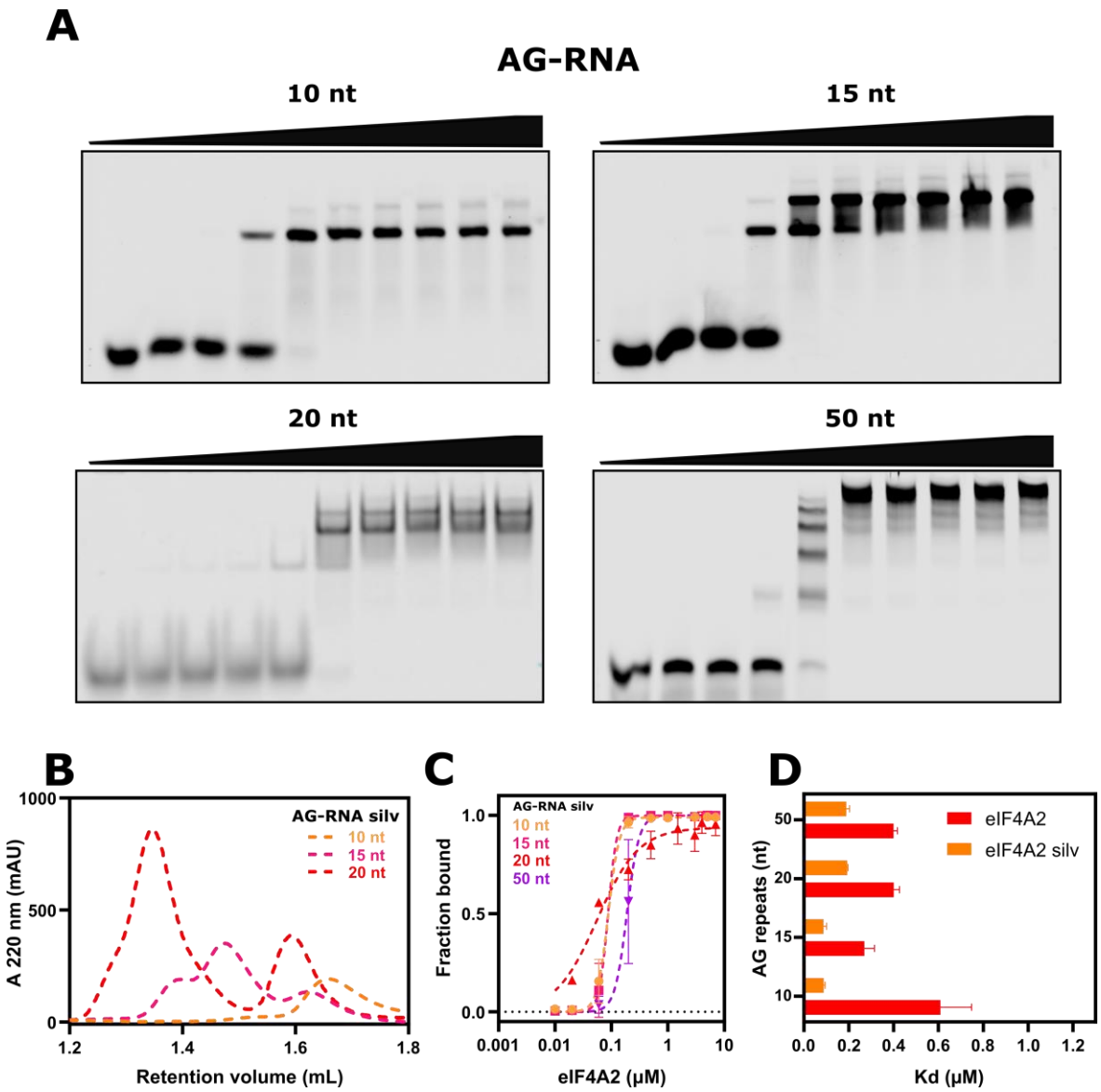

Figure 3.9-2 Silvestrol enhances eIF4A2 RNA binding affinity and induces oligomerisation on short RNA substrates

- **A.** Representative (n = 3) EMSAs of titration eIF4A2 (indicated as the triangles above each gel, 0 to 7 μM eIF4A2) on (25 nM) Dy780 labelled RNA substrate containing various lengths of AG stretches (10, 15, 20, 50 nt) in presence of silvestrol. Samples prepared, resolved, and visualised in the same way as described in **Figure 3.9-1**. Silvestrol induced oligomerisation on shorter RNA substates.
- **B.** Representative (n = 3) aSEC of 16 μM eIF4A2 and 4 μM AG RNA (10, 15, 20 nt) performed in the same way as in **Figure 3.5-4**, panel A, in presence of silvestrol. Silvestrol induces formation of oligomers.
- **C.** Quantification of RNA binding from EMSAs (n = 3), as presented in panel **A**. Fit – hill equation, error bar – SEM.
- **D.** Dissociation (K_D) constant obtained from fitted Hill equation to the data in panel **B**, compared to the K_D from **Figure 3.5-4**, panel B and C, in DMSO conditions. Silvestrol improves the binding affinity of eIF4A2 to polypurine RNA regardless of their length. Error bar – SEM.

It has been reported previously in a publication by Iwasaki, Floor and Ingolia, 2016 that eIF4A1 in presence of RocA (rocaglamide inhibitor) binds AG-RNA regardless of presence of AMP-PNP. Additionally, it has been shown that eIF4A2 has a natural preference for AG-RNA and in this aspect behaves like inhibited eIF4A1 (Wilczynska *et al.*, 2019). However, whether eIF4A2 can bind the AG-RNA without the presence of nucleotide and how the possible outcome influences oligomerised eIF4A2 has not been explored.

To test the influence of nucleotide as well as silvestrol eIF4A2 was pre-incubated with either $(AG)_{10}$, $(CAA)_6CA$, or A_{20} in presence of either DMSO (control) or silvestrol with **1)** no nt, **2)** 1 mM ADP + Pi, **3)** 1 mM AMP-PNP. $(AG)_{10}$ is the same polypurine RNA as used in previous reports (Iwasaki, Floor and Ingolia, 2016) that was demonstrated to be bound by eIF4A1 in presence of silvestrol without nt. In the same study $(CAA)_6CA$ was shown not to promote binding in the same conditions. As an additional control A_{20} was employed, that was shown in this thesis to induce formation of oligomers, however the previously measured K_D was higher than the one for $(AG)_{10}$ and $(CAA)_6CA$ (see **Figure 3.5-2**).

The RNA binding capacity was then visualised with an EMSA (**Figure 3.9-3**, panel A). It was observed, that eIF4A2, similarly to eIF4A1 was capable of silvestrol-induced, ATP-independent binding only to the AG-RNA substrate. However, silvestrol enhanced both binding, and oligomerisation on $(CAA)_6CA$ and A_{20} RNA substrates in presence of AMP-PNP. This ATP-independent binding to the AG-RNA, was further proved using an additional technique, fluorescence polarisation. eIF4A2, again, bound the AG-RNA, regardless of presence of AMP-PNP in the silvestrol condition (**Figure 3.9-3**, panel B).

In all, this suggests silvestrol influences eIF4A2 binding capacity in a similar manner to eIF4A1. The complexes formed on $(AG)_{10}$ in the -nt and ADP + Pi conditions corresponded to at least a dimer. Additionally, silvestrol stimulated formation of oligomers in presence of AMP-PNP on $(CAA)_6CA$ and A_{20}.

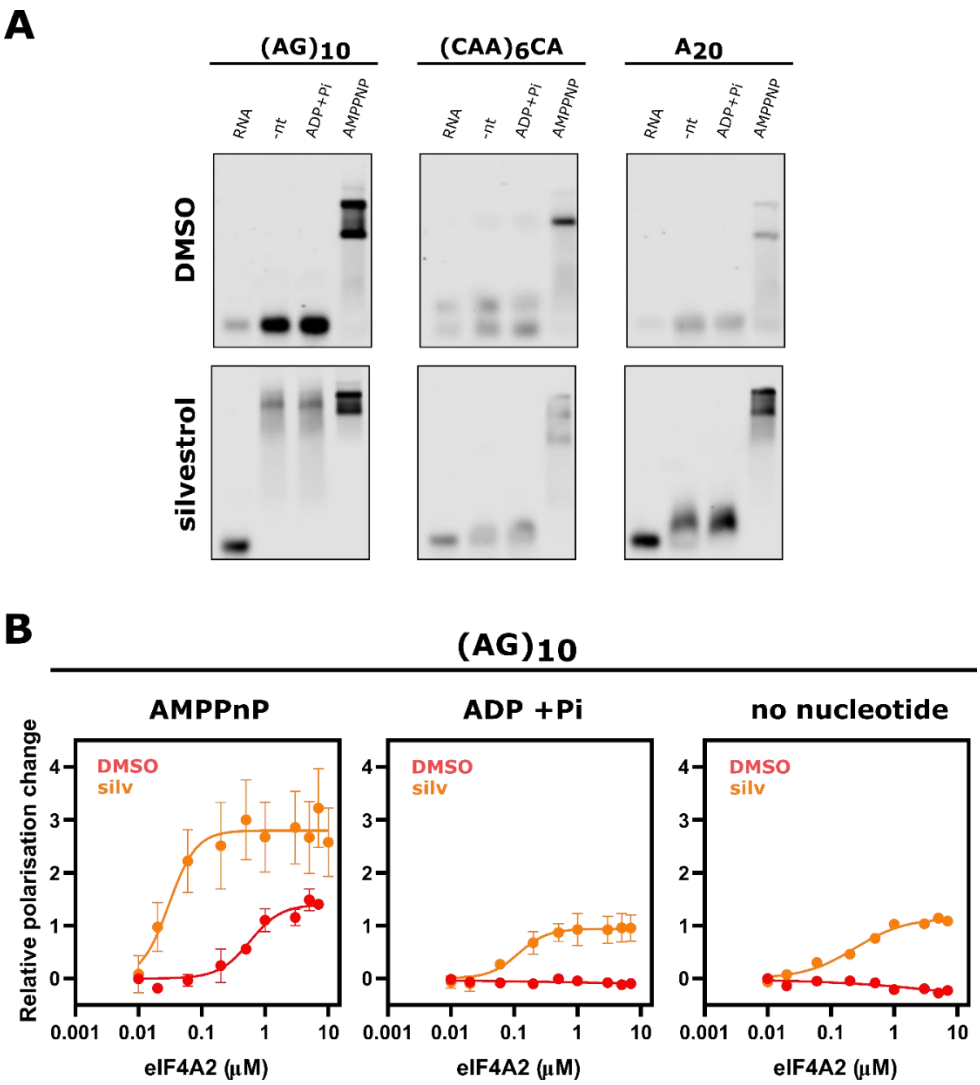

Figure 3.9-3 Silvestrol induces eIF4A2 RNA binding to polypurine RNA regardless of presence of ATP derivatives

A. Representative (n = 2) EMSAs of eIF4A2 (5 μM) to (25 nM) RNA substrate (D780 labelled $(AG)_{10}$, Dy680 labelled $(CAA)_6CA$, Dy780 A_{20}) in presence of DMSO (control; *top panel*) and silvestrol (*bottom panel*). The use of ATP analogue or lack of it is indicated above each lane. eIF4A2 binds RNA only in the presence of AMP-PNP in DMSO conditions, silvestrol induces RNA binding regardless of presence of nucleotide on polypurine RNA only.

B. Representative (n = 3) eIF4A2 RNA binding measured by fluorescence polarisation to 50 nM FAM-labelled $(AG)_{10}$ RNA substrate. Samples were prepared in the same manner as in panel **A**. Silvestrol induces polypurine RNA binding of eIF4A2 in presence of ADP + Pi and no nucleotide. Error – SEM from technical duplicate, fit – Hill equation.

Both higher oligomerisation and higher affinity of eIF4A2 towards AG-RNA were correlated with higher unwinding and ATPase activities (see **Figures 3.8-2**, **3.8-3**, and **Table 3.8-1**). As silvestrol improved both the oligomerisation and K_D of eIF4A2 on AG-RNA a question was asked how it potentially influences eIF4A2 catalytic capacities (see **Figures 3.9-1**, **3.9-2**). As silvestrol is an inhibitor that acts on eIF4A1 the expectation would be that it inhibits eIF4A activities especially in the cancer setting.

Here, eIF4A2 unwinding and ATPase reactions in presence of silvestrol were explored. As shown in the **Figure 3.9-4**, panel A, eIF4A2 unwinding activity was greater on both the $(AG)_{10}$ and $(CAA)_6CA$ 5'overhang substrates. Silvestrol enhanced not only the amount of unwound substrate but also the velocity with which the unwinding was performed for $(AG)_{10}$ 5'overhang RNA (**Figure 3.9-4**, panel B, **Table 3.9-1**). The same trend was observed for the ATPase activity (**Figure 3.9-4**, panel C and **Table 3.9-1**).

As silvestrol is an inhibitor the improvement of activities seemed contra intuitive. However, it has been reported previously that another eIF4A inhibitor – pateamine A – stimulated eIF4A1 RNA binding, unwinding and ATPase activities (Bordeleau *et al.*, 2005). Additionally, the observed earlier improvement of binding (**Figure 3.9-2**) seems to correlate with increase of the catalytic activities.

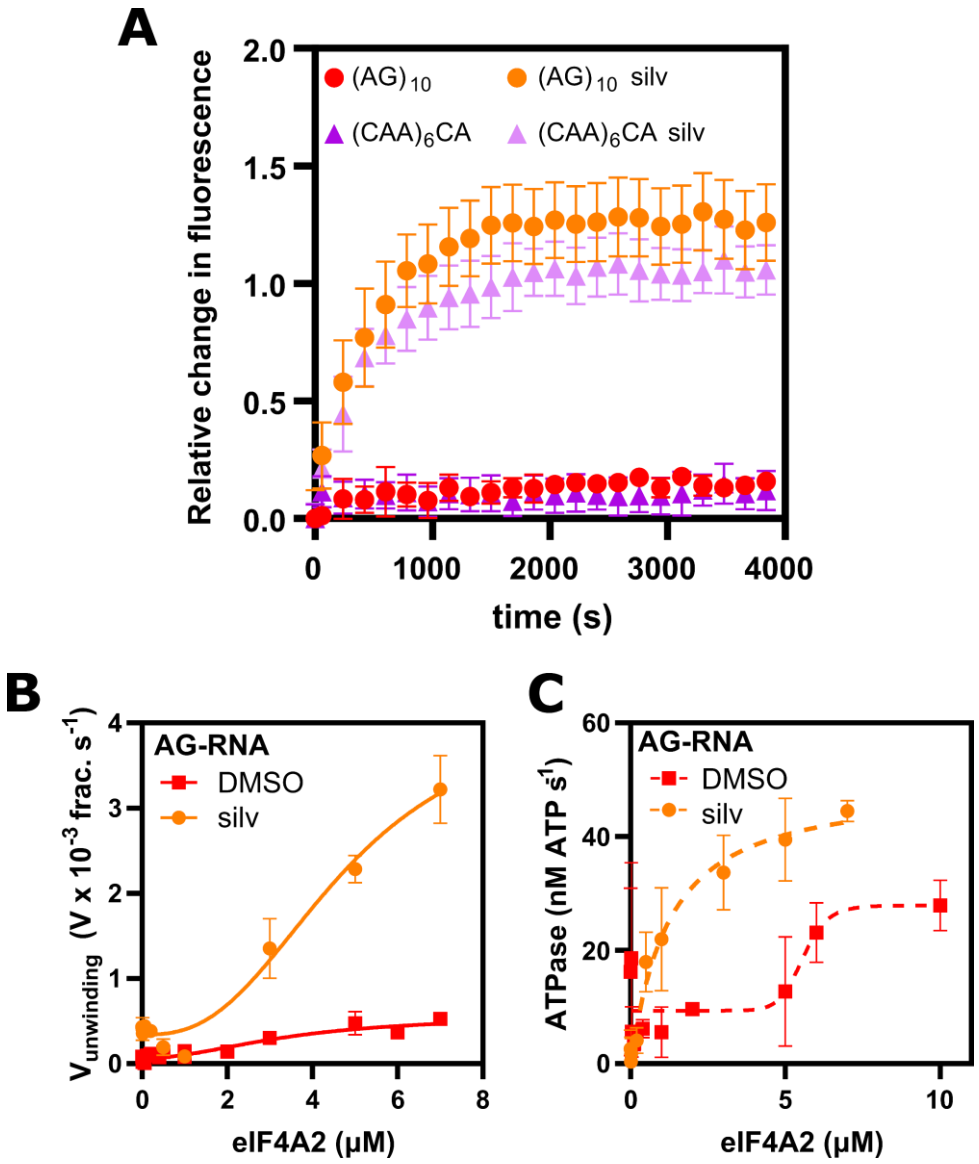

Figure 3.9-4 Silvestrol enhances eIF4A2 catalytic activities

A. Representative (n = 3) unwinding activity of 5 μM eIF4A2 in presence and absence of silvestrol on double-stranded RNA substrates containing 5' single-stranded overhang consisting of either $(AG)_{10}$ or $(CAA)_6CA$ RNA stretch. The graph is presented as relative change in fluorescence (change was measured by dividing the measured fluorescence by the starting value – before the start of the reaction, and subsequently subtracting the obtained (=1) starting value) over time. Silvestrol induces greater unwinding regardless of RNA substrate. Error bars – SEM from a technical duplicate.

B. Comparison of velocity of unwinding for an RNA substrate with $(AG)_{10}$ single-stranded 5'overhang over the concentration of eIF4A2 in presence of either DMSO (red) or silvestrol (orange). Error bars - SEM, n = 3, fit - Hill equation. Silvestrol induces greater velocity for each tested eIF4A2 concentration.

C. Comparison of ATPase activity presented as velocity of ATPase over eIF4A2 concentration (0 to 14 μM) in presence of DMSO (red) and silvestrol (orange) on RNA substrate containing 5' single stranded overhang consisting of $(AG)_{10}$. Silvestrol induces higher ATP conversion. N = 3, error bars - SEM, fit - Hill equation.

Table 3.9-1 Velocity of unwinding and ATPase of 5 μM eIF4A2 on AG-RNA substrates

5'$(AG)_{10}$ 24BP RNA	V x 10^{-3} frac. s^{-1}	nM ATP s^{-1}
DMSO	0.426 ± 0.004	12.800 ± 2.300
silvestrol	1.950 ± 0.201	39.966 ± 4.561

In all, the gathered data indicates that both hippuristanol and silvestrol exert their function on eIF4A2. Hippuristanol abrogated RNA binding almost completely. The further exploration of silvestrol influence on eIF4A2 suggested that silvestrol enhances both the RNA binding as well as oligomerisation, even on the less optimal RNA substrates. Additionally, similarly as reported in the literature (Iwasaki, Floor and Ingolia, 2016), silvestrol induced ATP-independent AG-RNA binding. This potentially opens a question on the effect of silvestrol on eIF4A2 activities in the cancer setting. Additionally, the catalytic capacities of eIF4A2 were enhanced by silvestrol, an induction of activities not unheard of for other eIF4A inhibitors (Bordeleau *et al.*, 2005).

3.10. Unwinding is performed by free and oligomerised eIF4A2

Throughout this thesis the formation of oligomeric eIF4A2 was thoroughly described. It has been explored what influences oligomerisation of eIF4A2 and what enzymatic capacities the oligomeric eIF4A2 has. Additionally, it was demonstrated that eIF4A2 may oligomerise in live cells (**Figure 3.7-3**). However, the existence of monomeric eIF4A2 in cells cannot be excluded. Moreover, on certain RNAs eIF4A2 formed mostly monomeric complexes (**Figures 3.5-2**, **3.5-6**). Therefore, the question about the activity of monomeric eIF4A2 remains open.

As described previously eIF4A2 forms oligomers only in the presence of RNA and, with the protein being in excess over the RNA substrate (**Figure 3.5-1**). Therefore, by modulating the protein to RNA ratio it should be possible to change the oligomerisation status of eIF4A2. The more RNA added should create a situation where the protein is in monomeric conditions. To test the monomeric eIF4A2 catalytic capacities, the unwinding and ATPase reactions thus should be performed with addition of competitor RNA. However, as the unwinding activity of eIF4A2 was measured on a fluorescently labelled RNA substrate (see **Figure 3.3-1**, panel A) and the use of more labelled RNA would influence the sensitivity of the detection, a non-labelled single-stranded RNA would be a better choice as a competitor RNA. Additionally, ATP is necessary for unwinding activity, therefore certain precautions need to be taken, to assure that eIF4A2 stays bound to the unwinding substrate.

As seen previously, silvestrol induced eIF4A2 binding to AG-RNA without the presence of ATP analogue (**Figure 3.9-3**). This could mean, that silvestrol could potentially serve as a tool, where eIF4A2-unwinding substrate complexes can be formed before the start of the reaction with ATP. Additionally, complexes formed with silvestrol are more stable, as the RNA strand release is much slower than in the control condition (**Figure 3.10-1**).

To test whether eIF4A2 would remain bound to the RNA substrate in presence of competitor RNA, eIF4A2 was first preincubated with Dy780 $(AG)_{10}$ RNA in presence of silvestrol. After the preincubation time has elapsed, increasing

amounts of unlabelled competitor RNA (either $(AG)_{10}$ or $(CAA)_6CA$) and 1mM AMP-PNP were added to the pre-formed complexes and incubated for equivalent amount of time. Subsequently the complexes were resolved using EMSA (**Figure 3.10-2**, panel A). As the hypothesis predicted, with increasing concentration of competitor RNA oligomerisation status of eIF4A2 has changed, however the protein remained fully bound to the labelled RNA.

Additionally, $(AG)_{10}$ competitor RNA had greater effect than $(CAA)_6CA$ which can be explained by higher K_D of eIF4A2 on $(CAA)_6CA$ (see **Table 3.8-1**) and possibly the different oligomerisation potential.

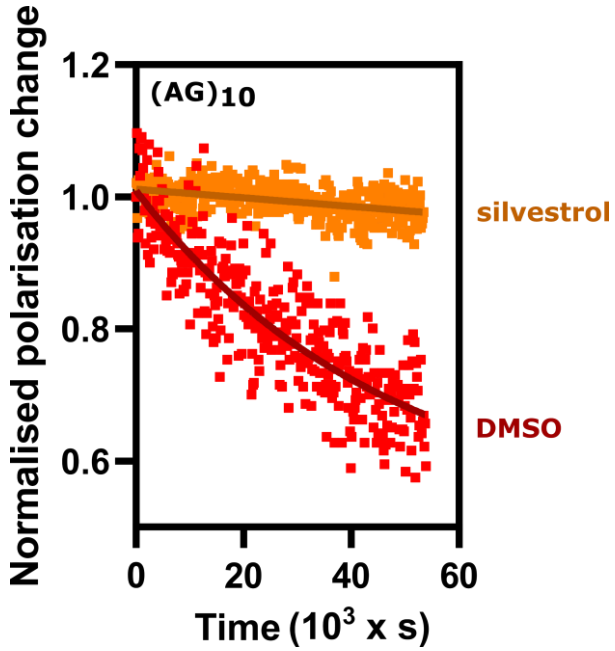

Figure 3.10-1 Silvestrol blocks the RNA strand release of eIF4A2

$(AG)_{10}$ RNA (50 nM) release experiment of 5 μM eIF4A2 in presence of DMSO (control) and silvestrol (100 μM) in presence of ATP measured by polarisation. The complexes were mixed in room temperature and immediately placed in a plate reader to observe the change in polarisation. Single, representative, technical replicate shown, for clarity of presentation, n = 3. Data normalised to starting value, and RNA only sample used as a baseline (0). Silvestrol prohibits RNA release in comparison to control conditions.

As it was possible to manipulate the oligomerisation status of eIF4A2, the catalytic activity of the scavenged complexes was assessed. Here, eIF4A2 was preincubated in presence of silvestrol with RNA substrate containing 5' single-stranded $(AG)_{10}$ overhang, representing the more traditional role of the helicase in unwinding from 5'-to-3' direction. Then the $(AG)_{10}$ or $(CAA)_6CA$ RNA competitor was added, and the samples were incubated for the same amount of time. Subsequently, the unwinding reactions were started by addition of ATP. Addition of $(AG)_{10}$ competitor RNA almost completely abolished the unwinding activity of eIF4A2 (**Figure 3.10-2**, panel B). The influence of the $(CAA)_6CA$ competitor RNA was less potent (**Figure 3.10-2**, panel C). The velocity of unwinding (**Figure 3.10-2**, panel D) was compared between the reactions with the two competitor RNAs. The velocity of unwinding decreased to almost 0%, however this change was not as consistent for the $(CAA)_6CA$ RNA. The difference here could stem from the mode of binding, as $(CAA)_6CA$ was not bound by eIF4A2 in presence of silvestrol without nt (see **Figure 3.9-3**, panel A). Therefore, the binding to the $(CAA)_6CA$ RNA could only occur in the presence of ATP, which would allow for the reaction to start on the already pre-formed complexes on the unwinding substrate.

It should be noted that the resolved complexes in the presence of AMP-PNP may not fully reflect what happens in a dynamic reaction in presence of ATP. Additionally, the decrease in activity was observed even for the $(AG)_{10}$ competitor RNA concentration that did not cause a large change in oligomerisation, and eIF4A2 was still in excess. Similar decrease in unwinding activity for comparable protein to RNA ratio was previously reported in the literature (Rogers, Lima and Merrick, 2001). Potentially, in this situation all of the protein is bound to the RNA in oligomeric conditions. A possible explanation could be that the unwinding activity is performed by the free eIF4A2 that is recruited to the double-stranded region by the already formed oligomer. In the case of $(CAA)_6CA$ competitor RNA not all of the free protein was scavenged, therefore the reduction in the unwinding activity was not as high.

Additionally, the influence of the competitor RNA on eIF4A2 ATPase activity was tested (**Figure 3.10-2**, panel E). For both of the tested competitor RNAs ATPase activity increased with increase of the concentration of competitor, indicating presence of enzymatically active eIF4A2.

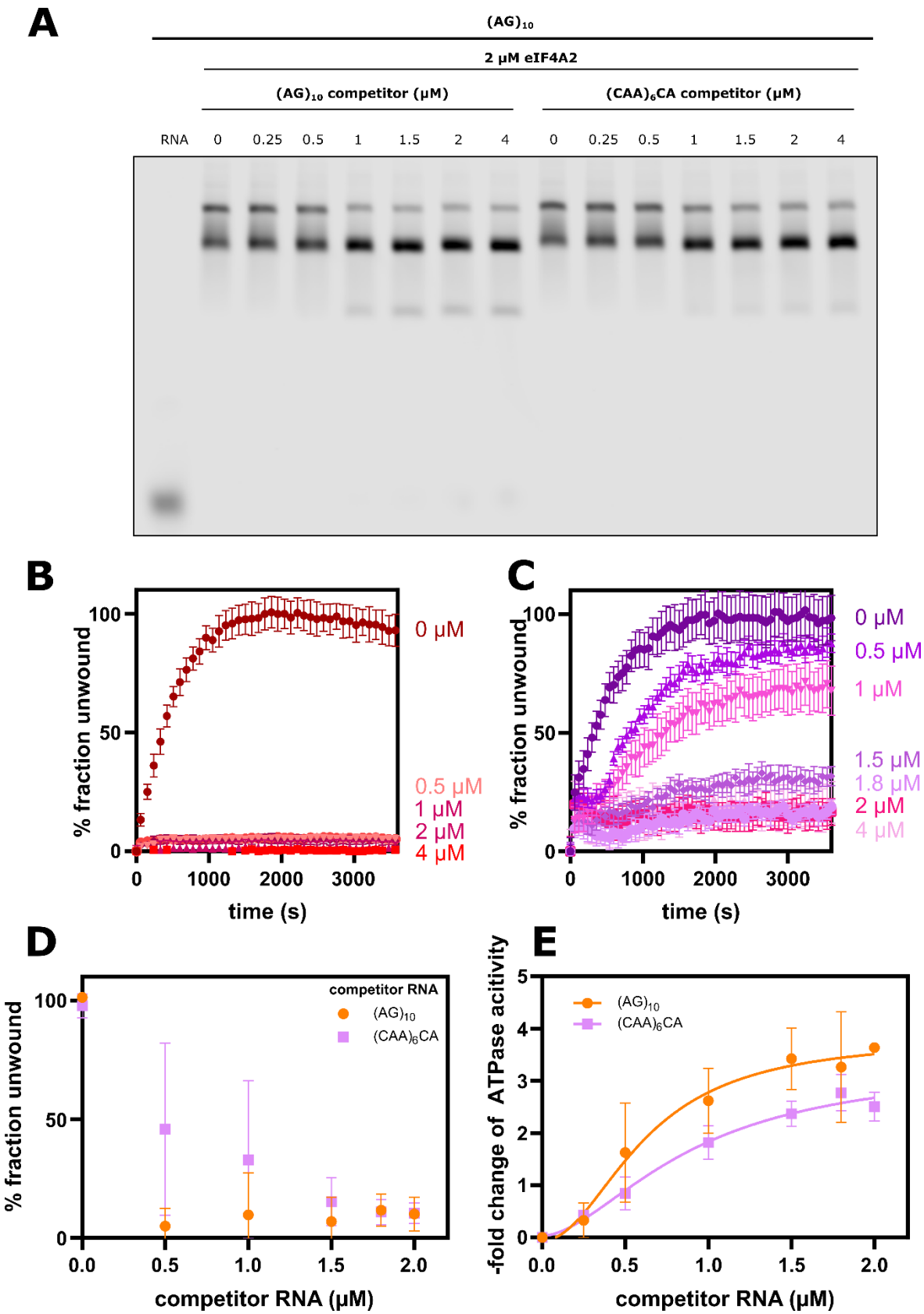

Figure 3.10-2 Unwinding activity is performed by excess of free and oligomerised eIF4A2

(figure legend on the next page)

A. Representative EMSA (n = 3) of (2 μM) eIF4A2 binding to (25 nM) Dy780 $(AG)_{10}$ RNA in presence of increasing concentration (0 to 4 μM) of unlabelled competitor RNA $(AG)_{10}$ and $(CAA)_6CA$. Competitor RNA induced change in oligomerisation status (more monomer formation) without releasing the RNA substrate. $(AG)_{10}$ - competitor RNA induced change in oligomerisation status to a greater extent than $(CAA)_6CA$ competitor.

B. Representative (n = 5) unwinding activity of eIF4A2 on RNA substrate with $(AG)_{10}$ single-stranded overhang and double-stranded region in presence of varying amounts of $(AG)_{10}$ competitor RNA. Samples prepared in the same way as in the panel **A**, reactions started with ATP (no AMP-PNP in this reaction). Fraction unwound by eIF4A2 without competitor was established as 100% fraction unwound, the percentage of other conditions was calculated using ratio of the unwound fractions to the 100%. eIF4A2 does not unwind double-stranded RNA in presence of single-stranded $(AG)_{10}$ competitor RNA. Error bars - SEM, technical duplicate presented.

C. Representative (n = 3) unwinding activity of eIF4A2 on RNA substrate with $(AG)_{10}$ single-stranded overhang and double-stranded region in presence of varying amounts of $(CAA)_6CA$ competitor RNA. Samples prepared and data analysed in the same manner as in panel **B**. eIF4A2 unwinding activity is reduced in presence of $(CAA)_6CA$ competitor RNA. Error bars - SEM, technical duplicate presented.

D. Fraction unwound in presence of competitor RNA. Graph created based on unwinding activity as presented in panels **B** and **C**. N = 5 for $(AG)_{10}$ competitor and n = 3 for $(CAA)_6CA$ competitor, error bar - SEM. Presence of competitor reduces unwinding activity of eIF4A2.

E. ATPase activity of 2 μM eIF4A2 in presence of competitor RNA. Reactions performed simultaneously as the unwinding reactions presented in panels **B** and **C** in reactions supplemented with NADH, PEP and LDH/PK mix. Graph presented as fold change of ATPase activity with ATPase activity of eIF4A2 without competitor RNA used as a starting value. N = 5 for $(AG)_{10}$ competitor and n = 3 for $(CAA)_6CA$ one. Error bars – SEM, fit – Hill equation.

In sum, in the previous subchapter (**Chapter 3.8**) unwinding activity was detected on all of the tested RNA substrates. This activity was observed for high excess of eIF4A2 over the RNA, which correlated with formation of oligomeric complexes. As shown here, the eIF4A2 oligomerisation status can be modulated by changing the concentration of RNA. However, in the tested conditions a fully monomerised eIF4A2 was not observed. Perhaps, due to dynamic nature of the unwinding reaction the true oligomerisation status could be different. As the almost complete abrogation of the unwinding activity was seen for $(AG)_{10}$ competitor to eIF4A2 ratio that in other tested conditions could potentially still promote oligomerisation (see **Figure 3.5-1**), the gathered data may indicate that the unwinding is performed by a cooperation between the oligomerised, RNA bound eIF4A2 and the free protein recruited to the double-stranded region.

3.11. Chapter discussion

This chapter was focused on a thorough biochemical characterisation of DEAD-box helicase eIF4A2, a highly similar paralogue of eIF4A1. As eIF4A1 is the more abundant paralogue it has been studied in a greater detail than eIF4A2 (Nielsen, McMaster and Trachsel, 1985; Nielsen and Trachsel, 1988; Galicia-Vazquez *et al.*, 2012). eIF4A1 overexpression has been implicated in many types of cancer and a mostly opposite correlation has been observed for eIF4A2 (Ji *et al.*, 2003; Yan *et al.*, 2011; Lomnytska *et al.*, 2012; Shaoyan *et al.*, 2013; Liang *et al.*, 2014; Modelska *et al.*, 2015). Therefore, a detailed biochemical characterisation of eIF4A2 was imperative to understand the mechanisms of actions governing eIF4A2 that could potentially help elucidate the differences between the two paralogues and allow for more specialised targeting in the future.

While investigating the biochemical characteristics of heterologously produced highly pure eIF4A2 (**Figure 3.2-1**) a novel oligomeric version of the helicase was discovered (**Figure 3.3-1**, **3.4-1**). The concept of oligomerisation in the context of eIF4A2 is unprecedented, however the phenomenon of multimerisation for other DEAD-box helicases has been previously observed (Putnam *et al.*, 2015; Kim and Myong, 2016; Sharma *et al.*, 2017) (see also **Chapter 1.5.1**).

This study explored how eIF4A2 oligomeric complexes are formed and the presented data suggest that the eIF4A2 oligomerisation is dependent both on the presence of RNA and protein being in excess (**Figure 3.5-1**). The necessity of presence of RNA for eIF4A2 oligomerisation is different to what has been previously described for Ded1p (Putnam *et al.*, 2015), suggesting a different mechanism involved in formation of those oligomeric complexes. However, the crystal structure of DDX3 (human ortholog of Ded1p) presented the oligomer only in presence of RNA (Song and Ji, 2019).

The requirement for eIF4A2 to be in excess over RNA in order to oligomerise has potential implication *in vivo*. eIF4A2 is thought to be less abundant in cells than eIF4A1, however its expression depends on the type of the tissue as well as the state of the cell (Galicia-Vazquez *et al.*, 2012, 2014). One example is a higher expression of eIF4A2 in differentiated cells (Williams-Hill *et al.*, 1997). Additionally, the relative abundance of eIF4A2 as quantified in Galicia-Vaquez *et*

al., 2012 is higher than eIF4A1 in foetal brain, heart, kidney and adult brain, skeletal muscles, ovaries and leukocytes. Depending on the local concentrations and abundance as well as the affinity towards the RNA it is possible that eIF4A2 oligomers are highly prevalent *in vivo*.

The oligomeric complexes were shown to form predominantly on AG-RNA (polypurine motifs) (**Figure 3.5-2**). As eIF4A2 has been shown previously **1)** to have the same preference to AG-RNA as inhibited eIF4A1, and **2)** to exert repression through binding to the AG-rich motifs in the 5'UTRs of mRNAs (Wilczynska *et al.*, 2019), it is possible that the oligomeric form of eIF4A2 takes part in the repression.

Additional features have been identified in mRNAs associated with eIF4A, i.e., long 5'UTRs and high GC content or only C content (Rubio *et al.*, 2014; Wolfe *et al.*, 2014; Modelska *et al.*, 2015; Waldron *et al.*, 2019). However, the previous studies either focused on eIF4A1 or did not differentiate between the two paralogues. Nevertheless, the studies presented in this thesis cannot exclude the involvement of eIF4A2 in either monomeric or oligomeric form on RNAs exerting the stated above features. The other tested RNA sequences promoted oligomerisation to varying extent. In line with the high GC content, $(GUGCU)_4$ RNA promoted formation of oligomers to a higher extent than $(CAA)_6CA$. Additionally, the oligomerisation was shown to not be correlated with eIF4A2 K_D to the tested RNAs (**Figures 3.5-2**, **3.5-6**). As the long uninterrupted stretches of AG motifs are uncommon in native mRNAs, the positioning of AGs within the RNA substrates was investigated. This showed that eIF4A2 requires at least four purines next to each other and an appropriate positioning of the flanking regions to readily oligomerise (**Figure 3.5-6**).

Moreover, both the RNA binding site and optimal RNA length for oligomerisation was investigated (**Figure 3.5-4**). The gathered data suggest that the optimal binding site increases from 10 to 15 nt, which is in agreement with previous studies (Abramson *et al.*, 1987; Alexandra Z. Andreou and Klostermeier, 2013). The available crystal structure presenting eIF4A1 bound to 10 nt long AG-RNA in presence of RocA (Iwasaki *et al.*, 2019) shows that eIF4A1 binds fully to the 10 nt, leaving no flanking regions that would allow for another protein to bind to the same RNA. The gathered data showed that silvestrol induced oligomerisation

on exactly the same 10 nt AG-RNA, which further supports RNA mediated protein-protein interaction dependent oligomerisation (**Figure 3.9-2**).

Moreover, in this chapter in-depth structural analysis of eIF4A2 using SAXS was presented. SAXS provides a structural information in solution and does not require any prior structural information (Tsutakawa *et al.*, 2007). The recently predicted eIF4A2 structure (AF-Q14240-F1) with AlphaFold 2.0 (Jumper *et al.*, 2021) features a similar elongated extension visible in apo-eIF4A2 SAXS envelope model (**Figure 3.6-3**, see also **Figure 1.5.1-1**). The positioning of the extension in the predicted structure differs, however the model of confidence in this region is low, which could suggest that the predicted structure resembles the envelope model to even higher degree. The gathered data demonstrated that RNA bound state is more folded than both the apo and AMP-PNP bound eIF4A2. The structural data gathered for the oligomeric eIF4A2 provides a direct evidence that eIF4A2 is able to form the oligomeric complexes, and that their dimensions differ from the monomeric ones (**Figure 3.6-2**, **Table 3.6-1**). The calculated R_g for the oligomeric complexes is larger than for the monomeric ones indicating larger radius from the centre of gravity in the oligomer, and possible different mass distribution. The envelope models of the monomers formed on $(AG)_{10}$, and $(CAA)_6CA$ RNAs, show high degree of similarity (**Figure 3.6-5**). However, the differences in the d_{max} as well as in the dimensionless Kratky plot could indicate a minor disparity in how eIF4A2 binds those two RNAs with different propensities to induce oligomer formation (**Figure 3.6-4**, **Table 3.6-1**).

Subsequently, both oligomeric and monomeric complexes on RNAs with double-stranded regions, differing only in length and sequence of 5'overhang were investigated. This analysis suggested differences in all paired monomers and oligomers with oligomers being less globular and folded (**Figure 3.6-7**). Moreover, $(AG)_{10}$ 24BP oligomer had a more defined and rigid structure than the $(CAA)_6CA$ 24BP eIF4A2 oligomer. The presence of oligomers on the $(AG)_5$ 24BP RNA substrate, a 10 nt single-stranded region that did not promote oligomer formation without the presence of inhibitor (**Figure 3.5-3**) suggests that there is at least a partial interaction with the double-stranded region. This has been suggested previously in the literature (Rogers, Lima and Merrick, 2001), however other reports contested this activity (Lorsch and Herschlag, 1998a). The

formation of eIF4A2 oligomers on both $(AG)_5$ 24BP and $(CAA)_6CA$ 24BP (**Appendix 1 Figures 1-5**, **1-6**) to a lower extent than on $(AG)_{10}$ 24BP RNA further emphasises the importance of the optimal binding site and the RNA sequence of the single-stranded overhang in oligomerisation. The effect of single-stranded RNA on the conformation and activities of eIF4A has been investigated for the yeast ortholog (Andreou, Harms and Klostermeier, 2019), further implicating the single-stranded RNA as a determinant of eIF4A behaviour. Additionally, the dissimilar complexes obtained on different RNAs are in stark contrast and provide evidence against the previously described lack of sequence specificity of eIF4A (Abramson *et al.*, 1987).

Furthermore, as the determination of the RNA position and influence in the modelled SAXS envelopes cannot be sufficiently distinguished from the protein in the formed complexes, a use of a different technique would be advisable. One example of a technique to use together with SAXS could be SANS (small-angle neutron scattering).

The potential of eIF4A2 to oligomerise was also investigated in live cells. As for the FLIM-FRET technique the protein of interest needs to be tagged with a fluorophore the influence of the tag on eIF4A2 oligomerisation was investigated. The tests on the tagged-eIF4A2 demonstrated that the tag does not prohibit formation of oligomers (**Figure 3.7-2**). The tagged-eIF4A2 had cytosolic localisation, visible in the fluorescence distribution in live cells (**Figure 3.7-3**), which suggested endogenous localisation. The change in fluorescence lifetime, i.e., the measurement indicating interaction, was only observed for tagged-eIF4A2 and not for the free fluorophores, suggesting eIF4A2-eIF4A2 interaction in cells. Additional control (**Figure 3.7-4**) showing co-precipitation of tagged-eIF4A2 and eIF4A2 WT in RNase 1 conditions indicated direct interactions between eIF4A2-eIF4A2. As eIF4A2 can form trimeric complexes, perhaps a use of modified FRET could provide additional information about the distribution of oligomeric complexes in cells. Methods described in Sun *et al.*, 2010; Hoppe *et al.*, 2013 suggest use of three-fluorophore system in which interactions between multiple proteins can be measured.

As shown in **Figure 1.3.2-2** eIF4G has two binding sites for eIF4A and although eIF4G is not the preferred interaction partner of eIF4A2, it has been shown

previously that overexpression of eIF4A2 causes it to associate with eIF4G (Wilczynska *et al.*, 2019). Taken together, the possibility of eIF4G-mediated in cell interaction between eIF4A2 cannot be excluded. However, the native concentrations of both eIF4A1 and eIF4A2 as well as the amount of tagged eIF4A2 should far exceed the in-cell concentration of eIF4G (see Bekker-Jensen *et al.*, 2017 for quantification of endogenous HeLa cell proteome). This suggests that at least part of the observed signal stems from eIF4A2-eIF4A2 eIF4G-independent interaction. For additional supporting evidence please refer to **Appendix 3 Figure 3-3**. Perhaps, in the future, using the above-mentioned three-fluorophore system could provide more evidence for eIF4G-independent interaction.

One of the disadvantages of FLIM-FRET is that it requires overexpression of the tagged proteins, which as mentioned-above could potentially change the in-cell interactions. However, there is a lack of specific methods that would detect homo-interacting proteins without using a tag. Antibody based methods as IP or PLA (proximity ligation assay) require a use of tagged proteins to detect homo-complexes. In this case, the performed Western Blot control demonstrated that WT and overexpressed eIF4A2 was on a comparable level (**Figure 3.7-3**) and the signs of cell death were not visible suggesting that overexpression of eIF4A2 was not detrimental to the cells and similar to what could be expected naturally.

As oligomeric complexes were detected on RNA substrates with double-stranded region, and co-operativity in the unwinding reaction was observed (**Figure 3.3-1**) the catalytic activities of eIF4A2 in conditions stimulating oligomerisation were investigated. Both the unwinding and ATPase activities were higher on RNA substrate with $(AG)_{10}$ than $(CAA)_6CA$ single-stranded overhang (**Figure 3.8-2**). However, this correlated both with the higher affinity towards the $(AG)_{10}$ RNA as well as the greater oligomerisation induction by this RNA. To determine what was the main predictor of the differences in the catalytic capacities of eIF4A2, additional RNA substrates were employed (**Figure 3.8-3**). eIF4A2 activity on the substrate with most similarities in its sequence to previously used $(AG)_{10}$ - $(AGUG)_5$ single-stranded overhang, exhibited the greatest unwinding potential. This again correlated with both the highest oligomerisation and the lowest K_D. However, for other tested substrates, this correlation was not observed. The difference between apparent K_D measured in presence of ATP and K_D in AMP-PNP

conditions for all the tested RNA substrates indicates possible different binding dynamics in presence of ATP (**Table 3.8-1**). Additional experiments could perhaps indicate whether possible differences in the dynamics of RNA binding (k_{on} and k_{off} rates) dictate the outcomes of the unwinding. Possibly the differences observed in the SAXS data for monomers formed on $(AG)_{10}$ and $(CAA)_6CA$ could also indicate different modes of binding to the tested RNA substrates. Worth noting is that the RNAs used in the unwinding assay have a relatively long double-stranded region (24 base-pairs). As the measured increase in fluorescence stems only from the fully unwound RNA substrate, potential small steps of unwinding could remain unnoticed. Additionally, there is a chance that the long duplex could reanneal, especially if the protein is no longer bound to it. Perhaps shorter dissociation rates of eIF4A2 from the RNA substrate could be responsible. Previous studies have explored different lengths of the double-stranded regions and often resolved to shorter stretches (Lorsch and Herschlag, 1998a; Rogers, Richter and Merrick, 1999; George W. Rogers, Lima and Merrick, 2001). Perhaps using RNA substrates with shorter double-stranded regions would provide a different or more specific result. Nonetheless, as the sequence of the double-stranded region is identical in the tested substrates the comparison between different RNA overhangs was possible. Finally, the unexpected 3'-to-5' helicase preference of eIF4A2 (**Table 3.8-2**, **Figure 3.8-5**), which was not observed for eIF4A1 (George W. Rogers, Lima and Merrick, 2001), could potentially correlate with roles more specific to eIF4A2.

The tested small-molecule inhibitor – silvestrol – induced the RNA binding, oligomerisation as well as catalytic activities of eIF4A2 (**Figures 3.9-1, 3.9-2**, **3.9-4**). This induction of eIF4A activities by an inhibitor has been previously reported in the literature (Bordeleau *et al.*, 2005). However, the induction of those activities does not preclude silvestrol for being a potent in cell inhibitor (Jin *et al.*, 2013; Wolfe *et al.*, 2014; Chen *et al.*, 2016; Biedenkopf *et al.*, 2017). The described function of inducing RNA clamping (Iwasaki, Floor and Ingolia, 2016) and creating a potential molecular roadblock for the ribosome still stands true in line with the concept of oligomerisation. The long RNA release time in presence of silvestrol was also observed (**Figure 3.10-1**). The imparted by silvestrol functions however point to the lack of specificity of the inhibitor towards one paralogue.

Finally, the potential differential roles of monomers were explored. Addition of competitor RNA induced change in oligomerisation status however full monomerisation was not observed (**Figure 3.10-2**). Another study in a similar manner has used competitor RNA to explore the capacities of a monomer, however a control of the conditions was not presented (Putnam *et al.*, 2015). Nonetheless, addition of $(AG)_{10}$ competitor RNA obliterated eIF4A2 unwinding activity. The change in activity was visible for a competitor concentration that did not induce change in oligomerisation. Similar change in activity was previously reported without investigation of the eIF4A complexes (G. W. Rogers, Lima and Merrick, 2001). The result differed for $(CAA)_6CA$ RNA, which did not induce oligomerisation to the same extent as $(AG)_{10}$ RNA, suggesting that the unwinding is potentially performed by a free protein recruited by the already bound oligomer. Perhaps, additional studies, exploring the regions of eIF4A2 responsible for oligomerisation could bring more answers.

In sum, this chapter provided detailed description of molecular functions of eIF4A2 and on the basis of this further studies into the wider implication of oligomerisation could be produced. Perhaps the eIF4A2 oligomerisation and unwinding activities could be part of uORF translation (Wilczynska *et al.*, 2019) (see also **Chapter 1.5.2**). Or maybe the recently found role of eIF4A in unwinding RNA secondary structures in stress granules (Tauber *et al.*, 2020), could be performed by the oligomeric eIF4A2 and thus inhibit mRNA storage of cancer cells.

4. Interaction partners influence activities of eIF4A2

4.1. Chapter introduction

The previous chapter focused on the activities of eIF4A2 without its auxiliary factors. However, the busy cellular environment provides multitude of opportunities for proteins to interact with one another.

Since eIF4A2 and eIF4A1 have been implicated in distinct translational processes (Meijer *et al.*, 2013) with eIF4A1 being the more abundant paralogue in many tissues (Nielsen and Trachsel, 1988; Galicia-Vazquez *et al.*, 2012) and the one most often recognised as responsible for cancer development and progression (Ji *et al.*, 2003; Yan *et al.*, 2011; Lomnytska *et al.*, 2012; Liang *et al.*, 2014; Modelska *et al.*, 2015; Tillotson *et al.*, 2017; Gao *et al.*, 2020) it has been studied in greater detail. In contrast, the enzymatic activities of eIF4A2 have rarely been explored and knowledge about regulation by its interaction partners is missing. Moreover, what the implications of this novel, oligomerisation potential of eIF4A2 on the interactions with auxiliary proteins remains uncovered.

Here, eIF4A2 activities were explored in presence of the canonical interaction partners of eIF4A1 (see also **Chapters 1.3.2, 1.4**): **1)** the small auxiliary protein eIF4H, implicated in enhancing the activities of eIF4A1 (Richter-Cook *et al.*, 1998; Richter *et al.*, 1999; Rogers, Richter and Merrick, 1999; Özeş *et al.*, 2011), **2)** eIF4G1, the scaffold protein of eIF4F complex (Grifo *et al.*, 1983), and **3)** PDCD4, the mTOR-regulated eIF4A inhibitor (Yang *et al.*, 2002; Suzuki *et al.*, 2008; Loh *et al.*, 2009; Dennis, Jefferson and Kimball, 2012).

Additionally, as eIF4A2 but not eIF4A1 is thought to interact with CNOT1, the scaffold protein of CCR4-NOT complex (Meijer *et al.*, 2013, 2019; Wilczynska *et al.*, 2019), (see also **Chapter 1.3.6**), the possible influence of short CNOT1 constructs on eIF4A2 activities was investigated.

To uncover possible interactions between eIF4A2 and eIF4G1, PDCD4, or CNOT1, both in cell and *in vitro* co-immunoprecipitations were employed in this chapter (see also **Chapters 2.3.7**, **2.4.5**).

Moreover, as this chapter was focused on the influence of interaction partners on enzymatic activities of eIF4A2, pivotal to this study was the purification of high-quality recombinant proteins. Next, using biochemical methods described and used throughout the previous chapter (**Chapter 3**), the influence of the auxiliary proteins on eIF4A2 unwinding and ATPase activities as well as on RNA binding and release was assessed.

Finally, as eIF4A2 has been shown to inhibit CNOT7 deadenylation activity on RNA substrates containing polyA tails in presence of longer CNOT1 constructs (Meijer *et al.*, 2019), the effect of eIF4A2 on CNOT7 in presence of shorter CNOT1 constructs was tested (see **Chapter 2.3.6**). Additionally, as DDX6 has been shown to interact strongly with CNOT1 (Chen *et al.*, 2014), it has been employed as a control for determination of CNOT1 imposed activities.

In all, this chapter focuses on the influence of potential auxiliary proteins on activities of eIF4A2 in oligomerisation stimulating conditions.

4.2. eIF4H stimulates unwinding activity of eIF4A2

eIF4H is found ubiquitously in human tissues, with varying degrees of mRNA as well as protein expression. Both the eIF4H mRNA and protein levels are high in skeletal muscle and brain (Richter *et al.*, 1999, Human Protein Atlas), tissues previously shown to have high eIF4A2 expression (Galicia-Vazquez *et al.*, 2012). Intriguingly, the expression of eIF4B, an initiation factor described to have similar, although more potent role than eIF4H *in vitro* (Özeş *et al.*, 2011), was lower in the brain (Richter *et al.*, 1999, Human Protein Atlas). Therefore, a question remains open whether the similar expression pattern of eIF4A2 and eIF4H could mean that the two proteins specifically interact with each other.

As previous studies described the enhancement of eIF4A1 helicase and ATPase activities by eIF4H without focusing on how it affects eIF4A2 a further scrutiny was needed.

First, to examine the influence of eIF4H on the catalytic capacities of eIF4A2, eIF4H was heterologously expressed. A previously cloned full length eIF4H construct containing a His-SUMO tag was expressed in *E. coli* strain BL21 DE3 RP codon+. Bacterial cells were grown, induced, harvested, and lysed as described above for eIF4A2 (**Chapter 3.2**). The cleared lysate was then applied to a Ni^{2+} column and the bound protein eluted in a linear imidazole gradient (**Figure 4.2-1**, panel A). Next, the pooled peak fractions were applied to ion exchange chromatography. As eIF4H has a calculated pI = 6.66 and is an RNA binding protein, a cation exchange column was used (**Figure 4.2-1**, panel B). Pooled peak fractions were subsequently applied on a size exclusion chromatography column (**Figure 4.2-1**, panel C). The eluted protein was concentrated, its concentration measured using a UV-VIS spectrometer and the purity was estimated through SDS-PAGE (**Figure 4.2-1**, panel D). In all, eIF4H was deemed to be of high purity to use in the subsequent studies in this chapter.

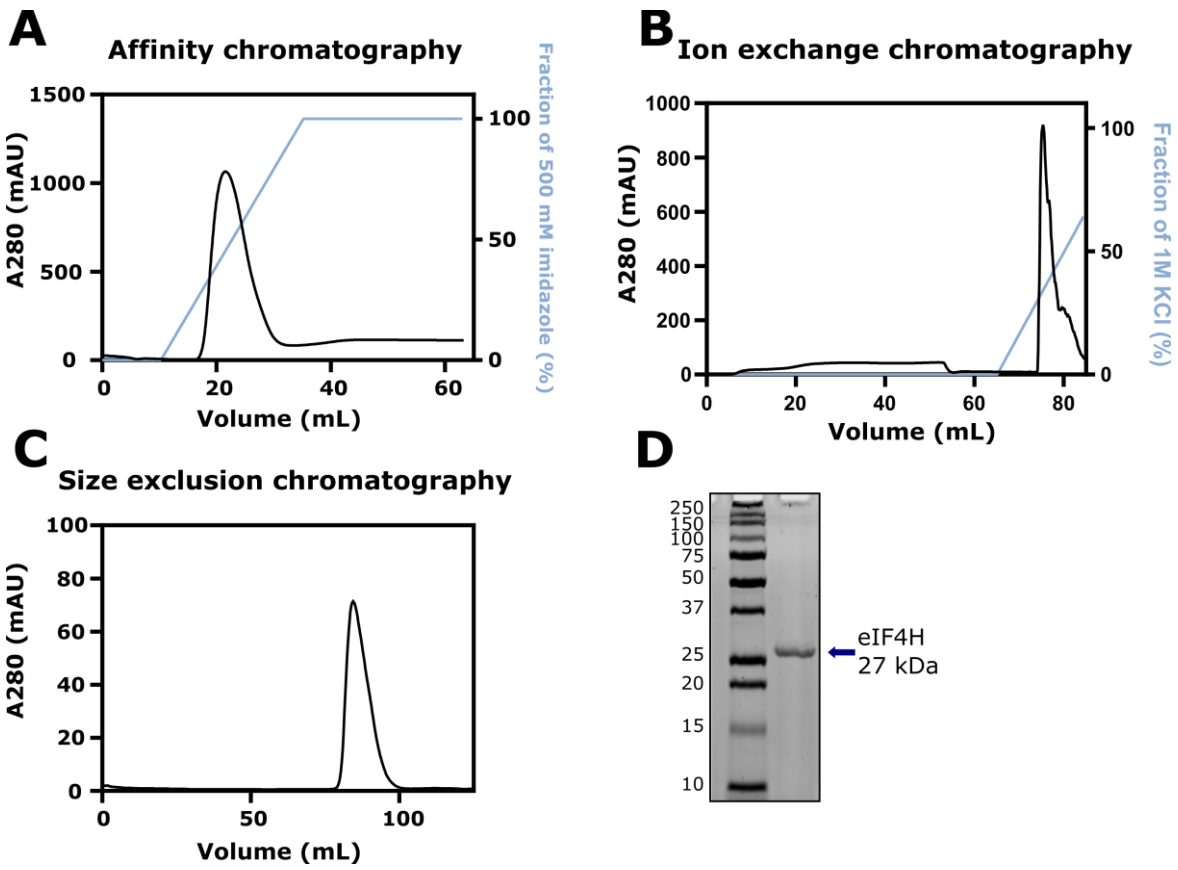

Figure 4.2-1 eIF4H purification

A. Representative chromatogram of an elution profile of His-SUMO eIF4H on a HisTrap HP column.

B. Representative chromatogram of an elution profile of pooled fractions containing eIF4H after tag cleavage using a HiTrap Heparin column.

C. Representative size exclusion chromatography elution profile. Purified eIF4H elutes at around 90 – 95 mL on a Superdex S200 HiLoad 16/600 column.

D. Representative Coomassie stained SDS-PAGE of purified, full length, tag free 27 kDa eIF4H. The numbers on the left of the gel indicate sizes of the protein marker in kDa.

Next, the influence of eIF4H on the unwinding and ATPase activity of eIF4A2 was tested. Here, the 5'$(AG)_{10}$ overhang RNA substrate was used for assays established in the previous chapter (**Chapter 3.8**). This revealed that eIF4H greatly stimulated eIF4A2 unwinding activity (**Figure 4.2-2**, panel A, **Table 4.2-1**). The mean unwinding velocity of 5 µM eIF4A2 was 11-fold greater in presence of eIF4H. Additionally, eIF4H stimulated eIF4A2 unwinding activity in a concentration dependent manner. Curiously, when the Hill equation was fitted to the data, it was found that eIF4H reduced the co-operativity between different eIF4A2 subunits in the oligomer in the unwinding reaction (**Figure 4.2-2**, panel B). This suggests that a functional sub-oligomeric eIF4A2 complex may exist when interacting with eIF4H.

In contrast to earlier reports (Richter-Cook *et al.*, 1998) eIF4H enhanced eIF4A2 ATPase activity only slightly in presence of both 0.5 µM and 5 µM eIF4H (**Figure 4.2-2**, panel C, **Table 4.2-1**).

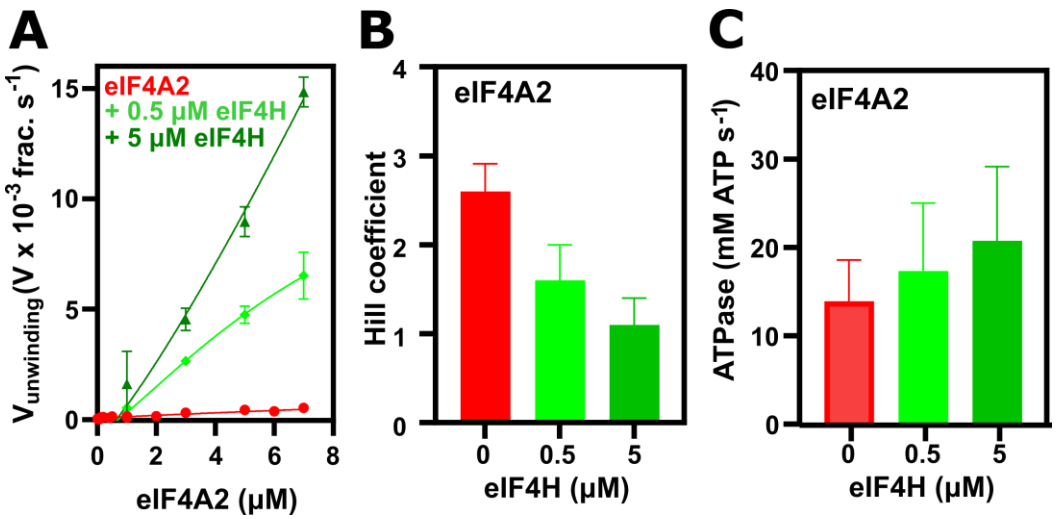

Figure 4.2-2 eIF4H enhances unwinding activity of eIF4A2 without increasing the ATPase activity

- **A.** Velocity of unwinding of indicated concentrations of eIF4A2 alone (*red*, n = 4), and in presence of 0.5 µM eIF4H (*light green*, n = 2), 5 µM eIF4H (*dark green*, n = 4). Error = SEM, fit – Hill equation. eIF4H enhances eIF4A2 unwinding activity to a higher degree than silvestrol.
- **B.** Hill coefficient of obtained from the fit in panel **A**. eIF4H reduces the cooperativity between eIF4A2.
- **C.** ATPase activity of 5 µM eIF4A2 concentration in presence of indicated eIF4H concentration. Colour scheme of samples, n and error as in panel **A**. eIF4H only slightly increases ATPase activity of 5 µM eIF4A2.

Next, as eIF4A2 showed a preference in the directionality of unwinding (see **Figure 3.8-5**), it was investigated if the presence of eIF4H affects directional specificity. Unwinding assays for double-stranded RNA with 5' or 3' single-stranded overhangs were performed as before (see **Figure 3.8-4**). The results show that eIF4A2 maintains its preference for unwinding in the 3'-to-5' direction also in presence of eIF4H on RNA substrates with AG-overhang (**Figure 4.2-3**, panel A, **Table 4.2-1**). However, the difference is not as large as for the free eIF4A2 (5 µM eIF4A2 with 0.5 µM eIF4H $V_{5'}$ 4.75 ± 0.39 in comparison to $V_{3'}$ = 5.53 ± 0.63). Moreover, the activity of free eIF4A2 was enhanced by the presence of eIF4H on both 3'$(AG)_{10}$ and 3'$(CAA)_6CA$ overhang substrates. The unwinding velocity increased 5-fold in presence of eIF4H for 5 µM eIF4A2 on 3'$(CAA)_6CA$. Similarly, to what was shown in **Figure 3.8-5**, the activation on 3'$(AG)_{10}$ RNA was greater than on 3'$(CAA)_6CA$ (**Figure 4.2-3**, panel B). However, this time, the unwinding activity in presence of eIF4H was greater on both the 5'- and 3'$(AG)_{10}$ overhang substrates than on the 3'$(CAA)_6CA$ (see **Figure 3.8-5**, **Table 4.2-1**).

Next, the contribution of eIF4H to eIF4A2 ATPase activity was tested. A slight reduction in the ATPase activity was detected when comparing ATPase of free eIF4A2 and in presence of eIF4H on both tested 3'overhang substrates (**Figure 4.2-3**, panel C, **Table 4.2-1**).

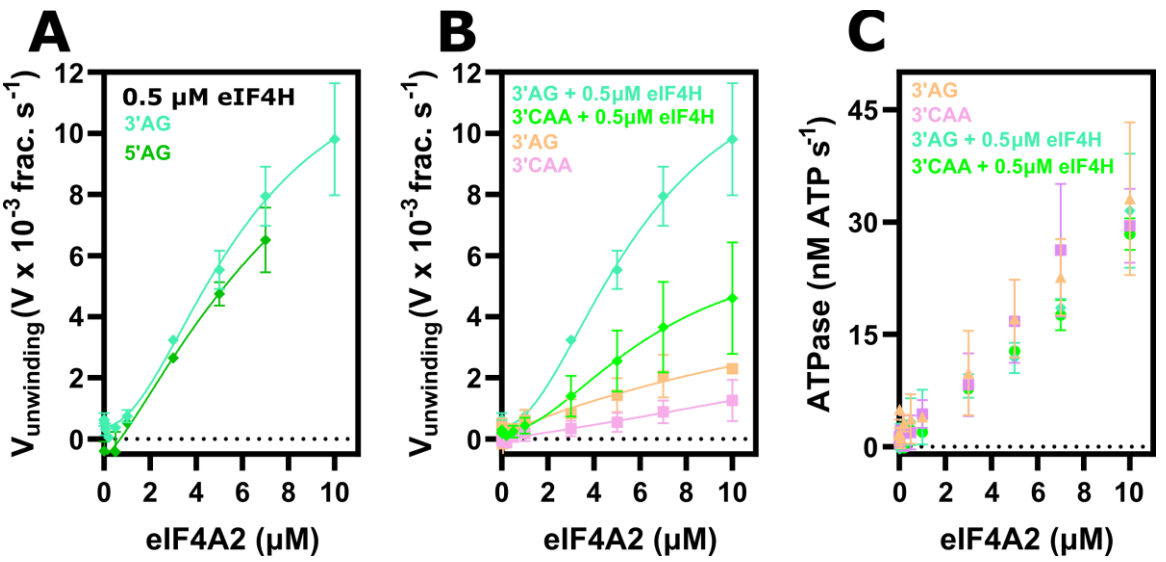

Figure 4.2-3 eIF4H enhances eIF4A2 unwinding activity on a substrate with 3'overhang to a greater extent than on the one with 5'overhang

A. Unwinding activity of eIF4A2 in presence of 0.5 μM eIF4H presented as velocity of unwinding versus eIF4A2 concentration. eIF4H enhances eIF4A2 unwinding activity on substrate with 3'$(AG)_{10}$ overhang (*light turquoise*, n = 3) more than on 5'$(AG)_{10}$ overhang (*green*, n = 2). Error = SEM, fit – Hill equation.

B. Unwinding activity of eIF4A2 presented as in panel **A** on 3'$(AG)_{10}$ overhang substrate without (*light orange*) and with 0.5 μM eIF4AH (*light turquoise*) and on 3'$(CAA)_6CA$ overhang substrate without (*light pink*) and with 0.5 μM eIF4AH (*green*). eIF4H enhances eIF4A2 activity on both substrates. N = 3, error = SEM, fit – Hill equation.

C. ATPase activity versus eIF4A2 concentration on the same RNA substrates as in panel **B**, colour scheme the same as in panel **B**. eIF4H slightly reduces the ATPase activity of eIF4A2 on 3'overhang RNA substrates. N = 3, error = SEM.

As **1)** eIF4H stimulated unwinding activity of eIF4A2 to a greater extent on both 3' and 5'$(AG)_{10}$ than on 3'$(CAA)_6CA$ overhang RNA, and **2)** in the previous chapter (**Chapter 3.8**), eIF4A2 was shown to have a greater preference to unwind RNA substrates in 3'-to-5' direction regardless of the overhang sequence of the tested RNA, a question was posed whether eIF4H itself could have a preference for the AG-RNA. It has been shown that eIF4H has an RNA recognition motif (RRM) (Richter *et al.*, 1999; Rogers *et al.*, 2001); however, as it has been reported previously, it is considered to only weakly bind to RNA (Richter-Cook *et al.*, 1998; Rozovsky, Butterworth and Moore, 2008). To explore whether eIF4H binds AG-RNA, polarisation-based RNA binding experiments were performed, and the binding affinity was quantified as K_D (**Figure 4.2-4**). Surprisingly, eIF4H showed a higher affinity for $(AG)_{10}$ RNA than eIF4A2 ($K_{D,\ eIF4H} < K_{D,\ eIF4A2}$). This could potentially lead to a possible mechanism for eIF4H-induced eIF4A2 unwinding activation. It has been shown in the literature that eIF4H improves RNA binding of eIF4A1 and that this induction happens through possible protein-protein interaction (Richter *et al.*, 1999; Rozovsky, Butterworth and Moore, 2008). Perhaps, here the stronger enhancement of eIF4A2 activity on 5'$(AG)_{10}$ than 3'$(CAA)_6CA$ could stem from the eIF4H binding itself to the AG-RNA. As the eIF4H reduced co-operativity between different eIF4A2 subunits in the oligomer, a possible explanation could be that eIF4H binds to the RNA and recruits eIF4A2, forming a distinct complex to oligomeric eIF4A2.

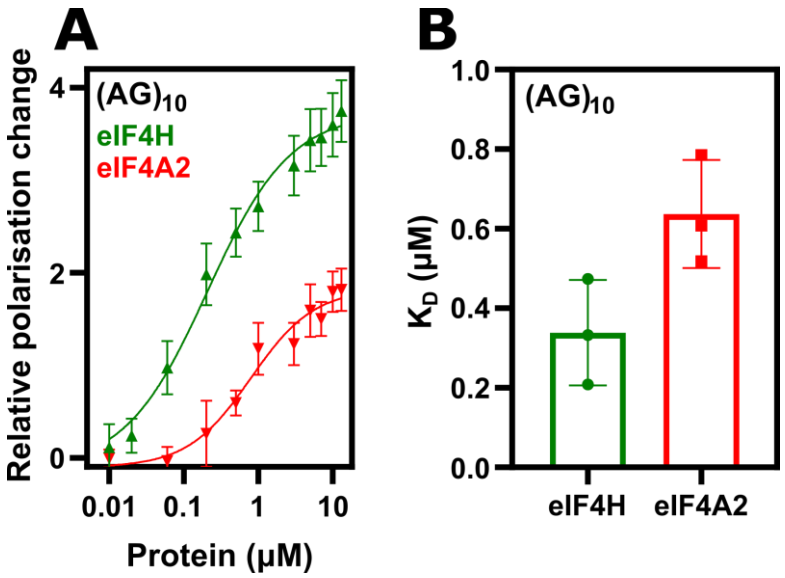

Figure 4.2-4 eIF4H binds AG-RNA with stronger affinity than eIF4A2

A. Representative binding of eIF4H (*green*) and eIF4A2 (*red*) to $(AG)_{10}$ RNA measured by polarisation. Values were normalised to the polarisation of free RNA, then baseline was removed (-1). N = 3, error = SEM from technical duplicate, fit – Hill equation.

B. Comparison of K_D obtained from Hill equation fitting of 3 replicates of polarisation experiment as presented in panel **A**. Each dot represents the K_D obtained from an individual replicate.

Table 4.2-1 Comparison of velocity of unwinding and ATPase of 5 μM eIF4A2 in presence of eIF4H

24BP RNA overhang	eIF4H (μM)	V x 10^{-3} frac. s^{-1}	nM ATP s^{-1}
5'$(AG)_{10}$	0	0.43 ± 0.00	12.80 ± 2.30
5'$(AG)_{10}$	0.5	4.75 ± 0.39	17.33 ± 4.43
3'$(AG)_{10}$	0	1.43 ± 0.56	17.10 ± 2.61
3'$(AG)_{10}$	0.5	5.53 ± 0.63	11.83 ± 1.17
3'$(CAA)_6CA$	0	0.54 ± 0.32	16.78 ± 3.21
3'$(CAA)_6CA$	0.5	2.55 ± 0.99	12.75 ± 0.05

In sum, this chapter described the influence of eIF4H on the catalytic activities of eIF4A2 in oligomerisation-inducing conditions. eIF4H stimulated the unwinding activity of eIF4A2. However, a decrease of co-operativity between eIF4A2 protomers in unwinding reaction in the presence of eIF4H was observed. This indicates possible different mechanism of unwinding in presence of eIF4H, where eIF4A2 relies more on the interaction with eIF4H than between protomers. Moreover, eIF4H-stimulated unwinding has a bidirectional nature. However, unlike for eIF4A2 alone (see **Figure 3.8-5**), the presence of eIF4H correlated with stronger activity on $(AG)_{10}$ RNA regardless of the position of single-stranded region. This could be perhaps further explained through the surprisingly high affinity of eIF4H towards $(AG)_{10}$ RNA (K_D = 0.34 ± 0.08), however eIF4H RNA binding to $(CAA)_6CA$ as well as eIF4A2 binding in presence of eIF4H should be evaluated to reach conclusion.

Finally, the assessment of the eIF4A2 ATPase activity indicated that the changes induced by eIF4H are less potent than its influence on unwinding activity. A slight increase was observed for the 5'$(AG)_{10}$ overhang substrate, however the opposite was observed for substrates with a 3'overhang. This suggested that the effects of ATPase and unwinding activities are not correlated.

4.3. eIF4G does not synergistically activate eIF4A2 in presence of eIF4H

eIF4G has been shown not to be the main interaction partner of eIF4A2 (Meijer *et al.*, 2013, 2019; Wilczynska *et al.*, 2019). However, none of the above-mentioned publications contested the eIF4A2-eIF4G interaction. In fact, in Wilczynska *et al.*, 2019 under the high overexpression of eIF4A2 a large increase of interaction with eIF4G was observed. This significant increase was not observed for overexpressed eIF4A1. Moreover, as presented in Wilczynska *et al.*, 2019 the regions responsible for interaction with eIF4G are highly identical between eIF4A1 and eIF4A2, with only one amino acid difference between them. Additionally, as presented in Meijer *et al.*, 2019 in fractions of cytoplasmic HeLa lysate containing eIF4A2, both the presence of CNOT1 and eIF4G was detected. Moreover, a more recent report (Robert *et al.*, 2020) has described existence of different variations of eIF4F complex, some of them containing eIF4A2. In all, the interaction between eIF4A2 and eIF4G cannot be dismissed. Perhaps, in cells with high eIF4A2 overexpression, or tissues in which eIF4A2 is the dominant paralogue it is the eIF4A2 that preferentially interacts with eIF4G.

First, to support the previous reports, immunoprecipitations of eIF4A1 and eIF4A2 were performed in HeLa cells lysed either in presence of Ribolock, to preserve RNA integrity, or RNase 1, to degrade the RNA (**Figure 4.3-1**). eIF4G1 co-precipitated strongly with eIF4A1, however in both RNA stabilising and RNA degrading conditions, a small fraction of eIF4G1 co-precipitated with eIF4A2 suggesting that at least a small fraction of eIF4A2 in non-overexpressing conditions can indeed interact with eIF4G1.

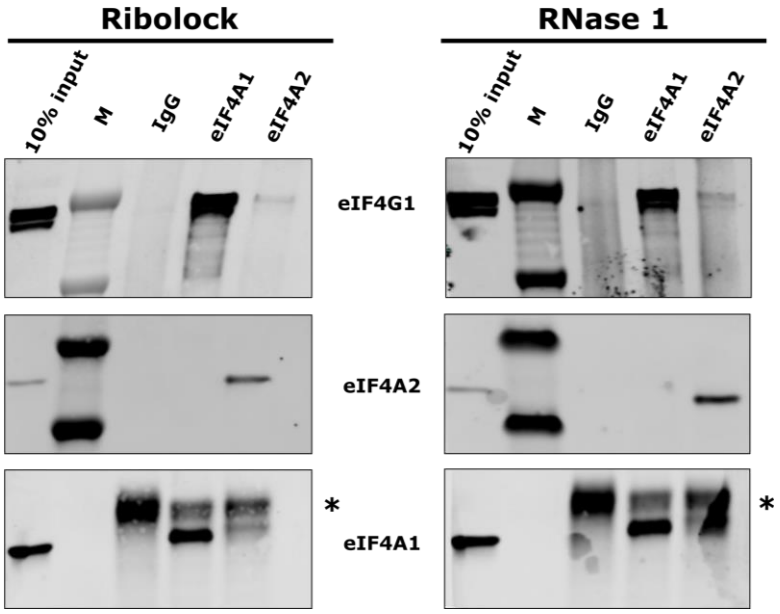

Figure 4.3-1 eIF4A2 interacts with eIF4G1

Co-immunoprecipitations of IgG, eIF4A1 and eIF4A2 in HeLa cells lysed in presence of Ribolock (*left*) and RNase 1 (*right*), probed with anti-eIF4G1 and anti-eIF4A2, and anti-eIF4A1 antibodies. eIF4G1 interacts strongly with eIF4A1, however co-precipitation of eIF4G1 with eIF4A2 is also visible. No unspecific bands were detected in IgG IP lane. Asterisk indicates denatured antibody chains.

As both the previous reports and data presented in **Figure 4.3-1** showed that eIF4A2 can interact with eIF4G1, the influence of eIF4G1 on catalytic activities of eIF4A2 was investigated. First, an N-terminally truncated eIF4G1 (amino acids 674 – 1599), called eIF4G-MC, previously cloned into petSUMO vector was expressed in a similar manner as described in **Chapter 4.2**. The lysate containing His-SUMO-eIF4G-MC was subjected to affinity chromatography and eluted in a linear imidazole gradient (**Figure 4.3-2**, panel A). Subsequently, the fractions containing the protein were pooled together and cleaved with ULP1 to remove His-SUMO tag. Next, the sample was applied onto cation exchange column, as the pI of eIF4G-MC is 7.89 (**Figure 4.3-2**, panel B, see also **Chapter 2.2**). The eluted peak was then subjected to size exclusion chromatography (**Figure 4.3-2**, panel C), and fractions eluted at around 70 mL were collected and concentrated. The purity of the obtained protein was investigated by SDS-PAGE (**Figure 4.3-2**, panel D) and UV-VIS spectrum indicated no nucleic acid contamination. In sum, eIF4G-MC was deemed to be of good purity level for use in further studies.

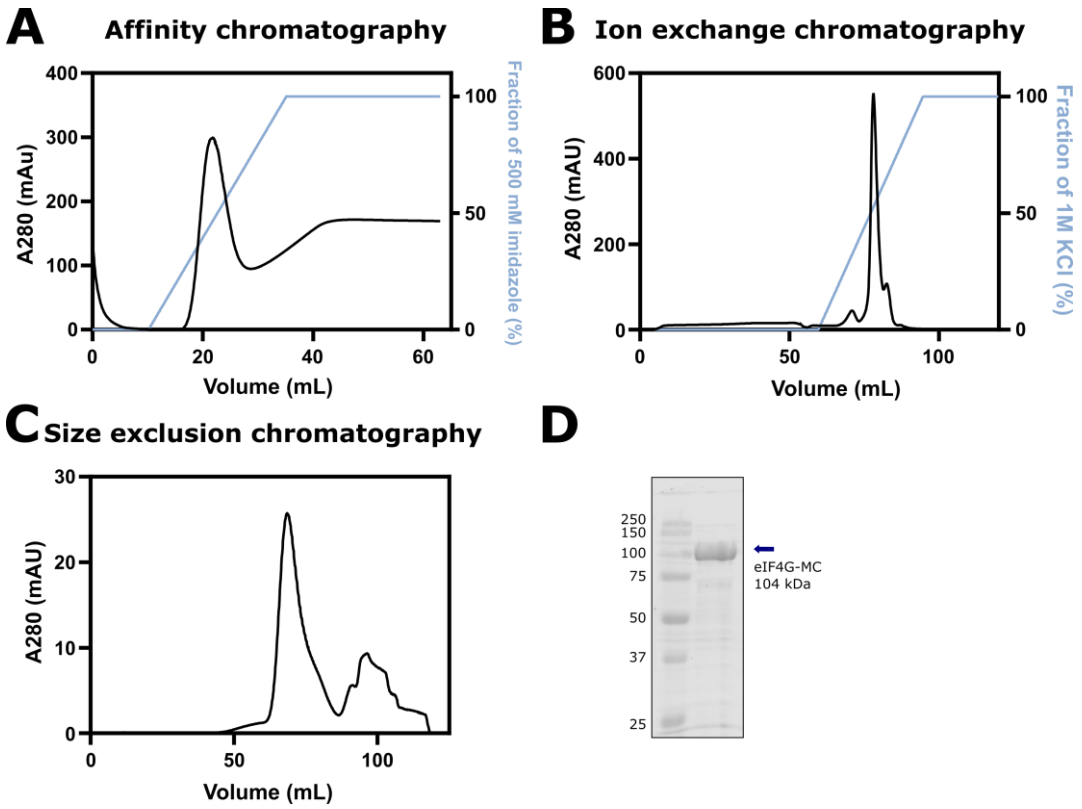

Figure 4.3-2 eIF4G-MC purification

- **A.** Affinity chromatography elution profile on 5 mL HisTrap HP column (Ni^{2+} resin). eIF4G-MC elutes in a linear imidazole gradient.
- **B.** Ion exchange chromatography – eIF4G-MC after ULP1 cleavage elutes in a linear gradient of KCl on cation exchange column (HiTrap Heparin column).
- **C.** SEC chromatogram of peak collected from heparin column in panel **C**. eIF4G-MC elutes at around 70 mL Superdex S200 HiLoad 16/600 column.
- **D.** Coomassie stained SDS-PAGE gel presenting purified eIF4G-MC (104 kDa). Protein marker sizes in kDa indicated on the left.

As the N-terminal truncation of eIF4G1 – eIF4G-MC contains both eIF4A binding sites but lacks the eIF4E binding site, rendering it eIF4E independent and functionally active (Feoktistova *et al.*, 2013), this construct can be used in assays without additional co-factors.

First the influence of eIF4G-MC was investigated on eIF4A2 unwinding and ATPase activity on 5'$(AG)_{10}$ overhang RNA substrate **(Figure 4.3-3**, panel A and B respectively). Similarly to what was described in the literature for eIF4A1 (Rogers *et al.*, 2001; Korneeva *et al.*, 2005; Nielsen *et al.*, 2011; Özeş *et al.*, 2011), a slight increase in the tested activities was detected. However, the observed change was less than previously described 2-fold increase.

As **1)** eIF4G-MC stimulated eIF4A2 activity only weakly, **2)** previous studies indicated synergistic activation of eIF4A(1) by eIF4G and eIF4B (Abramson, Dever and Merrick, 1988; Nielsen *et al.*, 2011), and **3)** eIF4H was found to be functionally similar to eIF4B *in vitro* (Rogers *et al.*, 2001), a question was posed whether eIF4A2 could be synergistically activated by eIF4H and eIF4G-MC.

This time, unwinding reactions were performed on 5'$(AG)_{10}$ RNA substrate with 0.5 μM eIF4G-MC and either 0.5 or 5 μM eIF4H (**Figure 4.3-3**, panel C, **Table 4.3-1**). Surprisingly, the enhanced velocity of unwinding of eIF4A2 induced by eIF4H was reduced in presence of eIF4G-MC at higher eIF4A2 concentrations. Intriguingly, this reduction in velocity was eIF4H concentration dependent, i.e., higher concentration of eIF4H correlated with higher unwinding activity. eIF4G-MC, similarly as eIF4H reduced cooperativity between eIF4A2 protomers, however to a lesser extent (**Table 4.3-2**). The cooperativity of eIF4A2 in presence of both eIF4H and eIF4G-MC cannot be determined as calculated error of the Hill coefficient was too high. Moreover, the functional binding affinity (presented as K_D) of eIF4A2 to RNA substrate decreased in presence of eIF4G-MC, whereas in presence of eIF4H K_D changed only slightly (**Table 4.3-2**). Interestingly, presence of both eIF4G-MC and eIF4H increased the affinity. As the functional binding of eIF4A2 was greater (lower K_D) in presence of both tested co-factors but the velocity was lower than the one in presence of eIF4H alone, the data might indicate a possible competition between eIF4H and eIF4G-MC for eIF4A2. Additional indication for the possible competition can stem from slight increase in activity in presence of both interaction partners for lower concentration of eIF4A2 (3 μM) in comparison to 0.5 μM eIF4H only.

Interestingly, the opposite effect was observed for eIF4A2 ATPase activity (**Figure 4.3-3**, panel D, **Table 4.3-1**). Presence of eIF4H in the reaction reduced the ATPase activity of eIF4A2 in eIF4H concentration dependent manner, visible at high eIF4A2 concentrations. In all, the presence of eIF4G-MC in the reaction changed the activity of eIF4A2, suggesting eIF4H and eIF4G-MC seemed to exert opposite effect on eIF4A2 activity.

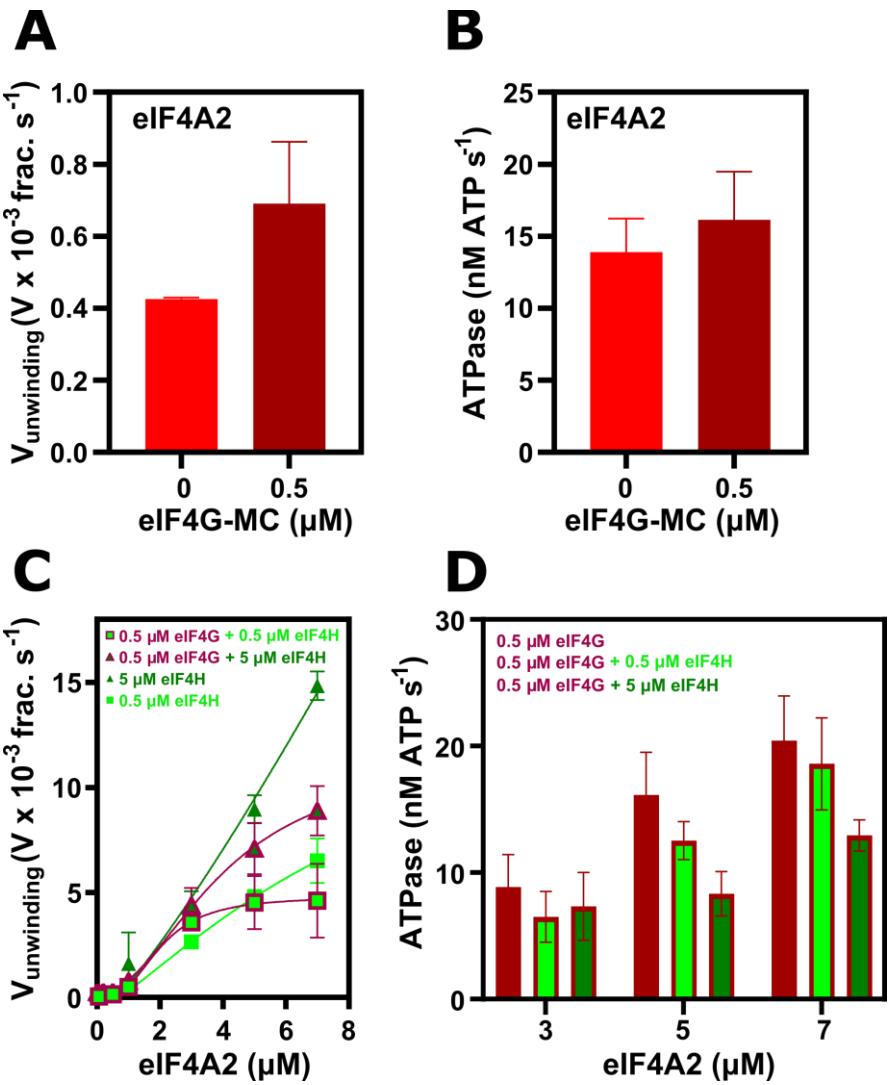

Figure 4.3-3 eIF4G does not strongly stimulate eIF4A2 catalytic activities and reduces the influence of eIF4H on unwinding activity

A. Unwinding activity of eIF4A2 presented as velocity of unwinding of 5 μM eIF4A2 on 5'$(AG)_{10}$ overhang substrate (*red*) and in presence of 0.5 μM eIF4G-MC (*burgundy*). Activity of eIF4A2 alone and in presence of eIF4G-MC is highly similar. N = 4, error = SEM.

B. ATPase activity of 5 μM eIF4A2 on $(AG)_{10}$ overhang RNA (*red*) and in presence of 0.5 μM eIF4G-MC (*burgundy*). ATPase with and without eIF4G-MC is similar. N = 4, error = SEM.

C. Velocity of unwinding versus eIF4A2 concentration on 5'$(AG)_{10}$ overhang RNA substrate in presence of: **1)** 0.5 μM eIF4H (*bright green*), n = 2, **2)** 5 μM eIF4H (*dark green*), n = 4, **3)** 0.5 μM eIF4G-MC and 0.5 μM eIF4H (*bright green with burgundy border*), n = 3, **4)** 0.5 μM eIF4G-MC and 5 μM eIF4H (*dark green with burgundy border*) n =3. Addition of eIF4G-MC reduces the increase in eIF4A2 unwinding activity exerted by presence of eIF4H. Error = SEM.

D. ATPase activity for indicated eIF4A2 concentrations on 5'$(AG)_{10}$ overhang RNA in presence of **1)** eIF4G (*burgundy*) n = 4, **2)** 0.5 μM eIF4G-MC and 0.5 μM eIF4H (*bright green with burgundy border*), n = 3, **3)** 0.5 μM eIF4G-MC and 5 μM eIF4H (*dark green with burgundy border*) n =3. Error = SEM. A reduction of ATPase activity in presence of eIF4H is visible.

eIF4G-MC seemed to stimulate eIF4A2 unwinding activity on 5'$(AG)_{10}$ overhang RNA only to a low extent. However, eIF4A2 showed a preference in unwinding from 3'-to-5' direction (see **Figure 3.8-5**), therefore the next step was to determine the effect of eIF4G-MC on 3'$(AG)_{10}$ overhang RNA. A very limited increase of eIF4A2 activity in presence of eIF4G-MC was detected in the 3'-to-5' unwinding direction (**Figure 4.3-4**, panel A). Additionally, the unwinding activity was lower than for the free eIF4A2 (compare **Table 4.2-1** and **4.3-1**). Moreover, the ATPase activity on the 3'overhang RNA was reduced in comparison to 5'overhang, similarly as in the case of eIF4H (**Figure 4.3-4**, panel B, see also **Table 4.2-1**).

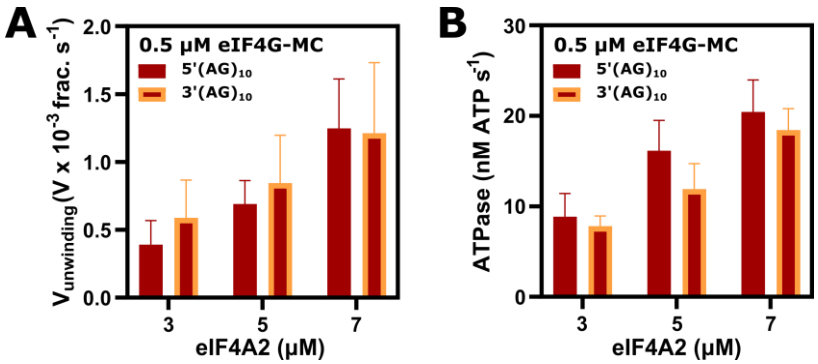

Figure 4.3-4 eIF4G reduces eIF4A2 activity on 3'overhang RNA substrate

- **A.** Comparison of unwinding velocity versus eIF4A2 concentration for eIF4A2 activity in presence of 0.5 μM eIF4G-MC on RNA substrates with $(AG)_{10}$ 5'- (*burgundy*, n = 4) and 3'- (*orange*, n = 3) overhangs. Activity on 3'$(AG)_{10}$ is only marginally increased in comparison to 5'overhang. Error = SEM.
- **B.** Comparison of ATPase activity versus eIF4A2 concentration in presence of 0.5 μM eIF4G-MC. Colour scheme, n, and error as in panel **A**.

Table 4.3-1 Comparison of velocity of unwinding and ATPase of 5 μM eIF4A2 in presence of eIF4G-MC

24BP RNA overhang	eIF4H (μM)	eIF4G-MC (μM)	V x 10^{-3} frac. s^{-1}	nM ATP s^{-1}
5'$(AG)_{10}$	0	0.5	0.69 ± 0.17	15.96 ± 2.61
5'$(AG)_{10}$	0.5	0.5	4.52 ± 1.27	12.53 ± 1.56
5'$(AG)_{10}$	5	0.5	7.08 ± 1.22	8.32 ± 1.75
3'$(AG)_{10}$	0	0.5	0.84 ± 0.35	11.91 ± 2.81

Table 4.3-2 Functional binding affinity and Hill coefficient of eIF4A2 for unwinding reactions in presence of interaction partners

24BP RNA overhang	eIF4H (µM)	eIF4G-MC (µM)	functional K_D (µM)	Hill coefficient
5'$(AG)_{10}$	0	0	4.9 ± 0.5	2.6 ± 0.3
5'$(AG)_{10}$	0.5	0	3.9 ± 0.6	1.6 ± 0.4
5'$(AG)_{10}$	5	0	5.3 ± 0.2	1.1 ± 0.3
5'$(AG)_{10}$	0	0.5	8.4 ± 0.7	1.9 ± 0.3
5'$(AG)_{10}$	0.5	0.5	1.9 ± 0.8	2.7 ± 1.9
5'$(AG)_{10}$	5	0.5	3.5 ± 0.3	2.6 ± 0.8

In sum, eIF4G1 can interact with eIF4A2, and similarly, as in the case of eIF4A1 (Rogers *et al.*, 2001; Korneeva *et al.*, 2005; Nielsen *et al.*, 2011; Özeş *et al.*, 2011), eIF4G-MC enhanced the catalytic activities of eIF4A2, however to a lower extent. Moreover, both eIF4G-MC and eIF4H seem to reduce the cooperativity between the eIF4A2 protomers, while exerting different outcomes on eIF4A2 activity. Additionally, the functional binding affinity of eIF4A2 was reduced in presence of eIF4G-MC. However, an increase of the functional binding affinity was observed when both eIF4G-MC and eIF4H were present in the reaction. In presence of both interaction partners eIF4A2 unwinding activity was greater than for the free eIF4A2, however the velocity was lower than in presence of eIF4H alone. However, the presence of eIF4H reduced the ATPase activity of eIF4A2-eIF4G-MC. This potentially suggest, a competition between the eIF4G-MC and eIF4H for eIF4A2. Finally, the tested activities in presence of eIF4G-MC showed a slight increase of unwinding and decrease in ATPase on 3'$(AG)_{10}$ in comparison to 5'$(AG)_{10}$ RNA substrate. Moreover, the activities of free eIF4A2 on 3'$(AG)_{10}$ RNA were reduced in presence of eIF4G-MC.

4.4. PDCD4 inhibits eIF4A2 catalytic activities

PDCD4 is thought to be a tumour suppressor that acts upon eIF4A helicase (Yang *et al.*, 2002, 2004; Chen *et al.*, 2003; LaRonde-LeBlanc *et al.*, 2006; Chang *et al.*, 2009; Loh *et al.*, 2009). Interestingly, despite the functional differences in protein translation between eIF4A1 and eIF4A2 (Meijer *et al.*, 2013), PDCD4 has been shown to interact with eIF4A2 (Yang *et al.*, 2002). Moreover, as eIF4A2 expression in the brain is higher than that of eIF4A1 (Galicia-Vázquez *et al.*, 2012), PDCD4 has been demonstrated to interact more preferentially with eIF4A2 in this organ (Yang *et al.*, 2002). Despite this interaction, previous studies exploring enzymatic activities in presence of PDCD4 have been focused solely on eIF4A1 and its co-factors (Yang *et al.*, 2002).

Moreover, in the study that explored *in vitro* inhibition of eIF4A1 by PDCD4, PDCD4 has been shown to inhibit eIF4A1 activation by eIF4B (Yang *et al.*, 2002). As **1)** PDCD4 and eIF4G1 share MA3 domain similarities (Suzuki *et al.*, 2008), **2)** PDCD4 has been shown to displace eIF4G from eIF4A (Suzuki *et al.*, 2008; Chang *et al.*, 2009), but **3)** no additive effect was observed between eIF4H and eIF4G-MC on eIF4A2 activity, (see **Figure 4.3-3**, panels C, D), a question whether eIF4H could still exert its function upon eIF4A2 in presence of PDCD4 was posed.

First, the interaction of eIF4A2 and PDCD4 was assessed by co-immunoprecipitation in HeLa cells (**Figure 4.4-1**, panel A). PDCD4 co-precipitated in both eIF4A1 and eIF4A2 lanes and not in IgG IP lane, indicating an association of eIF4A2 with PDCD4.

Therefore, the effect of PDCD4 on catalytic activities of eIF4A2 was assessed. First, full length PDCD4 cloned into petSUMO vector was expressed in *E. coli* as described previously (see **Chapters 2.2**, **3.2**, **4.2**). The cleared lysate was applied on a HisTrap HP column and fractions containing bound proteins were eluted in a linear imidazole gradient (**Figure 4.4-1**, panel B). Next, the His-SUMO tag was cleaved off with ULP1 and the sample was subjected to anion exchange chromatography as calculated pI of PDCD4 is 5.07 (**Figure 4.4-1**, panel C). PDCD4 eluted in linear KCl gradient and the pooled fractions containing the protein were applied to size exclusion chromatography (**Figure 4.4-1**, panel D). PDCD4 eluted around 85 mL on Superdex S200 HiLoad 16/600 column. The

concentration of protein was determined using UV-VIS spectrum and calculated extinction coefficient and the purity was estimated by SDS-PAGE (**Figure 4.4-1**, panel D, *left*). In all, the obtained PDCD4 protein was assessed to be of good purity to be used in subsequent studies.

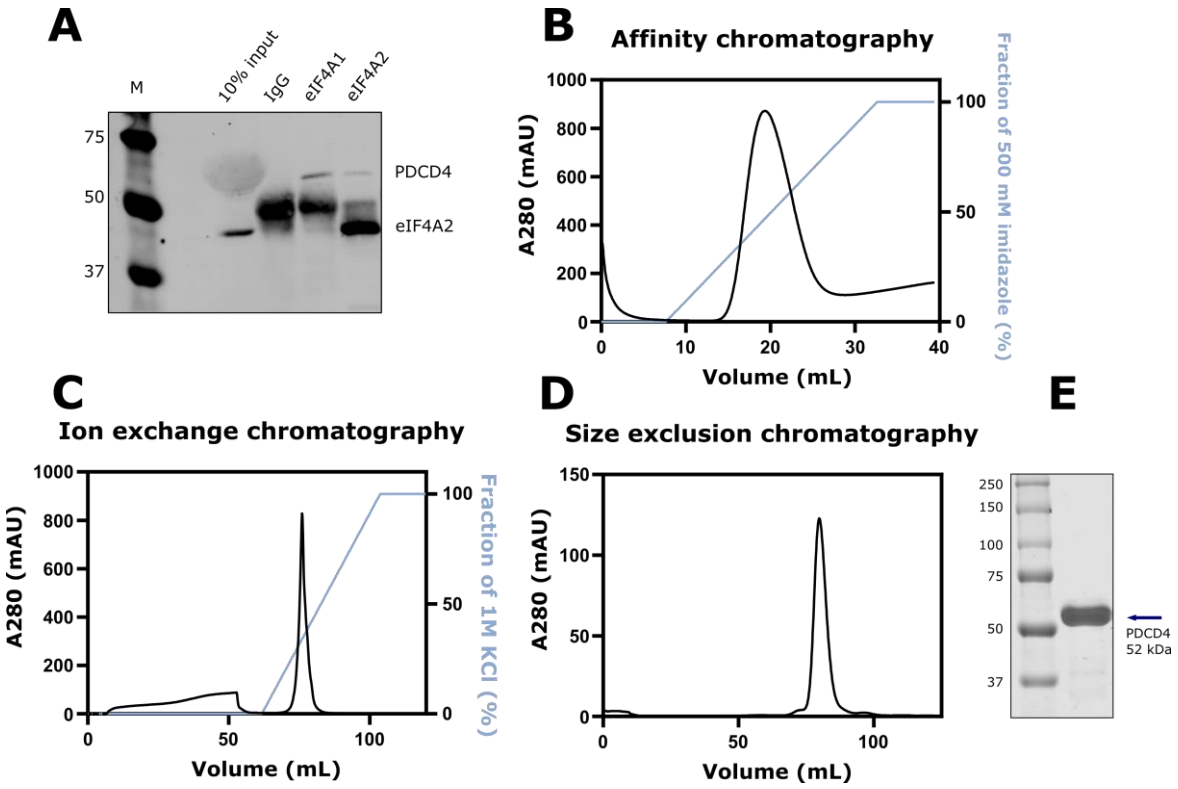

Figure 4.4-1 PDCD4 purification

- **A.** Co-immunoprecipitations of IgG, eIF4A1 and eIF4A2 in HeLa cells, probed with anti-PDCD4 and anti-eIF4A2 antibodies. PDCD4 co-precipitated in both eIF4A1 and eIF4A2 IP lanes. No unspecific bands were detected.
- **B.** Representative elution profile of PDCD4 in a linear imidazole gradient on a HisTrap HP column.
- **C.** Representative chromatogram of PDCD4 protein sample after ULP1 treatment. PDCD4 elutes in a linear KCl gradient on a ResourceQ column.
- **D.** Representative size exclusion chromatography column of PDCD4. PDCD4 elutes around 85 mL on a Superdex S200 HiLoad 16/600 column.
- **E.** Coomassie stained SDS-PAGE gel presenting purified PDCD4 (52 kDa). Protein marker sizes indicated on the left in kDa.

Next, the effect of PDCD4 on eIF4A2 unwinding and ATPase activities was tested on 5'$(AG)_{10}$ overhang RNA. Similarly, as what was previously described for eIF4A1 (Yang *et al.*, 2002), PDCD4 inhibited eIF4A2 unwinding activity in a concentration dependent manner (**Figure 4.4-2**, panel A); here even a 4-fold excess of PDCD4 did not inhibit fully the unwinding activity of 5 μM eIF4A2. However, as this reaction was performed in presence of eIF4H, its influence on the inhibition could not be excluded. Contrary to what was reported for eIF4A1, eIF4B and PDCD4 (Yang *et al.*, 2002), eIF4H in presence of equimolar PDCD4 and eIF4A2 concentrations still stimulated eIF4A2 unwinding activity (**Figure 4.4-2**, panel B, *left*). To exclude possible batch issues, this experiment was replicated with PDCD4 from a new protein purification. The obtained results were identical (± SEM), suggesting that eIF4H can stimulate eIF4A2 in presence of PDCD4. To exclude a role of eIF4H in prevention of eIF4A2 inhibition by PDCD4, the same experiments were performed in absence of eIF4H (**Figure 4.4-2**, panel B, *left*). Note, that the reaction performed with free eIF4A2 is only a technical duplicate. Similarly, as in the presence of eIF4H, equimolar concentration of PDCD4 did not fully inhibit eIF4A2 activity (**Figure 4.4-2**, panel B, *left*). Since the activity of eIF4A2 is a lot lower than in presence of eIF4H a direct comparison is difficult to make. Therefore, the obtained results were normalised to the respective starting value with 0 μM PDCD4 (**Figure 4.4-2**, panel B, *right*). The PDCD4 inhibition followed a similar trend both in presence and absence of eIF4H. Additionally, PDCD4 inhibition of eIF4A2 ATPase activity was correlated with the inhibition of unwinding (**Figure 4.4-2,** panel C).

In all, PDCD4 interacts with eIF4A2 even in cells in which eIF4A2 is not the dominant paralogue. Moreover, PDCD4 inhibits eIF4A2 in concentration dependent manner, however a full inhibition of both unwinding and ATPase activity requires excess of PDCD4. Additionally, eIF4H stimulates eIF4A2 unwinding activity even in equimolar PDCD4 to eIF4A2 ratio. Finally, the inhibition of both catalytic activities of eIF4A2 is correlated.

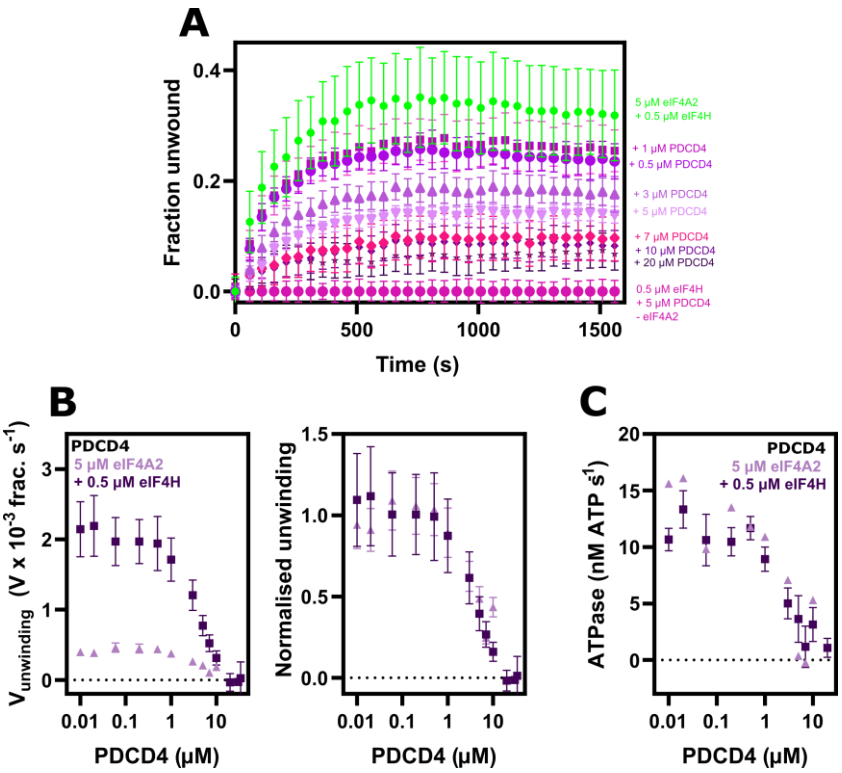

Figure 4.4-2 PDCD4 completely inhibits eIF4A2 unwinding and ATPase activities when in excess over eIF4A2

A. Unwinding activity of 5 μM eIF4A2 in presence of 0.5 μM eIF4H and indicated concentration of PDCD4, presented as fraction unwound over time. Activity of eIF4A2 decreases with increase of PDCD4 concentration. N = 6, error bar – SEM.

B. **Left**: eIF4A2 velocity of unwinding versus PDCD4 concentration for 5 μM eIF4A2 (*light purple*, n = 1), and in presence of 0.5 μM eIF4H (*dark purple*, n = 6). **Right**: Normalisation of unwinding from the graph on the left to the result obtained for 0 μM PDCD4 concentration. The influence of PDCD4 on eIF4A2 activity is the same both with and without presence of eIF4H. Error – SEM.

C. ATPase activity of 5 μM eIF4A2 alone (*light purple* = 1) and in presence of 0.5 μM eIF4H (*dark purple*, n = 6) in increasing concentration of PDCD4. Error – SEM.

4.5. CNOT1 reduces eIF4A2 affinity for RNA

Recent reports have shown that eIF4A2 plays a role in translational repression, through association with CNOT1, a large scaffold protein of CCR4-NOT complex (Meijer *et al.*, 2013, 2019; Wilczynska *et al.*, 2019). However, this interaction has also been contested (Chen *et al.*, 2014). This subchapter's aim was to explore the potential interaction and what could modulate it, as well as to test the previously unexplored possible influence of CNOT1 on eIF4A2 enzymatic activities.

As purification of a longer construct of CNOT1 spanning both MA3 and MIF domains turned out to be problematic (see selected examples **Appendix 2 Figures 2-1**, **2-2**), two shorter constructs were purified (**Figure 4.5-1**).

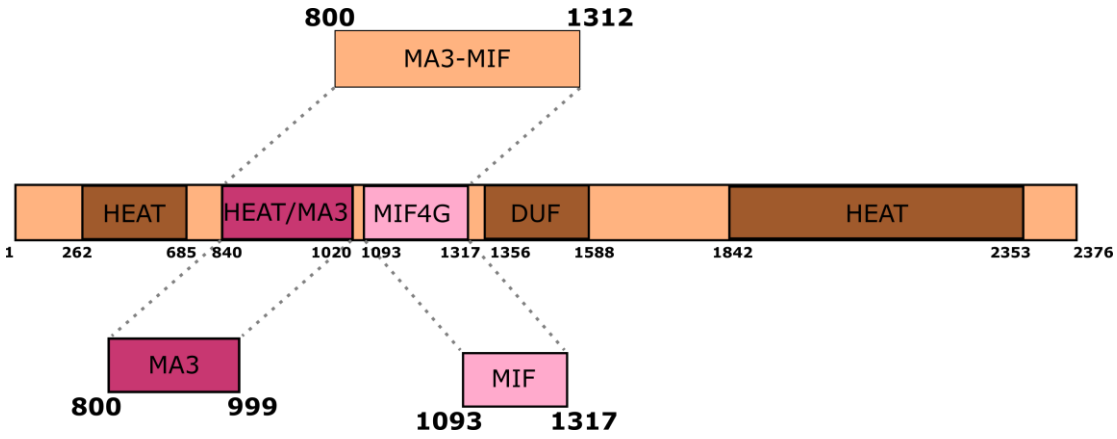

Figure 4.5-1 CNOT1 constructs

CNOT1 constructs used in this thesis. Numbers indicate start and end residues of the domains and constructs. Domains' residue numbers taken from (Hagkarim and Grand, 2020).

First His-SUMO-CNOT1-MIF4G construct (further called as MIF – amino acids 1093 – 1317; generated by Dr Tobias Schmidt) was expressed in *E. coli* strain BL21 DE3 RP codon+. The precleared bacterial lysate was treated in the same manner as for the other proteins in this chapter (see also **Chapter 2.2**). First, His-SUMO-MIF was eluted in a linear imidazole gradient from HisTrap HP affinity column (**Figure 4.5-2**, panel A, *top left*), next after ULP1 cleavage the fractions containing MIF protein were applied to a ResourceQ column (**Figure 4.5-2**, panel A, *top right*; see SDS-PAGE *bottom right*). Even though the calculated pI of MIF was 6.62 the protein did not bound to the anion exchange column in pH 7.5. Therefore, flow through (FT) was collected, concentrated, and applied on a Superdex S200 HiLoad 16/600 size exclusion column (**Figure 4.5-2**, panel A, *bottom left*). The fractions containing proteins that eluted at around 100 mL retention volume were collected and resolved on an SDS-PAGE (**Figure 4.5-2**, panel A, *bottom right*). This time, contaminants were visible in the sample and additional purification steps were performed. As most of the contaminants visible on a Coomassie stained gel corresponded in size to His-SUMO tag a reverse affinity chromatography was performed (**Figure 4.5-2**, panel B, *top*). This time, flow through from the HisTrap HP column contained MIF protein and contaminants were eluted in a linear imidazole gradient (**Figure 4.5-2**, panel B, *bottom left*). Finally, the flow through from reverse affinity chromatography was concentrated and applied again on a Superdex S200 HiLoad 16/600 column. This time, the sample did not contain contaminants, and MIF eluted in earlier fractions - 95 mL (**Figure 4.5-2**, panel B, *bottom right*). Finally, the concentration of MIF was determined by measuring its absorbance and the purity was assessed using SDS-PAGE (**Figure 4.5-2**, panel B, *bottom right*). In all, MIF domain was deemed to be of good purity to be used in subsequent studies.

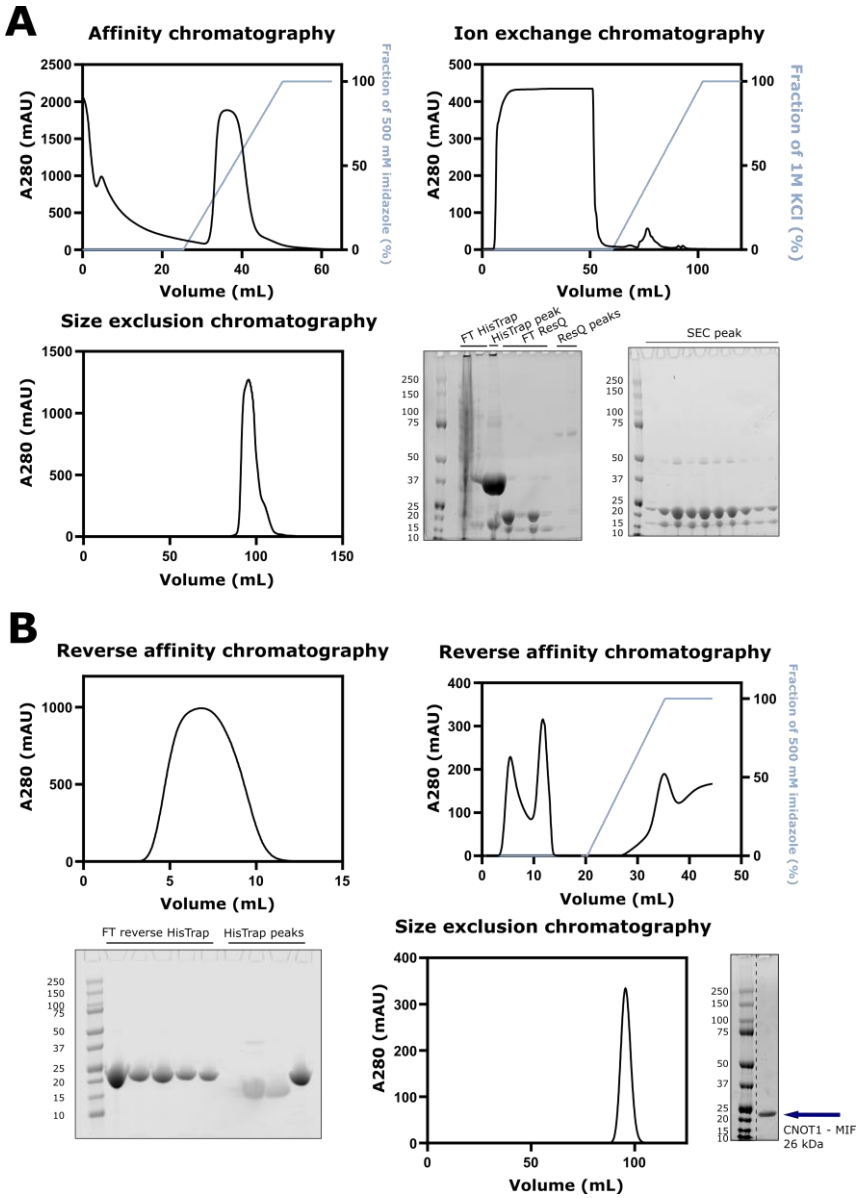

Figure 4.5-2 CNOT1 MIF domain purification

A. Purification of CNOT1 MIF domain (amino acids 1093-1317). Representative chromatograms. MIF elution in imidazole gradient on HisTrap HP (affinity chromatography) – *top left*. ULP1 treated MIF did not bound to anion exchange column (ResQ), the flow through was collected and concentrated – *top right* panel. The 26 kDa MIF eluted at around 100 mL on Superdex S200 HiLoad 16/600 column – *bottom left* panel. Coomassie stained gels from MIF purification – *bottom right*, fractions presented on the gels indicated above each lane, marker sizes in kDa indicated on the side. FT – flow through. MIF construct was deemed not pure enough (contamination of cleaved tag and other proteins visible).

B. Further purification of pooled fractions from size exclusion chromatography visible in panel **A**. The pooled fractions were of large volume, therefore double application on HisTrap HP column was needed – *top panels*. Collected flow through (FT) from HisTrap HP resolved on Coomassie stained gel visible in the *bottom left panel* – samples indicated on the top of the gel, marker sizes in kDa indicated on the side. Size exclusion chromatography of concentrated FT fractions from reverse affinity (Superdex S200 HiLoad 16/600 column), with Coomassie stained gel indicating final product (*bottom right*).

Next, CNOT1 MA3 domain (amino acids 800 - 999; cloned by Dr Lori Buetow) in petSUMO vector was expressed in *E. coli* strain BL21 DE3 RP codon+. It should be noted that there are 93 amino acids uncovered between both MIF and MA3 constructs, however purification of longer MA3 domain, including linker was unsuccessful (see **Appendix 2 Figure 2-3**). First, pre-cleared lysate was applied to a HisTrap HP column, and the bound protein eluted in a linear imidazole gradient (**Figure 4.5-3**, panel A). Next, a protocol described in Fabian *et al.*, 2013 was followed. However, the construct did not bind to an anion exchange column both in the pH conditions described previously (Fabian *et al.*, 2013) as well as in increased pH of the buffer (**Figure 4.5-3**, panel B, *left*). As the collected flow-through contained both the MA3 domain and the cleaved His-SUMO tag (**Figure 4.5-3**, panel B, *middle*), reverse affinity chromatography was performed using a peristaltic pump. The absorbance of collected FT was measured and the final product purity was determined based on Coomassie stained gel (**Figure 4.5-3**, panel B, *right*). In sum, the MA3 domain was deemed to be of good quality to be used in further studies.

In this subchapter CNOT1 constructs are referred to as MIF (amino acids 1093 – 1317), MA3 (amino acids 800 - 999), MIF + MA3, when used together. Additionally, longer construct spanning both domains (amino acids 800 – 1312) was gifted by Dr Lori Buetow and is referred to as MA3-MIF (see **Appendix 2 Figure 2-4**). It should be noted that the longer MA3-MIF construct was limited in both concentration (due to aggregation issues) and amount therefore it could not be tested in all of the activities.

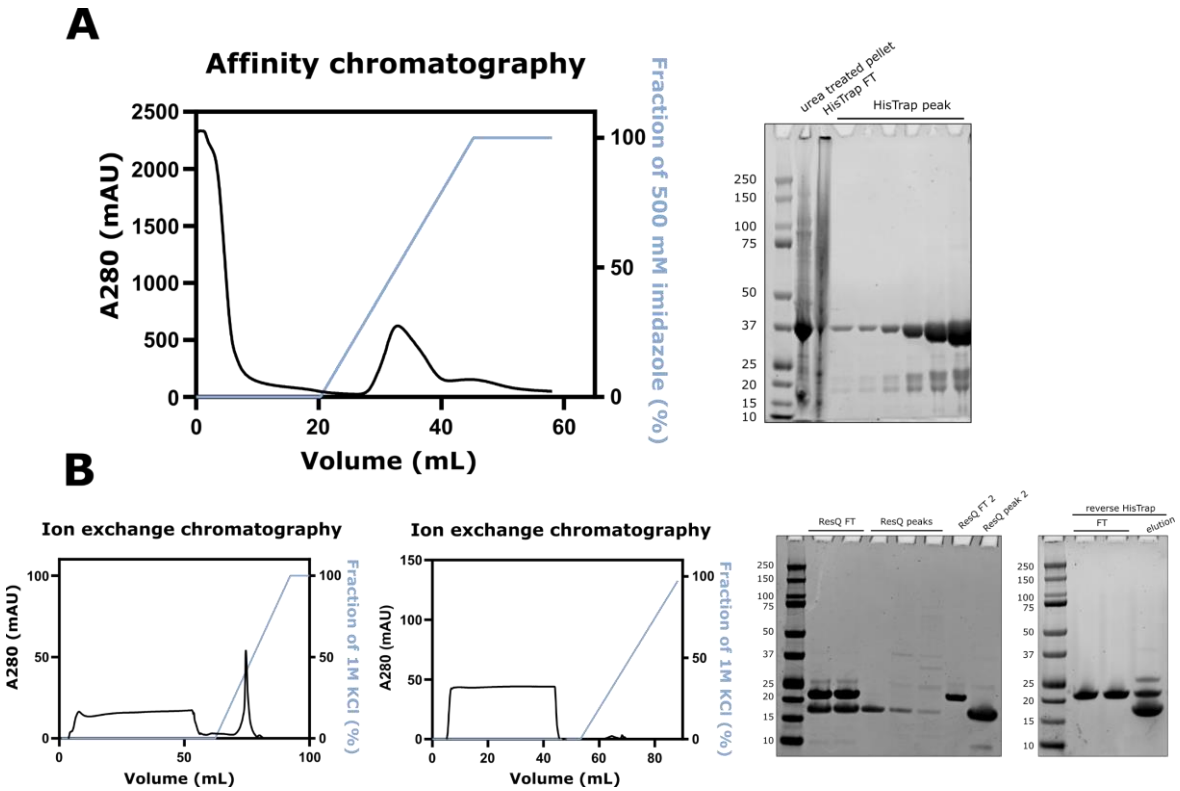

Figure 4.5-3 CNOT1 MA3 domain purification

A. Elution profile of CNOT1 MA3 (amino acids 800 – 999) in a linear imidazole gradient on HisTrap HP column – *left*, and a Coomassie stained gel representing fractions from this step of purification (marker sizes in kDa indicated on the side of the gel). Flow through – FT.

B. MA3 elution profile on a heparin column in increasing concentration of KCl in pH = 7.5 (*left*) and collected flow through (FT) applied again in pH = 8.5 (*middle*). Coomassie stained gels from purification (*right*), with marker size indicated on the side of the gel. Each time, MA3 fraction was found in FT. Gel on the right indicates additional purification steps – reverse affinity chromatography – done with a peristaltic pump – FT fractions contained clean protein.

Next, the interactions between the purified CNOT1 constructs and eIF4A2 were examined through immunoprecipitations of recombinant proteins (see also **Chapter 2.3.7**). As interaction between MIF domain and DDX6 has been previously described (Chen *et al.*, 2014), DDX6 was used as a control. For DDX6 purification see **Appendix 2 Figure 2-5**. The proteins for IPs were mixed in equimolar concentrations in binding buffer supplemented with IGEPAL CA-630 (see **Chapter 2.3.7**). MIF domain precipitated weakly with eIF4A2, however the precipitation with DDX6 was only 1.5-fold stronger, quantified as signal intensity from the gel (**Figure 4.5-4**, panel A). No interaction between eIF4A2 and MA3

was detected in the tested conditions, and 10-fold lower interaction was observed for MA3 and DDX6 than for MIF and DDX6.

As it has been described that **1)** CNOT1 stimulates ATPase activity of DDX6 and modulates its conformation, with the structure indicating that bound DDX6 is ATPase competent (Mathys *et al.*, 2014), **2)** the ATPase competent conformation of DDX6 is similar to the one observed for yeast eIF4A in presence of eIF4G (Schutz *et al.*, 2008), **3)** eIF4A undergoes conformational changes during ATP conversion and RNA binding (Lorsch and Herschlag, 1998b), the interaction between eIF4A2 and MIF was explored in presence of RNA and three stages of ATP conversion, i.e., AMP, ADP + Pi, AMPPNP (**Figure 4.5-4**, panel B). Indeed, presence of RNA and different adenosine phosphates influenced the interaction. The strongest, albeit still rather weak, interaction between eIF4A2 and MIF was observed in presence of ADP + Pi. Free proteins interacted to lower extent, and a low intensity band was detected for AMP condition.

As presence of ATP derivatives and RNA seemed to change the interaction between MIF and eIF4A2, it was tested whether both MIF and MA3 could co-precipitate in AMP and ADP + Pi conditions (**Figure 4.5-4**, panel C). MIF domain again coprecipitated with eIF4A2 in the tested conditions, however this time MIF domain interacted with eIF4A2 the strongest when both MIF and MA3 were present in ADP + Pi conditions. Moreover, a co-precipitation of MA3 was observed in ADP + Pi condition.

In all, both MIF and MA3 domains can interact with eIF4A2 to a low extent. Moreover, this interaction can be modulated by presence of RNA and different stages of ATP conversion, suggesting this interaction might be conformation dependent.

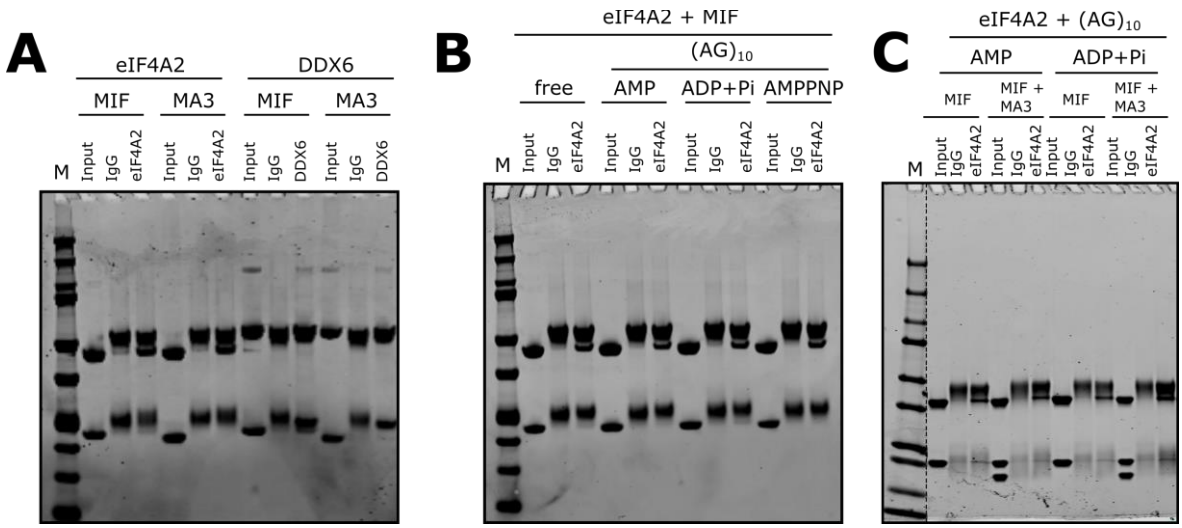

Figure 4.5-4 MIF domain of CNOT1 interacts with eIF4A2 more strongly than MA3 domain

- **A.** Coomassie stained gel of IPs on recombinant proteins representing interactions of eIF4A2 and DDX6 with MIF and MA3 domains. Both MIF and MA3 domains co-precipitated with DDX6, MA3 to a lower extent. Only MIF domain of CNOT1 co-precipitated with eIF4A2. 100 µL of 5 µM of each protein was used per IP.
- **B.** Coomassie stained gel of IP on recombinant proteins representing co-precipitation of CNOT1 MIF domain and eIF4A2 in 4 conditions: 1) free proteins, 2) 1 µM $(AG)_{10}$ RNA and 1 µM AMP, 3) 1 µM $(AG)_{10}$ RNA and 1 µM ADP + Pi, 4) 1 µM $(AG)_{10}$ RNA and 1 µM AMP-PNP. 100 µL of 5 µM of each protein was used per IP. eIF4A2 precipitated in eIF4A2 IP in all conditions, MIF co-precipitation visible in all conditions except the AMP-PNP one.
- **C.** Coomassie stained gel of IP on recombinant proteins representing co-precipitation of CNOT1 MIF and MA3 domains and eIF4A2 in 1 µM $(AG)_{10}$ RNA and 1 µM AMP and 1 µM $(AG)_{10}$ RNA and 1 µM ADP + Pi conditions. 100 µL of 5 µM of each protein was used per IP. Lanes with conditions unrelated to this experiment were removed. MIF domain co-precipitated with eIF4A2 in all tested conditions, weak co-precipitation of MA3 domain is visible only in ADP + Pi condition with all the tested proteins present.

Next, as the interaction between MIF, MA3 and eIF4A2 was established, the influence of both domains on eIF4A2 RNA unwinding was investigated. Here, free eIF4A2 unwinding activity was set as 100% and the activity in presence of MA3, MIF, and MA3-MIF was normalised to this value (**Figure 4.5-5**, panel A). None of the tested domains influenced significantly eIF4A2 activity. A small reduction (less than 5 %) can be seen in presence of MIF, and less than 10% in presence of MA3-MIF.

As the influence on eIF4A2 unwinding activity was not striking, the same CNOT1 constructs were tested with DDX6 (**Figure 4.5-5**, panel B). As MIF domain induced DDX6 unwinding to a high extent, the unwinding activity of free DDX6 and in presence of other CNOT1 constructs was normalised to this value, similarly as in **Figure 4.5-5,** panel A. DDX6 unwinding activity was undetectable, and MA3 did not activate DDX6 unwinding activity. MA3-MIF activated DDX6 however to about 30% of the activation observed in presence of MIF. It should be noted however, that previous experiments in the Bushell lab, indicated a greater activation of DDX6 unwinding in presence of a longer construct (amino acids 842 – 1317). This could possibly indicate, **1)** that the longer construct used in this experiment (amino acids MA3-MIF 800 – 1312) acts differently than the one previously used in the Bushell lab (amino acids 842 – 1317), **2)** the gifted MA3-MIF is a mixture of both active and inactive protein, **3)** small amounts of contaminants present in MA3-MIF sample led to inaccurate determination of concentration. However, the constructs were active, and used in the further studies.

As eIF4G and CNOT1 share sequence similarities (Rouya *et al.*, 2014), and eIF4G-MC reduced functional affinity of eIF4A2 (see **Table 4.3-2**), it was tested whether CNOT1 constructs could influence eIF4A2 RNA binding affinity. Interestingly, all of the tested CNOT1 constructs reduced eIF4A2 binding affinity (**Figure 4.5-5**, panel C). Intriguingly, only the affinity towards the AG-motifs RNAs, i.e., $(AG)_{10}$, $(AGUG)_5$ could be measured, as either no binding or not well quantifiable affinity (above 20 µM and unreliable) was detected for $(CAA)_6CA$, $(UCUC)_5$, $(UGUU)_5$. Additionally, as only MA3-MIF was shown to exert any RNA binding on its own, and only towards $(AG)_{10}$ and $(AGUG)_{10}$ (**Figure 4.5-5**, panel D), the observed decrease in affinity possibly stems from protein-protein interaction and not competition for RNA binding.

Next, as a reduction of eIF4A2 affinity was observed in presence of CNOT1 constructs, it was examined whether RNA release by eIF4A2 could also be influenced. Since MIF and MA3 did not bind RNA, the signal observed in RNA release experiment stems from eIF4A2 activity (**Figure 4.5-5**, panel E). Despite the change in affinity, no change in RNA release was observed.

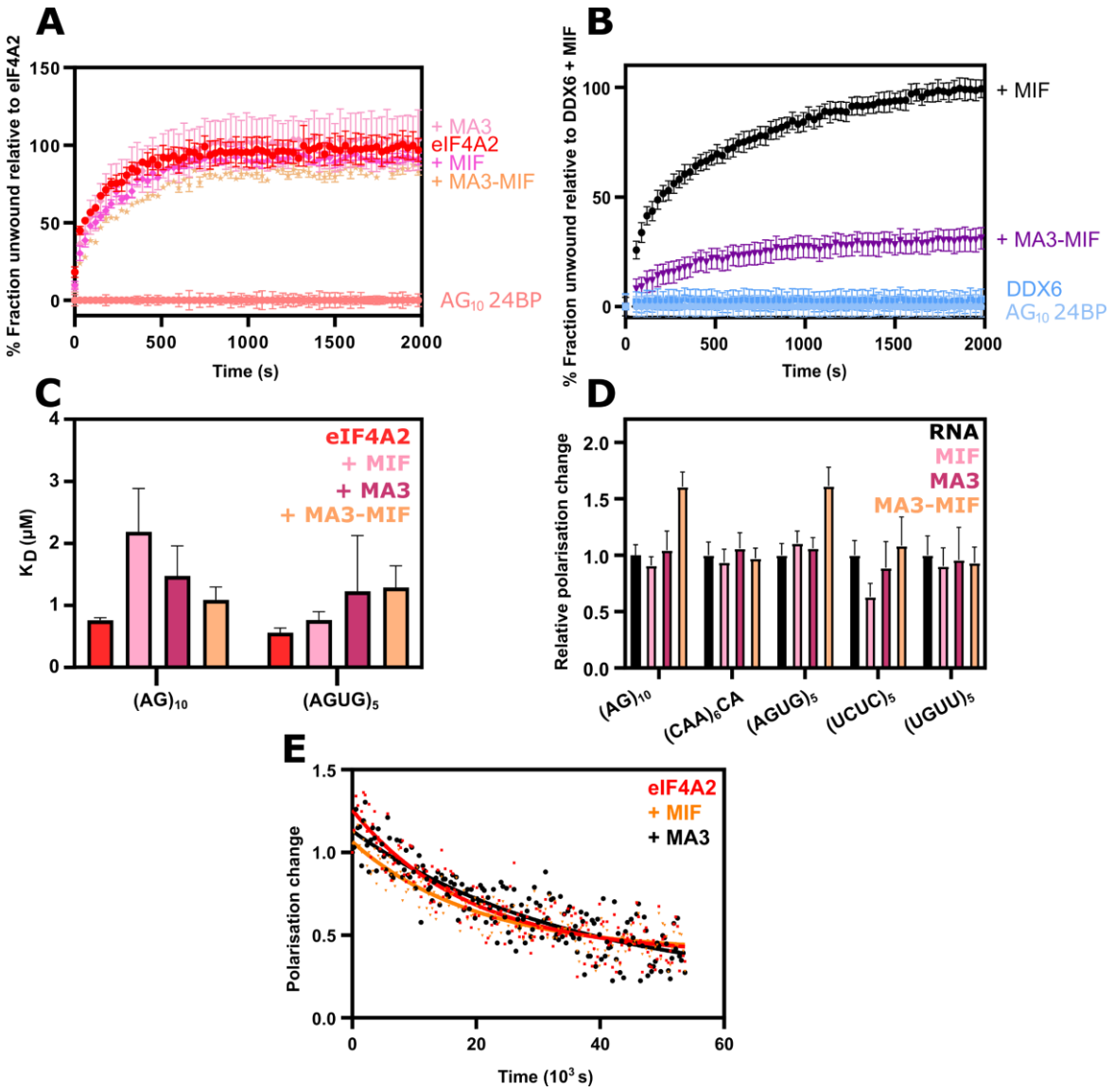

Figure 4.5-5 CNOT1 reduces eIF4A2 binding affinity

A. Unwinding activity of eIF4A2 alone (*red*) and in presence of 0.5 μM CNOT1 constructs: MIF (*purple*), MA3 (*light pink*), and the longer MA3-MIF (*yellow*). Representative graph (n = 3), normalisation to the activity of 5 μM eIF4A2 – set as 100 %, error – STD from technical duplicate. MIF and MA3 constructs do not change eIF4A2 unwinding activity. Slight reduction of unwinding activity visible in MA3-MIF.

B. Unwinding activity of 5 μM DDX6 alone (*blue*) and in presence of 0.5 μM MIF (*black*) and 0.5 μM MA3-MIF (*purple*). Normalisation to the unwinding activity of 5 μM DDX6 in presence of 0.5 μM MIF – set as 100 %. MA3 did not change the unwinding activity of DDX6 (points omitted for clarity). MIF strongly enhanced the activity of DDX6. The longer construct induced unwinding to only about 30 % of what was observed for MIF. Error – STD from technical duplicate, n = 2.

C. K_D of eIF4A2 measured by polarisation for eIF4A2 alone (*red*, n = 4) and in presence of 0.5 μM MIF (*pink*, n =2), 0.5 μM MA3 (*purple*, n = 2) and 0.5 μM MA3-MIF (*yellow*, n = 3) for $(AG)_{10}$ and $(AGUG)_5$ RNAs. K_D of eIF4A2 increases in presence of all tested CNOT1 constructs. Error – SEM, measured in presence of AMP-PNP, RNA concentration 50 nM.

(figure legend continues on the next page)

D. RNA binding of 0.5 µM of each MIF (*pink*, n =3), MA3 (*purple,* n = 3), MA3-MIF (*yellow*, n = 3). Relative polarisation for each free RNA (*black*), polarisation measured for each construct divided by polarisation of free RNA. Only visible change for $(AG)_{10}$ and $(AGUG)_5$ RNA for longer construct MA3-MIF, indicates RNA sequence specific binding. Error – SEM.

E. $(AG)_{10}$ RNA release of 5 µM eIF4A2 (*red*) in presence of 0.5 µM MIF (*orange*), 0.5 µM MA3 (*black*). The tested domains do not influence RNA release. Technical duplicate presented, error bars omitted for clarity, fit – exponential decay, n = 3.

So far, the only influence of the tested CNOT1 constructs on eIF4A2 was observed in the RNA binding affinity. As CNOT1 interacts with deadenylases CNOT6 and CNOT7, and eIF4A2 has been shown to inhibit CNOT7 deadenylation activity through interaction with longer CNOT1 construct (Meijer *et al.*, 2019), it was explored whether similar activity can be observed for shorter (MIF and MA3) constructs. For purification of CNOT7 see **Appendix 2 Figure 2-6**.

Here, no deadenylation activity of CNOT7 was observed in presence of eIF4A2 and MIF, MA3, or both MIF + MA3 (**Figure 4.5-6** *top*). In contrast, strong deadenylation was observed in presence of DDX6 and MIF or both MIF + MA3 (**Figure 4.5-6** *middle*). However, no deadenylation was detected in presence of MA3 and DDX6, indicating that what was previously observed for the longer CNOT1 construct (Meijer *et al.*, 2019), was mediated through MIF domain. Additionally, no deadenylation activity was detected for either CNOT7 alone, or in presence of MIF, MA3, both MIF + MA3 without DDX6. As deadenylation activity has been observed for longer construct of CNOT1 and CNOT7 in absence of the helicases (Meijer *et al.*, 2019), the lack of deadenylation in presence of MIF indicates that a longer CNOT1 construct is needed for stimulation of CNOT7.

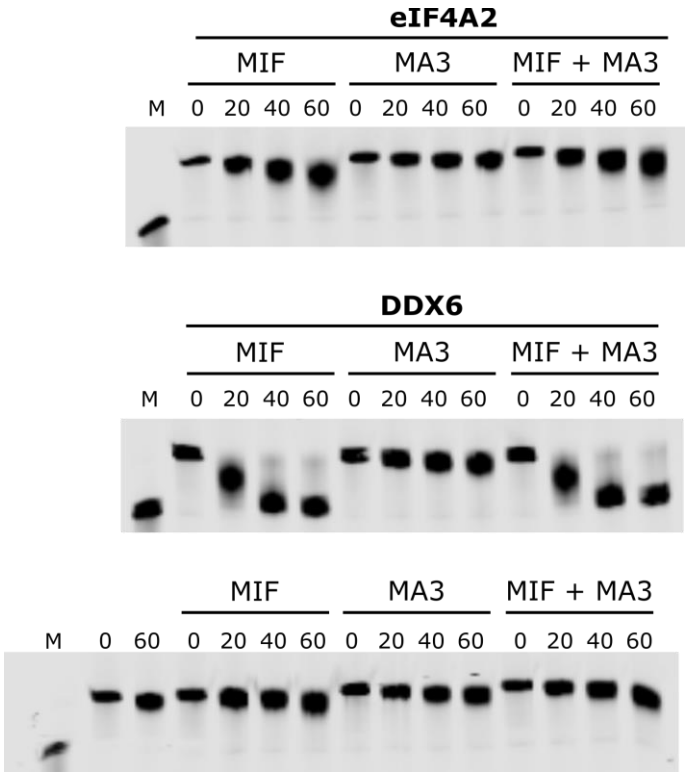

Figure 4.5-6 eIF4A2 do not influence deadenylation activity of CNOT7 in presence of short CNOT1 constructs

Deadenylation activity of 0.5 µM CNOT7 with 3 µM of indicated proteins on 1 µM deadenylation substrate in presence of 1 mM AMP-PNP. Timepoints indicated as numbers above the lanes in minutes, sample at timepoint 0 contains no CNOT7. M stands for fully deadenylated marker. Short constructs of CNOT1 do not induce deadenylation activity of CNOT7. DDX6 enhances deadenylation only in presence of MIF domain or both MIF and MA3 but not with MA3 only. eIF4A2 do not induce deadenylation.

In summary, eIF4A2 was shown to interact with MIF and MA3 CNOT1 constructs *in vitro*, and this interaction was modulated by presence of RNA and ATP derivatives. MIF interacted with eIF4A2 to a greater extent than MA3, which interaction was detected only when both MIF and MA3 were present in the reaction. Moreover, ADP + Pi bound state of eIF4A2 seemed to be the most favourable for the interaction with the tested constructs. In contrast to DDX6, the CNOT1 constructs did not greatly change eIF4A2 unwinding activity, and the largest effect was observed on RNA binding affinity of eIF4A2. All of the tested constructs reduced eIF4A2 binding affinity for RNAs, with only detectable binding for the AG-motifs. Furthermore, this reduced affinity possibly did not stem from competition for RNA substrate as only MA3-MIF had a measurable binding to $(AG)_{10}$ and $(AGUG)_5$ RNAs. The reduced binding affinity however did not correlate with faster or changed RNA release by eIF4A2. Finally, eIF4A2 did not influence deadenylation of CNOT7 in presence of MIF and MA3, while opposite effect was observed for MIF and DDX6.

4.6. Chapter discussion

In this chapter the influence of potential interaction partners on activities of eIF4A2 was explored. As previous studies have focused on the effect of interaction partners exerted on eIF4A1, and none of the previous reports investigated their influence on the novel, oligomerised eIF4A, a thorough examination of eIF4A2 in presence of auxiliary proteins was necessary.

First, the effect of eIF4H on eIF4A2 was investigated. Both the unwinding and ATPase activities of eIF4A2 on 5'$(AG)_{10}$ overhang RNA were stimulated (**Figure 4.2-2**). However, the increase in ATPase activity, contradictory to previous reports on the effect on eIF4A1, was minimal (Richter-Cook *et al.*, 1998). Moreover, eIF4H seemed to reduce the cooperativity between eIF4A2 protomers in the unwinding reaction in concentration dependent manner. This could potentially indicate, that eIF4A2 achieves the enhanced activity by either creating sub-oligomeric complexes or by each individual protomer interacting more with eIF4H than with another eIF4A2.

Moreover, the unwinding activity in 3'-to-5' direction in presence of eIF4H was investigated (**Figure 4.2-3**). Contrary to what was previously reported for eIF4A1 (Rogers *et al.*, 2001), the activity on 3'-to-5' direction was further stimulated, albeit not to a high extent. This time, a stronger preference towards AG-RNA was observed in both direction than to 3'$(CAA)_6$CA overhang as was detected for free eIF4A2 (**Figure 4.2-3**). Additionally, a slight decrease in ATPase activity was observed on 3'overhang RNA substrates (**Table 4.2-1**). This suggests that eIF4A2 unwinding activity in presence of eIF4H on 3'overhang RNA is more productive per unit of ATP.

Next, to understand what could drive the stronger preference of eIF4A2 in presence of eIF4H towards AG-RNA than to the position of the overhang itself, eIF4H binding affinity towards $(AG)_{10}$ was investigated. Conversely to what has been described in the literature (Richter-Cook *et al.*, 1998; Rozovsky, Butterworth and Moore, 2008), eIF4H bound to $(AG)_{10}$ with higher affinity than eIF4A2. Perhaps eIF4H could enhance the affinity of eIF4A2 itself in the reaction, however a strong increase (K_D reduction) in functional binding affinity was not observed (**Table 4.3-2**). Another reason for this AG-specific stimulation could

stem from both the decrease in cooperativity between eIF4A2 protomers and the affinity of eIF4H towards $(AG)_{10}$. Possibly eIF4H binds strongly to the AG-RNA and recruits eIF4A2 forming a distinct oligomeric complex. Additional explanation could be what was speculated before (Assen Marintchev *et al.*, 2009), that eIF4H could stabilise the single-stranded RNA region and prevent duplex reannealing. Perhaps additional tests for eIF4H binding to the duplex region, or the single-stranded region created after strand dissociation and to other RNA substrate sequences could yield more answers.

Next, the influence of eIF4G1 was investigated. As eIF4G1 has been shown to not be the main interaction partner of eIF4A2 (Meijer *et al.*, 2019; Wilczynska *et al.*, 2019), the interaction of the two proteins was investigated in HeLa cells. In HeLa cells, where eIF4A2 is not the dominant paralogue (Roger Duncan and Hershey, 1983; Bekker-Jensen *et al.*, 2017), an interaction was observed (**Figure 4.3-1**).

Therefore next, constitutively active eIF4G-MC (amino acids 674 – 1599) was purified (Feoktistova *et al.*, 2013). Here, in contrast to eIF4A1 (Rogers *et al.*, 2001; Korneeva *et al.*, 2005; Nielsen *et al.*, 2011; Özeş *et al.*, 2011) a stimulation of the eIF4A2 unwinding and ATPase activities in presence of eIF4G-MC was limited (**Figure 4.3-3**). This in turn could suggest a different interaction mechanism between eIF4G-MC and eIF4A1 or eIF4A2. Next, whether eIF4H and eIF4G-MC can impart synergistic effect on eIF4A2, similarly to what has been shown for eIF4A1, eIF4G and eIF4B was investigated (Abramson, Dever and Merrick, 1988; Nielsen *et al.*, 2011). Again, a dissimilar effect to the one described for eIF4A1 was observed, further suggesting that eIF4G-MC acts differently upon eIF4A2 (**Figure 4.3-3**). Moreover, a reduction in eIF4H stimulation was observed in the unwinding reaction. This reduction however was not due to competition for RNA binding or lack of eIF4G-eIF4A2 interaction. In fact, eIF4G-MC reduced eIF4A2 functional binding affinity for RNA substrate (**Table 4.3-2**), however presence of both cofactors increased the affinity of eIF4A2 for RNA. This indicates, that despite lower activity detected for eIF4A2 in presence of both interaction partners than just eIF4H, eIF4A2 bound tighter to the RNA substrate. Moreover, eIF4G-MC, similarly as eIF4H reduced cooperativity between eIF4A2 protomers however to a lower extent, suggesting that in the presence of sub-molar concentrations of eIF4G-MC, the eIF4A2 protomers work together.

In the ATPase reaction, the opposite effect to what was observed in unwinding was detected. With addition of eIF4H the ATPase activity decreased in eIF4H concentration-dependent manner in comparison to ATPase of eIF4A2 and eIF4G-MC complex (**Figure 4.3-3**). This indicates, that both cofactors exert different effect on eIF4A2 and in fact do not act in a synergistic manner. Additionally, a similar reduction in ATPase activity was observed for eIF4G-MC eIF4A2 on RNA substrate with 3'$(AG)_{10}$ (**Figure 4.3-4**). Moreover, regardless of the slight increase in the eIF4A2 unwinding activity in presence of eIF4G-MC in 3'-to-5' direction versus 5'-to-3', the observed activity was lower than for eIF4A2 alone (compare **Table 4.2-1** and **Table 4.3-1**). This could potentially suggest that eIF4A2 while bound to eIF4G-MC loses its 3'-to-5' directional preference. Perhaps, a competition experiments on a substrate with single-stranded region in the middle, and two differently labelled double stranded region would provide more information about the eIF4A2 preference when faced with a choice of direction, especially in presence of auxiliary proteins.

Last of the canonical interaction partners of eIF4A tested on eIF4A2 was the tumour suppressor, mTOR-regulated eIF4A inhibitor – PDCD4 (Yang *et al.*, 2002, 2004; Chen *et al.*, 2003; Dennis, Jefferson and Kimball, 2012; Jin *et al.*, 2013; Modelska *et al.*, 2015). Despite the previously reported interaction between eIF4A2 and PDCD4 (Yang *et al.*, 2002), this interaction was re-examined in HeLa cells. Indeed, even in cells preferentially overexpressing eIF4A1 (Duncan and Hershey, 1983), interaction between the two proteins was observed (**Figure 4.4-1**).

Next, the PDCD4 imposed inhibition of RNA unwinding and ATPase activity was tested *in vitro (***Figure 4.4-2**). PDCD4, in agreement to previous reports on eIF4A1 (Yang *et al.*, 2002) inhibited eIF4A2 in concentration dependent manner. Similarly, a full inhibition was not observed for equimolar concentrations of both proteins. This however, is in contrast with the available crystal structures of PDCD4 in complex with eIF4A1 (Chang *et al.*, 2009; Loh *et al.*, 2009), where a 1:2 interaction of PDCD4 to eIF4A1 was suggested, which could be interpreted as PDCD4 binding an oligomeric version of eIF4A. However, the full inhibition of both eIF4A2 activities was not observed for PDCD4 concentrations exceeding eIF4A2 concentration. Additionally, the previously observed low protein levels of PDCD4 in cells would not be sufficient to inhibit all of the free eIF4A (Vikhreva,

Kalinichenko and Korobko, 2017). Perhaps, the suggested previously mechanism of translation inhibition in which PDCD4 directly binds to mRNAs in the nucleus (Singh *et al.*, 2011; Vikhreva, Kalinichenko and Korobko, 2017), could be the main explanation for the reduction of translation in cells. Possibly, because the experiments performed in this chapter were started by preincubation of the proteins before adding the RNA substrate, the full inhibition was not observed. Another speculation about PDCD4 mediated translational inhibition could be recruitment of eIF4A2 to already bound by PDCD4 mRNA, and subsequently recruitment of CCR4-NOT complex.

Additionally, PDCD4 in conducted experiments did not inhibit stimulation imposed by eIF4H, which again could potentially indicate different modes of actions of on eIF4A2.

Finally, the influence of CNOT1 on eIF4A2 was investigated. For this short constructs of CNOT1 spanning 800 – 999 amino acids (MA3), and 1093 – 1317 amino acids (MIF) were purified. As the purification of a longer CNOT1 construct was problematic (see **Appendix 2 Figures 2-1**, **2-2**, **2-3**) due to aggregation and contaminants, only a small amount of longer construct spanning 800 – 1312 amino acids (MA3-MIF) was obtained as a gift and used in this study.

Contrary to the contested interaction between eIF4A2 and CNOT1 (MIF) (Chen *et al.*, 2014), an interaction between eIF4A2 and MIF was observed (**Figure 4.5-4**). Additionally, both MIF and MA3 co-precipitated with eIF4A2 in presence of ADP + Pi indicating that this interaction, similarly to what was described for both CNOT1 and DDX6 (Mathys *et al.*, 2014), as well as yeast eIF4A and eIF4G (Schutz *et al.*, 2008), could be dependent on conformational change of eIF4A2.

Next, the influence of CNOT1 on eIF4A2 was tested. Despite the strong stimulation of DDX6 unwinding activity by both MIF and MA3-MIF constructs, almost no change in eIF4A2 unwinding activity was detected (**Figure 4.5-5**).

Interestingly, eIF4A2 binding affinity was decreased in presence of all of the tested CNOT1 constructs (**Figure 4.5-5**). Additionally, the binding affinity was only observed for the AG-RNAs, i.e., $(AG)_{10}$ and $(AGUG)_5$ as for the other tested sequences either no binding or unreliable K_D values were measured. This increase in K_D is similar to what was observed for functional binding in presence of eIF4G-MC (**Table 4.3-2**), suggesting a possible similar mechanism imposed by

the two proteins. However, when interpreting the lack of eIF4A2 binding to certain RNA sequences in presence of CNOT1, caution need to be taken as **1)** those binding affinities were measured in presence of AMP-PNP, and **2)** for some of the tested sequences, i.e., $(UCUC)_5$, $(UGUU)_5$ eIF4A2 had higher affinity in presence of ATP (see **Table 3.8-1**). Furthermore, the change in binding affinity in presence of MIF and MA3 did not reflect the RNA release, as no change was detected on $(AG)_{10}$ RNA (**Figure 4.5-5**). Perhaps, investigating different RNA sequences and using the longer MA3-MIF construct would yield a different outcome.

More importantly, RNA binding to AG-motifs was detected for the longer construct, which has not been previously shown. Only in Baltz *et al.*, 2012, CNOT1 was indicated as possible mRNA binder with 50 % confidence. As both MIF and MA3 alone did not exhibit RNA binding, possibly the linker between two domains (between 1000 and 1092 amino acids) or a change in conformation is responsible for binding to mRNA.

Lastly, influence of eIF4A2 on CNOT7 deadenylation activities was examined in presence of MIF and MA3 domains (**Figure 4.5-6**). In contrast to DDX6, which induced deadenylation in presence of MIF, no induction of this activity was observed in presence of eIF4A2. Previously eIF4A2 was implicated in inhibition of CNOT7 deadenylation activity (Meijer *et al.*, 2019), however as this time as MIF domain did not induce CNOT7 deadenylation on its own, it cannot be concluded whether it was lack of activity or its inhibition. Furthermore, with the tested deadenylation substrate, i.e., $(CAA)_6CA\text{-}C_{20}\text{-}A_{20}$ in presence of MIF and AMP-PNP no binding by eIF4A2 should be expected. However, as shown in Meijer *et al.*, 2019, the inhibition of CNOT7 deadenylation was independent of eIF4A2 RNA binding capacity. Moreover, the greater interaction between eIF4A2 and MIF was observed in presence of ADP + Pi (**Figure 4.5-4**), however how that could be affected by addition of CNOT7 was not investigated. Perhaps, additional studies into different deadenylation RNA substrates, and different ATP analogues could potentially provide more information about the role of eIF4A2 in this process.

In all, in this chapter interactions of eIF4A2 with both the canonical eIF4A1 interaction partners as well as the CNOT1 from the translational repression complex was demonstrated. Moreover, the influence of eIF4G-MC was dissimilar

to the one previously described for eIF4A1. Perhaps, eIF4A2 exerts a dual activity, one in initiating translation (and possibly pro-tumourigenic), and the other in translational repression. After all, in Wilczynska *et al.*, 2019, mRNAs bound by both eIF4A1 and eIF4A2 were not shifted more towards the translating polysomal fractions, nor towards the repressed subpolysomal fractions. This in turn, may indicate that eIF4A2 behaviour is modulated by its interaction partners and by the bound mRNAs themselves.

5. The eIF4A paralogues and cross-species comparison

5.1. Chapter introduction

The differences on the effect on protein translation exerted by the highly identical eIF4A1 and eIF4A2 in the cellular and tumour environment are supported by the growing body of research (Galicia-Vazquez *et al.*, 2012; Meijer *et al.*, 2013; Modelska *et al.*, 2015; Wilczynska *et al.*, 2019; Gao *et al.*, 2020), (see also **Chapters 1.3**, **1.5**). However, how these different activities are achieved remains largely unknown. Therefore, the aim of the final results chapter of this thesis was to elucidate potential molecular differences between eIF4A1 and eIF4A2.

For this, different properties of eIF4A1 and eIF4A2 were compared including oligomerisation, unwinding, ATPase activity, and RNA binding. In particular, the effect of cofactors eIF4H and eIF4G on eIF4A1 and eIF4A2 was compared, as earlier reports about eIF4A1 (Abramson, Dever and Merrick, 1988; Nielsen *et al.*, 2011) and findings about eIF4A2 from this study (**Chapters 4.2**, **4.3**) indicated distinct cofactor activity upon the eIF4A paralogues.

As one of the major differences between the paralogues was observed in their RNA binding sequence-selectivity in a previous study from the Bushell lab (Wilczynska *et al.*, 2019), this was further explored. Identification of the responsible region for eIF4A2's strong binding sequence-selectivity could support determining the molecular differences between the paralogues and help our understanding how eIF4A1 and eIF4A2 establish their biological functions. Moreover, as the eIF4A2 binding-selectivity was implicated in translational repression, further understanding of which regions of those highly identical paralogues are responsible for this activity could potentially lead to targeting specific regions of the helicases in the future. Here, to identify regions responsible for this molecular divergence, a mutational analysis of the paralogues was performed.

As an additional approach to understand how differences between eIF4As can result in divergent functions, the *Saccharomyces cerevisiae* eIF4A (*Sc* eIF4A) was examined. Many previous studies exploring the activities of eIF4A were performed in yeast (Caruthers, Johnson and McKay, 2000; Schutz *et al.*, 2008;

Andreou and Klostermeier, 2013; 2014; Andreou, Harms and Klostermeier, 2019). However, it is not known whether the *Sc* eIF4A can oligomerise or has activities similar to one or both of the human eIF4A paralogues. Often yeast and human proteins exhibit striking similarities, i.e., synergistic stimulation of yeast eIF4A by their interaction partners (Andreou and Klostermeier, 2014). However, eIF4A2 activity was often in contrast with the literature. Moreover, yeast eIF4G, in contrast to human orthologue, has only one eIF4A binding site (Schutz *et al.*, 2008). Therefore here, the main focus was on the RNA binding capacity of *Saccharomyces cerevisiae* eIF4A, and the possible differences in K_D for different RNA sequences both alone and in presence of *S. cerevisiae* eIF4G.

In all, this chapter is focused on bringing together the data describing the activity of eIF4A2 alone (**Chapter 3**), and in presence of its interaction partners (**Chapter 4**) and comparing it to its highly identical paralogue eIF4A1, and further exploring how those activities could relate to yeast eIF4A.

5.2. eIF4A1 is a less efficient helicase than eIF4A2 in vitro

As a previous study from the Bushell lab (Wilczynska *et al.*, 2019) identified differences in the binding preferences of the two paralogues, with eIF4A2 preferentially binding AG-RNA, a question was posed how additional activities of both paralogues can be affected by this RNA in light of the newly described oligomerisation potential of eIF4A2 (**Chapter 3**).

To compare eIF4A1 and eIF4A2 activities *in vitro*, first full length eIF4A1 was heterologously produced and purified (see **Chapter 2.2**). Briefly, a previously cloned full length His-SUMO-eIF4A1 protein construct was produced in *E. coli* strain BL21 DE3 RP codon+. The prepared bacterial lysate was applied to a HisTrap column (**Figure 5.2-1**, panel A), and the bound protein was eluted in a linear imidazole gradient. Next, the pooled fractions containing His-SUMO-eIF4A1 were subjected to SUMO-tag cleavage with ULP1 and applied to a Resource Q column (**Figure 5.2-1**, panel B), (eIF4A1 pI = 5.32). The peak fractions were combined and applied on a size exclusion chromatography column (**Figure 5.2-1**, panel C). The eluted protein was concentrated, and its purity was assessed by SDS-PAGE (**Figure 5.2-1**, panel C) and UV-VIS spectrum. In sum, eIF4A1 was determined to be of high purity for use in further studies.

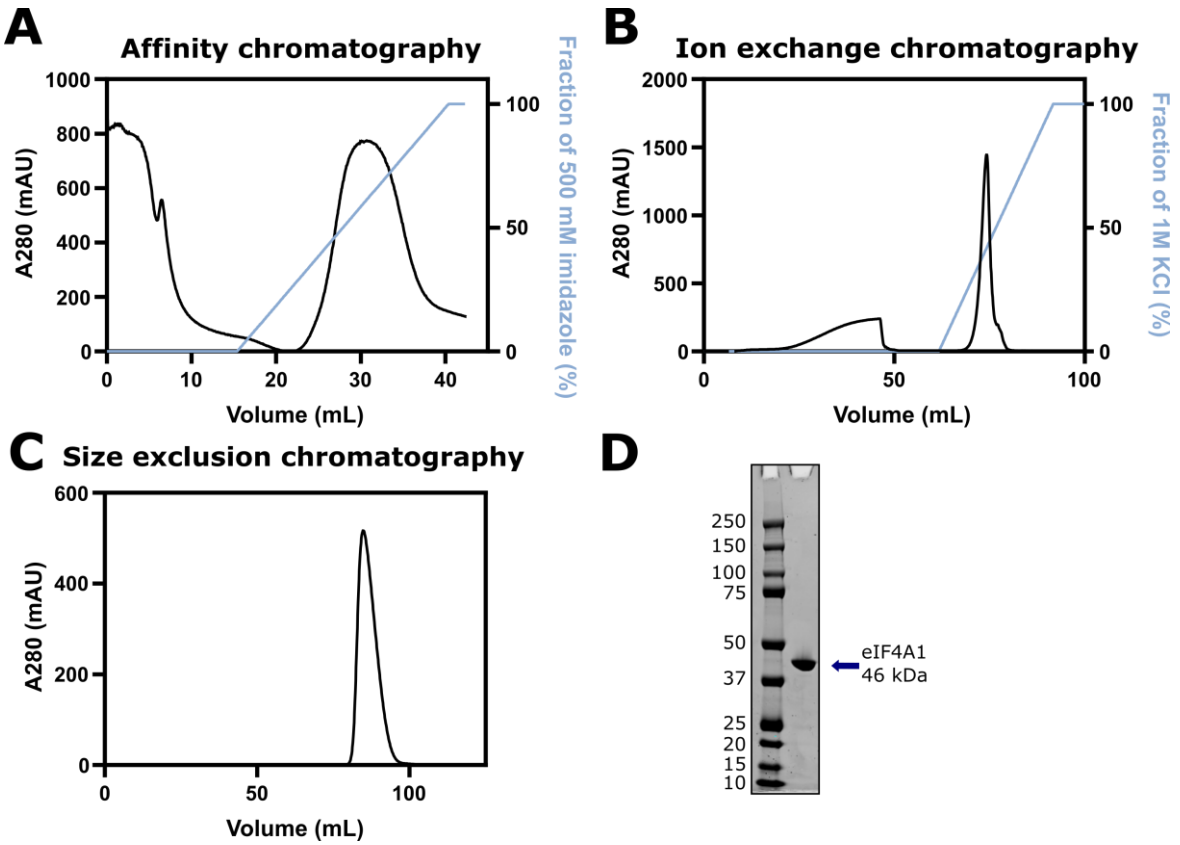

Figure 5.2-1 eIF4A1 purification

A. Representative chromatogram of His-SUMO eIF4A1 elution in a linear imidazole gradient on a HisTrap HP column.

B. Representative elution profile of eIF4A1 after ULP1 cleavage on a ResourceQ anion exchange column.

C. Representative chromatogram of eIF4A1 on a Superdex S200 HiLoad 16/600 column. eIF4A1 elutes around 80-85 mL.

D. Coomassie stained gel of purified full length, 46 kDa eIF4A1. Numbers on the left side of the gel indicate protein marker sizes in kDa.

As the novel propensity of eIF4A2 to form oligomeric complexes has not been characterised for the paralogue eIF4A1, therefore its oligomerisation potential was tested utilising the same methods as used for eIF4A2, i.e., EMSAs and aSEC (see **Chapter 3.5**). Since **1)** eIF4A2 formed oligomers due to protein-protein interactions, and **2)** silvestrol, a small molecule eIF4A inhibitor (Bordeleau *et al.*, 2008), stimulated oligomer formation even on a short RNA substrate (see **Figure 3.9-2**), eIF4A1 oligomerisation potential was tested on RNA substrates with varying length of AG-repeats in presence and absence of silvestrol (**Figure 5.2-2**, panel A). eIF4A1, similarly to eIF4A2, formed trimeric complexes only on 20 nt AG-RNA. Moreover, silvestrol induced oligomerisation of eIF4A1, and stimulated oligomer formation on 10 nt AG-RNA. This suggest, that both paralogues can form oligomers, and oligomer formation is supported through protein-protein interactions.

To visualise eIF4A1 oligomerisation side by side with eIF4A2 EMSA was used (**Figure 5.2-2**, panel B, see also **Chapter 2.3.1.1**). Here, eIF4A2 seemed to exhibit greater oligomerisation potential *in vitro* than eIF4A1. Moreover, silvestrol enhanced oligomerisation of both paralogues on AG-RNA (**Figure 5.2-2**, panel C). However, in contrast to eIF4A2, eIF4A1 failed to support oligomerisation on $(CAA)_6CA$ RNA in this assay. This suggests that eIF4A1 is more selective in its preference for oligomerisation-inducing RNA sequence.

Next, the K_D of eIF4A1 binding to different lengths of AG-RNA was quantified in the same way as for eIF4A2 (see **Figure 3.5-4** and **Figure 5.2-2**, panel B). In contrast to eIF4A2, eIF4A1 demonstrated the highest affinity (lowest K_D) to 20 nt AG-RNA (**Figure 5.2-2**, panel D, *left*). The same was observed in presence of silvestrol, which increased the affinity of both paralogues for AG-RNA (**Figure 5.2-2**, panel D, *right*). Similar silvestrol-induced increase of affinity was previously described in literature (Iwasaki, Floor and Ingolia, 2016; Wilczynska *et al.*, 2019). The difference in observed minimal K_D of both paralogues (20 nt for eIFA1, 15 nt for eIF4A2), indicates that eIF4A2 binds more strongly to shorter RNA substrates. That suggests that eIF4A2's mechanism of RNA binding is distinct to eIF4A1. Additionally, the K_D of eIF4A2 in DMSO conditions is lower for each RNA length than the K_D of eIF4A1 showing that eIF4A2 binds more strongly to AG-RNA than eIF4A1 (**Figure 5.2-2**, panel D, *left*).

Additionally, eIF4A1, similarly to eIF4A2, was observed to oligomerise in live cells using FLIM-FRET (**Appendix 3 Figure 3-1**). Moreover, eIF4A1 oligomerisation was eIF4G independent in cells (**Appendix 3 Figures 3-2**, **3-3**, **3-4**) and there was no requirement for all of the protomers in the oligomer to have RNA binding capacity (**Appendix 3 Figure 3-1**).

In all, both paralogues can form oligomeric complexes, with eIF4A2 having greater propensity to oligomerise *in vitro*, and being less selective to oligomerisation-inducing RNA sequence.

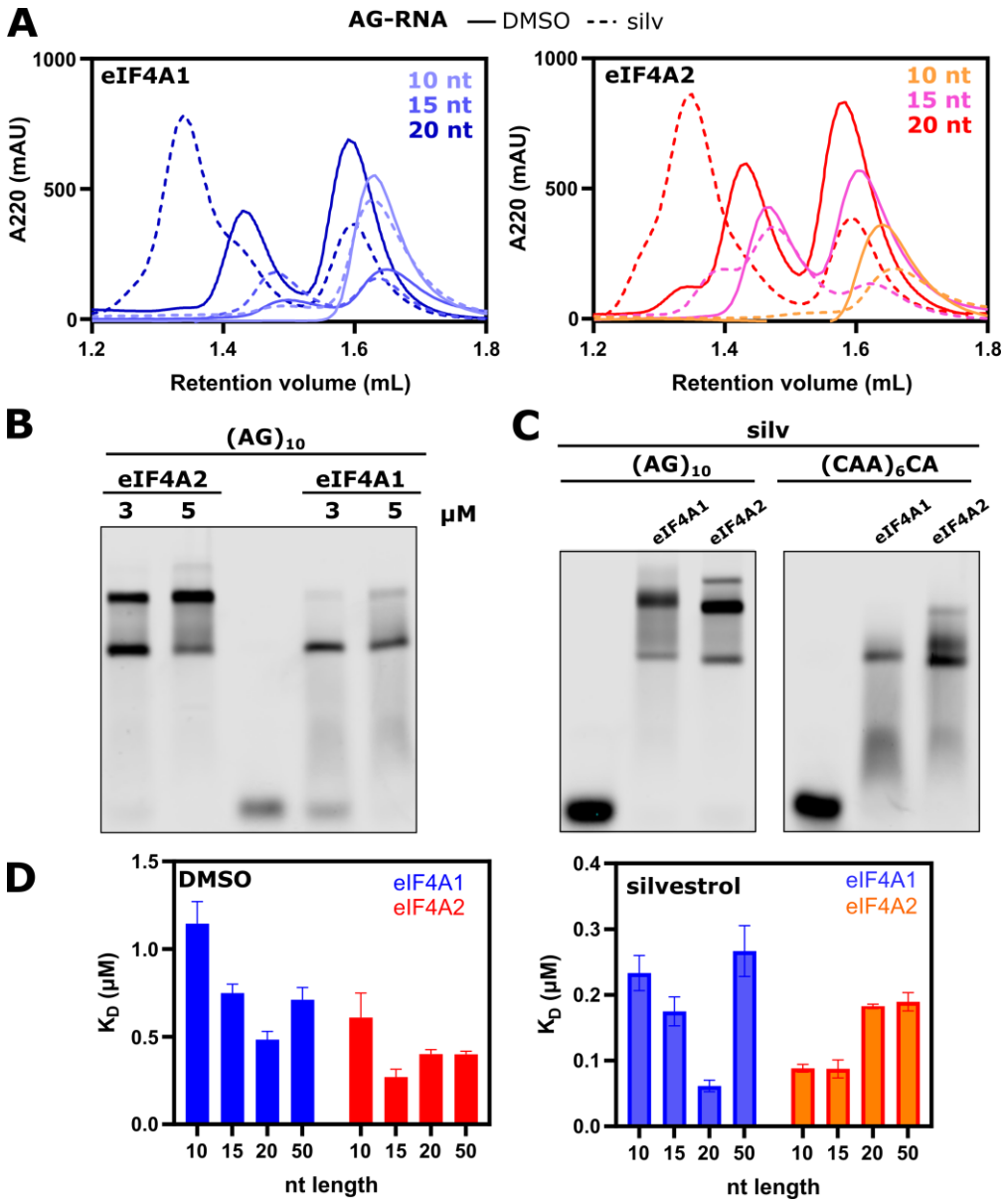

Figure 5.2-2 eIF4A2 has better oligomerisation potential than eIF4A1 *in vitro*

A. Representative chromatograms of eIF4A1 (*left*) and eIF4A2 (*right*) complexes formed on AG-RNA (10, 15, 20 nt) in presence of DMSO (*full line*) or silvestrol (*dashed line*). Both paralogues form oligomeric complexes, and silvestrol induces oligomerisation. N = 3.

B. Representative EMSA of eIF4A2 and eIF4A1 binding to $(AG)_{10}$ RNA in DMSO conditions at indicated protein concentrations. eIF4A2 forms oligomers more readily than eIF4A1. N = 3.

C. Representative EMSA of 5 µM eIF4A1 and eIF4A2 binding to $(AG)_{10}$ (*left*) and $(CAA)_6CA$ (*right*) in presence of silvestrol. Both proteins bind to $(AG)_{10}$ as oligomers, however only eIF4A2 oligomers are detected in the tested conditions on $(CAA)_6CA$ RNA. N = 3.

D. K_D of eIF4A1 and eIF4A2 in DMSO (*left*) and silvestrol (*right*) conditions. Quantification from measured fraction bound on from individual EMSAs (n = 3 for each condition), Hill equation applied to the data. eIF4A1 has lower affinity than eIF4A2 in DMSO conditions. 20 nt RNA length is preferred by eIF4A1, and 15 nt by eIF4A2.

Furthermore, as **1)** eIF4A1 was shown to oligomerise (**Figure 5.2-2**), and **2)** similarly to eIF4A2, eIF4A1 did not exhibit unwinding activity in monomerisation-inducing conditions (**Appendix 3 Figure 3-5**), the catalytic capacities of both paralogues under oligomerisation-inducing conditions were assessed.

As both of the helicases had a preference to AG-RNA (see **Table 3.8-2**, and Iwasaki, Floor and Ingolia, 2016; Wilczynska *et al.*, 2019), and previous studies of eIF4A1 have focused mostly on the canonical 5'-to-3' unwinding activity, the data presented in **Figure 5.2-3** correspond to experiments performed on 5'$(AG)_{10}$ overhang RNA.

Here, the activity of eIF4A1 was compared to the activity of eIF4A2 in the same conditions (**Figure 5.2-3**, panel A). eIF4A2 had higher unwinding activity than eIF4A1, both alone and in the presence of eIF4G-MC. Since the increase in eIF4A2 activity caused by eIF4G-MC was only minimal (see **Figure 4.3-3**), the higher activity of eIF4A2 than eIF4A1 in presence of eIF4G-MC was possibly due to the higher activity of eIF4A2 itself. Both the activity of eIF4A2 in presence of eIF4H alone, and eIF4H with eIF4G-MC seemed to be greater than the unwinding activity of eIF4A1 in those conditions. However, caution needs to be taken when interpreting these data as the error bars for eIF4A2 activity is high. Nevertheless, eIF4A1 unwinding activity in presence of both eIF4H and eIF4G-MC seems to be closer to the activity of eIF4A2, supporting the previously described synergistic activation of eIF4A1 (Abramson, Dever and Merrick, 1988; Nielsen *et al.*, 2011).

Next, to better compare the effect of the cofactors on eIF4A1 and eIF4A2 unwinding activity was assessed (**Figure 5.2-3**, panel B). For this, the unwinding activity of 5 μM eIF4A1 or eIF4A2 in absence of cofactors was used as a baseline. eIF4A1 unwinding activity was enhanced to a greater extent by the presence of cofactors than eIF4A2. Moreover, for eIF4A1 an additive activation by eIF4H and eIF4G-MC was observed, which was not observed for eIF4A2 (see also **Figure 4.3-3**).

To further understand the additive activation of eIF4A1 by eIF4H and eIF4G-MC and compare it to the observed apparent lack of synergy in case of eIF4A2, a titration of eIF4G-MC in the unwinding reaction was performed (**Figure 5.2-3**, panel C). Here, a lower concentration of the helicases was used (2 μM) and an

equimolar concentration of eIF4H. The collected data were normalised to the activity of the respective helicase in absence of eIF4G-MC. At concentrations of eIF4G-MC lower than eIF4A1-eIF4H (<2 μM) eIF4A1 was activated. However, at equimolar concentration of all proteins in the reaction (2 μM) a slight decrease in the velocity of unwinding was observed, which further decreased at higher eIF4G-MC concentrations. It should be noted that eIF4A2 activity was only measured in single replicate. Nonetheless, the obtained result indicates that an increase in activity as observed for eIF4A1 may not be apparent. This is further supported by data presented in (**Figure 4.3-3**, panel C and **Figure 5.2-3**, panel A). Similarly, as was observed for eIF4A1, at high concentrations of eIF4G-MC, eIF4A2 activity became inhibited. In all, this suggests that the cofactor concentrations play a crucial role in the activation, possibly indicating that eIF4A2 has different optimum for cofactor activation than eIF4A1. Moreover, as previously mentioned eIF4G has two binding sites for eIF4A (see also **Figure 1.3.2-2**), the sub-molar optimum of eIF4G concentration for eIF4A1 activation indicates that when a single eIF4A1 is bound to eIF4G its main function could be different to RNA unwinding.

Lastly, the ATPase activity of both helicases in presence of interaction partners was compared to the activity of free eIF4A1 and eIF4A2, respectively (**Figure 5.2-3**, panel D). The activity of eIF4A2 was less subjected to change in presence of interaction partners, than the activity of eIF4A1 in the tested conditions. Surprisingly, in stark contrast to what was previously observed in the literature (Rogers *et al.*, 2001; Korneeva *et al.*, 2005; Nielsen *et al.*, 2011; Özeş *et al.*, 2011), the ATPase activity of eIF4A1 seemed to decrease in conditions containing eIF4G-MC. This is further discussed in **Chapter 5.5**.

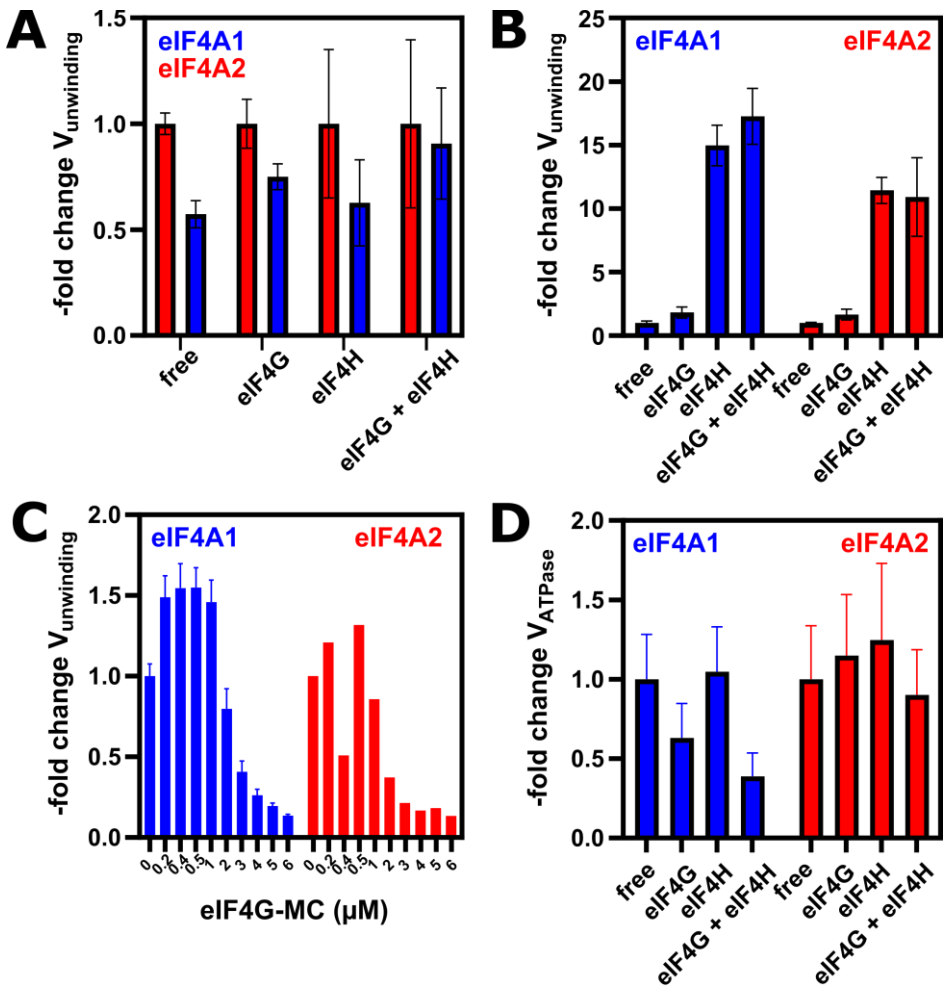

Figure 5.2-3 eIF4A2 is a faster helicase than eIF4A1

A. Fold change of velocity of unwinding normalised to eIF4A2 activity in each category. Helicases at 5 μM, interaction partners at 0.5 μM. All samples n = 3, apart from eIF4A2 and eIF4A2 with eIF4G n = 4, eIF4A2 with eIF4H n = 2. Error – SEM. eIF4G label corresponds to construct used in a previous chapter – eIF4G-MC. eIF4A2 activity seems to be higher than the one of eIF4A in all tested conditions, however error for eIF4A2 activity in presence of eIF4H and both eIF4H and eIF4G-MC is high, therefore accurate determination of change between eIF4A2 and eIF4A1 is not possible in those conditions.

B. Fold change of velocity of unwinding on 5'$(AG)_{10}$ overhang RNA in presence of cofactors normalised to activity of 5 μM eIF4A1 (*left*, *blue*) and 5 μM eIF4A2 (*right*, *red*). Replicate number, error, RNA, the proteins used and their concentrations as in panel **A**. All of the interaction partners enhance eIF4A1 activity to a greater extent than the one of eIF4A2. Synergistic effect of eIF4H and eIF4G is visible in the case of eIF4A1.

C. Fold change of unwinding velocity on 5'$(AG)_{10}$ overhang RNA of 2μM eIF4A1 (*blue*) and 2μM eIF4A2 (*red*) in presence of 2μM eIF4H and indicated concentrations of eIF4G-MC, normalised to the activity at 0 μM eIF4G-MC. eIF4A1 n = 3, eIF4A2 n = 1. eIF4A1 is synergistically activated by eIF4H and eIF4G-MC at sub-molar eIF4G-MC concentrations. This effect is not as pronounced for eIF4A2.

D. Fold change of ATPase activity (V_{ATPase} = nM ATP x s^{-1}) on 5'$(AG)_{10}$ overhang RNA for eIF4A1 (*blue*) and eIF4A2 (*red*) in presence of indicated co-factors, normalised to the activity of the respective free helicase. Replicate number, error, the proteins used and their concentrations as in panel **A**.

To sum up, both eIF4A1 and eIF4A2 can oligomerise in cells and *in vitro* (**Appendix 3 Figure 3-1** and **Figures 3.7-3**, **5.2-2**). Additionally, the oligomerisation of both paralogues can be further enhanced by silvestrol. One of the most noticeable differences was the preferred AG-RNA length. eIF4A2 exhibited greater affinity towards shorter RNA substrates than eIF4A1, suggesting preference of eIF4A2 for shorter RNA substrates. Moreover, this difference in the preferred RNA length could potentially indicate that the two paralogues have different RNA binding interface. Another striking difference between the helicases was the lack of eIF4A1 oligomers on $(CAA)_6CA$ RNA in the tested conditions, indicating that eIF4A1 is potentially more selective then eIF4A2 when it comes to the oligomerisation-promoting RNA sequence.

Furthermore, eIF4A2 showed a trend to unwind RNA substrates with greater velocity then eIF4A1 in the tested conditions (**Figure 5.2-3**). Interestingly, cofactors eIF4G and eIF4H stimulated the activity of eIF4A1 more than eIF4A2. Additionally, eIF4A1 was synergistically activated by eIF4H and eIF4G-MC, while this was not observed for eIF4A2. This suggest a different role of eIF4A1 and eIF4A2 when in complex with the tested co-factors, in which eIF4A2 unwinding activity is not stimulated. Finally, the ATPase activity of eIF4A2 was relatively unchanged in all of the tested conditions, while eIF4A1 activity decreased in presence of eIF4G-MC. In all, the influence of the co-factors on the helicases activity on different RNA substrates could potentially yield more information about the role of the helicases in the different complexes.

5.3. Mutational analysis of the paralogues identifies regions responsible for lack of sequence-specific binding selectivity of eIF4A1

The investigations presented in the previous subchapter elucidated disparities between the highly identical paralogues eIF4A1 and eIF4A2, thus the next question was what drives those differences. To identify which divergent regions in the amino acid sequence of the two paralogues play a role in the different behaviour of eIF4A1 and eIF4A2, mutations were introduced into the two paralogues.

Previously, several eIF4A mutants were generated to elucidate the difference between the paralogues in cells (Wilczynska *et al.*, 2019). However, it is not clear how these mutations change the biochemical properties of both helicases. These mutants include: **1)** eIF4A1 1-18 A2; an eIF4A1 mutant with the first 18 amino acids exchanged for those from eIF4A2, **2)** eIF4A2 1-18 A1; an eIF4A2 mutant with the first 18 amino acids exchanged for those from eIF4A1, **3)** eIF4A1 Δ N-20; eIF4A1 with a 20 amino acids N-terminal truncation, **4)** eIF4A2 Δ N-21; eIF4A2 with a 21 amino acids N-terminal truncation, **5)** eIF4A2-7-mut; eIF4A2 with 7 mutations exchanging residues for the corresponding amino acids in eIF4A1: N34S K41S E101A N143A A150M S207N I208T (**Figure 5.3-1**). The eIF4A2-7-mut was previously shown to switch off the eIF4A2 translation repressive function due to its association with eIF4G (Wilczynska *et al.*, 2019).

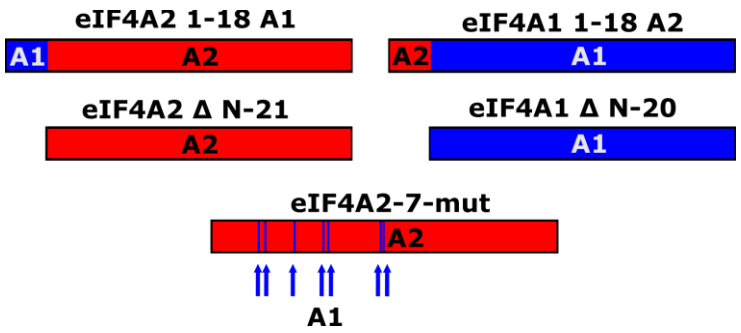

Figure 5.3-1 Schematic of eIF4A1 and eIF4A2 mutants

Schematic of mutants used in this study: **1)** eIF4A2 with exchanged first 18 amino acids with eIF4A1 (*top left*), **2)** eIF4A1 with exchanged first 18 amino acids with eIF4A2 (*top right*), **3)** eIF4A2 with N-terminal truncation (*middle left*), **4)** eIF4A1 with N-terminal truncation (*middle right*), **5)** eIF4A2 with 7 mutations exchanging residues for the ones corresponding to eIF4A1 (*bottom*).

First, the eIF4A mutants constructs were cloned into petSUMO vector for expression in *E. coli* BL21 DE3 RP codon+. The bacteria were treated in the same way as described previously (see **Chapter 2.2**). Next, the precleared bacterial lysates were applied on HisTrap HP columns, and the bound proteins were eluted in a linear imidazole gradient (**Figure 5.3-2**, *left in panels A-D*, see figure legend for each mutant). Next, the pooled fractions were treated with ULP1 to cleave off the His-SUMO tag. As the pI of the mutants did not differ greatly from WT proteins, the samples were applied on anion exchange chromatography (**Figure 5.3-2**, *middle left in all panels*). Fractions corresponding to main peaks were subsequently subjected to size exclusion chromatography (**Figure 5.3-2**, *middle right in all panels*). All of the mutants eluted at a similar retention volume as WT eIF4A1 and eIF4A2, suggesting that the expressed proteins are correctly folded. The purified proteins were visualised using SDS-PAGE (**Figure 5.3-2**, *right in all panels*), and their UV-VIS spectrum was measured. In all, the quality of the purified proteins was deemed to be high, and all the purified eIF4A mutants could be used in subsequent experiments.

Additionally, used in this study, eIF4A1 Δ N-20 protein, was obtained as a gift from Dr Tobias Schmidt.

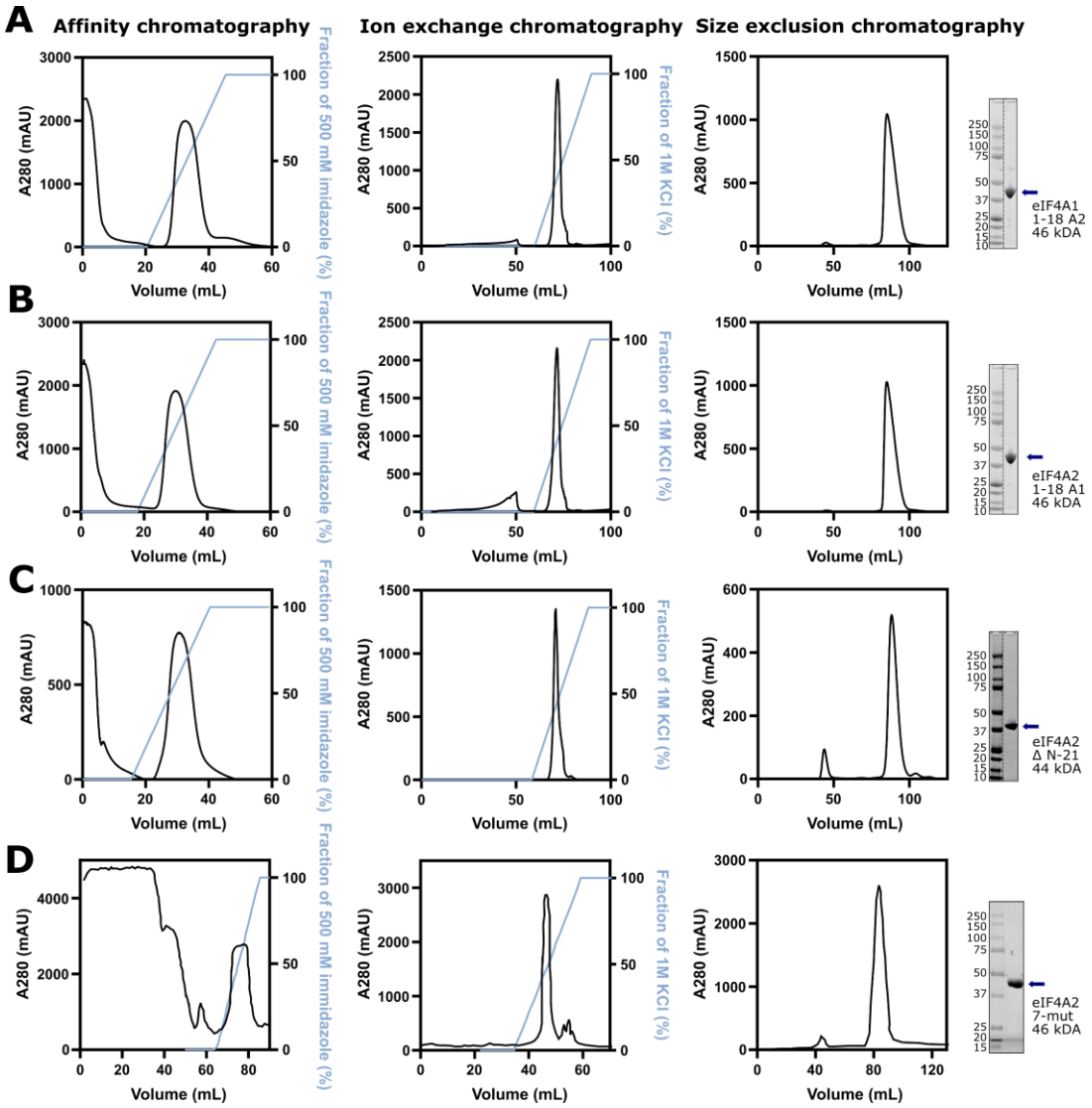

Figure 5.3-2 Purification of eIF4A1 and eIF4A2 mutants

Purification of eIF4A1 and eIF4A2 mutants: **1)** affinity chromatography on HisTrap HP column – *left*, **2)** anion exchange chromatography on Resource Q column after ULP1 cleavage – *middle left*, **3)** size exclusion chromatography on Superdex S200 HiLoad 16/600 column – *middle right*, **4)** Coomassie stained gels of final purification products with schematic of mutations; protein marker sizes in kDa indicated on the left of the gel; unrelated lanes removed from gels – *right*. Amino acid – aa.

- **A.** eIF4A1 with exchanged 1 - 18 aa for eIF4A2 (labelled eIF4A1 1-18 A2),
- **B.** eIF4A2 with exchanged 1 - 18 aa for eIF4A1 (labelled eIF4A2 1-18 A1),
- **C.** eIF4A2 with removed first 21 aa (labelled eIF4A2 Δ N-21),
- **D.** eIF4A2 with 7 mutations for eIF4A1 residues: N34S K41S E101A N143A A150M S207N I208T (labelled eIF4A2-7-mut). Chromatograms for eIF4A2-7-mut traced using (Plot Digitizer) from a photocopy.

One of the interesting differences between eIF4A1 and eIF4A2 was the previously described RNA sequence specificity (Wilczynska *et al.*, 2019). The authors of that work have observed that eIF4A2, unlike eIF4A1, exhibits a preference towards AG-RNA under competitive conditions. Most intriguingly, this activity could be artificially induced in eIF4A1 by silvestrol. The authors speculated that this selectivity of eIF4A2 drives its role in translational repression through the AG-motifs on a given mRNA.

As the nature of this observation has implications in the outcome of protein translation, the question of what drives the natural selectivity of eIF4A2 was explored. First, the selectivity experiment was replicated and expanded by utilisation of eIF4A1 and eIF4A2 mutants (**Figure 5.3-3**, panel A, note the different scale of Y axis in the top and bottom panels). Similarly to what was observed previously (Wilczynska *et al.*, 2019), eIF4A2, in contrast to eIF4A1, did not change the affinity towards AG-RNA even in the presence of large excess (50-fold) of competitor RNA. The exact numbers are slightly different than in the published work (Wilczynska *et al.*, 2019) as eIF4A1 did not exhibit an increase in K_D for $(AG)_{10}$ in presence of equimolar competitor RNA (2 out of 3 replicates). However, the overall trend remained unchanged. Strikingly, data collected for the N-terminal eIF4A1 mutants (eIF4A1 1-18 A2 and eIF4A1 Δ N-20) suggest that this is the region responsible for lack of selectivity in eIF4A1. Both the truncation, and the exchange of amino acids with those from eIF4A2, caused eIF4A1 to behave in a selective manner, akin to eIF4A2. Intriguingly, the eIF4A2 Δ N-21 mutant exhibited similar preference to AG-RNA as WT eIF4A2, suggesting that eIF4A2 N terminus is not responsible for eIF4A2 selectivity. Conversely, the eIF4A2 1-18 A1 affinity to AG-RNA was reduced, albeit the competitor concentration dependent increase of K_D was not observed. The last mutant tested in these conditions, i.e., eIF4A2-7mut, was observed to have an increased K_D in the presence of 10-fold competitor RNA. However, due to high discrepancy between the calculated K_D of eIF4A2-7-mut for each replicate in the 50-fold excess of competitor RNA condition, whether the selectivity of eIF4A2 was completely lost could not be determined. In all, these data suggest that it is the N-terminal region of eIF4A1 that is responsible for lack of RNA binding selectivity. However, the data suggest that another region within eIF4A2 is responsible for its RNA sequence preferences. Perhaps, combining eIF4A2 1-18

A2 and eIF4A2-7-mut mutations could lead to complete loss of selectivity associated with eIF4A2.

As a striking difference was observed for eIF4A1 N-terminal truncation and substitution in comparison to eIF4A1 WT in RNA binding selectivity, next question was to understand whether those regions could influence how the two paralogues bind and release the RNA. For this RNA release experiments in non-competitive conditions, employing eIF4A mutants were performed (**Figure 5.3-3**, panel B). Here, a distinct behaviour of both eIF4A1 Δ N-20 and eIF4A2 Δ N-21 compared to WT of both paralogues was observed. Both mutants exhibited longer duration of the RNA-bound state compared to wild type on both $(AG)_{10}$ and $(CAA)_6CA$ RNA. Additionally, the fractions bound for both N-terminally truncated mutants were greater than for the WT paralogues. The biggest difference was observed for eIF4A1 Δ N-20 on $(AG)_{10}$ RNA. Its RNA-bound state half-life doubled, and the $(AG)_{10}$ release was only minimal, equating to the starting points of eIF4A1 WT. The eIF4A1 1-18 A2 and eIF4A2 1-18 A1 followed a similar trend to WT proteins in the first 20 * 10^3 s of reaction, with greater RNA release at further time points. Moreover, the half-lives of both N-terminally exchanged mutants decreased in comparison to WT. The half-life for eIF4A1 1-18 A2 was 62% and 74% of eIF4A1 WT on $(AG)_{10}$ and $(CAA)_6CA$ RNAs, respectively; for eIF4A2 1-18 A1 these values were 76% and 51% of eIF4A2 WT. Interestingly, eIF4A2-7-mut, released RNA the most with half-lives 46% and 43% of the WT on $(AG)_{10}$ and $(CAA)_6CA$ RNAs, respectively. Intriguingly, those numbers for eIF4A2-7-mut were 45% and 55% in comparison to eIF4A1 WT, implying that this mutant has a shorter RNA-bound state than both WT paralogues. Although these data cannot be directly compared to the selectivity experiment (**Figure 5.3-3**, panel A) due to lack of the competitor RNA and use of hydrolysable ATP, it can be concluded that RNA release does not influence RNA binding selectivity. Hence these studies brought insights into which regions are responsible for distinct activities of the two paralogues.

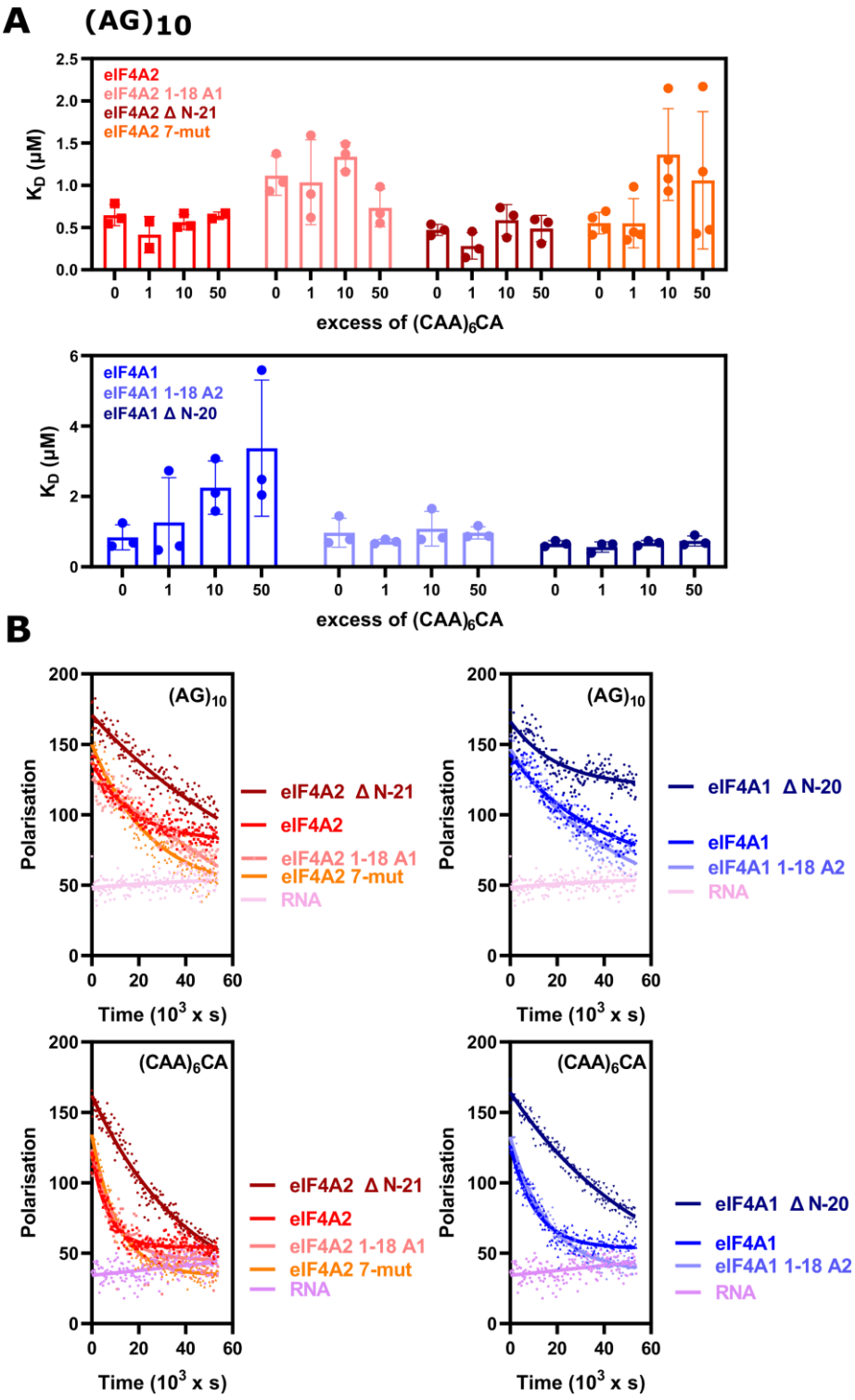

Figure 5.3-3 eIF4A2 has a distinct preference to AG-RNA

A. Comparison of K_D measurements of eIF4A2 and its mutants (*top*) and eIF4A1 and its mutants (*bottom*) in presence of excess of $(CAA)_6CA$ RNA. All measurements n = 3, eIF4A2 7-mut n = 4. K_D values obtained from fitting Hill equation to the helicase titration experiments.

B. RNA release – $(AG)_{10}$ (*top*) and $(CAA)_6CA$ (*bottom*) in presence of ATP in non-competitive conditions. Decrease of signal correlates with RNA release up to the signal of free RNA. eIF4A1, eIF4A2 n = 3, mutants n = 2. Fit – exponential decay. N-terminally truncated mutants follow a different pattern to the WT.

Next to address a question whether oligomerisation could influence the distinct RNA binding preferences of the paralogues, the influence of the mutations on the oligomerisation potential of eIF4A1 and eIF4A2 was explored. As described in the previous subchapter (see **Figure 5.2-2**, panel D), eIF4A1 formed oligomeric complexes more specifically on AG-RNA. Therefore, this time an EMSA was performed on the different eIF4A paralogues and mutants on a single gel, exploring oligomerisation potential on $(AG)_{10}$ and $(CAA)_6CA$ RNA (**Figure 5.3-4**). This time, a distinct higher species was detected on $(CAA)_6CA$ for eIF4A1 and not observed for eIF4A2. These higher order species were occasionally observed on different EMSAs; however, its presence was not consistent, suggesting possible lower stability of this complex. Moreover, the elution profiles of both eIF4A1 and eIF4A2 on AG-RNA in presence of silvestrol could potentially indicate a formation of an even higher order species (see **Figure 5.2-2**, panel A), indicating that depending on the conditions both paralogues could potentially form complexes greater than trimeric. These higher complexes were detected on $(CAA)_6CA$ RNA for both eIF4A1 1-18 A2 and eIF4A2 1-18 A1 (**Figure 5.3-4**), suggesting that the N-terminal region of eIF4A1 is sufficient to induce this activity in eIF4A2. However, exchange of this region in eIF4A1 is not enough to deplete eIF4A1 of this capacity. Moreover, both N-terminally exchanged mutants behaved more similar to eIF4A1 than eIF4A2 on AG-RNA. Next, the N-terminally truncated eIF4A2, i.e., eIF4A2 Δ N-21 exhibited similar activity to eIF4A2 WT on $(CAA)_6CA$ RNA, however it had a greater oligomerisation potential on $(AG)_{10}$ RNA, indicating that lack of N-terminal region promotes oligomerisation of eIF4A2. Lastly, eIF4A2-7-mut displayed similar oligomerisation potential to eIF4A2 WT, with slightly greater ratio of trimeric to monomeric complex on $(AG)_{10}$. Additionally, half of each sample applied on an EMSA was resolved on SDS PAGE (**Figure 5.3-4**, *bottom*), indicating similar protein load in for each tested condition.

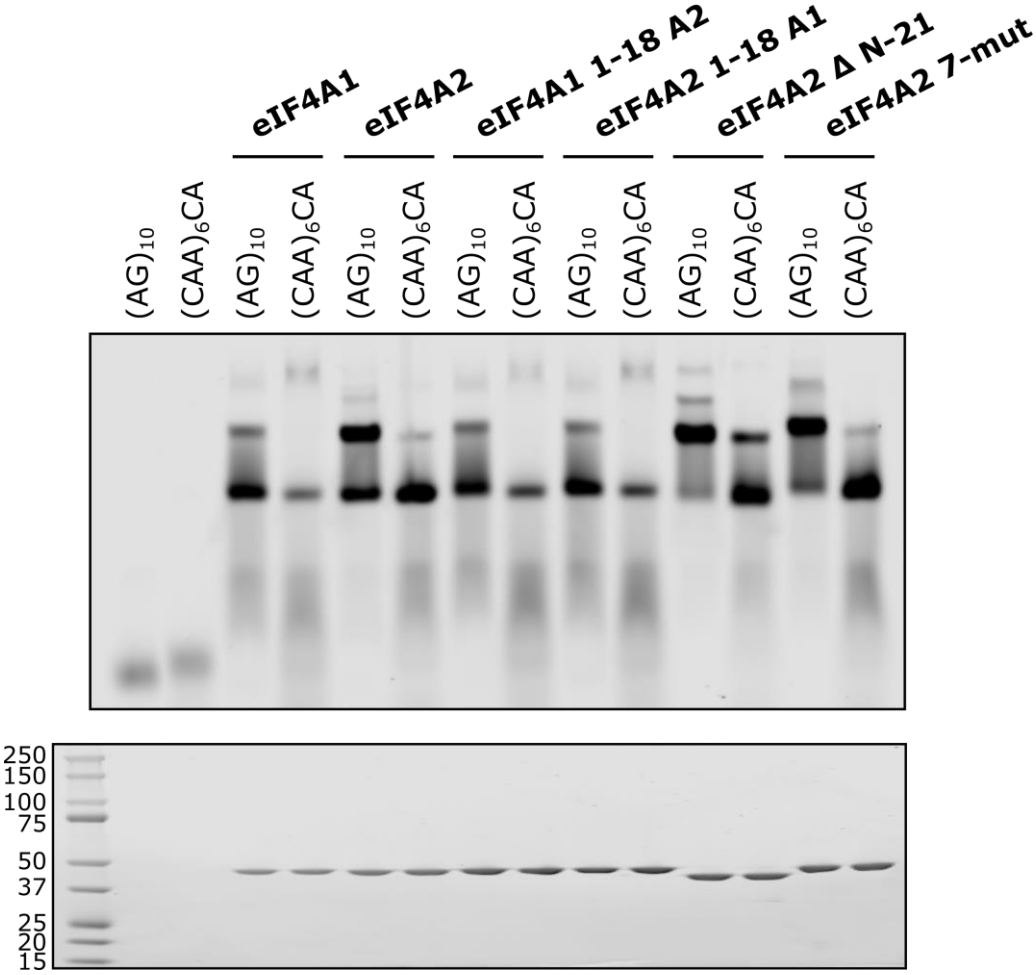

Figure 5.3-4 eIF4A mutants have distinct oligomerisation potential

Representative (n = 2) EMSA of Dy780 $(AG)_{10}$ and Dy680 $(CAA)_6CA$ binding to 5 μM eIF4A1, eIF4A2, eIF4A1 1 – 18 aa eIF4A2, eIF4A2 1 – 18 aa eIF4A1, eIF4A2 Δ N-21, eIF4A2 7-mut (*top*), and a Coomassie stained gel of the same samples as in the top panel, representing loaded proteins (*bottom*). Numbers on the side indicate protein marker sizes in kDa. Both eIF4A1 and eIF4A2 with swapped 18 aa behave similarly to eIF4A1 WT. Both eIF4A2 Δ N-21 and eIF4A2 7-mut behave similarly to eIF4A2, however the mutants seem to exhibit greater oligomerisation potential on $(AG)_{10}$ RNA. aa – amino acid.

In sum, the previously described distinct RNA sequence selectivity of eIF4A1 and eIF4A2 (Wilczynska *et al.*, 2019) was replicated (**Figure 5.3-3**, panel A). Moreover, the collected data suggested that it is the N-terminal region of eIF4A1 that is responsible for lack of binding selectivity towards the AG-RNA. In contrast, the truncation of eIF4A2 N-terminal region did not change its propensity to selectively bind AG-RNA. Moreover, the eIF4A2 1-18 A1 mutant similarly did not exhibit loss of AG-RNA selectivity, albeit its K_D to AG-RNA even in non-competitive conditions was increased in comparison to WT. The most visible loss of eIF4A2 selectivity was observed in the eIF4A2-7-mut mutant; however, due to high error in the measured K_D in the presence of 50-fold excess of competitor RNA, a strong conclusion cannot be made. Moreover, this mutant exhibited the greatest RNA release from all the tested proteins (**Figure 5.3-3**, panel B). However, as **1)** loss of selectivity was not observed for eIF4A2 1-18 A1, **2)** the eIF4A1 1-18 A2 mutant gained the selective behaviour, and **3)** the RNA-bound state half-lives of the N-terminally exchanged mutants were decreased, the selectivity might not be related to RNA release. An interesting observation was made for the N-terminally truncated mutants, especially eIF4A1 Δ N-20, which almost completely lost the ability to release $(AG)_{10}$ RNA. However, as mentioned above, the direct comparison between the RNA release and selectivity experiments cannot be made due to the differences in the tested conditions. Finally, the oligomerisation potential of the mutants was explored (**Figure 5.3-4**). Here, a higher oligomeric species than previously detected was observed for eIF4A1 bound to $(CAA)_6CA$ RNA. Moreover, similar oligomerisation potential was observed for eIF4A1 1-18 A2 and eIF4A2 1-18 A1. Additionally, eIF4A2-7-mut exhibited almost identical oligomerisation as the eIF4A2 WT, whereas eIF4A2 Δ N-21 oligomerised to a greater extent on $(AG)_{10}$ RNA. In all, both the similarities in the oligomerisation potential, i.e., between the N-terminally exchanged mutants and eIF4A1, as well as dissimilarities, i.e., eIF4A2 and eIF4A2 Δ N-21 do not explain the differences observed in selectivity experiment, suggesting that eIF4A2 selectivity, and its gain in the case of eIF4A1 mutants is oligomerisation independent.

5.4. Yeast eIF4A is distinct from both eIF4A1 and eIF4A2

The previous two subchapters elucidated some substantial differences between the two closely related eIF4A paralogues. However, in the literature there is a plethora of data regarding yeast eIF4A, but there is a lack of direct comparisons between the activity of yeast and human eIF4As. Therefore, the final aspect of this thesis was to uncover potential discrepancies in the activities of human and yeast eIF4As.

First, a sequence alignment of human eIF4A1, eIF4A2 and *Saccharomyces cerevisiae* eIF4A (*Sc* eIF4A) was performed using an online software PRALINE (Simossis and Heringa, 2003, 2005) (**Figure 5.4-1**). Overall, similarities were identified between all three helicases, with 66% identity between eIF4A1 and *Sc* eIF4A, and 65% identity between eIF4A2 and *Sc* eIF4A. Additionally, a large proportion of non-identical residues had a high degree of similarity (score 7 or higher in **Figure 5.4-1**). However, significant differences in key conserved motifs of the DEAD-box helicases (see **Figure 1.5.1-1**) were also observed, i.e., **1)** the substitution of basic lysine in human paralogues for acidic glutamic acid in the Q motif responsible for ATP binding and hydrolysis, **2)** substitution of hydrophobic, branched isoleucine and leucin in eIF4A1 and eIF4A2 for the thiol side chain bearing cysteine in the Motif IV responsible for RNA binding. In all, differences between the human and yeast orthologues, especially in the conserved motifs, suggest possible differences in the activities of the helicases.

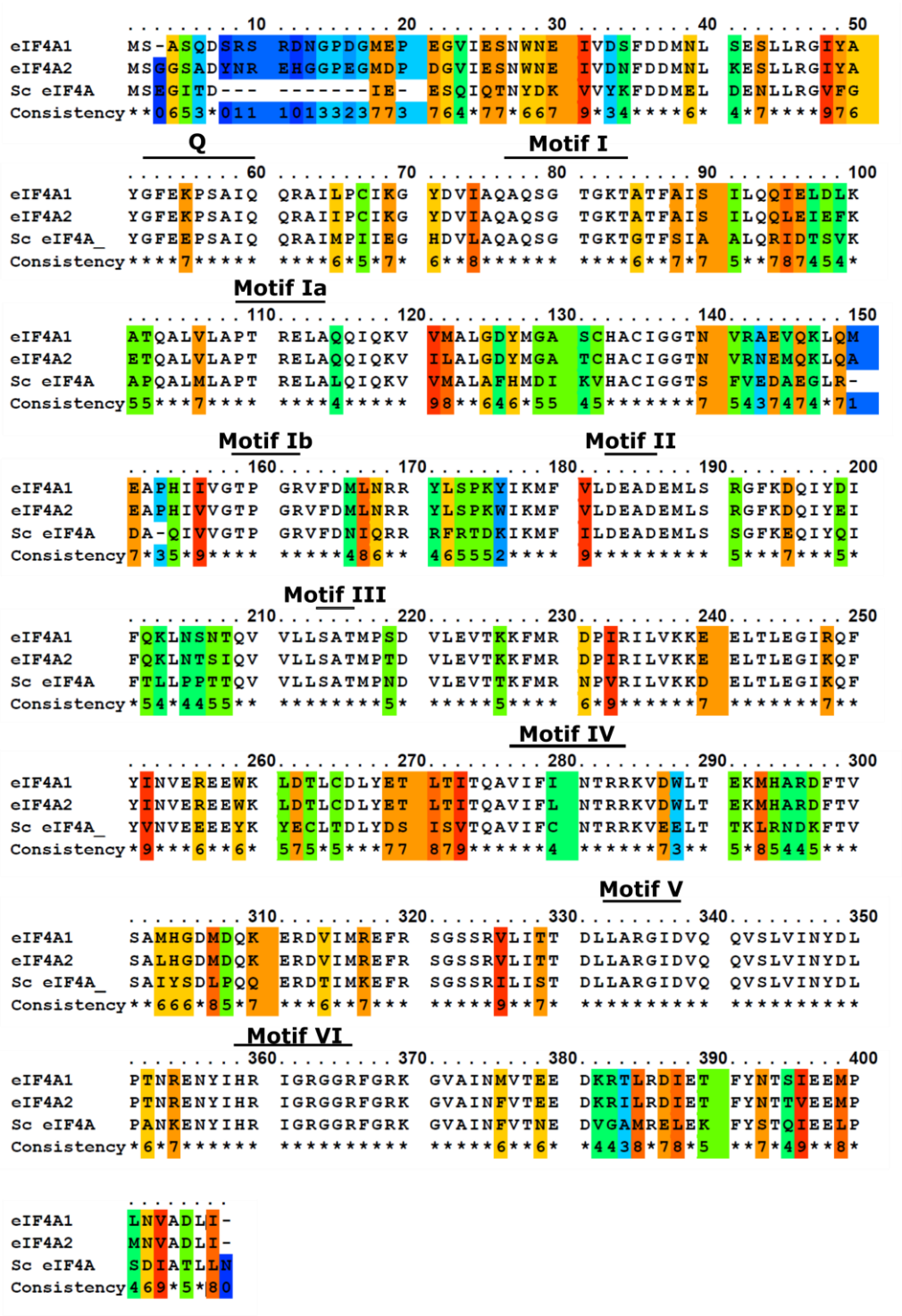

Figure 5.4-1 Alignment of human eIF4A1, eIF4A2, and Saccharomyces cerevisiae eIF4A

Alignment of an amino acid sequence between human eIF4A1, eIF4A2 and S. cerevisiae eIF4A performed using online software PRALINE (PRALINE, Centre for Integrative Bioinformatics VU) (Simossis and Heringa, 2003, 2005). Identical residues – not coloured and labelled with an asterisk, most similar residues indicated by red colour and higher number, least similar aa in blue and presented with the lowest score (number). DEAD-box helicase motives marked on the top of the sequences.

As assessment of the sequences of the helicases elucidated key differences despite large overall similarity, the next step was to compare the activities of eIF4A orthologues *in vitro*. For this, recombinant full length *Saccharomyces cerevisiae* eIF4A was obtained as a gift from Dr Tobias Schmidt. Moreover, as previously the activities of both human eIF4A paralogues were explored in presence of its interaction partners, this time the influence of yeast eIF4G was also assessed.

For this, plasmid containing full length *S. cerevisiae* eIF4G1 was purchased from Addgene (Mitchell *et al.*, 2010). Next, two constructs of *Sc* eIF4G1 were cloned into pet-SUMO vector, i.e., Sc eIF4G-M (amino acids 572 -853) and *Sc* eIF4G-MC (amino acids 572 - 952). Selection of the regions was based on the previously published data on yeast eIF4F complex (Andreou and Klostermeier, 2014). Next, the *Sc* eIF4G constructs were expressed in *E. coli* strain BL21 DE3 RP codon+ and treated in the same manner as other proteins in this thesis (see **Chapter 2.2**). The precleared bacterial lysates were applied on affinity chromatography column and the fractions containing bound proteins were eluted in a linear imidazole gradient (**Figure 5.4-2**, panel A, B, *left*). Next, the His-SUMO tag was cleaved using ULP1, and the samples were applied again on the HisTrap column (**Figure 5.4-2**, panel A, B, *middle*). As the proteins were subjected to ULP1 activity, only the free tag and possible uncleaved fraction bound the column. Subsequently, the FT from reverse affinity chromatography was concentrated and samples were applied to a size exclusion column (**Figure 5.4-2**, panel A, B, *right*). The shorter *Sc* eIF4G-M (32 kDa) eluted at around 90 mL retention volume on the Superdex S200 HiLoad 16/600 column, and the longer *Sc* eIF4G-MC (43 kDa) at around 85 mL. After concentration, the purity of the proteins was estimated by SDS-PAGE (**Figure 5.4-2**, panel C), and UV-VIS spectrum measurement. In all, the proteins were assessed to be of good quality to use in the subsequent experiments.

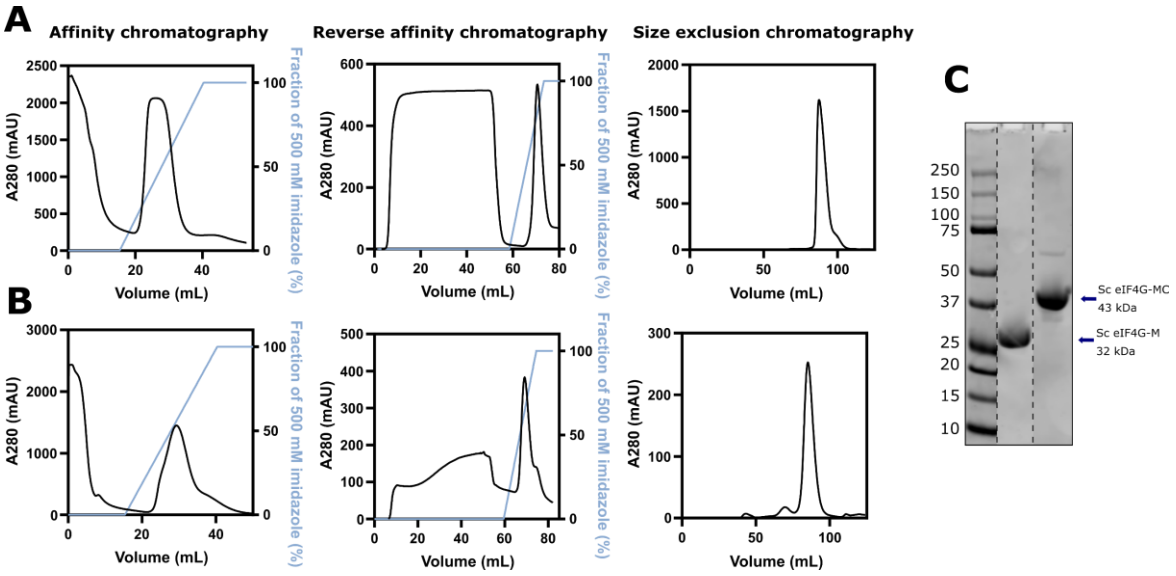

Figure 5.4-2 Purification of S. cerevisiae eIF4G domains

A., B. Purification of Saccharomyces cerevisiae short eIF4G constructs: *Sc* eIF4G-M (amino acids 572 -853) – panel **A**, and *Sc* eIF4G-MC (amino acids 572 - 952) – panel **B**. Affinity chromatography chromatogram on the *left* on a HisTrap HP column, reverse affinity chromatography after ULP1 cleavage on a HisTrap HP column – *middle*, size exclusion chromatography of flow through samples from a reverse affinity chromatography on a Superdex S200 HiLoad 16/600 column – *right*.

C. Coomassie stained gel of purified eIF4G-M and eIF4G-MC. Unrelated lanes removed from the gel. Numbers on the left indicate sizes of protein marker in kDa, arrows point to the protein and indicate the size.

As the novel oligomerisation potential described here for eIF4A1 and eIF4A2 was not previously observed for the *Sc* eIF4A, first this aspect was explored. The RNA binding capacity of *Sc* eIF4A was investigated using EMSA (**Figure 5.4-3**, panel A). In contrast to the previous experiments on eIF4A1 and eIF4A2 (see **Chapters 3.3**, **3.5**, **5.2**) no binding to RNA was detected in presence of the non-hydrolysable ATP analogue, AMP-PNP (**Figure 5.4-3**, panel A, *left*). Therefore, following the previous studies (Andreou, Harms and Klostermeier, 2019) *Sc* binding was investigated in presence of ATP. Here, only weak binding to AG-RNA was observed and no oligomeric complexes were apparent (**Figure 5.4-3**, panel A, *middle*), which indicated a major difference between the human and yeast orthologues. However, the same image of an EMSA with increased contrast, suggested possible weak dimer formation (**Appendix 3 Figure 3-6**). Moreover, use of silvestrol stimulated oligomerisation of *Sc* eIF4A (**Figure 5.4-3**, panel A, *right*). This suggested that the yeast eIF4A has the capacity and amino acid residues responsible for potential oligomerisation, however the extent of the oligomerisation is greatly diminished in comparison to the human eIF4As.

Next, the *Sc* eIF4A binding affinity for different RNA substrates was measured and compared to the human eIF4As (**Figure 5.4-3**, panel B). As the *Sc* eIF4A did not exhibit binding in presence of AMP-PNP, the experiments were performed with use of ATP. Yeast eIF4A exhibited higher K_D than the human orthologues for $(AG)_{10}$, $(CAA)_6CA$, $(AGUG)_5$ and lower for the $(UCUC)_5$ and $(UGUG)_5$. Interestingly, the last two sequences, were the ones for which eIF4A2 displayed lower K_D in presence of ATP than AMP-PNP (see **Table 3.8-1**). Similarly, as the human eIF4A, the yeast eIF4A showed highest affinity (lowest K_D) for AG-motif RNAs, i.e., $(AG)_{10}$ and $(AGUG)_5$. This suggested that the high affinity for AG-RNA could potentially be universal of eIF4A regardless of the species.

Next, as **1)** eIF4G-MC reduced the functional binding affinity of eIF4A2 to RNA substrate in the unwinding reaction (see **Table 4.3-2**), and **2)** all of the tested CNOT1 constructs had a similar effect in the binding experiments (see **Figure 4.5-5**, **Table 5.4-1**), whether *Sc* eIF4G could exert similar effect on *Sc* eIF4A was explored (**Figure 5.4-3**). Intriguingly, both the shorter *Sc* eIF4G-M and longer *Sc* eIF4G-MC increased *Sc* eIF4A affinity towards the tested RNAs, with the most striking difference observed for AG-motif RNAs (10-fold affinity increase, see **Table 5.4-1**). As this was in contrast with what was observed for eIF4A2, next

the question of what influence eIF4G-MC has on eIF4A1 binding affinity was posed (**Figure 5.4-3**, panel D). eIF4A1 binding affinity was greatly reduced (increase of K_D) in presence of eIF4G-MC. These data suggest a potential different mechanism of *Sc* eIF4A activation by *Sc* eIF4G. Last, the RNA binding capacity of *Sc* eIF4G constructs was explored. Similarly, as in the case of CNOT1 (see **Figure 4.5-5**), which contains MIF4G domain as eIF4G, only the longer construct exhibited a slight binding capacity towards the AG-RNA.

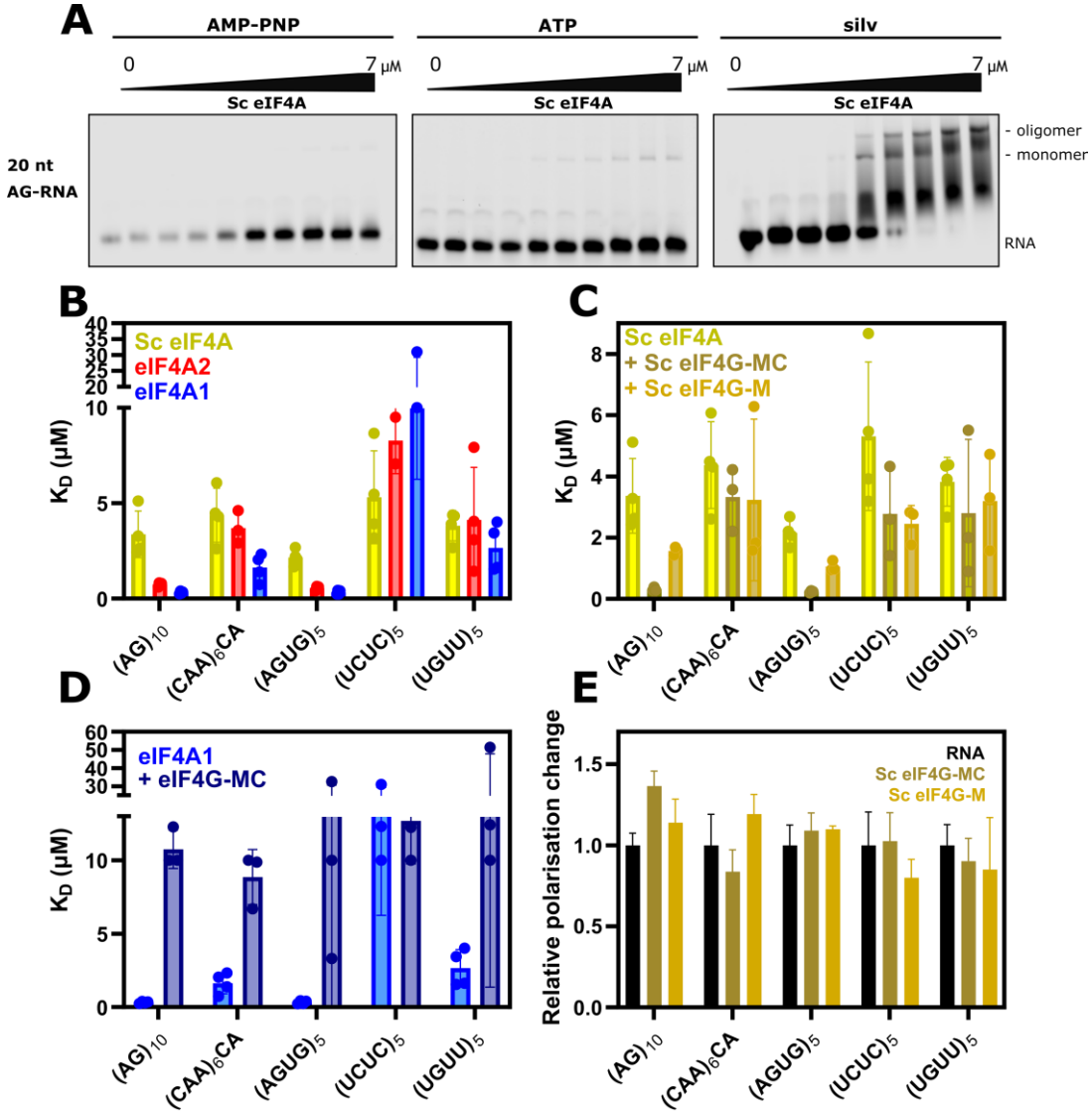

Figure 5.4-3 Sc eIF4A affinity is improved by Sc eIF4G constructs

Sc eIF4A – yeast eIF4A; eIF4A1, eIF4A2 – human paralogues; *Sc* eIF4G-MC, *Sc* eIF4G-M yeast eIF4G constructs; eIF4G-MC – human eIF4G construct

- **A.** EMSAs of *S. cerevisiae* eIF4A binding to Dy780 $(AG)_{10}$ RNA in presence of AMP-PNP, *left* (n = 2), ATP, *middle* (n = 1), silvestrol (silv) *right* (n = 2). Almost no binding detected in the presence of AMP-PNP, monomeric band visible in the ATP conditions, silvestrol induced oligomer formation.
- **B.** K_D of Sc eIF4A, eIF4A1 and eIF4A2 for indicated RNA sequences. Measurements for eIF4A1 and eIF4A2 done in presence of AMP-PNP, and for Sc eIF4A in presence of ATP. N = 3. K_D measurements for eIF4A1 performed by Dr Tobias Schmidt. K_D values obtained from fitting Hill equation to the titration data.
- **C.** Comparison of K_D measurements of Sc eIF4A and Sc eIF4A in presence of 0.5 µM of eIF4G constructs and ATP. K_D values obtained from fitting Hill equation to the titration data. N = 3. Yeast eIF4G improves the binding affinity of eIF4A.
- **D.** Comparison of K_D measurements of eIF4A1 and eIF4A1 in presence of 0.5 µM of human eIF4G-MC and AMP-PNP. N = 3. Measurements performed by Dr Tobias Schmidt. Human eIF4G decreases eIF4A1 affinity (increase K_D) to RNA.
- **E.** Relative polarisation change of yeast 0.5 µM eIF4G-MC and yeast eIF4G-M. Slight increase in $(AG)_{10}$ polarisation for eIF4G-MC in comparison to free RNA may indicate RNA binding. N = 3 for eIF4G-MC and n = 2 for eIF4G-M.

Table 5.4-1 K_D (μM) of eIF4A1, eIF4A2 and *Sc* eIF4A alone and in presence of interaction partners on various RNA sequences

Protein	$(AG)_{10}$	$(CAA)_6CA$	$(AGUG)_5$	$(UCUC)_5$	$(UGUU)_5$
eIF4A1	0.32 ± 0.03	1.63 ± 0.35	0.33 ± 0.05	17.77 ± 6.65	2.66 ± 0.63
eIF4A1 + eIF4G-MC	10.76 ± 0.76	8.86 ± 1.08	15.29 ± 8.85	12.69 ± 1.70	24.62 ± 13.43
eIF4A2	0.75 ± 0.05	3.24 ± 0.32	0.53 ± 0.12	8.27 ± 1.22	5.02 ± 1.47
eIF4A2 + CNOT1 MA3-MIF	1.08 ± 0.21	n.d.	1.29 ± 0.35	n.d.	10.73 ± 4.56
Sc eIF4A	3.36 ± 0.61	4.34 ± 0.71	2.16 ± 0.21	5.31 ± 1.21	3.82 ± 0.40
Sc eIF4A + Sc eIF4G-MC	0.31 ± 0.04	3.33 ± 0.59	0.23 ± 0.02	2.78 ± 0.84	2.80 ± 1.39

n.d. – not determined

In all, this subchapter elucidated that despite above 60% identity between human and yeast eIF4A (**Figure 5.4-1**), the propensity of *Sc* eIF4A to bind RNA and oligomerise is in stark contrast to what was observed for human paralogues (**Figure 5.4-3**, panels A, B). The gathered data suggest, that *Sc* eIF4A potentially exist mostly in the monomeric form, however the ability to oligomerise is not absent (**Appendix 3 Figure 3-6**). Furthermore, *Sc* eIF4A exhibits lower affinity for $(AG)_{10}$, $(CAA)_6CA$, and $(AGUG)_5$ RNAs than the human helicases. Albeit, out of the tested RNAs, *Sc* eIF4A similarly to human eIF4As has greatest affinity for AG-motif RNAs. Intriguingly, the stark difference was observed in presence of eIF4G constructs. While the human eIF4G-MC reduced eIF4A1's affinity (30-fold for AG-RNA) as well as eIF4A2's apparent affinity, the yeast eIF4G orthologue increased the affinity of *Sc* eIF4A to RNA (**Figure 5.4-3**, panel C, see also **Tables 4.3-2, 5.4-1**). The large decrease of affinity of eIF4A1 in presence of eIF4G-MC puts in perspective the only 2-fold affinity decrease of eIF4A2 in presence of CNOT1 MA3-MIF, suggesting that possibly eIF4A2 activity in presence of CNOT1 could be more akin to the activity of the yeast eIF4A. Taken together, this subchapter elucidated major differences between the eIF4A orthologues, with potential implication of how the data obtained for yeast complexes may not be related to the activities of human proteins.

5.5. Chapter discussion

This chapter was focused on biochemical comparison of the human eIF4A1 and eIF4A2 and their yeast orthologue eIF4A to elucidate potential differences.

First the oligomerisation potential of eIF4A1 was explored. Similarly, to what was discovered for eIF4A2 (see **Chapter 3.5**), eIF4A1 was found to oligomerise *in vitro* (**Figure 5.2-2**, panels A, B). However, its potential to oligomerise was lower than that of eIF4A2, revealing a major distinction between the two paralogues. Further dissimilarities were found for binding affinities, where eIF4A1 binding affinity was the highest for 20 nt RNA, supporting the full oligomerisation inducing interface (**Figure 5.2-2**, panels A, D). This finding is in contrast to what is described in the literature, where the binding interface of both human and yeast eIF4A was shown to be around 15 nt (Abramson *et al.*, 1987; A. Z Andreou and Klostermeier, 2013).

Furthermore, eIF4A1 oligomerisation was shown to exist in cells (**Appendix 3 Figure 3-1**). As human eIF4G1 has 2 eIF4A binding sites and was previously described to bind two eIF4A molecules (Korneeva *et al.*, 2001; Imataka and Sonenberg, 2015) the possibility of the eIF4G-induced eIF4A oligomerisation had to be examined. For this eIF4G-binding-deficient eIF4A1 mutants were utilised (mutations based on Oberer, Marintchev and Wagner, 2005), which contested the idea of eIF4G-induced interaction (**Appendix 3 Figure 3-2**, **3-3**, **3-4**). However, it should be noted that the cellular localisation of this mutant was not restricted to cytoplasm. As endogenous eIF4A1 is in far excess of endogenous eIF4G and is exclusively cytoplasmic, this change in not likely due to the loss of eIF4G binding and instead suggests that this mutant causes localisation defect. Importantly, the *in vitro* assays show that this mutant is capable of RNA binding, similar to WT eIF4A1. Additional use of RNA binding deficient eIF4A1 mutant supported the described model for eIF4A2 (see **Chapters 3.5**, **3.9**), in which oligomerisation happens through protein-protein interactions and the RNA contact is not required for all of the protomers in the oligomer (**Appendix 3 Figure 3-1**).

Next, the catalytic activities of eIF4A1 and eIF4A2 alone and in presence of interaction partners were compared. The activity of eIF4A2 in comparison to

eIF4A1 in all the tested conditions, both alone and with interaction partners, was higher (**Figure 5.2-3**, panel A). However, the enhancement of unwinding activity by eIF4H and eIF4G-MC was greater for eIF4A1 than eIF4A2 (**Figure 5.2-3**, panel B). Albeit the absolute effect was still greater for eIF4A2, which could be due to a higher activity of free oligomeric eIF4A2 than eIF4A1, as eIF4G-MC enhanced eIF4A2 activity only about 1.5-fold (see **Figure 4.3-3**). The observed stimulation for eIF4A1 unwinding activity is in agreement with the literature (Rogers, Richter and Merrick, 1999; Korneeva *et al.*, 2005; Nielsen *et al.*, 2011; Özeş *et al.*, 2011).

Intriguingly, eIF4A1 unwinding activity was synergistically stimulated by eIF4H and eIF4G similarly to the published data for human and yeast eIF4A (Abramson, Dever and Merrick, 1988; Nielsen *et al.*, 2011; Andreou and Klostermeier, 2014). Contrary to this observation, the additive effect on eIF4A2 activity was not as strong (**Figure 5.2-3**, panel C, see also **Figure 4.3-3**). Interestingly, there is only one amino acid difference between the two paralogues in the canonical region responsible for eIF4G binding. However, as eIF4A2 does not preferentially interact with eIF4G1 in cells (Meijer *et al.*, 2013, 2019; Wilczynska *et al.*, 2019) a possibility of different regions responsible for full eIF4G-eIF4A interaction could explain observed differences. In additional experiments, these data could be further expanded through the use of the eIF4A2-7-mut mutant described in this chapter, which was previously shown to restore the full interaction with eIF4G1 in cells (Wilczynska *et al.*, 2019). Potentially, experiments employing eIF4A2-7-mut could explain the lack of strong synergistic activation of eIF4A2 by eIF4H and eIF4G.

Moreover, a surprising decrease in eIF4A1 ATPase activity in presence of eIF4G-MC, and subsequent decrease in presence of both eIF4G-MC and eIF4H was observed (**Figure 5.2-3**, panel D). This observation is in stark contrast to what was described previously in the literature (Nielsen *et al.*, 2011). However, it should be noted that the previous observations included RNA substrates of different lengths of both single- and double-stranded regions, as well as different sequences. Moreover, a relation between the RNA length and ATPase activity was previously observed for yeast eIF4A (Andreou, Harms and Klostermeier, 2019). Perhaps, testing the eIF4A1 ATPase activity on different RNA substrates could explain the observed discrepancy. In contrast, eIF4A2

ATPase activity was not subjected to great change regardless of presence of the interaction partners. Albeit a slight decrease of eIF4A2 ATPase activity was detected in presence of both eIF4G-MC and eIF4H (**Figure 5.2-3**, panel D, see also **Figure 4.3-3**, panel D). This was also visible when comparing eIF4A1 ATPase in presence of eIF4G-MC and both eIF4G-MC and eIF4H, indicating that eIF4H in a reaction containing eIF4A-eIF4G complexes could potentially decrease the ATP turnover of eIF4A.

As differences in both oligomerisation potential and the catalytic activities between the two paralogues were observed, next part of this chapter focused on additional dissimilarities previously described in the literature (Wilczynska *et al.*, 2019). Here, the previous work showing selective binding of eIF4A2 to AG-RNA in the presence of a competitor RNA and the lack of this activity in eIF4A1 was expanded by use of eIF4A mutants. The goal was to uncover what potential regions of eIF4A are responsible for this distinct binding preference of the two helicases. The gathered data suggest that the N-terminal region of eIF4A1 drives the lack of selectivity (**Figure 5.3-3**, panel A). Intriguingly, for eIF4A2, loss or exchange of N-terminal region with eIF4A1, did not cause the loss of selectivity. This suggested that for eIF4A2, additional regions are responsible for its selective behaviour. The eIF4A2-7-mut mutant exhibited the largest change, resembling the activity of WT eIF4A1; however, the extent of this change was lower, and due to a large error between the replicates, strong conclusions could not be made. Taken together, these data suggest that the divergent N-terminal region of eIF4A1 is the primary driver of the differences in RNA binding between the paralogues. Moreover, additional regions in eIF4A2 make it distinct to eIF4A1, and resistant to the loss of its natural activity. These discoveries about the role of the divergent N-terminal region, and the previously described translational repression by eIF4A2 related to its selective behaviour (Wilczynska *et al.*, 2019), could aid in future developments into targeting the specific paralogue and its activity in a cancer setting.

Next, RNA release from WT and mutants of eIF4A1 was tested (**Figure 5.3-3**, panel B). Although a direct comparison between the experiments presented in this thesis and the ones described in Wilczynska *et al.*, 2019 could not be made due to uncompetitive nature of the RNA release experiments presented here certain conclusions could be drawn. The excess of competitor RNA used in the

previous study induced a faster RNA strand release, with both eIF4A1 and eIF4A2 exchanging labelled for non-labelled AG-RNA, whereas only eIF4A2 readily exchanged labelled $(CAA)_6CA$ for unlabelled $(AG)_{10}$. Here, in the non-competitive conditions both paralogues released the $(CAA)_6CA$ RNA in a similar manner, even in the starting phase of the reaction. The discrepancy between the data presented here and the previously published can additionally stem from the use of hydrolysable ATP in **Figure 5.3-3**, panel B, as AMP-PNP is thought to lock the proteins onto RNA. Moreover, eIF4A2 exhibited a longer duration in an RNA-bound state on AG-RNA in contrast to eIF4A1, eIF4A2-7-mut, eIF4A2 1-18 A1 and eIF4A1 1-18 A2. Interestingly, the N-terminally truncated mutants of both paralogues exhibited the longest half-lives, with eIF4A1 Δ N-20 showing almost no AG-RNA release in the tested conditions. These data further emphasise the differences between the paralogues and indicates that the RNA release is at least partially mediated through the N-terminal region. As an important aside, this discovery indicates that caution needs to be taken with interpretation of experiments that use N-terminally tagged or truncated eIF4A. Additionally, as the previously solved RNA-bound crystal structure of eIF4A1 represents N-terminal truncation of eIF4A1 (Iwasaki *et al.*, 2019), the findings presented here invoke a new question whether a more accurate structure of RNA-bound eIF4A1 should be determined with the full N-terminus present.

Moreover, distinct oligomerisation potential was observed for the two paralogues and their mutants (**Figure 5.3-4**). However, the oligomerisation and the preference to form larger oligomeric species on specific RNA sequences was not correlated with the RNA sequence selective binding. This suggested that the RNA binding selectivity might be independent of which species, i.e., monomeric, or oligomeric, are bound to the RNA substrate.

The final aspect of this chapter was the comparison of the human eIF4A paralogues and the yeast eIF4A. As *Saccharomyces cerevisiae* shares above 60% sequence identity with both eIF4A1 and eIF4A2 (**Figure 5.4-1**) the functions of exerted by *Sc* eIF4A are often thought to be similar for its orthologues.

The data presented here elucidated some large differences between the yeast and human eIF4A helicases. The biggest difference was observed in how *Sc* eIF4A binds RNA, with almost no RNA-binding activity detected in presence of AMP-PNP

and weak binding in presence of ATP (**Figure 5.4-3**, panel A). Moreover, almost no oligomeric species were detected for yeast eIF4A. Although *Sc* eIF4A has the potential to form oligomers, as silvestrol was shown to induce this activity (**Figure 5.4-3**, panel A).

Moreover, *Sc* eIF4A K_D for $(AG)_{10}$, $(CAA)_6CA$, $(AGUG)_5$ is larger than the one observed with human paralogues (**Figure 5.4-3**, panel B). However, this difference could potentially stem from the K_D measurements of *Sc* eIF4A in presence of hydrolysable ATP. This means that *Sc* eIF4A ATPase activity could influence the measured K_D. Additionally, as observed in **Table 3.8-1** eIF4A2 exhibited higher K_D values for the same RNAs in presence of ATP than AMP-PNP. Next, **1)** as CNOT1 fragments decreased eIF4A2 affinity for all tested RNA sequences (see **Figure 4.5-5**, **Table 5.4-1**), and **2)** eIF4G-MC decreased the functional binding affinity of eIF4A2 for 5'$(AG)_{10}$ overhang RNA (see **Table 4.3-2**), therefore a question was posed what influence the truncated fragments of *Sc* eIF4G have on *Sc* eIF4A binding affinities. Interestingly an opposite effect was observed for *Sc* eIF4A (**Figure 5.4-3** panel, **Table 5.4-1**). Here, both tested *Sc* eIF4G constructs increased affinity of *Sc* eIF4A to all tested RNA substrates, with the largest difference visible for AG-motif RNAs. Next, this data were compared to the affinities of eIF4A1 with and without eIF4G-MC (**Figure 5.4-3**, panel D, **Table 5.4-1**). Human eIF4G-MC caused above 30-fold increase in the K_D of eIF4A1 for $(AG)_{10}$ and $(AGUG)_5$ RNAs. This large difference puts in perspective the only 2-fold increase of K_D exerted by CNOT1 MA3-MIF on eIF4A2. This potentially indicates that eIF4A2 in presence of CNOT1 behaves in a more similar manner to the yeast orthologues than eIF4A1. The RNA binding capacity of yeast eIF4G constructs was examined (**Figure 5.4-3**, panel E) as human eIF4G-MC fragment was previously shown to bind RNA (Nielsen *et al.*, 2011), and a weak binding to AG-motif RNAs was observed for CNOT1 MA3-MIF fragment (**Figure 4.5-4**, panel D). Here a very weak binding of *Sc* eIF4G-MC to AG-RNA was detected which might relate to the previously identified three RNA binding regions on yeast eIF4G (Berset *et al.*, 2003). Moreover, only the longer *Sc* eIF4G-MC contains one of the RNA binding regions and for full binding activity all three regions need to be present. This could possibly indicate greater similarities between *Sc* eIF4A and eIF4A2 in presence of their main interaction partners. Additional similarity between eIF4A2 and CNOT1 interaction and the one

between *Sc* eIF4A and *Sc* eIF4G could potentially be drawn from the nature of the interaction. *Sc* eIF4G has been shown to modulate conformational change of *Sc* eIF4A (Andreou and Klostermeier, 2014). Additionally, the crystal structure of *Sc* eIF4A in complex with *Sc* eIF4G has been shown to resolve with the greatest quality, with less variation in the sample, in presence of both AMP and ADP (Schutz *et al.*, 2008). This could possibly be related to the greater co-immunoprecipitation of MIF and both MIF and MA3 domains of CNOT1 with eIF4A2 in presence of AMP and ADP + Pi (see **Figure 4.5-4**). Perhaps, further studies could focus on use of different stages of ATP hydrolysis to elucidate the inner workings of the formed complexes.

In all, this chapter emphasised the molecular differences between the highly identical human eIF4A paralogues, and highlighted the need for further studies, that could dissect the activities of eIF4A1 and eIF4A2. Moreover, the data presented here stressed the importance of studying human proteins for further progress in medical studies, as despite certain similarities between the orthologues their molecular mechanisms can differ.

6. Thesis discussion and future prospects

The high identity between eIF4A1 and eIF4A2 has led many scientists to believe that the two paralogues are functionally redundant, therefore most previous studies focused solely on exploration of the mechanisms of eIF4A1. However, the observation that upon knock out of eIF4A1, eIF4A2 is overexpressed without rescuing eIF4A1 role in translation initiation (Galicia-Vazquez *et al.*, 2012) has put eIF4A2 on the scientific map. The recent discoveries implicating eIF4A2 in a translationally repressive role (Meijer *et al.*, 2013, 2019; Wilczynska *et al.*, 2019) brought to light the need to investigate this molecularly unexplored eIF4A paralogue.

In this thesis, biochemical, structural, and imaging methods were used to uncover the molecular mechanisms that drive eIF4A2. Moreover, the activities conferred through the interaction partners were explored and the divergent functions between eIF4A1 and eIF4A2 were compared on a biochemical level. These findings led to creation of a model which could explain the new activities of the paralogues (**Figure 6-1**). This chapter brings together the most important discoveries described in this thesis and proposes future directions.

The discovery that both eIF4A1 and eIF4A2 can form oligomers *in vitro* and in cells (**Figures 3.4-1**, **3.7-3**, **5.2-2**, and **Appendix 3 Figure 3-1**) can have broader implications for our understanding of how protein translation is regulated. Both paralogues oligomerised preferentially on RNAs with AG-motifs (**Figures 3.5-2**, **5.2-2**), however eIF4A2 displayed more flexibility in this aspect, oligomerising on different sequences. Although it could not be determined whether the higher unwinding activity of eIF4A2 was correlated with oligomerisation potential or its affinity for specific RNA sequence (**Figure 3.8-3**), both eIF4A2 and eIF4A1 did not display RNA unwinding when oligomerisation potential and free exchange of protomers in the oligomer were abrogated (**Figure 3.10-2** and **Appendix 3 Figure 3-5**). Interestingly, independent investigation in the Bushell lab, has shown that the unwinding activity of eIF4A1 is the highest on AG-RNA, and translation of structured RNAs in reticulocyte assays is greater when the AG-motifs are present in a reporter mRNA. It is well known that efficient translation of mRNAs with highly structured 5'UTRs requires

helicase activity. In fact, depletions of helicases such as DDX3 or DHX36 have been shown to reduce translation of mRNAs with highly structured 5'UTRs (Pisareva *et al.*, 2008; Calviello *et al.*, 2021). Similar observations were made for inhibition of eIF4A (Rubio *et al.*, 2014; Waldron, Raza and Le Quesne, 2018; Waldron *et al.*, 2019); however, the interpretation of eIF4A inhibition could be more complicated, due to its unwinding-independent activity in mRNA loading onto the 43S ribosomal subunit (Sokabe and Fraser, 2017). Interestingly, the gain of function inhibitor, silvestrol used in this thesis induced oligomerisation of both paralogues as well as their unwinding activity (**Figures 3.9-1**, **3.9-4**, **5.2-2**). However, despite the observed gain of function, other studies using silvestrol have reported translational inhibition (Kogure *et al.*, 2013; Wolfe *et al.*, 2014; Chen *et al.*, 2016; Biedenkopf *et al.*, 2017). This could be due to the previously described (Iwasaki, Floor and Ingolia, 2016) and observed here (**Figure 3.10-1**) clamping mechanism, which leaves eIF4A locked onto the RNA. As explained in the publication from Ingolia lab (Iwasaki, Floor and Ingolia, 2016), the presence of eIF4A bound to the mRNA could physically disturb the scanning mechanism of the 40S ribosomal subunit. Alternatively, all available eIF4A could be scavenged by clamping it in monomeric form to the RNA, leaving no free eIF4A to perform other functions.

Curiously, the eIF4G-MC, containing both eIF4A binding sites, reduced the apparent affinity of eIF4A2 for RNA substrate in the unwinding reaction, as well as the cooperativity between the protomers in the oligomer (**Table 4.3-2**). A similar observation was made for eIF4A1, which displayed reduced binding affinity in presence of eIF4G-MC (**Table 5.4-1**). Importantly, eIF4G-MC greatly reduced the unwinding activity of both eIF4A1 and eIF4A2 when present in equal or greater molar concentration than the helicases (**Figure 5.2-3**). Moreover, an eIF4A1 mutant incapable of binding eIF4G, oligomerised both *in vitro* and in cells (**Appendix 3 Figures 3-2**, **3-3**, **3-4**). Of special importance was also the observed lack of synergistic activation of eIF4A2 by eIF4H and eIF4G-MC (**Figure 5.2-3**), suggesting that eIF4A2, forms complexes of distinct activity. Taken together, this indicates that the main function of both eIF4As when in complex with eIF4G is independent of unwinding activity. Therefore, it could be proposed that in cells the unwinding activity is performed by a population of the non-eIF4F-associated, free, oligomerised eIF4A. In fact, there are more molecules of

eIF4A than ribosomes present in cell, with a 3 to 1 ratio of the helicase to the ribosome (Roger Duncan and Hershey, 1983). Intriguingly, a recent landmark publication further supports the concept that there may be two pools of eIF4A in the cell. An atomic resolution structure of the entire 48S ribosomal initiation complex solved by CryoEM from the Ramakrishnan lab (Querido *et al.*, 2020) presented single eIF4A in the eIF4F complex at the 40S ribosomal subunit mRNA exit channel. This suggested that the canonical role of eIF4A in the eIF4F complex could be in the mRNA loading and supported the 'ratchet' model of translation initiation (as described in **Chapter 1.3.2**). However, the authors of that work did not exclude the possibility of additional, separate population of eIF4A existing outside of the eIF4F complex at the 40S mRNA entry channel, where it could perform the unwinding activity. Perhaps, the eIF4A2 preference to unwind RNA substrates in 3'-to-5' direction (**Figure 3.8-5**, **Table 3.8-2**) could play a role here. Moreover, investigation of the conditions in which the 48S was assembled (Querido *et al.*, 2020), suggests that the authors would not be able to obtain oligomeric eIF4A, as 1 to 2 eIF4G to eIF4A ratio was used. Additionally, the authors (Querido *et al.*, 2020) used ATP analogue, ATP-γ-S, which has been previously shown to be hydrolysed by eIF4A (Peck and Herschlag, 2003). Implication of that is that eIF4A could shift through conformational cycle, and it is currently unknown how transient are the oligomeric complexes.

Importantly, data collected for the *Sc* eIF4A additionally support a model in which oligomerised eIF4A is needed for unwinding activity. *Sc* eIF4A was demonstrated to mostly exist in monomeric form, however the potential to oligomerise was not absent (**Figure 5.4-3** and **Appendix 3 Figure 3-6**). Interestingly, the yeast mRNAs have significantly shorter and less structured 5'UTRs than human mRNAs (Leppek, Das and Barna, 2018). Furthermore, *Sc* eIF4A has been also shown to have unwinding-independent activity in mRNA loading on the 43S (Yourik *et al.*, 2017). That indicates, that *Sc* eIF4A role could be predominantly unwinding-independent, which correlates with its weaker oligomerisation potential.

However, to understand the exact role of oligomeric eIF4A, further investigations are necessary. The exact residues responsible for oligomerisation of eIF4A1 and eIF4A2 should be determined, either through crystallisation of oligomeric complexes, hydrogen-deuterium exchange (HDX), or mutational

analysis. The latter two have their limitations. In HDX, hydrogen atoms that are accessible to the solution are exchanged for deuterium. Therefore, using two separate samples of monomeric and oligomeric eIF4A, one can determine the regions which are accessible in monomeric complex and no longer available for the exchange in the oligomer. However, this kind of experiment, provides only broad regions that could be involved in oligomer formation. The mutational analysis requires prior knowledge, therefore can be coupled with HDX. Albeit creation of multiple mutations and testing them both *in vitro* and in cells can be time consuming. Therefore, obtaining exact atomic resolutions of oligomeric eIF4A is critical. However, crystallisation of the oligomeric complexes could be in itself a rather daunting task. As eIF4A oligomerisation is dependent on two factors: presence of RNA and protein being in excess over RNA (**Figure 3.5-1**), this often leads to formation of multiple species in one sample. In fact, crystal structure of eIF4A1 in presence of AG-RNA and RocA (Iwasaki *et al.*, 2019), was obtained in 3 to 1 excess of RNA over the protein. This ratio was perhaps chosen, to avoid mixed population in the sample with free and RNA-bound eIF4A. However, such a ratio would never lead to obtaining oligomeric complexes. Perhaps, deriving from another approach, that has been used in this thesis is needed. In the SAXS experiments (**Chapter 3.6**) the complexes were subjected to size exclusion chromatography and then exposed to X-ray radiation. This way, analysis of separate complexes was possible. Crystallisation of separate complexes eluted from size exclusion column would yield the most homogenous samples. As another approach, CryoEM could be used to obtain a more native state of the complexes at atomic resolution without the requirement for crystal formation.

Further, the impact of abrogation of oligomerisation should be assessed in cells, or mouse models. As overexpression of eIF4A1 and occasionally eIF4A2 is associated with poor prognosis for cancer patients (see **Table 1.5.1-1**) and many oncogenic proteins have highly structured 5'UTRs, the correlation between oligomerisation and cancer is rather alluring. However, testing whether lack of oligomerisation could be detrimental to normal cells should be a priority. Moreover, the next step should be to understand which mRNAs are dependent on the eIF4A oligomeric state, and to determine whether the disruption of oligomerisation of eIF4A reduces proliferation of cancer cells. If that is the case,

finding small molecule inhibitors that could disrupt the oligomerisation should be a priority. However, as eIF4A2 has been implicated in miRNA-mediated translational repression (Meijer *et al.*, 2013), and sometimes overexpression of eIF4A2 is beneficial for cancer patients (see **Table 1.5.1-1**), finding inhibitors that target the specific paralogue is of utmost importance.

Moreover, understanding in which form, oligomeric or monomeric, eIF4A2 exists in complex with CNOT1, and therefore performs its repressive function is needed. However, as described in this thesis (**Chapter 4.5** and **Appendix 2**), obtaining large quantities of pure, non-aggregated longer construct of CNOT1 is problematic. In fact, the difficult linker region between MA3 and MIF domains of CNOT1 is highly post-translationally modified through phosphorylation, acetylation and most importantly glycosylation (PhosphoSite, Hornbeck *et al.*, 2015). Perhaps, changing from the favoured by many biochemists bacterial protein expression system into the mammalian one would be beneficial. In fact, understanding what influence the post-translational modifications can have on the catalytical properties of eIF4A1 and eIF4A2 could be the next step. Advantageously, none of the possible post-translational modifications have an effect on eIF4A oligomerisation, as FLIM-FRET assays were performed in human HeLa cells (**Chapter 3.6** and **Appendix 3**).

Interestingly, virtually no RNA binding of eIF4A2 was observed for sequences without AG-motifs in presence of CNOT1, indicating that CNOT1 confers even more selectivity on eIF4A2 (**Figure 4.5-5** and **Table 5.4-1**). This discovery is in agreement with previous work from the Bushell lab (Wilczynska *et al.*, 2019), in which eIF4A2 induced repression through the AG-motifs in RNA. Perhaps the selective high unwinding of eIF4A1 in presence of AG-motifs, and the repression exerted by eIF4A2 through the same motifs act as a sort of a feedback loop to keep the translational control. Moreover, this enhanced RNA sequence preference, despite the slight increase in K_D for AG-motifs, was imparted by CNOT1, regardless of its own RNA binding properties (**Figure 4.5-5**). In fact, while investigating the influence of CNOT1 on eIF4A2, a discovery about CNOT1 RNA binding potential was made. As neither MA3 nor MIF domains themselves exhibited RNA binding (**Figure 4.5-5**), the AG-motif RNA binding of CNOT1 has to be attributed to the disordered linker between the two domains. This could have

possible implications on different studies, in which constructs lacking RNA binding functions were used.

Furthermore, despite the previously disputed eIF4A2-CNOT1 association (Chen *et al.*, 2014), both eIF4A2 and DDX6 interacted with CNOT1 MIF construct (**Figure 4.5-4**). Interestingly, the authors (Chen *et al.*, 2014) who contested eIF4A2-CNOT1 interaction and observed eIF4A2-eIF4G association used non-native levels of eIF4A2. As has been shown previously (Wilczynska *et al.*, 2019) overexpression of eIF4A2 causes its preferential association with eIF4G. Here, equimolar concentrations of recombinant eIF4A2 and CNOT1 constructs were used. Moreover, in this thesis the activation of CNOT7 deadenylation activity through association with CNOT1 MIF was only observed for DDX6 and not eIF4A2 (**Figure 4.5-6**). This supports the previously observed inhibition of CNOT7 deadenylation in presence of eIF4A2 (Meijer *et al.*, 2019). The lack of deadenylation in presence of eIF4A2 verifies a model in which eIF4A2 bound mRNAs can be translationally repressed but not degraded. The implication of that could be that the eIF4A2 bound messages targeted for repression are stored.

Interestingly, eIF4A2-mediated mRNA storage could fit into a model proposed by the Parker lab (Tauber *et al.*, 2020), in which eIF4A1 modulated RNA condensates. Interestingly, in that publication concentration of eIF4A1 which would support oligomerisation was used. Moreover, ATP-dependent dissolving of RNA condensates induced by eIF4A1 was observed. Possibly, the unwinding activity of oligomerised eIF4A1 played a role in this observation. Perhaps expanding that study (Tauber *et al.*, 2020) by use of eIF4A2 and different concentrations of both paralogues to obtain both monomeric and oligomeric conditions, would yield more definite answer about the role of eIF4A in phase separation. Interestingly another landmark study (Hondele *et al.*, 2019) which explored roles of DEAD-box helicases in phase separation postulated that eIF4A does not form RNA condensates. The condensation was suggested to happen mostly through low-complexity regions in the structures of DEAD-box proteins, which both eIF4A1 and eIF4A2 lack (Hondele *et al.*, 2019). However, an example of condensate-localised DDX39B (UAP56), which lacks low complexity domains was presented (Hondele *et al.*, 2019). Moreover, only the yeast eIF4A was explored in the aspect of phase-separation in that publication. Taken together, this captivating avenue of additional regulatory roles of eIF4As in protein

translation should be explored in context of both monomeric and oligomeric versions of eIF4A1 and eIF4A2.

Overall, this study provided in-depth investigation of both paralogues, however many more aspects of eIF4As' activities remain to be determined. Finally, out of the scope of this thesis, the possibility of eIF4A1 and eIF4A2 to form hetero oligomers was identified. As shown in Wilczynska *et al.*, 2019 there is a large group of mRNAs bound by both eIF4A1 and eIF4A2. Perhaps future investigations into exact roles of hetero oligomers could explain why in certain cancers eIF4A2 overexpression could have a negative effect on cancer patients.

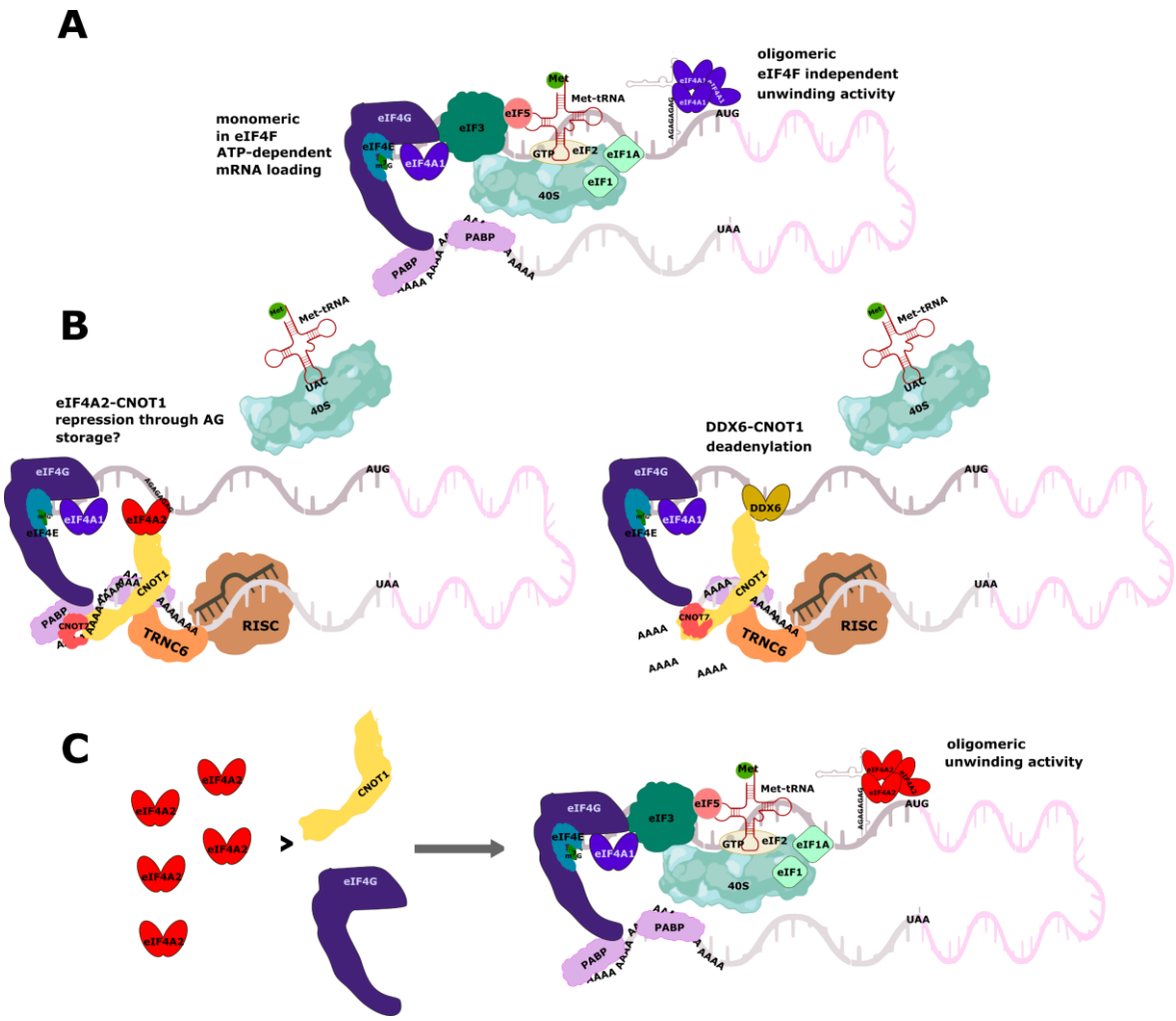

Figure 6-1 Oligomerisation-dependent model of translational control

A. Monomeric (or two independent eIF4A1) associate with eIF4F through eIF4G and perform function in mRNA loading onto the 40S ribosomal subunit. eIF4F-independent eIF4A1 unwinding secondary structures in the 5'UTR through oligomerisation at AG-motifs.

B. eIF4A2 in complex with CCR4-NOT represses translation through AG-motifs without mRNA degradation, possible role in mRNA storage. DDX6 in CCR4-NOT enhances CNOT7 deadenylation activities.

C. eIF4A2 if in excess of CNOT1 and possibly eIF4G can oligomerise on its own and unwind secondary structures either through association of AG-motifs or other sequences.

Appendix 1

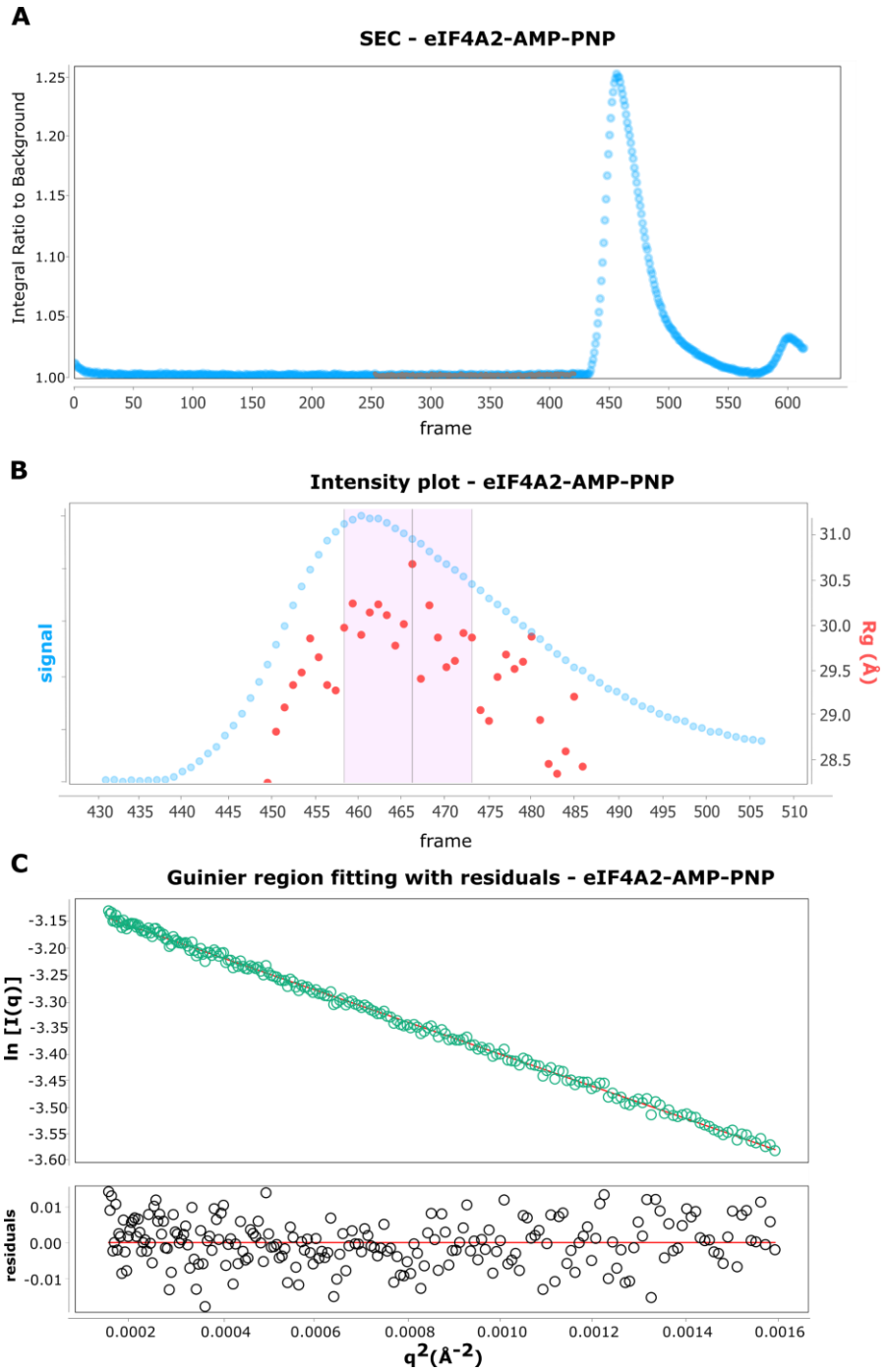

Appendix 1 Figure 1-1 AMP-PNP bound eIF4A2 remains monomeric in solution

A. Size exclusion chromatography (Superdex 200 increase 3.2) of the sample containing 100 µM eIF4A2 and 1 mM AMPPNP in binding buffer (20 mM HEPES pH 7.5, 100 mM KCl, 2 mM $MgCl_2$, 1 mM DTT) run at the Diamond Light Source (Oxford, UK) before the sample was subjected to X-ray radiation, frame corresponds to fraction collected during SAXS. Monomeric peak is visible, eluting around 470 frames. Grey region corresponds to buffer subtracted as background.

B. Intensity plot of the sample presented in panel **A**. Frames with most constant R_g (red dots) selected for further analysis (marked in light pink).

C. Guinier region fitting (*top*) with residuals (*bottom*) of the sample from panel **A**, presenting linearisation of scattering data in the region close to 0 for the scattering angle.

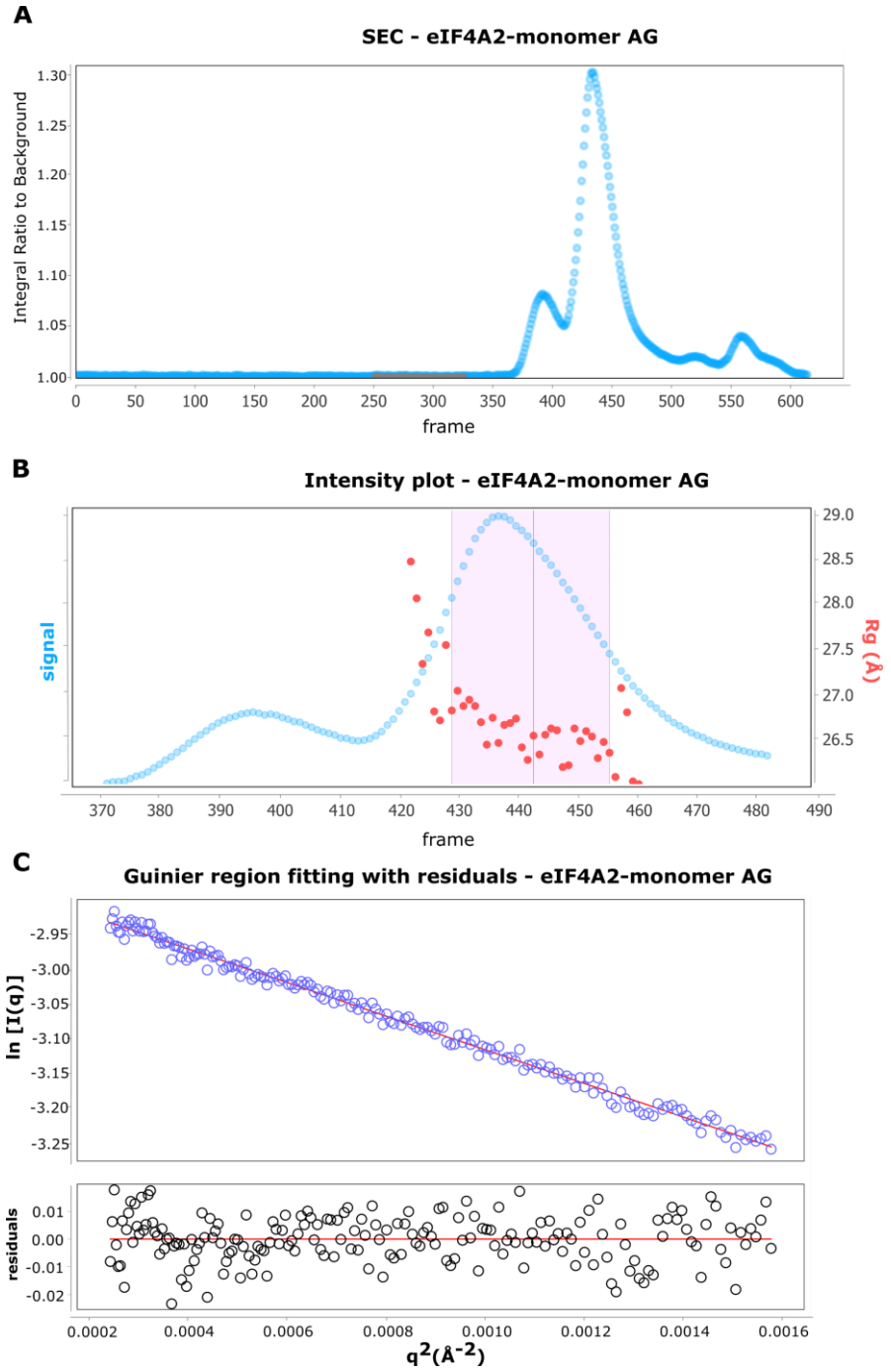

Appendix 1 Figure 1-2 eIF4A2 bound to equimolar amounts of $(AG)_{10}$ RNA remains predominantly monomeric

- **A.** Size exclusion chromatography (Superdex 200 increase 3.2) of the sample containing 90 µM eIF4A2, 90 µM $(AG)_{10}$ RNA, and 1 mM AMPPNP in binding buffer (20 mM HEPES pH 7.5, 100 mM KCl, 2 mM $MgCl_2$, 1 mM DTT) run at the Diamond Light Source (Oxford, UK) before the sample was subjected to X-ray radiation, frame corresponds to frames collected during SAXS. A main peak detected at 450 frames and a small peak at 400 frames are detected corresponding to eIF4A2 monomer and dimer, respectively. The grey region corresponds to buffer subtracted as background.
- **B.** Intensity plot of the sample presented in panel **A**. Frames with most constant R_g (red dots), corresponding to the monomer, selected for further analysis (marked in light pink).
- **C.** Guinier region fitting (*top*) with residuals (*bottom*) of the sample from panel **A**.

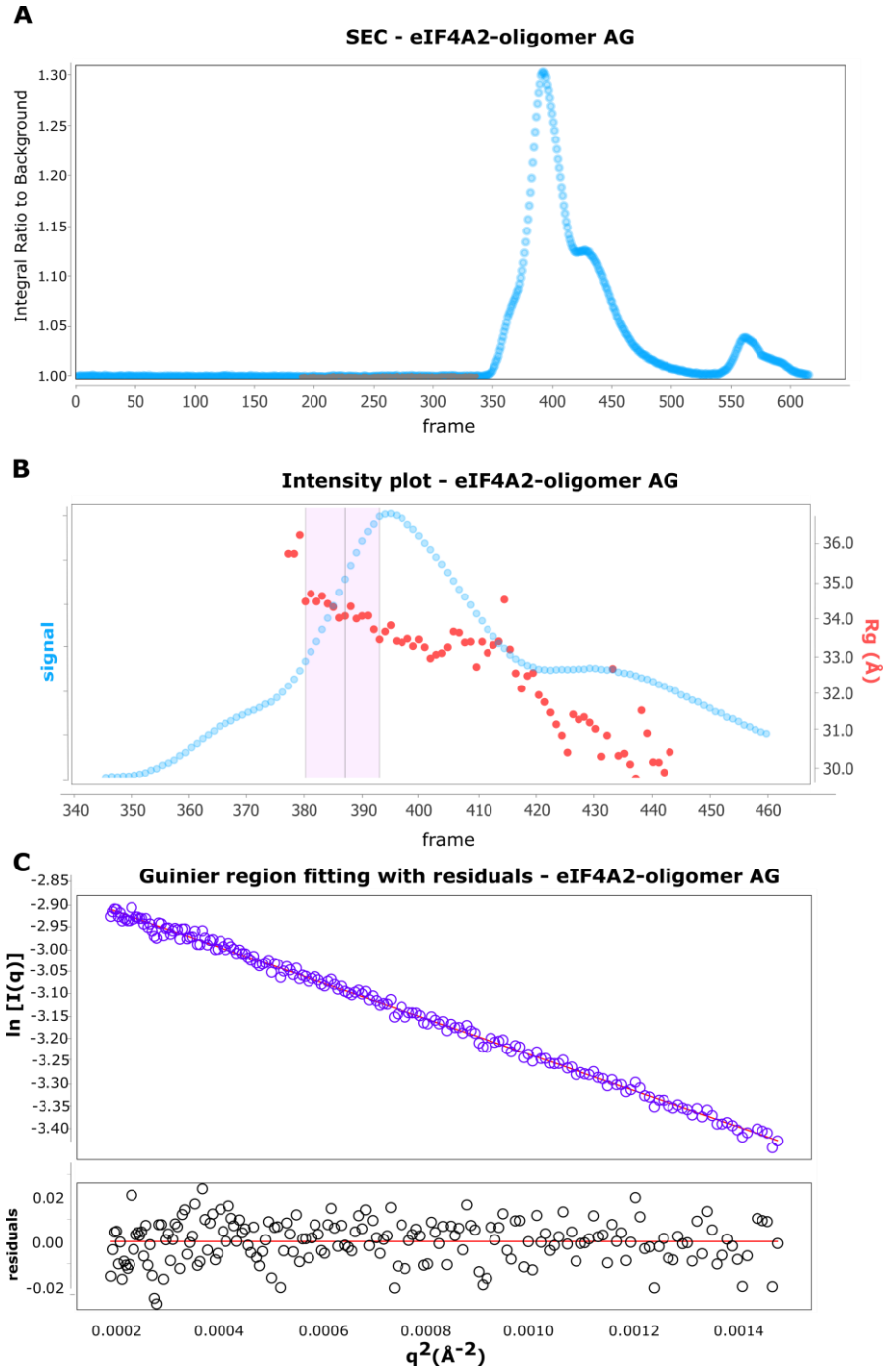

Appendix 1 Figure 1-3 eIF4A2 forms oligomers on polypurine RNA when in excess over RNA substrate

A. Size exclusion chromatography of the sample containing 90 µM eIF4A2, 30 µM $(AG)_{10}$ RNA, and 1 mM AMPPNP in binding buffer (20 mM HEPES pH 7.5, 100 mM KCl, 2 mM $MgCl_2$, 1 mM DTT) run at the Diamond Light Source (Oxford, UK) before the sample was subjected to X-ray radiation, frame corresponds to frames collected during SAXS. Three peaks are visible, monomer at 450 frames, and a small peak for oligomer (dimer) at 400 frames and oligomer (timer) at 360 frames. Grey region corresponds to buffer subtracted as background.

B. Intensity plot of the sample presented in panel **A**. Frames with most constant R_g (red dots), corresponding to the oligomer (dimer), selected for further analysis (marked in light pink). Not enough data was collected for frames corresponding to the peak around 360 frames.

C. Guinier region fitting (*top*) with residuals (*bottom*) of the sample from panel **A**.

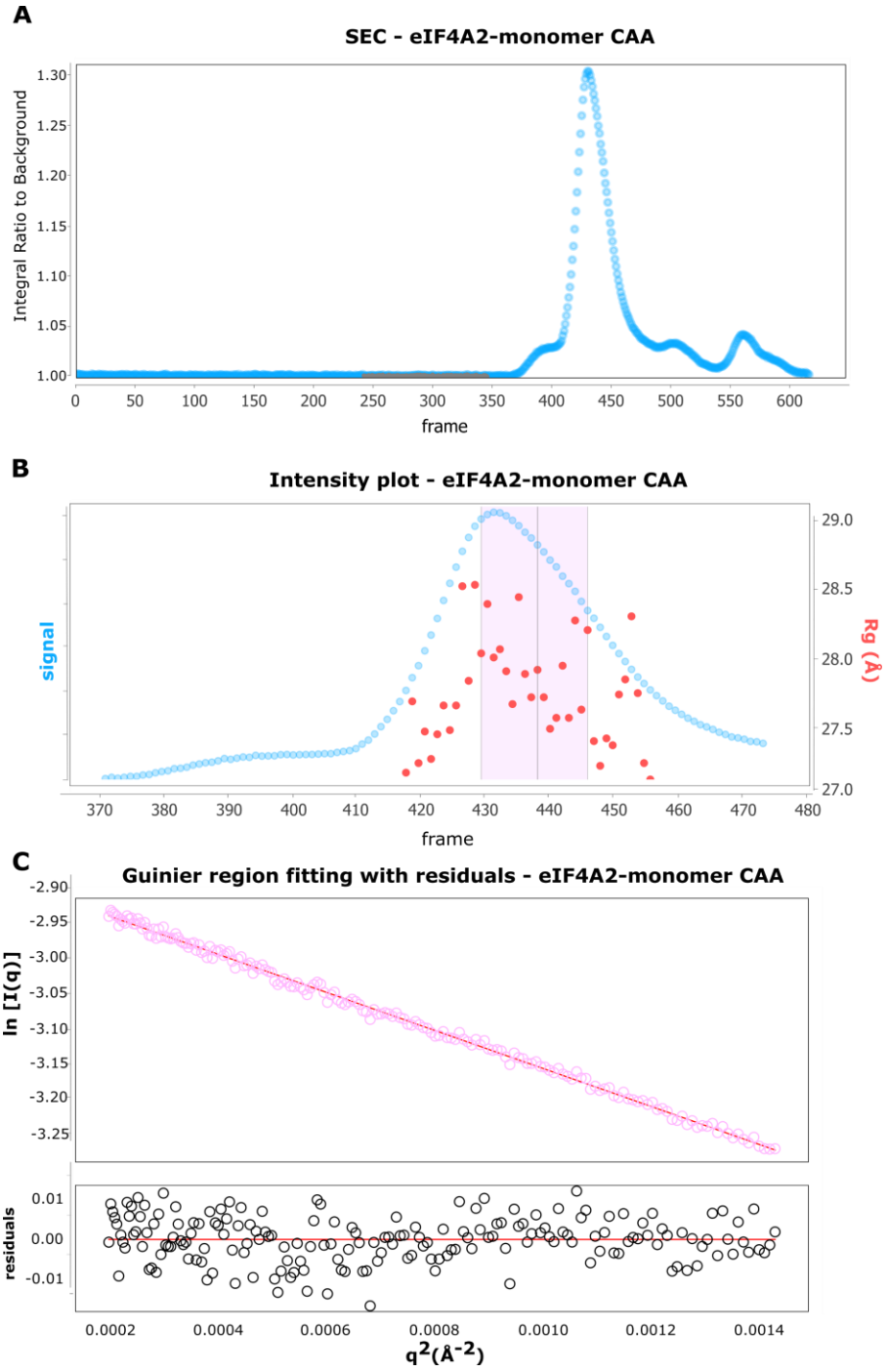

Appendix 1 Figure 1-4 eIF4A2 in presence of equimolar amounts of $(CAA)_6CA$ RNA remains mostly monomeric

- **A.** Size exclusion chromatography of the sample containing 90 µM eIF4A2, 90 µM $(CAA)_6CA$ RNA, and 1 mM AMPPNP in binding buffer (20 mM HEPES pH 7.5, 100 mM KCl, 2 mM $MgCl_2$, 1 mM DTT) run at the Diamond Light Source (Oxford, UK) before the sample was subjected to X-ray radiation, frame corresponds to frames collected during SAXS. Two peaks are visible, monomer at 450 frames, and a small peak for oligomer (dimer) at 400 frames. Grey region corresponds to buffer subtracted as background.
- **B.** Intensity plot of the sample presented in panel **A**. Frames with most constant R_g (red dots), corresponding to the monomer, selected for further analysis (marked in light pink).
- **C.** Guinier region fitting (*top*) with residuals (*bottom*) of the sample from panel **A**.

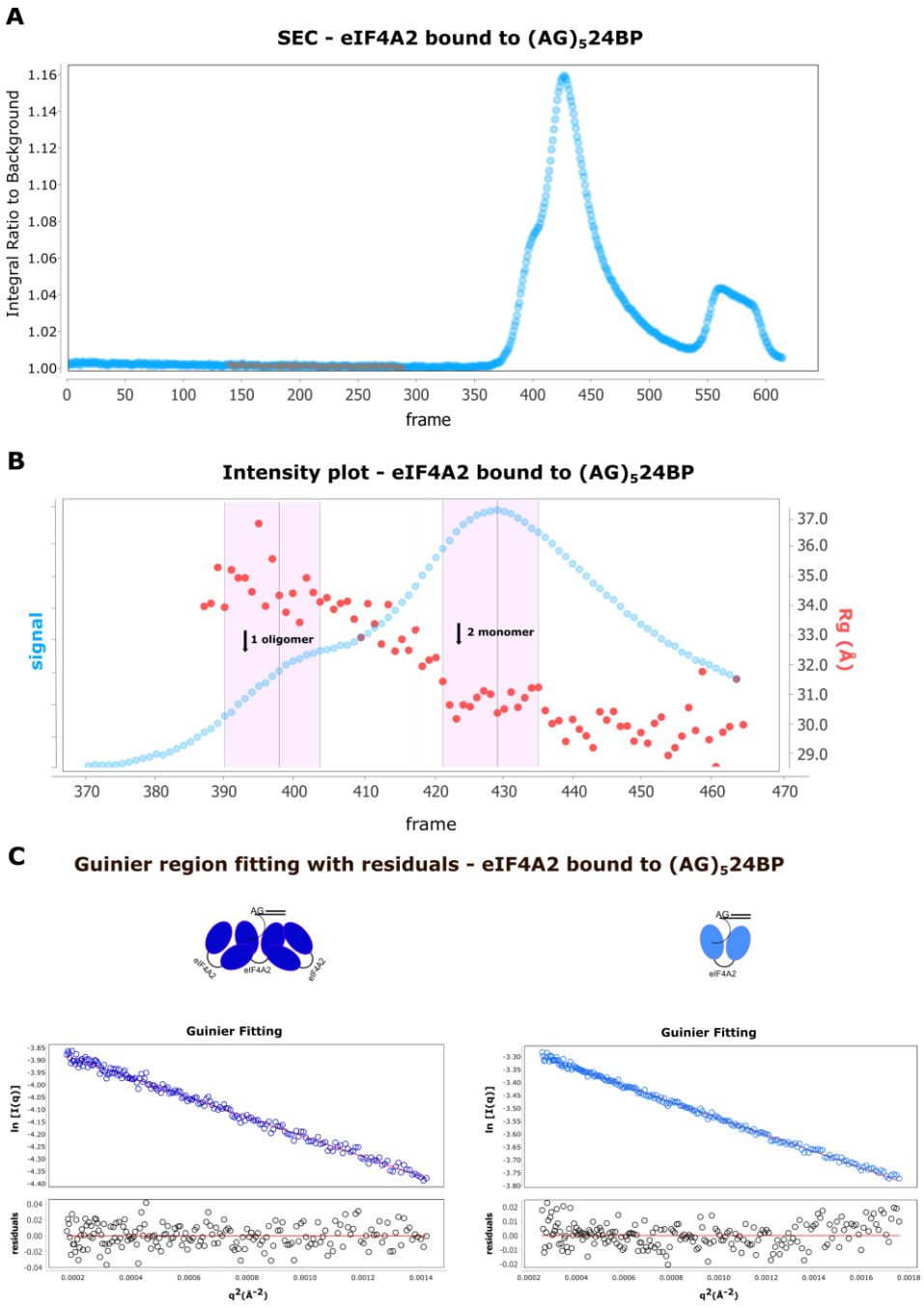

Appendix 1 Figure 1-5 Shorter single stranded region on an RNA substrate with double stranded region induces oligomerisation to a lower extent

A. Size exclusion chromatography of the sample containing 90 µM eIF4A2, 30 µM $(AG)_5$ 24BP RNA, and 1 mM AMPPNP in binding buffer (20 mM HEPES pH 7.5, 100 mM KCl, 2 mM $MgCl_2$, 1 mM DTT) run at the Diamond Light Source (Oxford, UK) before the sample was subjected to X-ray radiation, frame corresponds to frames collected during SAXS. Two peaks are visible, spanning, monomer at 450 and oligomer (dimer) at 400 frames. Grey region corresponds to buffer subtracted as background.

B. Intensity plot of the sample presented in panel **A**. Frames with most constant R_g (red dots), corresponding to the monomer, and oligomer, selected for further analysis (marked in light pink).

C. Guinier region fitting (*top*) with residuals (*bottom*) of the samples from panel **A**, oligomer on the left (*navy blue*) and monomer on the right (*blue*).

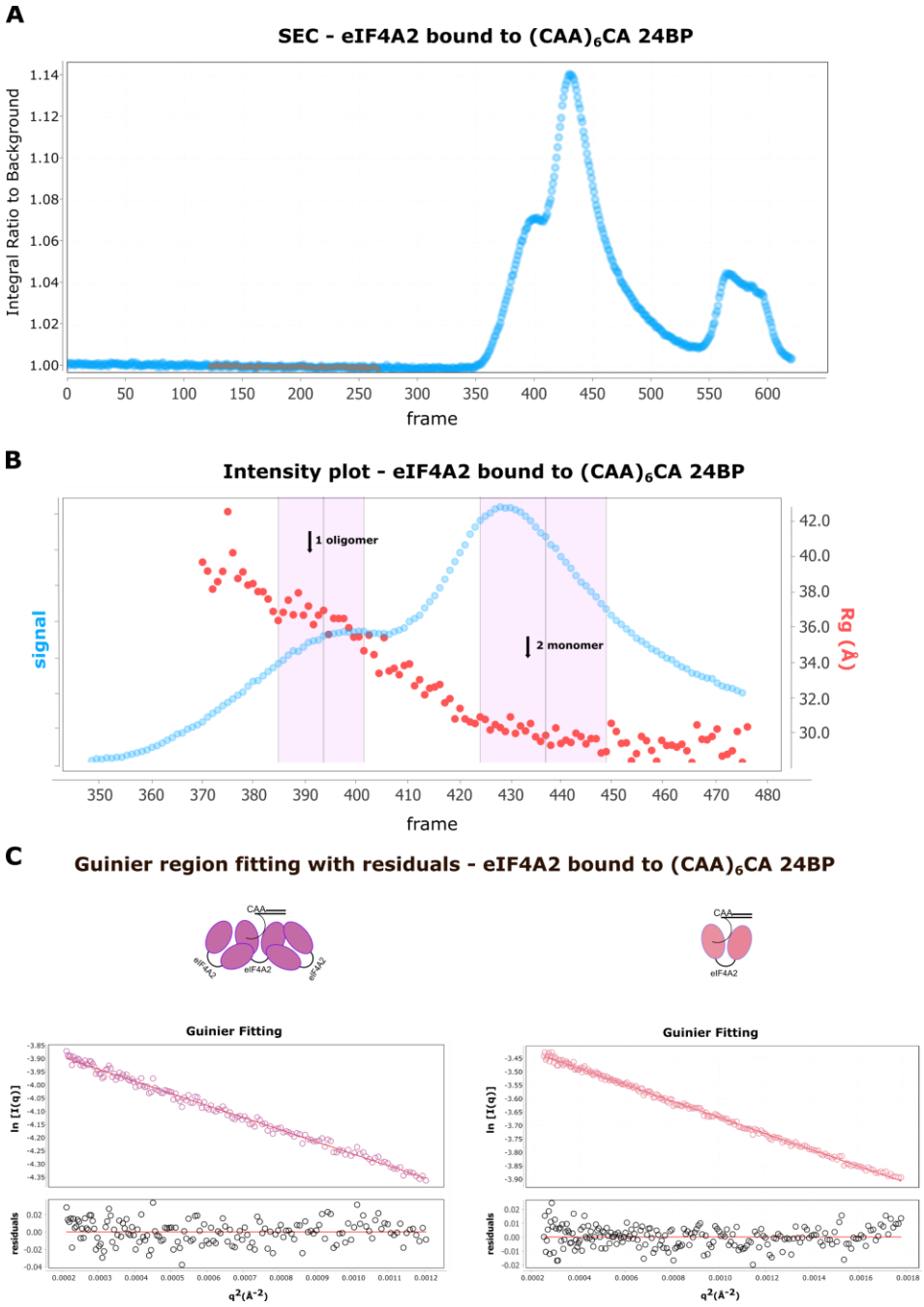

Appendix 1 Figure 1-6 $(CAA)_6CA$ 24BP RNA substrate supports formation of oligomeric complexes

A. Size exclusion chromatography of the sample containing 90 μM eIF4A2, 30 μM $(CAA)_6CA$ 24BP RNA, and 1 mM AMPPNP in binding buffer (20 mM HEPES pH 7.5, 100 mM KCl, 2 mM $MgCl_2$, 1 mM DTT) run at the Diamond Light Source (Oxford, UK) before the sample was subjected to X-ray radiation, frame corresponds to frames collected during SAXS. Two peaks are visible, spanning from 350 to 450 frames. Grey region corresponds to buffer subtracted as background.

B. Intensity plot of the sample presented in panel **A**. Frames with most constant R_g (red dots), corresponding to the monomer, and oligomer, selected for further analysis (marked in light pink).

C. Guinier region fitting (*top*) with residuals (*bottom*) of the samples from panel **A**, oligomer on the left (*deep pink*) and monomer on the right (*pink*).

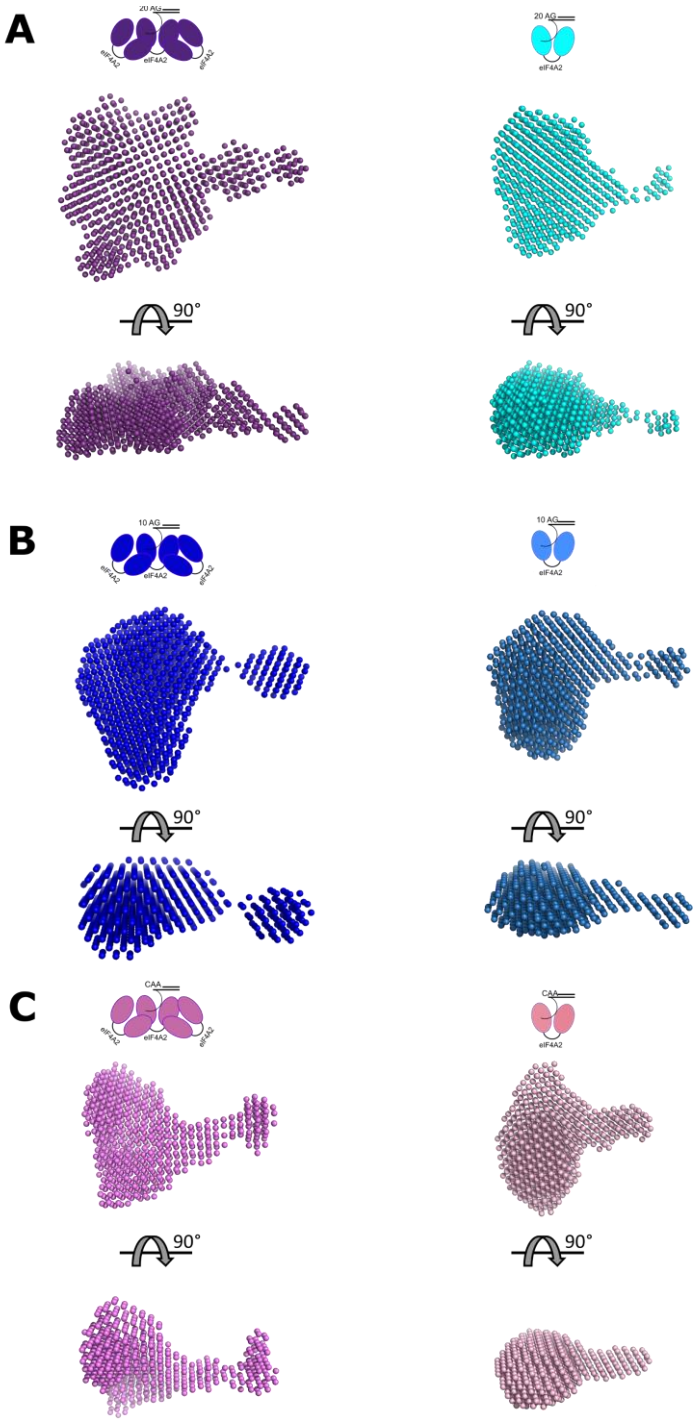

Appendix 1 Figure 1-7 eIF4A2 adopts different conformation based on RNA substrate and oligomerisation status

Envelope models (dummy atom model fitting using DAMMIF and DAMAVER packages from ATSAS 3.0.3) – for more information about analysis please refer to **Chapter 2.3.5** section.

- **A.** Envelope models formed on $(AG)_{10}$ 24 BP RNA substrate: oligomer on the left (*deep purple*) and monomer on the right (*cyan*).
- **B.** Envelope models formed on $(AG)_5$ 24 BP RNA substrate: oligomer on the left (*navy blue*) and monomer on the right (*blue*).
- **C.** Envelope models formed on $(CAA)_6CA$ 24 BP RNA substrate: oligomer on the left (*dark pink*) and monomer on the right (*pink*).

Appendix 2

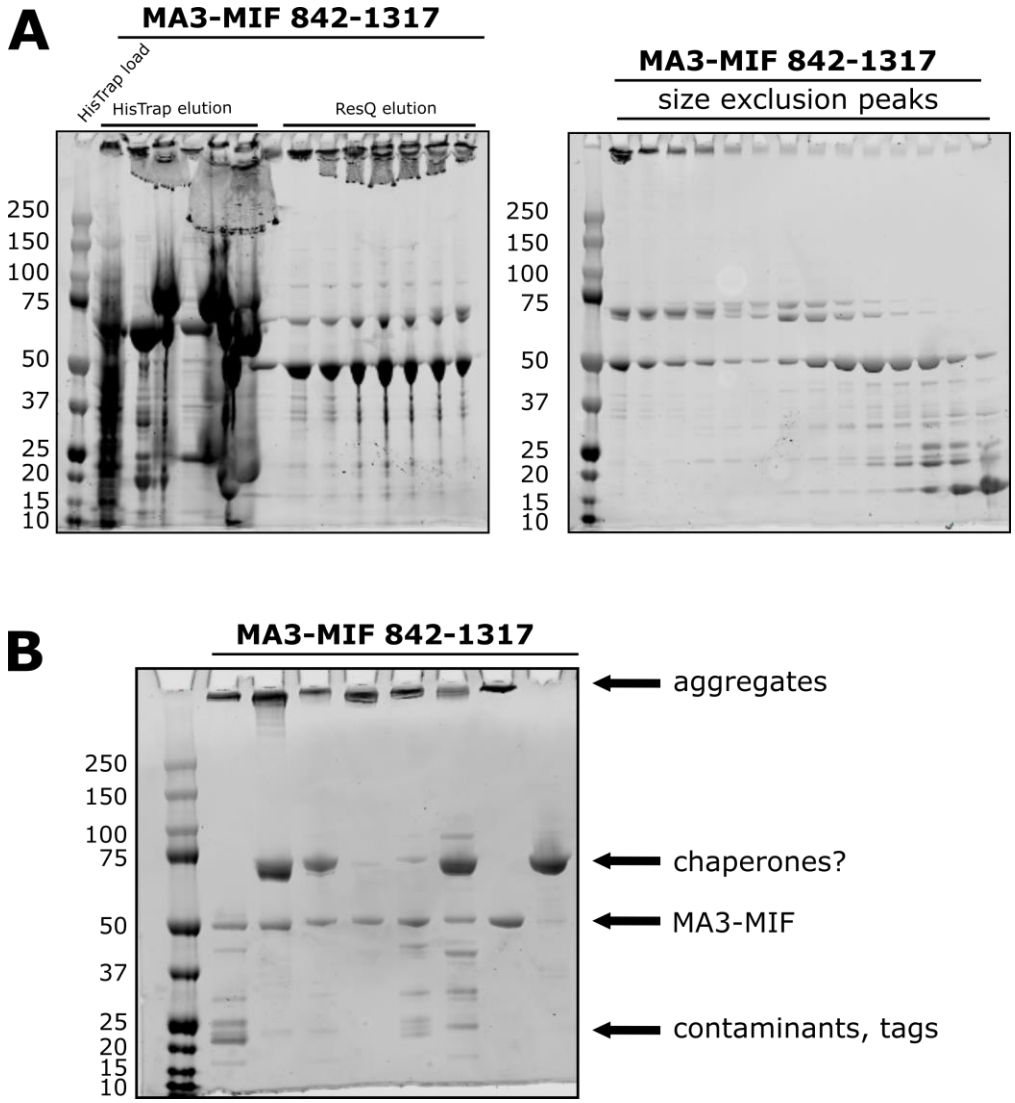

Appendix 2 Figure 2-1 Purification of MA3-MIF 842-1317 aa CNOT1 constructs

Protein marker sizes in kDa indicated on the left of the gel; aa – amino acid

- **A.** Coomassie stained gel from an example of purification. Here purification was performed with addition of CHAPS (Thermo Scientific 28299) in the lysis buffer (5 g per 200 mL of buffer). Protein of interest found throughout all peaks in the elution profile from size exclusion column (from 50 to 120 mL on Superdex S200 HiLoad 16/600), indicating either elution in complexes with other proteins (as visible on the gel) and/or the protein of interest was additionally misfolded. Samples show signs of aggregation, as well as presence of additional contaminants.
- **B.** Final products of purifications of individual batches of CNOT1 MA3-MIF 842-1317. All samples contain aggregates (except of the last one which does not contain the correct protein), some additionally contain chaperones (or possibly uncleaved material), and additional contaminants. Contaminants influenced activity of the purified proteins in ATPase assays (CNOT1 constructs alone should not have ATPase activity). None of the purified proteins were suitable for use in further experiments.

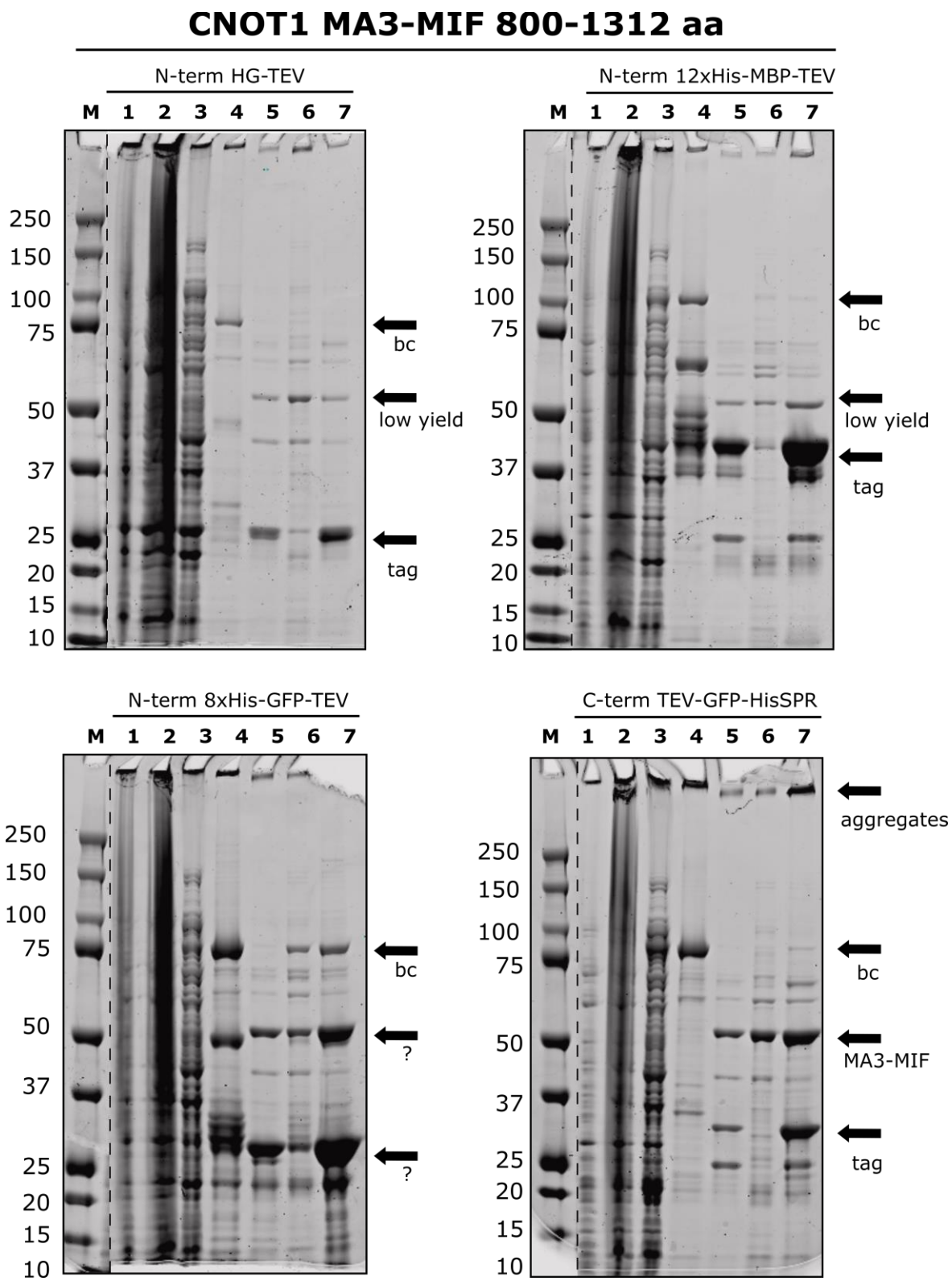

Appendix 2 Figure 2-2 Purification of MA3-MIF 800-1312 aa CNOT1 construct

Constructs cloned by Dr Lori Buetow with longer N-terminal limit and different tags (and their position) were assessed in test expression. Here, selected 4 constructs with different tags (tag and position indicated above each Coomassie stained gel; N-term – N-terminal tag, C-term – C-terminal tag) are shown. aa – amino acid. Unrelated lanes from each gel removed.

(figure legend continues on the next page)

The proteins were purified using agarose Ni^{2+} resin and numbers above each lane signify purification step: **1** – lysate (see **Chapter 2.2** for lysate preparation) that was applied on agarose resin, **2** – flow through from the agarose resin, **3** -wash from the resin (wash 1 out of 3 washes) (for buffer conditions see **Chapter 2.2.2**), **4** – elution from the resin (agarose resin split in two before elution), **5** – elution subjected to TEV cleavage to remove tags at 4°C over-night, **6** – TEV cleavage on the resin (the same condition as for cleavage of elution), **6** – elution after cleavage on the agarose resin. Arrows indicate proteins found in the lanes 4 to 7; bc – before cleavage or uncleaved product, low yield – correct protein but low yield in comparison to tag and contaminants, tag – the cleaved tag, MA3-MIF – the correct construct with acceptable yield, ? – unidentified contaminates (for example proteins that are of the size of cleaved final product but were already visible in lane 4 – before cleavage, signifying that this was not the final product). Other tests were performed, and the most promising construct C-term TEV-GFP-HisSPR (*bottom right corner*) was used for large scale purification however, final product that could be used in assays was not obtained. Finally, the longer construct used in this thesis was obtained as a gift from Dr Lori Buetow (see **Appendix 2 Figure 2-4** for Coomassie stained gel of the construct used in this thesis).

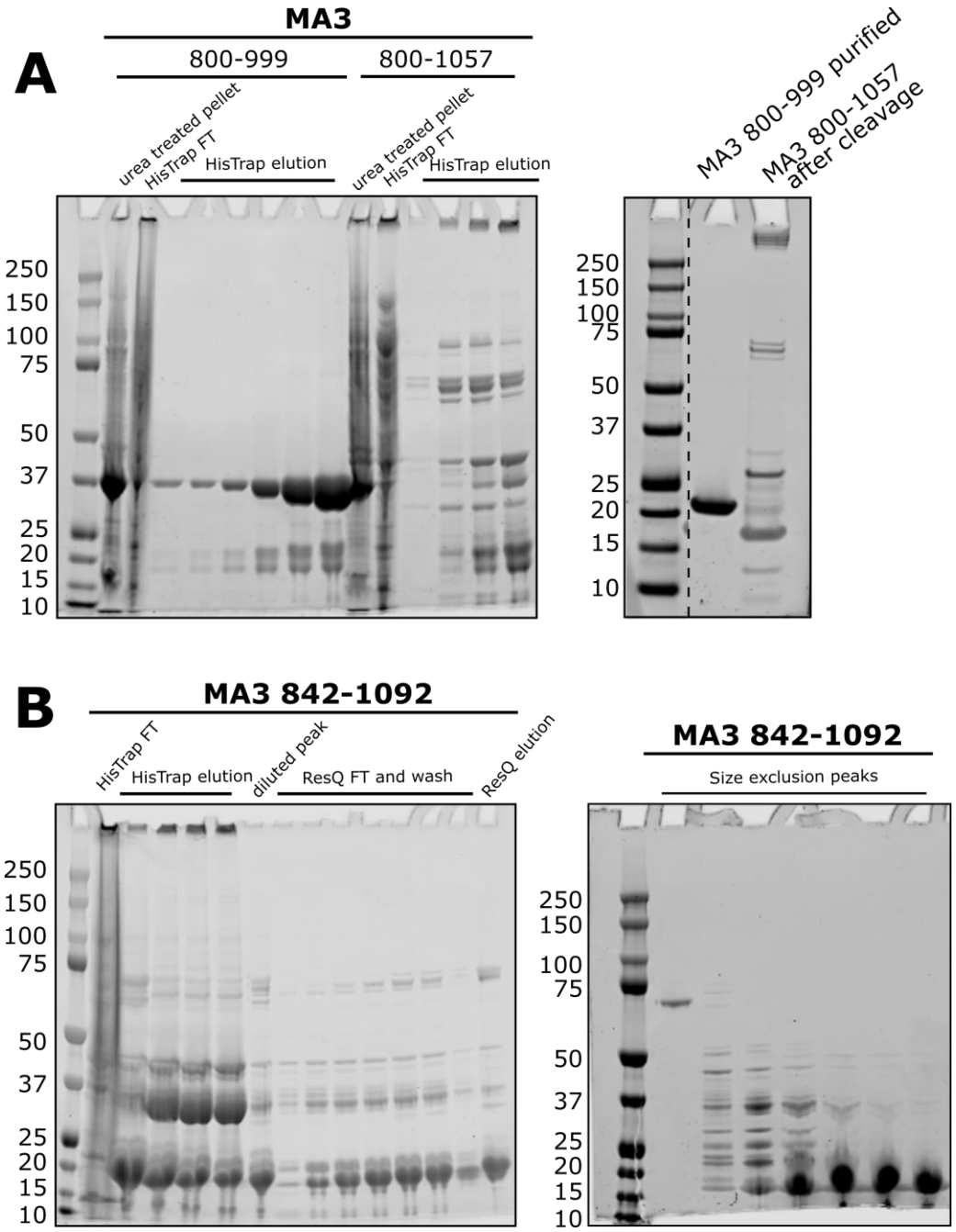

Appendix 2 Figure 2-3 Linker between MA3 and MIF domains of CNOT1 is responsible for aggregation issues

Protein marker sizes in kDa indicated on the left of the gel. FT – flow through, aa – amino acid, ResQ – ResourceQ anion exchange column.

A. Comparison of purification of MA3 construct 800-999 aa, without the linker between the two domains, and MA3 construct 800-1057. Longer construct showed signs of aggregation and multiple proteins eluted with it from HisTrap HP (gel on the *left*). Purified MA3 800-999 aa used as a comparison for MA3 800-1057, which cleavage was inefficient (additionally precipitation of protein was observed in the sample) (gel on the *right*).

B. Purification of MA3 construct 842-1092 aa, which also contains linker between the two domains. Protein showed signs of aggregation in first steps of purification (*left*). Cleavage was inefficient and multiple contaminants were observed (*right*).

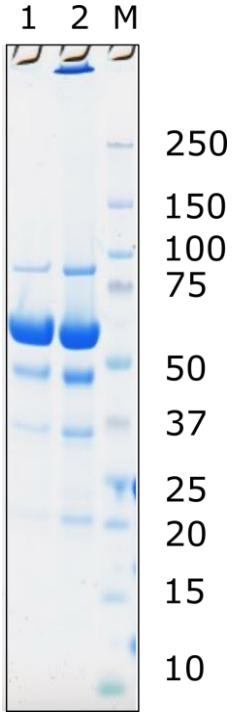

Appendix 2 Figure 2-4 CNOT1 MA3-MIF construct used in this thesis
Gel performed by Dr Lori Buetow; construct purified by Dr Lori Buetow. This CNOT1 construct was expressed with N-terminal His-SUMO-CL7-HRV3C tag and purified using Ni^{2+} agarose resin then a IM7 column with His-SUMO cleavage on the column, then cleavage of HRV3C tag by HRV3C protease and another run on IL7 column (flow through and wash were collected and concentrated), and final run on a size exclusion column. Lane 1 indicates protein eluted from the SEC column and used for subsequent studies (contaminations were present in the sample but no visible aggregation and ratio of proteins to contaminants is in favour of the protein), lane 2 indicates protein from lane 1 subjected to concentration. Concentration caused the CNOT1 construct to aggregate, which caused problems with the available concentration (as well as amount) of MA3-MIF construct for testing.

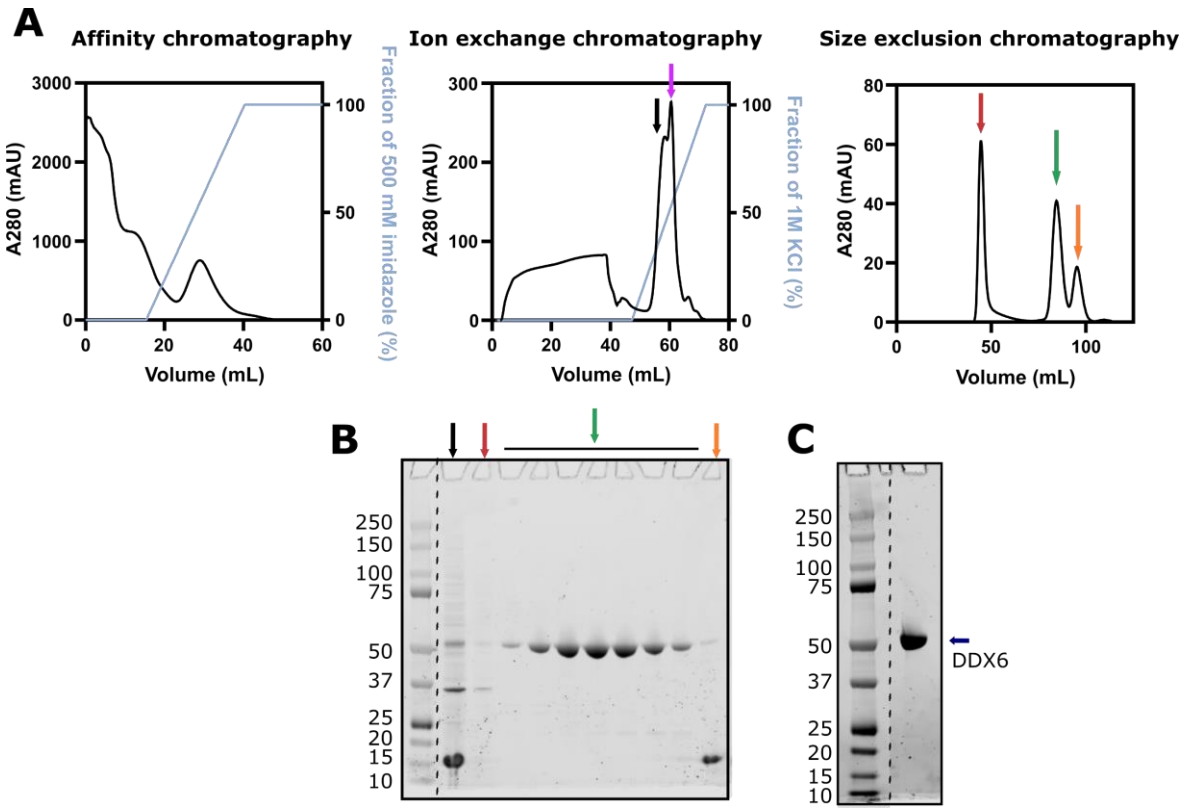

Appendix 2 Figure 2-5 Purification of DDX6

A. Elution profiles of DDX6 from affinity chromatography (HisTrap HP column, *left*), cation exchange chromatography (HiTrap Heparin column, *middle*), and size exclusion chromatography (Superdex S200 HiLoad 16/600, *right*). Arrows indicate peak samples run on an SDS-PAGE. Purple arrow in ion exchange chromatogram indicates a peak that was pooled and run on a size exclusion column (this was based on an elution profile and concentration of KCl at which DDX6 was previously purified in the Bushell lab).

B. Coomassie stained gel from purification of DDX6 (arrows correspond to the arrows in panel **A**). Protein marker sizes in kDa indicated on the left of the gel.

C. Purified DDX6 protein on a Coomassie stained gel. Protein marker sizes in kDa indicated on the left of the gel.

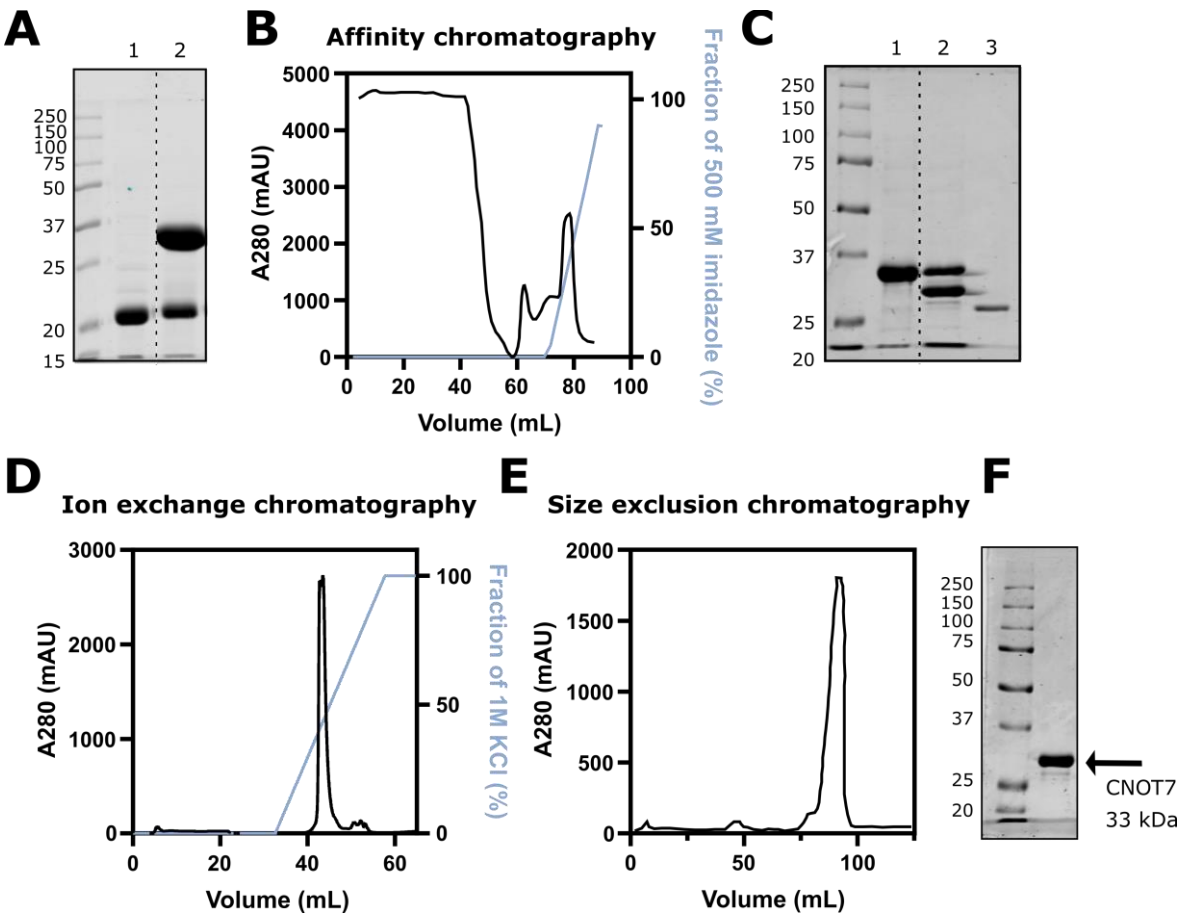

Appendix 2 Figure 2-6 Purification of CNOT7

Coomassie stained gels presented with protein marker on the left of each gel, sizes in kDa. Unrelated lanes removed. Chromatograms plotted using Plot Digitizer from a lab book photocopy.

- **A.** As the His-SUMO tag did not cleave of CNOT7 (lane 1 represents ULP1 protease, lane 2 represents His-SUMO-CNOT7 subjected to ULP1 cleavage), CNOT7 was purified with His-TEV tag.
- **B.** Affinity chromatography on HisTrap HP column of His-TEV-CNOT7. Tagged CNOT7 eluted in a linear imidazole gradient.
- **C.** Coomassie stained gel of His-TEV-CNOT7 cleavage using TEV protease. Lane 1 – tagged CNOT7 before cleavage, lane 2 – CNOT7 after overnight digestion, lane 3 – TEV protease.
- **D.** Ion exchange chromatography using ResourceQ column, of cleaved CNOT7. CNOT7 eluted in a linear KCl gradient.
- **E.** Size exclusion chromatography of cleaved CNOT7 on Superdex S200 HiLoad 16/600.
- **F.** Coomassie stained gel presenting purified CNOT7.

Appendix 3

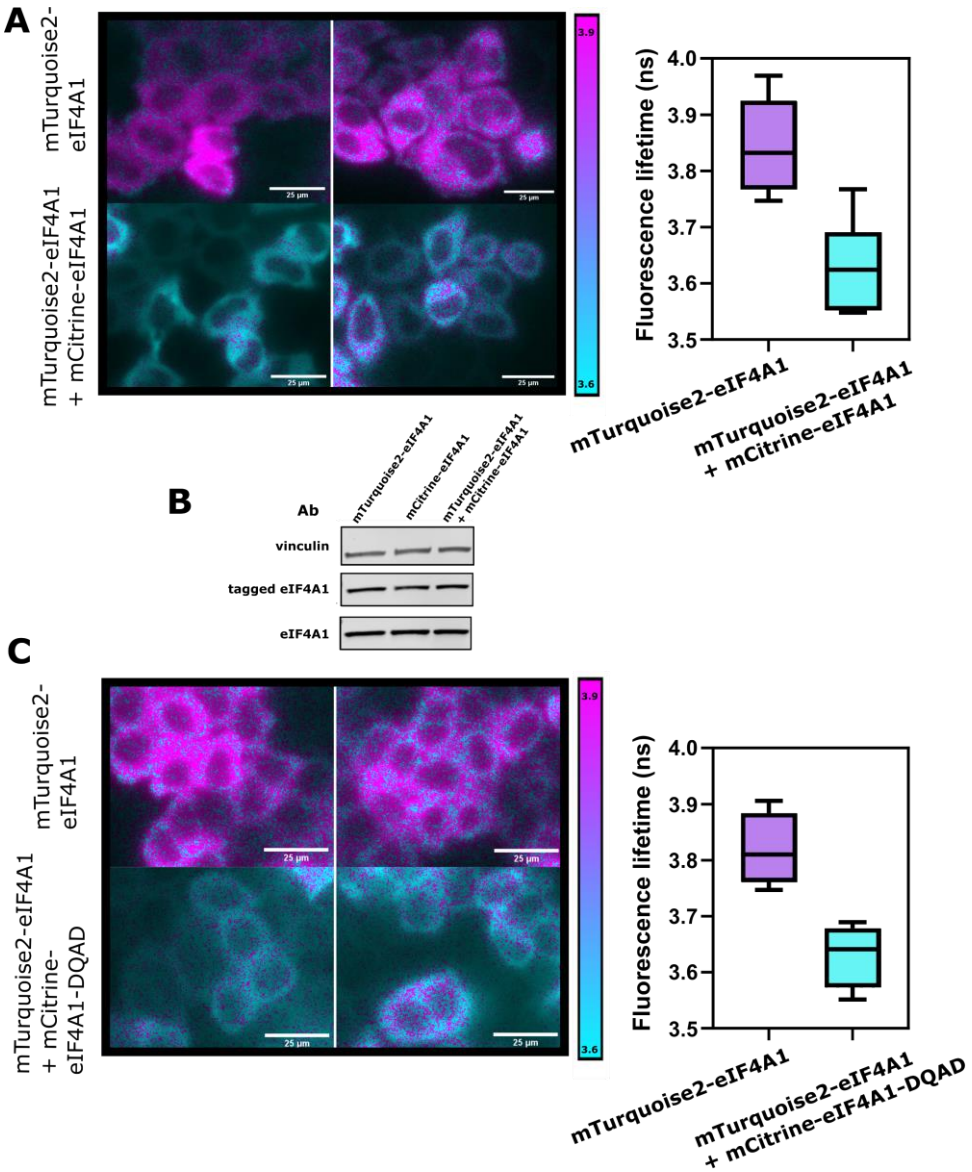

Appendix 3 Figure 3-1 eIF4A1 oligomerises in live cells through protein-protein interaction

A. Fluorophore tagged eIF4A1 oligomerises in live cells. On the left side of the panel, representative images from two independent paired (*top* and *bottom*) experiments are shown with a scale bar of 25 µm (right bottom corner of each image). Images are presented in the magenta fluorescence lifetime scale from 3.9 to 3.6 ns; the change in the colour from magenta (*top*, donor-eIF4A1) to cyan (*bottom*, eIF4A1 with both donor and acceptor), corresponds to the decreased fluorescence lifetime of the donor in presence of acceptor. On the right side, averages of all fluorescence lifetimes from 9 individual experiments (2 technical duplicates each) are presented in a form of a box plot with a median (black bar). Total of 339 and 338 cells were measured for mTurqoise2-eIF4A1 and for co-transfection of mTurqoise2-eIF4A1 and mCitrine-eIF4A1, respectively. The p-value = $2.7 * 10^{-5}$ was calculated using T-test (two-tailed distribution, two-sample equal variance) and the results were assessed to be statistically significant. (figure legend continues on the next page)

B. Transfection efficiency was assessed by Western botting, anti-vinculin antibody was used as a loading control. Transfected tagged-eIF4A1 levels were consistent for each combination of fluorophore and of similar expression level to WT.

C. To understand whether eIF4A1-eIF4A1 interaction in cells happens through protein-protein interaction and knowing that the oligomerisation of eIF4A occurs only in presence of RNA, HeLa cells were either transfected with mTurqoise2-eIF4A1 or co-transfected with mTurqoise2-eIF4A1 and mCitrine-eIF4A1. Presentation of the data in panel **C** is the same as in panel **A**. For these conditions, 4 individual experiments (two technical duplicates per experiment) were performed, with the total of 171 and 129 cells measured for donor and both donor and acceptor, respectively. p-value was calculated in the same manner as in panel **A** and the collected data were statistically significant (p-value = 0.0051).

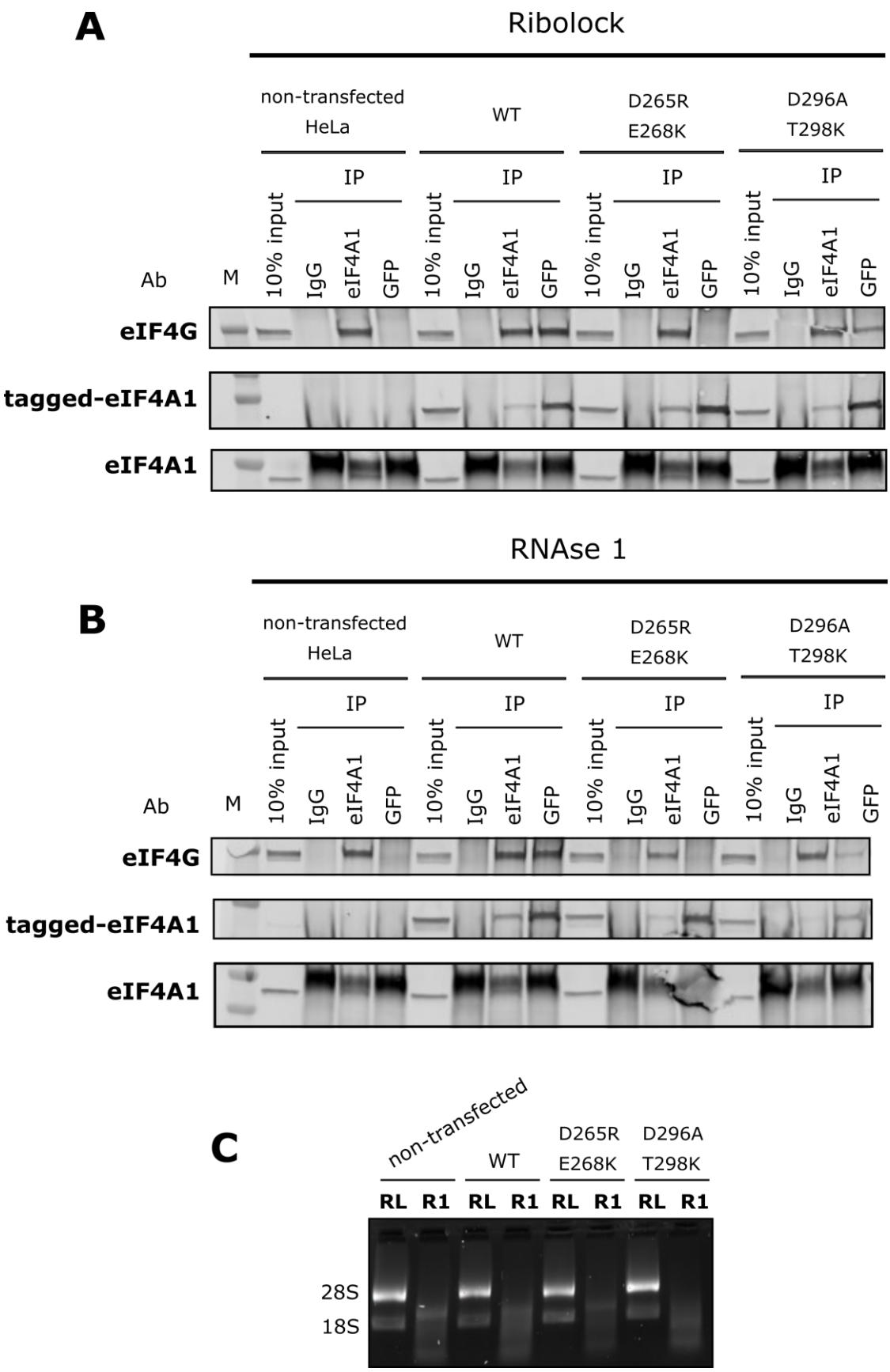

Appendix 3 Figure 3-2 Investigation of eIF4G-binding deficient mutants of eIF4A1

To test whether eIF4A1-eIF4A1 oligomerisation is mediated in cells by eIF4G, eIF4A1 mutants deficient in eIF4G binding were used for further studies.

(figure legend continues on the next page)

A. Immunoprecipitations (IP) with indicated antibodies of cell lysates from non-transfected HeLa cells, and HeLa cells transfected with donor and acceptor tagged WT eIF4A1, as well as the eIF4G-binding deficient mutants D265R E268K and D296A T298K (mutations responsible for loss of eIF4G binding identified in Oberer, Marintchev and Wagner, 2005). Cell lysis performed in presence of Ribolock to preserve RNA integrity. Co-precipitation of eIF4A1 and eIF4G1 in eIF4A1 IP lane and no precipitation in GFP IP was detected for non-transfected HeLa cells. For the tagged eIF4A1 WT transfection, eIF4G1 co-precipitated with eIF4A1 in both eIF4A1 and GFP IP lanes. For the eIF4A1 mutants, eIF4G1 co-precipitated with eIF4A1 in eIF4A1 IP lanes. No co-precipitation of eIF4G1 with eIF4A1 in GFP IP lane was observed for eIF4A1 D265R E268K, however eIF4G1 co-precipitated with eIF4A1 in GFP IP lane for. No unspecific precipitation was detected in the IgG IP lanes.

B. As eIF4G1 co-precipitation was detected in GFP IP lane for D296A T298K eIF4A1 mutant, it was tested whether this interaction can be RNA mediated. For this IPs were performed in the same way as in panel **A**, however instead of Ribolock, RNase 1 was used to digest RNA. The obtained result was the same for all the IP lanes as in panel **A**, except the D296A T298K eIF4A1 mutant GFP IP lane. Upon RNA digestion, lower co-precipitation of eIF4G1 in GFP IP lane was detected. However, the amount of precipitated tagged-eIF4A1 D296A T298K mutant was also lower in the RNase 1 condition. Therefore, eIF4A1 D296A T298K mutant possibly retained its ability to interact with eIF4G1.

C. RNA integrity test, for Ribolock (RL) and RNase 1 (R1) condition for the samples from panels **A** and **B**. All samples with RL had good quality of RNA, and RNA degradation was observed in R1 conditions.

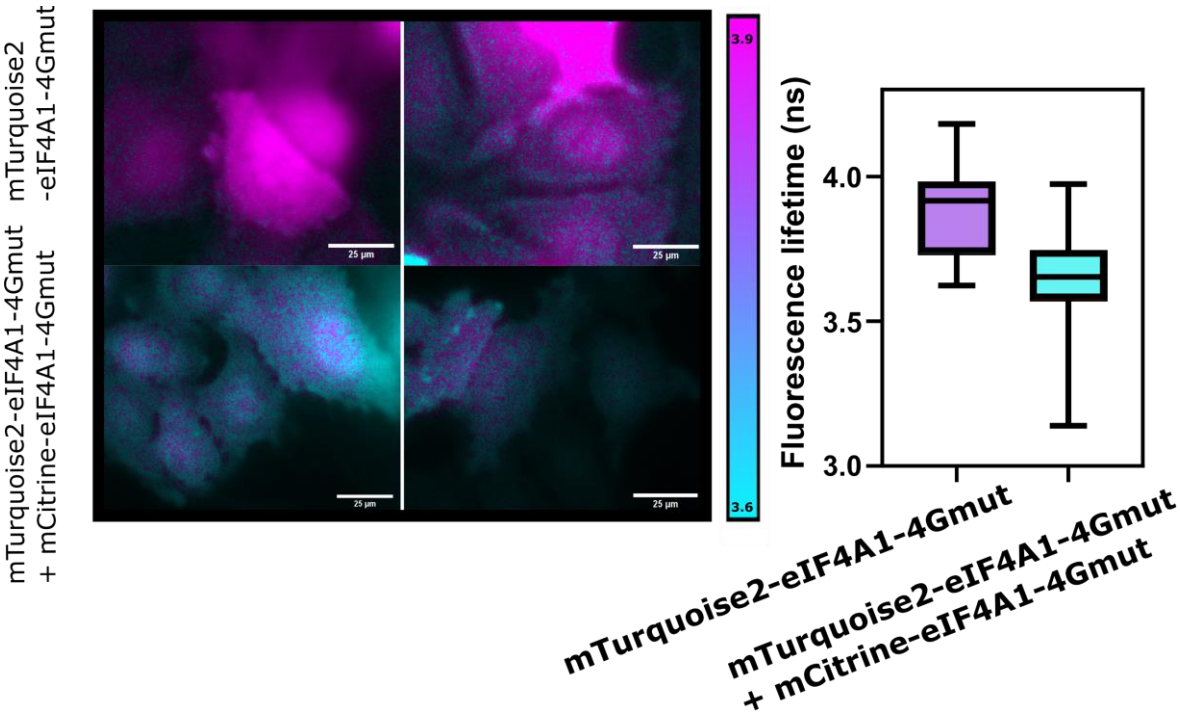

Appendix 3 Figure 3-3 eIF4A1 4G-mut oligomerises in live cells

As in **Figure Appendix** 3-2 for eIF4A1 D265R E268K mutant (from now on designated as eIF4A1 4G-mut) no co-precipitation of eIF4G1 was observed, this mutant was used to study whether eIF4A1 can interact in cells without the influence of eIF4G1. Here, HeLa cells were transfected as described in **Chapter 2.4.7**, with the fluorophore-tagged eIF4A1 4G-mut. On the left side of the panel, representative images from two independent paired (*top* and *bottom*) experiments are shown with a scale bar of 25 µm. As in **Appendix 3 Figure 3-1**, the images are presented in the magenta fluorescence lifetime scale from 3.9 to 3.6 ns. On the right side, all fluorescence lifetimes from 2 individual experiments (2 technical duplicates each) are presented in a form of a box plot with a median (black bar). Total of 38 and 59 cells were measured for the donor-eIF4A1 4G-mut, and for the co-transfection, respectively. The p-value = $2.3 * 10^{-11}$ was calculated using T-test (two-tailed distribution, two-sample equal variance) and the results were assessed to be statistically significant. It should be noted however, that the cellular localisation of eIF4A1 4G-mut was in contrast to known localisation of eIF4A1 WT (see nuclear both nuclear and cytoplasmic localisation of the mutant). Moreover, in case of co-transfection the change of fluorescence lifetime was mostly observed in the cytoplasm, this could mean that while in nucleus eIF4A1 does not perform the same function as in cytoplasm. This change of localisation and the large range of the measured fluorescence lifetimes could indicate that while the eIF4A1 4G-mut can oligomerise in cells its functions can be influenced by the mutation.

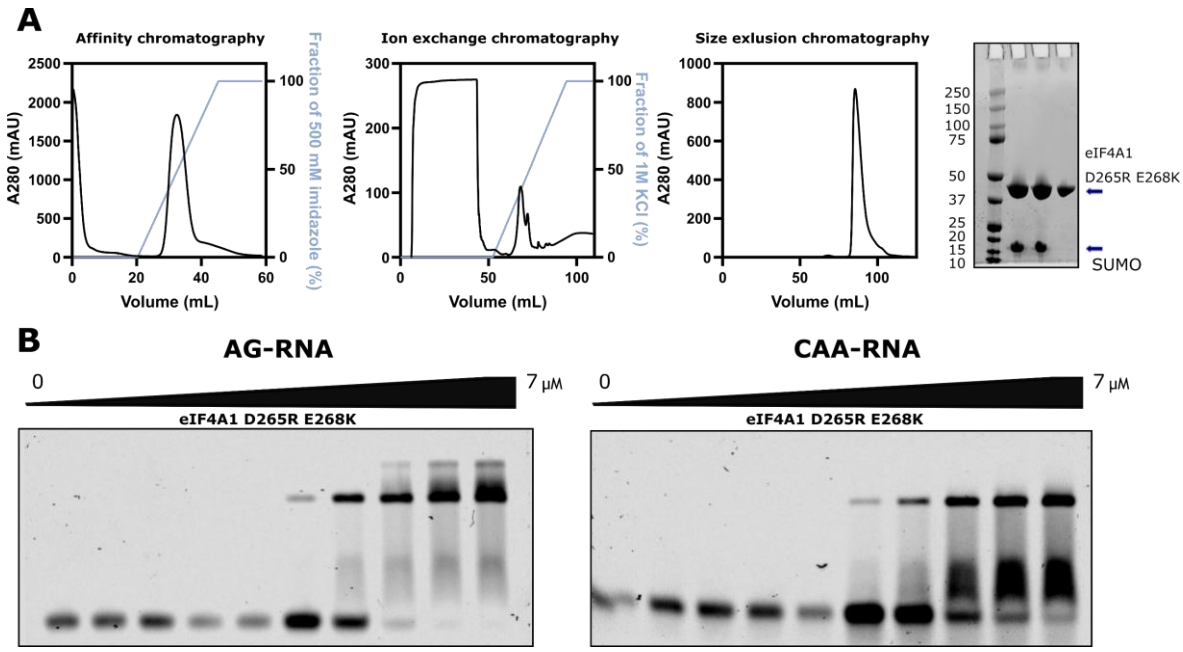

Appendix 3 Figure 3-4 eIF4A1 mutant deficient in eIF4G binding can form oligomeric complexes

As eIF4A1 4G-mut mutant localisation in cells was not restricted to the cytoplasm as is the case for WT eIF4A1, and the range of measured fluorescence lifetimes (**Appendix 3 Figure 3-3**) was larger, the eIF4A1 4G-mut oligomerisation potential was investigated *in vitro*.

A. Purification of eIF4A1 D265R E268K mutant (eIF4A1 4G-mut). Pre-cleared bacterial lysate was applied on HisTrap HP column (*left*), and the bound proteins were eluted in a linear imidazole gradient. Subsequently, the pooled fractions were subjected to His-SUMO tag cleavage by ULP1. Next, anion exchange chromatography was performed using ResourceQ column (*middle left*). eIF4A1 4G-mut did not bind to the column resin as WT, instead flow-through was collected and concentrated. Then, the concentrated sample was loaded onto Superdex S200 HiLoad 16/600 (*middle right*). The eluted sample contained cleaved His-SUMO tag, visible on Coomassie stained gel in 1st and 2nd lane on the right from the marker (*right*). The sample was run on the HisTrap HP column again (using peristaltic pump) and flow through was collected (most right lane in the gel on the *right*). Protein concentration was measured (see **Chapter 2.2**) and it was deemed to be of good quality to use in subsequent experiments. Protein marker kDa size indicated on the left of the gel.

B. Determination of eIF4A1 4G-mut RNA binding capacity and oligomerisation potential *in vitro*. EMSAs of eIF4A1 4G-mut titration on $(AG)_{10}$ RNA (*left*) and $(CAA)_6CA$ RNA (*right*). Oligomers of eIF4A1 4G-mut similarly to eIF4A1 WT were detected on $(AG)_{10}$ RNA and not on $(CAA)_6CA$ RNA. However, the calculated K_D (from gel image quantification, see **Chapter 2.3.1.1**) was higher (lower affinity) than the WT (eIF4A1 4G-mut $K_D(AG)_{10}$ = 1.13 and $K_D(CAA)_6CA$ 3.43).

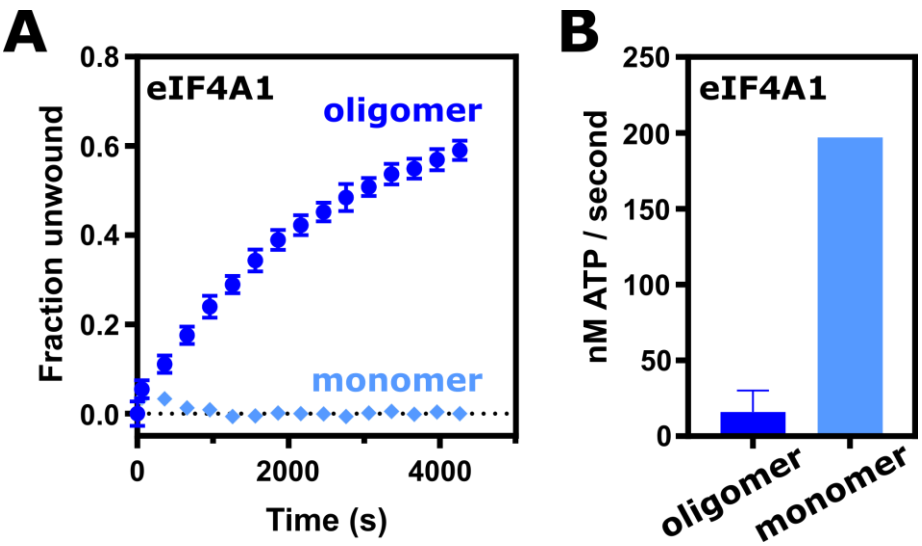

Appendix 3 Figure 3-5 Monomeric eIF4A1 does not exhibit unwinding activity

A. Unwinding activity of eIF4A1 in monomeric and oligomeric conditions presented as fraction unwound versus time. Monomeric eIF4A1 does not exhibit unwinding activity. Representative reactions (n = 3) for 2 μ eIF4A1 in presence of silvestrol on 5'$(AG)_{10}$ overhang RNA shown with standard deviation from technical duplicate. Monomeric conditions created by adding excess of unlabelled $(AG)_{10}$ RNA to the reaction.

B. ATPase activity of 5 μM eIF4A1 in oligomeric and monomeric conditions. Similarly, as is the case for eIF4A2 (**Figure 3.10-2**) monomeric eIF4A1 has greater ATPase activity than oligomer. High ATPase activity of monomer and lack of unwinding signifies that all eIF4A1 is active in the monomeric conditions, and lack of activity is specific only to unwinding.

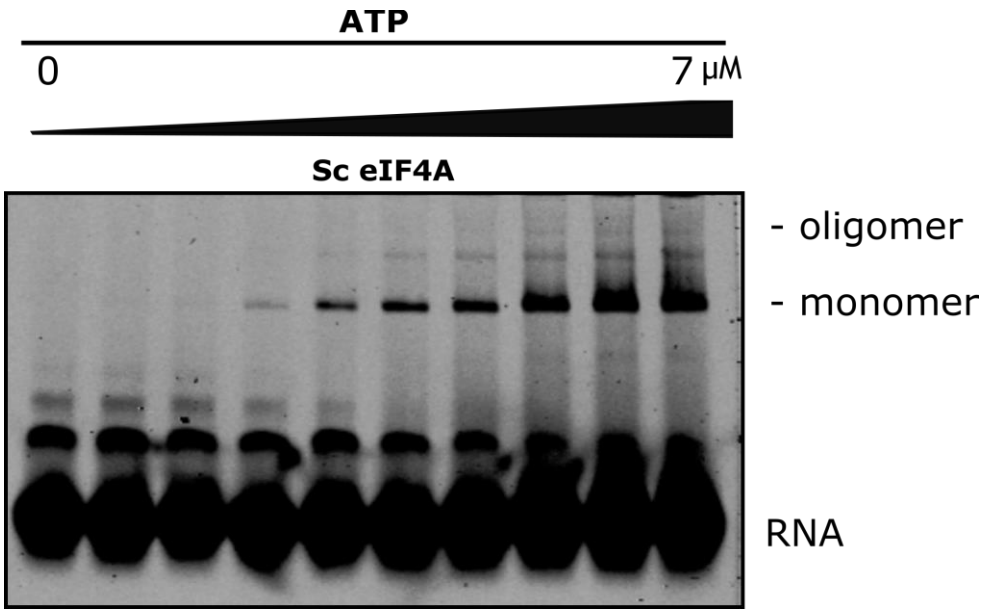

Appendix 3 Figure 3-6 *Sc* eIF4A can form oligomers

Increased contrast of the same EMSA image as in **Figure 5.4-3**, panel A *right*. *Sc* eIF4A binds RNA weaker than human eIF4A and its oligomerisation propensity is also lower, however the possibility to form oligomeric complexes is conserved.

Bibliography

Abdelhaleem, M. (2002) 'The novel helicase homologue DDX32 is down-regulated in acute lymphoblastic leukemia', *Leukemia Research*, 26, pp. 945–954. doi: 10.1016/s0145-2126(02)00040-1.

Abecasis, G. R. *et al.* (2012) 'An integrated map of genetic variation from 1,092 human genomes.', *Nature*, 491(7422), p. 56. doi: 10.1038/nature11632.An.

Abramson, R. D. *et al.* (1987) 'The ATP-dependent interaction of eukaryotic initiation factors with mRNA.', *Journal of Biological Chemistry*, 262(8), pp. 3826–3832.

Abramson, R. D., Dever, T. E. and Merrick, W. C. (1988) 'Biochemical evidence supporting a mechanism for cap-independent and internal initiation of eukaryotic mRNA', *Journal of Biological Chemistry*, 263(13), pp. 6016–6019. doi: 10.1016/s0021-9258(18)68741-1.

Acker, M. G. *et al.* (2009) 'Kinetic Analysis of Late Steps of Eukaryotic Translation Initiation', *Journal of Molecular Biology*. Elsevier Ltd, 385(2), pp. 491–506. doi: 10.1016/j.jmb.2008.10.029.

Aitken, C. E. and Lorsch, J. R. (2012) 'A mechanistic overview of translation initiation in eukaryotes', *Nature Structural & Molecular Biology*. Nature Publishing Group, 19(6). doi: 10.1038/nsmb.2303.

Alard, A. *et al.* (2019) 'Differential regulation of the three eukaryotic mRNA translation initiation factor (eIF) 4Gs by the proteasome', *Frontiers in Genetics*, 10(MAR), pp. 1–9. doi: 10.3389/fgene.2019.00254.

Albrecht, A. C. (1961) 'Polarizations and assignments of transitions: The method of photoselection', *Journal of Molecular Spectroscopy*, 6(C), pp. 84–108. doi: 10.1016/0022-2852(61)90234-X.

Alekhina, O. M. *et al.* (2020) 'Functional Cyclization of Eukaryotic mRNAs', *International Journal of Molecular Sciences Article*. doi: 10.3390/ijms21051677.

Algire, M. A., Maag, D. and Lorsch, J. R. (2005) 'Pi Release from eIF2 , Not GTP Hydrolysis , Is the Step Controlled by Start-Site Selection during Eukaryotic Translation Initiation', *Molecular Cell*, 20, pp. 251–262. doi:

10.1016/j.molcel.2005.09.008.

Alkalaeva, E. Z. *et al.* (2006) 'In Vitro Reconstitution of Eukaryotic Translation Reveals Cooperativity between Release Factors eRF1 and eRF3', *Cell*, 125(6), pp. 1125–1136. doi: 10.1016/j.cell.2006.04.035.

Alles, J. *et al.* (2019) 'An estimate of the total number of true human miRNAs', *Nucleic Acids Research*, 47(7), pp. 3353–3364. doi: 10.1093/nar/gkz097.

Anantharaman, V., Koonin, E. V and Aravind, L. (2002) 'Comparative genomics and evolution of proteins involved in RNA metabolism', *Nucleic Acids Research*, 30(7), pp. 1427–1464.

Andrei, M. A. *et al.* (2005) 'A role for eIF4E and eIF4E-transporter in targeting mRNPs to mammalian processing bodies', *RNA*, 11, pp. 717–727. doi: 10.1261/rna.2340405.5.

Andreou, A. Z., Harms, U. and Klostermeier, D. (2019) 'Single-stranded regions modulate conformational dynamics and ATPase activity of eIF4A to optimize 5′-UTR unwinding', *Nucleic Acids Research*. Oxford University Press, 47(10), pp. 5260–5275. doi: 10.1093/nar/gkz254.

Andreou, A. Z. and Klostermeier, D. (2012) *Conformational changes of DEAD-Box helicases monitored by single molecule fluorescence resonance energy transfer*. 1st edn, *Methods in Enzymology*. 1st edn. Elsevier Inc. doi: 10.1016/B978-0-12-396546-2.00004-8.

Andreou, A. Z and Klostermeier, D. (2013) 'The DEAD-box helicase eIF4A: Paradigm or the odd one out?', *RNA Biology*, 10(1), pp. 19–32. doi: 10.4161/rna.21966.

Andreou, A. Z. and Klostermeier, D. (2014) 'EIF4B and eIF4G jointly stimulate eIF4A ATPase and unwinding activities by modulation of the eIF4A conformational cycle', *Journal of Molecular Biology*. doi: 10.1016/j.jmb.2013.09.027.

Artieri, C. G. and Fraser, H. B. (2014) 'Accounting for biases in riboprofiling data indicates a major role for proline in stalling translation', *Genome Research*, 24, pp. 2011–2021. doi: 10.1101/gr.175893.114.

Asano, K. *et al.* (2000) 'A multifactor complex of eukaryotic and initiator tRNA

Met is an important translation initiation intermediate in vivo', *Genes and Development*, 14, pp. 2534–2546. doi: 10.1101/gad.831800.in.

Aviv, H. *et al.* (1976) 'Biosynthesis and stability of globin mRNA in cultured erythroleukemic friend cells', *Cell*, 8(4), pp. 495–503. doi: 10.1016/0092-8674(76)90217-8.

Avni, D., Biberman, Y. and Meyuhas, O. (1997) 'The 5′ Terminal Oligopyrimidine Tract Confers Translational Control on Top Mrnas in a Cell Type-and Sequence Context-Dependent Manner', *Nucleic Acids Research*, 25(5), pp. 995–1001. doi: 10.1093/nar/25.5.995.

Bajar, B. T. *et al.* (2016) 'A guide to fluorescent protein FRET pairs', *Sensors (Switzerland)*, 16(9), pp. 1–24. doi: 10.3390/s16091488.

Balbo, P. . and Bohm, A. (2007) 'Mechanism of Poly(A) Polymerase: Structure of the enzyme- MgATP–RNA ternary complex and kinetic analysis', *Structure.*, 15(9), pp. 1117–1131.

Baltz, A. G. *et al.* (2012) 'The mRNA-Bound Proteome and Its Global Occupancy Profile on Protein-Coding Transcripts', *Molecular Cell*. doi: 10.1016/j.molcel.2012.05.021.

Banroques, J. *et al.* (2011) 'Analyses of the functional regions of DEAD-box RNA "helicases" with deletion and chimera constructs tested in vivo and in vitro', *Journal of Molecular Biology*. Elsevier Ltd, 413(2), pp. 451–472. doi: 10.1016/j.jmb.2011.08.032.

Barault, L. *et al.* (2008) 'Mutations in the RAS-MAPK, PI(3)K (phosphatidylinositol-3-OH kinase) signaling network correlate with poor survival in a population-based series of colon cancers.', *International journal of cancer*. United States, 122(10), pp. 2255–2259. doi: 10.1002/ijc.23388.

Barrell, B. G., Bankier, A. T. and Drouin, J. (1979) 'A different genetic code in human mitochondria', *Nature*, 282(November), pp. 189–194.

Bartlam, M. and Yamamoto, T. (2010) 'The structural basis for deadenylation by the CCR4-NOT complex', *Protein & Cell*, 1(5), pp. 443–452. doi: 10.1007/s13238-010-0060-8.

Bastiaens, P. I. H. and Squire, A. (1999) ‘Fluorescence lifetime imaging microscopy: Spatial resolution of biochemical processes in the cell’, *Trends in Cell Biology*, 9(2), pp. 48–52. doi: 10.1016/S0962-8924(98)01410-X.

Bazzini, A. A. *et al.* (2014) ‘Identification of small ORFs in vertebrates using ribosome footprinting and evolutionary conservation’, *The EMBO journal*, 33(9), pp. 981–993.

Behrens, A., Rodschinka, G. and Nedialkova, D. D. (2021) ‘High-resolution quantitative profiling of tRNA abundance and modification status in eukaryotes by mim-tRNAseq’, *Molecular Cell*. Elsevier, 81(8), pp. 1802-1815.e7. doi: 10.1016/j.molcel.2021.01.028.

Behrens, M. A. *et al.* (2012) *Structural analysis of RNA helicases with small-angle X-ray scattering*. 1st edn, *Methods in Enzymology*. 1st edn. Elsevier Inc. doi: 10.1016/B978-0-12-396546-2.00031-0.

Bekker-Jensen, D. *et al.* (2017) ‘An Optimized Shotgun Strategy for the Rapid Generation of Comprehensive Human Proteomes’, *Cell Systems*. Elsevier Inc., 4(6), pp. 587-599.e4. doi: 10.1016/j.cels.2017.05.009.

Benne, R. and Hershey, J. W. (1978) ‘The mechanism of action of protein synthesis initiation factors from rabbit reticulocytes.’, *The Journal of biological chemistry*. United States, 253(9), pp. 3078–3087.

Berget, S. M., Moore, C. and Sharp, P. A. (1977) ‘Spliced segments at the 5 ’ terminus of adenovirus 2 late mRNA’, *Proc. Natl. Acad. Sci.*, 74(8), pp. 3171–3175.

Berset, C. *et al.* (2003) ‘RNA-binding activity of translation initiation factor eIF4G1 from Saccharomyces cerevisiae’, *RNA*, 9, pp. 871–880. doi: 10.1261/rna.5380903.lysis.

Bertolin, G. *et al.* (2019) ‘Optimized FRET Pairs and Quantification Approaches to Detect the Activation of Aurora Kinase A at Mitosis’, *ACS Sensors*, 4(8), pp. 2018–2027. doi: 10.1021/acssensors.9b00486.

Bhat, M. *et al.* (2015) ‘Targeting the translation machinery in cancer’, *Nature Rev. Drug Discov.* doi: 10.1038/nrd4505.

Bhattacharyya, S. N. *et al.* (2006) 'Relief of microRNA-Mediated Translational Repression in Human Cells Subjected to Stress', *Cell*, 125, pp. 1111–1124. doi: 10.1016/j.cell.2006.04.031.

Biberman, Y. and Meyuhas, O. (1999) 'TOP mRNAs are translationally inhibited by a titratable repressor in both wheat germ extract and reticulocyte lysate.', *FEBS letters*. England, 456(3), pp. 357–360. doi: 10.1016/s0014-5793(99)00983-7.

Biedenkopf, N. *et al.* (2017) 'The natural compound silvestrol is a potent inhibitor of Ebola virus replication', *Antiviral Research*. Elsevier B.V, 137, pp. 76–81. doi: 10.1016/j.antiviral.2016.11.011.

Bienroth, S., Keller, W. and Wahle, E. (1993) 'Assembly of a processive messenger RNA polyadenylation complex', *EMBO Journal*, 12(2), pp. 585–594. doi: 10.1002/j.1460-2075.1993.tb05690.x.

Bioisis: Tutorial. n.d. *Bioisis: Tutorial*. https://www.bioisis.net/tutorials

Bohlen, J. *et al.* (2020) 'Selective 40S Footprinting Reveals Cap-Tethered Ribosome Scanning in Human Cells ll ll Article Selective 40S Footprinting Reveals Cap-Tethered Ribosome Scanning in Human Cells', *Molecular Cell*, 79, pp. 561–574. doi: 10.1016/j.molcel.2020.06.005.

Bol, G. M. *et al.* (2015) 'Targeting DDX3 with a small molecule inhibitor for lung cancer therapy.', *EMBO molecular medicine*, 7(5), pp. 648–669. doi: 10.15252/emmm.201404368.

Bordeleau, M.-E. *et al.* (2008) 'Therapeutic suppression of translation initiation modulates chemosensitivity in a mouse lymphoma model', *The Journal of Clinical Investigation*, 118(7), pp. 2651–2660. doi: 10.1172/JCI34753.4E-BPs.

Bordeleau, M. *et al.* (2005) 'Stimulation of mammalian translation initiation factor eIF4A activity by a small molecule inhibitor of eukaryotic translation.', *PNAS*, 102, pp. 10460–10465. doi: 10.1073/pnas.0504249102.

Bordeleau, M. *et al.* (2006) 'Functional characterization of IRESes by an inhibitor of the RNA helicase eIF4A', *Nature Chemical Biology*, 2(4), pp. 213–220. doi: 10.1038/nchembio776.

Bordeleau, M. E. *et al.* (2006) 'RNA-Mediated Sequestration of the RNA Helicase eIF4A by Pateamine A Inhibits Translation Initiation', *Chemistry and Biology*,

13(12), pp. 1287–1295. doi: 10.1016/j.chembiol.2006.10.005.

Bostrom, K. *et al.* (1986) 'Pulse-chase studies of the synthesis and intracellular transport of apolipoprotein B-100 in Hep G2 cells', *Journal of Biological Chemistry*, 261(29), pp. 13800–13806. doi: 10.1016/s0021-9258(18)67090-5.

Botlagunta, M. *et al.* (2008) 'Oncogenic role of DDX3 in breast cancer biogenesis.', *Oncogene*, 27(28), pp. 3912–3922. doi: 10.1038/onc.2008.33.

Bourgeois, C. F., Mortreux, F. and Auboeuf, D. (2016) 'The multiple functions of RNA helicases as drivers and regulators of gene expression', *Nature Reviews Molecular Cell Biology*. doi: 10.1038/nrm.2016.50.

Bousquet-Antonelli, C., Presutti, C. and Tollervey, D. (2000) 'Identification of a regulated pathway for nuclear pre-mRNA turnover', *Cell*, 102(6), pp. 765–775. doi: 10.1016/S0092-8674(00)00065-9.

Braun, J. E. *et al.* (2011) 'GW182 proteins directly recruit cytoplasmic deadenylase complexes to miRNA targets.', *Molecular cell*. United States, 44(1), pp. 120–133. doi: 10.1016/j.molcel.2011.09.007.

Brengues, M., Teixeira, D. and Parker, R. (2005) 'Movement of Eukaryotic mRNAs Between Polysomes and Cytoplasmic Processing Bodies', *Science*, 310(5747), pp. 486–489.

Brosey, C. A. and Tainer, J. A. (2019) 'Evolving SAXS versatility: solution X-ray scattering for macromolecular architecture, functional landscapes, and integrative structural biology', *Current Opinion in Structural Biology*. Elsevier Ltd, 58, pp. 197–213. doi: 10.1016/j.sbi.2019.04.004.

Bushell, M. *et al.* (2001) 'Disruption of the Interaction of Mammalian Protein Synthesis Eukaryotic Initiation Factor 4B with the Poly (A) -binding Protein by Caspase- and Viral Protease-mediated Cleavages', *Journal of Biological Chemistry..*, 276(26), pp. 23922–23928. doi: 10.1074/jbc.M100384200.

Bushell, M. and Sarnow, P. (2002) 'Hijacking the translation apparatus by RNA viruses', *Journal of Cell Biology*, 158(3), pp. 395–399. doi: 10.1083/jcb.200205044.

Cai, W. *et al.* (2017) 'Wanted DEAD / H or Alive : Helicases Winding Up in Cancers', *JNCI J Natl Cancer Inst*, 109(6), pp. 1–15. doi: 10.1093/jnci/djw278.

Calviello, L. *et al.* (2021) 'DDX3 depletion represses translation of mRNAs with complex 5' UTRs', *Nucleic Acids Research*. Oxford University Press, 49(9), pp. 5336–5350. doi: 10.1093/nar/gkab287.

Calvo, S. E., Pagliarini, D. J. and Mootha, V. K. (2009) 'Upstream open reading frames cause widespread reduction of protein expression and are', *PNAS*, 106(18), pp. 7507–7512.

Caruthers, J. M., Johnson, E. R. and McKay, D. B. (2000) 'Crystal structure of yeast initiation factor 4A, a DEAD-box RNA helicase', *Proceedings of the National Academy of Sciences*, 97(24), pp. 13080–13085. doi: 10.1073/pnas.97.24.13080.

Causevic, M. *et al.* (2001) 'Overexpression and poly-ubiquitylation of the DEAD-box RNA helicase p68 in colorectal tumours.', *Oncogene*. England, 20(53), pp. 7734–7743. doi: 10.1038/sj.onc.1204976.

Cencica, R. and Pelletier, J. (2016) 'Hippuristanol - A potent steroid inhibitor of eukaryotic initiation factor 4A', *Translation*. Taylor & Francis, 4(1), pp. 1–14. doi: 10.1080/21690731.2015.1137381.

Chan, C.-H. *et al.* (2019) 'DNA Damage, Liver Injury, and Tumorigenesis: Consequences of DDX3X Loss.', *Molecular cancer research : MCR*. United States, 17(2), pp. 555–566. doi: 10.1158/1541-7786.MCR-18-0551.

Chan, C. C. *et al.* (2004) 'eIF4A3 is a novel component of the exon junction complex', *Rna*, 10(2), pp. 200–209. doi: 10.1261/rna.5230104.

Chan, K. *et al.* (2019) 'eIF4A supports an oncogenic translation program in pancreatic ductal adenocarcinoma', *Nature Communications*. Springer US, 10(1), pp. 1–16. doi: 10.1038/s41467-019-13086-5.

Chang, J. H. *et al.* (2009) 'Crystal structure of the eIF4A-PDCD4 complex', *Proceedings of the National Academy of Sciences*, 106(9), pp. 3148–3153. doi: 10.1073/pnas.0808275106.

Chekulaeva, M. *et al.* (2011) 'miRNA repression involves GW182-mediated recruitment of CCR4-NOT through conserved W-containing motifs.', *Nature structural & molecular biology*, 18(11), pp. 1218–1226. doi: 10.1038/nsmb.2166.

Chen, J. *et al.* (2012) 'Unraveling the Dynamics of Ribosome Translocation', *Curr Opin Struct Biol*. doi: 10.1016/j.sbi.2012.09.004..

Chen, J. *et al.* (2020) 'Pervasive functional translation of non-canonical human open reading frames', *Science*, 367(6482), pp. 1140–1146. doi: 10.1126/science.aay0262.

Chen, R. H., Chen, Y. H. and Huang, T. Y. (2019) 'Ubiquitin-mediated regulation of autophagy', *Journal of Biomedical Science*. Journal of Biomedical Science, 26(1), pp. 1–12. doi: 10.1186/s12929-019-0569-y.

Chen, W. L. *et al.* (2016) 'Silvestrol induces early autophagy and apoptosis in human melanoma cells', *BMC Cancer*. BMC Cancer, 16(1), pp. 1–10. doi: 10.1186/s12885-015-1988-0.

Chen, W., Smeekens, J. M. and Wu, R. (2016) 'Systematic study of the dynamics and half-lives of newly synthesized proteins in human cells', *Chemical Science*. Royal Society of Chemistry, 7(2), pp. 1393–1400. doi: 10.1039/c5sc03826j.

Chen, Y. *et al.* (2003) 'Loss of PDCD4 expression in human lung cancer correlates with tumour progression and prognosis', *Journal of Pathology*, 200(March), pp. 640–646. doi: 10.1002/path.1378.

Chen, Y. *et al.* (2014) 'A DDX6-CNOT1 Complex and W-Binding Pockets in CNOT9 Reveal Direct Links between miRNA Target Recognition and Silencing', *Molecular Cell*, 54(5), pp. 737–750. doi: 10.1016/j.molcel.2014.03.034.

Chen, Z. *et al.* (2019) 'Eukaryotic initiation factor 4A2 promotes experimental metastasis and oxaliplatin resistance in colorectal cancer', *Journal of Experimental & Clinical Cancer Research*,38(196), pp. 1-18, doi: 10.1186/s13046-019-1178-z

Cho, B. *et al.* (2003) 'Promoter hypomethylation of a novel cancer/testis antigen gene CAGE is correlated with its aberrant expression and is seen in premalignant stage of gastric carcinoma', *Biochemical and Biophysical Research Communications 307*, 307, pp. 52–63. doi: 10.1016/S0006-291X(03)01121-5.

Cho, E. J. *et al.* (1997) 'mRNA capping enzyme is recruited to the transcription complex by phosphorylation of the RNA polymerase II carboxy-terminal domain', *Genes and Development*, 11(24), pp. 3319–3326. doi: 10.1101/gad.11.24.3319.

Cho, W. C. S. (2007) ‘OncomiRs: The discovery and progress of microRNAs in cancers’, *Molecular Cancer*, 6, pp. 1–7. doi: 10.1186/1476-4598-6-60.

Chu, J. *et al.* (2019) ‘Amidino-Rocaglates: A Potent Class of eIF4A Inhibitors’, *Cell Chemical Biology*. Elsevier Ltd., pp. 1–8. doi: 10.1016/j.chembiol.2019.08.008.

Ciechanover, A. *et al.* (1980) ‘ATP-dependent conjugation of reticulocyte proteins with the polypeptide required for protein degradation.’, *Proceedings of the National Academy of Sciences of the United States of America*, 77(3), pp. 1365–1368. doi: 10.1073/pnas.77.3.1365.

Copeland, P. R. (2003) ‘Regulation of gene expression by stop codon recoding: selenocysteine’, *Gene.*, 23(1), pp. 1–7.

Corbalenya, E. and Koonin, E. V (2007) ‘Helicases : amino acid sequence comparisons relationships and of Medical’, *Annu. Rev. Biochem*.

Cougot, N., Babajko, S. and Séraphin, B. (2004) ‘Cytoplasmic foci are sites of mRNA decay in human cells’, *JBC*, 165(1), pp. 31–40. doi: 10.1083/jcb.200309008.

Crick, F. (1970) ‘Central Dogma of Molecular Biology’, *Nature*. doi: 10.1007/978-1-4020-6754-9_2672.

Cunningham, T. A., Chapman, E. and Schatz, J. H. (2018) ‘EIF4A inhibition: Ready for primetime?’, *Oncotarget*, 9(85), pp. 35515–35516. doi: 10.18632/oncotarget.26268.

Debdyuti, M. and Howard, R. (2007) ‘Proteasome-Independent Functions of Ubiquitin in Endocytosis and Signaling’, *Science*. American Association for the Advancement of Science, 315(5809), pp. 201–205. doi: 10.1126/science.1127085.

Dennis, M. D., Jefferson, L. S. and Kimball, S. R. (2012) ‘Role of p70S6K1-mediated Phosphorylation of eIF4B and PDCD4 Proteins in the Regulation of Protein Synthesis *’, *Journal of Biological Chemistry*. Â© 2012 ASBMB. Currently published by Elsevier Inc; originally published by American Society for

Biochemistry and Molecular Biology., 287(51), pp. 42890–42899. doi: 10.1074/jbc.M112.404822.

Dever, T. E. and Green, R. (2012) 'Phases of Translation in Eukaryotes', *Cold Spring Harbor Perspectives in Biology Perspect Biology*, 4, pp. 1–16.

Didiano, D. and Hobert, O. (2006) 'Perfect seed pairing is not a generally reliable predictor for miRNA-target interactions', *Nature Structural and Molecular Biology*, 13(9), pp. 849–851. doi: 10.1038/nsmb1138.

Djuranovic, S., Nahvi, A. and Green, R. (2012) 'miRNA-mediated gene silencing by translational repression followed by mRNA deadenylation and decay.', *Science (New York, N.Y.)*, 336(6078), pp. 237–240. doi: 10.1126/science.1215691.

Dominissini, D. *et al.* (2012) 'Topology of the human and mouse m6A RNA methylomes revealed by m6A-seq', *Nature*. Nature Publishing Group, 485(7397), pp. 201–206. doi: 10.1038/nature11112.

Dorrello, N. V. *et al.* (2006) 'S6K1- and betaTRCP-mediated degradation of PDCD4 promotes protein translation and cell growth.', *Science (New York, N.Y.)*. United States, 314(5798), pp. 467–471. doi: 10.1126/science.1130276.

Dreyfuss, G., Kim, V. N. and Kataoka, N. (2002) 'Messenger-RNA-binding proteins and the messages they carry', *Nature Reviews Molecular Cell Biology*, 3(3), pp. 195–205. doi: 10.1038/nrm760.

Duncan, R. and Hershey, J. W. (1983) 'Identification and quantitation of levels of protein synthesis initiation factors in crude HeLa cell lysates by two-dimensional polyacrylamide gel electrophoresis.', *Journal of Biological Chemistry*. © 1983 ASBMB.., 258(11), pp. 7228–7235. doi: 10.1016/j.ymssp.2012.11.002.

Duncan, Roger and Hershey, J. W. B. (1983) 'Identification and Quantitation of Levels of Protein Synthesis Initiation Factors in Crude HeLa Cell Lysates by Two-dimensional Polyacrylamide Gel Electrophoresis', *Journal of Biological Chemistry.*, 258(11), pp. 7228–7235. doi: 10.1016/S0021-9258(18)32356-1.

Duncan, R., Milburn, S. C. and Hershey, J. W. B. (1987) 'Regulated phosphorylation and low abundance of HeLa cell initiation factor eIF-4F suggest

a role in translational control. Heat shock effects on eIF-4F', *Journal of Biological Chemistry*, 262(1), pp. 380–388.

Duvaud, S. *et al.* (2021) 'Expasy , the Swiss Bioinformatics Resource Portal , as designed by its users', *Nucleic Acids Research*, 49(April), pp. 216–227.

Ebada, S. S. *et al.* (2011) 'Chemistry and biology of rocaglamides (= flavaglines) and related derivatives from aglaia species (meliaceae).', *Progress in the chemistry of organic natural products*, 94, pp. 1–58. doi: 10.1007/978-3-7091-0748-5_1.

Effector Therapeutics. 2020-. *Intravenous Zotatifin in Adults With Mild or Moderate COVID-19 (PROPEL) NCT04632381.* https://clinicaltrials.gov/ct2/show/NCT04632381.

Eisenstein, M. (2006) 'A look back: Adventures in the matrix', *Nature Methods*, 3(5), p. 410. doi: 10.1038/nmeth0506-410.

Elfakess, R. *et al.* (2011) 'Unique translation initiation of mRNAs-containing TISU element', *Nucleic Acids Research*, 39(17), pp. 7598–7609. doi: 10.1093/nar/gkr484.

Elfakess, R. and Dikstein, R. (2008) 'A Translation Initiation Element Specific to mRNAs with Very Short 5'UTR that Also Regulates Transcription', *plos one*, 3(8). doi: 10.1371/journal.pone.0003094.

Ernst, J. T. *et al.* (2020) 'Design of Development Candidate eFT226, a First in Class Inhibitor of Eukaryotic Initiation Factor 4A RNA Helicase', *Journal of Medicinal Chemistry*, 63(11), pp. 5879–5955. doi: 10.1021/acs.jmedchem.0c00182.

Ezkurdia, I. *et al.* (2014) 'Multiple evidence strands suggest that theremay be as few as 19 000 human protein-coding genes', *Human Molecular Genetics*, 23(22), pp. 5866–5878. doi: 10.1093/hmg/ddu309.

Fabian, M. R. *et al.* (2011) 'MiRNA-mediated deadenylation is orchestrated by GW182 through two conserved motifs that interact with CCR4-NOT', *Nature Structural and Molecular Biology*. Nature Publishing Group, 18(11), pp. 1211–1217. doi: 10.1038/nsmb.2149.

Fabian, M. R. *et al.* (2013) 'Structural basis for the recruitment of the human CCR4 – NOT deadenylase complex by tristetraprolin', *Nature Structural &*

Molecular Biology. Nature Publishing Group, 20(6), pp. 735–740. doi: 10.1038/nsmb.2572.

Fairman-Williams, M., Guenther, U.-P. and Jankowsky, E. (2011) 'SF1 and SF2 helicases: family matters', *Curr Opin Struct Biol.*, 20(3), pp. 313–324. doi: 10.1016/j.sbi.2010.03.011.SF1.

Fay, M. M. *et al.* (2014) 'Enhanced arginine methylation of programmed cell death 4 protein during nutrient deprivation promotes tumor cell viability', *Journal of Biological Chemistry*, 289(25), pp. 17541–17552. doi: 10.1074/jbc.M113.541300.

Feoktistova, K. *et al.* (2013) 'Human eIF4E promotes mRNA restructuring by stimulating eIF4A helicase activity', *Proceedings of the National Academy of Sciences*, 110(33), pp. 13339–13344. doi: 10.1073/pnas.1303781110.

Filipowicz, W. *et al.* (1976) 'A protein binding the methylated 5'-terminal sequence, m7GpppN, of eukaryotic messenger RNA', *Proc. Natl. Acad. Sci.* doi: 10.1146/annurev.bi.43.070174.003201.

Floor, S. N. *et al.* (2016) 'Autoinhibitory interdomain interactions and subfamilyspecific extensions redefine the catalytic core of the human DEAD-box protein DDX3', *Journal of Biological Chemistry*, 291(5), pp. 2412–2421. doi: 10.1074/jbc.M115.700625.

Fonseca, B. D. *et al.* (2015) 'La-related Protein 1 (LARP1) Represses Terminal Oligopyrimidine (TOP) mRNA Translation Downstream of mTOR Complex 1 (mTORC1)', *Journal of Biological Chemistry*, 290(26), pp. 15996–16020. doi: 10.1074/jbc.M114.621730.

Förster, T. (1948) 'Zwischenmolekulare Energiewanderung und Fluoreszenz', *annalen der physik*.

FPbase . n.d. https://www.fpbase.org/fret/.

Franke, D. and Svergun, D. I. (2009) 'DAMMIF, a program for rapid ab-initio shape determination in small-angle scattering', *Journal of Applied Crystallography*. International Union of Crystallography, 42(2), pp. 342–346. doi: 10.1107/S0021889809000338.

Fraser, C. S. *et al.* (2007) 'eIF3j Is Located in the Decoding Center of the Human

40S Ribosomal Subunit', *Molecular Cell*, 26(6), pp. 811–819. doi: 10.1016/j.molcel.2007.05.019.

Fried, M. and Crothers, D. (1981) 'Equlibibria and kinetics of Lac Repressor', *Nucleic acids research*, 9(23), pp. 6505–6525.

Frolova, L. *et al.* (1996) 'Eukaryotic polypeptide chain release factor eRF3 is an eRF1- and ribosome-dependent guanosine triphosphatese', *RNA*.

Fu, Q. and Yuan, Y. A. (2013) 'Structural insights into RISC assembly facilitated by dsRNA-binding domains of human RNA helicase A (DHX9)', *Nucleic Acids Research*, 41(5), pp. 3457–3470. doi: 10.1093/nar/gkt042.

Fukao, A. *et al.* (2014) 'MicroRNAs trigger dissociation of eIF4AI and eIF4AII from target mRNAs in humans', *Molecular Cell*. Elsevier Inc., 56(1), pp. 79–89. doi: 10.1016/j.molcel.2014.09.005.

Fukuchi-Shimogori, T. *et al.* (1997) 'Malignant transformation by overproduction of translation initiation factor eIF4G.', *Cancer research*. United States, 57(22), pp. 5041–5044.

Galicia-Vazquez, G. *et al.* (2012) 'A cellular response linking eIF4AI activity to eIF4AII transcription', *RNA*, 18, pp. 1373–1384. doi: 10.1261/rna.033209.112.

Galicia-Vazquez, G. *et al.* (2014) 'Regulation of eukaryotic initiation factor 4AII by MyoD during murine myogenic cell differentiation', *PLoS ONE*, 9(1), pp. 1–9. doi: 10.1371/journal.pone.0087237.

Galicia-Vázquez, G. *et al.* (2012) 'A cellular response linking eIF4AI activity to eIF4AII transcription', *Rna*, 18(7), pp. 1373–1384. doi: 10.1261/rna.033209.112.

Gao, C. *et al.* (2020) 'High intratumoral expression of eIF4A1 promotes epithelial-to-mesenchymal transition and predicts unfavorable prognosis in gastric cancer', *Acta Biochimica et Biophysica Sinica*, 52(3), pp. 310–319. doi: 10.1093/abbs/gmz168.

Garner, M. M. and Revzin, A. (1981) 'A gel electrophoresis mothod for quantifying the binding of proteins to specific DNA regions', *Nucleic Acids Research*, 9(13), pp. 3047–3060.

Gartmann, M. *et al.* (2010) 'Mechanism of eIF6-mediated Inhibition of

Ribosomal', *The Journal of Biological Chemistry*, 285(20), pp. 14848–14851. doi: 10.1074/jbc.C109.096057.

Gasteiger, E. *et al.* (2005) 'Protein Identification and Analysis Tools on the ExPASy Server', in Walker, J. (ed.) *The Proteomics Protocols Handbook*. Humana Press Inc., pp. 571–608. doi: 10.1385/1592598900.

Gatza, M. L. *et al.* (2014) 'An integrated genomics approach identifies drivers of proliferation in luminal-subtype human breast cancer', *Nature genetics*. 2014/08/24, 46(10), pp. 1051–1059. doi: 10.1038/ng.3073.

Gerashchenko, M. V, Su, D. and Gladyshev, V. N. (2010) 'CUG start codon generates thioredoxin/glutathione reductase isoforms in mouse testes.', *The Journal of biological chemistry*, 285(7), pp. 4595–4602. doi: 10.1074/jbc.M109.070532.

Germain, D. R. *et al.* (2011) 'DEAD box 1: a novel and independent prognostic marker for early recurrence in breast cancer.', *Breast cancer research and treatment*. Netherlands, 127(1), pp. 53–63. doi: 10.1007/s10549-010-0943-7.

Gingold, H. *et al.* (2014) 'A dual program for translation regulation in cellular proliferation and differentiation.', *Cell*. Elsevier Inc., 158(6), pp. 1281–1292. doi: 10.1016/j.cell.2014.08.011.

Gingras, A. *et al.* (1999) 'Regulation of 4E-BP1 phosphorylation : a novel two-step mechanism', *Genes and Development*, 13, pp. 1422–1437.

Gingras, A., Raught, B. and Sonenberg, N. (1999) 'eIF4 initiation factors: effectors of mRNA recruitment to ribosomes and regulators of translation', *Annu. Rev. Biochem.*, 68, pp. 913–963. doi: 0066-4154/99/0701-0913.

Giraldo, J. (2008) 'On the fitting of binding data when receptor dimerization is suspected', *British Journal of Pharmacology*, 155(1), pp. 17–23. doi: 10.1038/bjp.2008.234.

Giraldo, J. (2013) 'Modeling cooperativity effects in dimeric G protein-coupled receptors', *Progress in Molecular Biology and Translational Science*, 115, pp. 349–373. doi: 10.1016/B978-0-12-394587-7.00008-7.

Glickman, M. H. and Ciechanover, A. (2002) 'The ubiquitin-proteasome proteolytic pathway: Destruction for the sake of construction', *Physiological*

Reviews, 82(2), pp. 373–428. doi: 10.1152/physrev.00027.2001.

Godwin, A. . *et al.* (2013) 'Kiss your tail goodbye: the role of PARN, Nocturnin, and Angel deadenylases in mRNA biology Alan', *Biochimica et Biophysica Acta*, 1829829(6–7), pp. 571–579. doi: 10.1016/j.bbagrm.2012.12.004.Kiss.

Goedhart, J. *et al.* (2012) 'Structure-guided evolution of cyan fluorescent proteins towards a quantum yield of 93%', *Nature Communications*. doi: 10.1038/ncomms1738.

Goldstein, G. *et al.* (1975) 'Isolation of a polypeptide that has lymphocyte differentiating properties and is probably represented universally in living cells', *Proceedings of the National Academy of Sciences of the United States of America*, 72(1), pp. 11–15. doi: 10.1073/pnas.72.1.11.

Griesbeck, O. *et al.* (2001) 'Reducing the environmental sensitivity of yellow fluorescent protein. Mechanism and applications.', *The Journal of biological chemistry*. United States, 276(31), pp. 29188–29194. doi: 10.1074/jbc.M102815200.

Grifo, J. A. *et al.* (1983) 'New initiation factor activity required for globin mRNA translation.', *Journal of Biological Chemistry*, 258(9), pp. 5804–5810. doi: 10.1016/s0021-9258(20)81965-6.

Grifo, J. A. *et al.* (1984) 'RNA-stimulated ATPase activity of eukaryotic initiation factors', *Journal of Biological Chemistry*. Â© 1984 ASBMB. Currently published by Elsevier Inc; originally published by American Society for Biochemistry and Molecular Biology., 259(13), pp. 8648–8654. doi: 10.1016/s0021-9258(17)39779-x.

Grishaev, A. (2012) 'Sample preparation, data collection, and preliminary data analysis in biomolecular solution X-ray scattering', *Current Protocols in Protein Science*, 1(SUPPL.70), pp. 1–20. doi: 10.1002/0471140864.ps1714s70.

Guinier, A., Fournet, G. and Yudowitch, K. L. (1955) 'Small-angle scattering of X-rays'. Wiley New York.

Hagkarim, N. C. and Grand, R. J. (2020) 'The Regulatory Properties of the Ccr4 – Not Complex', *Cells*, 9(2379), pp. 1–45.

Hammond-Martel, I., Yu, H. and Affar, E. B. (2012) 'Roles of ubiquitin signaling

in transcription regulation', *Cellular Signalling*, 24(2), pp. 410–421. doi: https://doi.org/10.1016/j.cellsig.2011.10.009.

Han, C. *et al.* (2014) 'Article The RNA-Binding Protein DDX1 Promotes Primary MicroRNA Maturation and Inhibits Ovarian Tumor Progression', *Cell Reports*. The Authors, 8(5), pp. 1447–1460. doi: 10.1016/j.celrep.2014.07.058.

Hanahan, D. and Weinberg, R. A. (2011) 'Review Hallmarks of Cancer : The Next Generation', *Cell*. Elsevier Inc., 144(5), pp. 646–674. doi: 10.1016/j.cell.2011.02.013.

Hannan, K. M. *et al.* (2003) 'mTOR-Dependent Regulation of Ribosomal Gene Transcription Requires S6K1 and Is Mediated by Phosphorylation of the Carboxy-Terminal Activation Domain of the Nucleolar Transcription Factor UBF†', *Molecular and Cellular Biology*, 23(23), pp. 8862–8877. doi: 10.1128/mcb.23.23.8862-8877.2003.

Hanson, G. and Coller, J. (2018) 'Translation and Protein Quality Control: Codon optimality, bias and usage in translation and mRNA decay', *Nature Reviews Molecular Cell Biology*. Nature Publishing Group, 19(1), pp. 20–30. doi: 10.1038/nrm.2017.91.

Hara, K. *et al.* (1998) 'Amino Acid Sufficiency and mTOR Regulate p70 S6 Kinase and eIF-4E BP1 through a Common Effector Mechanism', *Journal of Biological Chemistry*. © 1998 ASBMB. Currently published by Elsevier Inc; originally published by American Society for Biochemistry and Molecular Biology., 273(23), pp. 14484–14494. doi: 10.1074/jbc.273.23.14484.

Harms, U. *et al.* (2014) 'EIF4B, eIF4G and RNA regulate eIF4A activity in translation initiation by modulating the eIF4A conformational cycle', *Nucleic Acids Research*. doi: 10.1093/nar/gku440.

Henn, A., Bradley, M. J. and De La Cruz, E. M. (2012) 'ATP utilization and RNA conformational rearrangement by DEAD-box proteins', *Annual Review of Biophysics*, 41(1), pp. 247–267. doi: 10.1146/annurev-biophys-050511-102243.

Herold, A. *et al.* (2000) 'TAP (NXF1) Belongs to a Multigene Family of Putative RNA Export Factors with a Conserved Modular Architecture', *Molecular and Cellular Biology*, 20(23), pp. 8996–9008. doi: 10.1128/mcb.20.23.8996-9008.2000.

Hershko, A. *et al*. (1980) ‘Proposed role of ATP in protein breakdown: conjugation of protein with multiple chains of the polypeptide of ATP-dependent proteolysis’, *Proceedings of the National Academy of Sciences*, 77(4), pp. 1783 LP – 1786. doi: 10.1073/pnas.77.4.1783.

Herzel, L. *et al*. (2017) ‘Splicing and transcription touch base: Co-transcriptional spliceosome assembly and function’, *Nature Reviews Molecular Cell Biology*. Nature Publishing Group, 18(10), pp. 637–650. doi: 10.1038/nrm.2017.63.

Herzog, V. A. *et al*. (2017) ‘Thiol-linked alkylation of RNA to assess expression dynamics’, *Nature Methods*, 14(12), pp. 1198–1204. doi: 10.1038/nmeth.4435.

Hesketh, J. (2005) ‘3’UTRs and Regulation’, *Encyclopedia of life sciences*, pp. 1–4. doi: 10.1038/npg.els.0005011.

Hilbert, M., Karow, A. R. and Klostermeier, D. (2009) ‘The mechanism of ATP-dependent RNA unwinding by DEAD box proteins’, *Biological Chemistry*, 390(12), pp. 1237–1250. doi: 10.1515/BC.2009.135.

Hill, A. . (1913) ‘The Combinations of Haemoglobin With Oxygen and With Carbon Monoxide. I’, *Biochemical Journal*, (7(5)), pp. 471–480.

Hinnebusch, A. G., Ivanov, I. P. and Sonenberg, N. (2016) ‘Translational control by 5′-untranslated regions of eukaryotic mRNAs’, *Science*, 352(6292), pp. 1413–1416. doi: 10.1126/science.aad9868.

Hinnebusch, A. G. and Lorsch, J. R. (2012) ‘The mechanism of eukaryotic translation initiation: New insights and challenges’, *Cold Spring Harbor Perspectives in Biology*, 4(10), pp. 1–25. doi: 10.1101/cshperspect.a011544.

Hoffmann, F., Chen, Y. and Campbell, R. E. (2018) ‘Integrative Biology Enhancing fluorescent protein photostability’, *Integrative Biology*. Royal Society of Chemistry, 10, pp. 419–428. doi: 10.1039/C8IB00063H.

Holzmann, K. *et al*. (2000) ‘A human common nuclear matrix protein homologous to eukaryotic translation initiation factor 4A.’, *Biochemical and biophysical research communications*. United States, 267(1), pp. 339–344. doi: 10.1006/bbrc.1999.1973.

Hondele, M. *et al*. (2019) ‘DEAD-box ATPases are global regulators of phase-separated organelles’, *Nature*. Springer US, 573(7772), pp. 144–148. doi:

10.1038/s41586-019-1502-y.

Hong, S. *et al.* (2017) 'LARP1 functions as a molecular switch for mTORC1-mediated translation of an essential class of mRNAs', *eLife*, 6, pp. 1–24. doi: 10.7554/eLife.25237.

Hoppe, A. D. *et al.* (2013) 'N-Way FRET Microscopy of Multiple Protein-Protein Interactions in Live Cells', *PLoS ONE*, 8(6). doi: 10.1371/journal.pone.0064760.

Hornbeck, P. V *et al.* (2015) 'PhosphoSitePlus, 2014: mutations, PTMs and recalibrations.', *Nucleic acids research*, 43(Database issue), pp. D512-20. doi: 10.1093/nar/gku1267.

Hosmillo, M. *et al.* (2016) 'The RNA Helicase eIF4A Is Required for Sapovirus Translation', *Journal of Virology*, 90(10), pp. 5200–5204. doi: 10.1128/jvi.03174-15.

Hosoda, N. *et al.* (2005) 'CBP80 promotes interaction of Upf1 with Upf2 during nonsense-mediated mRNA decay in mammalian cells', *Nature Structural & Molecular Biology*, 12(10), pp. 893–901. doi: 10.1038/nsmb995.

Hsieh, A. C. *et al.* (2012) 'The translational landscape of mTOR signalling steers cancer initiation and metastasis.', *Nature*, 485(7396), pp. 55–61. doi: 10.1038/nature10912.

Hu, W. *et al.* (2009) 'Co-translational mRNA decay in Saccharomyces cerevisiae', *Nature*. Nature Publishing Group, 461(September), pp. 225–230. doi: 10.1038/nature08265.

Huang, J.-S. *et al.* (2004) 'Diverse cellular transformation capability of overexpressed genes in human hepatocellular carcinoma.', *Biochemical and biophysical research communications*. United States, 315(4), pp. 950–958. doi: 10.1016/j.bbrc.2004.01.151.

Iacono, M., Mignone, F. and Pesole, G. (2005) 'uAUG and uORFs in human and rodent 5'untranslated mRNAs.', *Gene*. Netherlands, 349, pp. 97–105. doi: 10.1016/j.gene.2004.11.041.

Iadevaia, V. *et al.* (2008) 'All translation elongation factors and the e, f, and h subunits of translation initiation factor 3 are encoded by 5'-terminal oligopyrimidine (TOP) mRNAs.', *RNA (New York, N.Y.)*, 14(9), pp. 1730–1736.

doi: 10.1261/rna.1037108.

Imataka, H., Gradi, A. and Sonenberg, N. (1998) ‘A newly identified N-terminal amino acid sequence of human eIF4G binds poly (A) -binding protein and functions in poly (A) -dependent translation’, *The EMBO journal*, 17(24), pp. 7480–7489.

Imataka, H., Olsen, H. S. and Sonenberg, N. (1997) ‘A new translational regulator with homology to eukaryotic translation initiation factor 4G’, *The EMBO journal*, 16(4), pp. 817–825.

Imataka, H. and Sonenberg, N. (2015) ‘Human eukaryotic translation initiation factor 4G (eIF4G) possesses two separate and independent binding sites for eIF4A.’, *Molecular and Cellular Biology*, 17(12), pp. 6940–6947. doi: 10.1128/mcb.17.12.6940.

Ingelfinger, D. *et al.* (2002) ‘The human LSm1-7 proteins colocalize with the mRNA-degrading enzymes Dcp1 / 2 and Xrn1 in distinct cytoplasmic foci’, *RNA*, 8, pp. 1489–1501.

Ingolia, N. T., Lareau, L. F. and Weissman, J. S. (2011) ‘Ribosome profiling of mouse embryonic stem cells reveals the complexity and dynamics of mammalian proteomes’, *Cell*. Elsevier Inc., 147(4), pp. 789–802. doi: 10.1016/j.cell.2011.10.002.

Inoki, K. *et al.* (2002) ‘TSC2 is phosphorylated and inhibited by Akt and suppresses mTOR signalling.’, *Nature cell biology*. England, 4(9), pp. 648–657. doi: 10.1038/ncb839.

International Human Genome Sequencing Consortium (2004) ‘Finishing the euchromatic sequence of the human genome’, *Nature*, 431(7011), pp. 931–945.

Isken, O. and Maquat, L. E. (2008) ‘The multiple lives of NMD factors: Balancing roles in gene and genome regulation’, *Nature Reviews Genetics*, 9(9), pp. 699–712. doi: 10.1038/nrg2402.

Ivanov, I. P. *et al.* (2011) ‘Identification of evolutionarily conserved non-AUG-initiated N-terminal extensions in human coding sequences’, *Nucleic Acids Research*, 39(10), pp. 4220–4234. doi: 10.1093/nar/gkr007.

Iwasaki, S. *et al.* (2019) ‘The Translation Inhibitor Rocaglamide Targets a

Bimolecular Cavity between eIF4A and Article The Translation Inhibitor Rocaglamide Targets a Bimolecular Cavity between eIF4A and Polypurine RNA', *Molecular Cell*. Elsevier Inc., pp. 1–11. doi: 10.1016/j.molcel.2018.11.026.

Iwasaki, S., Floor, S. N. and Ingolia, N. T. (2016) 'Rocaglates convert DEAD-box protein eIF4A into a sequence-selective translational repressor', *Nature*, 534(7608):, pp. 558–561. doi: 10.1038/nature17978.

Izaurralde, E. *et al.* (1992) 'A cap binding protein that may mediate nuclear export of RNA polymerase II-transcribed RNAs', *Journal of Cell Biology*, 118(6), pp. 1287–1295. doi: 10.1083/jcb.118.6.1287.

Izaurralde, E. *et al.* (1995) 'A cap-binidng protein complex mediating U snRNA export', 376(August), pp. 709–712.

Jackson, R. ., Hellen, C. U. . and Pestova, T. . (2010) 'The mechanism of eukaryotic translation initiation and principles of its regulation', *Nature Reviews Molecular Cell Biology*. Nature Publishing Group, 10(February), pp. 113–127. doi: 10.1038/nrm2838.

Jackson, R., Hellen, C. and Pestova, T. (2010) 'The mechanism of eukaryotic translation initiation and priciples of its regulation', *Nat Rev Mol Cell Biol.*, 2, pp. 113–127.

Jackson, R. J. (2013) 'The current status of vertebrate cellular mRNA IRESs.', *Cold Spring Harbor perspectives in biology*, 5(2). doi: 10.1101/cshperspect.a011569.

Jackson, R. J., Hellen, C. U. T. and Pestova, T. V. (2012) *Termination and post-termination events in eukaryotic translation*. 1st edn, *Advances in Protein Chemistry and Structural Biology*. 1st edn. Elsevier Inc. doi: 10.1016/B978-0-12-386497-0.00002-5.

Jalkanen, A. L., Coleman, S. J. and Wilusz, J. (2014) 'Determinants and Implications of mRNA Poly(A) Tail Size - Does this Protein Make My Tail Look Big?', *Semin Cell Dev Biol.*, pp. 24–32. doi: 10.1016/j.semcdb.2014.05.018.Determinants.

Jankowsky, E. (2012) 'RNA Helicases at work: binding and rearranging', *Trends Biochem Sci.*, 36(1), pp. 19–29. doi: 10.1016/j.tibs.2010.07.008.RNA.

Jenuwein, T. and Allis, C. D. (2001) ‘Translating the histone code’, *Science*, 293(5532), pp. 1074–1080. doi: 10.1126/science.1063127.

Ji, P. *et al.* (2003) ‘MALAT-1, a novel noncoding RNA, and thymosin β4 predict metastasis and survival in early-stage non-small cell lung cancer’, *Oncogene*, 22(39), pp. 8031–8041. doi: 10.1038/sj.onc.1206928.

Jiang, C. *et al.* (2019) ‘Targeting the N Terminus of eIF4AI for Inhibition of Its Catalytic Recycling’, *Cell Chemical Biology*, 26, pp. 1–10. doi: 10.1016/j.chembiol.2019.07.010.

Jin, C. *et al.* (2013) ‘Targeting the eIF4A RNA helicase blocks translation of the MUC1-C oncoprotein’, *Oncogene*. Nature Publishing Group, 32(17), pp. 2179–2188. doi: 10.1038/onc.2012.236.

Johannes, G. and Sarnow, P. (1998) ‘Cap-independent polysomal association of natural mRNAs encoding c-myc, BiP, and eIF4G conferred by internal ribosome entry sites’, *Rna*, 4(12), pp. 1500–1513. doi: 10.1017/S1355838298981080.

Jovanovic, M. *et al.* (2015) ‘Immunogenetics. Dynamic profiling of the protein life cycle in response to pathogens.’, *Science*, 347(6226), p. 1259038. doi: 10.1126/science.1259038.

Jumper, J. *et al.* (2021) ‘Highly accurate protein structure prediction with AlphaFold’, *Nature*. doi: 10.1038/s41586-021-03819-2.

Kachala, M., Valentini, E. and Svergun, D. I. (2015) *Application of SAXS for the Structural Characterization of IDPs*, *Advances in Experimental Medicine and Biology in. Springer, Cham, pp. 261–289. doi: 10.1007/978-3-319-20164-1_8.* doi: 10.1007/978-3-319-20164-1_14.

Kanellis, D. C. *et al.* (2021) ‘The exon-junction complex helicase eIF4A3 controls cell fate via coordinated regulation of ribosome biogenesis and translational output’, *Science Advances*, 7(August).

Kapp, L. D. and Lorsch, J. R. (2004) ‘The molecular mechanics of eukaryotic translation’, *Annual Review of Biochemistry*, 73, pp. 657–704. doi: 10.1146/annurev.biochem.73.030403.080419.

Karousis, E. D. and Mühlemann, O. (2016) ‘Nonsense-mediated mRNA decay : novel mechanistic insights and biological impact’, *WIREs RNA*, 7(October), pp.

661–682. doi: 10.1002/wrna.1357.

Kashima, I. *et al.* (2006) 'Binding of a novel SMG-1 – Upf1 – eRF1 – eRF3 complex (SURF) to the exon junction complex triggers Upf1 phosphorylation and nonsense-mediated mRNA decay', *Genes and Development*, 20, pp. 355–367. doi: 10.1101/gad.1389006.phenotype.

Kearse, M. G. and Wilusz, J. E. (2017) 'Non-AUG translation: A new start for protein synthesis in eukaryotes', *Genes and Development*, 31(17), pp. 1717–1731. doi: 10.1101/gad.305250.117.GENES.

Khong, A. *et al.* (2017) 'The stress granule transcriptome reveals principles of mRNA accumulation accumulation in stress granules', *Mol. Cell*, 68(4), pp. 808–820. doi: 10.1016/j.molcel.2017.10.015.The.

Kieft, J. S. (2008) 'Viral IRES RNA structures and ribosome interactions.', *Trends in biochemical sciences*, 33(6), pp. 274–283. doi: 10.1016/j.tibs.2008.04.007.

Kikhney, A. G. and Svergun, D. I. (2015) 'A practical guide to small angle X-ray scattering (SAXS) of flexible and intrinsically disordered proteins', *FEBS Letters*, 589(19), pp. 2570–2577. doi: 10.1016/j.febslet.2015.08.027.

Kim, Y. and Myong, S. (2016) 'RNA Remodeling Activity of DEAD Box Proteins Tuned by Protein Concentration, RNA Length, and ATP', *Molecular Cell*. doi: 10.1016/j.molcel.2016.07.010.

Knight, J. R. P. *et al.* (2021) 'MNK inhibition sensitizes KRAS-Mutant colorectal cancer to mTORC1 inhibition by reducing eIF4E phosphorylation and C-MYC expression', *Cancer Discovery*, 11(5), pp. 1228–1247. doi: 10.1158/2159-8290.CD-20-0652.

Kocaturk, N. M. and Gozuacik, D. (2018) 'Crosstalk between mammalian autophagy and the ubiquitin-proteasome system', *Frontiers in Cell and Developmental Biology*, 6(OCT), pp. 1–27. doi: 10.3389/fcell.2018.00128.

Kogure, T. *et al.* (2013) 'Therapeutic Potential of the Translation Inhibitor Silvestrol in Hepatocellular Cancer', *PLoS ONE*, 8(9), pp. 1–14. doi: 10.1371/journal.pone.0076136.

Kolupaeva, V. G. *et al.* (2005) 'Binding of eukaryotic initiation factor 3 to ribosomal 40S subunits and its role in ribosomal dissociation and anti-

association', *RNA*, 11, pp. 470–486. doi: 10.1261/rna.7215305.resulting.

Kornberg, R. D. (1999) 'Eukaryotic transcriptional control', *Trends in Biochemical Sciences*, 24(12), pp. 46–49. doi: 10.1016/S0968-0004(99)01489-9.

Korneeva, N. L. *et al.* (2001) 'Characterization of the Two eIF4A-binding Sites on Human eIF4G-1', *Journal of Biological Chemistry*, 276(4), pp. 2872–2879. doi: 10.1074/jbc.M006345200.

Korneeva, N. L. *et al.* (2005) 'Interaction between the NH 2 -terminal Domain of eIF4A and the Central Domain of eIF4G Modulates RNA-stimulated ATPase Activity *', *Journal of Biological Chemistry*. Â© 2005 ASBMB. Currently published by Elsevier Inc; originally published by American Society for Biochemistry and Molecular Biology., 280(3), pp. 1872–1881. doi: 10.1074/jbc.M406168200.

Koutmou, K. S., Radhakrishnan, A. and Green, R. (2015) 'Synthesis at the Speed of Codons', *Trends in Biochemical Sciences*. Elsevier Ltd, 40(12), pp. 717–718. doi: 10.1016/j.tibs.2015.10.005.

Kozak, M. (1986) 'Point Mutations Define a Sequence Flanking the AUG Initiator Codon That Modulates Translation by Eukaryotic Ribosomes', *Cell*, 44, pp. 283–292.

Kozak, M. (1989) 'The Scanning Model for Translation: An Update', *The Journal of Cell Biology*, 108(February), pp. 229–241.

Kozak, M. (2001) 'Constraints on reinitiation of translation in mammals', *Nucleic Acids Research*, 29(24), pp. 5226–5232.

Kozak, M. (2002) 'Pushing the limits of the scanning mechanism for initiation of translation.', *Gene*, 299(1–2), pp. 1–34. doi: 10.1016/s0378-1119(02)01056-9.

Kozin, M. B. and Svergun, D. I. (2001) 'Automated matching of high- and low-resolution structural models', *Journal of Applied Crystallography*, 34(1), pp. 33–41. doi: 10.1107/S0021889800014126.

Kryukov, G. V *et al.* (2003) 'Characterization of Mammalian Selenoproteomes', *Science*, 300(5624), pp. 1439–1443. doi: 10.1126/science.1083516.

Kuzuoğlu-Öztürk, D. *et al.* (2016) ' mi RISC and the CCR 4– NOT complex silence mRNA targets independently of 43S ribosomal scanning ', *The EMBO Journal*,

35(11), pp. 1186–1203. doi: 10.15252/embj.201592901.

Kwon, S. C. *et al.* (2016) 'Structure of Human DROSHA', *Cell*. Elsevier Inc., 164(1–2), pp. 81–90. doi: 10.1016/j.cell.2015.12.019.

Lagos-Quintana, M. *et al.* (2001) 'Identification of novel genes coding for small expressed RNAs.', *Science (New York, N.Y.)*. United States, 294(5543), pp. 853–858. doi: 10.1126/science.1064921.

Lahr, R. M. *et al.* (2015) 'The La-related protein 1-specific domain repurposes HEAT-like repeats to directly bind a 5'TOP sequence', *Nucleic Acids Research*, 43(16), pp. 8077–8088. doi: 10.1093/nar/gkv748.

Lahr, R. M. *et al.* (2017) 'La-related protein 1 (LARP1) binds the mRNA cap, blocking eIF4F assembly on TOP mRNAs', *eLife*, 6, pp. 1–15. doi: 10.7554/eLife.24146.

Lakowicz, J. R. (2006) *General features of protein fluorescence*, *Principles of Fluorescence Spectroscopy.*, *Springer*

Lambert Instruments . n.d. https://www.lambertinstruments.com/technologies-1/2014/12/4/frequency-domain-flim-for-beginners.

Lamphear, B. J. *et al.* (1995) 'Mapping of Functional Domains in Eukaryotic Protein Synthesis Initiation Factor 4G (eIF4G) with Picornaviral Proteases', *Journal of Biological Chemistry.*, 270(37), pp. 21975–21983. doi: 10.1074/jbc.270.37.21975.

Lander, E. S. *et al.* (2001) 'Initial sequencing and analysis of the human genome', *Nature*, 412(6846), pp. 565–566. doi: 10.1038/35087627.

LaRonde-LeBlanc, N. *et al.* (2006) 'Structural Basis for Inhibition of Translation by the Tumor Suppressor Pdcd4', *Molecular and Cellular Biology*, 27(1), pp. 147–156. doi: 10.1128/mcb.00867-06.

Larsson, O. and Nadon, R. (2013) 'Re-analysis of genome wide data on mammalian microRNA-mediated suppression of gene expression.', *Translation*, 1(1), p. e24557. doi: 10.4161/trla.24557.

Lathe, G. H. and Ruthven, C. R. (1955) 'The separation of substances on the basis of their molecular weights, using columns of starch and water.', *The Biochemical journal*, 60(4).

Lattmann, S. *et al.* (2010) 'Role of the amino terminal RHAU-specific motif in the recognition and resolution of guanine quadruplex-RNA by the DEAH-box RNA helicase RHAU', *Nucleic Acids Research*, 38(18), pp. 6219–6233. doi: 10.1093/nar/gkq372.

Lazaris-Karatzas, A., Montine, K. S. and Sonenberg, N. (1990) 'Malignant transformation by a eukaryotic initiation factor subunit that binds to mRNA 5′ cap', *Nature*, 345(6275), pp. 544–547. doi: 10.1038/345544a0.

Le, H. *et al.* (1997) 'Translation initiation factors eIF-iso4G and eIF-4B interact with the poly(A)-binding protein and increase its RNA binding activity.', *The Journal of biological chemistry*. United States, 272(26), pp. 16247–16255. doi: 10.1074/jbc.272.26.16247.

Lea, W. A. and Simeonov, A. (2011) 'Fluorescence polarization assays in small molecule screening', *Expert Opinion on Drug Discovery*, 6(1), pp. 17–32. doi: 10.1517/17460441.2011.537322.

Lee, C. and Seydoux, G. (2019) 'Dynamics of mRNA entry into stress granules', *Nature Cell Biology*, 21(February), pp. 114–121.

Lembo, A., Di Cunto, F. and Provero, P. (2012) 'Shortening of 3'UTRs correlates with poor prognosis in breast and lung cancer.', *PloS one*, 7(2), p. e31129. doi: 10.1371/journal.pone.0031129.

Leppek, K., Das, R. and Barna, M. (2018) 'Functional 5′ UTR mRNA structures in eukaryotic translation regulation and how to find them', *Nat Rev Mol Cell Biol*. Nature Publishing Group, 19(3), pp. 158–174. doi: 10.1038/nrm.2017.103.Functional.

Levy, S. *et al.* (1991) 'Oligopyrimidine tract at the 5' end of mammalian ribosomal protein mRNAs is required for their translational control.', *Proceedings of the National Academy of Sciences of the United States of America*, 88(8), pp. 3319–3323. doi: 10.1073/pnas.88.8.3319.

Lewis, B. P., Burge, C. B. and Bartel, D. P. (2005) 'Conserved seed pairing, often flanked by adenosines, indicates that thousands of human genes are microRNA targets', *Cell*, 120(1), pp. 15–20. doi: 10.1016/j.cell.2004.12.035.

Li, J. and Liu, C. (2019) 'Coding or noncoding, the converging concepts of RNAs',

Frontiers in Genetics, 10(MAY), pp. 1–10. doi: 10.3389/fgene.2019.00496.

Li, W., Belsham, G. J. and Proud, C. G. (2001) 'Eukaryotic Initiation Factors 4A (eIF4A) and 4G (eIF4G) Mutually Interact in a 1:1 Ratio in Vivo', *Journal of Biological Chemistry*, 276(31), pp. 29111–29115. doi: 10.1074/jbc.C100284200.

Liang, S. *et al.* (2014) 'Decreased expression of EIF4A1 after preoperative brachytherapy predicts better tumor-specific survival in cervical cancer', *International Journal of Gynecological Cancer*, 24(5), pp. 908–915. doi: 10.1097/IGC.0000000000000152.

Liberman, N. *et al.* (2015) 'DAP5 associates with eIF2β and eIF4AI to promote Internal Ribosome Entry Site driven translation', *Nucleic Acids Research*, 43(7), pp. 3764–3775. doi: 10.1093/nar/gkv205.

Lim, J. *et al.* (2018) 'Mixed tailing by TENT4A and TENT4B shields mRNA from rapid deadenylation', *Science*, 361(6403), pp. 701–704. doi: 10.1126/science.aam5794.

Lin, Y. *et al.* (2018) 'Systematic Analysis of Gene Expression Alteration and Co-Expression Network of Eukaryotic Initiation Factor 4A-3 in Cancer', *Journal of Cancer*, 9, pp. 1–10. doi: 10.7150/jca.27655.

Linder, P. *et al.* (1989) 'Birth of the D-E-A-D box', *Nature*, 24, pp. 8–9.

Linder, P. and Jankowsky, E. (2011) 'From unwinding to clamping — the DEAD box RNA helicase family', *Nature Publishing Group*. Nature Publishing Group, 12(August). doi: 10.1038/nrm3154.

Lindqvist, L. *et al.* (2008) 'Selective pharmacological targeting of a DEAD box RNA helicase', *PLoS ONE*, 3(2). doi: 10.1371/journal.pone.0001583.

Ling, J. *et al.* (2020) 'Targeting eIF4A3 as a multifunctional translation initiation factor for breast cancer therapy', *Cancer Research*. American Association for Cancer Research, 80(16 Supplement), p. 2461. doi: 10.1158/1538-7445.AM2020-2461.

Liu, H., Luo, M. and Wen, J. K. (2014) 'mRNA stability in the nucleus', *Journal of Zhejiang University: Science B*, 15(5), pp. 444–454. doi: 10.1631/jzus.B1400088.

Liu, M. *et al.* (2019) 'MicroRNA-5195-3p enhances the chemosensitivity of triple-

negative breast cancer to paclitaxel by downregulating EIF4A2', *Cellular and Molecular Biology Letters*. Cellular & Molecular Biology Letters, 24(1), pp. 1–11. doi: 10.1186/s11658-019-0168-7.

Liu, N., Han, H. and Lasko, P. (2009) 'Vasa promotes Drosophila germline stem cell differentiation by activating mei-P26 translation by directly interacting with a (U)-rich motif in its 3' UTR.', *Genes & development*, 23(23), pp. 2742–2752. doi: 10.1101/gad.1820709.

Lobanov, A. V *et al.* (2010) 'Dual functions of codons in the genetic code.', *Critical reviews in biochemistry and molecular biology*, 45(4), pp. 257–265. doi: 10.3109/10409231003786094.

Loh, P. G. *et al.* (2009) 'Structural basis for translational inhibition by the tumour suppressor Pdcd4', *EMBO Journal*, 28(3), pp. 274–285. doi: 10.1038/emboj.2008.278.

Lomnytska, M. I. *et al.* (2012) 'Impact of genomic stability on protein expression in endometrioid endometrial cancer', *British Journal of Cancer*, 106(7), pp. 1297–1305. doi: 10.1038/bjc.2012.67.

Longtin, R. (2004) 'A forgotten debate: Is selenocysteine the 21st amino acid?', *Journal of the National Cancer Institute*, 96(7), pp. 504–505. doi: 10.1093/jnci/96.7.504.

Lorsch, J. R. and Dever, T. E. (2010) 'Molecular View of 43 S Complex Formation and Start Site Selection in Eukaryotic Translation Initiation', *Journal of Biological Chemistry*. Â© 2010 ASBMB. Currently published by Elsevier Inc; originally published by American Society for Biochemistry and Molecular Biology., 285(28), pp. 21203–21207. doi: 10.1074/jbc.R110.119743.

Lorsch, J. R. and Herschlag, D. (1998a) 'The DEAD box protein eIF4A. 1. A minimal kinetic and thermodynamic framework reveals coupled binding of RNA and nucleotide', *Biochemistry*, 37(8), pp. 2180–2193. doi: 10.1021/bi972430g.

Lorsch, J. R. and Herschlag, D. (1998b) 'The DEAD box protein eIF4A. 2. A cycle of nucleotide and RNA-dependent conformational changes', *Biochemistry*, 37(8), pp. 2194–2206. doi: 10.1021/bi9724319.

Lykke-andersen, J., Shu, M. and Steitz, J. A. (2000) 'Human Upf Proteins Target

an mRNA for Nonsense-Mediated Decay When Bound Downstream of a Termination Codon', *Cell*, 103, pp. 1121–1131.

Lykke-Andersen, S. and Jensen, T. H. (2007) 'Overlapping pathways dictate termination of RNA polymerase II transcription', *Biochimie*, 89(10), pp. 1177–1182. doi: 10.1016/j.biochi.2007.05.007.

Lyu, S. *et al.* (2020) 'High expression of eIF4A2 in esophageal squamous cell carcinoma is associated with poor prognosis', *Oncology Letters*, 98(37), pp. 1–8. doi: 10.1097/MD.0000000000017104.

Ma, L. *et al.* (2005) 'Phosphorylation and functional inactivation of TSC2 by Erk implications for tuberous sclerosis and cancer pathogenesis.', *Cell*. United States, 121(2), pp. 179–193. doi: 10.1016/j.cell.2005.02.031.

Mackowiak, S. D. *et al.* (2015) 'Extensive identification and analysis of conserved small ORFs in animals', *Genome Biology*. Genome Biology, 16(179), pp. 1–21. doi: 10.1186/s13059-015-0742-x.

Mader, S. *et al.* (1995) 'The translation initiation factor eIF-4E binds to a common motif shared by the translation factor eIF-4 gamma and the translational repressors 4E-binding proteins', *Molecular and Cellular Biology*, 15(9), pp. 4990–4997. doi: 10.1128/mcb.15.9.4990.

Manalastas-Cantos, K. *et al.* (2021) 'ATSAS 3.0: Expanded functionality and new tools for small-angle scattering data analysis', *Journal of Applied Crystallography*. International Union of Crystallography, 54, pp. 343–355. doi: 10.1107/S1600576720013412.

Maquat, L. E., Tarn, W. Y. and Isken, O. (2010) 'The pioneer round of translation: Features and functions', *Cell*, 142(3), pp. 368–374. doi: 10.1016/j.cell.2010.07.022.

Marcotrigiano, J. *et al.* (1999) 'Cap-Dependent Translation Initiation in Eukaryotes Is Regulated by a Molecular Mimic of eIF4G', *Molecular Cell*, 3, pp. 707–716.

Marintchev, A *et al.* (2009) 'Topology and regulation of the human eIF4A/4G/4H helicase complex in translation initiation.', *Cell*, 136(3), pp. 447–460.

Marintchev, Assen *et al.* (2009) 'Topology and regulation of the human

eIF4A/4G/4H helicase complex in translation initiation.', *Cell*, 136(3), pp. 447–460. doi: 10.1016/j.cell.2009.01.014.

Marintchev, A. (2013) 'Roles of Helicases in Translation Initiation: A Mechanistic View', *Biochim Biophys Acta.*, 1829(8), pp. 799–809. doi: 10.1016/j.bbagrm.2013.01.005.

Mark, C. A., Lan, F. and F., D. T. (1988) 'tRNAimet Functions in Directing the Scanning Ribosome to the Start Site of Translation', *Science*. American Association for the Advancement of Science, 242(4875), pp. 93–97. doi: 10.1126/science.3051379.

Martelange, V. *et al.* (2000) 'Identification on a Human Sarcoma of Two New Genes with Tumor-specific Expression', *Cancer Research*, 60(29), pp. 3848–3855.

Mateju, D. *et al.* (2020) 'Single-Molecule Imaging Reveals Translation of mRNAs Localized to Stress Granules ll ll Article Single-Molecule Imaging Reveals Translation of mRNAs Localized to Stress Granules', *Cell*. Elsevier Inc., 183(7), pp. 1801–1812. doi: 10.1016/j.cell.2020.11.010.

Mathonnet, G. *et al.* (2007) 'MicroRNA inhibition of translation initiation in vitro by targeting the cap-binding complex eIF4F.', *Science (New York, N.Y.)*. United States, 317(5845), pp. 1764–1767. doi: 10.1126/science.1146067.

Mathys, H. *et al.* (2014) 'Structural and Biochemical Insights to the Role of the CCR4-NOT Complex and DDX6 ATPase in MicroRNA Repression', *Molecular Cell*. doi: 10.1016/j.molcel.2014.03.036.

Matsuda, D. *et al.* (2007) 'Failsafe nonsense-mediated mRNA decay does not detectably target eIF4E-bound mRNA', *Nature Structural & Molecular Biology*, 14(10), pp. 974–979. doi: 10.1038/nsmb1297.

Matsui, M. *et al.* (2007) 'Bioinformatic analysis of post-transcriptional regulation by uORF in human and mouse.', *FEBS letters*. England, 581(22), pp. 4184–4188. doi: 10.1016/j.febslet.2007.07.057.

Mauer, J. *et al.* (2017) 'Reversible methylation of m 6 A m in the 5 ′ cap controls mRNA stability', *Nature Publishing Group*. Nature Publishing Group, 541(7637), pp. 371–375. doi: 10.1038/nature21022.

Mayr, C. and Bartel, D. (2009) 'Widespread shortening of 3′UTRs by alternative

cleavage and polyadenylation activates oncogenes in cancer cells', *Cell*, 138(4). doi: 10.1016/j.cell.2009.06.016.Widespread.

McMahon, M. *et al.* (2019) 'A single H/ACA small nucleolar RNA mediates tumor suppression downstream of oncogenic RAS', *eLife*, 8, pp. 1–26. doi: 10.7554/eLife.48847.

Medina-Muñoz, S. G. *et al.* (2021) 'Crosstalk between codon optimality and cis-regulatory elements dictates mRNA stability', *Genome Biology*. Genome Biology, 22(1), pp. 1–23. doi: 10.1186/s13059-020-02251-5.

Meijer, H. A. *et al.* (2013) 'Translational Repression and eIF4A2 Activity Are Critical for MicroRNA-Mediated Gene Regulation', *Science*. doi: 10.1126/science.1231197.

Meijer, H. A. *et al.* (2019) 'DEAD-box helicase eIF4A2 inhibits CNOT7 deadenylation activity', *Nucleic Acids Research*. Oxford University Press, pp. 1–15. doi: 10.1093/nar/gkz509.

Methot, N., Song, M. and Sonenberg, N. (1996) 'A Region Rich in Aspartic Acid , Arginine , Tyrosine , and Glycine (DRYG) Mediates Eukaryotic Initiation Factor 4B (eIF4B) Self-Association and Interaction with eIF3', *Molecular and Cellular Biology*, 16(10), pp. 5328–5334.

Meyer, K. D. *et al.* (2012) 'Comprehensive analysis of mRNA methylation reveals enrichment in 3′ UTRs and near stop codons', *Cell*, 149(7), pp. 1635–1646. doi: 10.1016/j.cell.2012.05.003.

Meyuhas, O. and Kahan, T. (2015) 'The race to decipher the top secrets of TOP mRNAs.', *Biochimica et biophysica acta*. Netherlands, 1849(7), pp. 801–811. doi: 10.1016/j.bbagrm.2014.08.015.

Miga, K. H. *et al.* (2020) 'Telomere-to-telomere assembly of a complete human X chromosome', *Nature*. Springer US, 585(7823), pp. 79–84. doi: 10.1038/s41586-020-2547-7.

Mignone, F. and Pesole, G. (2018) 'mRNA Untranslated Regions (UTRs)', *eLS*, pp. 1–6. doi: 10.1002/9780470015902.a0005009.pub3.

Miluzio, A. *et al.* (2009) 'Eukaryotic initiation factor 6 mediates a continuum between 60S ribosome biogenesis and translation', *EMBO reports*, 10(5), pp.

459–465. doi: 10.1038/embor.2009.70.

Mitchell, S. F. *et al.* (2010) 'The 5'-7-Methylguanosine Cap on Eukaryotic mRNAs Serves Both to Stimulate Canonical Translation Initiation and to Block an Alternative Pathway', *Molecular Cell*. Elsevier Inc., 39(6), pp. 950–962. doi: 10.1016/j.molcel.2010.08.021.

Mitkevich, V. A. *et al.* (2006) 'Termination of translation in eukaryotes is mediated by the quaternary eRF1•eRF3•GTP•Mg2+ complex. The biological roles of eRF3 and prokaryotic RF3 are profoundly distinct', *Nucleic Acids Research*, 34(14), pp. 3947–3954. doi: 10.1093/nar/gkl549.

Mix, H., Lobanov, A. V and Gladyshev, V. N. (2007) 'SECIS elements in the coding regions of selenoprotein transcripts are functional in higher eukaryotes', *Nucleic Acids Research*, 35(2), pp. 414–423. doi: 10.1093/nar/gkl1060.

Modelska, A. *et al.* (2015) 'The malignant phenotype in breast cancer is driven by eIf4A1-mediated changes in the translational landscape', *Cell Death and Disease*. doi: 10.1038/cddis.2014.542.

Mollet, S. *et al.* (2008) 'Translationally Repressed mRNA Transiently Cycles through Stress Granules during Stress', *Molecular Biology of the Cell*, 19, pp. 4469–4479. doi: 10.1091/mbc.E08.

Morales, C. R., Kwon, Y. K. and Hecht, N. B. (1991) 'Cytoplasmic localization during storage and translation of the mRNAs of transition protein 1 and protamine 1, two translationally regulated transcripts of the mammalian testis.', *Journal of cell science*. England, 100 (Pt 1, pp. 119–131.

Mozziconacci, J. *et al.* (2017) 'P-Body Purification Reveals the Condensation of Repressed mRNA Regulons Article P-Body Purification Reveals the Condensation of Repressed mRNA Regulons', *Molecular Cell*, 68(October), pp. 144–157. doi: 10.1016/j.molcel.2017.09.003.

Mugridge, J. S., Coller, J. and Gross, J. D. (2018) 'Structural and molecular mechanisms for the control of eukaryotic 5′–3′ mRNA decay', *Nature Structural & Molecular Biology*. Springer US, 25(December). doi: 10.1038/s41594-018-0164-z.

Müller, C. *et al.* (2020) 'Comparison of broad-spectrum antiviral activities of the synthetic rocaglate CR-31-B (−) and the eIF4A-inhibitor Silvestrol', *Antiviral*

Research. Elsevier B.V., 175, p. 104706. doi: 10.1016/j.antiviral.2020.104706.

Naineni, S. K. *et al*. (2020) 'A Comparative Study of Small Molecules Targeting eIF4A', *RNA*, p. rna.072884.119. doi: 10.1261/rna.072884.119.

Nakagawa, Y. *et al*. (1999) 'Overexpression of rck/p54, a DEAD box protein, in human colorectal tumours.', *British journal of cancer*, 80(5–6), pp. 914–917. doi: 10.1038/sj.bjc.6690441.

Nielsen, K. H. *et al*. (2011) 'Synergistic activation of eIF4A by eIF4B and eIF4G', *Nucleic Acids Research*. doi: 10.1093/nar/gkq1206.

Nielsen, P. J., McMaster, G. and Trachsel, H. (1985) 'Nucleic Acids Research Nucleic Acids Research', *Nucl*.

Nielsen, P. J. and Trachsel, H. (1988) 'The mouse protein synthesis initiation factor 4A gene family includes two related functional genes which are differentially expressed.', *The EMBO journal*, 7(7), pp. 2097–2105. doi: 10.1002/j.1460-2075.1988.tb03049.x.

Northcote, P. T., Blunt, J. W. and Munro, M. H. G. (1991) 'Pateamine: a potent cytotoxin from the New Zealand Marine sponge, mycale sp.', *Tetrahedron Letters*, 32(44), pp. 6411–6414. doi: https://doi.org/10.1016/0040-4039(91)80182-6.

Nott, A., Le Hir, H. and Moore, M. J. (2004) 'Splicing enhances translation in mammalian cells: An additional function of the exon junction complex', *Genes and Development*, 18(2), pp. 210–222. doi: 10.1101/gad.1163204.

O'Leary, C. A. *et al*. (2019) 'RNA structural analysis of the MYC mRNA reveals conserved motifs that affect gene expression', *PLOS ONE*. Public Library of Science, 14(6), p. e0213758. Available at: https://doi.org/10.1371/journal.pone.0213758.

Oberer, M., Marintchev, A. and Wagner, G. (2005) 'Structural basis for the enhancement of eIF4A helicase activity by eIF4G', *Genes and Development*, 19(18), pp. 2212–2223. doi: 10.1101/gad.1335305.

Ohnishi, S. *et al*. (2009) 'Solution structure of the GUCT domain from human RNA helicase II/Guß reveals the RRM fold, but implausible RNA interactions', *Proteins: Structure, Function and Bioinformatics*, 74(1), pp. 133–144. doi:

10.1002/prot.22138.

Osborne, M. J. *et al.* (2013) 'EIF4E3 acts as a tumor suppressor by utilizing an atypical mode of methyl-7-guanosine cap recognition', *Proceedings of the National Academy of Sciences of the United States of America*, 110(10), pp. 3877–3882. doi: 10.1073/pnas.1216862110.

Özeş, A. R. *et al.* (2011) 'Duplex unwinding and ATPase activities of the DEAD-box helicase eIF4A are coupled by eIF4G and eIF4B', *Journal of Molecular Biology*, 412(4), pp. 674–687. doi: 10.1016/j.jmb.2011.08.004.

Özeş, A. R. *et al.* (2014) 'Real-time fluorescence assays to monitor duplex unwinding and ATPase activities of helicases', *Nature Protocols*, 9(7), pp. 1645–1661. doi: 10.1038/nprot.2014.112.

Pan, Q. *et al.* (2008) 'Deep surveying of alternative splicing complexity in the human transcriptome by high-throughput sequencing', *Nature Genetics*, 40(12), pp. 1413–1415. doi: 10.1038/ng.259.

Park, J. E. *et al.* (2011) 'Dicer recognizes the 5′ end of RNA for efficient and accurate processing', *Nature*. Nature Publishing Group, 475(7355), pp. 201–205. doi: 10.1038/nature10198.

Parker, R. and Song, H. (2004) 'The enzymes and control of eukaryotic mRNA turnover', *Nature Structural & Molecular Biology*, 11(2), pp. 121–127. doi: 10.1038/nsmb724.

Parsyan, A. *et al.* (2009) 'The helicase protein DHX29 promotes translation initiation , cell proliferation , and tumorigenesis', *PNAS*, 106(52), pp. 22217–22222.

Parsyan, A. *et al.* (2011) 'MRNA helicases: The tacticians of translational control', *Nature Reviews Molecular Cell Biology*, 12, pp. 235–245. doi: 10.1038/nrm3083.

Passmore, L. A. *et al.* (2007) 'The Eukaryotic Translation Initiation Factors eIF1 and eIF1A Induce an Open Conformation of the 40S Ribosome', *Molecular Cell*, 26, pp. 41–50. doi: 10.1016/j.molcel.2007.03.018.

Pause, A. *et al.* (1994) 'Insulin-dependent stimulation of protein synthesis by phosphorylation of a regulator of 5'-cap function', *Nature*, 371(October), pp.

762–767.

Pavlov, M. Y. *et al.* (2009) 'Slow peptide bond formation by proline and other N-alkylamino acids in translation', *PNAS*, 106(1), pp. 50–54.

Peck, M. L. and Herschlag, D. (1999) 'Effects of oligonucleotide length and atomic composition on stimulation of the ATPase activity of translation initiation factor eIF4A', *RNA*, 5(9), pp. 1210–1221. doi: 10.1017/S1355838299990817.

Peck, M. L. and Herschlag, D. (2003) 'Adenosine 5′-O-(3-thio)triphosphate (ATPγS) is a substrate for the nucleotide hydrolysis and RNA unwinding activities of eukaryotic translation initiation factor eIF4A', *Rna*, 9(10), pp. 1180–1187. doi: 10.1261/rna.2103703.

Pelechano, V. *et al.* (2015) 'Widespread Co-translational RNA Decay Reveals Ribosome Dynamics Article Widespread Co-translational RNA Decay Reveals Ribosome Dynamics', *Cell*. Elsevier Inc., 161(6), pp. 1400–1412. doi: 10.1016/j.cell.2015.05.008.

Pelletier, J. and Sonenberg, N. (1985) 'Insertion mutagenesis to increase secondary structure within the 5′ noncoding region of a eukaryotic mRNA reduces translational efficiency', *Cell*, 40(3), pp. 515–526. doi: 10.1016/0092-8674(85)90200-4.

Pelletier, J. and Sonenberg, N. (1988) 'Internal initiation of translation of eukaryotic mRNA directed by a sequence derived from poliovirus RNA', *Nature*, 334(6180), pp. 320–325. doi: 10.1038/334320a0.

Pesole, G. *et al.* (2001) 'Structural and functional features of eukaryotic mRNA untranslated regions', *Gene*, 276, pp. 73–81.

Pestova, T. V *et al.* (2000) 'The joining of ribosomal subunits in eukaryotes requires eIF5B', *Nature*, 403(JANUARY), pp. 4–7.

Pestova, T. V, Borukhov, S. I. and Hellen, C. U. T. (1998) 'Eukaryotic ribosomes require initiation factors 1 and 1A to locate initiation codons', *Nature*, 394(August), pp. 854–859.

Phillips, T., and K. Shaw. 2008. "Chromatin Remodeling in Eukaryotes." *Nature Education*.

PhysiologyWeb. n.d. *PhysiologyWeb*. https://www.physiologyweb.com/calculators/hill_equation_interactive_graph.html.

Pisarev, A. V. *et al.* (2010) 'The Role of ABCE1 in Eukaryotic Posttermination Ribosomal Recycling', *Molecular Cell*, 37(2), pp. 196–210. doi: 10.1016/j.molcel.2009.12.034.

Pisareva, V. P. *et al.* (2006) 'Kinetic analysis of interaction of eukaryotic release factor 3 with guanine nucleotides', *Journal of Biological Chemistry*. Â© 2006 ASBMB. Currently published by Elsevier Inc; originally published by American Society for Biochemistry and Molecular Biology., 281(52), pp. 40224–40235. doi: 10.1074/jbc.M607461200.

Pisareva, V. P. *et al.* (2008) 'Translation Initiation on Mammalian mRNAs with Structured 5'UTRs Requires DExH-Box Protein DHX29', *Cell*. Elsevier Ltd, 135(7), pp. 1237–1250. doi: 10.1016/j.cell.2008.10.037.

Plot Digitizer. n.d. https://plotdigitizer.com/.

Poliseno, L. *et al.* (2010) 'A coding-independent function of gene and pseudogene mRNAs regulates tumour biology', *Nature*. Nature Publishing Group, 465(7301), pp. 1033–1038. doi: 10.1038/nature09144.

PRALINE, Centre for Integrative Bioinformatics VU. n.d. *PRALINE*. https://www.ibi.vu.nl/programs/pralinewww/.

Pratt, A. J. and MacRae, I. J. (2009) 'The RNA-induced silencing complex: A versatile gene-silencing machine', *Journal of Biological Chemistry*, 284(27), pp. 17897–17901. doi: 10.1074/jbc.R900012200.

Prinz, H. (2010) 'Hill coefficients, dose-response curves and allosteric mechanisms', *Journal of Chemical Biology*, 3(1), pp. 37–44. doi: 10.1007/s12154-009-0029-3.

Prior, I. A., Lewis, P. D. and Mattos, C. (2012) 'A comprehensive survey of Ras mutations in cancer.', *Cancer research*, 72(10), pp. 2457–2467. doi: 10.1158/0008-5472.CAN-11-2612.

Proud, C. G. (2005) 'eIF2 and the control of cell physiology.', *Seminars in cell & developmental biology*. England, 16(1), pp. 3–12. doi: 10.1016/j.semcdb.2004.11.004.

Putnam, A. A. *et al.* (2015) 'Division of labor in an oligomer of the DEAD-box RNA helicase Ded1p', *Molecular Cell*, 59(0), pp. 923–930. doi: 10.1016/j.clinbiochem.2015.06.023.Gut-Liver.

Putnam, C. D. *et al.* (2007) 'X-ray solution scattering (SAXS) combined with crystallography and computation: Defining accurate macromolecular structures, conformations and assemblies in solution', *Quarterly Reviews of Biophysics*, 40(3), pp. 191–285. doi: 10.1017/S0033583507004635.

Pyronnet, S. *et al.* (1999) 'Human eukaryotic translation initiation factor 4G (eIF4G) recruits Mnk1 to phosphorylate eIF4E', *The EMBO journal*, 18(1), pp. 270–279.

Querido, J. B. *et al.* (2020) 'Structure of a human 48S translational initiation complex', *Science*, 369(6508), pp. 1220–1227. doi: 10.1126/science.aba4904.Structure.

Rambo, R. P. and Tainer, J. A. (2011) 'Characterizing flexible and intrinsically unstructured biological macromolecules by SAS using the Porod-Debye law', *Biopolymers*, 95(8), pp. 559–571. doi: 10.1002/bip.21638.

Rana, T. M. (2007) 'Illuminating the silence: Understanding the structure and function of small RNAs', *Nature Reviews Molecular Cell Biology*, 8(1), pp. 23–36. doi: 10.1038/nrm2085.

Rau, M. *et al.* (1996) 'A Reevaluation of the Cap-binding Protein , eIF4E , as a Rate-limiting Factor for Initiation of Translation in Reticulocyte Lysate', *Journal of Biological Chemistry*. Â© 1996 ASBMB. Currently published by Elsevier Inc; originally published by American Society for Biochemistry and Molecular Biology., 271(15), pp. 8983–8990. doi: 10.1074/jbc.271.15.8983.

Reich, S. H. *et al.* (2018) 'Structure-based Design of Pyridone-Aminal eFT508 Targeting Dysregulated Translation by Selective Mitogen-activated Protein Kinase Interacting Kinases 1 and 2 (MNK1/2) Inhibition', *Journal of Medicinal Chemistry*, 61(8), pp. 3516–3540. doi: 10.1021/acs.jmedchem.7b01795.

Richter-Cook, N. J. *et al.* (1998) 'Purification and characterization of a new eukaryotic protein translation factor: Eukaryotic initiation factor 4h', *Journal of Biological Chemistry*. Â© 1998 ASBMB. Currently published by Elsevier Inc; originally published by American Society for Biochemistry and Molecular

Biology., 273(13), pp. 7579–7587. doi: 10.1074/jbc.273.13.7579.

Richter, N. J. *et al.* (1999) 'Further biochemical and kinetic characterization of human eukaryotic initiation factor 4H', *Journal of Biological Chemistry*. Â© 1999 ASBMB. Currently published by Elsevier Inc; originally published by American Society for Biochemistry and Molecular Biology., 274(50), pp. 35415–35424. doi: 10.1074/jbc.274.50.35415.

Robert, F. *et al.* (2020) 'RNA-tethering assay and eIF4G : eIF4A obligate dimer design uncovers multiple eIF4F functional complexes', *Nucleic Acids Research*. Oxford University Press, 48(15), pp. 8562–8575. doi: 10.1093/nar/gkaa646.

Rogers, G. W. *et al.* (2001) 'Modulation of the Helicase Activity of eIF4A by eIF4B, eIF4H, and eIF4F', *Journal of Biological Chemistry*. doi: 10.1074/jbc.M100157200.

Rogers, George W., Lima, W. F. and Merrick, W. C. (2001) 'Further characterization of the helicase activity of eIF4A. Substrate specificity', *Journal of Biological Chemistry*. Â© 2001 ASBMB. Currently published by Elsevier Inc; originally published by American Society for Biochemistry and Molecular Biology., 276(16), pp. 12598–12608. doi: 10.1074/jbc.M007560200.

Rogers, G. W., Lima, W. F. and Merrick, W. C. (2001) 'Further Characterization of the Helicase Activity of eIF4A', *The Journal of Biological Chemistry*, 276(16), pp. 12598–12608. doi: 10.1074/jbc.M007560200.

Rogers, G. W., Richter, N. J. and Merrick, W. C. (1999) 'Biochemical and kinetic characterization of the RNA helicase activity of eukaryotic initiation factor 4A', *Journal of Biological Chemistry*. Â© 1999 ASBMB. Currently published by Elsevier Inc; originally published by American Society for Biochemistry and Molecular Biology., 274(18), pp. 12236–12244. doi: 10.1074/jbc.274.18.12236.

Ross, J. and Sullivan, T. D. (1985) 'Half-lives of beta and gamma globin messenger RNAs and of protein synthetic capacity in cultured human reticulocytes', *Blood*. American Society of Hematology, 66(5), pp. 1149–1154. doi: 10.1182/blood.v66.5.1149.1149.

Rouya, C. *et al.* (2014) 'Human DDX6 effects miRNA-mediated gene silencing via direct binding to CNOT1', *RNA*, 20, pp. 1398–1409. doi: 10.1261/rna.045302.114.4.

Rozen, F. *et al.* (1990) 'Bidirectional RNA helicase activity of eucaryotic translation initiation factors 4A and 4F.', *Molecular and cellular biology*, 10(3), pp. 1134–44. doi: 10.1128/MCB.10.3.1134.

Rozovsky, N., Butterworth, A. C. and Moore, M. J. (2008) 'Interactions between eIF4AI and its accessory factors eIF4B and eIF4H', *Rna*, 14(10), pp. 2136–2148. doi: 10.1261/rna.1049608.

Rubio, C. A. *et al.* (2014) 'Transcriptome-wide characterization of the eIF4A signature highlights plasticity in translation regulation', *Genome Biology*, 15(476), pp. 1–19.

Rudolph, M. G. and Klostermeier, D. (2015) 'When core competence is not enough: Functional interplay of the DEAD-box helicase core with ancillary domains and auxiliary factors in RNA binding and unwinding', *Biological Chemistry*, 396(8), pp. 849–865. doi: 10.1515/hsz-2014-0277.

Ruggero, D. *et al.* (2004) 'The translation factor eIF-4E promotes tumor formation and cooperates with c-Myc in lymphomagenesis', *Nature Medicine*, 10(5), pp. 484–486. doi: 10.1038/nm1042.

Ryu, I. *et al.* (2013) 'eIF4GI Facilitates the MicroRNA-Mediated Gene Silencing', *PLoS ONE*, 8(2). doi: 10.1371/journal.pone.0055725.

Sabatini, D. M. *et al.* (1994) 'RAFT1: A mammalian protein that binds to FKBP12 in a rapamycin-dependent fashion and is homologous to yeast TORs', *Cell*, 78(1), pp. 35–43. doi: 10.1016/0092-8674(94)90570-3.

Saha, A., Wittmeyer, J. and Cairns, B. R. (2006) 'Chromatin remodelling: The industrial revolution of DNA around histones', *Nature Reviews Molecular Cell Biology*, 7(6), pp. 437–447. doi: 10.1038/nrm1945.

Saikia, M. *et al.* (2016) 'Codon optimality controls differential mRNA translation during amino acid starvation', *Rna*, 22(11), pp. 1719–1727. doi: 10.1261/rna.058180.116.

Salzberg, S. L. (2018) 'Open questions: How many genes do we have?', *BMC Biology*. BMC Biology, 16(1), pp. 10–12. doi: 10.1186/s12915-018-0564-x.

Saulière, J. *et al.* (2012) 'CLIP-seq of eIF4AIII reveals transcriptome-wide mapping of the human exon junction complex', *Nature Structural and Molecular*

Biology. Nature Publishing Group, 19(11), pp. 1124–1131. doi: 10.1038/nsmb.2420.

Schmidt, C. *et al.* (2016) 'The cryo-EM structure of a ribosome-Ski2-Ski3-Ski8 helicase complex.', *Science (New York, N.Y.)*. United States, 354(6318), pp. 1431–1433. doi: 10.1126/science.aaf7520.

Schnell, J. D. and Hicke, L. (2003) 'Non-traditional functions of ubiquitin and ubiquitin-binding proteins', *Journal of Biological Chemistry*. Â© 2003 ASBMB. Currently published by Elsevier Inc; originally published by American Society for Biochemistry and Molecular Biology., 278(38), pp. 35857–35860. doi: 10.1074/jbc.R300018200.

Schutz, P. *et al.* (2008) 'Crystal structure of the yeast eIF4A-eIF4G complex: An RNA-helicase controlled by protein-protein interactions', *Proceedings of the National Academy of Sciences*, 105(28), pp. 9564–9569. doi: 10.1073/pnas.0800418105.

Schütz, P. *et al.* (2010) 'Comparative structural analysis of human DEAD-Box RNA helicases', *PLoS ONE*, 5(9), pp. 1–11. doi: 10.1371/journal.pone.0012791.

Schwanhüusser, B. *et al.* (2011) 'Global quantification of mammalian gene expression control', *Nature*, 473(7347), pp. 337–342. doi: 10.1038/nature10098.

Selbach, M. *et al.* (2008) 'Widespread changes in protein synthesis induced by microRNAs', *Nature*, 455(7209), pp. 58–63. doi: 10.1038/nature07228.

Sendoel, A. *et al.* (2017) 'Translation from unconventional 5' start sites drives tumour initiation.', *Nature*, 541(7638), pp. 494–499. doi: 10.1038/nature21036.

Shah, P. *et al.* (2013) 'Rate-limiting steps in yeast protein translation', *Cell*. Elsevier, 153(7), p. 1589. doi: 10.1016/j.cell.2013.05.049.

Shahbazian, D. *et al.* (2006) 'The mTOR/PI3K and MAPK pathways converge on eIF4B to control its phosphorylation and activity', *EMBO Journal*, 25(12), pp. 2781–2791. doi: 10.1038/sj.emboj.7601166.

Shaoyan, X. *et al.* (2013) 'Downregulation of EIF4A2 in Non e Small-Cell Lung Cancer Associates with Poor Prognosis', *Clinical Lung Cancer*. Elsevier Inc, 14(6), pp. 658–665. doi: 10.1016/j.cllc.2013.04.011.

Sharma, D. *et al*. (2017) 'Biochemical Differences and Similarities between the DEAD-Box Helicase Orthologs DDX3X and Ded1p', *J Mol Biol.*, 429(23), pp. 3730–3742. doi: 10.1186/s40945-017-0033-9.Using.

Shatkin, A. J. (1976) 'Capping of eucaryotic mRNAs', *Cell*, 9(4 PART 2), pp. 645–653. doi: 10.1016/0092-8674(76)90128-8.

Shatsky, I. N. *et al*. (2014) 'Transcriptome-wide studies uncover the diversity of modes of mRNA recruitment to eukaryotic ribosomes', *Critical Reviews in Biochemistry and Molecular Biology*. Taylor & Francis, 49(2), pp. 164–177. doi: 10.3109/10409238.2014.887051.

Sheth, U. and Parker, R. (2003) 'Decapping and Decay of Messenger RNA Occur in Cytoplasmic Processing Bodies', *Science*, 300(5620), pp. 805–808.

Shin, S. *et al*. (2007) 'Involvement of RNA helicases p68 and p72 in colon cancer.', *Cancer research*. United States, 67(16), pp. 7572–7578. doi: 10.1158/0008-5472.CAN-06-4652.

Shirai, Y. *et al*. (2014) 'Multifunctional roles of the mammalian CCR4 – NOT complex in physiological phenomena', *Frontiers in Genetics*, 5(August), pp. 1–11. doi: 10.3389/fgene.2014.00286.

Silvera, D. *et al*. (2009) 'Essential role for eIF4GI overexpression in the pathogenesis of inflammatory breast cancer.', *Nature cell biology*. England, 11(7), pp. 903–908. doi: 10.1038/ncb1900.

Simossis, V. A. and Heringa, J. (2003) 'The PRALINE online server : optimising progressive multiple alignment on the web', *Computational Biology and Chemistry*, 27, pp. 511–519. doi: 10.1016/j.compbiolchem.2003.09.002.

Simossis, V. A. and Heringa, J. (2005) 'PRALINE : a multiple sequence alignment toolbox that integrates homology-extended and secondary structure information', *Nucleic Acids Research*, 33, pp. 289–294. doi: 10.1093/nar/gki390.

Sims, R. J., Mandal, S. S. and Reinberg, D. (2004) 'Recent highlights of RNA-polymerase-II-mediated transcription', *Current Opinion in Cell Biology*, 16(3), pp. 263–271. doi: 10.1016/j.ceb.2004.04.004.

Singh, P. *et al*. (2011) 'Pdcd4 directly binds the coding region of c-myb mRNA and suppresses its translation', *Oncogene*, 30(49), pp. 4864–4873. doi:

10.1038/onc.2011.202.

Singleton, M. R., Dillingham, M. S. and Wigley, D. B. (2007) 'Structure and Mechanism of Helicases and Nucleic Acid Translocases', *Annu. Rev. Biochem.*, 76, pp. 23–50. doi: 10.1146/annurev.biochem.76.052305.115300.

Smith, E. M. *et al.* (2021) 'The mTOR regulated RNA-binding protein LARP1 requires PABPC1 for guided mRNA interaction', *Nucleic Acids Research*. Oxford University Press, 49(1), pp. 458–478. doi: 10.1093/nar/gkaa1189.

Sokabe, M. and Fraser, C. S. (2017) 'A helicase-independent activity of eIF4A in promoting mRNA recruitment to the human ribosome', *Proceedings of the National Academy of Sciences of the United States of America*, 114(24), pp. 6304–6309. doi: 10.1073/pnas.1620426114.

Sokabe, M., Fraser, C. S. and Hershey, J. W. B. (2012) 'The human translation initiation multi-factor complex promotes methionyl-tRNA i binding to the 40S ribosomal subunit', *Nucleic Acids Research*, 40(2), pp. 905–913. doi: 10.1093/nar/gkr772.

Sonenberg, N. and Hinnebusch, A. G. (2009) 'Regulation of Translation Initiation in Eukaryotes: Mechanisms and Biological Targets', *Cell*. Elsevier Inc., 136(4), pp. 731–745. doi: 10.1016/j.cell.2009.01.042.

Song, H. *et al.* (2000) 'The crystal structure of human eukaryotic release factor eRF1 - Mechanism of stop codon recognition and peptidyl-tRNA hydrolysis', *Cell*, 100(3), pp. 311–321. doi: 10.1016/S0092-8674(00)80667-4.

Song, H. and Ji, X. (2019) 'The mechanism of RNA duplex recognition and unwinding by DEAD-box helicase DDX3X', *Nature Communications*. Springer US, 10(1), p. 3085. doi: 10.1038/s41467-019-11083-2.

Spiegel, J. D. *et al.* (2016) 'Failure of the IDA in FRET Systems at Close Inter-Dye Distances Is Moderated by Frequent Low κ 2 Values', *The Journal of physical chemistry*, 120, pp. 8845–8862. doi: 10.1021/acs.jpcb.6b05754.

Spriggs, K. A. *et al.* (2008) 'Re-programming of translation following cell stress allows IRES-mediated translation to predominate.', *Biology of the cell*. England, 100(1), pp. 27–38. doi: 10.1042/BC20070098.

Strahl, B. D. and Allis, C. D. (2000) 'The language of covalent histone

modifications', *Nature*, 403(6765), pp. 41–45. doi: 10.1038/47412.

Sudo, K., Takahashi, E. and Nakamura, Y. (1995) 'Isolation and mapping of the human EIF4A2 gene homologous to the murine protein synthesis initiation factor 4A-II gene Eif4a2', *Cytogenetics and Cell Genetics*. Switzerland, 71(4), pp. 385–388. doi: 10.1159/000134145.

Sun, Y. *et al.* (2010) 'Three-color spectral FRET microscopy localizes three interacting proteins in living cells', *Biophysical Journal*. Biophysical Society, 99(4), pp. 1274–1283. doi: 10.1016/j.bpj.2010.06.004.

Sun, Y. *et al.* (2014) 'Single-molecule kinetics of the eukaryotic initiation factor 4AI upon RNA unwinding', *Structure*. Elsevier Ltd, 22(7), pp. 941–948. doi: 10.1016/j.str.2014.04.014.

Suzuki, C. *et al.* (2008) 'PDCD4 inhibits translation initiation by binding to eIF4A using both its MA3 domains', *PNAS*.

Svergun, D. I. (1999) 'Restoring low resolution structure of biological macromolecules from solution scattering using simulated annealing', *Biophysical Journal*. Elsevier, 76(6), pp. 2879–2886. doi: 10.1016/S0006-3495(99)77443-6.

Svergun, D. I. and Stuhrmann, H. B. (1991) 'New developments in direct shape determination from small-angle scattering. 1. Theory and model calculations', *Acta Crystallographica Section A*. International Union of Crystallography, 47(6), pp. 736–744. doi: 10.1107/S0108767391006414.

Tajirika, T. *et al.* (2018) 'DEAD-Box Protein RNA-Helicase DDX6 Regulates the Expression of HER2 and FGFR2 at the Post-Transcriptional Step in Gastric Cancer Cells', *International Journal of Molecular Sciences*, 19(7). doi: 10.3390/ijms19072005.

Takata, A. *et al.* (2012) 'A miRNA machinery component DDX20 controls NF-κB via microRNA-140 function.', *Biochemical and biophysical research communications*. United States, 420(3), pp. 564–569. doi: 10.1016/j.bbrc.2012.03.034.

Taliaferro, J. M. *et al.* (2016) 'RNA Sequence Context Effects Measured In Vitro Predict In Vivo Protein Binding and Regulation', *Molecular Cell*. Elsevier Inc., 64(2), pp. 294–306. doi: 10.1016/j.molcel.2016.08.035.

Tanaka, K. *et al.* (2009) 'DDX1 is required for testicular tumorigenesis, partially through the transcriptional activation of 12p stem cell genes.', *Oncogene*. England, 28(21), pp. 2142–2151. doi: 10.1038/onc.2009.89.

Tang, J. *et al.* (2018) 'DEAD-box helicase 27 promotes colorectal cancer growth and metastasis and predicts poor survival in CRC patients', *Oncogene*. Springer US, pp. 3006–3021. doi: 10.1038/s41388-018-0196-1.

Tange, T., Nott, A. and Moore, M. J. (2004) 'The ever-increasing complexities of the exon junction complex', *Current Opinion in Cell Biology*, 16(3), pp. 279–284. doi: 10.1016/j.ceb.2004.03.012.

Taniguchi, K. *et al.* (2018) 'Oncogene RNA helicase DDX6 promotes the process of c-Myc expression in gastric cancer cells.', *Molecular carcinogenesis*. United States, 57(5), pp. 579–589. doi: 10.1002/mc.22781.

Tanner, N. K. *et al.* (2003) 'The Q Motif : A Newly Identified Motif in DEAD Box Helicases May Regulate ATP Binding and Hydrolysis', *Molecular Cell*, 11, pp. 127–138.

Tanner, N. K. and Linder, P. (2001) 'DExD / H Box RNA Helicases : From Generic Motors to Specific Dissociation Functions', 8, pp. 251–262.

Tat, T. T. *et al.* (2016) 'Cotranslational microRNA mediated messenger RNA destabilization', *eLife*, pp. 1–18. doi: 10.7554/eLife.12880.

Tauber, D. *et al.* (2020) 'Modulation of RNA Condensation by the DEAD-Box Protein eIF4A', *Cell*.

Temperley, R. J. *et al.* (2010) 'Human mitochondrial mRNAs-like members of all families, similar but different', *Biochimica et Biophysica Acta - Bioenergetics*, 1797(6–7), pp. 1081–1085. doi: 10.1016/j.bbabio.2010.02.036.

The 1000 Genomes Project Consortium (2015) 'A global reference for human genetic variation', *Nature*. doi: 10.1038/nature15393.A.

The UniProt Consortium (2021) 'UniProt : the universal protein knowledgebase in 2021', *Nucleic Acids Research*. Oxford University Press, 49(November 2020), pp. 480–489. doi: 10.1093/nar/gkaa1100.

Theissen, B. *et al.* (2008) 'Cooperative binding of ATP and RNA induces a closed

conformation in a DEAD box RNA helicase', *Proceedings of the National Academy of Sciences of the United States of America*, 105(2), pp. 548–553. doi: 10.1073/pnas.0705488105.

Thoreen, C. C. *et al.* (2012) 'A unifying model for mTORC1-mediated regulation of mRNA translation.', *Nature*, 485(7396), pp. 109–113. doi: 10.1038/nature11083.

Tillotson, J. *et al.* (2017) 'ATP-competitive, marine derived natural products that target the DEAD box helicase, eIF4A', *Bioorganic and Medicinal Chemistry Letters*. doi: 10.1016/j.bmcl.2017.07.045.

Tomek, W. and Wollenhaupt, K. (2012) 'The "closed loop model" in controlling mRNA translation during development', *Animal Reproduction Science*. Elsevier B.V., 134(1–2), pp. 2–8. doi: 10.1016/j.anireprosci.2012.08.005.

Torrent, M. *et al.* (2018) 'Cells alter their tRNA abundance to selectively regulate protein synthesis during stress conditions', *Science Signaling*, 11(546), pp. 1–10. doi: 10.1126/scisignal.aat6409.

Torres, A. G. *et al.* (2019) 'Differential expression of human tRNA genes drives the abundance of tRNA-derived fragments', *Proceedings of the National Academy of Sciences of the United States of America*, 116(17), pp. 8451–8456. doi: 10.1073/pnas.1821120116.

Travers, A. (1974) 'RNA Polymerase-Promoter Interactions: Some General Principles', *Cell*, 3(October), pp. 97–104.

Tropberger, P. and Schneider, R. (2013) 'Scratching the (lateral) surface of chromatin regulation by histone modifications', *Nature Structural and Molecular Biology*. Nature Publishing Group, 20(6), pp. 657–661. doi: 10.1038/nsmb.2581.

Truitt, M. L. *et al.* (2015) 'Differential Requirements for eIF4E Dose in Normal Development and Cancer', *Cell*, 162(1), pp. 59–71. doi: 10.1016/j.cell.2015.05.049.

Tsutakawa, S. E. *et al.* (2007) 'Structural analysis of flexible proteins in solution by small angle X-ray scattering combined with crystallography', *Journal of Structural Biology*, 158, pp. 214–223. doi: 10.1016/j.jsb.2006.09.008.

Tuukkanen, A. T., Kleywegt, G. J. and Svergun, D. I. (2016) 'Resolution of ab

initio shapes determined from small-angle scattering', *IUCrJ*. International Union of Crystallography, 3, pp. 440–447. doi: 10.1107/S2052252516016018.

Ueda, T. *et al*. (2010) 'Combined deficiency for MAP kinase-interacting kinase 1 and 2 (Mnk1 and Mnk2) delays tumor development', *Proceedings of the National Academy of Sciences of the United States of America*, 107(32), pp. 13984–13990. doi: 10.1073/pnas.1008136107.

Valasek, L. *et al*. (2004) 'Interactions of Eukaryotic Translation Initiation Factor 3 (eIF3) Subunit NIP1 / c with eIF1 and eIF5 Promote Preinitiation Complex Assembly and Regulate Start Codon Selection', *Molecular and Cellular Biology*, 24(21), pp. 9437–9455. doi: 10.1128/MCB.24.21.9437.

Vattem, K. M. and Wek, R. C. (2004) 'Reinitiation involving upstream ORFs regulates ATF4 mRNA translation in mammalian cells', *PNAS*, 101(31), pp. 11269–11274.

Vikhreva, P. N., Kalinichenko, S. V. and Korobko, I. V. (2017) 'Programmed cell death 4 mechanism of action: The model to be updated?', *Cell Cycle*. Taylor & Francis, 16(19), pp. 1761–1764. doi: 10.1080/15384101.2017.1371881.

Volkov, V. V. and Svergun, D. I. (2003) 'Uniqueness of ab initio shape determination in small-angle scattering', *Journal of Applied Crystallography*, 36(3 I), pp. 860–864. doi: 10.1107/S0021889803000268.

Voorhees, R. M. *et al*. (2010) 'The mechanism for activation of GTP hydrolysis on the ribosome', *Science*. doi: 10.1126/science.1194460.The.

Voorhees, R. M. and Ramakrishnan, V. (2013) 'Structural basis of the translational elongation cycle', *Annual Review of Biochemistry*, 82, pp. 203–236. doi: 10.1146/annurev-biochem-113009-092313.

Wagner, S. *et al*. (2020) 'Selective Translation Complex Profiling Reveals Staged Initiation and Co-translational Assembly of Initiation Factor Complexes ll Selective Translation Complex Profiling Reveals Staged Initiation and Co-translational Assembly of Initiation Factor', *Molecular Cell*, 79, pp. 546–560. doi: 10.1016/j.molcel.2020.06.004.

Waldron, J. A. *et al*. (2019) 'MRNA structural elements immediately upstream of the start codon dictate dependence upon eIF4A helicase activity', *Genome*

Biology. Genome Biology, 20(1), pp. 1–23. doi: 10.1186/s13059-019-1901-2.

Waldron, J. A., Raza, F. and Le Quesne, J. (2018) 'eIF4A alleviates the translational repression mediated by classical secondary structures more than by G-quadruplexes', *Nucleic Acids Research*. Oxford University Press, 46(6), pp. 3075–3087. doi: 10.1093/nar/gky108.

Wang, D. W. *et al*. (2015) 'The different roles of selective autophagic protein degradation in mammalian cells', *Oncotarget*, 6(35), pp. 37098–37116. doi: 10.18632/oncotarget.5776.

Wang, G. ., Allis, C. . and Ping, C. (2007) 'Chromatin remodeling and cancer, part II: ATP-dependent chromatin remodeling', *Trends Mol Med*. doi: 10.1016/j.molmed.2007.07.004.Chromatin.

Wei, X. *et al*. (2004) 'Analysis of the RNA helicase A gene in human lung cancer', *Oncol Rep*. Institute of Pathology, University Hospital Charité, Berlin, Germany null, 11(1), pp. 253–258. doi: 10.3892/or.11.1.253.

Weingarten-Gabbay, S. *et al*. (2016) 'Systematic discovery of cap-independent translation sequences in human and viral genomes', *Science*, 351(6270), p. aad4939. doi: 10.1126/science.aad4939.

Wells, S. E. *et al*. (1998) 'Circularization of mRNA by Eukaryotic Translation Initiation Factors', *Molecular Cell*, 2, pp. 135–140.

Wendel, H. G. *et al*. (2007) 'Dissecting eIF4E action in tumorigenesis', *Genes and Development*, 21(24), pp. 3232–3237. doi: 10.1101/gad.1604407.

Wilczynska, A. *et al*. (2019) 'eIF4A2 drives repression of translation at initiation by Ccr4-Not through purine-rich motifs in the 5′ UTR', *Genome Biology*. Genome Biology, 20(262), pp. 1–21. doi: 10.1186/s13059-019-1857-2.

Wilczynska, A. and Bushell, M. (2015) 'The complexity of miRNA-mediated repression', *Cell Death and Differentiation*, 22, pp. 22–33. doi: 10.1038/cdd.2014.112.

Will, C. . and Luhrmann, R. (2011) 'Spliceosome Structure and Function', *Cold Spring Harbor Perspectives in Biology*. doi: 10.3858/emm.2008.40.6.686.

Williams-Hill, D. M. *et al*. (1997) 'Differential Expression of the Murine

Eukaryotic Translation Initiation Factor Isogenes eIF4A I and eIF4A II Is Dependent upon Cellular Growth Status', *ARCHIVES OF BIOCHEMISTRY AND BIOPHYSICS*, 338(BB969804), pp. 111–120.

Wisdom, R. and Lee, W. (1991) 'The protein-coding region of c-myc mRNA contains a sequence that specifies rapid mRNA turnover and induction by protein synthesis inhibitors', *Genes and Development*, 5(2), pp. 232–243. doi: 10.1101/gad.5.2.232.

Wolfe, A. L. *et al.* (2014) 'RNA G-quadruplexes cause eIF4A-dependent oncogene translation in cancer.', *Nature*. doi: 10.1038/nature13485.

Wortham, N. C. *et al.* (2009) 'The DEAD-box protein p72 regulates ERalpha-/oestrogen-dependent transcription and cell growth, and is associated with improved survival in ERalpha-positive breast cancer.', *Oncogene*, 28(46), pp. 4053–4064. doi: 10.1038/onc.2009.261.

Wu, D.-W. *et al.* (2016) 'DDX3 enhances oncogenic KRAS-induced tumor invasion in colorectal cancer via the ß-catenin/ZEB1 axis.', *Oncotarget*, 7(16), pp. 22687–22699. doi: 10.18632/oncotarget.8143.

Wu, D. *et al.* (2011) 'An alternative splicing isoform of eukaryotic initiation factor 4H promotes tumorigenesis in vivo and is a potential therapeutic target for human cancer.', *International journal of cancer*. United States, 128(5), pp. 1018–1030. doi: 10.1002/ijc.25419.

Wu, Q. *et al.* (2020) 'Translation of small downstream ORFs enhances translation of canonical main open reading frames', *The EMBO journal*, 39, pp. 1–13. doi: 10.15252/embj.2020104763.

Wurm, J., Glowacz, K. and Sprangers, R. (2021) 'Structural basis for the activation of the DEAD-box RNA helicase DbpA by the nascent ribosome', *PNAS*, 118(36), pp. 1–10. doi: 10.1073/pnas.2105961118/-/DCSupplemental.Published.

Yadav, M. *et al.* (2021) 'The KH domain facilitates the substrate specificity and unwinding processivity of DDX43 helicase', *Journal of Biological Chemistry*. Elsevier B.V, 296(10), p. 100085. doi: 10.1074/jbc.RA120.015824.

Yamashita, A. *et al.* (2005) 'Concerted action of poly (A) nucleases and decapping enzyme in mammalian mRNA turnover', *Nature Structural &*

Molecular Biology, 12(12), pp. 1054–1063. doi: 10.1038/nsmb1016.

Yan, L. X. *et al.* (2011) 'Knockdown of miR-21 in human breast cancer cell lines inhibits proliferation, in vitro migration and in vivo tumor growth', *Breast Cancer Research*, 13(1), pp. 1–14. doi: 10.1186/bcr2803.

Yang, H.-S. *et al.* (2002) 'The Transformation Suppressor Pdcd4 Is a Novel Eukaryotic Translation Initiation Factor 4A Binding Protein That Inhibits Translation', *Molecular and Cellular Biology*, 23(1), pp. 26–37. doi: 10.1128/mcb.23.1.26-37.2003.

Yang, H. *et al.* (2004) 'A Novel Function of the MA-3 Domains in Transformation and Translation Suppressor Pdcd4 Is Essential for Its Binding to Eukaryotic Translation Initiation Factor 4A', *Molecular & Cellular Biology*, 24(9), pp. 3894–3906. doi: 10.1128/MCB.24.9.3894.

Yang, L., Lin, C. and Liu, Z.-R. (2005) 'Phosphorylations of DEAD box p68 RNA helicase are associated with cancer development and cell proliferation.', *Molecular cancer research : MCR*. United States, 3(6), pp. 355–363. doi: 10.1158/1541-7786.MCR-05-0022.

Yi, H. *et al.* (2018) 'PABP Cooperates with the CCR4-NOT Complex to Promote mRNA Deadenylation and Block Article PABP Cooperates with the CCR4-NOT Complex to Promote mRNA Deadenylation and Block Precocious Decay', *Molecular Cell*. Elsevier Inc., 70(6), pp. 1081–1088. doi: 10.1016/j.molcel.2018.05.009.

Yoder-Hill, J. *et al.* (1993) 'The p46 Subunit of Eukaryotic Initiation Factor (eIF)-4F Exchanges with eIF-4A', *THE JOURNAL OF BIOLOGICAL CHEMISTRY*.

Yourik, P. *et al.* (2017) 'Yeast eIF4A enhances recruitment of mRNAs regardless of their structural complexity', *eLife*. doi: 10.7554/eLife.31476.

Yu, C. H. *et al.* (2015) 'Codon Usage Influences the Local Rate of Translation Elongation to Regulate Co-translational Protein Folding', *Molecular Cell*. Elsevier Inc., 59(5), pp. 744–754. doi: 10.1016/j.molcel.2015.07.018.

Yuan, T. L. and Cantley, L. C. (2008) 'PI3K pathway alterations in cancer: variations on a theme.', *Oncogene*, 27(41), pp. 5497–5510. doi: 10.1038/onc.2008.245.

Zaccara, S. and Jaffrey, S. R. (2020) ‘A Unified Model for the Function of YTHDF Proteins in Regulating m6A-Modified mRNA’, *Cell*. Elsevier, 181(7), pp. 1582-1595.e18. doi: 10.1016/j.cell.2020.05.012.

Zhang, J. *et al.* (1998) ‘Intron function in the nonsense-mediated decay of b - globin mRNA : Indications that pre-mRNA splicing in the nucleus can influence mRNA translation in the cytoplasm’, *RNA*, 4, pp. 801–815.

Zhang, W. *et al.* (2019) ‘Intercepted Retro-Nazarov Reaction: Syntheses of Amidino-Rocaglate Derivatives and Their Biological Evaluation as eIF4A Inhibitors’, *Journal of the American Chemical Society*. American Chemical Society, 141(32), pp. 12891–12900. doi: 10.1021/jacs.9b06446.

Zhang, W., Dunkle, J. and Cate, J. H. D. (2009) ‘Structures of the ribosome in intermediate states of ratcheting’, *Science*. doi: 10.1126/science.1175275.Structures.

Zhu, C. *et al.* (2020) ‘Integrated Analysis of DEAD-Box Helicase 56: A Potential Oncogene in Osteosarcoma’, *Frontiers in Bioengineering and Biotechnology*, 8, p. 588. doi: 10.3389/fbioe.2020.00588.

Zhu, Y., Ren, C. and Yang, L. I. (2021) ‘Effect of eukaryotic translation initiation factor 4A3 in malignant tumors (Review)’, *Oncology Letters*, 21. doi: 10.3892/ol.2021.12619.

Zinder, J. C. and Lima, C. D. (2017) ‘Targeting RNA for processing or destruction by the eukaryotic RNA exosome and its cofactors’, *Genes and Development*, 31, pp. 88–100. doi: 10.1101/gad.294769.116.

Zinoni, F. *et al.* (1986) ‘Nucleotide sequence and expression of the selenocysteine-containing polypeptide of formate dehydrogenase (formate-hydrogen-lyase-linked) from Escherichia coli’, *Proceedings of the National Academy of Sciences*, 83(13), pp. 4650 LP – 4654. doi: 10.1073/pnas.83.13.4650.